PHD

Transition metal complexes partnered with the highly alkylated carborane anion, [1-H-CLOSO-CB11Me11]

Ingleson, Michael James

Award date:
2004

Awarding institution:
University of Bath

TRANSITION METAL COMPLEXES PARTNERED WITH THE HIGHLY ALKYLATED CARBORANE ANION, [1-H-*CLOSO*-$CB_{11}Me_{11}$]$^-$.

Michael James Ingleson

A thesis submitted for the degree of Doctor of Philosophy

University of Bath

Department of Chemistry

September 2004

ProQuest LLC
789 East Eisenhower Parkway
P.O. Box 1346
Ann Arbor, MI 48106-1346

CONTENTS

Chapter 3 - Full and Half Sandwich Metallocenes Partnered with [1-H-*closo*-$CB_{11}Me_{11}$]$^-$

Chapter 4 – [1-H-*closo*-$CB_{11}Me_{11}$]$^-$ as a Weakly Coordinating Anion susceptible to B-C bond Cleavage

Chapter 5 - The Hydrogenation of Group 9 Metal Di-olefin Complexes Partnered with [1-H-*closo*-$CB_{11}Me_{11}$]$^-$ and [BAr_F]$^-$.

Chapter 6 - High Hydride Content Octahedral Clusters from the Decomposition of Rhodium Dihydrogen Complexes.

Chapter 7 – Experimental

Appendix - Publications

Acknowledgements

Andy (Dr Weller) is thanked for being so enthusiastic throughout and providing me with the help and guidance without which this would not have been possible. Many thanks go to Dr Mary Mahon and Dr Gabriele Kociok-Köhn for their work in collecting and refining all the crystal structures in this thesis and teaching me the basics. Dr Gus Ruggerio is thanked for the DFT calculations on a number of systems and Professor Paul Raithby is thanked for the Hydex analysis on the clusters. Dr Adam Clarke and Dr Jonathon Rourke are thanked for performing the 2D NMR Spectrum in Chapters Two and Three. The EPSRC are thanked for funding this PhD. I would like to thank everyone who I have shared a lab with, including, Nathan, Adem, Mark, Nico, Eduardo, Viccy, Gary, Amanda, and last but certainly not least big thanks to Susie and Jamie for being there inside and outside work, cheers for all the fun. Thanks to for all the guys who I've played squash and football with in my lunch hours, it saved me taking out my chemistry frustrations on the glassware!

Finally loads of appreciation to my parents for helping me out over the last few years and just for being there in general, it's much appreciated.

Abbreviations

Å	Angstrom (1×10^{-10} metres)
$[BAr_F]^-$	$[B(3,5\text{-}C_6H_3(CF_3)_2)_4]^-$
COD	Cyclooctadiene
Cp	Cyclopentadiene
Cp*	Pentamethylcyclopentadiene
Cy	Cyclohexyl
c.v.e.	Cluster Valence Electron
DAP	Double A Frame Porphyrin
δ	Chemical Shift
Δ	Difference
ES	Electro-Spray
Et	CH_2CH_3
FAB	Fast Atom Bombardment
Fc	Ferrocene
HOMO	Highest Occupied Molecular Orbital
Hz	Hertz
IR	InfraRed
k	Rate constant
K	Equilibrium Constant
kie	Kinetic Isotope Effect
L	Ligand
LUMO	Lowest Unoccupied Molecular Orbital
M	Metal
Me	CH_3
NBD	Norbornadiene
NMR	Nuclear Magnetic Resonance
Nuc	Nucleophile
OTf	Trifluromethanesulfonate
PAC	Photo-Acoustic Calorimetry
Ph	C_6H_5
ppm	Parts per Million
R	Alkyl Group
SBI	*rac*-$Me_2Si(Indenyl)_2$
Tp	Trispyrazolylborate
TMS	Trimethylsilyl
TRIR	Time Resolved Infra Red

Abstract

Synthetically useful salts of the mono-anionic, highly alkylated carborane, [1-H-*closo*-$CB_{11}Me_{11}$]$^-$ have been synthesised and used to introduce this anion to the coordination sphere of transition metal complexes. Partnering [1-H-*closo*-$CB_{11}Me_{11}$]$^-$ with a number of phosphine stabilised silver salts led to intimate ion pair formation, involving Ag···H_3C interactions in both the solid-state and solution. These Ag···H_3C interactions were shown to be weak, with the anion readily displaced by other poor Lewis-bases. Solid-state cation···anion interactions were also ascertained for the zirconocene complexes, Cp'$_2$ZrMe(1-H-*closo*-$CB_{11}Me_{11}$) (Cp' = C_5H_5 or C_5H_4Me) and equally shown to persist in solution. A Co···anion intimate ion pair has also been partially characterised. These complexes can be viewed as models for the catalytically important metal σ alkane interaction. The weak nucleophilicity of [1-H-*closo*-$CB_{11}Me_{11}$] has been shown by the retarded metathesis reactions involving the $[Ag]^+$ and $[Cs]^+$ salts.

A number of metal complexes where weak σ donors bind in favour to [1-H-*closo*-$CB_{11}Me_{11}$]$^-$ have been isolated. Including, solvent separated ion pairs which can undergo decomposition via anion B-C/solvent activation to generate a number of functionalised anions via a neutral, internally charge compensated borenium ylide, [1-H-*closo*-$CB_{11}Me_{11}$]. Several agostic complexes have also been synthesised with [1-H-*closo*-$CB_{11}Me_{11}$]$^-$ as the counter ion and one, $[PtMe(^iPr_3P)_2]^+$ demonstrated to undergo acid catalysed cyclometallation. Finally, dihydrogen also binds preferably over [1-H-*closo*-$CB_{11}Me_{11}$]$^-$ to $\{(PR_3)_2Rh(H)_2\}^+$ fragments (R = ^{i}Pr or Cy), generating complexes of the general formula, $[(PR_3)_2Rh(H_2)_x(H)_2]^+$ (x = 1or 2). These, by the heterolytic cleavage of dihydrogen, form the novel high hydride content rhodium octahedra, $[(PR_3)_6Rh_6H_Y]^{2+}$ (Y = 10, 12 or 14), that reversibly bind dihydrogen.

1. Introduction

1.1 Alkane Complexes of Transition Metals

1.1.1: Background:

The selective activation of inert C-H bonds, particularly the transformation of methane to methanol, has become a key aspiration in organometallic chemistry, with the potential to convert this most abundant hydrocarbon resource to a useful, transportable and valuable product. Currently the industrial uses of alkanes are either inefficient (*e.g.*, thermal dehydrogenation) or indirect (*e.g.*, steam reforming of methane to produce synthesis gas: carbon monoxide and hydrogen). It is not in the unreactivity of alkanes that lays the difficulty, but rather in the selectivity and the avoidance of the thermodynamically favourable products from over-oxidation (CO_2 and H_2O). Controlled and catalytic functionalisation would therefore make methane an invaluable chemical precursor. To achieve this, breaking one of the most inert bonds in nature, the sp^3 C-H linkage, would need to be overcome. Arene C-H activation has been known since 1965[1] and the first reported oxidative addition of alkanes appeared independently from the groups of Bergmann (Ir)[2] and Graham (Rh) in 1982 (Figure 1).[3]

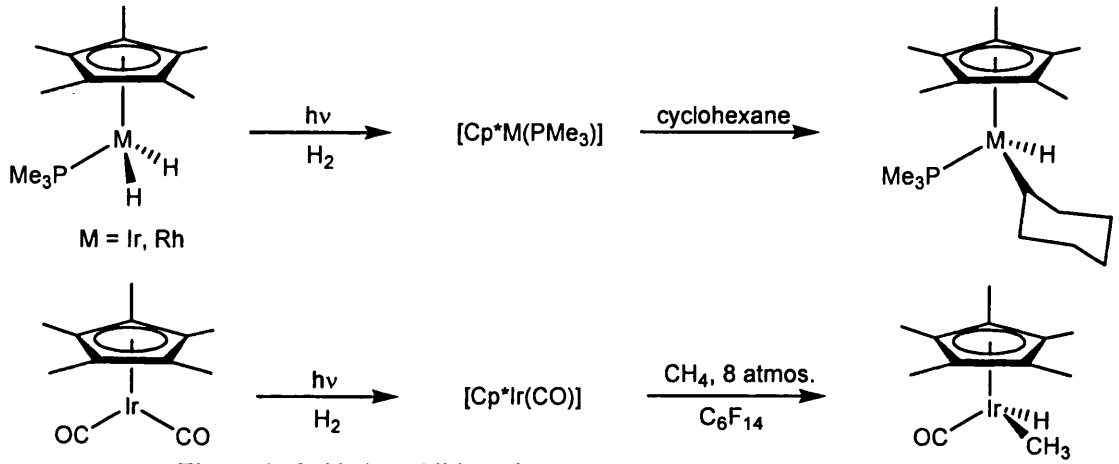

Figure 1: Oxidative addition of saturated alkanes to late transition metals.

Since this seminal work an increasingly large number of organometallic systems that activate alkane C-H bonds have been documented, spanning virtually the entirety of the transition metals.[4] This plethora of research has revealed that the homogeneous C-H activation of alkanes by organotransition metal complexes can be divided into two sub-areas: (i) the radical based C-H activation (similar to that carried out by a variety of enzymes) that does not involve any direct metal-alkane contact, and (ii) systems where there is a direct interaction between the alkane and the metal centre resulting in the breaking of the C-H bond (usually by an oxidative addition or a σ bond metathesis mechanism).[5] The latter type has been more extensively studied due to the predominantly diamagnetic complexes, two-electron chemistry and superior C-H functionalisation selectivities. From the numerous synthetic, kinetic, mechanistic and theoretical studies the intermediacy of an alkane directly bound to the metal centre has been firmly established and is outlined in Figure 2.

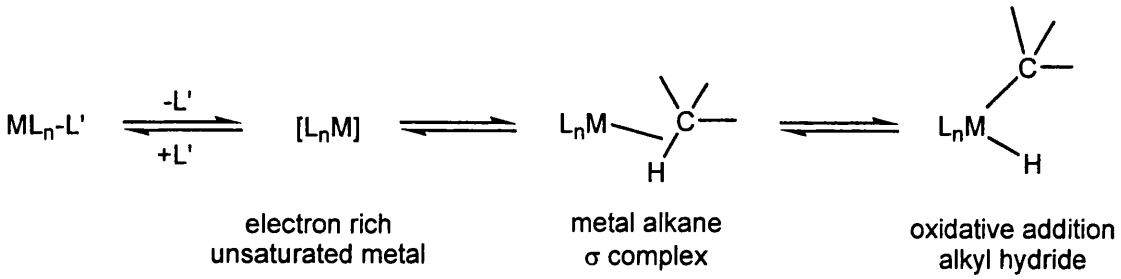

Figure 2: Oxidative Addition pathway for late transition metals.

The concept of an alkane as a ligand is counterintuitive as the HOMO of the alkane C-H σ bond is low lying, thus poorly electron donating, whilst the σ^* LUMO is high in energy therefore unsuitable for accepting electron density. Despite these adverse properties there is a large body of evidence, both indirectly and by direct spectroscopic measurements, that proves beyond doubt the importance of the metal-alkane intermediate.[6] For arenes the initial complex on the oxidative addition pathway has been shown to be an η^2 – arene complex;[7-9] however, for alkanes the σ complex (Figure 2)

has not been unambiguously experimentally determined (i.e. jointly by spectroscopic and solid state methods) and a number of geometries are possible as shown in Figure 3. The following nomenclature will be used throughout.

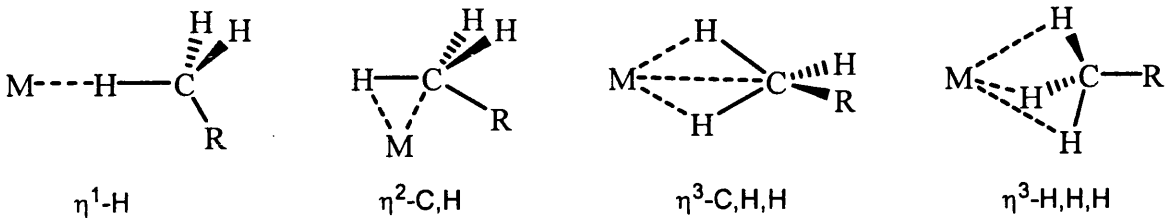

Figure 3: Possible bonding modes of an alkane to a metal centre.

The purpose of this introduction will be to concentrate on the chemistry of R-CH_3···M interactions in the homogeneous media, as this is the area of focus of the research reported herein. The extensive fields of alkane complexation with heterogeneous metal surfaces, gas phase systems and naked metal cations will not be discussed here – but are covered in a number of recent reviews.[4, 6]

1.1.2: Indirect Evidence for σ Alkane complexes:

There are two key methods that have provided indirect evidence for the existence of alkane complexes. The first is H/D scrambling occurring between a metal deuteride complex and its alkyl substituent, prior to alkane reductive elimination,[10] as demonstrated by the repeated migration and insertion of the {$C_5Me_5Rh(PMe_3)$} fragment into a transient σ alkane complex (Figure 4).[10]

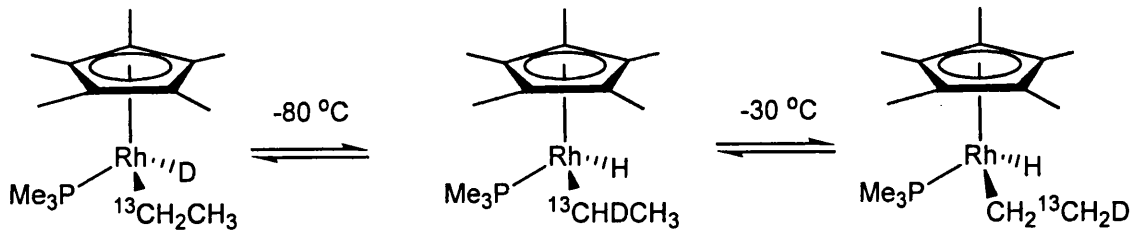

Figure 4: Exchange processes in $Cp^*Rh(PMe_3)(C_2H_5)D$.

A combination of ^{13}C and ^{2}H labelling NMR studies revealed two distinct processes. At temperatures below -30°C, H/D exchange occurred purely at the α position on the ethyl ligand. At higher temperatures, a second process follows where the deuterium is incorporated at the β position. In all instances the ^{2}H remains associated with the labelled ^{13}C, indicative of the intramolecular reversible formation of a σ alkane complex that at higher temperatures dissociates, rotates and reattaches to the metal through the non labelled CH_3 interaction (Figure 5).

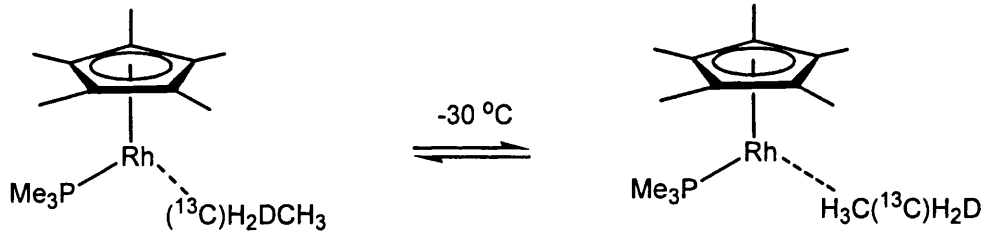

Figure 5: Incorporation of deuterium into the β position of the ethyl group at temperatures above -30°C.

Reductive elimination is the microscopic reverse of oxidative addition and thus proceeds along the same reaction trajectory with identical transition states and intermediates.[11] The majority of the indirect studies into transient alkane complexes have investigated the reductive elimination of an alkane from a metal alkyl/hydride. Included in this are a number of systems that by analogous H/D scrambling experiments clearly implicate the presence of a metal σ - alkyl complex.[12-14] Recently, Gross and Girolami have reported the first example of a transition metal compound,

$[Cp^*Os(dmpm)CH_3(H)]^+$, where the equilibrium between a σ alkane complex and the metal alkyl/hydride is dynamic on the NMR time scale (Figure 6).[15] Spin saturation transfer experiments provided definitive evidence that the hydrogen atoms in the Os-H and the Os-Me groups were undergoing rapid exchange. The rate constant at -100°C (calculated using both line shape analysis techniques and spin saturation experiments) revealed that an alkane complex is being formed reversibly at ~160 times a second. At -120°C the fluxionality is halted, giving rise to independent Os-CH_3 and Os-H signals, whilst above -95°C irreversible reductive elimination occurs.

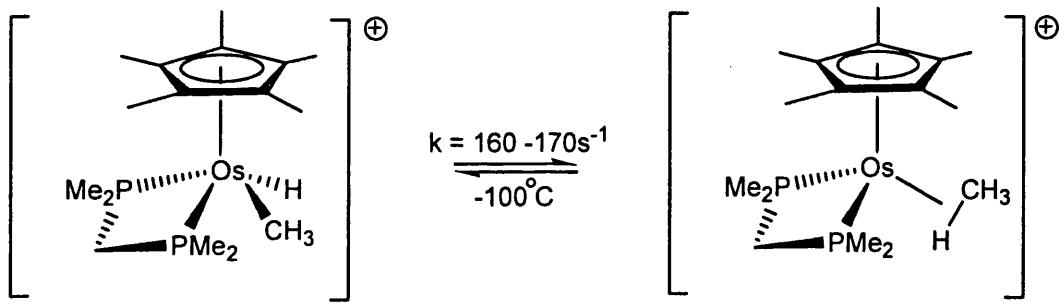

Figure 6: The dynamic equilibrium between an Osmium alkyl/hydride and its respective σ alkane complex.

Complimentary to the H/D scrambling experiments further evidence of the central role of the σ complex comes from the inverse kinetic isotope effect (kie) for the reductive elimination of an alkane from an alkyl hydride complex.[16] Here the relative rates of reductive elimination for *perprotio* and *perdeuterio* samples are compared. In the vast majority of cases for this process the kie measured is inverse (i.e. less than unity). This is a non standard value as deuterium compounds generally give slower rates of reaction due to their stronger bonds, and a 'normal' kie is >1.[10, 12, 13, 17] To elucidate the origin of this effect we need to first realise that the isotope effect is predominantly associated with the bond making/breaking step with little or no contribution from the dissociation of the formed σ alkane complex. In the intermediate (i.e., the product-like

metal σ alkane complex) the deuterium experiences a higher force constant compared to that in the reactant (the metal alkyl/hydride), due to the relative strengths of C-H (or C-D) and M-H (or M-D) resulting in the difference in zero point energies being greater in the reactive intermediate than in the reactant (Figure 7).[6] As this first step is reversible and rapid compared to the alkane dissociation step there is a higher pre-equilibrium concentration of the *deuterio* alkane complex compared to the *protio* analogue, thus a greater overall rate for reductive elimination and a $k_H/k_D < 1$.

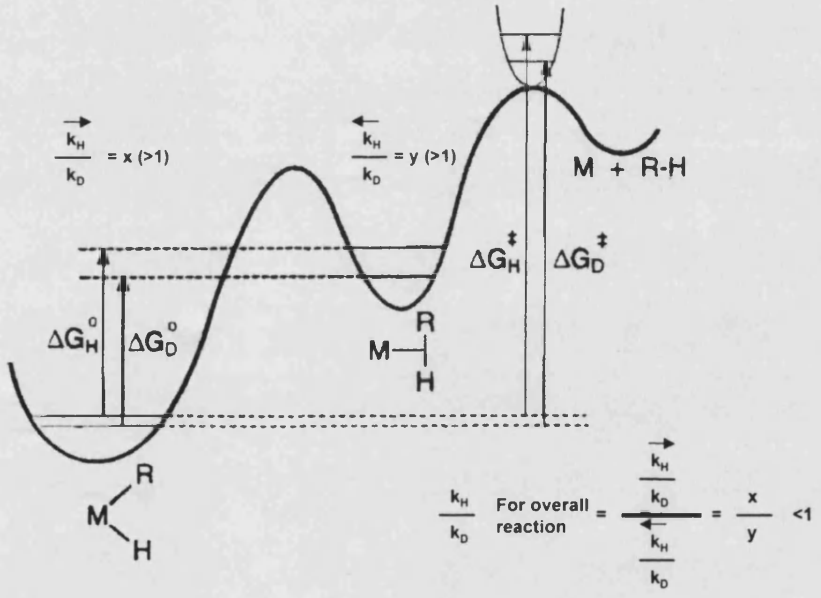

Figure 7: Reaction coordinate for the reductive elimination of an alkane from a metal alkyl hydride. This shows the larger zero point energy difference between hydrogen and deuterium analogues in the products relative to the reactants.

Interestingly, recent work by Jones' group on the Tp*Rh(CNR)(alkyl)^{n}H (n = 1 or 2) system has shown that the origin of the different equilibrium concentrations for the *deuterio* and *protio* systems is in fact due to an inverse kinetic equilibrium effect between the alkyl hydride and the σ alkane complex.[18] In this equilibrium there are normal isotope effects in both directions, but the kie is greater for the oxidative addition of the coordinated alkane than for the reductive coupling of the metal hydride/alkyl to

generate the metal σ alkane complex (Figure 7), thereby generating the overall inverse kie for this process.

1.1.3: Direct Evidence of Metal σ Alkane Complexes:

Direct evidence for the coordination of alkanes to metal centres was first documented in the 1970's and was achieved by the photoexpulsion of CO from $M(CO)_6$ (M = Cr, Mo, or W) in low temperature alkane matrices. Time Resolved Infra Red (TRIR) and UV/Vis spectroscopy were used to demonstrate the solvation of the 16-electron fragment $\{Cr(CO)_5\}$ with the matrix host. Mixed matrix experiments proved this solvation to be the specific solvation of the metal fragment with the matrix host acting as a weak sixth ligand.[19] Use of a methane matrix at 12K thus resulted in the coordination of a CH_4 molecule as the sixth ligand. In an argon matrix doped with ~2% CH_4 the shift of the a_1 maximum for the CO stretch was similar, although less than that found for the equivalent $(CO)_5CrXe$ complex (both exhibit a small down frequency shift) but is drastically different to the complexes $Cr(CO)_5(\eta^2\text{-}H_2)$ and $Cr(CO)_5(\eta^1\text{-}N_2)$ which show a large high frequency shift. This demonstrates that methane is a significantly poorer acceptor of electron density than H_2 or N_2.[20] More recently the intermediacy of an alkane (neopentane) complex in a C-H activating process utilising the $Cp^*Rh(CO)_2$ system has been directly observed using similar methods in liquid krypton.[21,22] Here initial excitation expels CO and generates two transient complexes that rapidly come to equilibrium. The relatively slow oxidative addition of a neopentane C-H bond (Figure 8) in one of these complexes then follows. Whilst matrix experiments allow for the characterisation of these short-lived compounds (*e.g.*, $Cp^*Rh(CO)((CD_3)_4C)$ has a lifetime of only *ca.* 1000μs) it provides scant information to quantify their structure or any further reactivity.

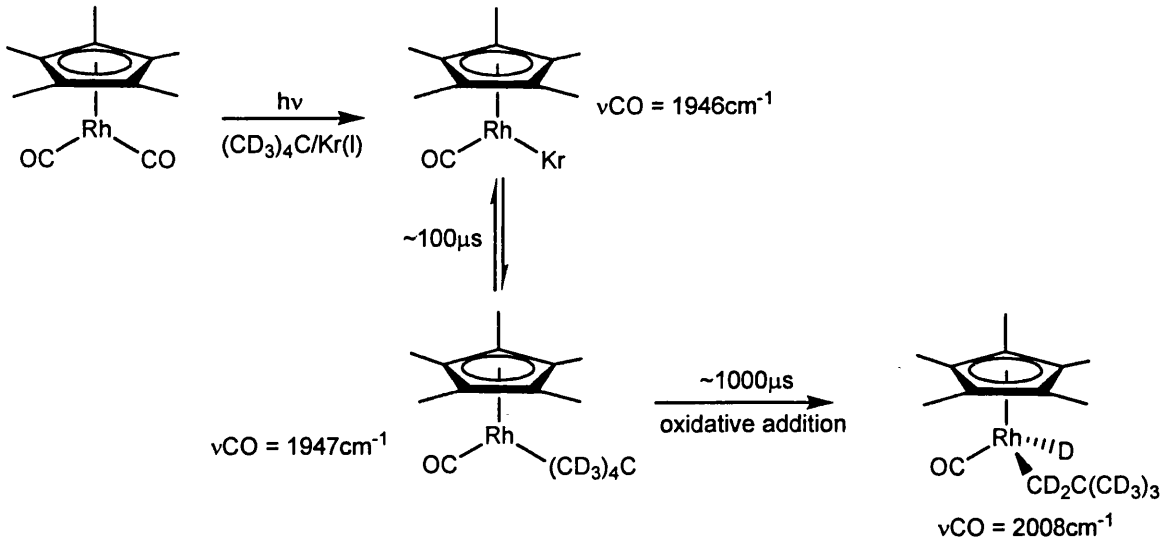

Figure 8: Pathway for the oxidative addition of an alkane as monitored by TRIR spectroscopy

To obtain kinetic and thermodynamic information on the metal alkane interaction, solution studies in alkane solvents were required. The energetics of alkane binding has been determined using Photo Acoustic Calorimetry (PAC). Flash photolysis of $M(CO)_6$ (M = Cr, Mo, W) is used to generate the transient alkane complex, with the resultant amplitude of the acoustic wave measured being directly dependent on the amount of heat liberated/absorbed from a chemical process.[23] This requires two assumptions, that the solvation of the product and the reactant are effectively identical, and that there is negligible volume change. The enthalpy change measured is then equal to the difference in the metal-carbonyl and metal alkane bond energies. As the metal carbonyl bond enthalpy is known from gas phase experiments, a range of bond enthalpies for M-alkanes has been calculated (Figure 9).

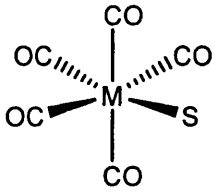

M = Cr, Mo, W, S = pentane, heptane, iso-octane or cyclohexane

M	Alkane	-ΔH (kcal/mol)
Cr	pentane	8.9 (3.2)
	heptane	9.6 (2.3)
	isooctane	11.0 (2.1)
	cyclohexane	12.6 (2.1)
Mo	heptane	8.7 (2.7)
W	heptane	13.4 (2.8)

Figure 9: Binding enthalpies for alkanes to $M(CO)_5$ (errors in parentheses to 1σ).

Significantly the binding enthalpy of cyclohexane is greater than for the linear alkanes, corresponding to a stronger σ bond and consequently a more stable metal alkane complex. The authors suggest that a secondary CH_2 sigma complex is energetically preferred over a primary CH_3, with the cyclohexane secondary CH bonds being more accessible than those in the linear alkanes. A possible electronic factor to explain this trend is that secondary CH bonds are more electron rich than their primary counterparts. Long and co-workers in a similar study proposed that this variation is not due to different binding enthalpies ($\Delta H^{\ddagger}$) which remained constant, but rather from changes in the entropy of binding ($\Delta S^{\ddagger}$).[24] On coordination of the alkane to the metal its freedom of motion is restricted, linear alkanes possessing a greater degree of freedom than their cyclic counterparts, effect a larger (unfavourable) entropic term. These energetics are, however, in contrast to metal insertion reactions that occur preferentially into primary CH bonds, this contrasting selectivity may arise from the σ complex being less sterically demanding than the resultant metal alkyl.[25]

Solution phase laser flash photolysis and ultrafast transient spectroscopy has provided an insight into the kinetics of alkane complexes and importantly some of the factors that control their solution lifetimes. Initial work demonstrated that photolysis of $Cr(CO)_6$ in cyclohexane lead to a broad absorption band in the UV/Vis spectrum similar to that found in the methane matrix experiments.[26] $Cr(CO)_5(C_6H_{12})$ is produced at ambient temperature within 50 ns of UV flash photolysis. The product is extremely reactive, decaying within 50 μs.[27] Further TRIR experiments have shown that the stability of organometallic alkane complexes increases both across and down Groups V, VI and VII (Figure 10).[28, 29] For the manganese and rhenium complexes, $CpM(CO)_2$(alkane), the lifetimes are appreciably longer for the cycloalkane complexes

than for the heptane analogues, in good agreement with the PAC measurements.[30] The decay rate of $CpRe(CO)_2$(heptane) in the absence of added ligand was only $40s^{-1}$ making it the longest measured lifetime of any alkane complex. It can be assumed that the cyclopentane analogue would persist in solution for even longer.[28]

Group V	Group VI	Group VII
$CpV(CO)_3$(heptane)	(Benzene)$Cr(CO)_2$(heptane)	$CpMn(CO)_2$(heptane)
1×10^8	2×10^6	8×10^5
$CpNb(CO)_3$(heptane)		$CpMn(CO)_2$(cyclopentane)
7×10^6		3×10^5
$CpTa(CO)_3$(heptane)		$CpRe(CO)_2$(heptane)
5×10^6		3×10^3
		$CpRe(CO)_2$(cyclopentane)
		1×10^3

Figure 10: Second order rate constants (mol^{-1} dm^3 s^{-1}) for the reaction of metal alkane complexes with CO in alkane solution at 298K.

A low temperature NMR investigation into the photolysis of a supersaturated solution of $CpRe(CO)_3$ in cyclopentane,[31] monitored the formation and reactivity of $CpRe(CO)_2(C_5H_{10})$ that had a lifetime of *ca.* 1 hour at 180K. This transient specie was characterised by ^1H NMR spectroscopy with continuous irradiation of the sample with a UV light in the probe maximising the concentration of the alkane complex. Photolysis at -80°C in cyclopentane produced two new resonances: a high field resonance at δ – 2.32 ppm, which had a fixed integral of 2H when compared to the correspondingly new Cp peak at δ 4.92 ppm (5H). These peaks are attributed to $CpRe(CO)_2$(cyclopentane), where the cyclopentane ring is coordinated to the rhenium centre via one of the methylene units. The highfield signal appears as a quintet with ^3J (HH) coupling of 6.6 Hz, fully consistent with four equivalent protons on the two adjacent carbons.

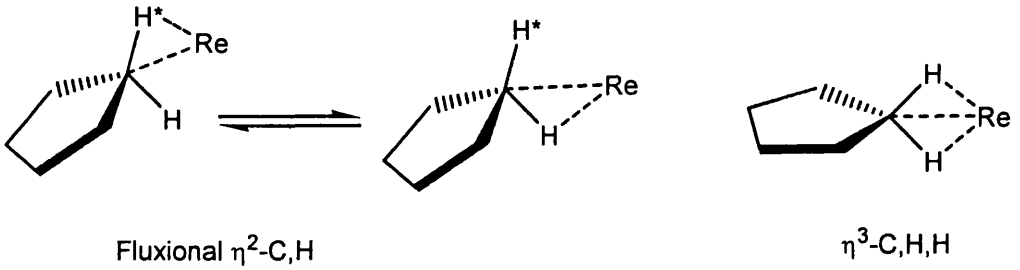

Figure 11: Possible bonding modes for cyclopentane to $CpRe(CO)_2$ as determined by ^1H NMR Spectroscopy.

The equivalence of the two protons involved implies that either they are both involved in the bonding via a η^3-C,H,H linkage or by a fluxional η^2-C,H motif (Figure 11). Using ^{13}C isotopically enriched cyclopentane the $^1J(CH)$ coupling constant for the resonance at –2.32 was found to be 112.9 Hz, compared to that of free cyclopentane (129.4 Hz). The expected reduction signifies a reduced bond order between the C and the H characteristic of σ donation to a metal centre.[32] Theoretical studies on a related alkane complex $W(CO)_5$(propane) found the lowest energy conformer to be a C-H from the methylene group bound in a η^2-C,H motif.[33] If a similar bonding mode is assumed in $CpRe(CO)_2$(cyclopentane) then the $^1J(CH)$ coupling constant is in fact an averaged value of one coordinated and one unbound C-H bond. The calculated $^1J(CH)$ of just the coordinated C-H bond is then approximately 95 Hz. This value is consistent with typical static agostic interactions that range between 60 and 90 Hz and implies a relatively weak interaction with the metal centre in the $\{CpRe(CO)_2\}$ complex.[34]

Crystallographic evidence for the coordination of an alkane to a metal centre has also been recently reported.[35] An iron (II) metal centre ligated by a double A frame porphyrin (Fe - DAP) on crystallisation from fluorobenzene/heptane displays two clear interactions with one heptane molecule. As opposed to all the previous structures of metal σ C-H bonding where there is an entropic advantage from their intramolecular

nature, the Fe-DAP utilises host/guest chemistry to enhance the weak bond between the metal and alkane. The backbone of the Fe-DAP complex creates a hydrophobic cavity of the correct size and shape for a heptane molecule to reside in (Figure 12).

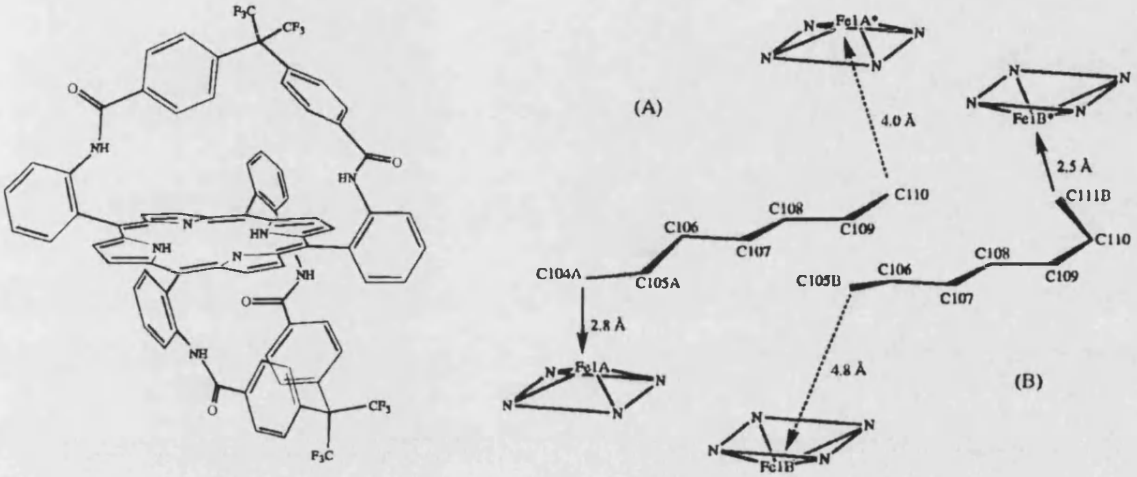

Figure 12: The double A –frame Porphyrin, and a representation of the two disordered heptane molecules interacting with Fe-DAP.

The coordination of heptane to the Fe^{II} centre is significant as indicated by the non-planarity of the iron porphyrin (the Fe^{II} is displaced out of the plane towards the terminal carbon of the heptane by 0.26 Å). This deviation unequivocally demonstrates that the heptane is not only bound in place by a host guest effect, although the additional stabilising effect provided is undoubtedly important. Crystallographically, the heptane molecule is disordered appearing as an *n*-octane molecule that can be readily modelled with half occupancy of the two terminal carbons. Each of the two terminal carbons is in contact with a single Fe(II) centre, with Fe-C distances of 2.5 and 2.8 Å, comfortably within the range expected for weak agostic interactions.[34,36] The structural disorder prevented free refinement of the hydrogens and hence the determination of the bonding mode in this metal alkane complex. Density functional calculations on a range of Fe (II) porphyrin – alkane interactions (four alkanes were studied, methane, ethane, propane and *n*-butane) all gave Fe···C distances between 2.62 and 2.65 Å, consistent with the

experimentally determined average Fe···C bonding separation of 2.65 Å. In each case the geometry of the Fe···C-H interaction calculated was an unsymmetrical bidentate structure with one close Fe-H distance (2.01 to 2.13 Å) and one longer (2.62 to 2.65 Å).

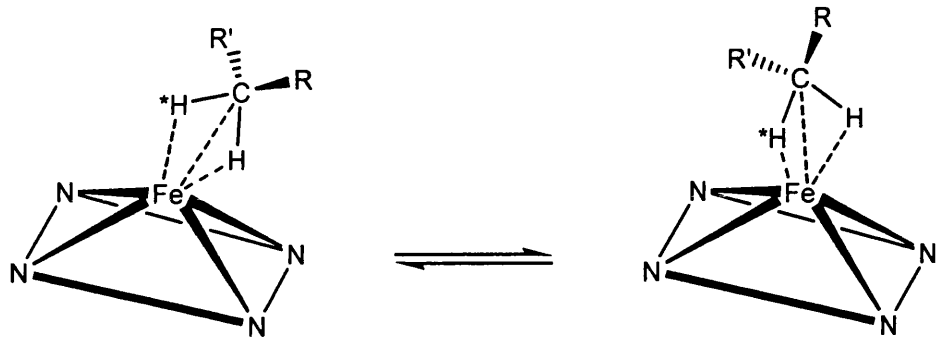

Figure 13: Calculated η^2 C-H unsymmetrical binding mode and possible fluxionality.

An asymmetric bonding arrangement is still consistent with the NMR study performed on $CpRe(CO)_2(C_5H_{10})$ if we assume fluxionality on the NMR timescale (Figure 13).[31] The computed binding energies ranged from 10.5 to 16.7 $KJmol^{-1}$ indicative of weak interactions that on the NMR timescale would be in fast exchange, thereby making equivalent all the terminal C-H bonds. Meaningful solution studies on the Fe – heptane interaction have proved impossible as there is insufficient solubility in non competing solvents and other weak donors (e.g. arenes) have been shown previously to readily bind to metalloporhyrins.[37]

A second, more recent, report has analysed by X- ray diffraction a series of alkane complexes of the unsaturated, tris-aryl oxide uranium (III) complex $[((ArO)_3tacn)U]$ (Figure 14).[38] In each case the apical position of the uranium coordination sphere is occupied by an alkane ligand. The uranium – carbon bond distances are between 3.731 and 3.798 Å, just within the sum of the van der Waals radii for a $U\text{-}CH_3$ contact (3.9 Å) suggestive of a bonding interaction.[39]

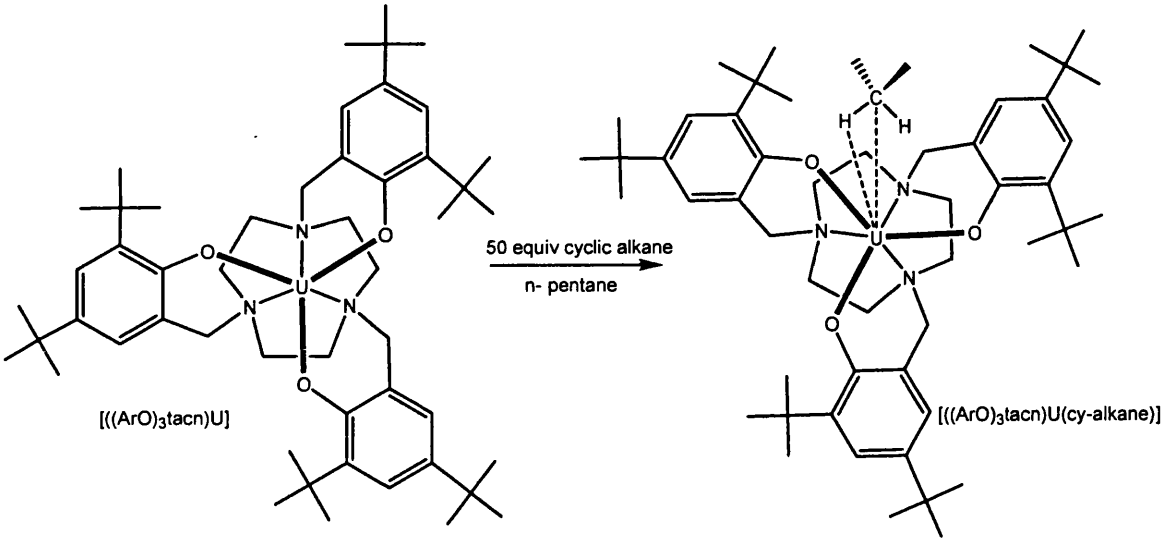

Figure 14: Coordination of an array of alkanes to [((ArO)$_3$tacn)U].

Significantly all the structures exhibited close contacts between the axial alkane and the peripheral tertiary butyl group from the tacn ligand (contacts from 2.12 to 2.71 Å). This implies that the metal C-H bonding interaction is supplemented by a host guest effect between the alkane and the ^{t}Bu groups of the macrocyclic ligand, in an analogous manner to the Fe-DAP heptane complexation. This does not discount that the axial alkane could be held in position solely through the metal-alkane interaction, or conversely solely by a host guest effect. Computational studies indicate the bonding contact has only a minor contribution from the C-H σ orbital (~2%) indicative of a very weak alkane to metal bond. Combined with the observed freely refined d(C-H) of 0.96 Å for the hydrogen atoms in proximity to the uranium centre (showing no lengthening of the C-H bond) perhaps indicates that host guest interactions predominate. Three of the structures were of sufficient quality to calculate hydrogen positions proximal to the uranium centre and all three freely refined as the η^2-C,H bonding mode, in good agreement with the calculated structures.

It is significant to note that still there remains a scarcity of experimental data on non-supported metal – alkane adducts that are accessible under ambient conditions. The stablest reported hitherto persists for less than 1 hour in solution at 180 K. Until this is remedied the isolation of the first true alkane complex will remain a key objective in organometallic chemistry.

1.1.4: Theoretical Studies on σ Alkane Complexes:

Complimentary to the progress made in the experimental investigations into these important intermediates a number of noteworthy theoretical examinations have been performed. Many of these specifically scrutinize areas where experimental information is scarce, i.e., the coordinating modes and the factors affecting the binding strength of CH_4 on metal centres. Studies on $CpRh(CO)(CH_4)$,[40] $[CpIr(PH_3)(CH_3)(CH_4)]^+$ [41] and $CpM(NO)(CH_2)(CH_4)$[42] (M = Mo, W) all predict a η^2-C,H alkane coordination, whereas the η^3-C,H,H mode is calculated to be energetically favourable for the 14 electron complexes $RhCl(PH_3)_2$ and $Ni(PH_3)_2$.[43, 44] An interesting comparison involved the *ab-initio* calculations on the binding energies of alkanes versus fluoroalkanes with respect to the fragment $\{W(CO)_5\}$.[33] The simple alkanes (CH_4 to C_3H_8) bond in the η^2-C,H manner as their lowest energy conformers, but the fluoroalkanes CH_nF_{4-n} preferentially bind via a C-F η^2 linkage (Figure 15). This is supported by experimental evidence with C-F activation of fluoromethane occurring in preference to C-H activation.

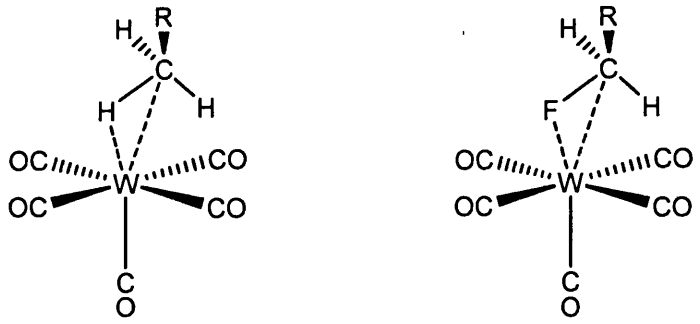

Figure 15: Calculated binding geometries of methane and fluoromethane to $W(CO)_5$.

The energy profile for all the η^2-C,H alkane interactions have very low barriers to rotation between the C-H positions on the contact carbon, inferring a rapid fluxional system with all the C-H bonds being in exchange with one another. The binding of the secondary CH_2 group in the propane analogue, $(CO)_5W$(propane) is calculated to be 1.37 kcal/mol energetically more favourable than through the primary CH_3 group, consistent with the PAC measurements and the relative stabilities of the Re···heptane/Re···cyclopentane complexes.[30] Another important trend noted is that alkane binding strengths increase with chain length, thus the most abundant and important alkane, methane will be the least stable adduct.

Reduced variational space analysis techniques by Cundari have indicated two factors that can be altered to improve alkane binding: the polarisation of CH_4 and the degree of charge transfer: $CH_4 \rightarrow M$.[45] Both are predominantly affected by the charge on the metal, with cationic compounds binding alkanes significantly stronger than their neutral counterparts. In addition to the metal's charge, the ligand set can also drastically alter alkane binding. A prime example involves the oxidative addition of CH_4 to the 14 electron fragment $IrX(PH_3)_2$ (X = Cl, H).[46] DFT calculations compute that the favourable binding mode is via the η^3-C,H,H interaction; however, its energetics are

extremely sensitive to the *trans* ligand, exemplified by a binding energy that is ~9 kcal/mol stronger for the X= Cl complex (Figure 16).

Figure 16: Relatives binding energies of the methane to two similar 14 electron Iridium fragments.

Seigbahn and Svensson have used *ab-initio* calculations to study the activation of methane with compounds that have triplet ground states (*e.g.*, {Rh(Cl)CO} and $\{RuH_2\}$) and related compounds that have singlet grounds states (*e.g.*, $\{Rh(H)(NH_3)\}$ and {Rh(H)(CO)}).[47] Promisingly, for the prospect of isolating a stable alkane complex, they found that a triplet ground state resulted in low barriers to oxidative addition but that singlet ground states are required for strong σ alkane binding. Complexes are available that have a low barrier to oxidative addition without forming a strong σ complex and thus it is possible that the inverse is true: that a strongly bound σ complex exists with a high barrier to oxidative addition. Computational theory also indicates that if a cationic complex can be solubilised into alkane solvents then, with the correct ligand set a stable alkane complex is an attainable goal.

With the current paucity of data relating to unsupported metal alkane complexes, systems that provide a model for the important M···H_3C-R interaction are vital and have been exploited to some extent. Model compounds have the advantage of a dramatically increased stability that allows for the isolation and full characterisation of an increasing number of σ-bonded complexes, including some involving M···H_3C-R interactions. A

variety of these will be introduced and discussed in the next section and their relevance to 'true' alkane complexes examined.

1.2: Models for Alkane σ Complexes:

1.2.1: Coordination of X-H σ bonds:

As well as alkanes, an electron deficient metal centre can react with other X-H bonds to readily generate σ complexes where X-H acts a two-electron donor (X = R_3B^-, R_2B, R_3Si, and H). The isolation of the M-(HX) adduct in the condensed phase as a stable entity is now feasible due to the altered energies of the X-H σ and σ^* orbitals in comparison to their alkane analogues. If X = R_3Si or H the X-H bond becomes more basic with a higher energy σ bond enhancing electron donation to the metal and concurrently, the σ^* is lowered in energy becoming more accessible for back donation. Furthermore, in dihydrogen complexes the steric hindrance is greatly reduced and the degree of back donation into the σ^* orbital can be significant.[32] When X = BR_2, the borane complexes have increased hydridic character and in the case of the borates (X = $[BR_3]^-$), there is the possibility of a significant ionic contribution to the bonding interaction making it debatable if they are true σ complexes.[48]

1.2.2: Coordination of B-H σ bonds:

$[BH_4]^-$ and R_3PBH_3 both form stable adducts with a range of metals and are isolobal with methane and the higher alkane homologues, giving precedent and valuable insights into alkane σ complexes (Figure 17).

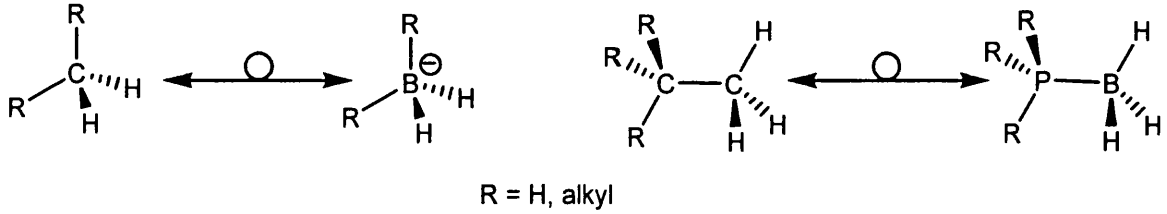

Figure 17: The isolobal relationship between alkanes and borates/phosphine-boranes.

For BH_4^- the most common coordination mode is the η^2-H,H, though η^1-H and η^3–H,H,H bonding motifs have all been characterised (Figure 18).[49-54]

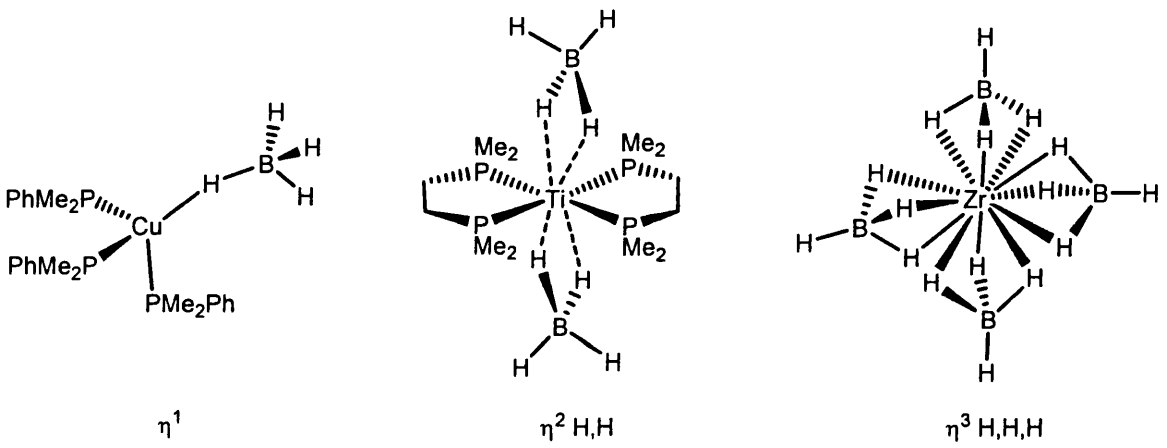

Figure 18: Examples of the three possible binding modes observed for $[BH_4]^-$, η^1,[54] η^2-H,H,[50] η^3-H,H,H.[49]

Moving to the borates of the general formula $[R_2BH_2]^-$, a very common binding motif crystallographically characterised is the η^2-H,H mode (*e.g.*, in $[Et_2BH_2]^-$ to $[RePh_2PCH_2CH_2P(Ph)CH_2CH_2P(Ph)CH_2CH_2PPh_2]$, $[H_2BR_2]^-$ (R = C_4H_8, C_5H_{10} and C_8H_{14}) to Cp_2ZrH and $[H_2BO_2C_6H_4]^-$ to Cp_2Nb).[55-58] With these compounds the degree of ionic bonding is uncertain and the end on bonding in $[(PMe_2Ph)_3Cu(\eta^1\text{-}H_4B)]$ is indicative of the increased polarisation of the $B^{\delta+}$-$H^{\delta-}$ bond. To remove this ambiguity, a neutral borane linkage is required. This has been achieved in two manners, firstly utilising the Lewis base adducts of BH_3, such as the phosphine boranes (Figure 17), pioneered by

Shimoi.[59-61] All the mono-phosphine boranes (R_3PBH_3) structurally characterised bind in an η^1-H motif (*e.g.*, $CpMo(CO)_2(\eta^1\text{-}H_3B{:}PMe_3)$, Figure 19). A 'bis' phosphine diborane [$Me_3P{:}BH_2BH_2{:}PMe_3$] (isolobal with butane) binds in a mode not previously seen for alkanes, i.e., via a η^2-H,B-B,H interaction from two adjacent borons (Figure 19).[62] It can, however, be viewed as a bidentate ligand, involving two individual η^1–H contacts. Alternatively, chelating mono phosphine boranes (general formula $Ph_2PCH_2P(Ph)_2BH_3$) have been shown to bind in a η^3-B,H,H fashion.[63, 64]

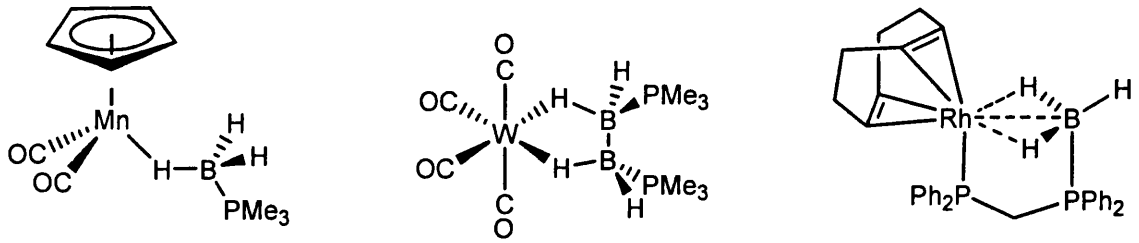

η^1-H η^2-H,B-B,H η^3-B,H,H

Figure 19: Examples of the three reported bonding modes for phosphine boranes.

In all of these compounds a significant decrease in the B-H coupling constant is observed analogous to that in $CpRe(CO)_2(C_5H_{10})$, suggesting a reduction in the B-H bond strength and some σ donation. As with the borohydride compounds, however, the boron is four coordinate and though neutral, the B-H bonds certainly have some hydridic character. An analogous system, $(CO)_5W(\eta^1\text{-}H_3Ga{\cdot}quinuclidine)$, based on the Lewis base adduct of GaH_3, has also been synthesised. [65] Structural studies demonstrate a similar end on η^1-H interaction with a 16 electron $\{W(CO)_5\}$ fragment as previously seen with the mono dentate phosphine boranes. Due to the increased electropositive nature of Ga there will be an even greater polarisation of the $Ga^{\delta+}\text{-}H^{\delta-}$ bond.

The second type of structurally characterised, neutral B-H σ-bonded systems involves the base-free three coordinate catechol and pinacol boranes ($C_6H_4O_2B$-H = HBcat, $(Me)_4C_2O_2B$-H = HBPin) such as Hartwig's $Cp_2Ti(HBcat)_2$ and Chaudret's $(PCy_3)_2Ru(H)(H_2BPin)(HBPin)$ (Figure 20). These systems are consistently bonded to the metal via a η^2-B,H mode, with the donating B-H bond approaching in a side – on geometry.[66-68] An unusual feature of these σ borane complexes is that as well as B-H to metal donation there is also significant M→B back donation. This is not into the σ^* orbital, as would be expected for an alkane complex, but is into the empty p_π orbital on the boron. The unusual side on geometry is adopted to strengthen the M-(B-H) interaction by maximising efficient metal d – boron p_π orbital overlap whilst not weakening the B-H bond.[69] This backbonding is not available in alkane complexes – somewhat limiting the comparability of σ boranes and σ alkane complexes.

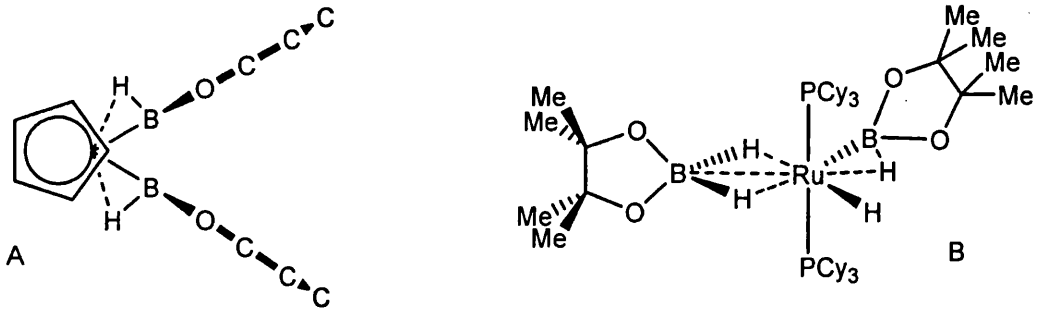

Figure 20: A: a borane structure exhibiting the side-on geometry in $Cp_2Ti(HBcat)_2$ (viewed down the Cp-Cp axis), B: a mixed η^3-B,H,H borate/η^2-B,H structure in $(PCy_3)_2Ru(H)(H_2Bpin)(HBpin)$.

1.2.3: Metal σ Dihydrogen Complexes:

The first metal dihydrogen (H_2) complex, $W(CO)_3(^iPr_3P)_2(H_2)$, was discovered and fully characterised nearly 20 years ago, firmly establishing the σ bond as an important ligand in organometallic chemistry.[70, 71] The H_2 molecule can be thought of as the zeroth member of the hydrocarbon series, with equivalent strong bond enthalpies (CH_3-H and H-H both ~104 kcal/mol), comparable bond polarities and frontier orbitals (σ and σ^*) of similar shape, energy and extent. The solid-state orientation of the

coordinated H_2 is side on in a η^2 binding mode in $W(CO)_3(^iPr_3P)_2(\eta^2\text{-}H_2)$ (a bonding mode universal in dihydrogen complexes).[32] The H-H bond distance in this complex was determined to be 0.89Å, slightly 'stretched' from that of free H_2 (0.75 Å) but still short enough to be indicative of an intact H-H bond. A wide range of (H-H) distances have since been reported, ranging from the 'unstretched' complexes (d(HH) < 1.00 Å) through to the severely stretched complexes (1.00Å < d(HH) < 1.4Å), where d(HH) is only slightly less than that found in some classical dihydrides (Figure 21).[32]

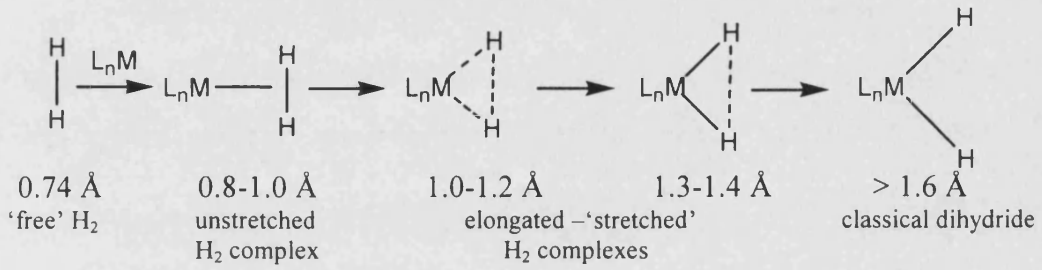

Figure 21: The continuum of H-H bond distances from crystallographic and NMR spectroscopy studies and the classification of the varying types of (η^2-H_2) metal complexes.

It has been from extensive studies on the nearly 600 different H_2 complexes spectroscopically and structurally characterised that much of the fundamental understanding of σ complexes (including alkane complexes) stemmed from.[32] This includes how σ bonding can be viewed in an analogous manner to the Dewar-Chatt-Duncanson model for π complexes (Figure 22).[72] The metal hydride bond becomes stronger with increasing M to σ^* back donation, along with a concomitant decrease in the H-H bond order resulting in the observed H-H elongation.

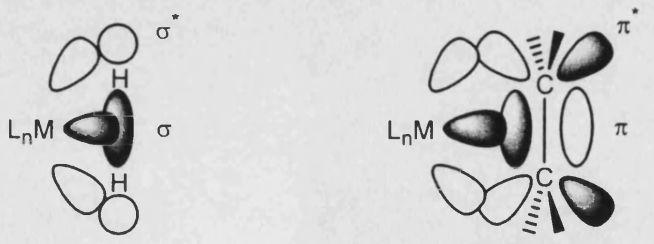

Figure 22: The analogous bonding interactions involving a metal fragment with (η^2-H_2) and (η^2-alkene).

The stability of the H_2 interaction in comparison to that of alkanes was thought to be controlled by the degree of back bonding from the metal, as a series of electron deficient metal fragments such as $M(CO)_5$ (M = Cr, W) formed very unstable dihydrogen adducts.[73] Alkanes, in contrast to H_2, do not have the ability to be stabilized by back donation (as it is disfavoured due to steric reasons) and therefore experience an intrinsically weaker interaction. However, more recent work has shown that H_2 can bind to very electron deficient metal centres where there is no significant contribution from back bonding (though heterolytic H-H cleavage can readily occur in these systems).[74, 75] Calculations on a number of models of these systems have demonstrated that for the highly electrophilic metals involved (*e.g.*, $[(PR_3)M(CO)_4]^+$ (M = Mn or Re, R = Cy, Ph or ^{i}Pr), $[Re(CO)_3(PR_3)_2]^+$ (R = Cy, Ph, ^{i}Pr), $[Fe(PH_3)_5]^{2+}$ and $[CpW(CO)_3]^+$) the reduction in back donation is almost completely offset by the increased electron donation from H_2.[32, 76-79] The binding of dihydrogen in these super-electrophilic systems can be considered as analogous to how alkanes would interact - exclusively through σ donation with no back donation involved. The prospect that alkanes can bind to these fierce electrophiles if other competing (and invariably superior) electron donors can be excluded is therefore reasonable.

1.2.4: Coordination of Si-H σ Bonds:

A large number of σ complexes involving silanes have been characterised and are important intermediates in the catalytic dehydropolymerisation of silane to polysilanes.[80, 81] All exhibit the η^2-Si,H bonding mode in the solid state, confirmed by neutron diffraction studies on selected compounds.[80, 82, 83] The structures predominantly resemble the oxidative addition product (i.e. d_{MH} and d_{MSi} are short characteristic of classically bonded ligands, with a concomitantly long – 'stretched' Si-H bond) as

opposed to an unstretched Si-H σ complex where Si-H bond lengths are 'normal'. Solution studies also support a significantly lengthened Si-H bond with the ^1J (SiH) coupling constant falling drastically on coordination (*e.g.*, 200 Hz for free $HSiPh_3$ decreasing to 65 Hz on coordination to the 16 electron $\{MeCpMn(CO)_2\}$).[84] The origin for this is twofold: (i) the greater basicity of the Si-H bond relative to the C-H (and H-H) bond results in better σ donor ability; and (ii) as a result a weaker Si-H bond which therefore lowers the energy of the σ^* orbital making it more accessible for back donation. By altering the metal/ligand set a sequence of (Si-H)-M interactions have been synthesised that produce a near continuum along the entirety of the oxidative addition pathway for σ silane complexes. The two disparate systems $Mo(CO)(depe)_2(\eta^2\text{-}HSi(H)_2Ph)$ and $[CpRu(PMe_3)_2(\eta^2\text{-}HSiCl_3)]^+$ are prime examples of unstretched and stretched Si-H bonds respectively (Figure 23).[82, 85]

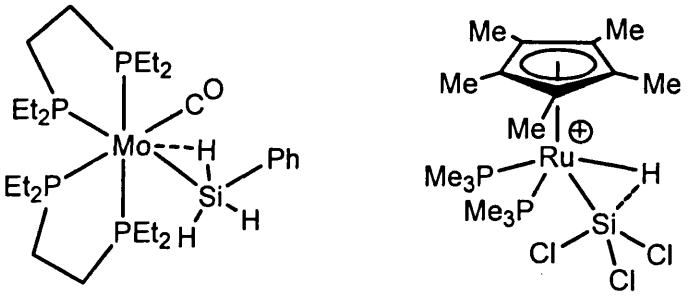

Figure 23: $Mo(CO)(depe)_2(\eta^2\text{-}HSi(H)_2Ph)$ and the cation $CpRu(PMe_3)_2(\eta^2\text{-}HSiCl_3)^+$.

The synthesis of metal silane σ complexes is readily achieved by a number of routes, including the addition of silanes to unsaturated metal centres (often generated by photolytic/thermolytic dissociation of CO), the displacement of weaker σ ligands (e.g. H_2 and agostic C-H), displacement of weakly coordinated solvent molecules and; more recently, by the protonation of metal silyl bonds.[85-87] Both neutral and cationic silane complexes are known, though cationic systems are rare due to their susceptibility to undergo heterolytic bond cleavage.[85, 88] A wide variety of different silanes, including the

simplest, SiH_4, and from the electron deficient $HSiCl_3$, to the electron rich bulky silanes (*e.g.*, $HSi(SiMe_3)_3$) have all been characterised, with the metals involved ranging from groups 5 to 10. The extensive number of stable isolated silane compounds compared with alkane complexes is indicative of the increased metal – silane stability arising from the better σ donating ability of the Si-H bond and the increased back donation into the Si-H σ^* orbital.[89]

1.2.5: Agostic C-H Interactions:

The agostic bond, where a metal's coordination sphere is completed by a ligand bending back and 'clasping itself' (agostic is derived from the Greek word αγοσός - meaning to hold oneself)[34] through donation of σ C-H electron density has been known since 1965.[90, 91] A large number of agostic compounds have been characterised ranging from main group metals (M = Li, Na, Mg, Ca, *e.g.* $[Li\{\mu\text{–}N(SiMe_3)_2\}_2Mg\{N(SiMe_3)_2\}]$ Figure 24),[92-94] d^0 transition metals (*e.g.*, M = Zr, Hf, Ti, Ta where the agostic interaction is a key intermediate in Ziegler-Natta alkene polymerisation catalysis, *e.g.* $[rac\text{-}C_2H_4(indenyl)_2ZrC(SiMe_3)=CMe_2]^+$ - Figure 24)[34, 92, 95-97] and all other transition metal d electron configurations.[32, 34, 92, 98-100]

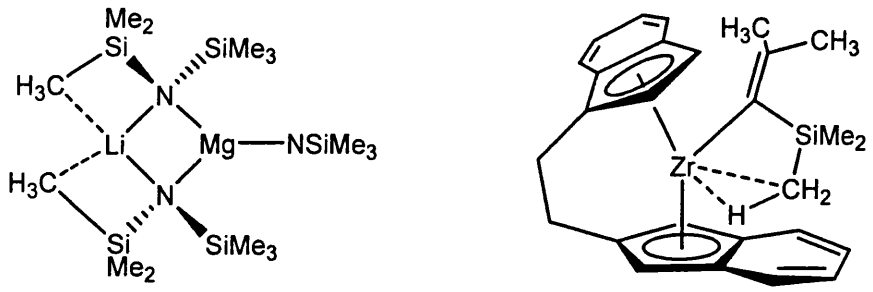

Figure 24: Agostic interactions in $[Li\{\mu\text{–}N(SiMe_3)_2\}_2Mg\{N(SiMe_3)_2\}]$ (left) and $[rac\text{-}C_2H_4(indenyl)_2ZrC(SiMe_3)=CMe_2]^+$.

From these numerous studies the interaction with the metal centre has been found to lie between two extremes, the η^3–C,H,H and the η^2–C,H bonding modes. These are connected by numerous asymmetrically bound η^3-C,H,H adducts (Figure 25).[101]

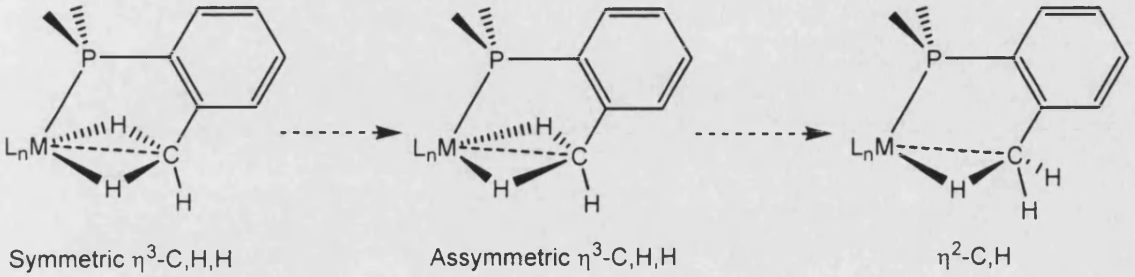

Figure 25: The continuum of possible agostic interaction.

The observed structural motif is highly dependant on the length and the freedom of motion in the arm that the intramolecular connectivity is through. A variety of possibilities from α through to δ positions have been observed to bind to the metal centre. In the small number of systems where the ligand has undergone little or no structural deformation to achieve the agostic interaction a symmetric η^3 C,H,H binding mode is favoured (verified by neutron diffraction techniques).[102, 103] These primarily involve a CH_3 δ position on phosphine ligands such as $PR_2(2,6\text{-}Me_2C_6H_3)$ (where R = Ph or Cy) for the agostic connection. This generates an agostic interaction with an unstrained six membered ring between the metal and the agostic arm of the ligand and it binds in favour over a number of β and χ sites available from the Ph or Cy arms. The solution NMR studies of these systems do not reach a static state and therefore the equivalence of the two coordinated C-H bonds cannot be confirmed.

The η^2-C,H agostic complexes are predominantly found for α and β compounds, where the required deformation of the ligand results in only one C-H bond approaching within close enough proximity for a bonding interaction to occur. Due to the

constrained nature, the M-H bond has to lie in the M-C_1-C_2 plane (i.e., M-C_2-C_1-H_1 torsion angle = 0°) otherwise the M-H distance is too great for a bonding interaction (Figure 26). If a torsional twist were to take place in the C_1-C_2 bond to present two C-H bonds towards the metal centres both M-H distances would be significantly longer than the single agostic M-H distance in the η^2-C,H mode as the C-H bonds now are above and below the M-C_1-C_2 plane. This prevents sufficient bonding overlap for this mode to be energetically favourable over the η^2-C,H mode (Figure 26).

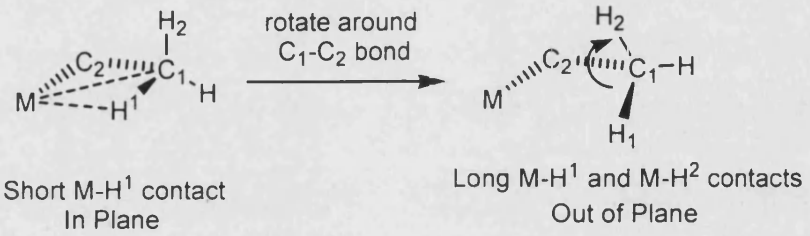

Figure 26: The favourable in plane bonding interaction and the twisted unfavourable interaction.

Moving to γ and δ systems the ligand is not so severely perturbed with larger M-C_1-C_2 angles. Torsional twist of the C-C bonds can now occur whilst maintaining the agostic binding interaction (i.e., short interatomic M-H distances), thus allowing the terminal CH_3 group to bind in an unconstrained manner to the metal centre (Figure 27). It is these examples that occupy the more symmetrical η^3-C,H,H end of the continuum.[101]

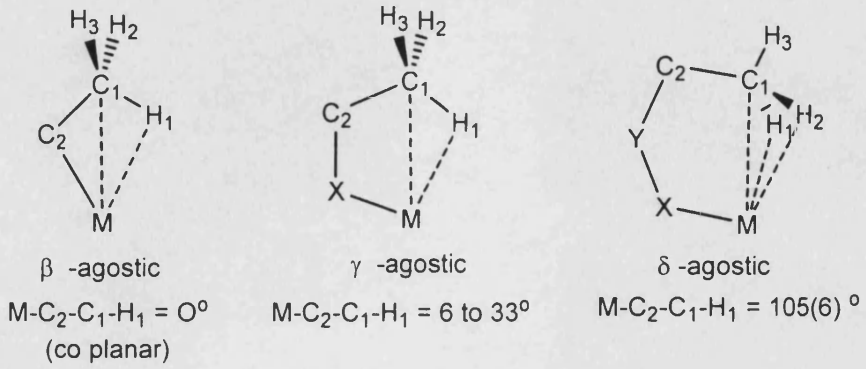

Figure 27: Schematic of β to δ agostic complexes, showing the degree of projection of the agostic bound H atom out of the M-C_1-C_2 plane.[101]

It therefore can be concluded that in the less strained, torsionally non-confined, agostic complexes the preferred geometry for the $CH_3\cdots M$ interaction is the symmetric or asymmetric η^3–C,H,H motif. This supports the limited experimental and more extensive theoretical data so far reported for the structural motif of true metal alkane σ complexes, which also show a η^3-C,H,H binding mode.

Apart from providing insight into the type of bonding mode C-H σ complexes favour, information can also be obtained on the C-H bond parameters in agostic interactions. Agostic bonds are elongated between 5 and 10% (by neutron diffraction studies) with respect to non-bridging hydrogens, implying a reduction in electron density in the C-H bond due to its transfer to the electrophilic metal.[92] Recently, the first example of a stretched agostic C-H interaction has been characterised in a 'pincer' ligand system (Figure 28).[104] The C-H elongation is 22% in the solid state when compared to the normal d_{CH} in benzene and is supported by solution NMR studies with the $^1J(CH)$ coupling constant of 50 Hz showing a significant reduction from the 120-130 Hz found in 'free' arene C-H bonds. The lengthened nature of the C-H bond indicates that it could be viewed as a step along the pathway to oxidative addition.

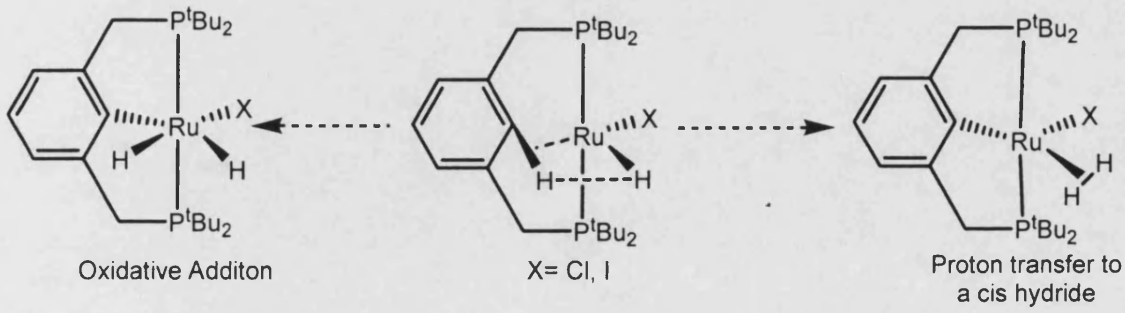

Figure 28: The possible initial step of the reaction elongated agostic pincer complex to give the observed trans-[(Cl)Ru(PCP)].

An alternative possibility is that arrested proton transfer to a *cis*-hydride is causing the geometry and elongation of the agostic interaction, with the C-H directed toward the *cis* hydride rather than the vacant site. Proton transfer reactions of coordinated dihydrogen are well documented and intermolecular dihydrogen bonding can be viewed as an intermediate on this reaction coordinate.[98, 105]

Work by Crabtree investigating the changes in the M-H agostic bond and the M-H-C angle generates a continuum of interactions, with an initial end on approach of the C-H bond that continues into a canted side on geometry with a concurrent increase in d_{CH} bond length (Figure 29).[99] This experimental trajectory for the oxidative addition of agostic complexes correlates well with the calculated reaction coordinate for the addition of CH_4 to the complexes $RhCl(PH_3)_3$ and $IrX(PH_3)_2$ (X = H, Cl).[46, 106]

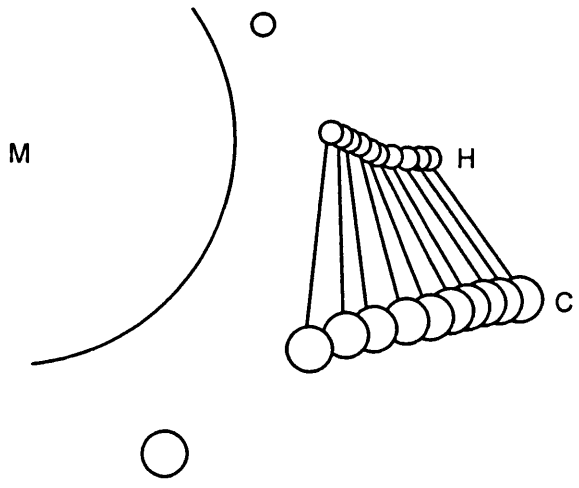

Figure 29: Proposed trajectory for the oxidative addition of agostic complexes.

However, with measured elongations in the range of only 5 –10% of the agostic C-H bond length only the initial stage on the oxidative addition reaction coordinate has been experimentally calculated, thus extrapolation to generate a mechanism for the oxidative addition with any confidence is not possible.

Agostic interaction energies have been revealed by experimental and computational studies to be weak (in the range 10 –15 kcal/mol), comparable to that calculated for the complexation of alkanes to $M(CO)_5$ (M = Cr, Mo, W)).[23, 107-110] The formation of the weak agostic bond is therefore very sensitive to a number of factors including ligand steric bulk. This is exemplified in non-bulky systems where the weak metal···H_3C interaction is insufficient to fix the pendant arm in the correct location (*e.g.*, $[Ir(H_2)(P^iPr_2Ph)_3]^+$ has no agostic bonding whilst solid state characterisation of the bulkier complex, $[Ir(H)_2(PCy_2Ph)_3]^+$, shows one agostic interaction),[111] whereas bulky phosphines 'trap' the C-H bond in the vicinity of the metal by steric effects.[112]

1.2.6: Intermolecular CH_3···M Interactions

1.2.6.1: Charge Neutral CH_3···M Interactions

An alternative method to model alkane coordination to transition metals involves the use of intermolecular bonding with either alkyl groups in the solid state (where crystal packing forces dominate) or with more polarised $E^{\delta+}$-$C^{\delta-}H_3$ groups in solution. There have been a number of examples of each published recently. Elegant work by Burns and Andersen provided a model for the η^3-H,H,H coordination motif of alkanes by using a CH_3X system where X was the electropositive {BeCp*} group, thereby increasing the electron density on the methyl group (Figure 30).[113] The Lewis acid – base adduct between Cp^*BeCH_3 and Cp^*_2Y exhibits a close Yb···C contact of 2.766(4)Å indicative of a significant interaction.

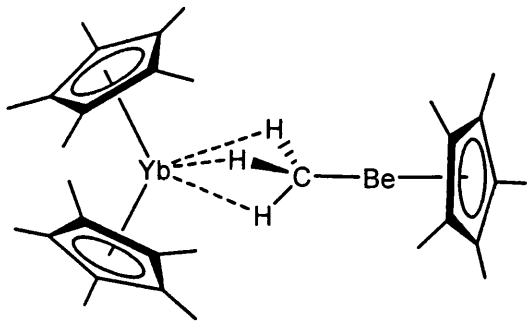

Figure 30: The Lewis base/acid adduct [$Cp^*_2Yb(\mu\text{-}Me)Be(C_5Me_5)$].

The geometry of the bridging methyl is symmetrical within errors (Y-H1 2.54(4), Y-H2 2.51(5) and Y-H3 2.71(6) Å), with the metal positioned over the tetrahedral face of the CH_3 group. The Yb-C distance (d_{YbC} = 2.766(4) Å) is close to the average found in the ethylene compound $(Cp^*)_2Yb(C_2H_4)$ (2.781(6) Å) and is shorter than the average in the alkyne complex $Cp^*_2Yb(MeC{\equiv}CMe)$ (2.85(1) Å).[114]

Another M···H_3C close contact has been reported in the rhodium dimer, [$Rh_2(\mu\text{-}O_2CC_6H_2{}^iPr_3)_4$] where each rhodium's coordination sphere is completed by an axial CH_3 interaction from an adjacent molecule in the extended structure (Figure 31).[115] The two independent Rh···H_3C interactions exhibited in the extended lattice both are of an asymmetrical η^3-H,H,H mode, with the metal capped by the tetrahedral face of the bridging methyl. No ^1H NMR data was reported. The Rh-C distances (2.80 Å and 2.74Å) are at the limit of the sum (2.81 Å) of the ionic radius for Rh(III) (0.81 Å) and the van der-Waals radius of CH_3 (2.00 Å) suggesting only a weak M···H_3C contact, with crystal packing forces dominating.

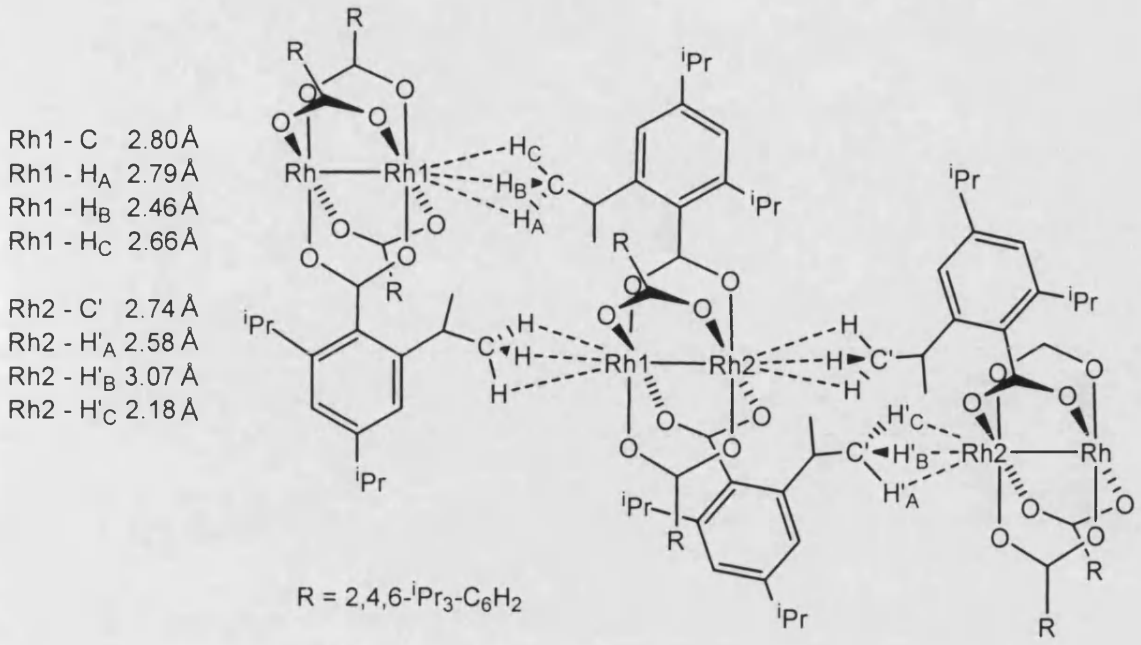

Figure 31: The Intermolecular Rh···H_3C interaction in the extended structure of [$Rh_2(\mu$-$O_2CC_6H_2{}^iPr_3)_4$] showing only the ^{i}Pr groups involved in the axial bonding.

A similar example comprises a cyclotriyne Ni(0) complex that crystallises in layers, analogous to graphite, with the nickel centre having two axial sites vacant.[116] Close examination revealed the presence of two intermolecular C-H contacts to two ligands, in a plane above and below (Figure 32).

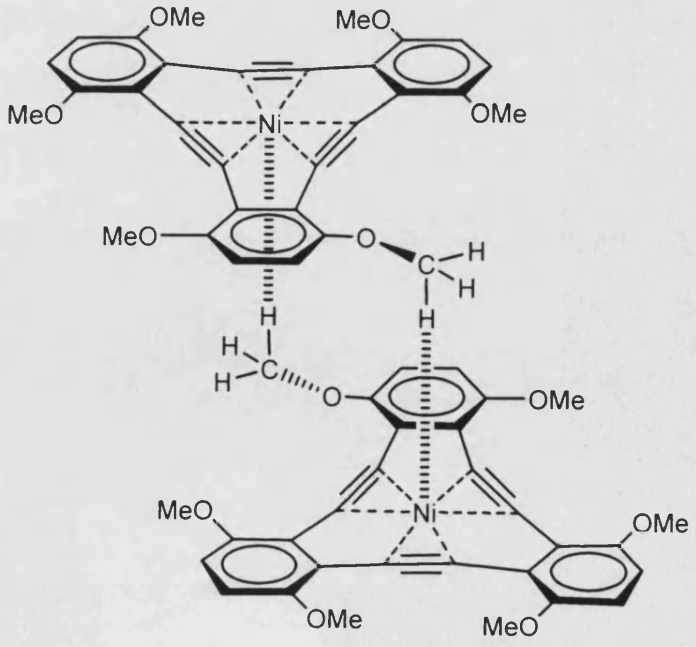

Figure 32: The intermolecular C-H···Ni interactions between layers of Ni(0) cyclotriynes.

The hydrogens on the methyl groups involved were refined isotropically and showed long, almost end, on contacts (Ni-H-C distance 2.822(1) Å and Ni-H-C angle 163.5°). The more reliable Ni-C distance at 3.750(4) Å lies outside the combined Van der Waals radii for Ni(0) (1.60 Å) and CH_3 (2.00 Å) suggesting that the crystal packing forces dominate with only a very weak σ contact, if any, present.

1.2.6.2: Electrostatic 'Enhanced' CH_3···M Interactions:

Other compounds that can be used as models for alkane σ coordination increase the interaction between the metal and the CH_3 moiety by introducing charge, thereby creating an additional electrostatic force between a cationic metal centre and the anion. This is exemplified by the solid state structure of $Li[BMe_4]$ determined by X- ray and neutron diffraction studies (Figure 33), where the electropositive Li is in close contact with the $[BMe_4]^-$ anion forming a one dimensional coordination polymer.[117, 118]

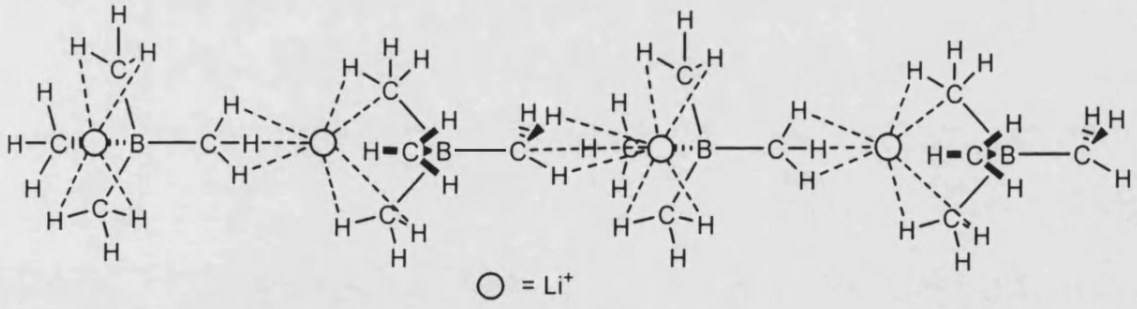

Figure 33: Schematic of the C-H···Li interactions in $LiBMe_4$ as determined by neutron diffraction.

Two bonding motifs are observed in the extended structure, an η^3-C,H,H and an η^4-C,H,H,H. In both motifs the Li···H_3C distance is within the sum (2.189(7) Å - 2.375(5) Å respectively) of the ionic radius for Li^+ (0.9 Å) and the van der-Waals radius for CH_3 (2.00 Å) implying a significant interaction.[119] The CH_3 geometry is slightly

distorted from tetrahedral (a compression of the H-C-H angle in the C-H bonds interacting with the lithium - average of H-C-H angle of 103.5°). No meaningful examination of the C-H bond lengths could be undertaken due to the large errors associated with low frequency methyl rotational amplitudes that occurred at the experimental temperature – thus, it is uncertain if there is any reduction in the C-H σ bond strength from C-H to M electron donation.

Further examples of CH_3 groups directly bound to a formally negative atom interacting with metal centres include the weakly coordinating methyl borates $[MeB(C_6F_5)_3]^-$ and the aluminates (*e.g.*, $[AlMe_4]^-$, $[Me_3AlE(R)AlMe_3]^-$).[120-126] Weakly coordinating anions such as $[MeB(C_6F_5)_3]^-$ (which will be discussed further in the introduction to Chapter 3) have found extensive use in organometallic chemistry and are used to generate highly Lewis acidic metal centres by forming loose, readily displaceable, interactions with the metal. The general use and specific properties of weakly coordinating anions will be reviewed later in this introduction. The generation of the $[MeB(C_6F_5)_3]^-$ anion occurs *in - situ* on the reaction of the highly Lewis acidic $B(C_6F_5)_3$ with a metal-methyl, the $M^{\delta+}$-$C^{\delta-}$ polarisation results in the abstraction of the formally negatively charged methyl forming the observed anion. In the absence of any Lewis basic molecules (such as THF) there is an interaction between the metal and the $[MeB(C_6F_5)_3]^-$ through the anion bound methyl group, a M···H_3C close contact (Figure 34). The bridging methyl moieties in these zwitterions can be regarded as an intermediate on the methyl abstraction reaction pathway and these complexes play an important role in homogeneous metallocene-catalysed olefin polymerisations.[126]

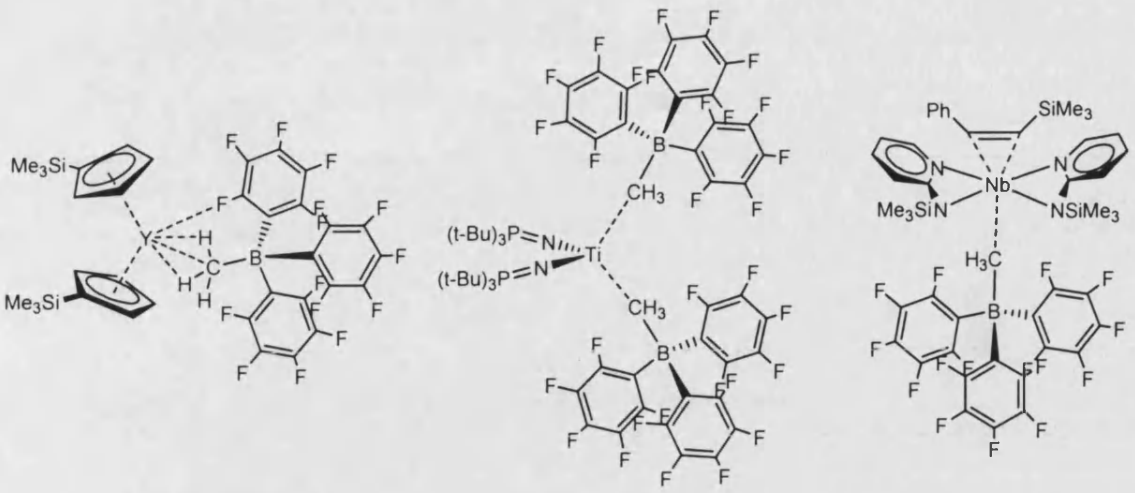

Figure 34: The zwitterionic complexes $[(Me_3Si\text{-}Cp)_2Y(\mu\text{-}Me\text{-}B(C_6F_5)_3]$,[122] $[(({}^tBu)_3P{=}N)_2Ti\{(\mu\text{-}Me\text{-}B(C_6F_5)_3\}_2]$[127] and $[(PhC{\equiv}CTMS)(\kappa^2\text{-}1\text{-}N(SiMe_3)\text{-}C_5H_4N)_2Nb(\mu\text{-}Me\text{-}B(C_6F_5)_3)]$.[128]

Calculations on a number of these systems show that electrostatic interactions dominate the bonding between the cationic metal and the bridging methyl group. They still, however, represent a pertinent model for M···alkane interactions.[129] The binding in the complexes where the hydrogens have been freely refined is the η^2 C,H,H mode.[121, 130] Solution studies on the coordination of $[MeB(C_6F_5)_3]^-$ to d^0 metal centres consistently show an up-field shift of the (μ-Me) moiety on coordination to the metal.[131]

For the aluminates (*e.g.*, $(O\text{-}{}^tBu_2C_6H_3)_2M(\mu\text{-}Me_2)AlMe_2$ (M = Y and Lu) and $\{(Cp^*)_2Yb(AlMe_3)_2\text{-}(S\text{-}p\text{-}C_6H_4Me)\}_2$ Figure 35),[124, 132] the hydrogen positions have been freely refined in only a limited number of these structures and the only bonding motif observed has been the η^3-H,H,H mode. The metal – H_3C distances in the ytterbium compound (2.670(7) Å and 2.667(6) Å) are well within the combined (3.04 Å) ionic radius of Y (1.04 Å) and the van der-Waals of CH_3 (2.00 Å).

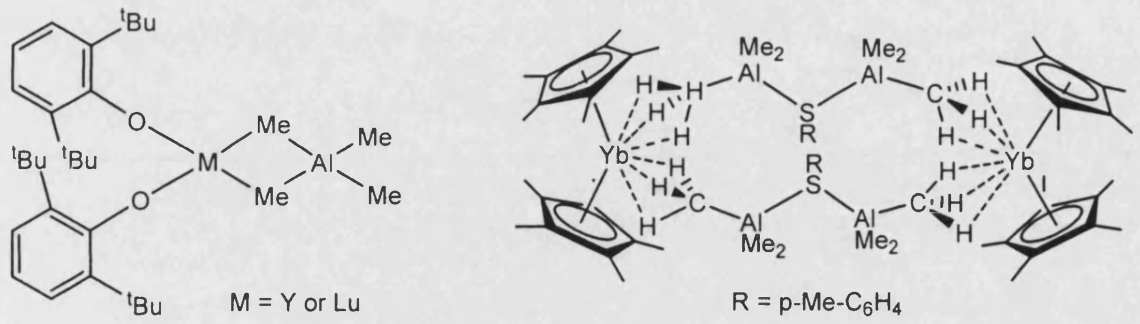

Figure 35: Molecular structures of the metal coordinated $[AlMe_4]^-$ and $[Me_3AlE(R)AlMe_3]^-$ anions.

A related anionic system with a CH_3 periphery has been recently developed by Michl and is based on the mono-anionic cluster [*closo*-$CB_{11}H_{12}]^-$ that has the advantage of a significantly more delocalised negative charge.[133] These anions are used in this thesis and the next section shall discuss these clusters and their bonding in depth.

1.3. Mono-Anionic Carboranes and their Alkylated Derivatives

1.3.1: The [*closo*-$CB_{11}H_{12}]^-$ Cluster

The mono-anionic carborane cluster [*closo*-$CB_{11}H_{12}]^-$ was first synthesized by Knoth in 1967.[134, 135] The icosahedral cluster core is extremely stable, having a delocalised σ bonding framework, a high HOMO-LUMO energy gap, a *closo* cluster core electron count and a high oxidation potential - making it conceptually a three dimensional analogue of benzene. These properties combined with its large size (~3.4 Å average B-B diameter), spherical shape, mono-anionic charge and lack of any lone pairs or π electron density leads to its relatively weak nucleophilicity and its potential as a weakly coordinating anion.[126, 136, 137]

Despite the inherent stability of the carborane core its periphery has a wide and versatile substitution chemistry that can lead to lower nucleophilicities, higher stabilities and increased solubilities in low dielectric solvents. The reactivity of the B-H bonds varies over the cluster due to the more electronegative carbon at position - 1 polarising the cage. The antipodal (B12) boron is the most reactive towards electrophilic attack, due to its increased hydridic nature, this is followed by the lower pentagonal belt B-H bonds (B7-11) with the upper pentagonal belt (B2-6) being the least susceptible to electrophilic attack.[138] The carbon at position - 1 has no reactivity to electrophiles.

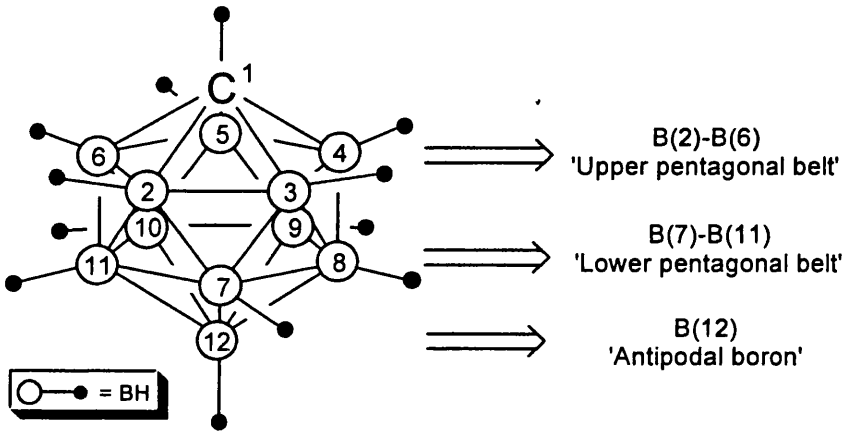

Figure 36: The labelling of [*closo*-$CB_{11}H_{12}$].

Controlled substitution of the three inequivalent boron vertices is possible, for example, in the halogenation reactions the B(12) position is functionalised under mild conditions (I_2, 20°C), the B(7-11) positions under harsh conditions (excess ICl, 20°C), while the B(2-6) vertices require forcing conditions (excess ICl, 200°C, 2 days).[138, 139]

Recent *ab-initio* calculations assist in the rationalisation of the observed reactivity of [*closo*-$CB_{11}H_{12}$]$^-$.[140] From Frontier Molecular Orbital theory it is known that the selectivity of electrophilic attack is highly dependant on the amplitude of the

HOMO at any particular position. In [*closo*-$CB_{11}H_{12}]^-$ the HOMO and HOMO –1 (both degenerate pairs of molecular orbitals) are relatively close in energy and thus both have to be examined when considering the cage's substitution patterns. The HOMO consists of orbitals at both the lower and upper pentagonal belts, whilst the HOMO-1 predominantly involves a large amplitude on the antipodal vertex and a smaller on B7-12 (Figure 37).

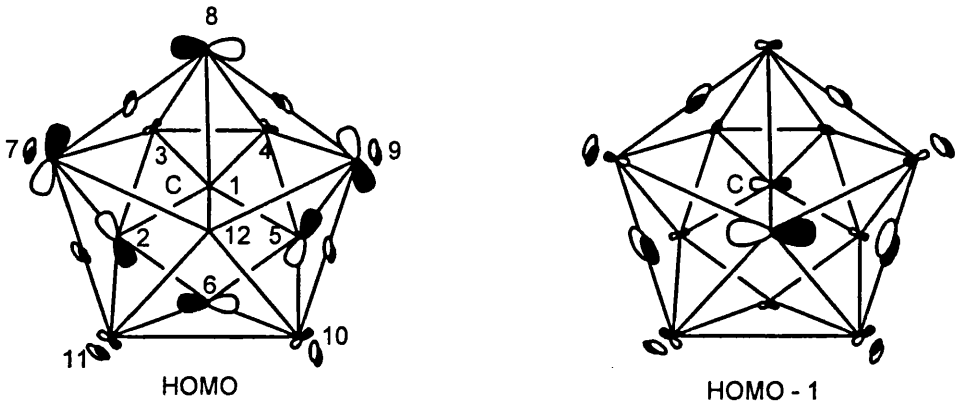

Figure 37: The HOMO and HOMO – 1 of [*closo*-$CB_{11}H_{12}]^-$ (only one of each degenerate pair is shown).

Further theoretical studies at the B3LYP/6-31G(d) level by McKee[141] on the Natural Population Analysis (NPA) Charges of [*closo*-$CB_{11}H_{12}]^-$ calculated that the vertices B(7-11) and B(12) carry partial negative charge (-0.13 and –0.11 respectively) whilst B(2-6) are slightly positive (0.03). An inferred order of reactivity with respect to E^+ can be postulated from these set of calculations of B(7-11) ≈ B(12) > B(2-6). The combination of these two investigations goes someway to accounting for the observed reactivity at each vertex.

The following mono-anionic compounds are all readily synthesised by electrophilic substitutions at some or all of the hydridic B-H bonds: [12-$(CH_3)_2S$-*closo*-$CB_{11}H_{11}$], [12-$CH_3SCH_2SCH_3$-*closo*-$CB_{11}H_{11}$], [12-X- *closo*-$CB_{11}H_{11}$] (X = F, Cl, Br or I), [7-I-*closo*-$CB_{11}H_{11}$], [7,12-X_2-*closo*-$CB_{11}H_{10}$] (X = Cl, Br or I), [7,8,9,10,11,12-X_6-

closo-$CB_{11}H_6$] (X = D, Cl, Br or I), [1-H-*closo*-$CB_{11}X_{11}$] (X = F, Cl, Br or I) and [12-CX_3COOHg-*closo*-$CB_{11}H_{11}$] (X = H or F).[138, 142] The halogenated derivatives of [*closo*-$CB_{11}H_{12}]^-$ have found extensive use in the stabilisation of reactive cationic complexes due to their robust nature and weakly coordinating properties.[143-148]

As opposed to the B-H bond's hydridic nature, the C-H bond is acidic and functionalisation is readily achieved via deprotonation and nucleophilic substitution reactions. The various C substituted carborane products include: [1-R-*closo*-$CB_{11}X_{11}$] (R = alkyl, aryl, halo, X = H, Cl, Br or I), [1-HS-*closo*-$CB_{11}H_{11}$], [1-COOH-*closo*-$CB_{11}H_{11}$] [1-R_3Si-*closo*-$CB_{11}H_{11}$], [1-Ph_2P-*closo*-$CB_{11}H_{11}$], [1-R(OH)CH-*closo*-$CB_{11}H_{11}$] (R = alkyl).[138, 149-151] These salts are generally characterized as the Cs^+ or R_3NH^+ salts. Simple salt metathesis reactions lead to the synthetically useful salts Ag^+, Tl^+, Ph_3C^+, R_3Si^+, and $H(OEt_2)^+$.[152]

1.3.2. Alkylated Carboranes:

The first example of a C-alkylated mono-anionic carborane was achieved by the deprotonation of the C-H vertex by a strong base followed by reaction with a series of alkyl halides to give a range of carboranes of the general formula [1-R-*closo*-$CB_{11}H_{11}$] (Figure 38).[149] The 1-alkyl systems are also readily accessible in the final step of the synthesis of the carborane cage, by a functionalised carbene insertion into the anion [*nido*-$B_{11}H_{14}]^-$ (albeit in low overall yield).[153]

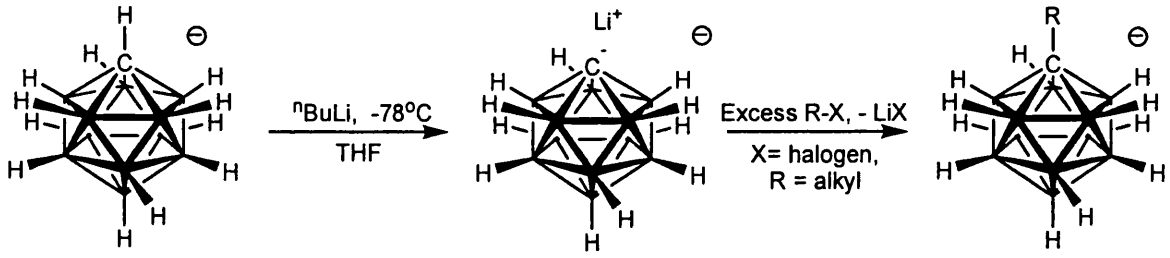

Figure 38: Preparation of [1-*closo*-R-$CB_{11}H_{11}$]$^-$ via deprotonation.

A mono-alkyl carborane anion has also been synthesised with a B-R vertex (R = aryl), in this case the 2-aryl derivative [2-Ph-1-*closo*-$CB_{11}H_{11}$]$^-$, which can be formed by the insertion of a functionalised boron into the [*nido*-$CB_{10}H_{11}$]$^{3-}$ anion.[154]

A number of B-alkyl derivatives have also been synthesised via the conversion of B-I vertices to B-C vertices by palladium catalysed alkylation with Grignard reagents.[155] This technique was initially developed by Hawthorne *et., al*,[156] for the alkylation of the [*closo*–$B_{12}H_{12}$]$^{2-}$ anion. The 1,12 dialkyl carborane derivatives [1-R-12-R'-*closo*-$CB_{11}H_{10}$]$^-$ are readily synthesised from [1-R-12-I-*closo*-$CB_{11}H_{11}$]$^-$ by this methodology (Figure 39). Partially methylated carboranes have also been prepared from the polyiodinated carboranes by a similar Pd catalysed cross coupling with CH_3MgI. No fully alkylated or hexa-alkylated derivatives were reported to be synthesised and isolated cleanly via this route for the mono anionic [CB_{11}]$^-$ cluster.[133]

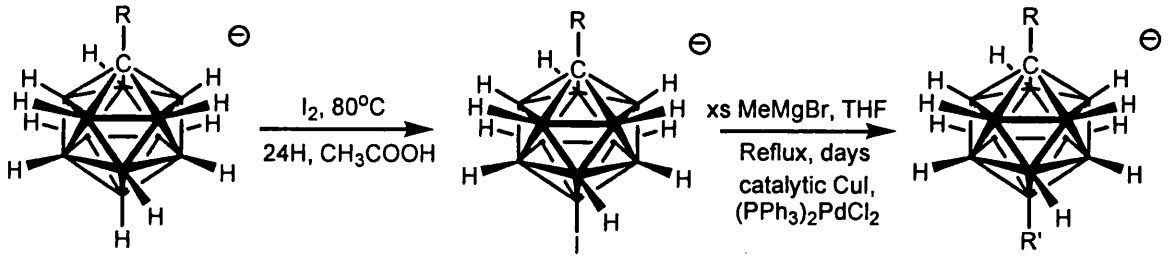

Figure 39: Formation of 1,12 dialkyl carboranes from [*closo*-$CB_{11}H_{12}$]$^-$.

The highly methylated derivative of the 10-vertex carborane [1-H-*closo*-CB_9Me_9]$^-$ has been synthesised from [1-H-*closo*-CB_9I_9]$^-$ using Pd catalysed cross coupling in a sealed tube reaction at high temperatures.[157]

The first successful peralkylation of the B-H vertices of a carborane was achieved in the neutral carborane analogue *para*-1,12-*closo*-$Me_2C_2B_{10}H_{10}$ that underwent permethylation with a methyl triflate – triflic acid mixture.[158] This reaction when carried out with the more reactive [*closo*-$CB_{11}H_{12}$]$^-$ lead to unspecified products, but not the desired permethylated derivative.[133] The first synthesis of a mono-anionic peralkylated carborane [*closo*-$CB_{11}Me_{12}$]$^-$, was achieved using excess methyl triflate in the presence of a hindered base (2,6-di-tert-butylpyridine) (Figure 40).[133]

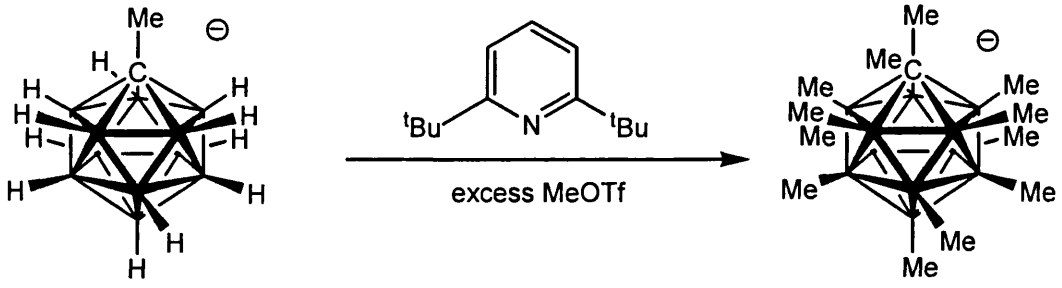

Figure 40: The formation of [*closo*-$CB_{11}Me_{12}$]$^-$ by reaction with excess methyl triflate.

The hindered base was required to react with the triflic acid produced as a by-product of the electrophilic substitution, thereby preventing unwanted side reactions and ultimately cage degradation. The permethylation reaction is self-catalysing ensuring that [*closo*-$CB_{11}Me_{12}$]$^-$ is the only functionalised carborane product. Initial mono-methylation activates the cage to further electrophilic substitutions due to the electron donating nature of the methyl substituents.[155] An improved synthesis of [*closo*-$CB_{11}Me_{12}$]$^-$ without the need for the expensive hindered base has also been recently published.[140] Salts of the permethyl carborane anion [*closo*-$CB_{11}Me_{12}$]$^-$ are air stable, stable to fragmentation in concentrated base and dilute acid, but cage degradation

occurs slowly on exposure to concentrated acid. This susceptibility to strong acid environments has been used to produce two mono fluorinated functionalised derivatives of [*closo*-$CB_{11}Me_{12}$]$^-$, the 12 and 7 isomers by reaction with HF.[159] A number of 1- alkyl derivatives can be produced with the general formula [1-R-*closo*-$CB_{11}Me_{11}$] by the methylation of [1-R-*closo*-$CB_{11}H_{12}$]$^-$ in an identical manner.[140]

An alternative route to peralkylated carborane anions is by the treatment of [*closo*-$CB_{11}H_{12}$]$^-$ with excess RBr (R = Me or Et) in a sealed tube under vacuum at raised temperatures.[160] This produces the peralkylated carborane anions [1-H-*closo*-$CB_{11}R_{11}$]$^-$ as the only boron-containing product (Figure 41). Attempts at peralkylation with more sterically demanding alkyl bromides, i.e. ^{i}PrBr, lead to a mixture of polyalkylated carboranes [1-H-*closo*-$CB_{11}H_{11-n}{}^iPr_n$] (n = 4 to 7); the incomplete nature of this reaction is due to the increased steric effects of the isopropyl groups.

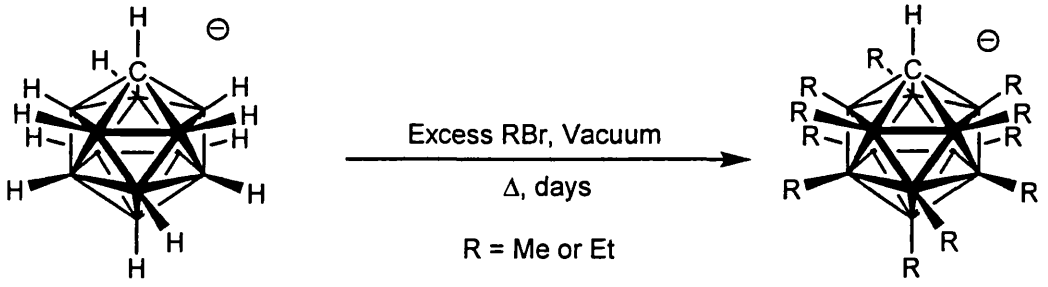

Figure 41: The formation of [1-H-*closo*-$CB_{11}R_{11}$]$^-$ via the 'sealed tube method'.

A direct result of the peralkylation of the monocarborane anion is an increased susceptibility to oxidation, owing to the alkyl substituents. *Ab-initio* calculations compute that permethylation reduces the ionisation potential (IP) from 5.19 eV ([*closo*-$CB_{11}H_{12}^-$]) to 4.32 eV, still a remarkably large value especially when compared to the experimental IP of F^- and Cl^- of 3.399 eV and 3.617 eV respectively.[141] Nevertheless the formation of the radical [*closo*-$CB_{11}Me_{12}$]$^\bullet$ by electrochemical (potentials greater that 1.2 V {vs Fc/Fc^+}) means or by reaction with PbO_2/CF_3COOH proceeds rapidly

producing an air stable black crystalline solid.[159] The radical $[CB_{11}Me_{12}]^{\bullet}$ is soluble in oxidation resistant non-polar solvents (*e.g.*, CCl_4, pentane); with its stability attributed to the steric protection provided by the peripheral encapsulating CH_3 groups.

[*closo*-$CB_{11}Me_{12}$][Y] (Y = group (I) cations excluding Li^+) are soluble in polar organic solvents (e.g. CH_2Cl_2, Et_2O), but sparingly in hydrocarbons. The cation has a significant contribution to the solubility properties of these anions, the lithium salts being the most soluble of all the simple cations, with a measurable solubility even in alkanes.[140] Replacement of the C-1 methyl group with higher alkyl homologues further improves solubilities of the lithium salts. Li[*closo*-$CB_{11}Me_{12}$] has also proved to be an active catalyst for Lewis acid catalysed pericyclic rearrangements, Diels Alder additions and ally and silyl ether solvolyses, showing that the Li^+ cation is highly Lewis acidic.[161]

A mixed halogen/methyl functionalised carborane, [1-H-2,3,4,5,6-Me-7,8,9,10,11,12-X-*closo*-CB_{11}]$^-$ (X = Cl, Br, or I) has been recently reported, which can also be readily synthesised in a two-step manner from [*closo*-$CB_{11}H_{12}$]$^-$ (Figure 42).[162]

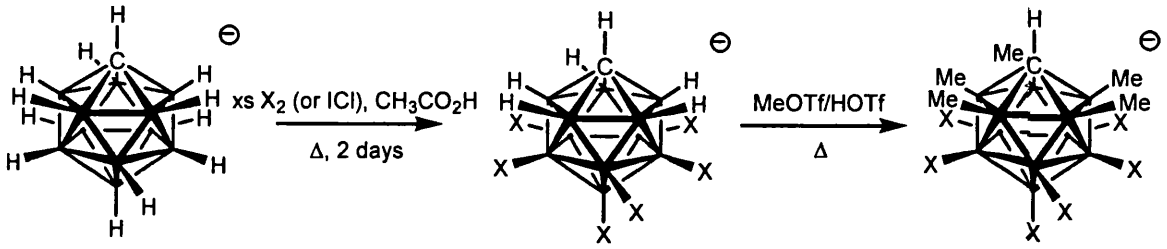

Figure 42: Formation of [1-H-*closo*-$CB_{11}X_6(CH_3)_5$]$^-$ from [*closo*-$CB_{11}H_{12}$]$^-$.

Pentamethylation renders the anion an order of magnitude greater solubility in toluene than the parent [*closo*-$CB_{11}H_6X_6$]$^-$ anion, without losing its chemical robustness – a drawback with the permethylated anion [*closo*-$CB_{11}Me_{12}$]$^-$. It is indefinitely stable in

neat triflic acid and more resistant to oxidation, it has in fact been described as the 'golden mean' between [*closo*-$CB_{11}H_6X_6$]$^-$ and [*closo*-$CB_{11}Me_{12}$]$^-$. A methyl reagent that is a stronger methylating agent than methyl triflate has been synthesised utilising this anion and used in the stoichiometric reaction of benzene with Me[1-H-*closo*-$CB_{11}Me_5Br_6$] to yield [C_6H_6Me][1-H-*closo*-$CB_{11}Me_5Br_6$]. Under identical conditions methyl triflate shows no significant conversion of benzene to the toluenium salt (Figure 43).

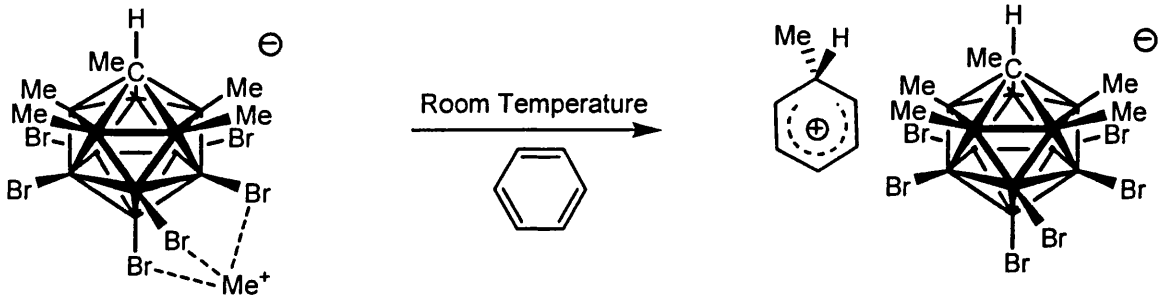

Figure 43: The isolation of a Wheland type intermediate by use of [1-H-*closo*-$CB_{11}Me_5Br_6$].

The potency of the Me^+ in Me[1-H-*closo*-$CB_{11}Me_5Br_6$] coupled with the robustness of its counter ion is further exemplified by the formation of [Me_3C][1-H-*closo*-$CB_{11}Me_5Br_6$] that is stable at room temperature under inert conditions (Figure 44).[163] The weakly coordinating nature of the [1-H-*closo*-$CB_{11}Me_5X_6$]$^-$ (X = Cl or Br) anion is clearly demonstrated by the absence of any close $C^+\cdots X$ contacts (in all complexes the interatomic distances are greater than the combined van der-Waals radii) and the sum of the C – C^+ - C angles being 360±0.1°.

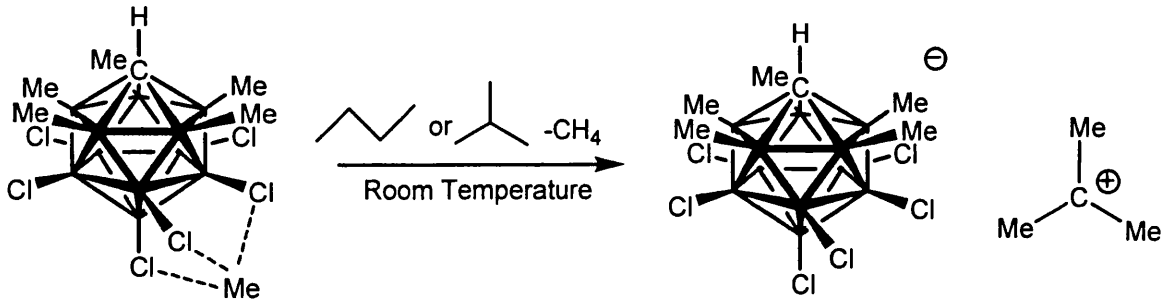

Figure 44: The synthesis of $[Me_3C][1\text{-H-}closo\text{-}CB_{11}Me_5Cl_6]$.

This anion appears to have the combined stability to strong acid/oxidising environments of the hexa-halogenated carborane derivatives, and to some extent the improved solubility characteristics of the permethylated carborane anions.

1.3.3: Coordination Chemistry of Alkylated Carboranes:

In contrast to the well-developed area of hexa-halogenated carborane chemistry,[137, 143-148, 162-171] there are relatively few reported metal complexes with the peralkylated carborane anions. The solid state structures of the thallium (I) and alkali (Li^+, Na^+, K^+, Rb^+ and Cs^+) salts of $[closo\text{-}CB_{11}Me_{12}]^-$ co-crystallised with arene solvents are known and display a number of different coordination motifs (**I** – **IV**, Figure 45).[172] The carbon vertex was not located in **(I)** and **(IV)** due to positional cage disorder, but is unambiguously assigned in structures **(II)** and **(III).** Methyl hydrogens were not located in any of the structures belaying any discussions on the $M\cdots H_3C$ coordination motifs.

In all four structural motifs the weak electrostatic interactions between the cation and $[closo\text{-}CB_{11}Me_{12}]^-$ necessitate strong cation – η^6 arene interactions. The Tl^+, Cs^+, Rb^+ and K^+ systems are all isomorphorous with the metal cation sandwiched between

two effectively parallel η^6-coordinated arenes, **(I)**. The geometry is *pseudo* octahedral with four equatorial contacts from adjacent cages completing the metal coordination sphere (all angles 90 ± 3°) Each anion in turn is coordinated to four metals in the extended structure. Processing up the alkali metal group to Na results in an alteration in the benzene/anion coordination motif to a *pseudo* tetrahedral geometry **(II)**. Displaying a tilted arene sandwich arrangement and two close anion contacts from the lower pentagonal belt (positions 7 and 9) that extend to produce a polymeric chain.

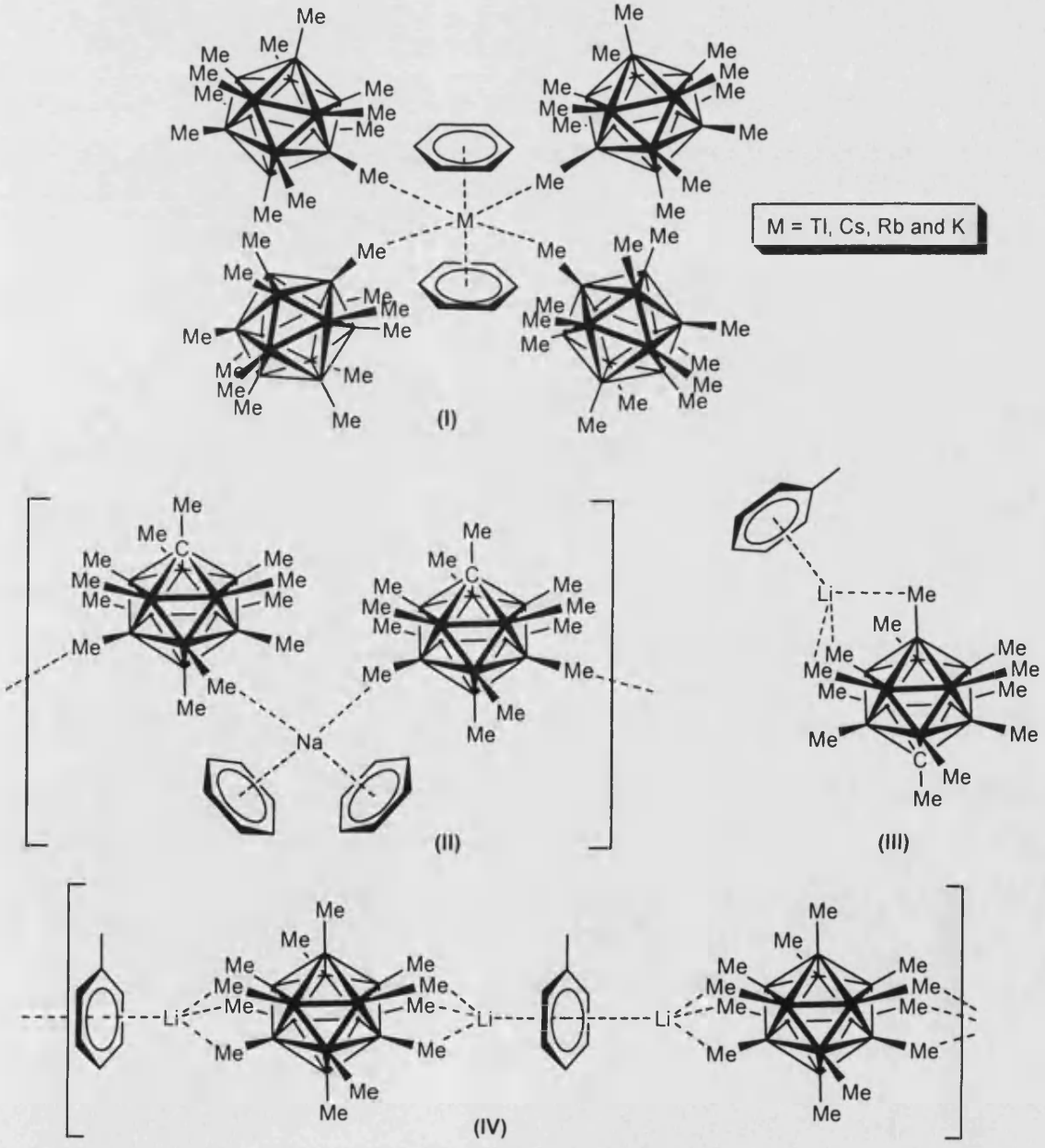

Figure 45: Structural bonding motifs for a series of simple metal cations partnered with [*closo*-$CB_{11}Me_{12}]^-$.

The Li^+ analogues contains two independent motifs in the solid state. In both the lithium is tetrahedrally coordinated by one η^6-arene and three CH_3 interactions from one cage anion. In **(III)** the Li^+ is coordinated to positions 7, 8 and 12 on one cage, and close examination revealed that these three methyl groups have been pushed apart slightly to improve the metal encapsulation. The Li-C distance (average 2.34 Å) is significantly shorter than the combined (2.90 Å) van der-Waals radius for CH_3 (2.00 Å) and the ionic radius of Li^+ (0.90 Å). These very close contacts and the anion methyl distortion (not observed for any other alkali salts) reflects a significant electrostatic interaction between the small lithium cation and the anion. In **(IV)** the Li interacts in a similar manner but consists of chains of half-occupancy η^6-toluene-Li^+ complexes on an inversion centre. The close contact ion pairing observed goes some way to explaining the improved solubility over other alkali salts in non-polar solvents.

The [*closo*-$CB_{11}Me_{12}]^-$ anion has been structurally characterised partnering a more complex cation, $[^nBu_3Sn]^+$. The reaction of two equivalents of the strong neutral oxidant [*closo*-$CB_{11}Me_{12}]^\bullet$ with *n*-Bu_6Sn_2 in an inert solvent (hexane) led to the ready formation of $[^nBu_3Sn]$[*closo*-$CB_{11}Me_{12}$] (Figure 46).[173]

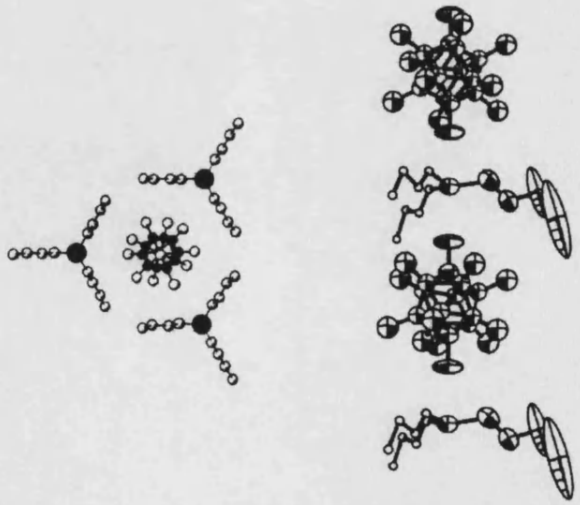

Figure 46 Structure of $^nBu_3Sn[CB_{11}Me_{12}]$, hydrogen atoms omitted.[173]

In the solid state there is a weak interaction between the $[^nBu_3Sn]^+$ cation and two methyl groups of the [*closo*-$CB_{11}Me_{12}]^-$ cage, resulting in a trigonal pyramidal geometry around the Sn. The B-CH_3···Sn contacts are significant, as judged by the close Sn-C distance (average 2.81 Å) lying comfortably within the combined van der-Waals radii for CH_3 (2.00 Å) and Sn (2.17 Å) of 4.17 Å. Crystallographic disorder of the cage anion prevented the determination of the carbon vertex and consequentially the identification of the position of the coordinated vertices (1 and 12 or 2 and 9) was not possible. Calculations at the B3LYP/SDD level on the ion pairing energies for the model complex Me_3Sn[*closo*-$CB_{11}Me_{12}$] gave the ordering of coordination energies as 12 > 7 > 2-6 >> 1 when there is only one cage···Sn contact. The calculated Natural Population Analyses produced a similar charge distribution, further supporting these computations.[141] However, due to each cage having two points of contact the 2,9 coordination motif is calculated to be more stable in the solid-state by 10.6 kcal/mol. The coordination persists in solution as demonstrated by the observed ^{119}Sn NMR chemical shift of 466 ppm. This is drastically further downfield than other trialkylstannyl cations, but it is still far lower than the calculated 1700 ppm shift of a truly free cation, suggesting a significant Sn-H_3C interaction.

1.4: Alkylated Carboranes as Weakly Coordinating Anions:

1.4.1: Background:

Weakly coordinating anions are vital in commercial olefin polymerisation processes, as electrolytes in lithium ion batteries, $[M]^+$ catalysed organic reactions, ionic liquids, extraction of radioactive cations from waste, photoacid generators and to

stabilise highly electrophilic (or oxidizing) cations.[174] A key property in these systems is an anion···metal interaction sufficiently weak that reactants or other poor electron donors can readily displace it.[136] The previously thought of 'non-coordinating anions' such as; $[ClO_4]^-$, $[OTf]^-$, $[BF_4]^-$, $[PF_6]^-$ and $[SbF_6]^-$ have all been reported to coordinate readily to Lewis acidic metal ions and are in fact weakly coordinating anions.[175-179] Out of this research came an improved understanding of the properties required to generate the next generation of 'non-coordinating' or more aptly 'super weakly coordinating anions' and they include:

- No basic or nucleophilic sites on the periphery (e.g. lone pairs, hydridic hydrogens, multiple bonds or easily polarised single bonds,
- Resistance to bond cleavage by super electrophilic metals,
- Kinetically and thermally stable,
- Delocalised charge distribution,
- Large size to minimize electrostatic attraction,
- Good solubility.

The leading candidates exemplifying the majority of these properties are the highly fluorinated tetraphenyl borates and halogenated derivatives of the $[closo\text{-}CB_{11}H_{12}]^-$ anion (Figure 47).[135, 138, 180]

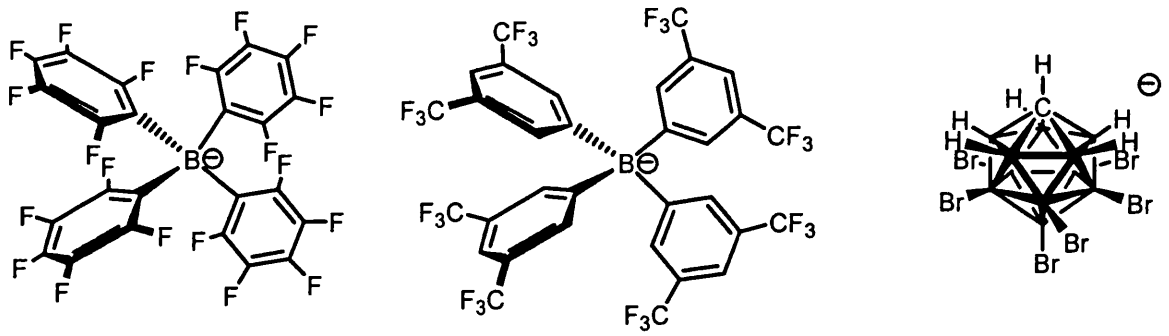

Figure 47: Commonly used Weakly Coordinating Anions.

These anions, especially the fluoroborates, have become ubiquitous throughout industrial and academic organometallic chemistry, being successfully utilised to isolate cationic transition metal complexes with very weak σ donors (i.e. CH_2Cl_2, CH_3Cl, Et_2O, H_2, N_2, R_3SiH and agostic C-H bonds), highly active olefin polymerisation catalysts and proving that there is no such thing as a non coordinating solvent.[35, 74, 75, 126, 181-183] They have also been used to stabilise reactive cations, including silylium cations, protonated arenes and other highly Lewis acidic organometallic fragments.[137, 184, 185] The major drawbacks in these systems have been their poor solubilities in non-polar organic solvents and particularly with the borate derivatives a tendency to form liquid clathrates thereby frustrating crystallisation.[162] These hindrances limit the prospects of these anions in attempts to isolate and structurally characterise stable alkane σ complexes.

1.4.2: [*closo*-$CB_{11}Me_{12}$]$^-$ - a Weakly Coordinating Anion?

Alkylated carborane mono-anions have the potential to attain the solubility criteria and thus solubilise reactive superelectrophiles into hydrocarbon media. The icosahedral [*closo*-CB_{11}]$^-$ cluster core seems ideal for weakly coordinating applications, with its large size, delocalised negative charge, no lone pairs and good stability. When

coupled with the improved solubility and reduced nucleophilicity inherent in peralkylation then these compounds could produce the ideal weakly coordinating anion.

A method to determine the coordinating ability of these anions relative to other commonly used anions involves the soft transition metal scale, based on $CpFe(CO)_2X$ (where X is the weakly coordinating anion). The average carbonyl stretching frequency correlates to the degree of back bonding which in turn is highly sensitive on the cationic character at Fe – thus an indirect measure of anion coordination (Figure 48).[137] The coordination ability determined from these stretching frequencies is that [*closo*-$CB_{11}Me_{12}]^-$ is more nucleophilic than [*closo*-$CB_{11}H_6Br_6]^-$, a result that appears counter intuitive implying that a lone pair is less coordinating than a C-H σ bond.

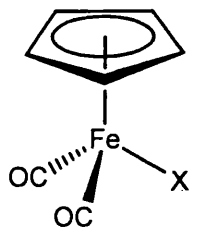

X	Average νCO in toluene (cm^{-1})
I^-	2016
ClO_4^-	2049
$CB_{11}H_{12}^-$	2049
$SbF6^-$	2050
$CB_9H_5Br_5^-$	2096
$CB_{11}Me_{12}^-$	2098
$CB_{11}H_6Br_6^-$	2108

Figure 48: The relative coordinating power of a series of anions based on the $CpFe(CO)_2^+$ system.

It has recently been reported that the *solvento* complex [$CpFe(CO)_2$(toluene)][*closo*-$CB_{11}Me_{12}$] is formed on the oxidation of the dimer $[CpFe(CO)_2]_2$ by the radical [*closo*-$CB_{11}Me_{12}$].[140] This is in contrast to a transition metal complex of the [1-H-*closo*-$CB_{11}H_5Br_6]^-$ anion that remains coordinated in the presence of arene solvents and has been structurally charcterised.[166] The combination of

these two reports cast doubt on the ordering of these anions and in fact suggests that the peralkylated carborane has the extremely weakly coordinating nature desired.[173] An alternative rating system is based on the ^{29}Si NMR chemical shift of $^{i}Pr_3Si[X]$; however, due to [*closo*-$CB_{11}Me_{12}$]$^-$ decomposition it is impossible to compare it using this scale (Figure 49).

Compound	δ(^{29}Si) ppm	Conditions	Compound	δ(^{29}Si) ppm	Conditions
$^{i}Pr_3Si(OSO_2CF_3)$	40	d_8-toluene	$^{i}Pr_3Si(1\text{-}H\text{-}CB_{11}Me_5Br_6)$	112	C_6D_6
$^{i}Pr_3Si(toluene)^+$ $(F_{20}\text{-}BPh_4)^-$	94	d_8-toluene	$^{i}Pr_3Si(1\text{-}H\text{-}CB_{11}Me_5Cl_6)$	113	C_6D_6
$^{i}Pr_3Si(1\text{-}H\text{-}CB_{11}H_5Br_6)$	100	C_6D_6	$^{i}Pr_3Si(1\text{-}H\text{-}CB_{11}Cl_{11})$	114	d_8-toluene
$^{i}Pr_3Si(1\text{-}H\text{-}CB_{11}H_5Cl_6)$	103	C_6D_6	$^{i}Pr_3Si(1\text{-}H\text{-}CB_{11}H_5Cl_6)$	115	solid state
$^{i}Pr_3Si(F_{20}\text{-}BPh_4)$	107	solid state	$^{i}Pr_3Si(1\text{-}Me\text{-}CB_{11}F_{11})$	120	d_8-toluene

Figure 49: Selected solution and solid state ^{29}Si Chemical Shifts for $^{i}Pr_3SiX$.

There has been no work at all reported on the coordination behaviour of the permethylated carborane anion partnered with transition metals and no further chemistry at all on the higher ethyl homologue [*closo*-$CB_{11}Et_{12}$]$^-$ due to its inaccessibility in usable quantities.[186]

In an analogous manner to the development of the $[BAr_F]^-$ anion to alleviate the coordinating ability of the BPh_4^- anion and prevent B-C bond cleavage, fluorination of the [*closo*-$CB_{11}Me_{12}$]$^-$ cluster has been successful.[136] The reaction of [*closo*-$CB_{11}Me_{12}$]$^-$ to give the fully fluorinated product [*closo*-$CB_{11}(CF_3)_{12}$]$^-$ has been achieved in a two-step process (Figure 50).[187] This anion is stable up to 250°C, in saturated base solutions and in concentrated H_2SO_4/triflic acid, whilst being electrochemically inert and having a large Van der-Waals diameter (~11Å).

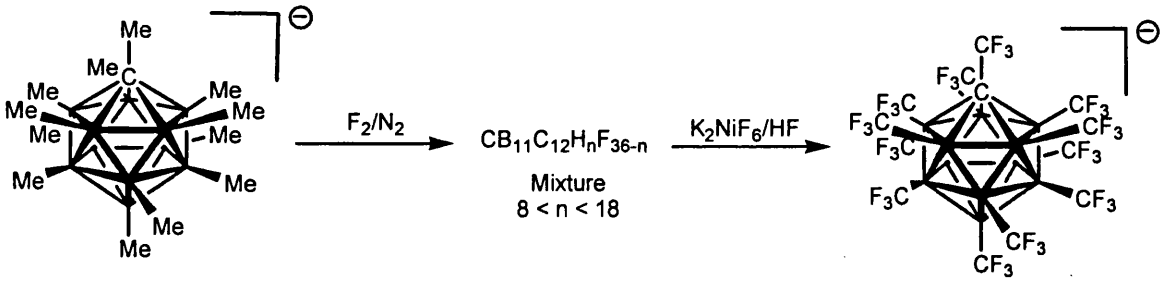

Figure 50: Synthesis of the fully fluorinated anion [*closo*-$CB_{11}(CF_3)_{12}]^-$.

[*closo*-$CB_{11}(CF_3)_{12}]^-$, however, is highly dangerous to use as it explodes upon scraping with a metal spatula, the products of the explosive decomposition are BF_3, $[BF_4]^-$, soot and CO_2. The high energy of decomposition is due to two factors, the large increase in the bond energy on the formation of a B-F bond relative to a C-F bond and the large strain energy due to the severe steric crowding of the perfluorinated carborane.

1.4.3 Anion Decomposition:

Along with anion coordination the other major limitation in the use of super weakly interacting anions is anion decomposition. The ubiquitous $[B(C_6F_5)_4]^-$ anion rapidly degrades in the presence of $[AlR_2]^+$ (though this cation has been isolated with [1-H-*closo*-$CB_{11}Me_5Br_6]^-$),[145] $[EtZn]^+$, $[H]^+$ (if no donor solvent is present) and open group 14 metallocenes.[126, 188, 189] The equally universally used $[BAr_F]^-$ anion has also been demonstrated to decompose in several systems. For example, attempts to partner it with $[(PPh_3)_2Pt(Me)(OEt_2)]^+$ and $[^iPr_3Si]^+$ resulted in B-C cleavage and fluoride abstraction respectively.[190, 191] The reaction with silylium cations is noteworthy as anion coordination to $^iPr_3Si^+$ is a methodology used to rank weakly coordinating anions.

It was whilst attempting to generate analogous silylium cations partnered with [*closo*-$CB_{11}Me_{12}$]$^-$ that its decomposition and susceptibility to strong electrophiles was discovered. The reaction of $^tBu_6Si_2$ with the radical [*closo*-$CB_{11}Me_{12}$]$^\bullet$ (in an analogous method to that successfully used in preparing $^nBu_3Sn$(*closo*-$CB_{11}Me_{12}$)) initially produced $^tBu_3SiMe$ and the neutral cage [*closo*-$CB_{11}Me_{11}$] (that is highly reactive to any nucleophiles present) rather than the expected [$^tBu_3Si$][*closo*-$CB_{11}Me_{12}$] (Figure 51).[140]

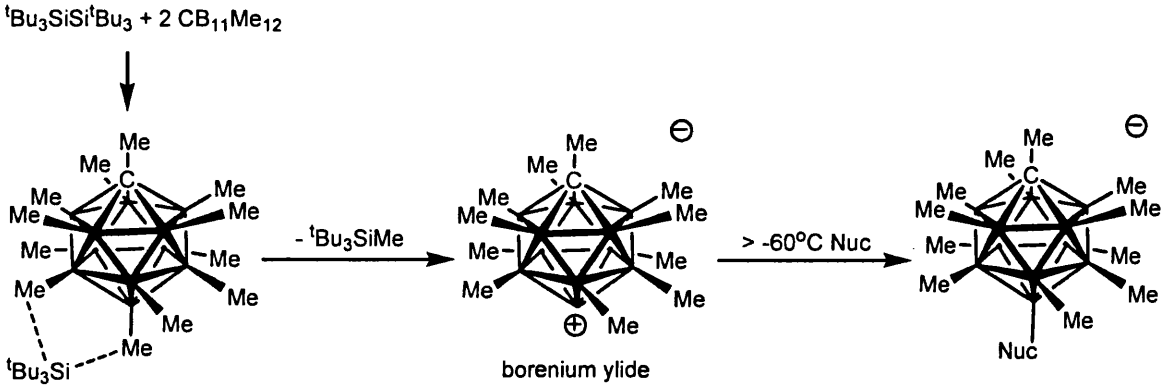

Figure 51: Proposed mechanism for the cage decomposition in the presence of silylium cations.

A plausible mechanism is proposed in Figure 51, with initial formation of the anion coordinated silylium complex, analogous to the characterised [$^nBu_3Sn$]$^+$ salt, that then abstracts the methyl in the antipodal position generating the borenium ylide *closo*-$CB_{11}Me_{11}$ (an anionic cage with eleven ligands and a positive centre at the 12 position)[140] and $^tBu_3SiMe$ - both of which are detected. The internally charge compensated borenium ylide is highly reactive, stable only below -60°C. Above this in the presence of even weak nucleophiles it reacts rapidly to yield a variety of 12-substituted products [12-Nuc-*closo*-$CB_{11}Me_{11}$].

A related reaction occurs when the lithium salt of the permethylated anion is heated in an aromatic solvent. With the simplest anion, [*closo*-$CB_{11}Me_{12}$]$^-$, multiple methyl/aryl exchange occurs to generate an intractable mixture.[192] An important point is

that the lithium salt is vital in mediating this exchange, as other alkali salts exhibit no activity, presumably due to lithium's greater Lewis acidity.[161] Aryl incorporation was found to be more specific when the C1 methyl is substituted for a dioxaborole ring (Figure 52); the lithium is now proposed to be partially coordinated to the oxygen atoms reducing its Lewis acidity and allowing for the selective 12 functionalisation.

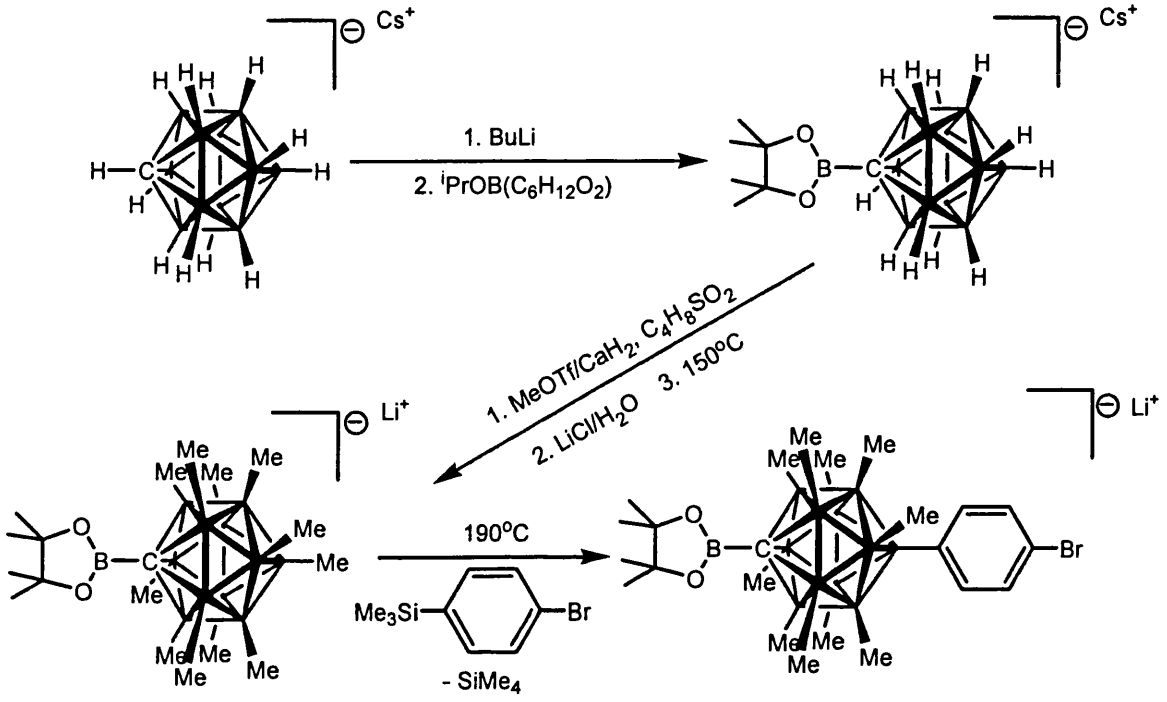

Figure 52: Schematic for the formation of $[1\text{-}(C_6H_{12}O_2)B\text{-}12\text{-}(4'\text{-}Br\text{-}C_6H_4)\text{-}closo\text{-}CB_{11}Me_{10}]^-$ from Cs-*closo*-$CB_{11}H_{12}$.

The reaction is postulated to proceed by one of two mechanisms: the first is S_E2, involving the abstraction by Li^+ of the antipodal methyl generating a borenium ylide which would then react with the arene by insertion into the Si-C bond followed by subsequent attack on the silicon centre by CH_3Li. An alternative feasible mechanism is that Li^+ coordination to the methyl in the 12 position activates it towards σ bond metathesis. This methodology has also been utilised to incorporate the anion onto a polymer support by the heating of Li[*closo*-$CB_{11}Me_{12}$] with polystyrene under a high vacuum.[140]

1.5. Scope of Thesis:

Whilst [*closo*-$CB_{11}Me_{12}$]$^-$ has been demonstrated to provide a degree of improved solubility in non-polar solvents (albeit highly cation dependent), its robustness in the presence of strong electrophiles can be deficient. It has though been reported to form stable, well-separated ion pairs (*solvento* complexes) with softer transition metal complexes and M···H_3C interactions with a number of alkali cations and [^{n}Bu_3Sn]$^+$. There is still a dearth in its coordination chemistry especially with respect to transition metals and therefore a need for further in-depth investigations into these highly attractive peralkylated carborane anions.

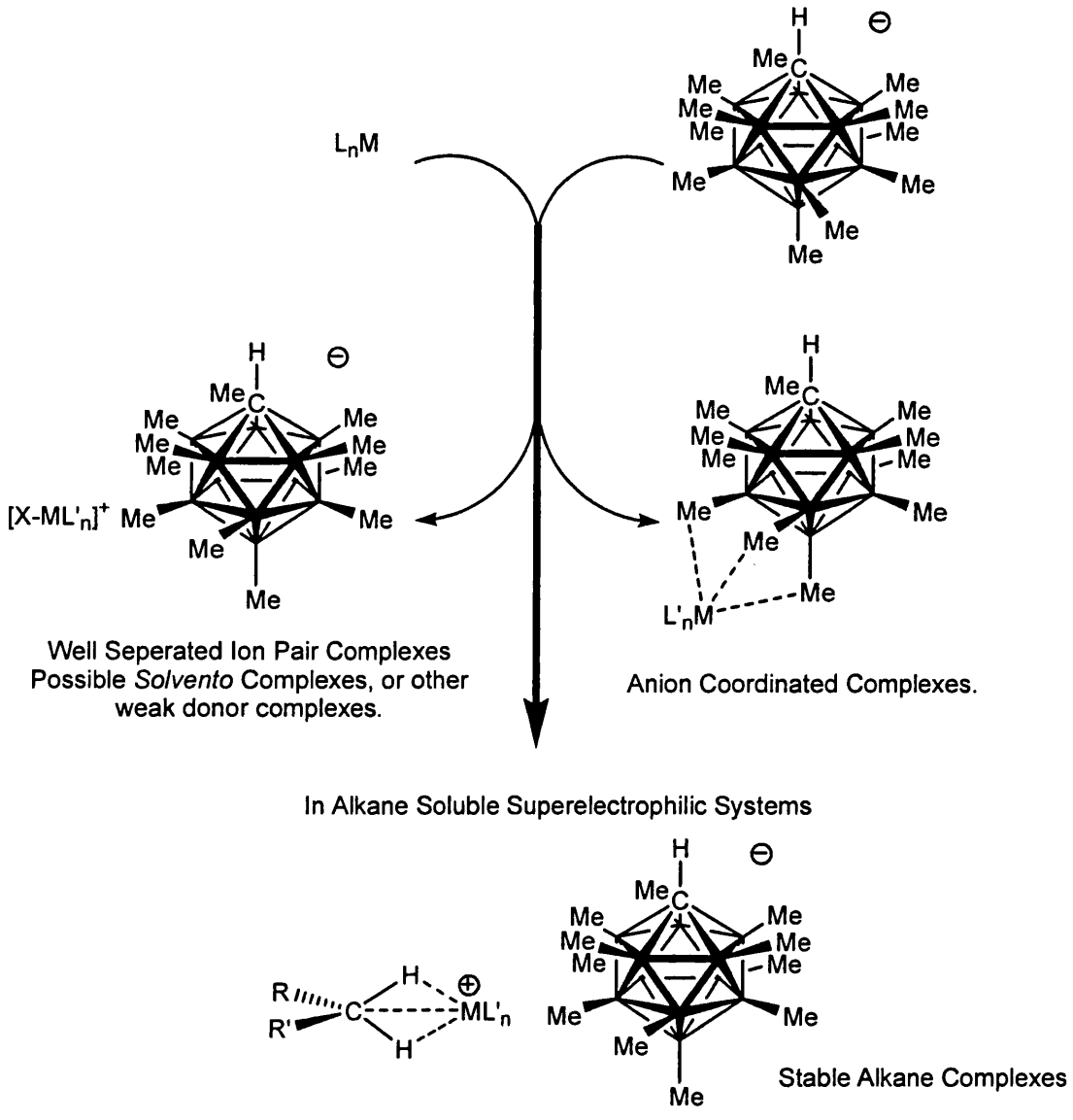

Figure 53: Possible outcomes from the partnering of [1-H-*closo*-$C_{11}Me_{11}$]$^-$ with varying metal complexes.

Any metal complexes formed may show either methyl interactions between the cage periphery and the metal centre (a model for alkane σ complexes) or interactions with solvent molecules and other weak donors whose chemistry would be of interest in their own right (Figure 53). Combination with the optimal cation/ligand combination may even grant access to alkane soluble superelectrophiles and a significant step towards generating an unsupported σ alkane complex.

In this thesis two major methodologies were followed to decide which cationic metal centres to investigate the coordination properties of the peralkylated carborane anion with, the first being based on known metal complexes of the closely related weakly coordinating anions [*closo*-$CB_{11}H_6Br_6$]$^-$ and [$MeB(C_6F_5)_3$]$^-$, where intimate anion···cation interactions have been previously unambiguously characterised *e.g.*, (R_3P)Ag(*closo*-$CB_{11}H_6Br_6$), *trans*-$(PPh_3)_2Ir(H)_2$(*closo*-$CB_{11}H_6Br_6$) and $Cp_2ZrMe(\mu\text{-}Me)B(C_6F_5)_3$ (Figure 54).[146, 148, 193]

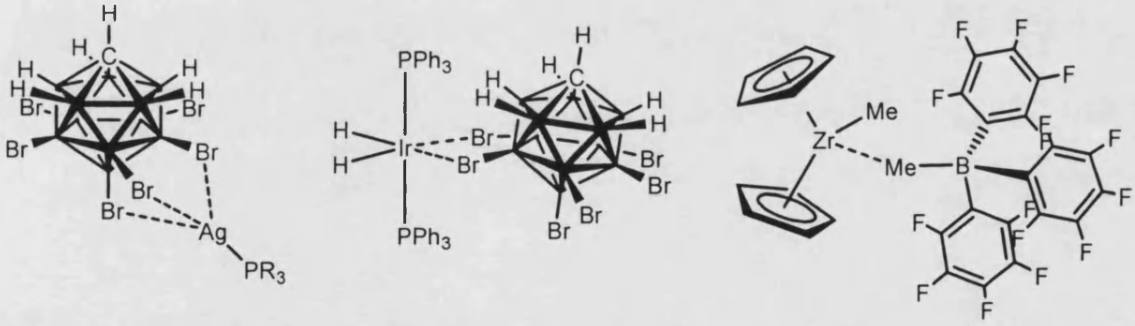

Figure 54: Anion bound metal complexes, whose [1-H-*closo*-$CB_{11}Me_{11}$]$^-$ analogues will be investigated.

In the second case, cationic complexes that are isolobal with the 16 electron fragment {$CpRe(CO)_2$} (that gives alkane complexes of the longest lifetimes thus documented), partnered with [1-H-*closo*-$CB_{11}Me_{11}$] were also investigated. The cationic charge on the metal centre should increase the binding strength of weak ligands (*e.g.*, the anion,

solvent or other weak donor) and a range of these complexes that were studied throughout this work are shown in Figure 55.

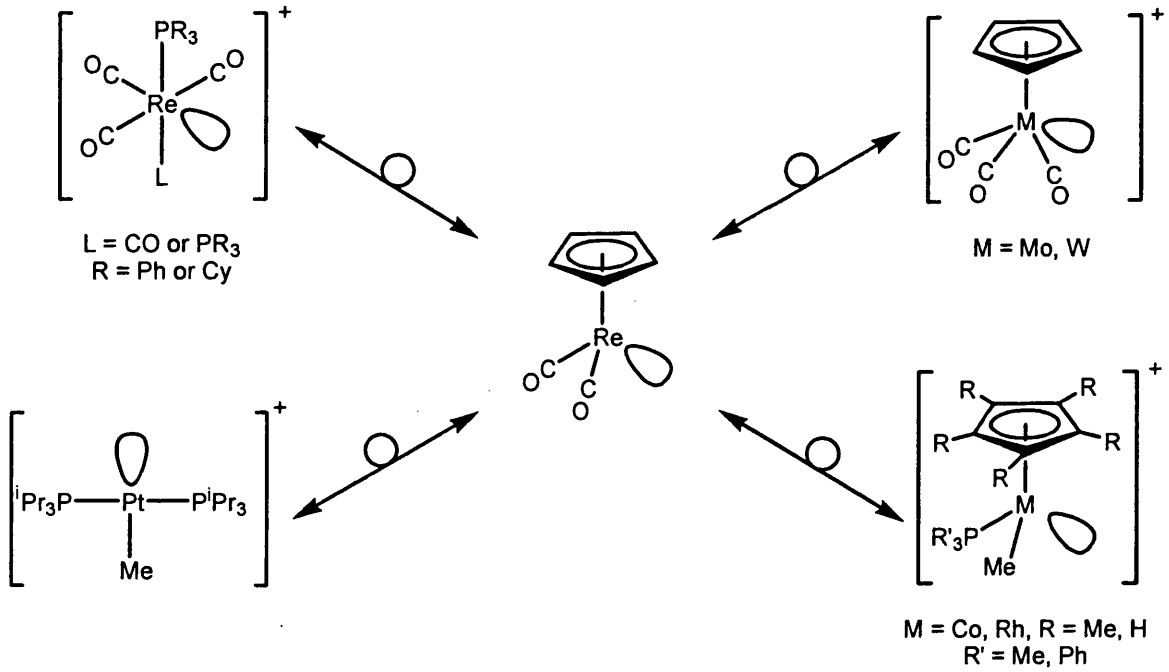

Figure 55: Cationic complexes formally isolobal with $\{CpRe(CO)_2\}$.

These complexes, as well as being cationic congeners of the $\{CpRe(CO)_2\}$ fragment, have all been the focus of related studies which have shown them to exist as either solvent coordinated, agostic, dihydrogen, or anion···cation zwitterionic complexes,[75-77, 182, 183, 194-198] thus making them attractive targets for the investigation of the coordination properties of $[1\text{-H-}closo\text{-}CB_{11}Me_{11}]^-$ when partnered with these cations.

1.6: References:

1 J. Chatt and J. M. J. Davidson, *J. Chem. Soc. A*, 1965, 843.
2 A. H. Janowicz and R. G. Bergmann, *J. Am. Chem. Soc.*, 1982, **104**, 352.
3 J. K. Hoyano and W. A. G. Graham, *J. Am. Chem. Soc.*, 1982, **104**, 3723.
4 A. E. Shilov and G. B. Shul'pin, 'Activation and Catalytic Reactions of Saturated Hydrocarbons in the Presence of Metal Complexes', Kluwer Academic, 2000.
5 R. H. Crabtree, *J. Chem. Soc., Dalton Trans.*, 2001, 2437

[6] C. Hall and R. N. Perutz, *Chem. Rev.*, 1996, **96**, 3125.
[7] S. T. Belt, L. Dong, S. B. Duckett, W. D. Jones, M. G. Partridge, and R. N. Perutz, *Chem. Commun.*. 1991, 266.
[8] S. T. Belt, S. B. Duckett, M. Helliwell, and R. N. Perutz, *Chem. Commun.*. 1989, 928.
[9] S. Reinhart, P. S. White, M. Brookhart, and J. L. Templeton, *J. Am. Chem. Soc.*. 2001, **123**, 12724.
[10] J. M. Buchanan, J. M. Stryker, and R. G. Bergmann, *J. Am. Chem. Soc.*, 1986, **108**, 1537.
[11] D. D. Wick, K. A. Reynolds, and W. D. Jones, *J. Am. Chem. Soc.*, 1999, **121**, 3974.
[12] R. M. Bullock, C. E. L. Headford, K. M. Hennesey, S. E. Kegley, and J. R. Northon, *J. Am. Chem. Soc.*, 1989, **111**, 3897.
[13] G. Parkin and J. E. Bercaw, *Organometallics*, 1989, **8**, 1172.
[14] G. L. Gould and D. M. Heinekey, *J. Am. Chem. Soc.*, 1989, **111**, 5502.
[15] C. L. Gross and G. S. Girolami, *J. Am. Chem. Soc.*, 1998, **120**, 6605.
[16] C. H. Wang, J. W. Ziller, and T. C. Flood, *J. Am. Chem. Soc.*, 1995, **117**, 1647.
[17] S. S. Stahl, J. A. Labinger, and J. E. Bercaw, *J. Am. Chem. Soc.*, 1996, **118**, 5961
[18] W. D. Jones, *Acc. Chem. Res.*, 2003, **36**, 140.
[19] J. J. Turner, J. K. Burdett, R. N. Perutz, and M. Poliakoff, *P. Appl. Chem.*, 1977, **49**, 271.
[20] R. N. Perutz and J. J. Turner, *J. Am. Chem. Soc.*, 1975, **97**, 47.
[21] R. H. Schultz, A. A. Bengali, M. J. Tauber, B. H. Weiller, E. P. Wasserman, K. R. Kyle, C. B. Moore, and R. G. Bergmann, *J. Am. Chem. Soc.*, 1994, **116**, 7369.
[22] A. A. Bengali, R. H. Schultz, C. B. Moore, and R. G. Bergmann, *J. Am. Chem. Soc.*, 1994, **116**, 9585
[23] J. M. Morse, G. H. Parker, and T. J. Burkey, *Organometallics*, 1989, **8**, 2471
[24] B. S. Creaven, M. W. George, A. G. Ginzburg, C. Hughes, J. M. Kelly, C. Long, I. M. McGrath, and M. T. Pryce, *Organometallics*, 1993, **12**, 3127.
[25] R. A. Periana and R. G. Bergmann, *J. Am. Chem. Soc.*, 1986, **108**, 7332
[26] J. M. Kelly, H. Hermann, and E. J. K. v. Gustorf, *Chem. Commun.*. 1973, **105**, 105.
[27] X. L. Xie and J. D. Simon, *J. Am. Chem. Soc.*, 1990, **112**, 1130.
[28] X. Z. Sun, D. C. Grills, S. M. Nikiforov, M. Poliakoff, and M. W. George, *J. Am. Chem. Soc.*, 1997, **119**, 7521.
[29] M. W. George, M. T. Haward, P. A. Hamley, C. Hughes, F. P. A. Popov, and M. Poliakoff, *J. Am. Chem. Soc.*, 1993, **115**, 2286.
[30] G. I. Childs, C. S. Colley, J. Dyer, D. C. Grills, X. Sun, J. Yang, and M. W. George, *J. Chem. Soc., Dalton Trans.*, 2000, 1901
[31] S. Geftakis and G. E. Ball, *J. Am. Chem. Soc.*, 1998, **120**, 9953.
[32] G. J. Kubas, 'Metal Dihydrogen and Sigma Bond Complexes. Structure, Theory and Reactivity.' Kluwer, 2001.
[33] S. Zaric and M. B. Hall, *J. Phys. Chem*, 1997, **101**, 4646.
[34] M. Brookhart, M. L. H. Green, and L. L. Wong, 'Progress in Inorganic Chemistry', 1988.
[35] D. R. Evans, T. Drovetskaya, R. Bau, C. A. Reed, and P. D. W. Boyd, *J. Am. Chem. Soc.*, 1997, **119**, 3633.
[36] R. H. Crabtree, E. M. Holt, M. Lavin, and S. M. Morehouse, *Inorg. Chem.*, 1985, **24**, 1986
[37] Z. Xie, R. Bau, and C. A. Reed, *Angew. Chem., Int. Ed. Engl.*, 1994, **33**, 2433

[38] I. Castro-Rodriguez, H. Nakai, P. Gantzel, L. N. Zakharov, A. L. Rheingold, and K. Meyer, *J. Am. Chem. Soc.*, 2003, **125**, 15734
[39] L. Pauling, 'The Nature of the Chemical Bond', Cornell University Press, 1960.
[40] J. Song and M. B. Hall, *Organometallics*, 1993, **12**, 3118.
[41] S. Niu and M. B. Hall, *Chem. Rev.*, 2000, **100**, 353.
[42] R. J. Poli and K. M. Smith, *Organometallics*, 2000, **19**, 2858.
[43] N. Koga and K. J. Morokuma, *J. Phys. Chem.*, 1990, **94**, 5454.
[44] N. Re, M. Rosi, A. Sgamelloti, C. Floriani, and M. F. Guest, *J. Chem. Soc., Dalton Trans.*, 1992, 1821.
[45] T. R. Cundari and T. R. Klinckmann, *Inorg. Chem.*, 1998, **37**, 5399.
[46] T. R. Cundari, *J. Am. Chem. Soc.*, 1994, **116**, 340.
[47] P. E. M. Siegbahn and M. Svensson, *J. Am. Chem. Soc.*, 1994, **116**, 10124.
[48] R. W. Parry and G. Kodama, *Coord. Chem. Rev*, 1993, **128**, 245.
[49] P. H. Bird and M. R. Churchill, *Chem. Commun.*. 1967, 403.
[50] J. A. Jensen, S. R. Wilson, Q. A. J. Schultz, and G. S. Girolami, *J. Am. Chem. Soc.*, 1987, **109**, 8094.
[51] M. V. Baker and L. D. Field, *Chem. Commun.*. 1984, 1160.
[52] J. A. Jensen and G. S. Girolami, *Chem. Commun.*. 1986, 1160.
[53] M. Mancini, P. Bougeard, R. C. Burns, M. Mlekuz, B. G. Sayer, J. I. A. Thompson, and M. J. McGlinchey, *Inorg. Chem.*, 1984, **23**, 1072.
[54] F. Takusagawa, A. Fumagalli, T. F. Koetzle, S. G. Shore, T. Schmitkons, A. V. Fratini, K. W. Morse, C. Wei, and J. R. Bau, *J. Am. Chem. Soc.*, 1981, **103**, 5165.
[55] J. F. Hartwig and S. R. DeGala, *J. Am. Chem. Soc.*, 1994, **116**, 3661.
[56] G. Jia, A. L. Lough, and R. H. Morris, *J. Organomet. Chem.*. 1993, **461**, 147.
[57] X. Chen, F.-C. Liu, C. E. Plecnik, S. Liu, B. Du, E. A. Meyers, and S. G. Shore, *Organometallics*, 2004, **23**, 2100.
[58] X. Chen, S. Liu, C. E. Plecnik, F.-C. Liu, G. Fraenkel, and S. G. Shore, *Organometallics*, 2003, **19**, 275.
[59] T. Kakizawa, Y. Kawano, and M. Shimoi, *Organometallics*, 2001, **20**, 3211.
[60] M. Shimoi, S. Nagai, M. Ichikawa, Y. Kawano, K. Katoh, M. Uruichi, and H. Ogion, *J. Am. Chem. Soc.*, 1999, **121**, 11707
[61] T. Yasue, Y. Kawano, and M. Shimoi, *Angew. Chem., Int. Ed. Engl.*, 2003, **42**, 1727
[62] K. Kinji, H. Ogino, and M. Shimoi, *Inorg. Chem.*, 1992, **31**, 670
[63] R. Macias, N. P. Rath, and L. Barton, *Angew. Chem., Int. Ed. Engl.*, 1999, **38**, 162.
[64] M. J. Ingleson, N. J. Patmore, G. D. Ruggiero, C. G. Frost, M. F. Mahon, M. C. Willis, and A. S. Weller, *Organometallics*, 2001, **20**, 4434
[65] K. Ueno, T. Yamaguchi, K. Uchiyama, and H. Ogino, *Organometallics*, 2002, **21**, 2347
[66] J. F. Hartwig, C. N. Muhoro, X. He, O. Eisenstein, R. Bosque, and F. J. Maseras, *J. Am. Chem. Soc.*, 1996, **118**, 10936.
[67] C. N. Muhoro, X. He, and J. F. Hartwig, *J. Am. Chem. Soc.*, 1999, **121**, 5033.
[68] V. Montiel-Palma, M. Lumbierred, B. Donnadieu, S. Sabo-Etienne, and B. Chaudret, *J. Am. Chem. Soc.*, 2002, **124**, 5624
[69] W. Lam and Z. Lin, *Organometallics*, 2000, **19**, 2625.
[70] G. J. Kubas, R. R. Ryan, B. I. Swanson, P. J. Vergamini, and H. J. Wasserman, *J. Am. Chem. Soc.*, 1984, **104**, 451.
[71] G. J. Kubas, *Acc. Chem. Res.*, 1988, **21**, 120.
[72] J. Chatt and L. A. Duncanson, *J. Chem. Soc.*, 1953, 2929.

[73] M. Poliakoff, J. J. Turner, and R. K. Upmacis, *J. Am. Chem. Soc.*, 1986, **108**, 3645.
[74] X. G. Fang, J. Huhmann-Vincent, B. L. Scott, and G. J. Kubas, *J. Organomet. Chem.*, 2000, **609**, 95.
[75] X. G. Fang, B. L. Scott, K. D. John, and G. J. Kubas, *Organometallics*, 2000, **19**, 4141.
[76] M. D. Heinekey, C. E. Radzewich, M. H. Voges, and B. M. Schomber, *J. Am. Chem. Soc.*, 1997, **119**, 4172.
[77] J. Huhmann-Vincent, B. L. Scott, and G. J. Kubas, *Inorg. Chem.*, 1999, **38**, 115.
[78] F. Maseras, M. Duran, A. Lledos, and J. Bertran, *J. Am. Chem. Soc.*, 1991, **113**, 2879.
[79] R. M. Bullock, J.-S. Song, and D. J. Szalda, *Organometallics*, 1996, **15**, 2504.
[80] U. Schubert, *Adv. Organomet. Chem*, 1990, **30**, 151.
[81] D. T. Tilley, *Acc. Chem. Res.*, 1993, **26**, 22.
[82] U. Schubert, G. Scholz, J. Muller, K. Ackermann, B. Worle, and R. F. D. Stansfield, *J. Organomet. Chem.*, 1986, **306**, 303
[83] U. Schubert, K. Ackermann, and B. Worle, *J. Am. Chem. Soc.*, 1982, **104**, 7378.
[84] K. Colomer, R. J. P. Corriu, C. Manzin, and A. Vioux, *Inorg. Chem.*, 1986, **21**, 368
[85] S. T. N. Freeman and F. R. Lemke, *Organometallics*, 2002, **21**, 2030
[86] X. L. Luo, G. J. Kubas, C. J. Burns, J. C. Bryan, and C. J. Unkefer, *J. Am. Chem. Soc.*, 1995, **117**, 1159.
[87] X. L. Luo, G. J. Kubas, J. C. Bryan, C. J. Burns, and C. J. Unkefer, *J. Am. Chem. Soc.*, 1994, **116**, 10312.
[88] E. Scharrer, S. Chang, and M. Brookhart, *Organometallics*, 1995, **14**, 5686
[89] J. Y. Corey and L. Braddock-Wilking, *J. Chem. Rev*, 1999, **99**, 175.
[90] S. J. LaPlaca and J. A. Ibers, *Inorg. Chem.*, 1965, **4**, 778.
[91] N. A. Bailey, J. M. Jenkins, R. Mason, and B. L. Shaw, *Chem. Commun.*. 1965, 237.
[92] D. Braga, F. Grepioni, K. Biradha, and G. Desiraju, *J. Chem. Soc., Dalton Trans.*, 1996, 3925.
[93] A. R. Kennedy, R. E. Mulvey, and R. B. Rowlings, *J. Organomet. Chem.*. 2002, 288.
[94] A. R. Kennedy, R. E. Mulvey, and R. B. Rowlings, *J. Am. Chem. Soc.*, 1998, **120**, 7816.
[95] H. Krauledat and H. H. Brintzinger, *Angew. Chem., Int. Ed. Engl.*, 1990, **29**, 1412.
[96] W. E. Piers and J. E. Bercaw, *J. Am. Chem. Soc.*, 1990, **112**, 9406.
[97] A. D. Horton and A. G. Orpen, *Organometallics*, 1991, **10**, 3910.
[98] R. H. Crabtree, P. E. M. Siegbahn, O. Eisenstein, and A. L. Rheingold, *Acc. Chem. Res.*, 1996, **29**, 348.
[99] R. H. Crabtree, *Angew. Chem., Int. Ed. Engl.*, 1993, **32**, 789
[100] G. J. Kubas, *Abs. Am. Chem. Soc.*, 2003, **226**, 312.
[101] W. Baratta, C. Mealli, E. Herdtweck, A. Ienco, S. A. Mason, and P. Rigo, *J. Am. Chem. Soc.*, 2004, **126**, 5549
[102] W. Baratta, E. Herdtweck, and P. Rigo, *Angew. Chem., Int. Ed. Engl.*, 1999, **38**, 1629.
[103] W. Baratta, S. Stoccoro, A. Doppiu, E. Herdtweck, A. Zucca, and P. Rigo, *Angew. Chem., Int. Ed. Engl.*, 2003, **42**, 105.
[104] D. M. Gusev, M. Madott, F. M. Dolgushin, K. A. Lyssenko, and M. Y. Antipin, *Organometallics*, 2000, **19**, 1734

105 R. H. Crabtree, *J. Organomet. Chem.*, 1998, **577**, 111.
106 N. Koga and K. Morokuma, *Chem. Rev.*, 1991, **91**, 823.
107 R. H. Crabtree, *Chem. Rev.*, 1985, **85**, 245.
108 B. J. Burger, M. E. thompson, W. D. Cotter, and J. E. Bercaw, *J. Am. Chem. Soc.*, 1990, **112**, 1566.
109 L. Deng, T. K. Woo, L. Cavallo, P. M. Margl, and T. Ziegler, *J. Am. Chem. Soc.*, 1997, **119**, 6177.
110 D. G. Musev, R. D. J. Froese, M. Svennson, and K. Morokuma, *J. Am. Chem. Soc.*, 1997, **119**, 367.
111 A. C. Cooper, E. Clot, J. C. Huffman, W. E. Streib, F. Maseras, O. Eisenstein, and K. G. Caulton, *J. Am. Chem. Soc.*, 1999, **121**, 97.
112 G. Ujaque, A. C. Cooper, F. Maseras, O. Eisenstein, and K. G. Caulton, *J. Am. Chem. Soc.*, 1998, **120**, 361
113 C. J. Burns and R. A. Andersen, *J. Am. Chem. Soc.*, 1987, **109**, 5853
114 C. J. Burns and R. A. andersen, *J. Am. Chem. Soc.*, 1987, **109**, 915
115 F. A. Cotton, E. A. Hillard, and C. A. Murillo, *J. Am. Chem. Soc.*, 2002, **124**, 5658.
116 W. L. Youngs, J. D. Kinder, J. D. Bradshaw, and C. A. Tessier, *Organometallics*, 1993, **12**, 2406
117 W. E. Rhine, G. Stucky, and S. W. J. Peterson, *J. Am. Chem. Soc.*, 1975, **97**, 6401.
118 D. Groves, W. E. Rhine, and G. Stucky, *J. Am. Chem. Soc.*, 1971, **93**, 1553.
119 J. E. Huheey and E. A. Keiter, 'Inorganic Chemistry: Principles of Structure and Reactivity', Harper Collins, 1993.
120 X. Yang, C. L. Stern, and T. J. Marks, *J. Am. Chem. Soc.*, 1991, **13**, 3623.
121 X. Yang, C. L. Stern, and T. J. Marks, *J. Am. Chem. Soc.*, 1994, **116**, 10015.
122 X. Song, M. Thorton-Pett, and M. Bochmann, *Organometallics*, 1998, **17**, 1004.
123 C. J. Burns and R. A. Andersen, *J. Am. Chem. Soc.*, 1987, **109**, 5853.
124 D. J. Berg and R. A. Andersen, *Organometallics*, 2003, **22**, 627.
125 F. Delpech, I. A. Guzei, and R. F. Jordan, *Organometallics*, 2002, **21**, 1167
126 E. Y. X. Chen and T. J. Marks, *Chem. Rev.*, 2000, **100**, 1391
127 F. Guerin and D. W. Stephan, *Angew. Chem., Int. Ed. Engl.*, 2000, **39**, 1298.
128 A. Spannenberg, H. Fuhrmann, P. Arndt, W. Baumann, and R. Kempe, *Angew. Chem., Int. Ed. Engl.*, 1998, **37**, 3363.
129 G. Lanza and T. J. Marks, *J. Am. Chem. Soc.*, 2000, **122**, 12764.
130 M. Bochmann, S. J. Lancaster, M. B. Hursthouse, and K. M. A. Malik, *Organometallics*, 1994, **13**, 2235.
131 C. L. Beswick and T. J. Marks, *Organometallics*, 1999, **18**, 2410
132 A. Fischbach, E. Herdtweck, R. Anwander, G. Eickerling, and W. Scherer, *Organometallics*, 2003, **22**, 499.
133 B. T. King, Z. Janousek, B. Gruner, M. Trammell, B. C. Noll, and J. Michl, *J. Am. Chem. Soc.*, 1996, **118**, 3313.
134 W. H. Knoth, *J. Am. Chem. Soc.*, 1967, **89**, 1274.
135 W. H. Knoth, *Inorg. Chem.*, 1971, **10**, 598.
136 S. H. Strauss, *Chem. Rev.*, 1993, **93**, 927.
137 C. A. Reed, *Acc. Chem. Res.*, 1998, **31**, 133.
138 T. Jelinek, J. Plesek, S. Hermanek, and B. Stibr, *Collect. Czech. Chem. Commun.*, 1985, **51**, 819.
139 Z. Xie, C. Tsang, E. T. P. Sze, Q. Yang, D. T. W. Chan, and T. C. W. Mak, *Inorg. Chem.*, 1998, **37**, 6444.
140 B. T. King, I. Zharov, and J. Michl, *Chemical Innovation*, 2001, **31**, 23.

141 M. L. McKee, *J. Am. Chem. Soc.*, 1997, **119**, 4220

142 T. Jelinek, J. Plesek, F. Mares, S. Hermanek, and B. Stibr, *Polyhedron*, 1987, **6**, 1981.

143 C. A. Reed, K. C. Kim, E. S. Stoyanov, D. Stasko, F. S. Tham, L. J. Mueller, and P. D. W. Boyd, *J. Am. Chem. Soc.*, 2003, **125**, 1796.

144 K. C. Kim, C. A. Reed, D. W. Elliott, L. J. Mueller, F. Tham, L. J. Lin, and J. B. Lambert, *Science*, 2002, **297**, 825.

145 K. C. Kim, C. A. Reed, G. S. Long, and A. Sen, *J. Am. Chem. Soc.*, 2002, **124**, 7662.

146 A. Rifat, G. Kociok-Kohn, J. W. Steed, and A. S. Weller, *Organometallics*, 2004, **23**, 428.

147 A. Rifat, N. J. Patmore, M. F. Mahon, and A. S. Weller, *Organometallics*, 2002, **21**, 2856.

148 N. J. Patmore, C. Hague, J. H. Cotgreave, M. F. Mahon, C. G. Frost, and A. S. Weller, *Chem. Eur. J.*, 2002, **8**, 2088.

149 T. Jelinek, P. Baldwin, W. R. Scheidt, and C. A. Reed, *Inorg. Chem.*. 1993, **32**, 1982.

150 L. I. Zakharkin, V. A. Ol'shevskaya, P. V. Petrovskii, and J. H. Morris, *Mendeleev Comminications*, 2000, 71.

151 V. A. Ol'shevskaya, R. P. Evstigneeva, V. N. Luzgina, M. A. Gyul'malieva, P. V. Petrovskii, J. H. Morris, and L. I. Zakharkin, *Mendeleev Comminications*, 2001, 14.

152 Z. W. Xie, T. Jelinek, R. Bau, and C. A. Reed, *J. Am. Chem. Soc.*, 1994, **116**, 1907.

153 A. Franken, B. T. King, J. Rudolph, P. Rao, B. C. Noll, and J. Michl, *Collect. Czech. Chem. Commun.*, 2001, **66**, 1238.

154 F. S. Mair, J. H. Morris, D. F. Gaines, and D. Powell, *J. Chem. Soc., Dalton Trans.*, 1993, 135.

155 B. Gruener, Z. Janousek, B. T. King, J. N. Woodford, C. H. Wang, V. Vsetecka, and J. Michl, *J. Am. Chem. Soc.*, 1999, **121**, 3122.

156 W. Jiang, C. B. Knobler, C. B. Curtis, C. E. Curtis, M. D. Mortimer, and M. F. Hawthorne, *Inorg. Chem.*, 1995, **34**, 3491.

157 C. W. Tsang, Q. Yang, E. T. P. Sze, T. C. W. Mak, D. T. W. Chan, and Z. Xie, *Inorg. Chem.*, 2000, **39**, 3582.

158 W. Jiang, C. B. Knobler, M. D. Mortimer, and M. F. Hawthorne, *Angew. Chem., Int. Ed. Engl.*, 1995, **34**, 1332.

159 B. T. King, B. C. Noll, A. J. McKinley, and J. Michl, *J. Am. Chem. Soc.*, 1996, **118**, 10902.

160 C. W. Tsang and Z. Xie, *Chem. Commun.*. 2000, **122**, 10253.

161 S. Moss, B. T. King, A. de Meijere, S. I. Kozhushkov, P. E. Eaton, and J. Michl, *Organic Letters*, 2001, **3**, 2375.

162 D. Stasko and C. A. Reed, *J. Am. Chem. Soc.*, 2002, **124**, 1148.

163 T. Kato and C. A. Reed, *Angew. Chem., Int. Ed. Engl.*, 2004, **43**, 2908

164 T. Muller, M. Juhasz, and C. A. Reed, *Angew. Chem., Int. Ed. Engl.*, 2004, **43**, 1543.

165 A. S. Larsen, J. D. Holbrey, F. S. Tham, and C. A. Reed, *J. Am. Chem. Soc.*, 2000, **122**, 7264.

166 A. Rifat, G. Kociok-Kohn, J. W. Steed, and A. S. Weller, *Organometallics*, 2004, **23**, 428.

167 A. Rifat, V. E. Laing, G. Kociok-Kohn, M. F. Mahon, G. D. Ruggiero, and A. S. Weller, *J. Organomet. Chem.*. 2003, **680**, 127.

[168] N. J. Patmore, M. J. Ingleson, M. F. Mahon, and A. S. Weller, *J. Chem. Soc., Dalton Trans.*, 2003, 2894.
[169] N. J. Patmore, M. F. Mahon, and A. S. Weller, *App. Organomet. Chem.*, 2003, **17**, 388.
[170] A. Rifat, M. F. Mahon, and A. S. Weller, *J. Organomet. Chem.*. 2003, **667**, 1.
[171] C. Hague, N. J. Patmore, C. G. Frost, M. F. Mahon, and A. S. Weller, *Chem. Commun.*. 2001, 2286
[172] B. T. King, B. C. Noll, and J. Michl, *Collect. Czech. Chem. Commun.*, 1999, **64**, 1001.
[173] I. Zharov, B. T. King, Z. Havlas, A. Pardi, and J. Michl, *J. Am. Chem. Soc.*, 2000, **122**, 10253.
[174] I. Krossing and I. Raebe, *Angew. Chem., Int. Ed. Engl.*, 2004, **43**, 2066
[175] N. M. N. Gowda, S. B. Naikar, and G. K. N. Reddy, *Adv. Inorg. Chem.. Radiochem.*, 1984, **28**, 255.
[176] G. A. Lawrence, *Chem. Rev.*, 1993, **93**, 17.
[177] W. H. Hersh, *Inorg. Chem.*, 1990, **29**, 713.
[178] R. V. Honeychuck and W. H. Hersh, *Inorg. Chem.*, 1989, **28**, 2869.
[179] K. Shelly, T. Bartczak, W. R. Scheidt, and C. A. Reed, *Inorg. Chem.*, 1985, **24**, 4325.
[180] A. G. Massey and A. J. Park, *J. Organomet. Chem.*, 1962, **2**, 245.
[181] O. Eisenstein, K. G. Caulton, V. Young, K. Folting, W. E. Streib, J. C. Bollinger, and D. J. Huang, *Organometallics*, 2000, **19**, 2281.
[182] J. Huhmann-Vincent, B. L. Scott, and G. J. Kubas, *J. Am. Chem. Soc.*, 1998, **120**, 6808.
[183] F. L. Taw, H. Mellows, P. S. White, F. J. Hollander, R. G. Bergmann, M. Brookhart, and M. D. Heinekey, *J. Am. Chem. Soc.*, 2002, **124**, 5100.
[184] J. B. Lambert, L. Lin, and V. Rassolov, *Angew. Chem., Int. Ed. Engl.*, 2002, **41**, 1429.
[185] J. B. Lambert and S. J. Zhang, *Chem. Commun.*. 1993, 383.
[186] Z. Xie, in 'Personal Communication', ed. A. S. Weller, 2003.
[187] B. T. King and J. Michl, *J. Am. Chem. Soc.*, 2000, **122**, 10255.
[188] M. Bochmann and M. J. Sarsfield, *Organometallics*, 1998, **17**, 5908.
[189] D. A. Walker, T. J. Woodman, D. L. Hughes, and M. L. Bochmann, *Organometallics*, 2001, **20**, 3772.
[190] W. V. Konze, B. L. Scott, and G. J. Kubas, *Chem. Commun.*. 1999, 1807.
[191] M. Kira, T. Hino, and H. Sakurai, *J. Am. Chem. Soc.*, 1992, **114**, 6697
[192] Z. Janousek, U. Lehmann, J. Castulik, I. Cisarova, and J. Michl, *J. Am. Chem. Soc*, 2004, **126**, 4060
[193] I. A. Guzei, R. A. S. Jr., and R. F. Jordan, *Acta Cryst. Sec. C*, 2000, **56**, 635.
[194] W. Beck and K. Sunkel, *Chem. Rev.*, 1988, **88**, 1405
[195] M. Appel, K. Schloter, J. Heidrich, and W. Beck, *J. Organomet. Chem.*, 1987, **322**, 77.
[196] G. F. Schmidt and M. Brookhart, *J. Am. Chem. Soc.*, 1985, **107**, 1443.
[197] M. D. Butts, B. L. Scott, and G. J. Kubas, *J. Am. Chem. Soc.*, 1996, **118**, 11831.
[198] M. D. Heinekey, B. M. Schomber, and C. E. Radzewich, *J. Am. Chem. Soc.*, 1994, **116**, 4515.

2: Silver Phosphine Complexes Partnered with [1-H-$CB_{11}Me_{11}]^-$.

2.1: Introduction:

The Ag(I) salts, especially those of anions that have a coordinating ability on par with weak donor solvents (*e.g,*. Et_2O or CH_2Cl_2), are of structural interest due to their potential for a diverse range of solvent coordinated or anion coordinated structures.[1-3] In addition, the utilisation of silver (I) salts for the metathesis of a halide with a weaker coordinating anion is a standard methodology for the formation of either cationic solvent or anion-coordinated metal complexes.[4] They are also an intermediate on the way to the formation of other synthetically useful salts.[5]

It is well documented that arenes readily bind to Ag(I) metals and this significantly improves their solubility in comparison to other simple salts.[6] Saturated chlorocarbon *solvento* Ag(I) complexes – particularly involving the 'polar but noncoordinating' dichloromethane are less widespread and have been characterised in only a handful of cases.[1, 7, 8] These have required anions based on the pentafluorooxotellurate and polyfluoroalkoxyaluminates moieties. Structures have been documented with up to three CH_2Cl_2 molecules interacting with a single silver centre (Figure 1).[1, 9]

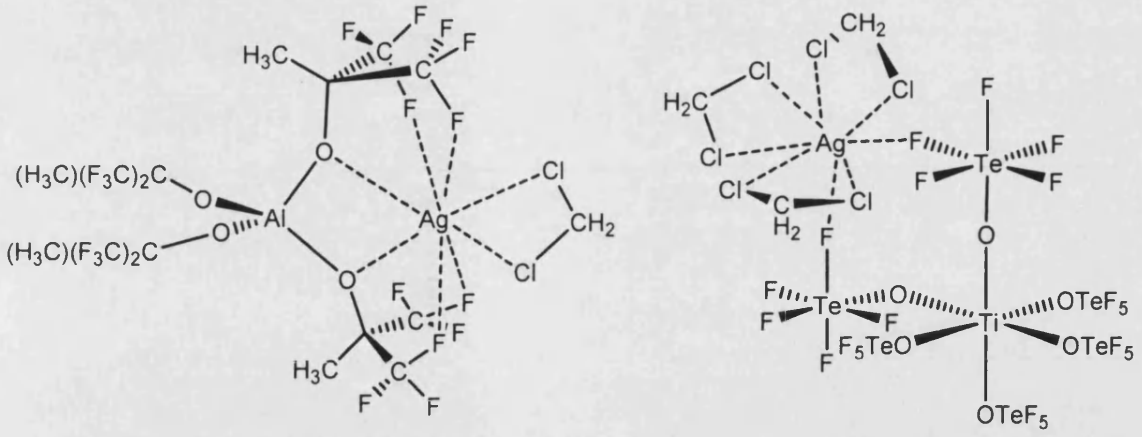

Figure 1: Solid state structures of silver (I) salts of weakly coordinating anions exhibiting mono and tris solvation of the Ag(I) cation by CH_2Cl_2

Silver (I) salts of the ubiquitous weakly coordinating anion, $[BAr_F]^-$, have been established by single crystal studies to comprise anion arene interactions, albeit with bidentate exo ligation from 1,2-di-iodobenzene or 2,2'-bipyridine.[10] In both complexes there is a bidentate bonding motif with the Ag cation sandwiched between two arene rings, one structure consisting of a symmetrical η^2-η^2 interaction whilst the other displays an unsymmetrical η^2-η^1 type (Figure 2).

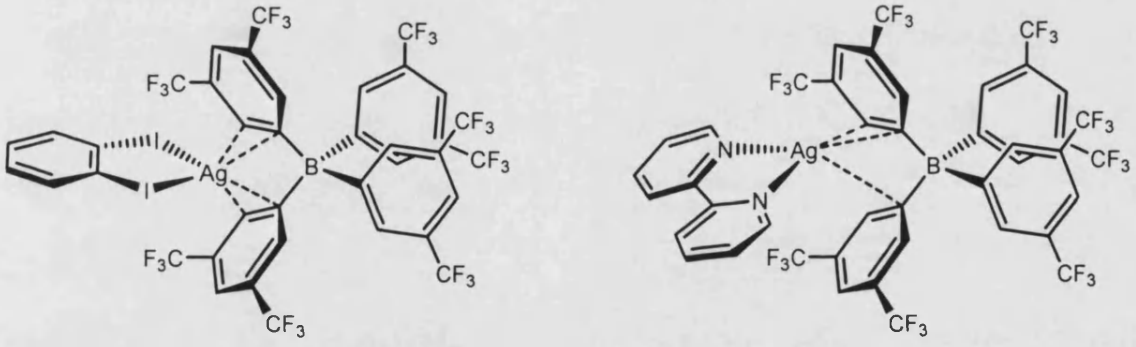

Figure 2: Solid-state structures of the symmetrical and asymmetrical bonding motifs of $L_2Ag(I)$ salts of the $[TFPB]^-$ anion.

It is suggested that the alteration in the bonding mode is due to the increase in steric bulk associated with moving from 1,2-diiodobenzene to the more bulky 2,2'-bipyridine.[10] The authors suggest that steric hindrance generated by the CF_3 substituents

is the principal origin of the weakly coordinating nature of $[BAr_F]^-$. This is exemplified by the ability of unencumbered cations to intercalate between two arene rings and form stable compounds, in contrast to the ready formation of solvent coordinated complexes when the metal-ligand set possesses significant steric volume.[11-14]

Halogenated derivatives of $[closo\text{-}CB_{11}H_{12}]^-$ have been demonstrated to have a coordinating ability comparable to that of the per-alkylated $[closo\text{-}CB_{11}Me_{12}]^-$ (see Introduction).[15] Coupled with their similar dimensions and spatial arrangement this affords a sequence of anions that provide for a better insight and comparison to the coordination properties of $[closo\text{-}CB_{11}Me_{12}]^-$ than the geometrically disparate $[BAr_F]^-$ anion. The silver salts of a range of hexa, per-halogenated and mixed halogenated mono anionic 12 – vertex *closo*-carboranes have been successfully synthesised and their solid-state configuration determinated.[5, 16, 17] All of the characterised structures consist of contact ion pairs with the anion coordinated to the Ag(I) cation through a lone pair from at least one halogen atom [*e.g.*, Figure 3 Ag(*closo*-$CB_{11}H_6Cl_6$)·(p-xylene) and Ag(*closo*-$CB_{11}H_6Br_6$].

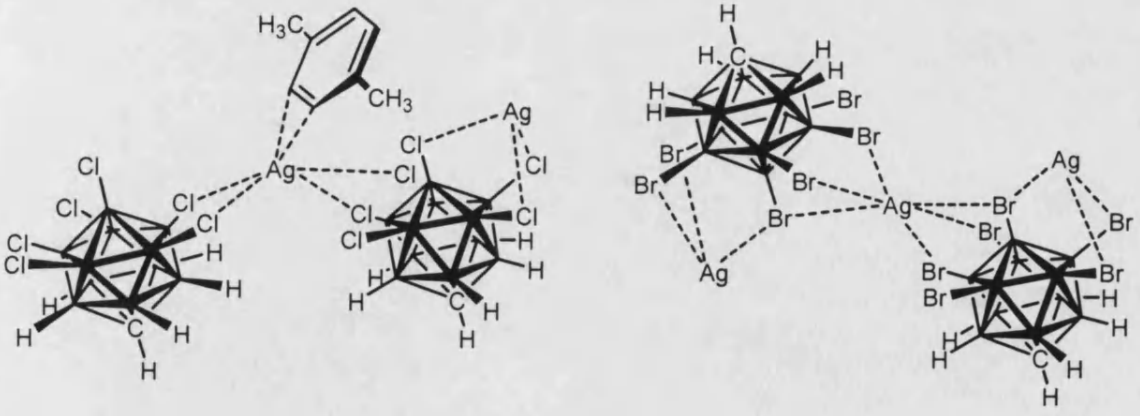

Figure 3: Solid state structures of [Ag(*closo*-$CB_{11}H_6Cl_6$)·(p-xylene)] and [Ag(*closo*-$CB_{11}H_6Br_6$)], hydrogen atoms not shown for clarity.

There are two major repeating motifs observed throughout these systems: (i) the anion bridging multiple Ag(I) centres forming a one dimensional co-ordination polymer and; (ii) discrete molecules with the silver encapsulated by one carborane anion and a number of arene interactions (Figure 5). In general, the systems are far from isostructural, involving a variety of mono-, bi-, tri dentate halogen atom binding, η^1 and η^2 arene interactions and silver coordination numbers from three to six. Silver (I) cations are thus able to exist in a wide variety of coordination environments provided there is efficient packing and charge compensation.

A method for the further reduction of the coordinating nature of these anions was observed in a 'dimeric unit', $[AgX_2]^-$ (X = [1-H-*closo*-$CB_{11}H_6Br_6$]$^-$) that has an even lower electrostatic attraction than the simple anion.[18] The effective charge is now halved by the coordination of a second [1-H-*closo*-$CB_{11}H_6Br_6$]$^-$. The lower nucleophilicity enabled the first isolation of the anion 'free' cation $[Fe(tpp)]^+$ (tpp = tetraphenylporphyrinate), where two molecules of p-xylene binds favourably over [(1-H-*closo*-$CB_{11}H_5Br_6)_2Ag]^-$ (Figure 4).

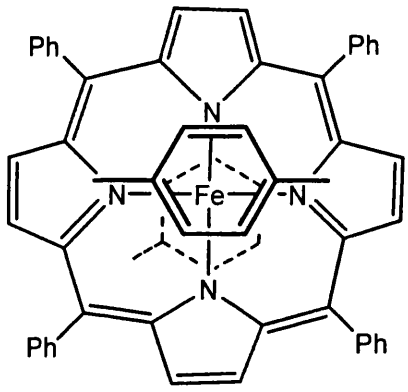

Figure 4: The cation $[Fe(tpp)]^+$ with axial coordination by two molecules of p-xylene.

A notable trend from the mixed halogenated carborane anions, [1-H-*closo*-$CB_{11}Br_5Cl_6]^-$, is the tendency for the cation to bind preferentially to the lower

pentagonal belt (B7 –12) and antipodal Cl lone pairs (Figure 5). This is counter intuitive given the presence of the better electron donor Br atoms in the upper pentagonal belt (B2-6) and contradicts the hard-soft acid-base principle.[16] The electron density polarisation across the cluster core caused by the electronegative carbon at C1 (see Chapter One) is still having a significant effect on the coordinating ability of the peripheral halogens – enough to reverse the chlorine/bromine ordering of lone pair accessibility.[19]

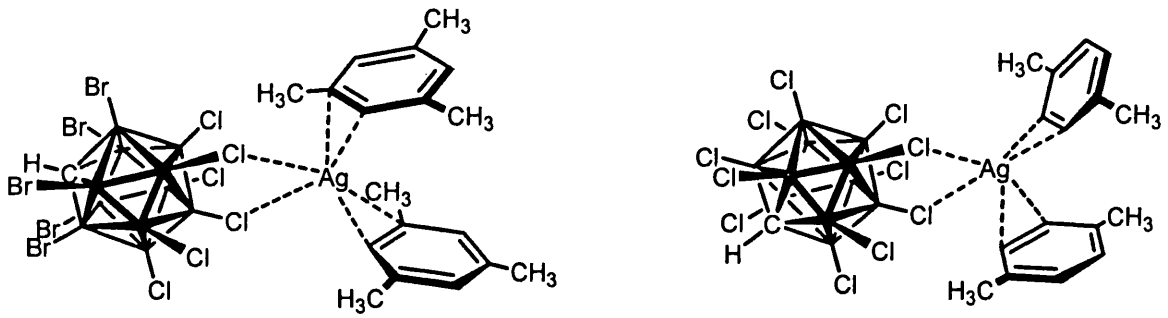

Figure 5: A series of bis-arene silver salts of **A**: [1-H-*closo*-$CB_{11}Br_5Cl_6$], **B**: [1-H-*closo*-$CB_{11}Cl_{11}$], all exhibiting coordination through {BX} vertices 7 through to 12.

Supporting evidence for this is provided by the coordination behaviour of the [1-H-*closo*-$CB_{11}X_{11}$]$^-$ anion (X = Cl or Br) that consistently interacts through the lower pentagonal and antipodal positions (*e.g.*, Figure 5).

In arene solvents the coordination persists and contact ion pairs similar to that observed in the solid state can be proposed, albeit not to the extent of one-dimensional polymers. This sustained interaction is characterised by a change in the chemical shift in the ^{11}B NMR spectroscopy in comparison with that of the 'free' anion in the caesium salt.[5, 17] In stronger donor solvents (e.g. acetone or acetonitrile) the ^{11}B NMR chemical shifts are similar to those observed for the non-coordinating Cs^+ salt, implying the

formation of *solvento*-complexes of the general formula $[Ag(solvent)_x]^+$. The solution NMR chemical shifts of these anions provide a valuable handle on their co-ordinating power with respect to common solvents.

It is noteworthy that there is no structural information available on the silver salts of what hitherto has been classified as the weakest coordinating member of the $[closo\text{-}CB_{11}H_{12}]^-$ derivatives, $[1\text{-}R\text{-}closo\text{-}CB_{11}F_{11}]^-$ (R = H or CH_3) (as determined by ^{29}Si NMR chemical shift of $^iPr_3Si^+$).[20, 21] The mono-fluorinated analogue Ag[12-F-*closo*-$CB_{11}H_{11}$] has been synthesised and the solid-state structure exhibits no close Ag···F contacts. Instead, the silver(I) coordination sphere is occupied by two benzene molecules and one terminal B-H contact.[22] This is in contrast to the structure of $Ag(C_6H_6)$[12-Br-*closo*-$CB_{11}H_{11}$] which contains a short Ag···Br distance of 2.642(1) Å implicit of a significant interaction (Figure 6).[23] By inference it would be expected that the Ag(I) salt of $[1\text{-}R\text{-}closo\text{-}CB_{11}F_{11}]^-$ would not involve any anion-Ag coordination and therefore would presumably lead to *solvento* complexes.

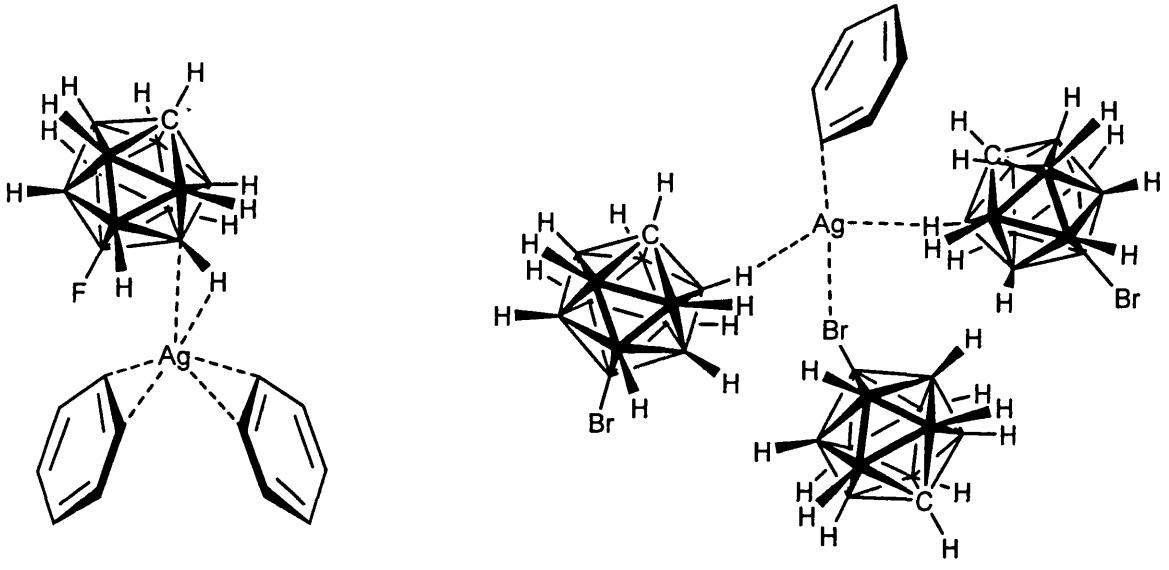

Figure 6: Structural motifs for the Ag(I) salt of $[12\text{-}F\text{-}closo\text{-}CB_{11}H_{11}]^-$ and $[12\text{-}Br\text{-}closo\text{-}CB_{11}H_{11}]^-$.

Phosphine stabilised silver (I) salts of mono carborane anions have previously been investigated and demonstrate excellent catalytic activity in hetero Diels Alder reactions.[24, 25] Solid-state studies have revealed that they form contact ion pairs in a variety of bonding modes that persist to some degree in non-interacting solutions (Figure 7). In the $(PPh_3)Ag(anion)$ complexes the positioning of the $\{Ag(PPh_3)\}^+$ fragment is consistently asymmetric over one triangular face of the carborane cluster. The Ag(I) coordination environment is completed by significantly longer intermolecular interactions with an anion or phenyl ring from an adjacent unit in the extended lattice.[26, 27]

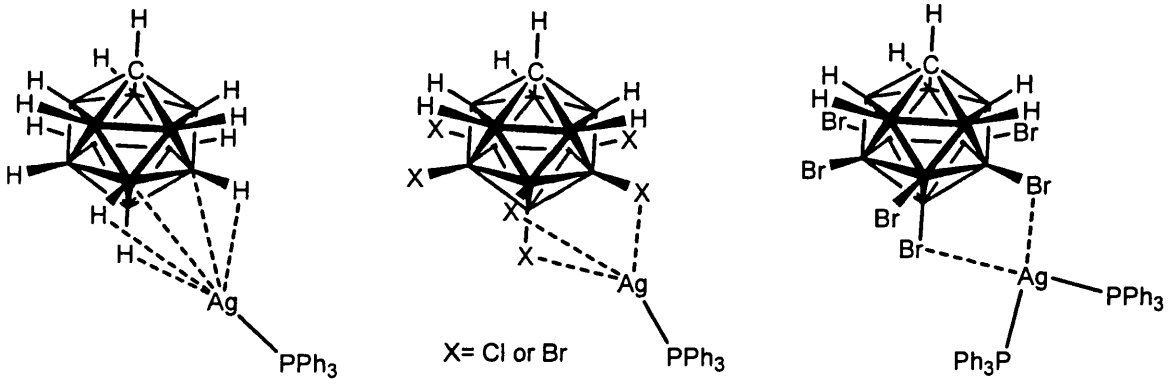

Figure 7: Solid state structures of the asymmetric units of a number of $Ag(PPh_3)_x$ (x = 1 or 2) coordinated to a series of carborane anions.

As seen previously for the non ligated simple silver salts an interaction persists in solution, again indicated by the change in the anion chemical shift in the ^{11}B NMR spectra. The C_{5V} symmetry of the cage on $\{Ag(PPh_3)\}^+$ coordination is maintained in solution, thus the cation fragment is fluxional over the surface of the cluster on the NMR timescale as found in other analogous exo-coordinated $Ag(PPh_3)$ carborane systems.[28, 29]

The strength of the Ag-P bond in these systems is a good measure of the degree of interaction between the anion and cationic fragment. In the $\{Ag(PPh_3)\}^+$ system it has furthermore been demonstrated that there is a good correlation between the solid-state determined Ag-P bond length and the $J_{average}(AgP)$ coupling constant. Both can be used to measure the strength of the cation-anion interaction (Table 1), with a stronger Ag-P bond (by a greater J(AgP) or a shorter solid-state Ag-P length) indicative of a weaker cation···anion interaction. Whilst this is a useful indicator, care has to be taken in the interpretation due to the variation in the binding motifs and observed silver coordination environments. The results do suggest a logical conclusion that the weakest coordinating anion by both techniques is the [*closo*-$CB_{11}H_6Cl_6$]$^-$.[26] A possible inconsistency in this system is in the relative ranking of [*closo*-$CB_{11}H_{12}$]$^-$ and [*closo*-$CB_{11}H_6Br_6$]$^-$ that contradicts several alternative rankings (this is probably an artefact of the different bonding observed in (PPh_3)Ag(*closo*-$CB_{11}H_{12}$) and (PPh_3)Ag(*closo*-$CB_{11}H_6Br_6$).[15]

Anion	J(AgP) Hz	Ag - P Bond distance (A)
$CB_{11}H_{12}$	743	2.3625(7)
$CB_{11}H_{11}Br$	621	2.39*
$CB_{11}H_6Br_6$	715	2.4032(3)
$CB_{11}H_6Cl_6$	770	2.314(2)

* average value of the two independent molecules present in the asymmetric unit

Table 1: Comparison of the solution and solid-state properties of a series of $[(Ag(PPh_3)]^+$ complexes.

A comparable method for the nucleophilic ranking of these anions in the $Ag(PPh_3)^+$ system is their catalytic activity in hetero Diels Alder reactions. Importantly, a number of classic, weakly coordinating anions have also been investigated and the

relative coordinating power demonstrated to increase, [*closo*-$CB_{11}H_6Br_6$]$^-$ < [*closo*-$CB_{11}H_{12}$]$^-$ < ClO_4^- ≈ OTf^- < BF_4^-. The relatively high coordinating power suggested by this methodology for BF_4^- is suspect and has been attributed to catalyst decomposition to inactive oxy-borates under the reaction conditions.[25]

Moving from PPh_3 to an analogous two electron donor, the carbene 1,3-dimesitylimidazol-2-ylidene (IMes), resulted in the isolation of the novel disproportionation compound [$Ag(IMes)_2]_2[Ag_2$(*closo*-$CB_{11}H_{12})_4$] as opposed to the expected [Ag(IMes)*closo*-$CB_{11}H_{12}$] compound (Figure 8).[30] Each Ag(I) centre in the dianionic portion is coordinated by three carborane anions only, in an approximately trigonal prismatic arrangement.

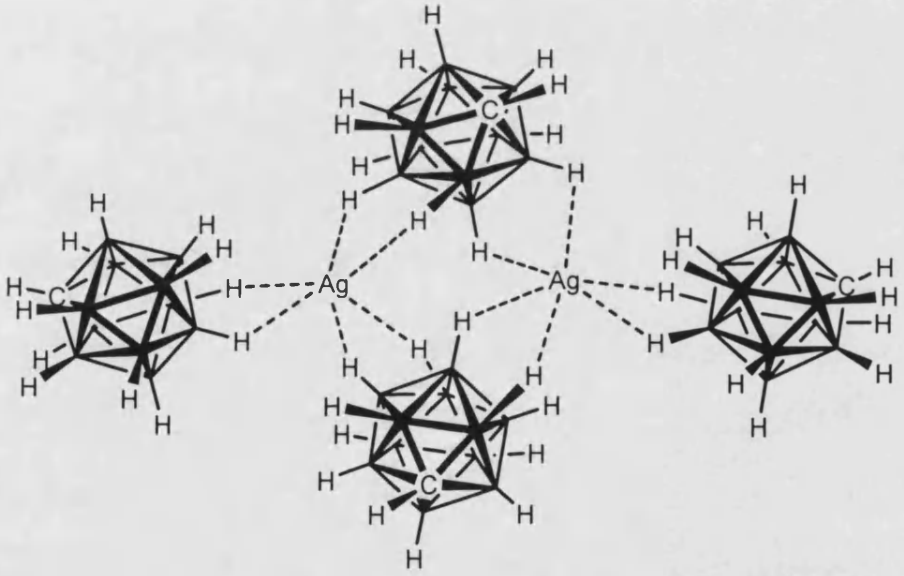

Figure 8: $[Ag_2(CB_{11}H_{12})_4]^{2-}$ solid-state structure omitting disorder in the bridging carborane clusters.

Solution studies on the bis-phosphine $Ag(PPh_3)_2^+$ complexes established a fluxional process which has been ascribed to an equilibrium between contact ion pairing (*e.g.*, as in the solid-state structure of $(PPh_3)_2AgX$ {X = [*closo*-$CB_{11}H_{12}$]$^-$ and [*closo*-$CB_{11}H_6Br_6$]$^-$ showing intimate anion cation ion pairing})[25, 26] and a linear [Ph_3P-Ag-

$PPh_3]^+$ cation with a well separated anion. This behaviour is indicative of weak Ag···anion interactions not persisting in solution. A noteworthy comparison is obtained from the analogous compound with the classic weakly coordinating anion BF_4^- as the counter ion. This produces a nearly linear solid state structure and no solution fluxionality,[31] allowing the conclusion that BF_4^- is less strongly interacting than the $[closo\text{-}CB_{11}H_{12}]^-$ and $[closo\text{-}CB_{11}H_6Br_6]^-$anions to $[Ag(PPh_3)_2]^+$.

2.1.1 Scope of Chapter

The coordination chemistry of the highly methylated carborane anion with $[Ag]^+$ and phosphine stabilised silver salts has not been studied. This anion with its periphery comprised entirely of methyl groups can be expected to be one of the weaker coordinating in the series of anionic derivatives of $[closo\text{-}CB_{11}H_{12}]^-$. Structural studies will therefore be interesting, as this anion will have a coordinating ability on par with weak donor solvents (*e.g.*, Et_2O and CH_2Cl_2) and can result in the formation of either intimate ion pairs or metal-solvent complexes (Figure 9). If there are close anion···cation interactions this will, by necessity, involve Ag···H_3C contacts – a model for the σ alkane bond. Alternatively, if solvent separated ion pairs result then this has the potential, if they are soluble in hydrocarbon solution, for the formation of true alkane σ complexes.

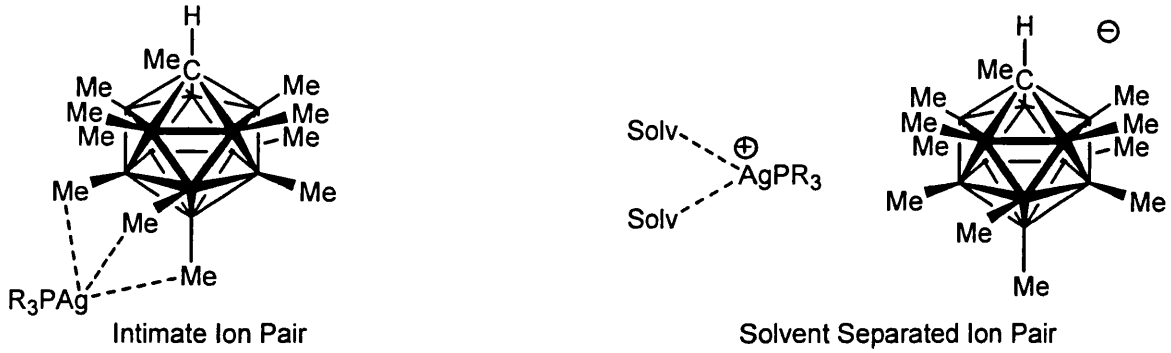

Figure 9: The two possible resultant products on the partnering of the highly alkylated carborane anion with cationic silver fragments.

2.2. Results and Discussion:

Michl and co-workers reported the synthesis of $NMe_4[closo\text{-}CB_{11}Me_{12}]$ by the complete methylation of $NMe_4[1\text{-}Me\text{-}closo\text{-}CB_{11}H_{11}]$ using methyl triflate followed by salt metathesis to prepare a range of other complexes $M[closo\text{-}CB_{11}Me_{12}]$ ($M = Li^+$, Tl^+, Ag^+, Na^+, K^+ and Cs^+).[32, 33] Consistently, the molecular structures generated by X-ray diffraction studies exhibited anion positional disorder, preventing the unequivocal location of the cage carbon (see Introduction) thus frustrating efforts to determine the B-CH_3 vertices involved in the metal contact.[19, 33, 34] To circumvent this and allow for unambiguous assignments of the cage vertices it was necessary to introduce a crystallographically prominent marker location to the cage periphery. A facile way to accomplish this without drastically altering the synthetic complexity and the chemical properties of the resultant anion is to leave the unique carbon vertex un-methylated. The synthesis of $Cs[1\text{-}H\text{-}closo\text{-}CB_{11}Me_{11}]$ is consistently achieved in reasonable yield (60 – 70%) starting from $Cs[closo\text{-}CB_{11}H_{12}]$, whilst avoiding the use of the expensive hindered base (Figure 10).[19]

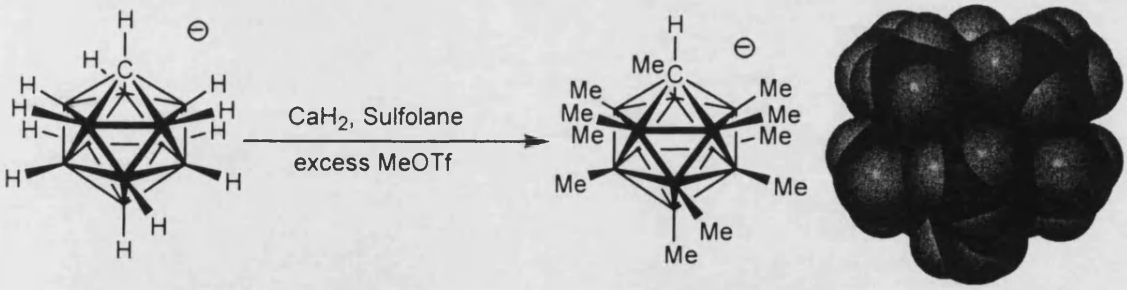

Figure 10: The synthesis and a space filling diagram of the $[1\text{-}H\text{-}closo\text{-}CB_{11}Me_{11}]^-$ anion.

Conversion of the caesium salt to other simple cations including $[HN(Me)_2Ph]^+$, $[NR_4]^+$ and Ag^+ is readily accomplished by the use of a two phase H_2O/Et_2O extraction methodology.[33] $Ag(1\text{-}H\text{-}closo\text{-}CB_{11}Me_{11})$ **(I)** can be converted to the mono phosphine

derivatives (R_3P)Ag(1-H-*closo*-$CB_{11}Me_{11}$) by the addition of one equivalent of R_3P (R = Ph, C_6H_{11} and 3,5-$Me_2C_6H_3$). The solid state structures of these four compounds will be discussed first followed by solution, DFT studies and finally their reactivity with additional Lewis bases.

2.2.1: Solid State Investigation into Ag^+ and $\{(R_3P)Ag\}^+$ complexes of [1-H-*closo*-$CB_{11}Me_{11}$]

2.2.1.1: Ag[1-H-*closo*-$CB_{11}Me_{11}$] (I):

Recrystallisation of the crude solid **(I)** by the slow diffusion of hexanes into a saturated CH_2Cl_2 solution afforded colourless crystals of suitable quality for X-ray diffraction studies. Complex **(I)** is stable in the solid state under an inert atmosphere though under prolonged exposure to light discolouration and ultimately decomposition occurs to give uncharacterised products. The solid-state structure of **(I)** exhibits no ambiguity in the location of the carbon vertex and only minor disorder in the hydrogen positions on C3 and C10 is found. This can be readily modelled by half occupancy of two separate sets. In the asymmetric unit the silver cation and the anion are not well separated (Figure 11). There is one close Ag···H_3C contact (Ag1···C7 2.6535(18) Å) from a methyl group on the lower pentagonal belt. This is within the combined (3.29 Å) van der-Waals radius of CH_3 (2.00 Å) and the ionic radius of Ag^+ (1.29 Å), suggesting a significant anion-cation interaction.[35] Similar close M···H_3C interatomic distances have been previously reported for a number of alkali salts of the related anion [*closo*-$CB_{11}Me_{12}]^-$.[33] The data was of sufficient quality to freely determine the C7 methyl hydrogen positions without any restraints and the refined bonding motif lies between

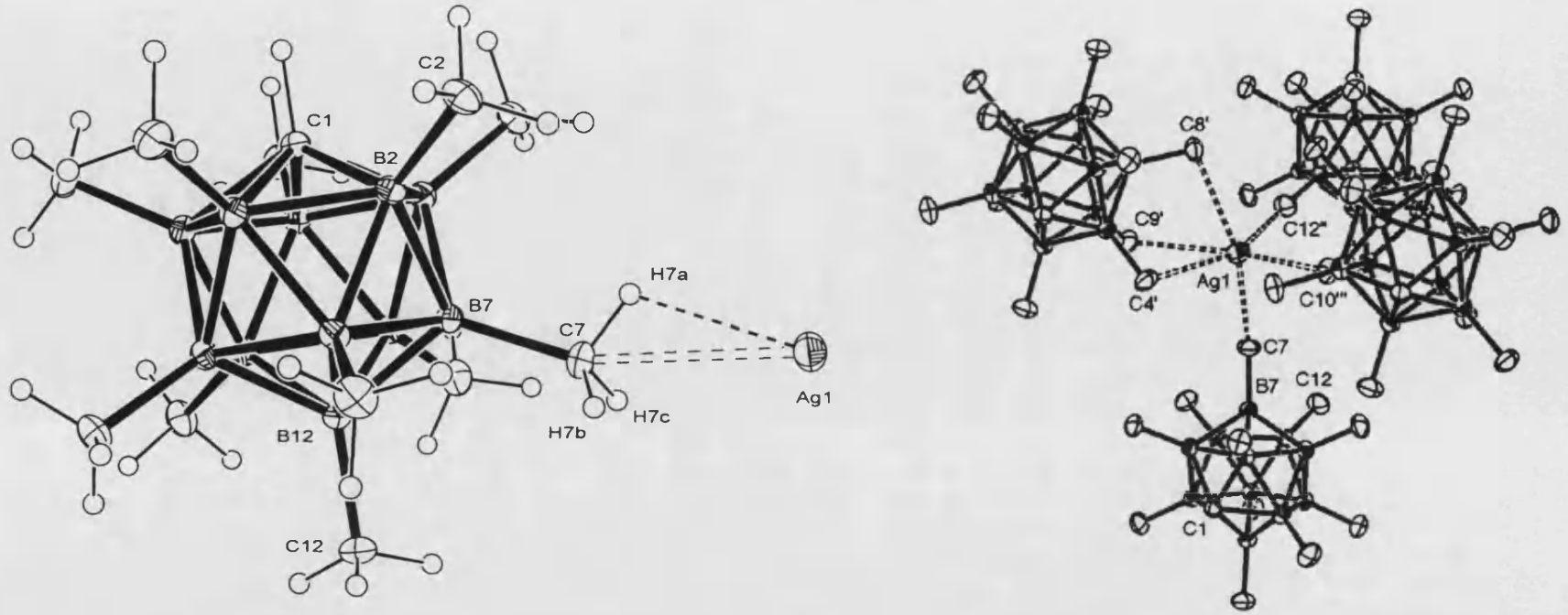

Figure 11: Molecular structure of the asymmetric unit of Ag[1-H-*closo*-$CB_{11}Me_{11}$] **(1)**, and the extended solid state structure showing all Ag···H_3C contacts in the unit cell. (ellipsoids drawn at the 30% probability level).

Ag1-C7	2.6535(18)	Ag1-C9'	3.089(2)	B9'-C9'-Ag1	95.86(10)	C4-B4	1.597(2)
Ag1-H7A	2.17(6)	Ag1-C12''	2.762(2)	B12''-C12''-Ag1	168.48(14)	C7-B7	1.601(2)
Ag1-H7B	2.49(4)	Ag1-C10'''	2.7716(18)	B10'''-C10'''-Ag1	156.05(12)	C8-B8	1.603(2)
Ag1-H7C	2.65(4)	B7-C7-Ag1	158.78(13)	C7-Ag1-C8'	161.87(5)	C9-B9	1.606(2)
Ag1-C4'	3.067(2)	B4'-C4'-Ag1	94.18(11)	C4'-Ag1-C12''	158.79(5)	C10-B10	1.611(2)
Ag1-C8'	2.832(2)	B8'-C8'-Ag1	101.08(11)	C3-B3	1.588(2)	C12-B12	1.608(2)

Table 2: Selected bond lengths (Å) and angles (°) for **(I)**.

the η^2-C,H and the η^4-C,H,H,H with one close (2.17(6) Å) and two longer (2.49(4) and 2.65(4) Å) H···Ag contacts (Figure 12).

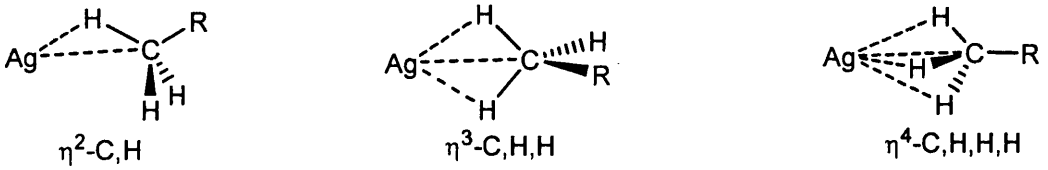

Figure 12: The three possible binding modes for the CH_3···M interaction (the continuum of asymmetric intermediates is not shown).

The close contact is at the upper limit of that previously reported for Ag-H contacts, albeit in Ag-H-M bridging units (1.4Å to 2.2 Å).[36, 37] The three C-H bonds exhibit no lengthening and the angles are close to expected for ideal sp^3 hybridisation (given the usual caveats associated with the free refinement of hydrogen positions using X-Ray diffraction data). The B7-C7 bond length is identical, within experimental errors to those of non-coordinating B-CH_3 vertices and the B7-C7-Ag1 angle (158.78(13)°) is significantly bent. These findings combine to exclude the possibility of any significant CH_3 σ donation. Definitive σ interactions studied by neutron diffraction all display some C-H bond lengthening.[38]

Inspection of the extended solid-state structure in **(1)** revealed the close proximity of three additional anions adjacent in the lattice (Figure 11). The overall coordination sphere of each Ag(I) in the lattice approaches *pseudo*-octahedral with a total of six Ag···H_3C methyl contacts (range of Ag··H_3C distances of 2.652(2) – 3.089(2) Å). These close contacts consist of mono-dentate (i.e. through one CH_3 vertex) to three anions and an unsymmetrical tri-dentate (through three vertices) association with the remaining anion. Both the octahedral coordination and the varying (mono- and tri-dentate) binding natures have precedence in the group 1 salts of the related anion

[*closo*-$CB_{11}Me_{12}]^-$, albeit with arene molecules in the apical positions of the distorted octahedron. The anion immediacy in these cases was attributed predominantly to crystal packing forces maximising anion···cation interactions.[33] In the absence of any observed deformation of the contact methyl groups it strongly suggests that this is also the case in the observed structure of **(I)**. These additional contacts explain the asymmetric nature of the interaction between the C7 methyl group and the Ag(I) in the asymmetric unit. The deviation from linearity (B7-C7-Ag(1) 158.78(13)°) is necessary to allow for the accommodation of the other cage anions. The arguments for a primarily electrostatic nature of the bonding in **(I)** are further strengthened by the examination of the extended packing diagram, which demonstrates that the Ag^+ cations occupy distorted tetrahedral holes formed by four approximately spherical anions (Figure 13), reminiscent of the structure of the classically ionic complex zinc sulfide (Wurtzite). The radius ratio (r_+/r_-) for the relative radii of Ag^+ (1.29 Å) and the approximately spherical [1-H-*closo*-$CB_{11}Me_{11}]^-$ (~3.5 Å) at 0.37 lies comfortably in the range permitted for tetrahedral coordination (0.22 – 0.41).[39]

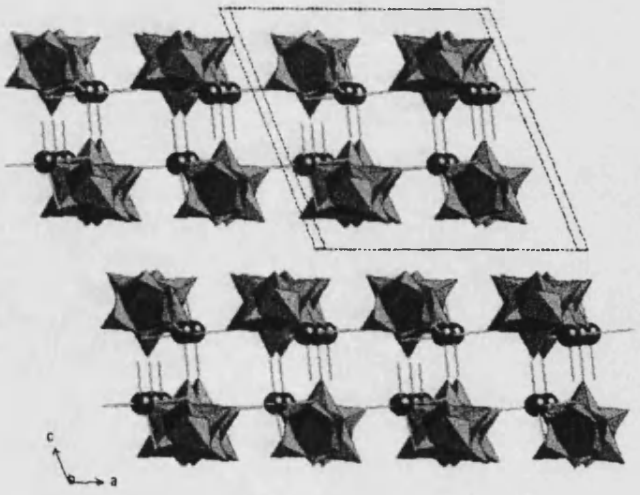

Figure 13: Packing diagram for **(1)** Carborane anions shown as polyhedra and Ag^+ cations as spheres of arbitrary radius.

An alternative way to view the structure of **(I)** is that each carborane anion is closely associated with four Ag^+ cations (Figure 14). The closest Ag···Ag distance at 6.567 Å is far too long to invoke any Ag···Ag interactions.[40, 41] These multiple interactions produce a three-dimensional coordination polymer in the crystal lattice. The longer Ag···H_3C contacts are associated with the tri-dentate bonded motif, as would be expected when compared to the mono-dentate, predominantly end on contacts. In the tri-dentate bonding motif there is a slight elongation of the C8 – C9 distance (C8 – C9 3.532 Å versus the average of the remainder of the anion, 3.471 Å). Presumably this is to permit the fuller encapsulation of the Ag(I) cations and a similar engulfing effect has been seen for the related complex Li(*closo*-$CB_{11}Me_{12}$).[33] Anion methyl distortion exemplifies the important point that highly alkylated carboranes are not regular rigid icosahedra.

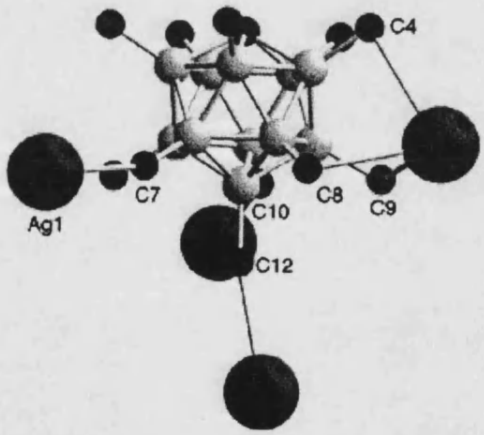

Figure 14: The coordination environment around a single carborane anion.

The observed silver binding locations (apart from a long contact to C4 in the tri-dentate interaction) all originate from the lower pentagonal belt or the antipodal cage vertices. Theoretical and experimental analysis on other derivatives of [*closo*-$CB_{11}H_{12}$]$^-$

have demonstrated an analogous positional preference and has been shown to arise from the increased negative charge residing on these vertices relative to the upper pentagonal belt. [16, 19, 42] A simplistic rationalization of this observation is to consider the origin of the dissimilar electron density magnitude at each inequivalent boron position. The cage carbon polarises the cluster principally by reducing the electron cloud associated with the upper pentagonal belt. This concurrently decreases the degree of electron density withdrawal to the connected peripheral groups (halogen or Me). The remoter lower pentagonal belt and antipodal boron positions experience this significantly less, permitting more of their associated electron density to be withdrawn to their relatively more electronegative periphery (Figure 15). The net effect is a greater partial negative charge on the vertices B7-12 leading to the energetic preference for cations to bind to the cage through these sites. A parallel effect in the [1-H-*closo*-$CB_{11}Me_{11}$]$^-$ anion is feasible and B3LYP/SDD calculations on the ion-pairing energies for the four inequivalent vertices in $^nBu_3Sn$(*closo*-$CB_{11}Me_{12}$) generate a similar trend in stabilities $12 \approx 7\text{-}11 > 2\text{-}5 >> 1$.[34]

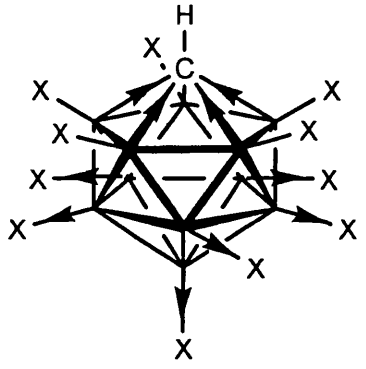

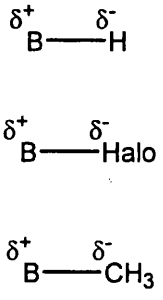

B	2.04		
H	2.20	Br	2.96
F	3.98	I	2.66
Cl	3.16	C	2.55

Figure 15: A simplified schematic demonstrating the major electron withdrawing effects in derivatives of [*closo*-$CB_{11}H_{12}$]$^-$, X = Halogen, H or CH_3. The Pauling scale electronegatives are also listed.[43]

The tight ion paring observed for **(I)** is in contrast to the Ag(I) salts of weakly coordinating anions based on the pentafluorooxotellurates and

polyfluoroalkoxyaluminates that form *solvento* complexes on recrystallisation from CH_2Cl_2 solutions (*e.g.*, $[Ti(OTeF_5)_6]^-$ and $[Al(O(CH_3)(CF_3)_2]^-$).[1, 7] Despite the saturated C-H exterior of [1-H-*closo*-$CB_{11}Me_{11}]^-$ the presence of close anion-cation contacts in the solid-state assign it as more coordinating than these anions.[1, 7, 9] The coordination polymers formed are, however, comparable to the halogenated derivatives of $[CB_{11}H_{12}]^-$.[5, 16, 17, 42] The solution behaviour of **(I)** will be discussed later and shows that these contacts are retained.

2.2.1.2: $(PPh_3)Ag$[1-H-*closo*-$CB_{11}Me_{11}$] (2):

$(PPh_3)Ag$(1-H-*closo*-$CB_{11}Me_{11}$) **(2)** is afforded in good yield by the reaction of equimolar CH_2Cl_2 solutions of **(I)** and PPh_3. Recrystallisation from the slow diffusion of hexanes into a saturated CH_2Cl_2 solution at -20°C provided colourless crystals of sufficient quality for X-ray diffraction analysis. Complex **(2)** crystallises with no positional disorder in the cage, allowing for the unambiguous assignment of the cage carbon atom. The asymmetric unit (Figure 16) consists of one $\{(PPh_3)Ag\}^+$ fragment and one [1-H-*closo*-$CB_{11}Me_{11}]^-$ anion in close contact through a single B-CH_3 vertex on the lower pentagonal belt of the cage (Ag1 – C7 2.544(2) Å). This is judged by the previously defined criteria of being closer than the combined van der-Waals radius of CH_3 and the ionic radius of Ag^+ (3.29 Å). The Ag1-C7 separation is significantly shorter than this 'outer limit' implying an appreciable interaction. The distance is considerably longer than that found in crystallographically characterised Ag-C single bonds (e.g., $(PPh_3)AgCH_2C_6F_5$ 2.144(5) Å)[44] but it is a of a comparable length to that reported for η^1-arene-Ag(I) interactions (*e.g.*, $AgCB_{11}H_{12}\cdot C_6H_6$ 2.400(7) Å),[45] where there is evidence for significant σ donor character.[46]

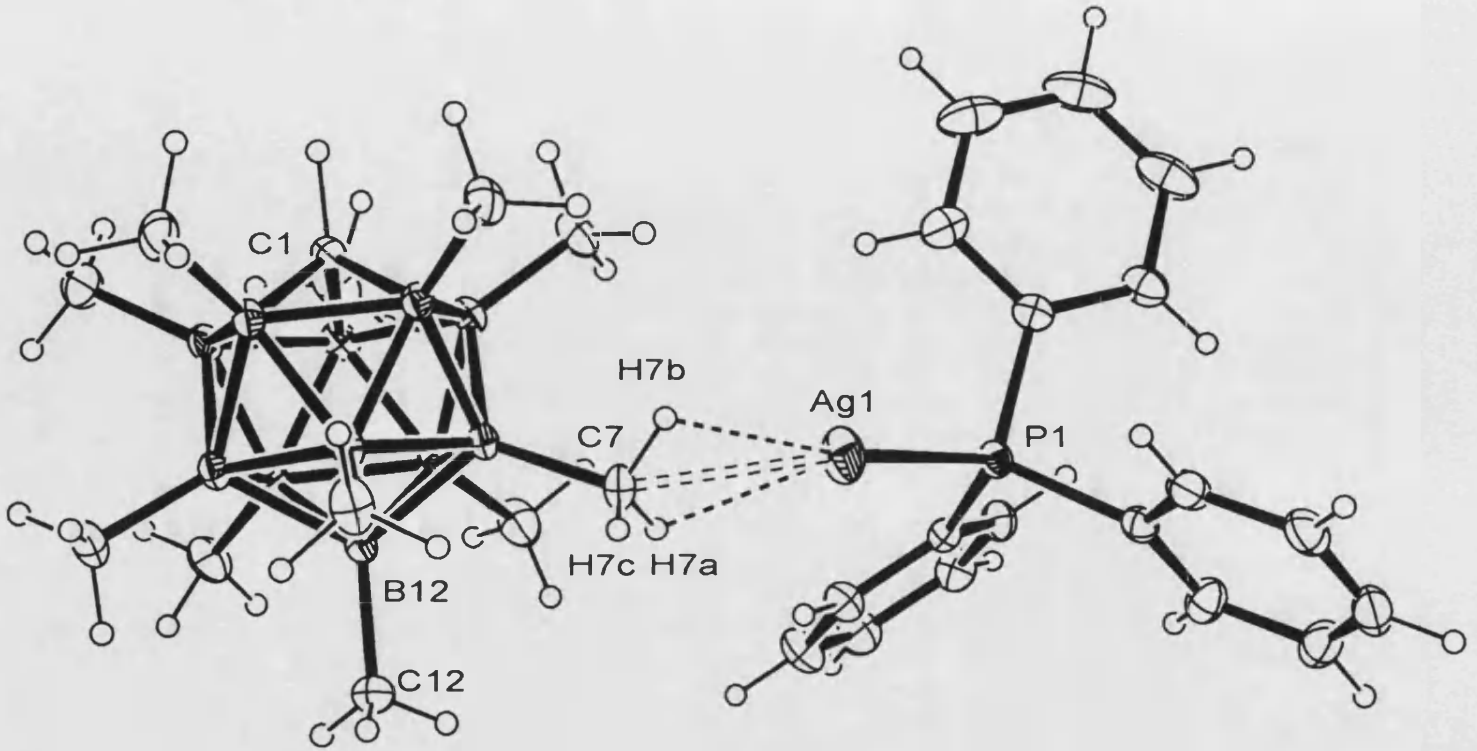

Figure 16: Molecular Structure of the asymmetric unit of $(PPh_3)Ag[1\text{-}H\text{-}closo\text{-}CB_{11}Me_{11}]$ **(2)**, thermal ellipsoids are shown at the 30% probability level.

Ag1-P1	2.3871(5)	C7-H7a	0.93(3)	P1-Ag-1-C7	152.21(6)	B7-C7-Ag1	138.88(15)
Ag1-C7	2.544(2)	C7-H7b	0.93(3)	H7a-C7-B7	108(2)	H7c-C7-H7a	116(3)
Ag1-H7a	2.19(3)	C7-H7c	0.93(4)	H7b-C7-B7	109(2)	H7b-C7-H7a	114(2)
Ag1-H7b	2.20(3)	C7-B7	1.606(3)	H7c-C7-B7	112(2)	H7c-C7-H7b	97(2)
Ag1-H7c	3.033(3)						

Table 3 Selected Bond Lengths (Å) and angles (°) for the asymmetric unit of **(2)**.

The hydrogen positions associated with the interacting vertex, C7, were freely refined without any constraints. Given the usual caveats inherent in the use of X-ray data for the assignment of hydrogen locations a number of observations can be made. The methyl group adopts a η^3-C,H,H motif involving two close Ag-H contacts that are identical within experimental error (Ag-H7a 2.19(3) Å and Ag-H7b 2.20(3) Å) and one considerably longer distance (Ag-H7c 3.03(3) Å). The Ag-H7 close contacts reside at the upper range for crystallographically characterised bridging Ag-H-M complexes (1.4 - 2.2 Å).[36, 37, 47] The asymmetry in this interaction is further illustrated by the B7-C7-Ag1 angle of 138.88(15)° being significantly perturbed from the expected 180° for a symmetric end on Ag···H_3C contact.[48] Similar metal-methyl bonding motifs have been previously characterised for a variety of systems including the anion coordinated compounds $LiBMe_4$[49] and $[\{1,3\text{-}(SiMe_3)_2C_5H_3\}_2ZrMe(\mu\text{-}Me)B(C_6F_5)_3]$[50] and a number of agostic interactions (see Chapter One).[51]

The C-H bond lengths (C7-H7a 0.93(3) Å, C7-H7b 0.93(3) Å and 0.93(4) Å) associated with the interacting moiety do not deviate from that expected for C-H bond lengths in methyl groups (0.98 Å). The H-C-H angles involved are also close to the ideal tetrahedral angle of 109.28° (116(3)°, 114(2)° and 97(2)°). Combined, these two sets of structural metrics rule out any significant contribution from σ bonding as this would be expected to result in a notable distortion in the methyl group away from pseudo-tetrahedral. The intermolecular bonding in **(2)** is dominated by ionic attractive forces as noted for the related anion coordinated systems involving $[BMe_4]^-$ and $[MeB(C_6F_5)_3]^-$ where there is equally no perturbation of the tetrahedral geometry about the interacting B-CH_3 moiety.[49, 50, 52, 53] Weak Ag···F interactions in low coordinate

silver phosphine complexes partnered with BF_4^- have also been described as being essentially electrostatic in origin.[31]

The silver phosphine bond length can be a useful indicator of the binding strength of anions to the cationic $\{(PPh_3)Ag\}^+$ fragment (see Introduction). In **(2)** the Ag-P distance of 2.3871(5) Å is of a comparable length to the analogous systems partnered with [*closo*-$CB_{11}H_{12}]^-$ and [*closo*-$CB_{11}H_6Br_6]^-$ (2.3625(7) Å and 2.4032(3) Å respectively) and even the NO_3^- anion (2.3918(4) Å), whilst being noticeably longer than that for the [*closo*-$CB_{11}H_6Cl_6]^-$ (2.314(2) Å).[25, 54] Again, over interpretation should be restricted due to the disparate binding motifs and degree of additional intermolecular interactions present - a better indicator of anion coordinating power, that of the solution ^1J(AgP) coupling constant, will be discussed later.

In an analogous manner to that observed for **(1)**, examination of the extended solid-state structure resulted in the characterisation of further close anion···Ag contacts from adjacent anions (Figure 17). Two additional, albeit significantly longer Ag···H_3C connectivities complete the coordination environment around Ag(I) - thus **(2)** has an extended three dimensional polymeric structure in the solid state. The additional contacts (Ag1-C9' 3.154(2) Å and Ag-C12'' 3.336(2) Å) are significantly longer in comparison to Ag1-C7 (2.3871(5) Å) and approach the 'interaction limit' of $\{Ag\}^+$···H_3C (3.29 Å). It is reasonable to assume that the source of the asymmetric binding mode between Ag1 and C7 are these long-range contacts, with the observed arrangement entirely dominated by the maximisation of electrostatic interactions. The contact methyl hydrogens (C9 and C12) were freely refined without restraints and equally display no elongation or angle deformation in comparison to sp^3 CH_3 moieties.

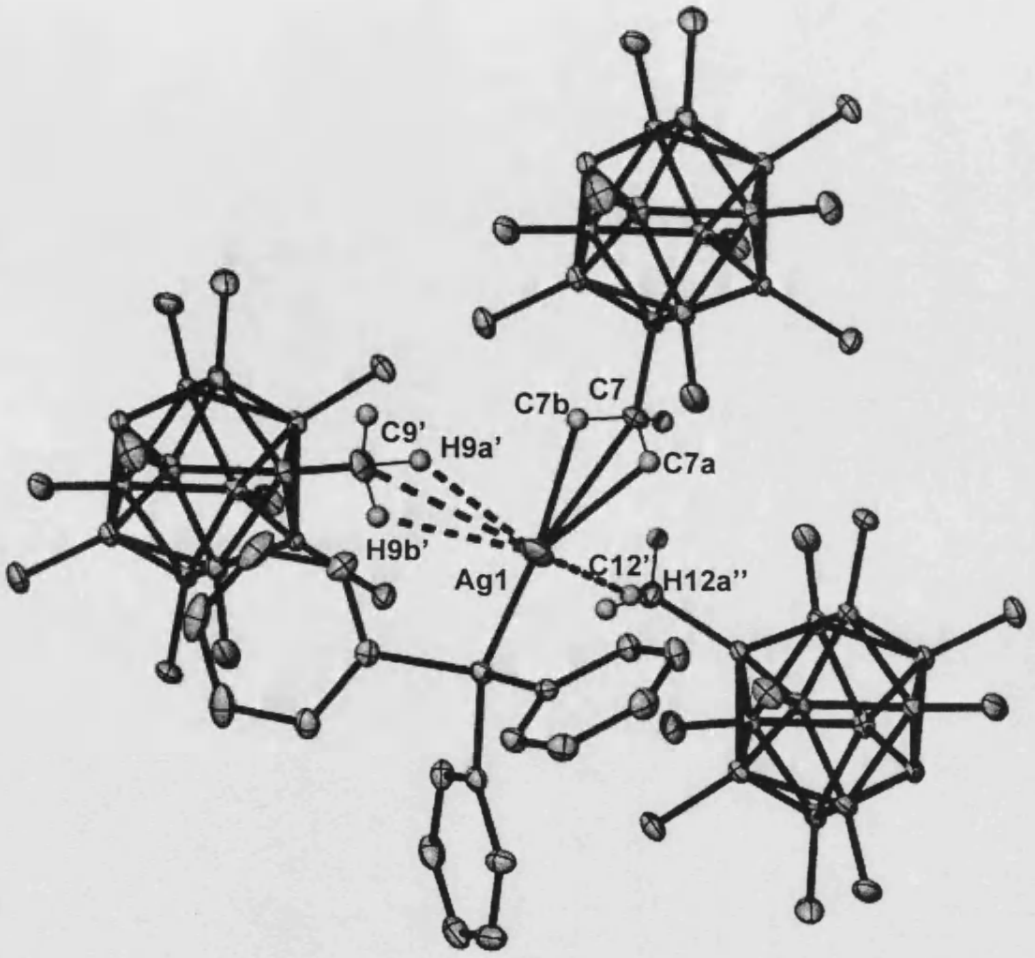

Figure 17: The Ag(I) coordination sphere for **(2)**. Hydrogen atoms omitted for clarity, except on C7, C9' C12''. Thermal ellipsoids shown at 30% probability level.

Ag1-C9'	3.154(2)	Ag1-C12''	3.336(2)
Ag1-H9a'	2.73(4)	Ag1-H12a''	2.45(3)
Ag1-H9b'	2.54(4)	Ag1-H12b''	3.434
Ag1-H9c'	3.338	Ag1-H12c''	3.546
C9-H9a	0.94(4)	C12-H12a	0.94(3)
C9-H9b	0.95(4)	C12-H12b	0.88(3)
C9-H9c	0.94(4)	C12-H12c	0.87(4)
C9-B9	1.600(3)	C12-B12	1.598(3)
H9a-C9-H9b	94(3)	H12a-C12-H12b	100(2)
H9b-C9-H9c	109(3)	H12b-C12-H12c	104(3)
H9a-C9-H9c	95(3)	H12a-C12-H12c	106(3)
H9a-C9-B9	114(2)	H12a-C12-B12	115(2)
H9b-C9-B9	120(2)	H12b-C12-B12	114(2)
H9c-C9-B9	120(2)	H12c-C12-B12	115(2)

Table 4: Selected bond lengths (Å) and angles (°) for the extended structure of **(2)**.

These additional binding motifs (Figure 17) are a second η^3-C,H,H and for the longest interaction an η^1-H. As the interactions are clearly best described as ionic, little insight can be taken from these motifs with respect to true σ interactions. Mixed binding modes in the extended structure observed in **(2)** are analogous to those previously determined by neutron diffraction studies for $LiBMe_4$ that shows a mixture of η^3-C,H,H and η^4-C,H,H,H interactions.[49]

A number of connections can be made between the solid-state structures of **(1)** and **(2)**. The interacting vertices in both originate predominantly from the lower pentagonal belt and antipodal positions – as expected from the relative negative charge densities. The bonding in each is mainly electrostatic with no visible indication of any σ orbital contribution. Structurally they are analogous (Figure 18) with the replacement of one of the globular [1-H-*closo*-$CB_{11}Me_{11}$]$^-$ anions for a PPh_3 ligand effecting only minor changes in the arrangement of the remaining three anions. The more bulky, less symmetrical, PPh_3 ligand results in a slightly more diffuse packing arrangement around the silver centre, as indicated by the longer secondary Ag···H_3C contacts relative to non ligated Ag[1-H-*closo*-$CB_{11}Me_{11}$]. Both **(1)** and **(2)** can be viewed as having a *pseudo* tetrahedral coordination around the silver centre (Figure 18).

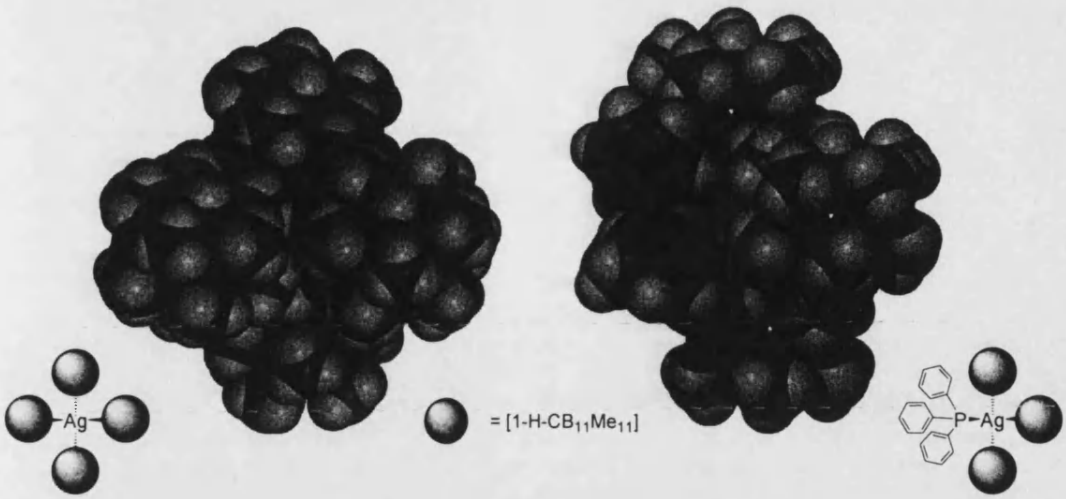

Figure 18: Space filling diagrams for **(1)** and **(2)**, at 100% van der-Waals radii.

It would be advantageous to limit the Ag···H_3C interactions to those involving only a single cage for a number of reasons: (i) to reflect more accurately the solution phase coordination as the longer contacts would not be expected to persist in the homogeneous environment; (ii) to allow closer comparison to gas phase DFT calculations (that do not take into account solution or solid-state effects); and (iii) an isolated interaction should reduce the complexity of any observed Ag···H_3C contacts. A straightforward method of approaching this is to increase the steric bulk associated with the phosphine ligand, thereby increasing the congestion at the Ag(I) centre in anticipation that this would make it less accessible to supplementary intermolecular interactions from the adjacent anions in the lattice.

2.2.1.3: $(PCy_3)Ag[1\text{-}H\text{-}\textit{closo}\text{-}CB_{11}Me_{11}]$ (3):

Use of the more bulky phosphine ligand tricyclohexyl phosphine (PCy_3) (a Tolman cone angle of 170° as opposed to PPh_3, 143°)[55] allows for the ready synthesis and isolation in moderate yield of $(PCy_3)Ag(1\text{-}H\text{-}\textit{closo}\text{-}CB_{11}Me_{11})$ **(3)** as a crystalline

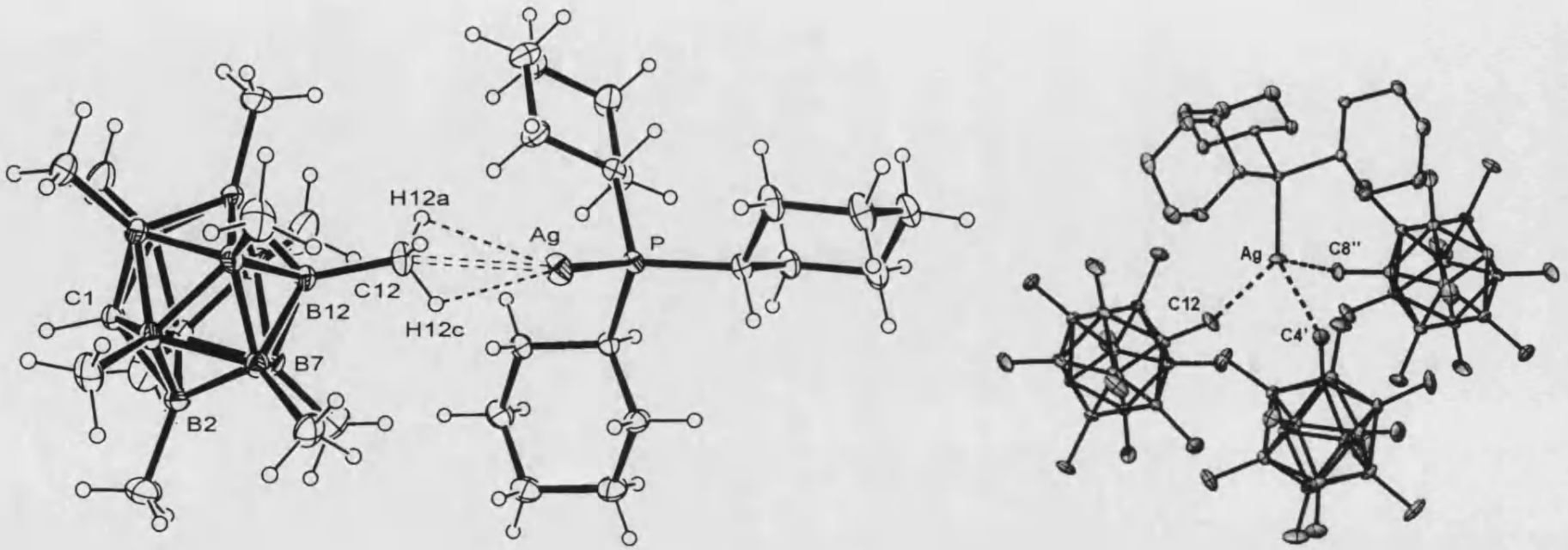

Figure 19: Molecular structure of the asymmetric unit of $(PCy_3)Ag[1\text{-}H\text{-}closo\text{-}CB_{11}Me_{11}]$ and the extended solid state structure showing all $Ag\cdots H_3C$ contacts (thermal ellipsoids shown at the 30% probability level). Hydrogen atoms omitted from the extended structure for clarity.

Table 5: Selected bond lengths (Å) and angles (°) for the extended structure of **(3)**.

Ag-P	2.3881(4)	C12-H12b	0.93(5)	Ag-C12	2.608(2)	B8''-C8''-Ag	153.41
Ag-H12a	2.38(4)	C12-H12c	1.02(5)	Ag-C4'	2.888(2)	C4'-Ag-C12	88.50(8)
Ag-H12b	2.74(5)	H12a-C12-H12b	108(3)	AgC8''	2.898(2)	C12-Ag-C8''	92.92(8)
Ag-H12c	2.21(5)	H12a-C12-H12c	120(4)	B12-C12-Ag	157.04(18)	C4'-Ag-C8''	97.73(7)
C12-H12a	0.92(4)	H12b-C12-H12c	80(3)	B4'-C4'-Ag	157.38		

solid in an analogous manner to that for **(2)**. The solid-state structure of **(3)** is shown in Figure 19. There is no positional disorder allowing for the unequivocal assignment of the cage carbon atom. As found for **(1)** and **(2)**, the asymmetric unit exhibits one close Ag···H_3C contact between the cationic silver fragment $\{(PCy_3)Ag\}^+$ and the anion [1-H-*closo*-$CB_{11}Me_{11}$]$^-$, this time via the antipodal, B12 cluster vertex. The Ag-C12 separation (2.608(2) Å) is comfortably within the previously stipulated upper limit indicative of a significant interaction (3.29 Å). The data set was also of sufficient quality to allow for the associated hydrogen atoms to be freely refined in the penultimate difference map. In a related manner to that exhibited in **(2)** there are two close H···Ag contacts that are identical within experimental error (Ag-H12c 2.21(5) Å, Ag-H12a 2.38(4) Å) and lie at the upper limit of bridging M-H-Ag units.[36, 37] The remaining C12-H bond is further away at 2.74(5) Å. The three C12-H bond lengths are all identical; there is, however, some deformation in the bonding angles associated with the contact methyl (H12a-C12-H12c 120(4)° and H12b-C12-H12c 80(3)°), with the widening of η^3-C,H,H bonding angle causing a concomitant compression of at least one of the other H12-C12-H12 angles. This could be suggestive of a degree of σ bonding character between the methyl group and the Ag. The absence of any elongation of the implicated C-H bonds and the high errors associated with any hydrogen positions determined by X-Ray diffraction data do not support this.

The silver phosphine fragment is not orientated end-on with respect to CH_3(12) but is slanted significantly away from linearity (B12-C12-Ag 157.04(18)°), though considerably less than that observed for **(2)** (B7-C7-Ag 138.88(15)°). The possible origin(s) of this difference are twofold – firstly an increased electron donation when moving from PPh_3 to PCy_3, or from increased σ donor contribution from the anion C-H

bonds could be instigating the change in geometry to achieve favourable orbital orientation. Alternatively, it could simply be due to packing effects to maximise electrostatic interactions. The latter is supported by the examination of the extended lattice that reveals the presence of a further two relatively close Ag-C distances to adjacent anions (Ag-C4' 2.888(2) Å and Ag-C8'' 2.898(2) Å). When viewed down the Ag-P axis, **(3)** appears to have *pseudo* C_3 symmetry with the immediate Ag(I) coordination being reminiscent of a propeller motif (Figure 20). The globular anions reside partially between each of the cyclohexyl rings thereby achieving a close proximity to the silver in order to maximise Coulombic interactions.

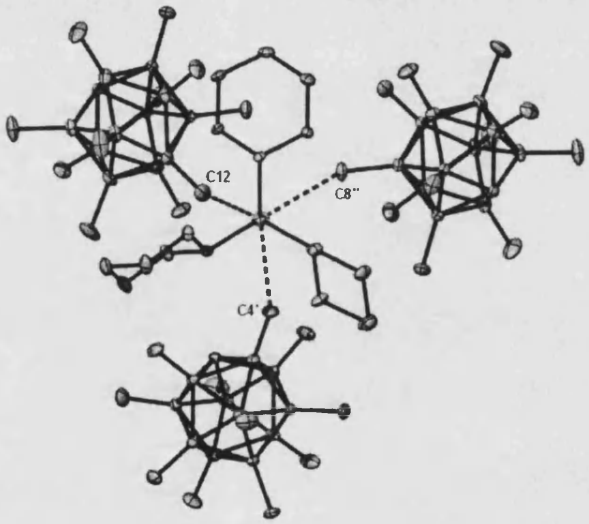

Figure 20: Complex **(3)** viewed down the Ag-P axis showing the *pseudo*-C_3 symmetry (thermal ellipsoids at 30% probability). All hydrogens are removed for clarity.

These further two close contacts are equally bent (B4'-C4'-Ag 157.38° and B8''-C8''Ag 153.41°). The bending of each B-C-Ag angle therefore originates due to steric interactions between the cyclohexyl rings and each of the three anions and the observed value presumably represents the energetic minimum achieved on reducing cyclohexyl – anion and anion – anion steric repulsions whilst maximising electrostatic Ag···cage interactions.

The Ag-P bond length (2.3881(4) Å) is longer than that found for three coordinate $(PCy_3)AgL_2$ complexes (e.g. 2.345(2) Å for $[(PCy_3)Ag(\mu\text{-}Cl)_2]$ and 2.351 Å for $[(PCy_3)Ag\{(pz_2B(pz)_2\}])$,[56, 57] but shorter than that found in four coordinate complexes (e.g., $[(PCy_3)AgI]_4$ average Ag-P distance 2.43(1)Å or $[(PCy_3)_2Ag(\eta^2\text{-}NO_2)$ 2.460(1)Å).[56, 58] Whilst increasing the steric bulk of the phosphine ligand has induced a shift from the geometry exhibited by **(1)** and **(2)**, the ability of the globular anions to partially intercalate between the cyclohexyl rings allows for the close approach of three anions and the subsequent failure to isolate the Ag···H_3C contacts to a single cluster.

In an attempt to increase further the steric hindrance associated with the ancillary phosphine ligand, an analogous synthesis was attempted with tri (*ortho*-tolyl) phosphine ($P(o\text{-}Tol)_3$, cone angle 198°). Numerous efforts at obtaining pure crystalline material of $(P(o\text{-}Tol)_3)Ag(1\text{-}H\text{-}closo\text{-}CB_{11}Me_{11})$ all failed. The only observed complexes involved stabilisation from solvent coordination (when solvents more Lewis basic than CH_2Cl_2 are utilised *e.g.*, acetone, Et_2O) or via phosphine disproportionation to yield $\{(P(o\text{-}Tol)_3)_2Ag\}^+$ (*vide infra.* – $^{31}P\{^1H\}$ NMR spectroscopy chemical shifts consistent with a linear bis phosphine adduct) and $Ag(1\text{-}H\text{-}closo\text{-}CB_{11}Me_{11})$ (again *vide infra.* with CH_3 signal broadening indicative of Ag···H_3C – discussed further in the solution studies section). This implies the phosphine is sterically shielding the Ag(I) centre enough that no single anion can approach to provide the apparently crucial stabilising anion-cation multiple interactions. (Figure 21). The prevention (or destabilisation) of close anion-cation contacts would generate an unsupported $\{(PR_3)Ag\}^+$ fragment (or only weakly supported by CH_2Cl_2 coordination) that without the close electrostatic intermolecular interactions appears inherently unstable.

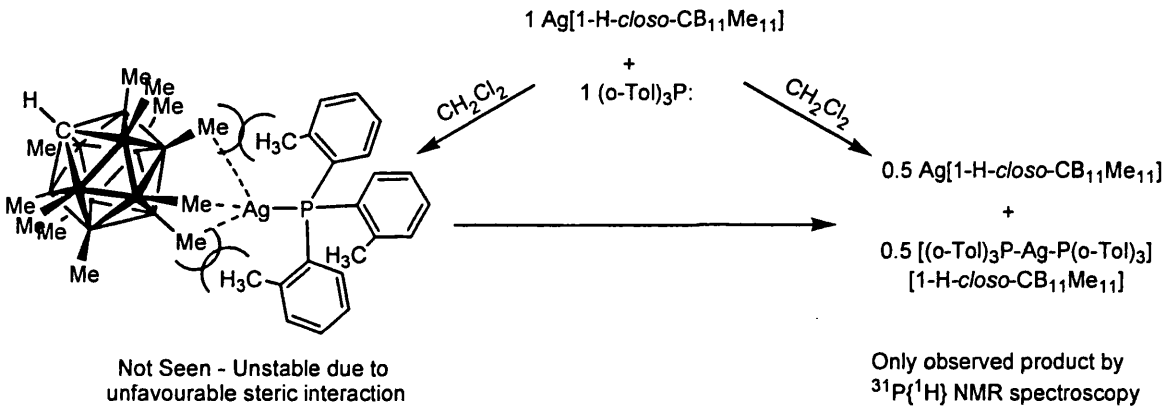

Figure 21: Dispropotionation mechanism for the formation of the observed products from the reaction of equimolar quantities of **(1)** and $(o\text{-}Tol)_3P$.

Complexes with less sterically demanding anions have been reported and are perfectly stable in the solution and the solid-state though even with anions as sterically unencumbered as NO_2^- the bulky $(o\text{-}Tol)_3P$ prevents any extended solid-state interactions and only monomers are observed.[58]

2.2.1.4:$(P(3,5\text{-}Me_2\text{-}C_6H_3)_3)Ag[1\text{-}H\text{-}closo\text{-}CB_{11}Me_{11}]$ (4):

Following the failure of increasing the phosphine cone angle as a methodology to eliminate the extended lattice contacts, an alternative but complementary approach was investigated. Re-examination of the extended structure of **(2)** (Figure 17) reveals that the *meta* – positions of the phenyl rings of the ancillary PPh_3 approach to within 3.6 Å to a number of CH_3 moieties on adjacent anions. It was thus reasoned that by the placement of suitable bulky groups in the 3,5 positions on the phenyl rings it would prevent external anions approaching and thus confine the Ag···H_3C interactions to a single carborane anion in the solid state. The slow addition of $P(3,5\text{-}Me_2\text{-}C_6H_3)_3$ to a slight excess (~1.1 equivalents) of **(1)** in CH_2Cl_2 and recrystallisation from CH_2Cl_2/pentane afforded extremely air and moisture sensitive crystals of lower than

desired quality. Despite repeated attempts, crystals of superior quality were unobtainable. A single crystal X-ray diffraction study was performed on the most likely candidate available and though they gave data of sufficient quality to define the gross features of **(4)** unambiguously (R_1 = 0.1008), it was inadequate for the free refinement of the hydrogen atoms.

The asymmetric unit of **(4)** (Figure 22) contains the $\{(P(3,5\text{-}Me_2\text{-}C_6H_3)_3)Ag\}^+$ fragment in close contact with a single [1-H-*closo*-$CB_{11}Me_{11}$]$^-$ anion. There is no positional disorder in the cluster allowing for the unequivocal assignment of the cage carbon. The silver centre is in relatively close proximity to two CH_3 vertices (Ag-C12 2.554(10) Å and Ag-C7 2.785(10) Å) and to one vertex by a longer connectivity (Ag-C8 3.166(10) Å). All fall within the combined ionic radius of Ag^+ and the van der-Waals radius of CH_3 (3.29 Å) and thus are considered to be significant. Inspection of the extended lattice reveals no anion approaches that are inside this stipulated limit; there is the possibility of one additional contact to an adjacent anion in the lattice (Ag-C2' 3.726 Å). This would be weak, if noteworthy at all, falling as it does outside the combined van der-Waals radii of CH_3 and Ag (3.70 Å).[35] Although this may still be the origin for the asymmetric orientation of the $\{PR_3Ag\}^+$ fragment over a triangular face of the anion. An alternative explanation for the asymmetric tridentate binding mode is possible, where the experimentally determined binding motif is energetically favourable compared to a symmetrical interaction over a triangular face. The approach of the C2' methyl observed in the extended lattice would then be attributable solely to efficient crystal packing. It would appear that increasing the steric bulk at the distal (with respect to Ag(I)) sites on the phenyl rings has switched off any major additional interactions. The reduction in electrostatic interactions is consequently compensated for by a

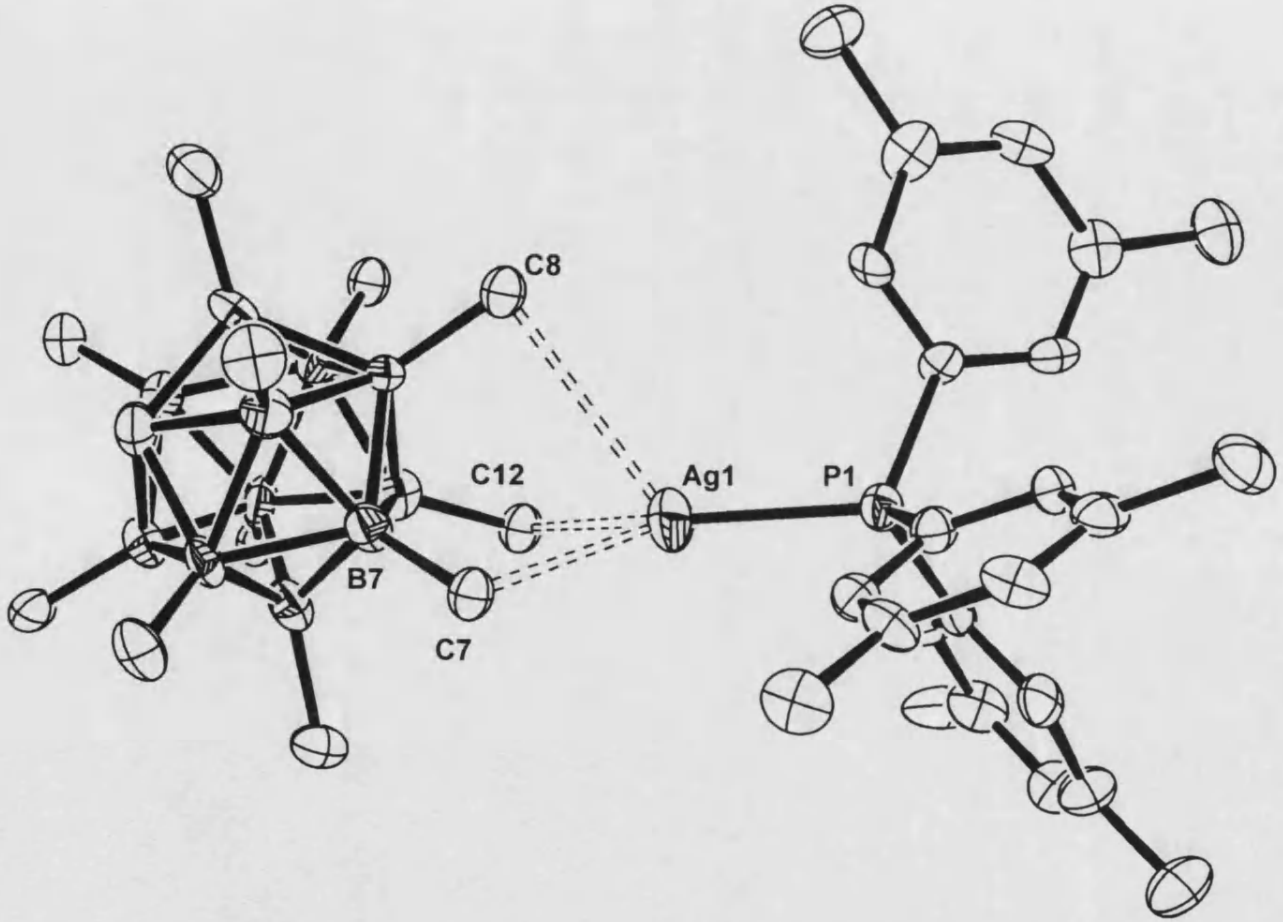

Figure 22: Molecular structure of $(P(3,5\text{-}Me_2\text{-}C_6H_3)_3)Ag[1\text{-}H\text{-}closo\text{-}CB_{11}Me_{11}]$ **(4)**, hydrogen positions removed for clarity (thermal ellipsoids at 30% probability level).

Ag-P	2.360(3)
Ag-C12	2.554(10)
Ag-C7	2.785(10)
Ag-C8	3.166(10)
C12-Ag-C7	83.5(3)
C12-Ag-C8	75.5(3)
C7-Ag-C8	71.7(3)
B12-C12-Ag	100.1(4)
B7-C7-Ag	96.5(5)
B8-C8-Ag	90.0(4)

Table 6: Selected bond lengths (Å) and angles (°) for **(4)**

reduction in the length (and concomitantly an increase in the strength) of the Ag-P bond in **(4)** (2.360(3)Å) compared to that established for **(2)** and **(3)** (2.3871(5)Å and 2.3881(4)Å respectively). Bearing in mind the significant associated errors, there appears to be no increase in the inter-methyl distances involved in the Ag connectivity in contrast to that observed for the simple lithium salt and to a degree in **(2)**.[19] The poor quality of the data set precludes any further meaningful investigation of the structural metrics associated with the anion cation interaction.

The gross structural silver coordination environment observed in **(4)** - namely an asymmetric tridentate motif is similar (albeit with closer Ag···H_3C contacts) to that observed in the extended structure of **(1)** and in that previously reported for [(η^6-C_6H_6)Li][*closo*-$CB_{11}Me_{12}$].[33] It is also not dissimilar to that noted for **(2)** and **(3)** both of which equally consist of three Ag···H_3C contacts. The main difference is that the steric blocking in **(4)** generates a situation where all three contacts can only originate from one anion. The structure of **(4)** provides further insight into the inherent instability of the analogous complex with ancillary *ortho*-tolyl phosphine ligation. Two of the phenyl *ortho* hydrogens are orientated towards the coordinated anion and are sufficiently close (3.181Å and 3.414Å – note that while high errors are associated due to the poor quality data set, they still indicate the close approach of the two groups) that on their replacement with CH_3 groups significant unfavourable steric interactions would be unavoidable. P-C bond rotation to project the ortho methyl groups away from the anion is not feasible due to the crowded environment created by the three-phenyl moieties in close proximity. As **(4)** is the only example where the interactions all stem from a single anion it is experimentally the closest to that expected to exist in the solution phase and

therefore can be viewed as a model for the solution behaviour of **(2)** to **(4)** as discussed next.

2.2.2: Ag···H_3C Interactions in the Solution Phase

The four complexes discussed so far all exhibit silver methyl interactions in the solid-state; it is of interest to investigate the behaviour of these compounds in weakly coordinating solutions. The use of a weak donor solvent would be expected to favour the formation of contact ion pairs whilst in acetone *solvento* complexes of the general formula [Ag(acetone)$_x$][Anion] would exist in preference.[5] A comparison of the $^1H\{^{11}B\}$ NMR spectra of **(1)** in a non-coordinating solvent (CD_2Cl_2, A) and a coordinating solvent (d_6 – acetone, B) is informative (Figure 23).

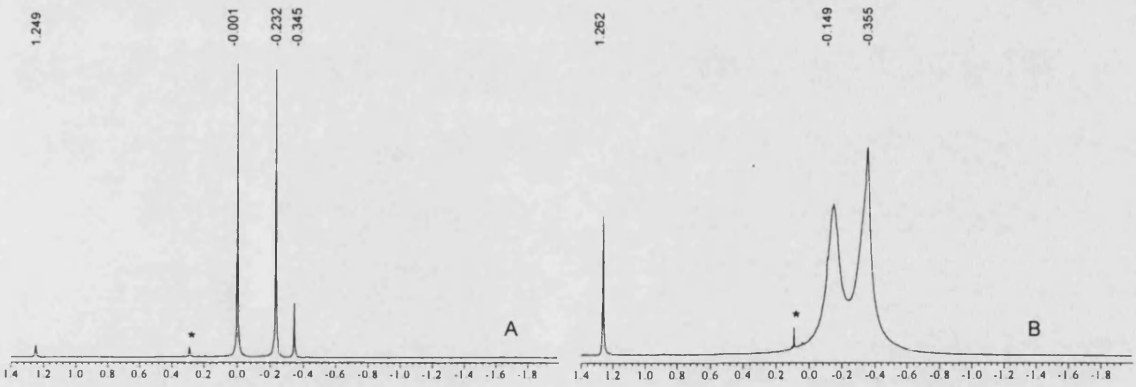

Figure 23: $^1H\{^{11}B\}$ NMR spectra of Ag[1-H-*closo*-$CB_{11}Me_{11}$] **(1)** in A: $(CD_3)_2C{=}O$ and B: CD_2Cl_2. * = minor impurity from silica grease.

For **(1)** in d_6 acetone, the anion CH_3 signals are sharp (frequency width at half magnitude (fwhm) ~ 1Hz) and the three inequivalent vertices are well resolved. The relative intensities observed are 15H:15H:3H as expected, with C_{5V} symmetry

maintained. This is further confirmed by examination of the ^{11}B NMR spectrum that consists of three singlets in a 1H:5H:5H ratio. In contrast the $^{1}H\{^{11}B\}$ spectrum of **(1)** in CD_2Cl_2 exhibits poorly defined signals for the three environments, significantly broadened (fwhm ~ 30Hz) suggesting that the Ag···H_3C interactions are persisting in solution. The signals for two of the inequivalent positions are coincident (most probably B7-11 and B12 methyl as these the most proximate) with observed relative intensities of 15H:18H. The ^{11}B NMR spectrum possessing C_{5V} indicates that on the NMR timescale the $\{(PPh_3)Ag\}^+$ is fluxional over the cluster periphery thereby making equivalent the pentagonal belt vertices. A comparison of the chemical shifts between A and B is not valid due to undetermined solvent effects inherent in NMR spectra collected in different solvents. A more suitable assessment of the chemical shift change of **(1)** in contact with the $\{(PPh_3)Ag\}^+$ fragment is possible using the relevant shifts from the non-coordinating salt $^{n}Bu_4N[1\text{-H-}closo\text{-}CB_{11}Me_{11}]$ in the same solvent, CD_2Cl_2 (Figure 24).

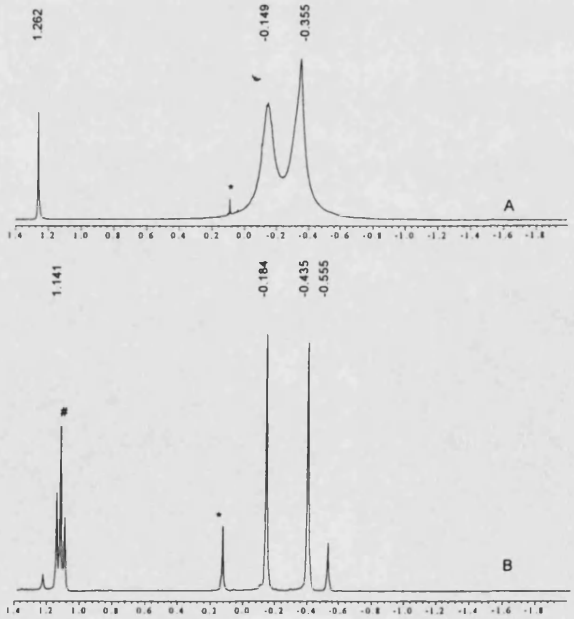

Figure 24: $^{1}H\{^{11}B\}$ NMR spectra of A: Ag[1-H-*closo*-$CB_{11}Me_{11}$] and B: [$^{n}Bu_4N$][1-H-*closo*-$CB_{11}Me_{11}$] in CD_2Cl_2 solutions. * = minor impurity from silicone grease, # = NCH_2 from ammonium cation.

Changing the cation from $[^nBu_4N]^+$ to Ag^+ results in the same broadening in the line widths associated with the B-CH_3 resonances as moving from acetone to CD_2Cl_2. Additionally, there is a small downfield shift, predominantly of the antipodal vertex (of –0.2ppm) and a related lesser shift of the lower pentagonal belt protons (assuming the signal at –0.355 is due to the BCH_3 (7-11) vertices see later), resulting in the compression of the signals related to the anion. The upper pentagonal belt proton chemical shift in **(1)**, by contrast, remains virtually identical to that observed for the non-interacting cation though it is significantly broadened. The exact unequivocal characterisation of each methyl resonance and in depth discussion of the behaviour is presented later for the mono phosphine complexes **(2)** to **(4)**.

The addition to CD_2Cl_2 solutions of **(1)** of less than two molar equivalents of a more coordinating solvent (e.g. toluene, MeCN, H_2O and Et_2O) reduces the broadening observed in the cluster methyl groups and a concomitant downfield shift in the solvent signal relative to 'free' non coordinated solvent. An exemplary example of this is in $^1H\{^{11}B\}$ NMR spectra of **(1)** in the presence of one equivalent of Et_2O. The etherate protons are deshielded by 1.12 ppm and 0.47 ppm (relative to non coordinated Et_2O in CD_2Cl_2, 3.48 and 1.20 ppm) indicative of metal coordination.[12, 13] A suggested structure is shown in Figure 25, with the reduced degree of coordination of the anion the likely source of the slightly sharper CH_3 resonances.

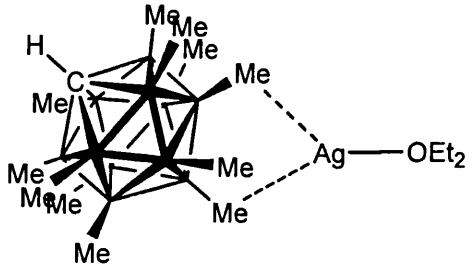

Figure 25: A plausible solution structure of Et_2O:Ag(1-H-*closo*-$CB_{11}Me_{11}$)

Similar anion displacement by Et_2O and MeCN has been reported in the mixed metal complex $[Me_2Pt(\mu\text{-}L)_2Ag_2(solv)_x][Y]_2$ (L = 2,6-bis(diphenylphosphino)pyridine, solv = Et_2O or MeCN, x = 1 or 2 and Y = ClO_4^- or BF_4^-) and both solvento complexes have been crystallographically characterised.[59] The reaction of $Ag[Al(OC(CF_3)_3)_4]^-$ with three stoichiometric equivalents of ethene in dichloromethane yielded the tri ligated product $(\eta^2\text{-}C_2H_4)_3Ag[Al(OC(CF_3)_3)_4]$[1] that can be viewed as a model for the solvated structures of Ag[1-H-*closo*-$CB_{11}Me_{11}$] in coordinating solvent and also exhibits a downfield shift of the ligated solvent.[2] Attempts to dissolve **(1)** in hydrocarbon solvents failed, with no detectable solubility even in hot cyclohexane. The same behaviour was observed for all the silver (I) salts compounds discussed in this chapter.

Analogous line broadening and downfield chemical shift changes are observed for compounds **(2)** to **(4)** and due to their related behaviour the three compounds will be discussed together. On comparison of the chemical shifts for **(2)**, **(3)** and **(4)** to [^{n}Bu$_4$N][1-H-*closo*-$CB_{11}Me_{11}$] all experience a line broadening effect and a downfield shift for the cluster methyl protons – as demonstrated for **(2)** by Figure 26 ((**3**) and **(4)** are effectively indistinguishable in this spectral region).

The key noteworthy points are: (i) the increase in line width to *ca.* 30 Hz (fwhm); and (ii) the ordering of the methyl region, with the relative intensities of each signal being 15H:3H:15H in contrast to that noted for the $[^nBu_4N]^+$ salt (15H:15H:3H). This correlates to a 5:1:5 ratio of the cluster methyl groups, with unequal shifting of the inequivalent positions. The C_{5V} symmetry apparent in the $^1H\{^{11}B\}$ NMR spectra is corroborated by the ^{11}B NMR spectra of each of these compounds that all have 1:5:5 comparative intensities.

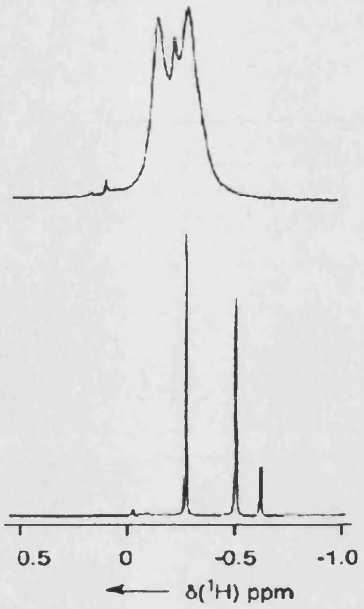

Figure 26: $^{1}H\{^{11}B\}$ NMR spectrum (CD_2Cl_2) of the methyl region of complex **(2)** (top) and [$^{n}Bu_4N$][1-H-*closo*-$CB_{11}Me_{11}$] (bottom).

There are only slight changes in the chemical shifts to higher field for **(2)** to **(4)** when compared to the ^{11}B NMR spectrum for [$^{n}Bu_4N$][1-H-*closo*-$CB_{11}Me_{11}$], demonstrating that the bonding interaction predominantly involves the peripheral methyl groups, with the interior boron cluster effectively screened. This is in contrast to metal complexes of the [*closo*-$CB_{11}H_{12}$]$^-$ anion where there are intimate B···M associations and correspondingly significant upfield shifts.[25, 26, 60] As expected in the ^{1}H NMR spectrum there is considerable additional line broadening due to quadrupolar relaxation from ^{11}B – this effect is also seen with non-interacting cations (e.g. Cs^+/NR_4^+ salts).

There are two possibilities that can equally account for the observed methyl signal arrangement in the $^{1}H\{^{11}B\}$ NMR spectrum: an ordering (low field to high field) of BCH_3(7-11), BCH_3(12) then BCH_3(2-6); or, alternatively, BCH_3(2-6), BCH_3(12) then

BCH_3(7-11). The antipodal signal is unequivocally characterised as the intermediate peak by its fivefold reduced integral. To resolve unambiguously the uncertainty in the identification of each pentagonal belt signal for complexes **(2)**, **(3)** and **(4)** two alternative yet complimentary experiments were undertaken: $^1H\{^{11}B_{selective}\}$ NMR spectroscopy and a combination of ^{11}B-^{11}B COSY and ^1H-^{11}B HMQC NMR spectroscopy. The need for the explicit identification of peak position is crucial as the degree of $CH_3\cdots Ag$ interaction in this system is defined by the scale of broadening and magnitude of the downfield chemical shift of the involved BCH_3 vertex. Therefore, identification of the individual resonances and the extent of the change in chemical shift (respective to the $[^nBu_4]^+$ salt) will give an indication to the degree of interaction of each inequivalent anion position (i.e. a larger chemical shift change implies a stronger $Ag\cdots H_3C$ associated with that vertex).

Regrettably the two complimentary methods do not corroborate each other. The $^1H\{^{11}B_{selective}\}$ spectrum of **(2)** appeared to give the sequence C7-11: C12: C2-6 (from downfield to highfield). This conclusion was reached by the extent of line sharpening of individual peaks on the decoupling of a specific boron signal. However, this experiment was somewhat ambiguous due to the overlapping signals and only small differences in respective line widths generating an inherent uncertainty in these results. The conclusions from the 2D correlation spectroscopy were found to be more reliable. To verify the validity of this methodology the experiment was initially performed on CD_2Cl_2 solutions of $[^nBu_4N]$ and $[Cs]^+$ [1-H-*closo*-$CB_{11}Me_{11}$] and both gave identical conclusions. The relevant spectra for the $[^nBu_4N]^+$ salt are shown in Figure 27.

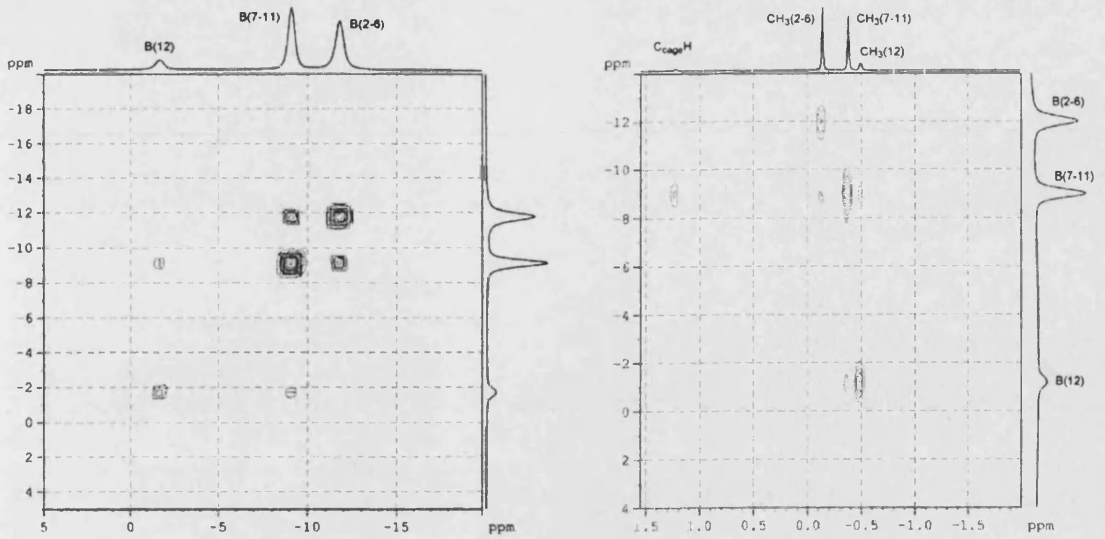

Figure 27: A standard ^{11}B-^{11}B COSY indistinguishable for all compounds (left), ^{1}H-^{11}B HMQC for $[^{n}Bu_4N][1\text{-H-}closo\text{-}CB_{11}Me_{11}]$

The boron vertices in the ^{11}B NMR spectra are easily assigned by the ^{11}B-^{11}B COSY experiment as B12, B7-11 and B2-6 (from downfield to high field), with only the B7-11 positions exhibiting a correlation to the other two resonances. The ^{1}H – ^{11}B HMQC experiment for $[^{n}Bu_4N][1\text{-H-}closo\text{-}CB_{11}Me_{11}]$ is equally clear-cut. The relative assignments from cross peaks are as follows (low field to high field) BCH_3(2-6), BCH_3(7-11) and BCH_3(12). It is interesting to note that the lower pentagonal belt borons (B7-11) have a long range correlation with the cage C-H vertex and all three inequivalent CH_3 positions in the cluster (albeit with a much reduced intensity to the correlation with its individual CH_3 resonance). Attempts to run HMQC experiments on **(2)** and **(3)** failed and so the assignment is solely from the analysis of **(4)**.

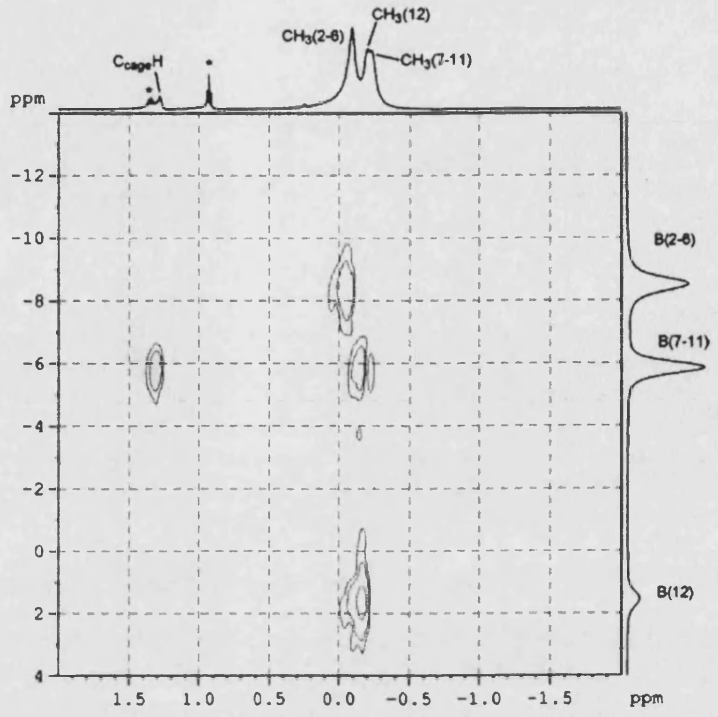

Figure 28: ^{1}H-^{11}B HMQC spectrum of complex **4**. Peaks marked with an asterisk arise from residual pentane from recrystallisation.

Figure 28 shows the ^{1}H-^{11}B HMQC for compound **(4)** and the assignment proceeds as follows: B12 correlates to the central CH_3 signal -supported by this integral measuring only to 3H. The B2-6 cross-peak connects with the methyl signal furthest down field unambiguously identifying this as CH_3(2-6). The remaining resonance (upfield 15H integral signal) by both the process of elimination and by correlation is therefore attributed to the protons CH_3(7-11). Again long range interactions between B7-11 and CH_3(2-6) and the cage C-H are observed, but due to their presence in the $[^{n}Bu_4N]^{+}$ spectra are not indicative of any metal coordination *per se*.

With the unequivocal assignment of the vertices achieved it is now possible to discuss the degree of chemical shift change for each compound in comparison to $[^{n}Bu_4N][1\text{-H-}closo\text{-}CB_{11}Me_{11}]$. All three methyl resonances are shifted downfield on

metal coordination, CH_3(2-6) the least (average 0.06 ppm), followed by CH_3(7-11) (av. 0.18 ppm). The most significant shift is that involving the antipodal position CH_3(12) (average 0.33 ppm). This has the effect of altering the relative positions of the three signals producing the experimental 5:1:5 integral ratio (Table 6).

Compound	Chemical Shift δ		
	CH_3(2-6)	CH_3(7-11)	CH_3(12)
$[^nBu_4N][1\text{-H-}CB_{11}Me_{11}]$	-0.18	-0.43	-0.55
$(PPh_3)Ag[1\text{-H-}CB_{11}Me_{11}]$	-0.14(0.04)	-0.28(0.15)	-0.22(0.33)
$(PCy_3)Ag[1\text{-H-}CB_{11}Me_{11}]$	-0.13(0.05)	-0.23(0.2)*	-0.23(0.32)*
$(P(3,5\text{-}Me_2\text{-}C_6H_3)_3)Ag[1\text{-H-}CB_{11}Me_{11}]$	-0.08(0.1)	-0.23(0.2)	-0.21(0.34)

Table 6: The chemical shift of the anion methyl resonances for **(2)**, **(3)**, **(4)** and $[^nBu_4N][1\text{-H-}closo\text{-}CB_{11}Me_{11}]$. Values in parentheses indicate degree of chemical shift relative to the 'free anion'. * =denotes coincidental signals.

A number of observations can be made from the data listed in Table 6 – firstly and perhaps most noteworthy is the similarity in the chemical shifts of **(2)**, **(3)** and **(4)** considering the disparate nature of their crystalline structures. This is a strong indicator that the solution $\{(PR_3)Ag\}^+\cdots$anion coordination in the three systems is indistinguishable, implying the loss of the extended interactions in **(2)** and **(3)** and a possible solution phase structure approximating to that of the solid-state structure of **(4)**. Examining the degree of chemical shift change it is noted that it increases in the direction CH_3(2-6) < CH_3(7-11) < CH_3(12), suggesting that the silver fragment experiences a greater interaction with the antipodal vertex in solution. That all resonances are broadened and shifted demonstrates that the $\{(PR_3)Ag\}^+$ moiety is in contact with each inequivalent position, a fluxional process over the entire BCH_3 periphery on the NMR time scale. The origin of the broadening effect on metal coordination remains ill-defined and could arise from unresolved $^{109/107}$Ag-H coupling or an undetermined relaxation mechanism associated with the proximate silver

phosphine fragment. Slow molecular tumbling induced broadening of the large contact ion pair can be discounted due to the sharp well-defined signals associated with the various phosphine ligands. In each case no ^{1}J (AgH) coupling was visible despite bridging hydrides have coupling constants of the magnitude of 70 – 20Hz.[61-63]

Definitive confirmation that the $CH_3\cdots Ag$ interactions are maintained in solution could not be provided by $^{1}H\{^{109}Ag\}$ NMR spectroscopy due to the failure to locate the silver signal despite numerous attempts. Instead the downfield shift and significant broadening do provide sufficient proof of the persistence of these contacts in the homogeneous environment. Additional confirmation is provided by the disruption of this interaction by the presence of any greater Lewis basic molecule (discussed shortly). $^{13}C\{^{1}H\}$ NMR studies on these systems revealed no pertinent information on the solution coordination – the BCH_3 resonance appear as a broad coincident signal with no chemical shift change compared to [$^{n}Bu_4N$][1-H-*closo*-$CB_{11}Me_{11}$] and no determinable coupling constants in the $^{13}C\{^{1}H\}$ NMR spectrum. Cooling CD_2Cl_2 solutions of **(2)** – **(4)** to 190K did not freeze out the fluxionality, with C_{5v} symmetry maintained. The broadening is reduced somewhat, (partially attributable to the thermal decoupling of boron) and there is a general upfield shift for signals corresponding to the methyl resonances to lie between that for **(2)** and [$^{n}Bu_4N$][1-H-*closo*-$CB_{11}Me_{11}$]. This data suggests that at low temperatures the $Ag\cdots H_3C$ interactions are reduced – possibly by the formation of a solvent complex of the type $(PPh_3)Ag(CH_2Cl_2)$(1-H-*closo*-$CB_{11}Me_{11}$). The gradual heating of **(2)** to temperatures above 40°C rapidly lead to complex decomposition by ^{1}H, ^{11}B and $^{31}P\{^{1}H\}$ NMR spectroscopy to unidentified and intractable products. The anion by both $^{1}H\{^{11}B\}$ and ^{11}B NMR spectroscopy was severely degraded with numerous cage environments visible. The metal coordination is

therefore activating the cage towards methyl abstraction and further reactivity, as observed for the lithium and silyl salts of the related anion [*closo*-$CB_{11}Me_{12}$]$^-$.[19, 64] Simple alkali salts of [1-H-*closo*-$CB_{11}Me_{11}$]$^-$ are stable in solution up to high temperatures and in the solid state to above 200°C.[32]

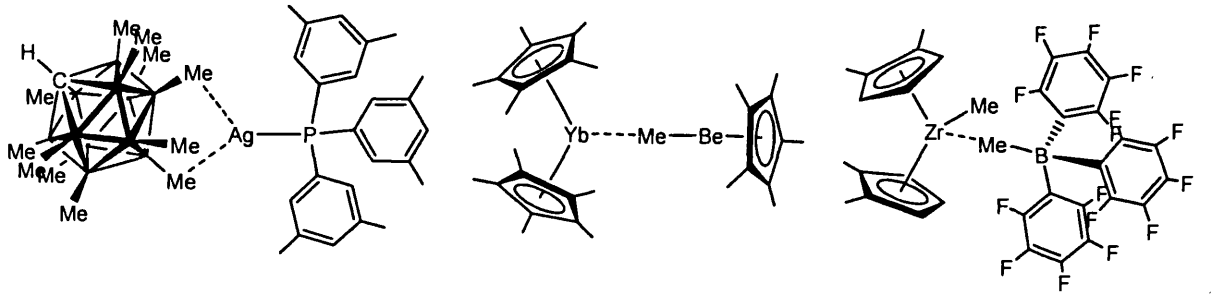

Figure 29: Examples of complexes that exhibit chemical shift changes of the metal coordinated methyl group, **(4)**, $Cp^*_2Yb(\mu\text{-}Me)BeCp^*$ and $(1,2\text{-}Me_2\text{-}C_5H_3)_2ZrMe(\mu\text{-}Me)B(C_6F_5)_3$.

Literature precedence for a downfield shift on methyl coordination to a metal comes from the complex $(\eta^5\text{-}C_5Me_5)_2Yb(\mu\text{-}Me)Be(\eta^5\text{-}C_5Me_5)$ (Figure 29), that has been crystallographically determined to involve an Yb-CH_3···Be bridging (μ-Me) motif. The similar downfield shift on coordination (compared to Me-Be(η^5-C_5Me_5)) of 0.1ppm was described as predominantly electrostatic in origin. In contrast, agostic interactions with metal complexes with a d electron count > 0, display upfield shifts of the coordinated CH_3 groups.[65] A more applicable comparison utilises the analogous intermolecular interaction between a metal centre and an anion bound methyl group in $[MeB(C_6F_5)_3]^-$. A CSD database search on structurally characterised contact ion pair complexes revealed 19 transition metal complexes with $L_nM\text{-}(\mu\text{-}Me)\text{-}B(C_6F_5)_3$ structures (M predominantly is Zr,[50, 66-77] but also includes Nb,[78] Ti,[79-81] Y,[52] and Hf[82]). In the solution studies these complexes all demonstrated an upfield shift of the (μ-Me) moiety in comparison to that of the free $[MeB(C_6F_5)_3]^-$ anion and in contrast to that observed in **(1)** to **(4)**.[83] This behaviour may be ascribed to the disparate metal involved,

with upfield shifts occurring with hard d^0 metals whilst for the softer $[Ag]^+$ d^{10} configuration a downfield shift is consistently observed. The behaviour of d^0 complexes and other polymerisation pre-catalysts with bridging (μ-Me) moieties will be discussed further in the Chapter Three.

Compounds **(2)** and **(3)** display the expected doublet of doublets in the room temperature $^{31}P\{^1H\}$ NMR spectrum (each single phosphorus environment is coupling to both ^{109}Ag and ^{107}Ag, I=½ relative abundance 51.8% and 48.2% respectively). The $^{31}P\{^1H\}$ NMR spectrum for complex **(4)** in contrast is a poorly defined doublet, with the individual $^{107/109}Ag$-P coupling not visible. The average J(AgP) at 731 Hz is less than that for **(2)** and **(3)**. As stated previously the $^{31}P\{^1H\}$ NMR of these complexes is indicative of the Ag-P bond strength and concomitantly the degree of Ag···anion interactions. The ^1J coupling constants for **(2)** and **(3)** at 824 Hz and 766 Hz respectively are amongst the highest reported for Ag(I) phosphine complexes,[84] indicative of very strong Ag-P bond and a low coordinate Ag(I) with a weak anion···cation interaction. A comparison of the coupling constant of complex **(2)** with $\{(PPh_3)Ag\}^+$ fragments partnered with related carborane mono anions positions **(2)** as the most weakly coordinating in this series with an average ^1J Ag-P significantly higher than that for the previously lowest nucleophilic carborane [*closo*-$CB_{11}H_6Cl_6]^-$ (761 Hz).[26] Broadened $^{31}P\{^1H\}$ signals are often indicative of fluxionality at room temperature on the NMR time scale – the observed broad, poorly resolved spectrum for **(4)** therefore suggests that there is an exchange process occurring here.[85] A plausible mechanism for this is that **(4)** is in equilibrium between an anion coordinated complex and a *solvento* complex (Figure 30). Support for this hypothesis comes from the isolation of stable Ag(I)···CH_2Cl_2 complexes with other weakly coordinating anions.[1, 7, 8]

Low temperature NMR data on **(2)**, where there is significant line sharpening indicative of less intimate Ag···H_3C contacts and (as will be discussed later) the displacement of [1-H-*closo*-$CB_{11}Me_{11}$]$^-$ by other weak donor solvents (*e.g.*, Et_2O).

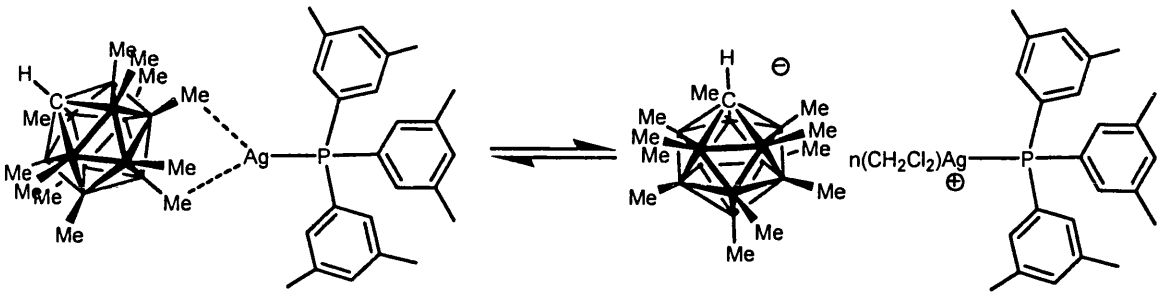

Figure 30: Possible solution behaviour of **(4)** an explanation for the observed fluxionality.

The distinct solution behaviour of **(4)** in comparison to **(2)** and **(3)** may be a result of its inability to form extended contacts to more than one anion. Although these can be expected to be weak they may result in [(PR_3)Ag(1-H-*closo*-$CB_{11}Me_{11}$)] (R = Ph or Cy) persisting as a dimer (or an oligomer) in solution. A dimeric solid-state structure has previously been reported for the related system [$(PPh_3)_2$Ag(*closo*-$CB_{11}H_{12}$)] so they are feasible entities.[27]

The solid state and solution infra-red spectra of **(2)** give little information. There is no decrease in the frequency of the major signals when **(2)** is compared to a non-interacting cation, signifying no weakening of the C-H bond. This is in line with a predominantly ionic contribution to the Ag···anion interaction.

2.2.3: DFT Calculations

DFT calculations on the isolated anion [1-H-*closo*-$CB_{11}Me_{11}$]$^-$ and complex **(2)** have been performed by Dr Gus Ruggerio (University of Bath) at the B3LYP/DZVP level. Calculated charges of the three inequivalent B-CH_3 vertices in [1-H-*closo*-$CB_{11}Me_{11}$]$^-$ closely correlate with that previously reported independently by McKee (B3LYP/6-31* level) and Michl and co-workers (B3LYP/SDD level).[34, 86] The lower pentagonal belt vertices (BCH_3 7-11) carry the greatest negative charge (-0.13), the antipodal only slightly less (-0.09) whilst the upper pentagonal belt B-CH_3 groups are positive (+0.07). Therefore, from a purely electrostatic approach, cations such as $\{(PR_3)Ag\}^+$ would be expected to interact most favourably with BCH_3(7-11). However, this does not take into account multiple M···H_3C interactions and any (albeit small) covalent contributions with a metal fragment.

	[1-H-*closo*-$CB_{11}Me_{11}H$]$^-$ charge (NBO)	[*closo*-$CB_{11}Me_{12}$]$^-$ (NPA) Charges	(NBO) Charges
vertex	BCH_3	BCH_3	BCH_3
12	-0.09	-0.1	-0.09
7 to 11	-0.13	-0.14	-0.15
2 to 6	0.07	0.05	0.11

Table 7: Comparison of Charges (from NBO/NPA) analysis on the anions [1-H-*closo*-$CB_{11}Me_{11}$]$^-$ and [*closo*-$CB_{11}Me_{12}$]$^-$.[34, 86]

Calculations by the Michl group have demonstrated that a simple electrostatic model does not predict the more stable isomer, with calculations on [Me_3Sn][*closo*-$CB_{11}Me_{12}$] finding that the 12-isomer is the energetic minimum even though the 7-11 vertices carry more negative charge. There are similar energetics reported for the unmethylated parent carborane anion [*closo*-$CB_{11}H_{12}$]$^-$, where calculations suggest a greater magnitude of electron density at the lower pentagonal belt but reactivity

(specifically the selective halogenation) suggests the 12 position is the most negative.[87] The calculated energies of the three possible monodentate isomers of [(PPh_3)Ag(1-H-*closo*-$CB_{11}Me_{11}$)] and a tridentate motif, as seen for **(4)**, are shown in Figure 30. In agreement with the calculations on Me_3Sn(*closo*-$CB_{11}Me_{12}$), the relative energies of the three mono-dentate structures for **(2)** show that the 12-isomer is marginally energetically favoured over the 7-isomer by 1.9 kcal mol^{-1}, with the 2-isomer a further 4.3 kcal mol^{-1} higher. The optimised geometries for these three bonding modes are all essentially end on with a slight elongation of the associated B-C bond (1.64 Å compared to an average 1.60 Å calculated in free anion and 1.589(4) – 1.606(4) Å in a number of experimentally determined structures) and a minor flattening of the B-C-H angles away from tetrahedral (106 -107°). The slight deformation of the bonding vertices are possibly an indication of a small sigma covalent interaction between H_3C and the Ag(I) cation. These geometries are not observed in the solid-state structures with the extended lattice interactions distorting the local Ag(I) environment and producing the observed packing arrangement in **(2)** and **(3)**. Complex **(4)** displays no such extended interactions existing in the crystalline phase as a triangular face bridged arrangement (μ-7,8,12) – albeit with a slight asymmetry in the binding towards the 7,8 positions. This structure is a better model for gas phase calculations, as it involves no intermolecular interactions.

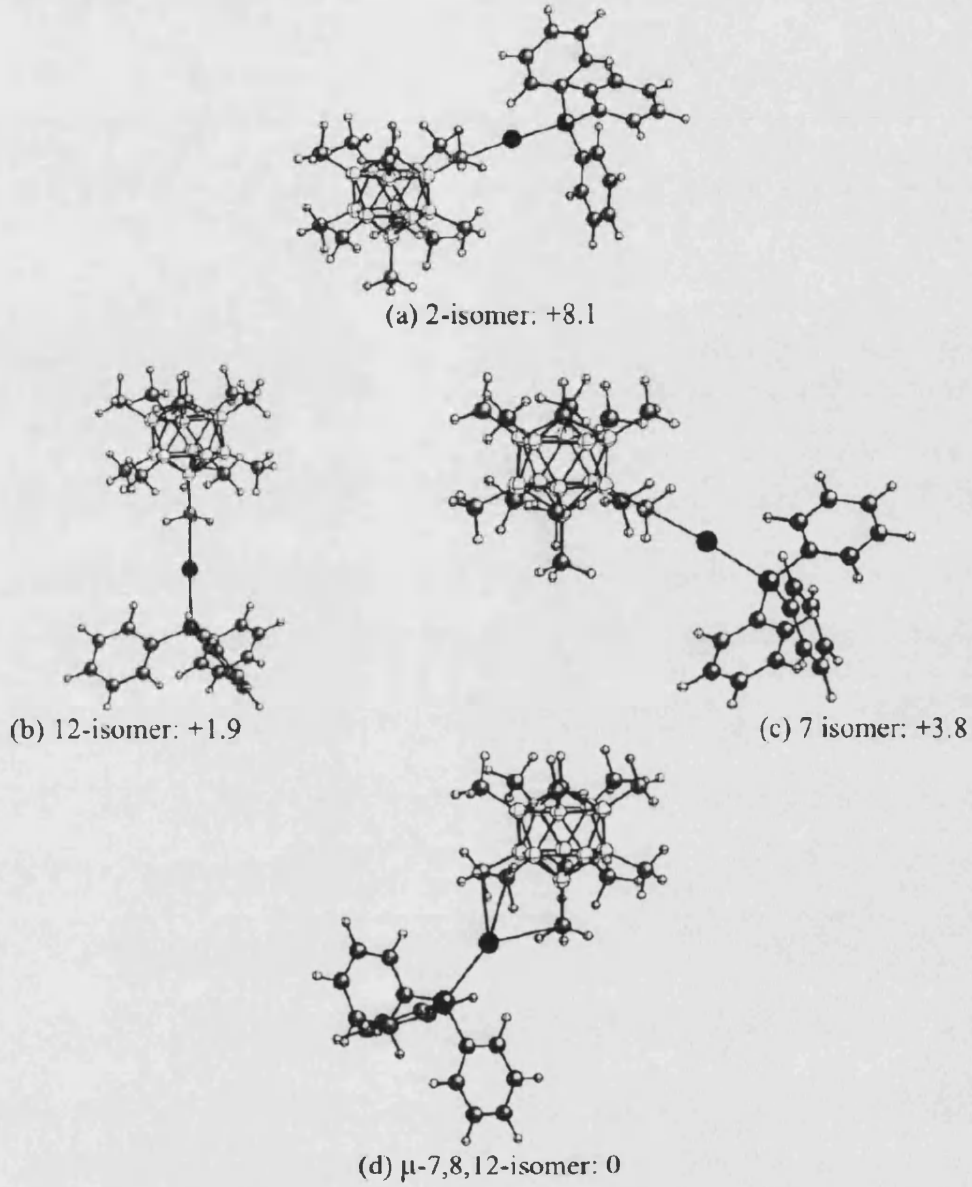

Figure 31: DFT optimised structures (B3LYP/DZVP level) of the isomers of **(2)**. Energies (kcal mol^{-1}) are given relative to the calculated most stable isomer, (μ-7,8,12-isomer).

Calculations on this isomeric form yielded a new energy minima 1.9 kcal mol^{-1} below that of the 12-isomer. The (μ-7,8,12) isomer exhibits no lengthening of the three complexed BCH_3 vertices when compared to the calculated structure of the free anion (1.60 Å) or structurally determined bond lengths. Specific comparisons between the structural metrics of the calculated (μ-7,8,12) isomer and those observed for **(4)** are not

warranted due to the high errors associated with **(4)** and the single extended contact in the solid state that may well have a small influence on the observed structure.

Transition state calculations on the potential energy surface between these isomeric forms were not carried out on this system due to the large number of atoms involved. The fact that the slow exchange regime is not reached even at 190 K is an indication of the low barriers inherent in the migration of the metal fragment over the cage periphery. This combined with the low energy difference between the tridentate and mono-dentate isomers provide a possible mechanism for fluxionality pathway and the observed C_{5V} symmetry (Figure 32).

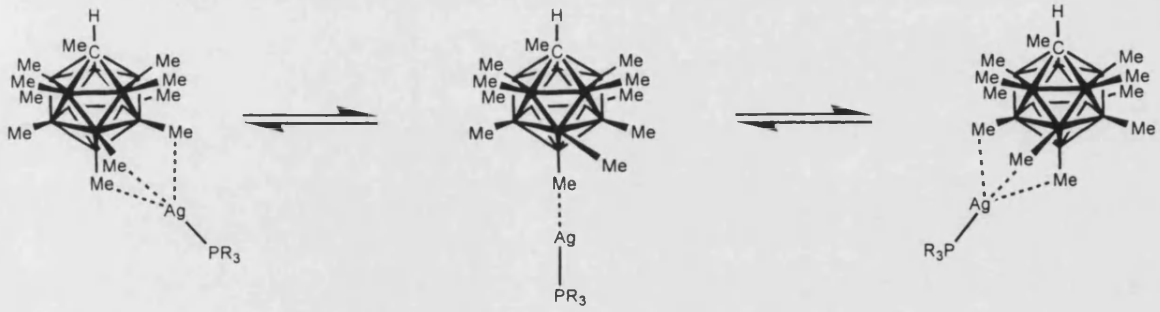

Figure 32: Possible mechanism for the solution fluxionality of $(PR_3)Ag(1\text{-H-}closo\text{-}CB_{11}Me_{11})$ supported by DFT calculations on low energy conformers.

A alternative mechanism via a bidentate coordinated $\{(PR_3)Ag\}^+$ fragment cannot be discounted – this type of bonding motif has not been computationally investigated. The low barriers to fluxionality and the small energy differences between all four isomers (maximum of 8.1 kcal mol^{-1}) explain the observed broadening of all three methyl vertices in the $^1H\{^{11}B\}$ NMR spectrum as each position is easily accessible. The 2-isomer, calculated as the energetically least favourable interaction, is supported by solution studies with this position exhibiting the least downfield chemical shift change. That the 12-isomer is perturbed to a greater extent than the 7-isomer is

again corroborated by the respective calculated energies – though the degree of shift for the 7-isomer may be artificially low due to averaging over the five equivalent positions (two vertices interacting and three innocent at any one time).

2.2.4. Reactions of $(PPh_3)Ag(1\text{-}H\text{-}closo\text{-}CB_{11}Me_{11})$ with Lewis bases

The reactivity of **(2)** with respect to other anions and additional Lewis bases was investigated to provide further information on the strength of the Ag···H_3C interaction. Initial studies examined the effect of solvents other than CH_2Cl_2 on the persistence of the anion cation interactions. The first indication for the ready displacement of [1-H-*closo*-$CB_{11}Me_{11}]^-$ came from the d_6-acetone solution of **(2)**. Unsurprisingly the methyl region of the ^1H NMR was now sharp (fwhm ~1Hz) with three well resolved resonances in a 15H:15H:3H integral ratio confirming that the anion has C_{5V} symmetry. This is verified by the ^{11}B NMR spectrum exhibiting a 1:5:5 ratio. The $^{31}P\{^1H\}$ NMR spectrum displays the expected concentric doublet of doublets but with a decrease in the $^1J(AgP)$ coupling (average $^1J(AgP)$ of 762 Hz), characteristic of the presence of a stronger coordinated ligand(s). Analogous anion displacement from the coordination environment of silver by excess acetone has previously been observed for the simple silver salt **(1)** and for related carborane mono anions.[5] The observed coupling constant falls between that for $(PPh_3)Ag(closo\text{-}CB_{11}H_6Br_6)$ (711 Hz) and $(PPh_3)Ag(closo\text{-}CB_{11}H_6Cl_6)$ (770 Hz) where, in each case the Ag(I) centre is tri-coordinated to the anion through three halogen atoms sharing a triangular face (see Introduction). Due to the similar electronegativities of Cl and O (3.16 and 3.44 respectively) and an analogous degree of polarisation of the $C^{\delta+}=O^{\delta-}$ bond (electronegativity difference 0.89) compared

to the $B^{\delta+}$-$Cl^{\delta-}$ bond (electronegativity difference 1.12)[43] the similar observed J(AgP) coupling constants in the solution structures of $(PPh_3)Ag(closo\text{-}CB_{11}H_6Cl_6)$ and $[(PPh_3)Ag(acetone)_n][1\text{-}H\text{-}closo\text{-}CB_{11}Me_{11}]$ must make them closely related.

On the addition of three equivalents of Et_2O to a CD_2Cl_2 solution of **(2)** an analogous switching off of the cage-metal interaction occurs by $^1H\{^{11}B\}$ NMR spectroscopy, along with a concomitant reduction in the $^1J(AgP)$ coupling constant to 801 Hz. Crystals suitable for X-ray diffraction analysis were obtained from the slow diffusion of pentane into a concentrated etherate solution of **(2)**. The asymmetric unit consists of two crystallographically independent $[(PPh_3)Ag][1\text{-}H\text{-}closo\text{-}CB_{11}Me_{11}]$ fragments, in which each Ag(I) cation is coordinated to two Et_2O molecules (Figure 33). The structural metrics for both independent molecules of $[(PPh_3)Ag(OEt_2)_2][1\text{-}H\text{-}closo\text{-}CB_{11}Me_{11}]$ **(5)** are essentially identical within errors and will be discussed together.

The coordination environment around the Ag(I) centres appears to be a distorted trigonal planar geometry, with the sum of angles around each silver (360.0(2)° and 358.4(2)°) approximating to 360°. The O-Ag-O angle, however, is significantly depressed (94.0(2)° and 89.4(2)°) in each moiety. Examination of the extended lattice environment proximate to the Ag(I) centres reveals close approaches of two adjacent anions to each silver. The distances (Ag1-C9' 3.466 Å, Ag1-C6'' 3.675 Å, Ag2-C24' 3.569 Å and Ag2-C21'' 4.235 Å) are all outside the earlier stated prerequisite for a significant interaction (3.29 Å). Three of the contacts do, however, fall within the combined (3.70Å) van der-Waals radii of CH_3 (2.00Å) and Ag (1.70Å) suggestive of a weak interaction.[43] The silver etherate orientation lend support to the existence and significance of this interaction. The Ag-O distances for the four coordinated ether

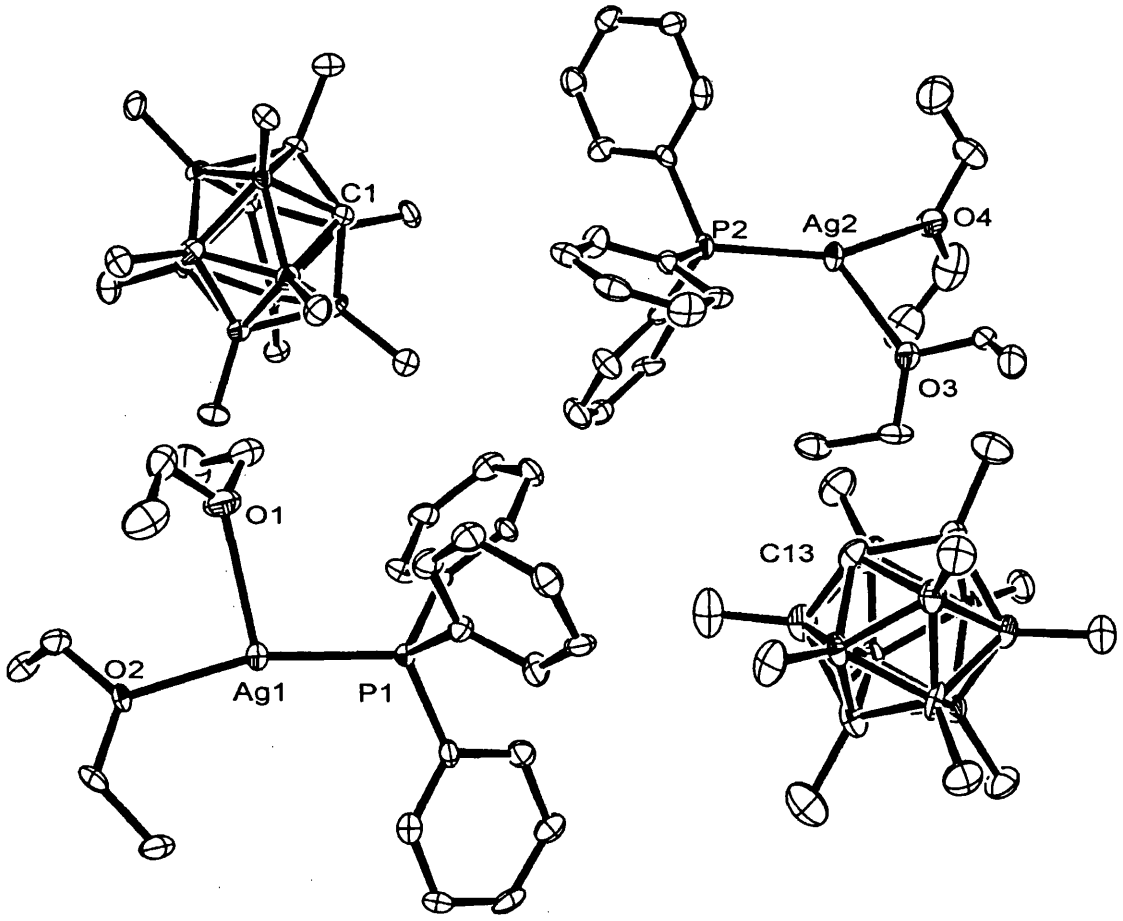

Ag1-P1	2.377(2)	Ag2-P2	2.362(2)
Ag1-O1	2.539(7)	Ag2-O3	2.418(6)
Ag1-O2	2.248(6)	Ag2-O4	2.291(8)
P1-Ag1-O1	103.13(19)	P2-Ag2-O3	122.70(18)
P1-Ag-1-O2	162.86(17)	P2-Ag2-O4	146.3(2)
O2-Ag-O1	94.0(2)	O3-Ag2-O4	89.4(2)
Sum of angles around Ag1	360.0(2)	Sum of angles around Ag2	358.4(2)

Table 8: Selected Bond Lengths (Å) and angles (°) for **(5)**

Figure 33: Molecular Structure of both crystallographically independent molecules in the asymmetric unit of $[(PPh_3)Ag(OEt_2)_2][1\text{-H-}closo\text{-}CB_{11}Me_{11}]$, **(5)**. Hydrogen atoms removed for clarity (thermal ellipsoids shown at 30% probability level).

molecules are disparate, involving one short contact (Ag1-O2 2.248(6) and Ag2-O4 2.291(8)Å) and one long contact (Ag1-O1 2.539(7) and Ag2-O3 2.418(6)Å). The inequivalent nature of the bound ethers is further demonstrated by a closer inspection of the immediate silver coordination sphere – which in fact approaches a trigonal bipyramidal structure.

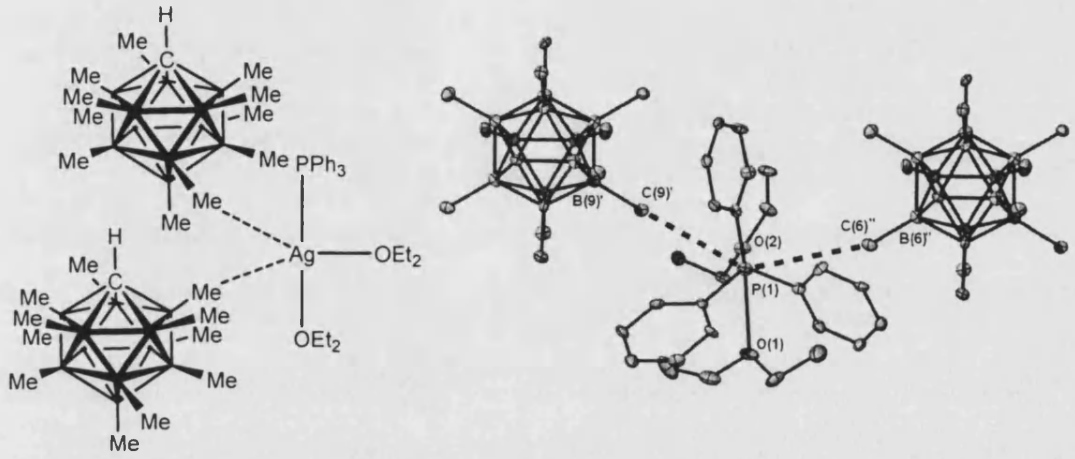

Figure 34: The pseudo trigonal pyramidal geometry of one of the independent molecules of **(5)**, viewed as a schematic (left) and along the Ag-P axis (right).

The closer Et_2O contact is approaching a *trans* position to the PPh_3 group (P1-Ag1-O2 162.86(17) and P2-Ag-2-O4 146.3(2)Å) whilst the longer is approximately *cis* to the phosphine (P1-Ag1-O1 103.13(19) and P2-Ag-O3 122.70(18)Å) and their increased bond lengths may partly be to minimise steric repulsion between the phenyl rings and the ethyl moieties. The pseudo-vacant site is then occupied by the two proximate anion contacts (Figure 34) producing a distorted trigonal bipyramidal geometry. The longer Ag-O bond lengths are comparable to the only other reported $LAg(OEt_2)$ complex ($[(CO)_3Fe(\mu$-2,6-bis(diphenylphosphino)pyridine) $Ag_2(Et_2O)][ClO_4]_2$ Ag-O 2.456(3) Å) and to Ag-O single bonds ($[Ag(O$-2-$C_6H_4Me)(PPh_3)_3]$ 2.386(5) Å), but the these are appreciably longer than the two short Ag-O bonds in **(5)** (2.248(6) Å and 2.291(8) Å) suggesting that these Et_2O are

significantly more tightly bound.[88] The P-Ag bond length (2.377(2) Å) is comparable to **(2)**, **(3)** and **(4)**, indicative of an equally strong Ag-P bond.[31]

Solution studies on crystalline **(5)** display an Et_2O : $(PPh_3)Ag(1\text{-}H\text{-}closo\text{-}CB_{11}Me_{11})$ ratio of 2:1 confirming the structure from X-ray diffraction. The C_{5v} symmetry of the cage is maintained at both room temperature and at 200 K by $^1H\{^{11}B\}$ and ^{11}B NMR spectroscopy. In the $^1H\{^{11}B\}$ spectrum the cage CH_3 resonances are sharp (fwhm ~ 1 Hz) and at positions close to that reported for the $[^nBu_4N]^+$ salt, suggesting that the long range anion···Ag contacts observed in the solid state do not persist in solution. The downfield shift observed in the $^1H\{^{11}B\}$ NMR spectrum for the Et_2O signals (3.55 and 1.26 ppm) is indicative of coordination to an electrophilic metal.[12, 14] The $^{31}P\{^1H\}$ NMR spectrum consists of the expected concentric doublet of doublets with a $J_{average}(AgP)$ coupling of 801 Hz. This implies that the etherate molecules are weakly bound in solution only interacting slightly more strongly than the anion $[1\text{-}H\text{-}closo\text{-}CB_{11}Me_{11}]^-$ ($J_{average}(AgP)$ 824 Hz). Addition of other weak ligands (10 equiv - 2,3 dimethyl butene, 5 equiv - MeCN) to **(2)** also results in the facile switching off of Ag···H_3C interactions (judged by the sharpening and upfield shift of the methyl resonances) further demonstrating the weakly coordinating nature of the $[1\text{-}H\text{-}closo\text{-}CB_{11}Me_{11}]^-$ anion and providing extra proof for close solution interactions between the $\{PR_3Ag\}^+$ fragment and the anion in **(2)**, **(3)** and **(4)**.

In addition to the reactivity of **(2)** with respect to neutral Lewis bases, the coordinating power of $[1\text{-}H\text{-}closo\text{-}CB_{11}Me_{11}]^-$ was investigated in comparison to a number of common weakly coordinating anions.[9, 15] The addition of one equivalent of $[^nBu_4N][closo\text{-}CB_{11}H_6Br_6]$ to a CD_2Cl_2 solution of **(2)** resulted in the immediate

formation of the known $(PPh_3)Ag(closo\text{-}CB_{11}H_6Br_6)$[27] and $[^nBu_4N][1\text{-}H\text{-}closo\text{-}CB_{11}Me_{11}]$ (Figure 35).

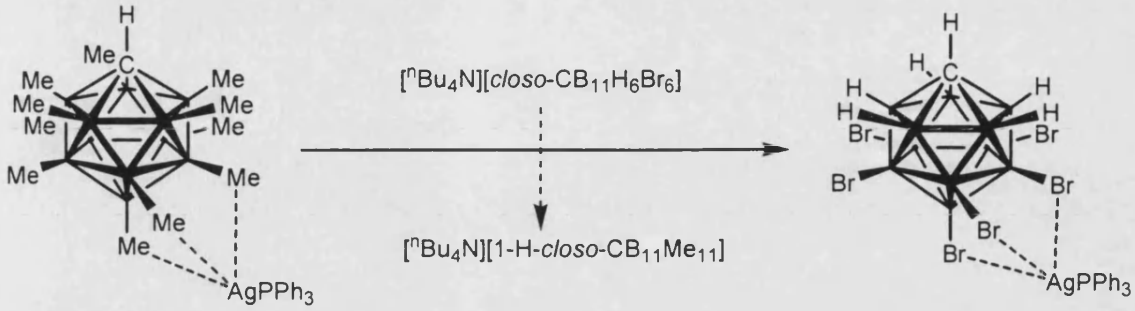

Figure 35: The displacement of $[1\text{-}H\text{-}closo\text{-}CB_{11}Me_{11}]^-$ from $\{Ag(PPh_3)\}^+$ by the addition of $[^nBu_4N][closo\text{-}CB_{11}H_6Br_6]$.

The anion exchange is unequivocally determined by the sharpening and upfield shift of the $[1\text{-}H\text{-}closo\text{-}CB_{11}Me_{11}]^-$ anion in the $^1H\{^{11}B\}$ NMR spectrum and by the change in the $J_{average}(AgP)$ coupling constant observed in the $^{31}P\{^1H\}$ NMR spectrum (824 Hz in **(2)** to 720 Hz) to that previously reported for $(PPh_3)Ag(closo\text{-}CB_{11}H_6Br_6)$.[24, 25] In contrast the analogous reaction with addition of $[^nBu_4N][B(C_6F_5)_4]$ resulted in no change in either the CH_3 region of the $^1H\{^{11}B\}$ NMR spectrum or in the $^{31}P\{^1H\}$ NMR spectrum, demonstrating the persistence of **(2)**. An anion coordinating power sequence with respect to the $\{Ag(PPh_3)\}^+$ fragment can therefore be proposed: $[closo\text{-}CB_{11}H_6Br_6]^- > [1\text{-}H\text{-}closo\text{-}CB_{11}Me_{11}]^- > [B(C_6F_5)_4]^-$. This ranks $[1\text{-}H\text{-}closo\text{-}CB_{11}Me_{11}]^-$ as less coordinating than one of the most weakly coordinating anions known, but more coordinating than $[B(C_6F_5)_4]^-$ in this system.[15, 21]

The addition of one equivalent of $[^nBu_4N][1\text{-}H\text{-}closo\text{-}CB_{11}Me_{11}]$ to a CD_2Cl_2 solution of **(2)** results in the observance of only one set of cage resonances. Although the CH_3 resonances remain somewhat broadened, there is a degree of sharpening (fwhm 18 Hz) and upfield shift on comparison to pure **(2)**. The observed $^1H\{^{11}B\}$ NMR cage

C-H signal at δ 1.20 ppm lies at the exact midpoint between that for **(2)** and [$^{n}Bu_4N$][1-H-*closo*-$CB_{11}Me_{11}$] (δ 1.26 and 1.14 ppm respectively). The $^{31}P\{^{1}H\}$ NMR spectrum displays a significantly broadened doublet in a similar region of the spectrum to that observed for **(2)**. These observations are consistent with an anion exchange process between a coordinated and a 'free' [1-H-*closo*-$CB_{11}Me_{11}$]$^-$ taking place rapidly on the NMR timescale.

Unsurprisingly, addition of one equivalent of the strong Lewis base PPh_3 to a CD_2Cl_2 solution of **(2)** resulted in the de-coordination of [1-H-*closo*-$CB_{11}Me_{11}$]$^-$, as determined by the standard line sharpening and upfield shift of the cage methyl resonances in the $^{1}H\{^{11}B\}$ NMR spectrum. Recrystallisation of the solution by the slow diffusion of pentanes into a CH_2Cl_2 solution at –20°C yielded colourless crystals suitable for X-ray diffraction study. This revealed the complex was the expected [$(PPh_3)_2$Ag][1-H-*closo*-$CB_{11}Me_{11}$], **(6)** (Figure 36). Complex **(6)** crystallises in the space group $P6_{3/m}$, containing only 1/6 of each anion and cation. The remaining portions of the cation and anion were generated by virtue of the 6-fold (identical to the 3/m symmetry operation) axis on which the silver and phosphorus atoms were located. The fraction of the anion contributing to the asymmetric unit contained four cage atoms (all treated as borons) and four methyl groups, all at half occupancy, affording one complete anion that is disordered equally over two sites. The disorder prevented the unambiguous location of the cage carbon in [1-H-*closo*-$CB_{11}Me_{11}$]$^-$.

The structure of **(6)** is linear by definition of the enforced symmetry in this Laue class, with a P1-Ag-P1' angle of 180°. This is in contrast to that reported for the related complex [$(PPh_3)_2$Ag][BF_4] (156.65(4)°), where the possibility of a weak dative bond or

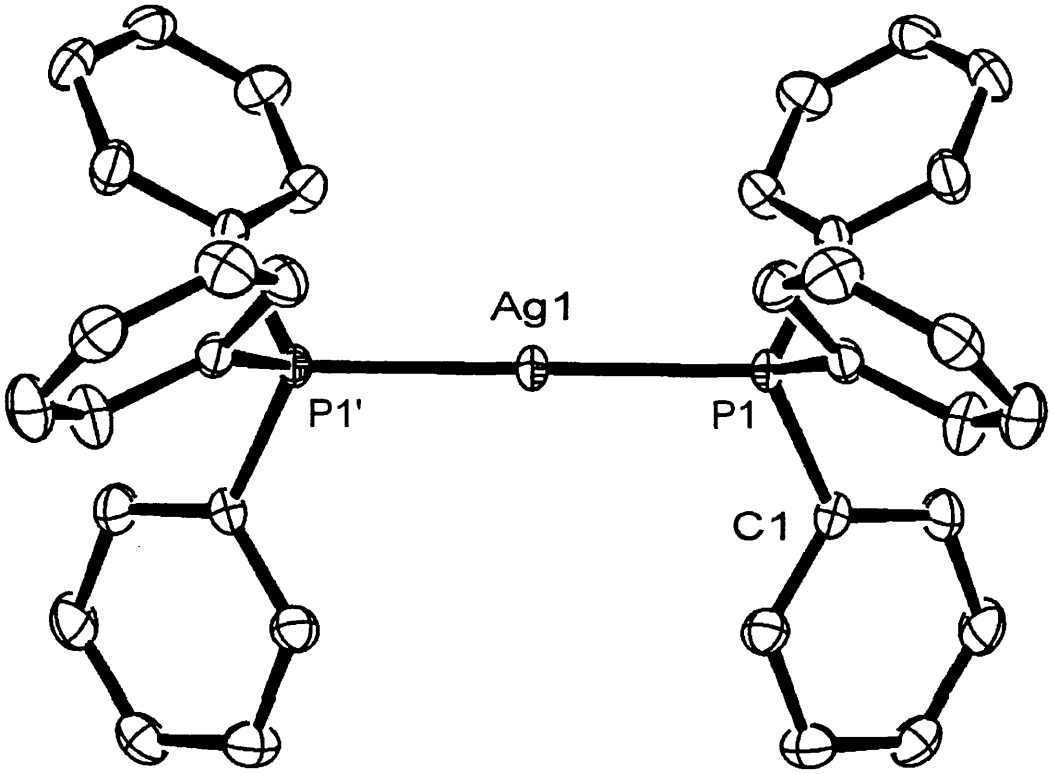

Figure 36: Molecular Structure of the cationic portion of $[(PPh_3)_2Ag][1\text{-H-}closo\text{-}CB_{11}Me_{11}]$, **(6)**. Thermal ellipsoids are shown at the 30% probability level. Symmetry transformations used to generate equivalent atoms: -x+y,-x+1,-z+1/2; -y+1,x-y+1,z; -x+y,-x+1,z; x,y,-z+3/2; -y+1,x-y+1,-z+3/2; -x+y,-x+1,-z+3/2. Hydrogens omitted for clarity.

Ag1-P1	2.4101(7)	P1-C1	1.8179(18)	P1-Ag1-P1'	180

Table 9: Selected Bond Lengths (Å) and angles (°) for **(6)**.

a significant electrostatic attraction between the Ag(I) centre and the anion is suggested.[31] The Ag···F distance in $[(PPh_3)Ag][BF_4]$ of 2.67 Å is well within the combined (2.79-2.89 Å) ionic radius of Ag(I) (1.29 Å) and the van der-Waals radius of F (1.5-1.6 Å) suggestive of a significant interaction.[43] Inspection of the extended lattice in **(6)** reveals the close approach of three proximal anions at a distance of 3.460 Å, longer than the previously defined 3.29 Å limit for a significant interaction, but within the combined (3.70Å) van der-Waals radii of Ag and H_3C. The close approach can be expected to be predominantly crystal packing in origin, with the most efficient space filling arrangement involving the assembly of the globular anions between the dumb bell like linear cations (Figure 37). A weak H_3C···Ag interaction cannot be ruled out however, with the lack of bending of the P-Ag-P bond then ascribed to the symmetric arrangement of the three proximate anions around the silver centre.

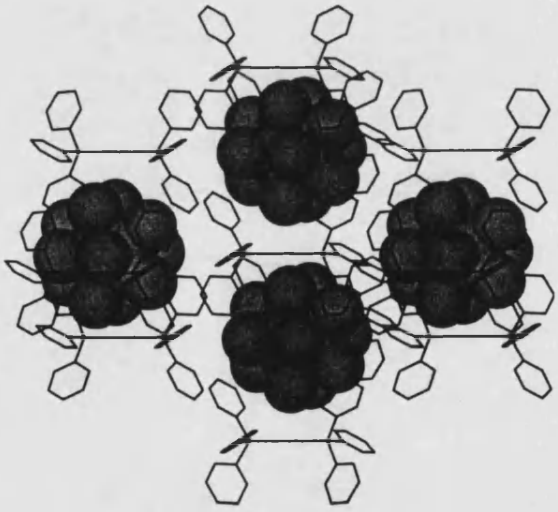

Figure 37: Packing diagram for compound **(6)**, [1-H-*closo*-$CB_{11}Me_{11}$]$^-$ anions shown at 100% van der-Waals radius.

Similar linear $[P\text{-}Ag\text{-}P]^+$ motifs have been previously achieved by the utilisation of bulkier phosphines to prevent any close anion/solvent contacts (*e.g.*, $[(Mes_3P)_2Ag][BF_4]^-$ and $[(Mes_3P)_2Ag][PF_6]$).[89, 90] A noteworthy comparison is with the solid-state structure of $(PPh_3)_2Ag(closo\text{-}CB_{11}H_6Br_6)$.[26] The Ag(I) environment in this

case is essentially tetrahedral with the intimate coordination of two bromine atoms from the anion resulting in a P1-Ag-P2 angle of 120.43(6)° (Figure 38).

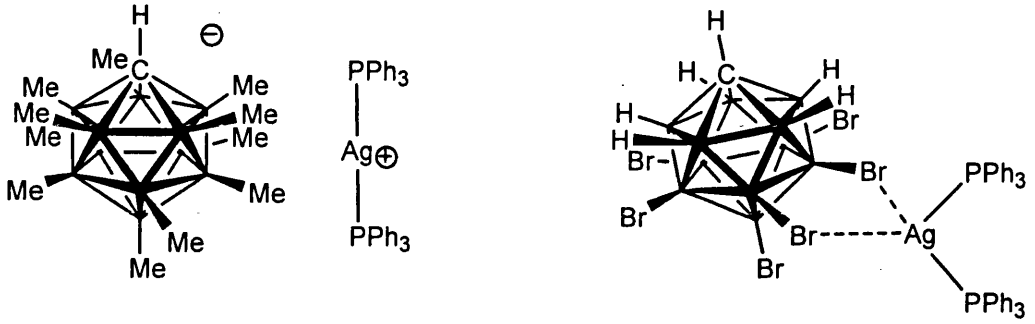

Figure 38: The solid state structures of $[(Ph_3P)_2Ag][1\text{-H-}closo\text{-}CB_{11}Me_{11}]$ and $(Ph_3P)_2PAg(closo\text{-}CB_{11}H_6Br_6)$ respectively.

This structural disparity suggests that the $[closo\text{-}CB_{11}H_6Br_6]^-$ anion is more strongly interacting with the metal, forcing the change in geometry. This ranks the $[1\text{-H-}closo\text{-}CB_{11}Me_{11}]^-$ as the weaker coordinating anion of the two (as expected from earlier studies in this chapter). The Ag-P bond length in **(6)** (2.4101(7) Å) is longer than that reported for the mono phosphine complexes **(2)** (2.3871(5) Å) and $(PPh_3)AgNO_3$ (2.369 Å). This is as expected as these complexes only involve one strongly Lewis basic molecule. It is comparable to that reported for $[(PPh_3)_2Ag][BF_4]$ (2.4177(12) Å and 2.4219(13) Å) implying that the anion interaction in both is equally weak. It is significantly shorter than the four coordinate complexes $(PPh_3)_2Ag(closo\text{-}CB_{11}H_6Br_6)$ (2.448(2) Å and 2.451(2)Å) and $(PPh_3)_2Ag(closo\text{-}CB_{11}H_{12})$ (2.4698(3) Å and 2.4741(3) Å).[26]

The $^1H\{^{11}B)$ NMR spectrum of **(6)** shows a 2:1 ratio of phosphine to cage, with C_{5V} symmetry of the anion maintained (^{11}B NMR spectroscopy also confirms the solution C_{5V} symmetry). The methyl cage resonances are sharp (fwhm ~ 1 Hz) and appear at chemical shifts close to $[^nBu_4N][1\text{-H-}closo\text{-}CB_{11}Me_{11}]$, demonstrating that the

long cation···anion contacts observed in the solid state do not persist in solution. The $^{31}P\{^{1}H\}$ NMR spectrum displays the expected concentric doublets from coupling to $^{107/109}Ag$, with an average J(AgP) coupling constant of 561 Hz. An identical spectra is also observed on the addition of two equivalents of PPh_3 to **(1)**. Analogous behaviour is observed on the addition of two equivalents of $(3,5\text{-}Me_2\text{-}C_6H_3)_3P$ to **(1)** (no broadening of CH_3 anion resonances in the $^{1}H\{^{11}B\}$ NMR spectrum and a $J_{average}(AgP)$ of 540 Hz). The magnitude of this coupling constant agrees well with that observed for other predominantly two coordinate species such as $[(PPh_3)_2Ag][BF_4]$ (550 Hz).[31] The $^{31}P\{^{1}H\}$ solution behaviour of related compounds that have close anion associations in the solid state (*e.g.*, $(PPh_3)_2Ag(closo\text{-}CB_{11}H_6Br_6)$, $((PPh_3)_2Ag)(closo\text{-}CB_{11}H_{12})$ and $(PPh_3)_2Ag(NO_3)$) are drastically different, displaying a broad singlet at room temperature indicative of rapid ligand exchange – an effect commonly seen in the $^{31}P\{^{1}H\}$ NMR spectra of $[(PPh_3)_2AgL_x]$ (x = 1 or 2, L in this case are the respective anions) complexes.[91, 92] In these cases it appears that the anion coordination to the silver centre is switching on the phosphine dissociation.

Fluxionality in $C_2D_2Cl_4$ solutions of **(6)**, though not observed at room temperature, can be induced by heating to temperatures above 40°C, with the $^{31}P\{^{1}H\}$ NMR resonance becoming a broad singlet indicative of phosphine exchange.[92] The mechanism of this exchange process is unclear, with an analogous anion coordination to cause fluxionality unlikely due to the lack of any close anion···cation interactions in the solid state and no observed shift or broadening of the anion methyl resonances in the $^{1}H\{^{11}B\}$ NMR spectrum at these raised temperatures. Cooling this sample back to temperatures below 40°C regenerates the concentric doublet of doublets. Heating may

result in the establishment of an equilibrium between the structurally characterised complex **(6)** and a disproportionation product produced by scission of an Ag-P bond.

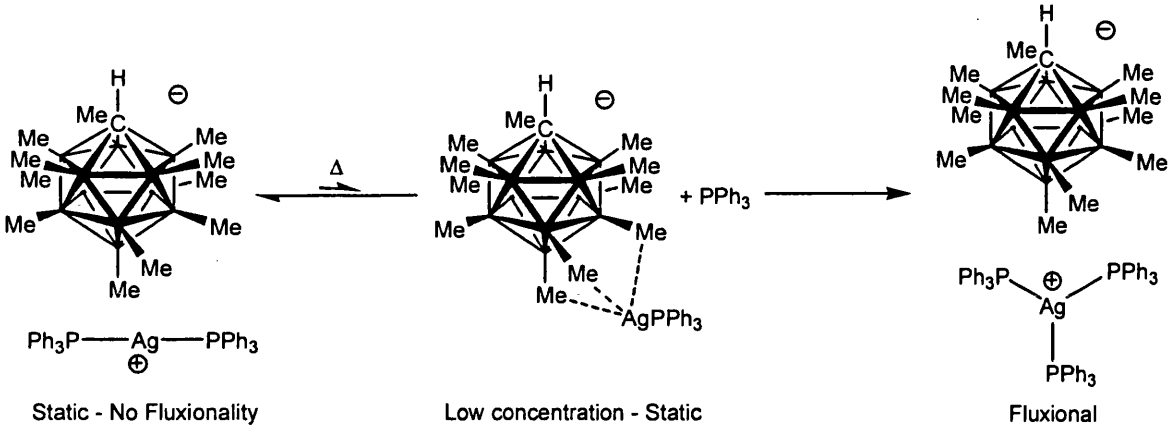

Figure 39: A possible initiation step in the thermally induced fluxionality observed in **(6)**.

Support for a disproportionation mechanism to explain the observed fluxionality is obtained on addition of 0.1 equivalents of PPh_3 to a CD_2Cl_2 solution of **(6)**. This results in a $^{31}P\{^1H\}$ NMR spectrum that displays a broad singlet at room temperature – confirming that the presence of a low concentration of uncoordinated phosphine is sufficient to induce fluxionality in this system. The $^1H\{^{11}B\}$ NMR spectrum of this solution displays no anion···cation interactions. Recrystallisation of this sample by the slow diffusion of pentanes yielded two colourless crystalline polymorphs suitable for X-ray diffraction studies, one set being complex **(6)**. A structure determination on the second polymorph revealed a complex with the same empirical formula to **(6)**, but the product of a disproportionation reaction, namely $[(PPh_3)_4Ag][(1\text{-H-}\textit{closo}\text{-}CB_{11}Me_{11})_2Ag]$ **(7)** (Figure 40). Complex **(7)** crystallises in the cubic space group F-3d, with the asymmetric unit containing only 1/12 of each anion and cation. The fraction of the anion contributing to the asymmetric unit contained only two cage atoms (both treated as borons) and two methyl groups. Due to the high symmetry inherent in this space group the unambiguous location of the cage carbon in $[1\text{-H-}\textit{closo}\text{-}CB_{11}Me_{11}]^-$ was

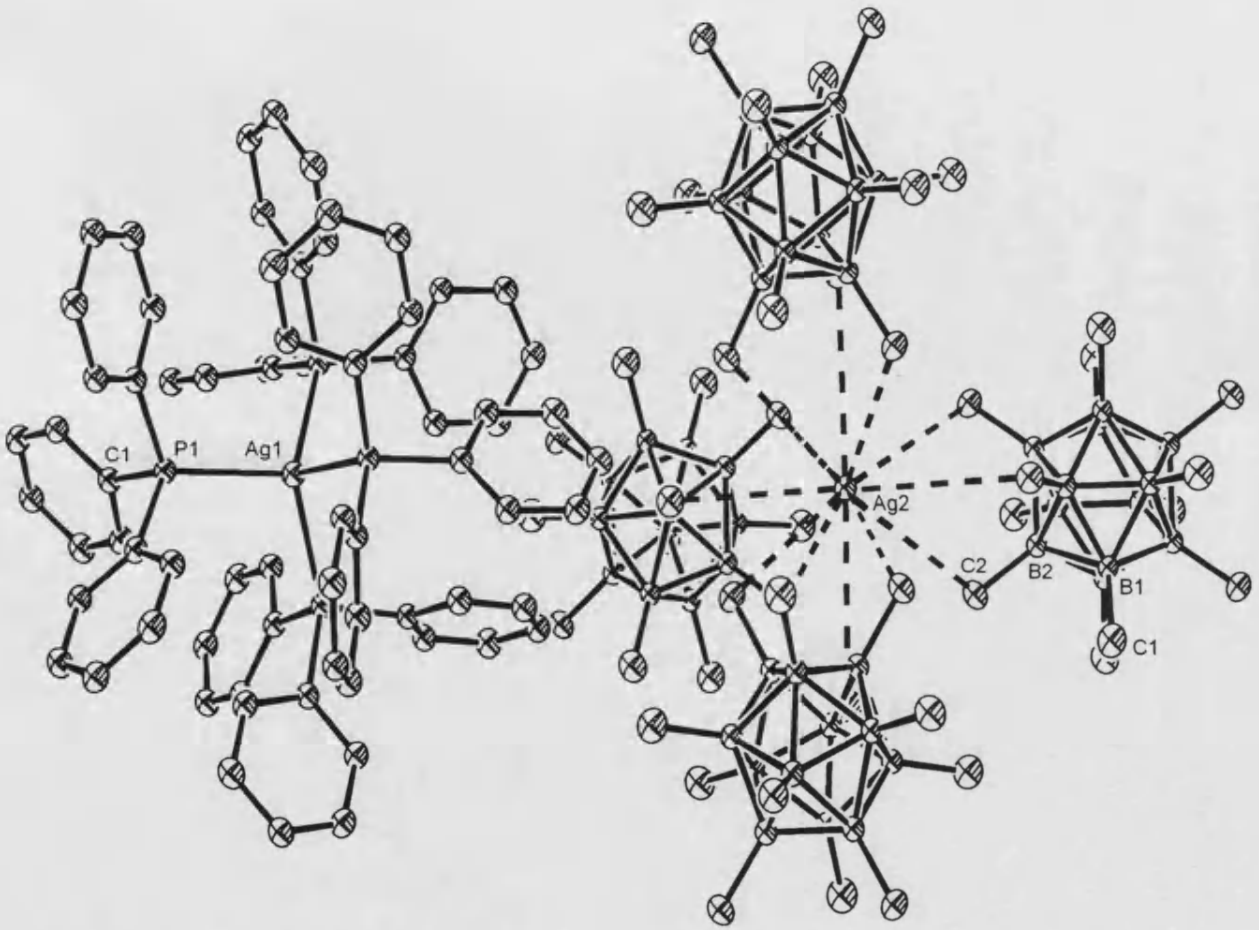

Figure 40: Molecular structure of $[(PPh_3)_4Ag][(1\text{-H-}closo\text{-}CB_{11}Me_{11})_2]$ **(7)**, showing the immediate environment around Ag2, including two proximal anions. Thermal ellipsoids are shown at 30% probability and hydrogens are omitted for clarity

P1-Ag1	2.6019(19)
P1-Ag1-P1'	109.47(1)
Ag2-C1	6.140(5)
Ag2-C2	3.868(5)
B1-C1	1.618(7)
B2-C2	1.601(7)

Table 10: Selected Bond Lengths (Å) and Angles (°) for **(7)**.

impossible. The cation $[(PPh_3)_4Ag]^+$ is tetrahedral (P1-Ag-P1' 109.47(1)) with an Ag-P bond length (2.6019(19) Å) similar to that previously reported for $[(PPh_3)_4Ag][X]$ (X = $[ClO_4]^-$ and $[NO_3]^-$, Ag-P distances in the range 2.643(3) Å to 2.671(4) Å).[93, 94] More noteworthy is the structure of the anion, which in the extended lattice is surrounded by four anions resulting in 12 Ag···H_3C contacts (Figure 40). The Ag···C distance is 3.868 Å (all 12 interactions are symmetrically equivalent) falling outside of the combined (3.70 Å) van der-Waals radii for Ag and CH_3. This is significantly longer than that found in the simple silver salt **(1)**, where a Ag(I) centre is likewise encapsulated by four anions, with the Ag···C distances ranging from 2.6535(18) Å to 3.089(2) Å. The packing observed around Ag2 in **(7)** is therefore not the most efficient way of minimising anion···cation distance and thereby maximising the electrostatic interaction and must be enforced by the high symmetry of the space group. The Ag2 coordination environment is essentially tetrahedral with the silver centre sitting symmetrically over four triangular faces (each made up of three methyl groups) thus the observed distance is likely to be the closest the Ag2 cation can get to each anion whilst still retaining the high symmetry. A similar tetrahedral geometry about the metal centre has been observed in $(\eta^6\text{-}C_6H_6)Na(closo\text{-}CB_{11}Me_{12})$.[33] The tetrahedral environment consists of two anions and two arenes; however, in this case the M···CH_3 contacts at 2.70 Å are within the combined (3.16 Å) ionic radius of Na^+ (1.16 Å) and the van der-Waals radius of CH_3 (2.00 Å). It thus appears that the packing arrangement is dominated by the highly symmetrical propeller like cations $[Ag(PPh_3)_4]^+$, with the vast majority of $[(PPh_3)_4Ag][X]$ salts possessing very high symmetry (*e.g.*, cubic when X = $[Mo_6O_{19}]^{2-}$ and rhombohedral when X= $[ClO_4]^-$, $[NO_3]^-$, $[PF_6]^-$ and $[SbF_6]^-$).[93-97]

A similar disproportionation reaction has been previously reported in the addition of one equivalent of IMes to Ag[*closo*-$CB_{11}H_{12}$]. The only product is[$(IMes)_2Ag$][Ag_2(*closo*-$CB_{11}H_{12})_4$], a dianion where the Ag(I) centres are surrounded solely by the carborane anion.[30] An analogous anion has also been reported with [*closo*-$CB_{11}H_6Br_6]^-$ which forms the [Ag(*closo*-$CB_{11}H_6Br_6)_2]^-$ anion on the reaction of Ag[*closo*-$CB_{11}H_6Br_6$] with [Fe(tpp)Br] (tpp = tetraphenylporphryinate).[18]

Dissolution of a crystalline sample of **(7)** into CD_2Cl_2 resulted in $^1H\{^{11}B\}$ and $^{31}P\{^1H\}$ NMR spectra essentially identical to that of **(6)** with no Ag···H_3C interactions visible in solution. The observed fluxionality induced in **(6)** on heating or by addition of a slight excess of PPh_3 is presumably an equilibrium between the linear [(PPh_3)-Ag-$(PPh_3)]^+$ cation and the disproportionation product. (Figure 41).

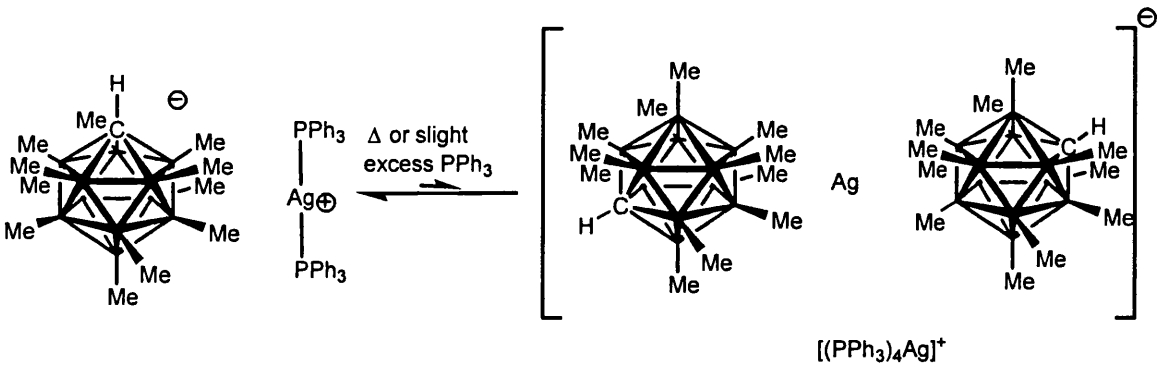

Figure 41: Possible solution equilibrium of **(6)** established on heating or by the addition of a slight excess of PPh_3.

On cooling a sample of **(6)** that has had a slight excess of PPh_3 added (i.e. is fluxional at room temperature as determined by a $^{31}P\{^1H\}$ NMR resonance that is a broad singlet) to -70°C three broad doublets are observed with J(AgP) coupling constants of 237 Hz, 320 Hz and 545 Hz. The major product at 237 Hz can be

characterised as the $[(PPh_3)_4Ag]^+$ cation by comparison to the related cation $[((p\text{-}MeC_6H_4)_3P)_4Ag]^+$ which has J(AgP) coupling constants in the range 224 Hz to 230 Hz.[85] In the $[(p\text{-}Me\text{-}C_6H_4)_3P]_4AgX$ systems ligand lability involving phosphine dissociation is observed at temperatures above -70°C. The behaviour of **(6)** here is analogous and the remaining two low temperature $^{31}P\{^1H\}$ doublets can, by further comparison to literature values, be readily assigned to the tris and bis phosphine adducts respectively.[85] Furthermore, contrasting the FAB+ mass spectrometry spectra of pure **(6)** and a 'fluxional sample' gives corroborating evidence for phosphine dissociation. Pure **(6)** only displays peaks due to $[(PPh_3)Ag]^+$ and $[(PPh_3)_2Ag]^+$ cations, whilst the fluxional sample consists of these two plus the $[(PPh_3)_3Ag]^+$ cation.

Addition of one equivalent of $[^nBu_4N][closo\text{-}CB_{11}H_6Br_6]$ or an excess of the cyclic sulphoxide complex $C_4H_8SO_2$ to a solution of **(6)** both also induce fluxionality – with the $^{31}P\{^1H\}$ NMR spectra consisting of only a broad singlet. Therefore any addition of a Lewis base stronger than the $[1\text{-}H\text{-}closo\text{-}CB_{11}Me_{11}]^-$ can coordinate to a Ag(I) centre instigating phosphine dissociation and fluxionality.

2.3: Summary.

Reported herein is the synthesis of the silver salt $Ag[1\text{-}H\text{-}closo\text{-}CB_{11}Me_{11}]$ and a number of $(PR_3)Ag(1\text{-}H\text{-}closo\text{-}CB_{11}Me_{11})$ complexes displaying $Ag\cdots H_3C$ interactions in the solid state. These are the first reported examples of $Ag\cdots H_3C$ contacts, and the first of a transition metal closely associated with a highly methylated carborane mono-anion. Variation in the phosphine results in extended coordination polymers that can be broken up into discrete contact ion pairs by increase of distal (with respect to the silver

centre) steric bulk. By a combination of structural analysis and DFT calculations it is concluded that the nature of the bonding interaction is predominantly electrostatic, although the presence of a small orbital contribution (i.e. a σ donor effect) cannot be ruled out. This is as previously observed for the Group I cations partnered with the related anion [*closo*-$CB_{11}Me_{12}$]$^-$ which also form intimate Ag···H_3C contacts that are attributed to electrostatic attraction.

These Ag···H_3C interactions have been unambiguously proven to persist in CD_2Cl_2 solution for all the complexes, demonstrating that these interactions are significant and not an artefact of crystal packing forces. Key spectroscopic indicators have been observed (primarily the considerable broadening and downfield shift of anion CH_3 groups) that will be useful markers in the development of the chemistry of these anions. The weakly coordinating nature of [1-H-*closo*-$CB_{11}Me_{11}$]$^-$ has also been unequivocally shown, with the coordinating power of the anion being less than [*closo*-$CB_{11}H_6Br_6$]$^-$, but more than the ubiquitous $[B(C_6F_5)_4]^-$ anion. The anion has also been readily demonstrated to be displaced from the Ag(I) coordination sphere by Lewis bases more donating than CD_2Cl_2.

The behaviour of $[(PPh_3)_2Ag]$[1-H-*closo*-$CB_{11}Me_{11}$] has been investigated and the solid state structure determined, which shows the first truly linear bis (PPh_3) silver adduct. Fluxionality in $[(PPh_3)_2Ag]$[1-H-*closo*-$CB_{11}Me_{11}$] has also been demonstrated to require the addition of an external Lewis base (be it anion or neutral ligand, or a donor solvent) to coordinate to the Ag(I) centre and initiate phosphine dissociation.

The investigations into Ag···H_3C interactions in both the solid-state and solution phase are important due to the role of metal alkane complexes as intermediates in numerous C-H activation reactions. The complexes characterised here can be presented as a model for these interactions (Figure 42) – especially those involving cationic Au(I) complexes, where a Au(I)···H_4C σ complex is postulated as an intermediate in the catalytic oxidation of methane to methanol.[98]

Model Complex Alkane σ Complex

Figure 42: A comparison between the model complexes discussed in this chapter and metal alkane complexes

2.4: References:

1 I. Krossing, *Chem. Eur. J.*, 2001, **7**, 490
2 I. Krossing and A. Reisinger, *Angew. Chem., Int. Ed. Engl.*, 2003, **42**, 5725
3 I. Krossing and I. Raebe, *Angew. Chem., Int. Ed. Engl.*, 2004, **43**, 2066
4 W. Beck and K. Sunkel, *Chem. Rev.*, 1988, **88**, 1405
5 Z. W. Xie, T. Jelinek, R. Bau, and C. A. Reed, *J. Am. Chem. Soc.*, 1994, **116**, 1907.
6 K. Shelly, D. C. Finster, Y. J. Lee, W. R. Scheidt, and C. A. Reed, *J. Am. Chem. Soc.*, 1985, **107**, 5955.
7 T. D. Newbound, M. R. Colsman, M. M. Miller, G. P. Wulfsberg, O. P. Anderson, and S. H. Strauss, *J. Am. Chem. Soc.*, 1989, **111**, 3762
8 D. M. Van-Seggen, P. K. Hurlburt, O. P. Anderson, and S. H. Strauss, *Inorg. Chem.*, 1995, **34**, 3453
9 S. H. Strauss, *Chem. Rev.*, 1993, **93**, 927.
10 J. Powell, A. Lough, and T. Saeed, *J. Chem. Soc., Dalton Trans.*, 1997, 4137
11 F. L. Taw, H. Mellows, P. S. White, F. J. Hollander, R. G. Bergmann, M. Brookhart, and M. D. Heinekey, *J. Am. Chem. Soc.*, 2002, **124**, 5100.
12 M. D. Butts, B. L. Scott, and G. J. Kubas, *J. Am. Chem. Soc.*, 1996, **118**, 11831.
13 J. Huhmann-Vincent, B. L. Scott, and G. J. Kubas, *J. Am. Chem. Soc.*, 1998, **120**, 6808.
14 J. Huhmann-Vincent, B. L. Scott, and G. J. Kubas, *Inorg. Chem.*, 1999, **38**, 115.

[15] C. A. Reed, *Acc. Chem. Res.*, 1998, **31**, 133.
[16] C.-W. Tsang, Q. Yang, E. T.-P. Sze, T. C. W. Mak, D. T. W. Chan, and Z. Xie, *Inorg. Chem.*, 2000, **39**, 5851
[17] Z. W. Xie, B. M. Wu, T. C. W. Mak, J. Manning, and C. A. Reed, *J. Chem. Soc., Dalton Trans.*, 1997, 1213.
[18] Z. Xie, R. Bau, and C. A. Reed, *Angew. Chem., Int. Ed. Engl.*, 1994, **33**, 2433
[19] B. T. King, I. Zharov, and J. Michl, *Chemical Innovation*, 2001, **31**, 23.
[20] S. V. Ivanov, J. J. Rockwell, O. G. Polyakov, C. M. Gaudinski, O. P. Anderson, K. A. Solntsev, and S. H. Strauss, *J. Am. Chem. Soc.*, 1998, **120**, 4224
[21] D. Stasko and C. A. Reed, *J. Am. Chem. Soc.*, 2002, **124**, 1148.
[22] S. V. Ivanov, A. J. Lupinetti, S. M. Miller, O. P. Anderson, K. A. Solntsev, and S. H. Strauss, *Inorg. Chem.*, 1995, **34**, 6419
[23] T. Jelinek, P. Baldwin, W. R. Scheidt, and C. A. Reed, *Inorg. Chem.*. 1993, **32**, 1982.
[24] C. Hague, N. J. Patmore, C. G. Frost, M. F. Mahon, and A. S. Weller, *Chem. Commun.*. 2001, 2286
[25] N. J. Patmore, C. Hague, J. H. Cotgreave, M. F. Mahon, C. G. Frost, and A. S. Weller, *Chem. Eur. J.*, 2002, **8**, 2088
[26] N. J. Patmore, 'Transition Metal Complexes of Icosahedral MonoCarborane Anions: Synthesis to Catalysis', Thesis, University of Bath, Bath, 2002.
[27] N. J. Patmore, C. Hague, J. H. Cotgreave, M. F. Mahon, C. G. Frost, and A. S. Weller, *Chem. Eur. J.*, 2002, **8**, 2088.
[28] D. D. Ellis, A. Franken, P. A. Jellis, J. A. Kautz, and G. A. Stone, *J. Chem. Soc., Dalton Trans.*, 2000, 2509.
[29] D. D. Ellis, J. C. Jeffrey, P. A. Jellis, J. A. Kautz, and F. G. A. Stone, *Inorg. Chem.*, 2001, **40**, 2041.
[30] M. A. Fox, M. F. Mahon, N. J. Patmore, and A. S. Weller, *Inorg. Chem.*, 2002, **41**, 4567.
[31] R. E. Bachmann and D. F. Andretta, *Inorg. Chem.*, 1998, **37**, 5657
[32] B. T. King, Z. Janousek, B. Gruner, M. Trammell, B. C. Noll, and J. Michl, *J. Am. Chem. Soc.*, 1996, **118**, 3313.
[33] B. T. King, B. C. Noll, and J. Michl, *Collect. Czech. Chem. Commun.*, 1999, **64**, 1001.
[34] I. Zharov, B. T. King, Z. Havlas, A. Pardi, and J. Michl, *J. Am. Chem. Soc.*, 2000, **122**, 10253.
[35] J. E. Huheey and E. A. Keiter, 'Inorganic Chemistry: Principles of Structure and Reactivity', Harper Collins, 1993.
[36] A. Albanati, C. Anklin, P. Janser, H. Lehner, D. Matt, and P. S. Pregosin, *Inorg. Chem.*, 1989, **28**, 1105.
[37] A. Albanati, F. Demartin, L. M. Venanzi, and M. K. Wolfer, *Angew. Chem., Int. Ed. Engl.*, 1988, **27**, 563 and ref therein.
[38] G. J. Kubas, 'Metal Dihydrogen and Sigma Bond Complexes. Structure, Theory and Reactivity.' Kluwer, 2001.
[39] A. G. Sharpe, 'Inorganic Chemistry', Longman, 1981.
[40] M. A. Omary, T. R. Webb, Z. Assefa, G. E. Shankle, and H. H. Patterson, *Inorg. Chem.*, 1998, **37**, 1380.
[41] G. W. Eastland, M. A. Mazid, D. R. Russell, and M. C. R. Symons, *J. Chem. Soc., Dalton Trans.*, 1980, 1682.
[42] C. W. Tsang, Q. Yang, E. T. P. Sze, T. C. W. Mak, D. T. W. Chan, and Z. Xie, *Inorg. Chem.*, 2000, **39**, 3582.

[43] L. Pauling, 'The Nature of the Chemical Bond', Cornell University Press, 1960.
[44] R. Uson, A. Laguna, A. Uson, P. G. Jones, and K. Meyer-Base, *J. Chem. Soc., Dalton Trans.*, 1988, 341.
[45] K. Shelly, D. C. Finster, Y. L. Lee, W. R. Scheidt, and C. A. Reed, *J. Am. Chem. Soc*, 1985, **107**, 5955.
[46] E. A. H. Griffith and E. L. Amma, *J. Am. Chem. Soc.*, 1974, **96**, 743.
[47] H. Brunner, M. Muschiol, T. Neuhierl, and B. Nuber, *Chem. Eur. J.*, 1998, **4**, 168.
[48] C. J. Burns and R. A. Andersen, *J. Am. Chem. Soc.*, 1987, **109**, 5853
[49] W. E. Rhine, G. Stucky, and S. W. J. Peterson, *J. Am. Chem. Soc.*, 1975, **97**, 6401.
[50] M. Bochmann, S. J. Lancaster, M. B. Hursthouse, and K. M. A. Malik, *Organometallics*, 1994, **13**, 2235.
[51] W. Baratta, C. Mealli, E. Herdtweck, A. Ienco, S. A. Mason, and P. Rigo, *J. Am. Chem. Soc.*, 2004, **126**, 5549
[52] X. Song, M. Thorton-Pett, and M. Bochmann, *Organometallics*, 1998, **17**, 1004.
[53] M. Bochmann and M. J. Sarsfield, *Organometallics*, 1998, **17**, 5908.
[54] R. A. Stein and C. Knobler, *Inorg. Chem.*, 1977, **16**, 242
[55] C. A. Tolman, *Chem. Rev.*, 1977, **77**, 313.
[56] G. A. Bowmaker, P. J. Harvey, P. C. Healy, B. W. Skelton, and A. H. White, *J. Chem. Soc., Dalton Trans.*, 1996, 2459.
[57] G. G. Lobbia, C. Pettinari, C. Santini, B. W. Skelton, and A. H. White, 1998, 2739.
[58] A. Cingolani, M. Pellei, Effendy, C. Pettinari, C. Santini, B. Skelton, and A. H. White, *Inorg. Chem.*, 2002, **41**, 6633.
[59] H.-B. Song, Z.-Z. Zhang, Z. Hui, C.-M. Che, and T. C. W. Mak, *Inorg. Chem.*, 2002, **41**, 3146
[60] A. Rifat, N. J. Patmore, M. F. Mahon, and A. S. Weller, *Organometallics*, 2002, **21**, 2856.
[61] A. T. Hutton, P. G. Pringle, and B. L. Shaw, *Organometallics*, 1983, **2**, 1889.
[62] H. Brunner, D. Mijolovic, B. Wrackmeyer, and B. Nuber, *J. Organomet. Chem.*. 1999, **579**, 298.
[63] M. B. Hursthouse, I. J. Colquhoun, W. McFarlane, and J. Murray, *J. Chem. Soc., Dalton Trans.*, 1988, 2787.
[64] Z. Janousek, U. Lehmann, J. Castulik, I. Cisarova, and J. Michl, *J. Am. Chem. Soc.*, 2004, **126**, 4060.
[65] M. Brookhart, M. L. H. Green, and L. L. Wong, 'Progress in Inorganic Chemistry', 1988.
[66] S. Beck, M.-H. Prosenc, H.-H. Brintzinger, and R. Goretzki, *J. Molecular Catalysis a: Chemical*, 1996, **111**, 67.
[67] I. A. Guzei, R. A. S. Jr, and R. F. Jordan, *Acta Cryst. Sec. C*, 2000, **56**, 635.
[68] R. Gomez, M. L. H. Green, and J. L. Haggit, *Chem. Commun.*. 1994, 2607.
[69] R. Gomez, M. L. H. Green, and J. L. Haggit, *J. Chem. Soc., Dalton Trans.*, 1996, 939.
[70] P. A. Chase, W. E. Piers, and B. O. patrick, *J. Am. Chem. Soc.*, 2000, **122**, 12911.
[71] G. C. Bazan, W. D. Cotter, Z. J. A. Komon, R. A. Lee, and R. J. Lachicotte, *J. Am. Chem. Soc.*, 2000, **122**, 1371.
[72] S. Beck, S. Lieber, F. Schaper, A. Geyer, and H.-H. Brintzinger, *J. Am. Chem. Soc.*, 2001, **123**, 1483.

[73] R. Baumann, W. M. Davis, and R. R. Schrock, *J. Am. Chem. Soc.*, 1997, **119**, 3830.
[74] X. Yang, C. L. Stern, and T. J. Marks, *J. Am. Chem. Soc.*, 1991, **13**, 3623.
[75] X. Yang, C. L. Stern, and T. J. Marks, *J. Am. Chem. Soc.*, 1994, **116**, 10015.
[76] Z. Lui, E. Somsook, and C. R. Landis, *J. Am. Chem. Soc.*, 2001, **123**, 2915.
[77] R. Choukroun, F. Wolff, C. Lorber, and B. Donnadieu, *Organometallics*, 2003, **22**, 2245.
[78] A. Spannenberg, H. Fuhrmann, P. Arndt, W. Baumann, and R. Kempe, *Angew. Chem., Int. Ed. Engl.*, 1998, **37**, 3363.
[79] F. Guerin and D. W. Stephan, *Angew. Chem., Int. Ed. Engl.*, 2000, **39**, 1298.
[80] A. Shafir and J. Arnold, *J. Am. Chem. Soc.*, 2001, **123**, 9212.
[81] H. Li, L. Li, T. J. Marks, L. Liable-Sands, and A. L. Rheingold, *J. Am. Chem. Soc.*, 2003, **125**, 10788.
[82] A. D. Sadow and T. D. Tilley, *J. Am. Chem. Soc.*, 2003, **125**, 9462.
[83] C. L. Beswick and T. J. Marks, *Organometallics*, 1999, **18**, 2410
[84] G. A. Bowmaker, J. V. Hanna, C. E. F. Rickard, and A. S. Lipton, *J. Chem. Soc., Dalton Trans.*, 2001, 20.
[85] E. L. Muetterties and C. W. Alegranti, *J. Am. Chem. Soc.*, 1972, **94**, 6386.
[86] M. L. McKee, *J. Am. Chem. Soc.*, 1997, **119**, 4220
[87] T. Jelinek, J. Plesek, S. Hermanek, and B. Stibr, *Collect. Czech. Chem. Commun.*, 1985, **51**, 819.
[88] D. A. Edwards, M. F. Mahon, K. C. Molloy, and V. Ogrodnik, *Inorg. Chim. Acta*, 2003, **349**, 37.
[89] A. Bayler, A. Schier, G. A. Bowmaker, and H. J. Schmidbaur, *J. Am. Chem. Soc.*, 1996, **118**, 7006.
[90] E. C. Alyea, G. Ferguson, and A. Somogyvari, *Inorg. Chem.*, 1982, **21**, 1369.
[91] A. Cingolani, Effendy, F. Marchetti, C. Pettinari, B. W. Skelton, and A. H. White, *J. Chem. Soc., Dalton Trans.*, 1999, 4047.
[92] L. Jager, C. Tretner, H. Hartung, and M. biedermann, *Eur. J. Inorg. Chem.*. 1998, 1051.
[93] P. F. Barren, J. C. Dyason, P. C. Healy, L. M. Engelhardt, B. W. Skelton, and A. H. White, *J. Chem. Soc., Dalton Trans.*, 1986, 1965.
[94] L. M. Engelhardt, C. Pakawatchai, A. H. White, and P. C. Healy, *J. Chem. Soc., Dalton Trans.*, 1985, 125.
[95] D.-L. Long, X.-Q. Xin, X.-M. Chen, and B.-S. Kang, *Polyhedron*, 1997, **16**, 1259.
[96] G. A. Bowmaker, P. C. Healy, L. M. Engelhardt, J. D. Kildea, B. W. Skelton, and A. H. White, *Aust. J. Chem.*, 1990, **43**, 1697.
[97] G. A. Bowmaker, Effendy, R. D. Hart, J. D. Kildea, E. N. de-Silva, B. W. Skelton, and A. H. White, *Aust. J. Chem.*, 1997, **50**, 539.
[98] C. J. Jones, D. Taube, V. R. Ziatdinov, R. A. Periana, R. J. Nielsen, J. Oxgaard, and W. A. Goddard-III, *Angew. Chem., Int. Ed. Engl.*, 2004, **43**, 4626.

3 Full and Half Sandwich Metallocenes Partnered with the [1-H-*closo*-$CB_{11}Me_{11}$]$^-$ anion.

3.1. Background.

The rapid recent expansion of new polymerisation catalysts based on single site, homogeneous organometallic complexes has centred on the improvement of catalyst activities and in the control of the key polymer properties.[1, 2] A major area of focus has been the group IV d^0 complexes, either as simple metallocenes (*e.g.*, Cp_2MX_2 (X = halide or alkyl, M = Ti, Zr or Hf)) or as 'constrained geometry' complexes *e.g.*, half sandwich complexes or *ansa*-metallocenes (Figure 1).

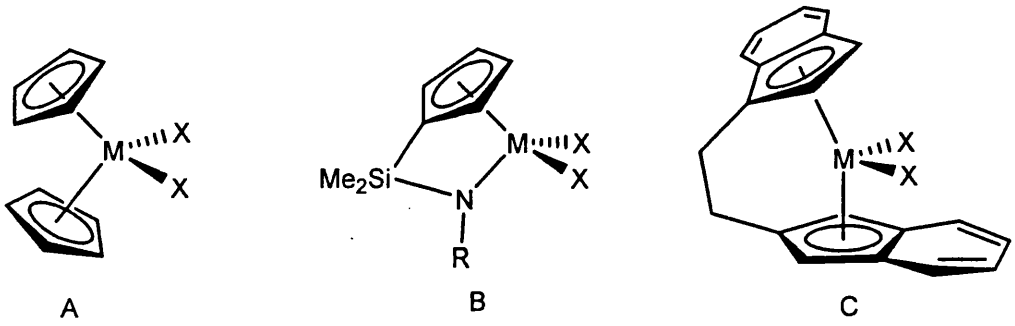

Figure 1: A = a standard metallocene, B = half sandwich amido complex (R = bulky alkane) and C = an *ansa* metallocene.

The complexes represented in Figure 1 are precatalysts for olefin polymerisation and require activation by a co-catalyst to generate the active complex. The putative active species for homogeneous polymerisation, is the cationic alkyl complex $[L_nMR]^+$ that is formally represented as having a 'vacant site' on the metal centre (Figure 2). In reality the unsaturation is generally alleviated by anion or solvent coordination (albeit a weak, easily displaced coordination). Therefore the term 'virtual' vacant site is more appropriate.[3] The most extensively studied metal precatalysts are the Group IV metallocenes and the following discussion will be based on these (M = Ti, Zr or Hf

unless otherwise specified). The concepts though are equally applicable to the constrained geometry, non-metallocene and non-Group IV metal complexes.

There are three main routes to access the catalytically active cation (Figure 2): (i) The activation of a di-halogen precursor: this is the most widely used industrially and predominantly uses aluminium alkyls as the co-catalysts. The co-catalyst role is two fold, initially alkylating the metallocene then initiating the polymerisation by Lewis acidic alkyl abstraction to form the active catalyst. MAO (methyl aluminoxane) is consistently used as a highly efficient activator for these systems.[4] Despite the success of the MAO co-catalyst in generating highly active metallocene polymerisation catalysts there remains an ambiguity over its role in the activation of the metal centre and the nature of the resultant anionic species formed despite extensive research in both academia and industry.[2, 5]

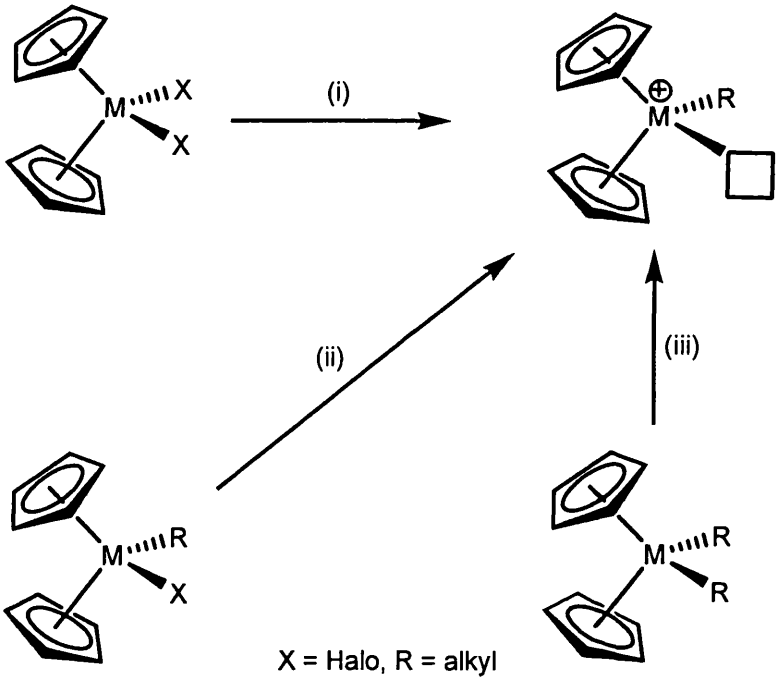

Figure 2: Common routes to generate the catalytically active complex for olefin polymerisation, '□' signifies a virtual vacant site.

(ii) Anion metathesis to precipitate an inorganic MX salt (M = Ag, Tl, Na and X = halide) and partner the metallocene with a weaker coordinating anion, *e.g.*, the halide abstraction reaction with $Na[BAr_F]$[6] (the co-catalyst in this case).[2] (iii) Activation of dialkyl metallocenes. This has received considerable interest due to its advantages over the ill-defined MAO based systems. These include the formation of well-defined characterisable ion-pair systems – allowing for reactivity trends to be studied in-depth and rationalised. The activation of dialkyl metallocenes can be further broken down to three distinct types (Figure 3).

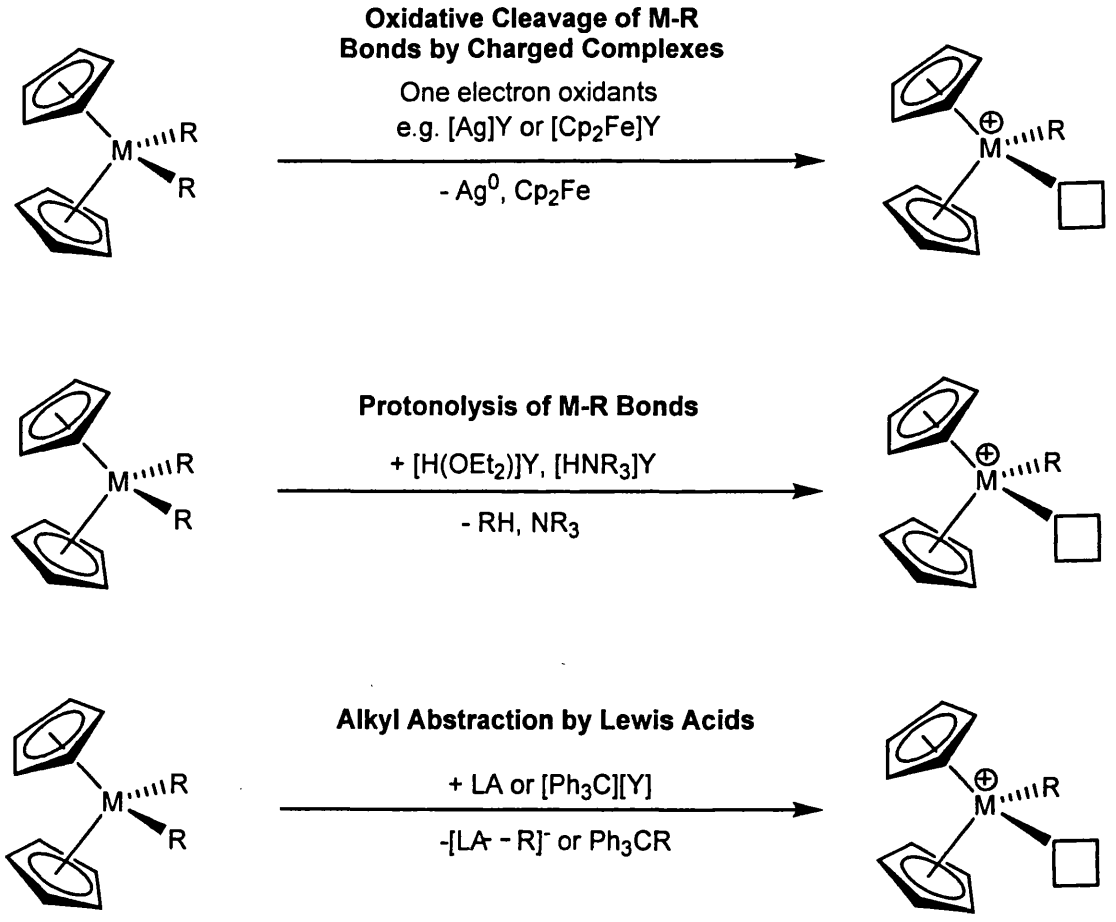

Figure 3: The various methods for the activation of the dialkyl metallocene pre-catalysts.

The reaction of Cp_2MR_2 with one electron (*e.g.*, Ag[Y] or Cp_2Fe[Y]) oxidants has been demonstrated to yield cleanly the desired active catalyst and when R = Me, ½ an equivalent of ethane (*e.g.*, the reaction of Ag[*closo*-$CB_{11}H_{12}$] with $(C_5H_4Me)_2ZrMe_2$, which cleanly yields $(C_5H_4Me)_2ZrMe(\eta^1$-*closo*-$CB_{11}H_{12})$, Figure 4).[7-10]

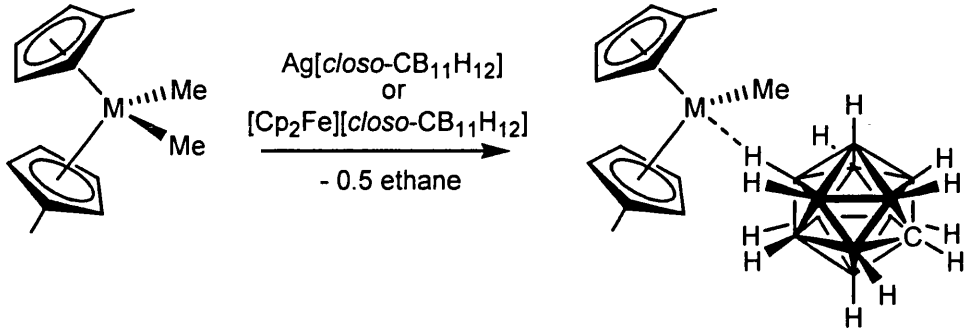

Figure 4: The oxidative cleavage of Zr-Me to generate the intimate ion pair $(C_5H_4Me)_2ZrMe(\eta^1$-*closo*-$CB_{11}H_{12})$.

Protonlysis of metal alkyl bonds has been extensively used to activate the pre-catalysts since Bochmann and co-workers reported the synthesis of $[Cp_2Ti(NH_3)Me]^+$ by the addition of ammonium salts to the dialkyl precursors.[11, 12] To prevent the coordination of the resultant amine (thereby reducing catalyst activity) bulky tri-alkyl ammonium cations were developed and used to synthesis a range of cationic complexes without the undesirable $R_3N\cdots M^+$ formation.[13-15] However, coordination of these bulky amines has still been observed for a number of systems *e.g.*, $[\kappa^2$-$Me_2Si(N^tBu)_2Zr(CH_2Ph)NMe_2Ph][B(C_6F_5)_4]$.[16, 17] The acidic carborane *nido*-$C_2B_9H_{13}$ can also protonate M-R bonds, generating a zwitterionic complex (Figure 5).[13, 15]

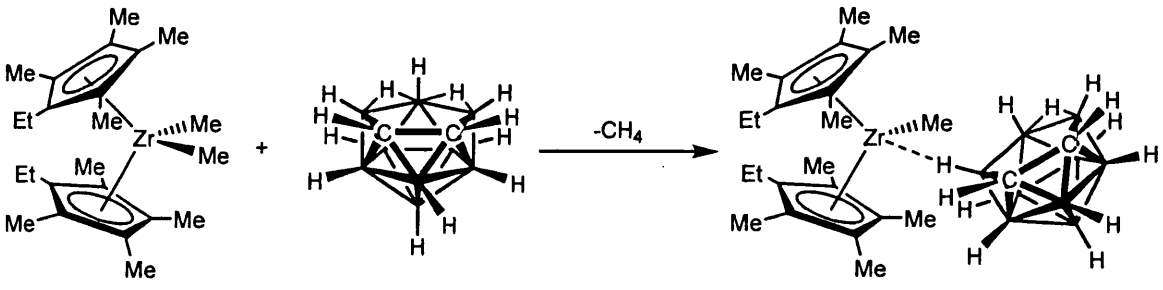

Figure 5: Protonation of a zirconium alkyl bond by the acidic *nido*-carborane $C_2B_9H_{13}$.

The final methodology outlined in Figure 3 involves the transfer of a methide (CH_3^-) from the metallocene to a suitable Lewis acid. Alkyl abstraction is readily achieved by the addition of the trityl $[CPh_3]^+$ cation, forming a neutral by-product (Ph_3C-Me when R = Me) that does not interfere with olefin polymerisation.[18-21] NMR investigations into the mechanism of alkyl abstraction (when R = Me) revealed that the initial product is the methyl bridged dimer $[(Cp_2ZrMe)_2(\mu\text{-Me})]^+$ that reacts with a further equivalent of $[Ph_3C]^+$ to generate the monomeric cationic complex (Figure 6).[22]

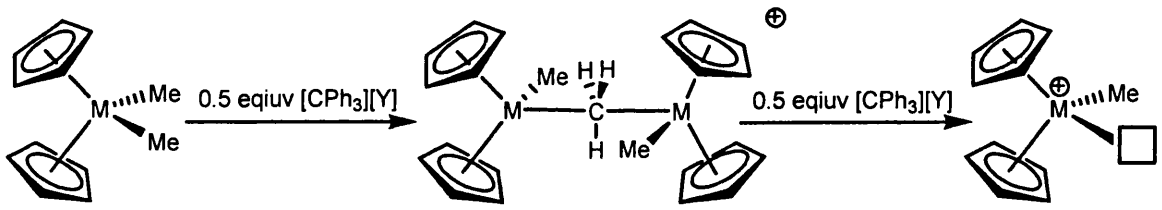

Figure 6: Reaction mechanism for the methyl abstraction by trityl salts. (Y = $[B(C_6F_5)_4]^-$)

The intermediate can be cleanly synthesised by the addition of ½ an equivalent of $[Ph_3C][B(C_6F_5)_4]^-$, and is in itself an active catalyst for olefin polymerisation (albeit with a lower turn-over frequency than the respective monomeric complex)[21]. The $[Ph_3C]^+$ cation has also been reported to act as one electron oxidant, though not with respect to d^0 metal alkyls, where alkyl abstraction is the only mode of activity documented.[23, 24]

The most commonly used neutral Lewis acid is $B(C_6F_5)_3$,[25-27] that on methide abstraction generates the anion, $[MeB(C_6F_5)_3]^-$. Other suitable Lewis acids demonstrated to activate Cp_2MR_2 complexes are dehydroxylated alumina,[28] $Al(C_6F_5)_3$[29] and numerous functionalised three coordinate boranes (Figure 7).[2, 30-32 33]

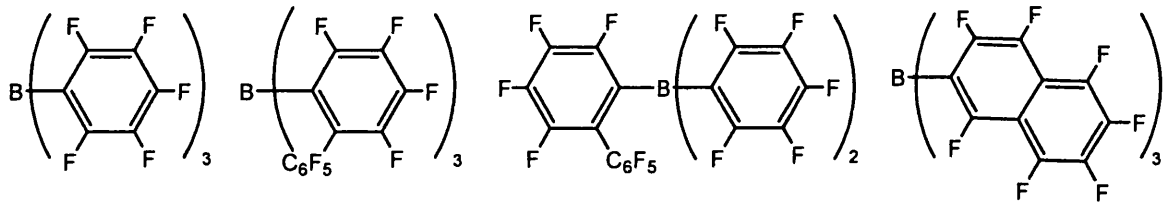

Figure 7: Common perfluorinated aryl boranes and their acronyms.

The reactions resulting in the formation of the $[MeB(C_6F_5)_3]^-$ anion are of particular interest, as in the absence of a stronger Lewis base the product formed is a contact ion pair. A range of these zwitterion complexes have been crystallographically characterised and the anion is bound to the metal centre through a bridging methyl moiety, *e.g.*, $(1,2\text{-}Me_2Cp)_2ZrMe(\mu\text{-}Me)B(C_6F_5)_3$ and $(C_6H_4N(^tBu))_2OZrMe(\mu\text{-}Me)B(C_6F_5)_3$ (Figure 8).[25, 26, 34]

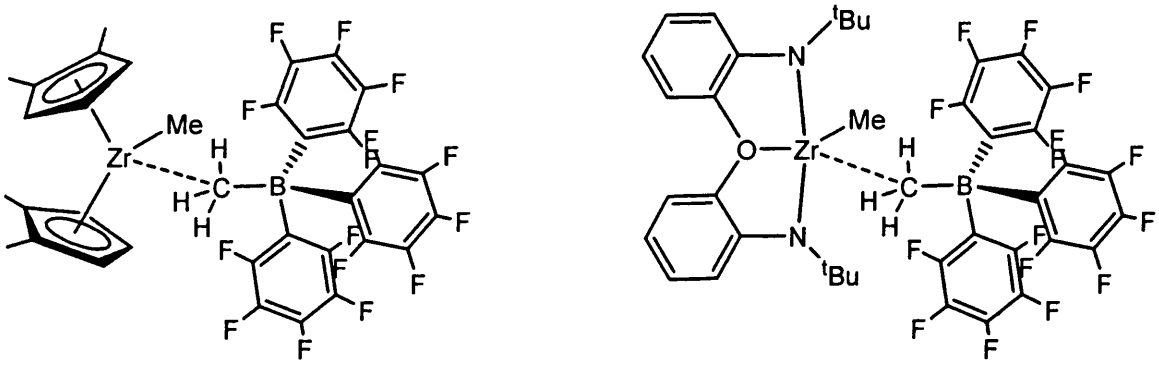

Figure 8: Examples of the zwitterion complexes exhibiting the bridging (μ-Me) moiety.

These isolated complexes are efficient catalysts for olefin polymerisation and require no additional MAO co-catalyst. The anion···cation binding motif (a M-Me-B

linkage) is reminiscent of the [1-H-*closo*-$CB_{11}Me_{11}$]$^-$ interaction with the simple alkali salts and the phosphine stabilised silver salts.[35-37] It can also be viewed as a model for the metal alkane σ bond, with a close M···H_3C contact implicit of a significant interaction (Zr···C distances ranging from 2.497(12) Å for the only non metallocene Zr-(μ-Me)-B, to between 2.549(3) Å and 2.640(7) Å for the zirconecenes).[25, 34, 38] The effect on the anion on its binding to a zirconium cation has been compared to that of the 'free' anion, with a slight elongation of the B-CH_3 bond occurring on coordination (from 1.638(5) Å to 1.66 Å - 1.69 Å). This suggests that the interaction with electrophilic zirconium is having a slight weakening effect on the B-CH_3 bond. The Zr-CH_3-B angle is generally non linear (ranging from 160 to 174°), whilst the geometry around the boron remains tetrahedral – suggesting a non-covalent interaction. The Zr-H contacts where reported (closest 2.25(3) Å) are longer than bridging hydrides (1.78(2) to 2.05(3) Å) and agostic interactions (2.16 Å), further demonstrating the weak nature of the Zr···H_3C connection.[21, 26] The solution behaviour of these zwitterions is also noteworthy, with an upfield shift of the methyl protons of [$MeB(C_6F_5)_3$]$^-$ in the ^{1}H NMR spectrum on coordination to a metal centre proving the persistence of the Zr···H_3C interaction in solution.[39] NMR studies on (1,2-$Me_2Cp)_2ZrMe(\mu\text{-}Me)B(C_6F_5)_3$ shows that the anion is firmly bound at room temperature, but on heating becomes fluxional by two processes, anion dissociation/reassociation (Zr-Me bond cleavage) and M-CH_3/BCH_3 exchange (B-Me bond cleavage, Figure 9).[25, 26]

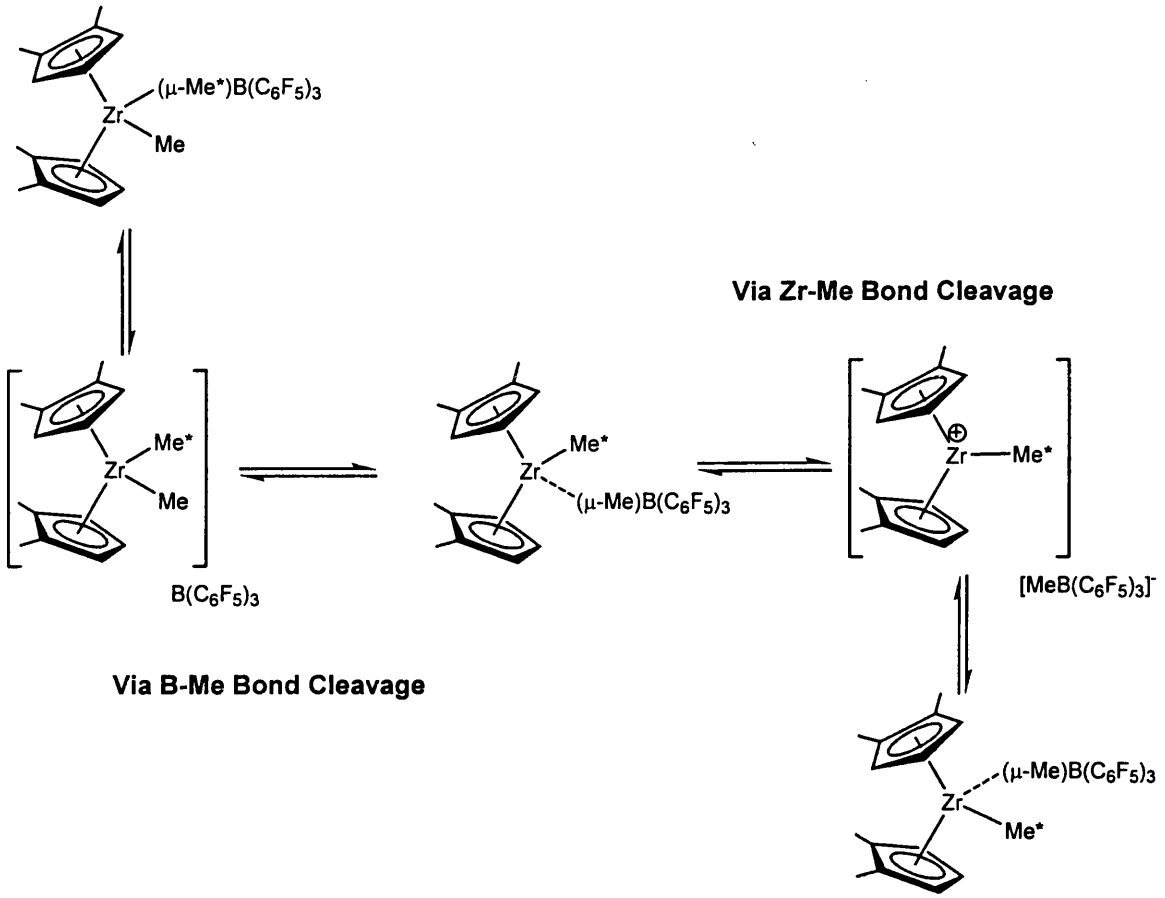

Figure 9: The two fluxional processes that take place on heating $[(1,2\text{-Me-}C_5H_3)_2ZrMe(\mu\text{-Me})B(C_6F_5)_3]$.

The weak binding of the $[MeB(C_6F_5)_3]^-$ anion and the reversible cleavage of the B-Me bond results in the sequential reaction of $Cp^*_2ZrMe(\mu\text{-Me})B(C_6F_5)_3$ with dihydrogen (Figure 10).[40] The anion is readily displaced from the metal coordination sphere to produce the dihydrogen adduct, that then undergoes stepwise hydrogenolysis to yield the mono- and dihydride complexes.

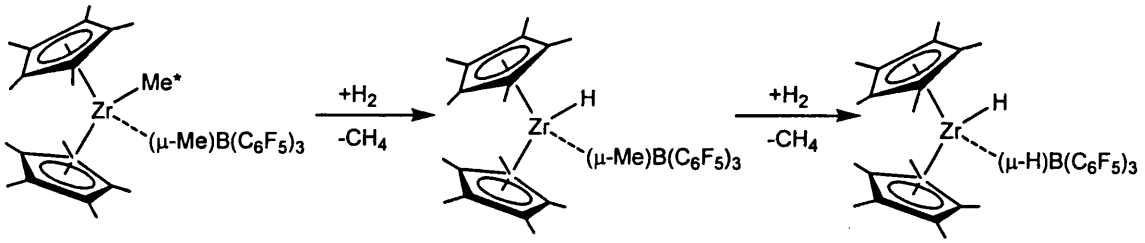

Figure 10: The stepwise hydrogenolysis of $Cp^*_2ZrMe(\mu\text{-Me})B(C_6F_5)_3$.

These $[MeB(C_6F_5)_3]^-$ complexes show a range of stabilities, $(C_6H_4N(^tBu))_2OZrMe(\mu\text{-}Me)B(C_6F_5)_3$ decomposes within hours at room temperature in hydrocarbon solvents (*e.g.* toluene), while in contrast the metallocene-derived products can be stable in solution for days.[2] Common decomposition routes (in hydrocarbon solvents) include anion B-C bond cleavage (C_6F_5 transfer to the metal) and fluoride abstraction from the anion by the electrophilic metal.[25, 41] In halocarbon solvents (*e.g.* CH_2Cl_2) rapid chloride abstraction can occur.[42]

The related bulkier Lewis acidic boranes (Figure 7) do not form zwitterionic complexes on methide abstraction, the unfavourable steric interactions prevent the close approach and the formation of the M-(μ-Me)-B bridge. Instead they form monomeric solvent separated ion pairs or the (μ-Me) bridged 'intermediate' zirconium dimers.[2] The reaction of less sterically hindered metal complexes (*e.g.* Cp^*ZrMe_3) with $B(C_6F_5)_3$ generates solvent separated ion pairs,[43, 44] whilst when R = benzyl (*e.g.*, in the *ansa* zirconocene *rac*-$(Me_2Si(indenyl)_2)ZrR_2$) alkyl abstraction leads to intramolecularly stabilised separated ion pair (Figure 11).[38]

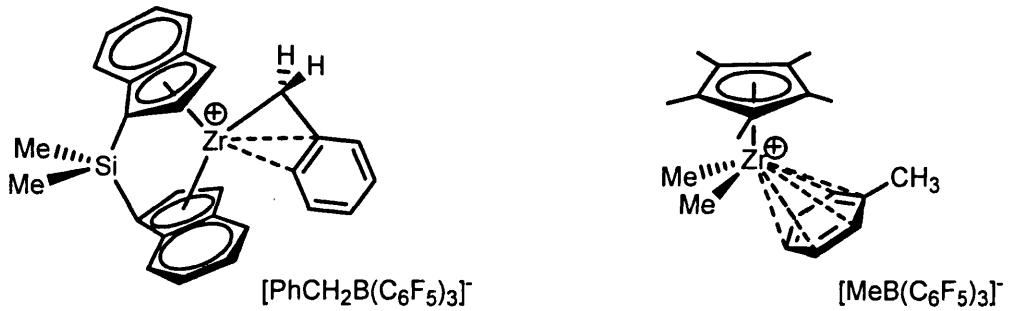

Figure 11: Examples of well-separated ion pair complexes resulting from alkyl abstraction.

In all these isolated systems there is an important balance that needs to be addressed. To prevent compound decomposition the metal centre needs to be stabilised by an interaction with a Lewis base; however; strong coordination reduces catalyst activity. Therefore the interaction must be sufficient to preserve the site in the absence of alkene, but weak enough to be easily displaced thus not suppressing activity. The effect of the anion is best exemplified by catalyst polymerisation activity data, with the order of coordinating power for a series of anions as $[MeB(C_6F_5)_3]^-$ > $[B(C_6F_4SiR_3)_4]^-$ > $[B(C_6F_5)_4]^-$ > $[CN\{B(C_6F_5)_3\}_2]^-$. The least coordinating anion produces catalysts with the lowest activation barrier for the displacement by the substrate and thus highest turn over frequencies.[22, 31, 41, 45]

Apart from the group IV metallocene based olefin polymerisation catalysts, there is a rapidly growing number of alternatives, particularly utilising late transition metal catalysts.[1, 46, 47] The unique properties of these systems, including, their ability to produce highly branched polymers and to incorporate highly polar monomers without catalyst deactivation make them a highly attractive alternative. One of the most extensively studied areas of these late transition metal systems is the CpCo (III) complexes, pioneered by Bergmann ($CpCo(PPh_3)_2Me_2$) and Brookhart ($[Cp^*Co(L)Et]^+$ L = C_2H_4, PMe_3 $P(OMe)_3$ and $P(C_6H_4R)_3$) (Figure 12). [48-55]

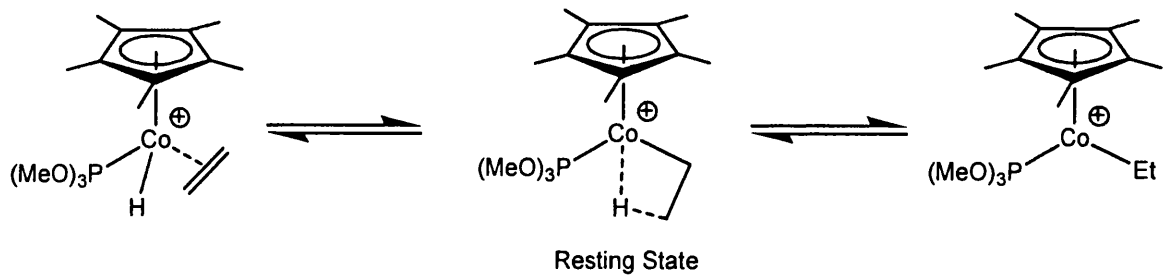

Figure 12: Dynamic processes involved in $[Cp^*Co(P(OMe)_3)Et][Y]$ (Y = $[BF_4]^-$ or $[BAr_F]^-$).

The polymerisation active state involves a cationic Co(III) alkyl complex $[CpCo(L)Me]^+$.[48, 56] Studies on the model complex $CpCo(PPh_3)Me_2$ demonstrated the reversible dissociation of PPh_3 to form the Co(III) complex $CpCoMe_2$, that is stable, yet electronically unsaturated. This complex readily undergoes methyl exchange with $CpCo(PPh_3)Me_2$ and interestingly with Cp_2ZrMe_2 via a methyl bridged dimer[54] - similar to that characterised previously for the cationic zirconocene methyl bridged dimers (Figure 13).[2]

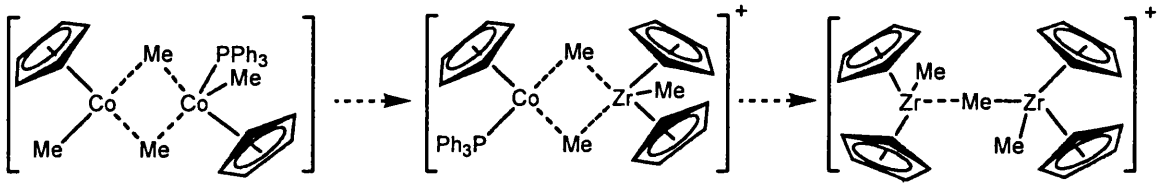

Figure 13: The methyl bridged dimers formed by the sequential replacement of an unsaturated $CpCoMe_2$ fragment for a $[Cp_2ZrMe]^+$.

The behaviour of the 16-electron fragment $\{CpCoMe_2\}$ is similar to that previously reported for the cation $[Cp_2ZrMe]^+$, both of which alleviate their coordinative unsaturation by the formation of methyl bridged dimers. In the absence of any Cp_2ZrMe_2, $[Cp_2ZrMe]^+$ has been shown to bind $[MeB(C_6F_5)_3]^-$. Thus a $[CpCo(L)Me]^+$ cation would be expected to behave similarly and in the exclusion of other Lewis bases form a contact ion pair – though no such compounds are currently known. Furthermore an isolobal relationship can be drawn between the d^6, 16 electron fragments, $\{CpCo(PR_3)Me^+\}$ and $\{CpRe(CO)_2\}$ (Figure 14), a complex that has been used to generate the stablest unsupported alkane complexes reported.[57, 58] The cationic charge in the $\{CpCo(PR_3)Me^+\}$ fragment should provide a significant supplementary force to aid the binding of weak donors.

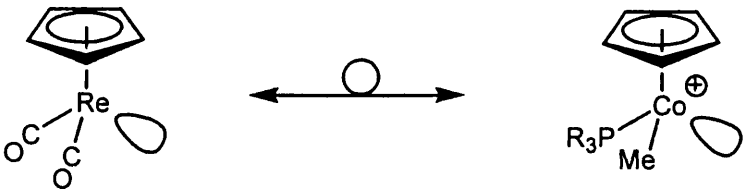

Figure 14: The isolobal relationship between the 16e⁻ fragments {$CpReCO_2$} and {$CpCo(PR_3)Me^+$}.

3.1.1: Scope of Chapter.

This chapter will discuss the synthesis of further reagents to introduce the [1-H-*closo*-$CB_{11}Me_{11}$]⁻ anion to the metal coordination sphere of cationic metal centres that are based on these polymerisation pre-catalysts. The partnering of [1-H-*closo*-$CB_{11}Me_{11}$]⁻ with a number of cationic zirconocene complexes will be discussed, including their solid-state characterisation and solution studies (*e.g.*, polymerisation activity, anion···cation interactions). The solid-state structure of intimate Zr···H_3C interactions is of interest as a model for the binding of alkanes to transition metals, as well as providing a comparison to the retarded methide abstraction complexes M···(μ-Me)$B(C_6F_5)_3$. Decomposition pathways have been investigated, including the identification of metal mediated cage activated products.

Attempts to partner the [1-H-*closo*-$CB_{11}Me_{11}$]⁻ anion with Co(III) complexes analogous to those used by Bergmann and Brookhart is also outlined, including a number of complexes formed from the reductive elimination of ethane from a transient Co(IV) complex. Finally, the initial characterisation of a Co···anion bound complex is presented which exhibits anion methyl chemical shift changes in the ^1H NMR spectrum indicative of metal···CH_3 contacts (see Chapter Two).

3.2. Results and Discussion:

3.2.1. Synthetically Useful Salts:

The synthesis of the $[HNMe_2Ph]^+$ salt of the [1-H-*closo*-$CB_{11}Me_{11}]^-$ anion is readily accomplished by the use of a two phase H_2O/Et_2O extraction methodology in an analogous manner to that used for Ag[1-H-*closo*-$CB_{11}Me_{11}]^-$. The neutral radical [1-H-*closo*-$CB_{11}Me_{11}]^\bullet$ can also be accessed utilising the synthesis previously reported for the related permethylated radical [*closo*-$CB_{11}Me_{12}]^\bullet$.[59] More importantly (for the activation of zirconocene polymerisation pre-catalysts) the $[Ph_3C]^+$ (trityl) cation is synthesised in a one step manner from the reaction of equimolar quantities of Cs[1-H-*closo*-$CB_{11}Me_{11}$] and Ph_3CBr in CH_2Cl_2 (Figure 15).

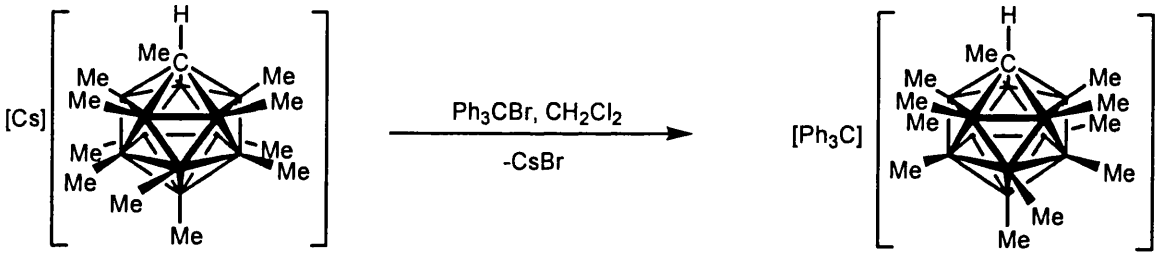

Figure 15: The reaction scheme for the formation of $[Ph_3C]$[1-H-*closo*-$CB_{11}Me_{11}$].

The resultant brown oil is recrystallised from the slow diffusion of hexanes into a saturated CH_2Cl_2 solution, yielding crystalline material suitable for an X-ray diffraction study (Figure 16). This confirmed that the compound composition was $[CPh_3]$[1-H-*closo*-$CB_{11}Me_{11}$] **(8)**. The asymmetric unit of **(8)** contains one trityl cation and one [1-H-*closo*-$CB_{11}Me_{11}]^-$ anion, with no observed disorder allowing for the unambiguous location of the cage carbon atom. The most significant feature of the structure is a close approach of an anion CH_3 vertex to the carbocation. The C7-C13 distance at 3.67 Å lies just within the sum (3.70 Å) of the van der-Waals radii of carbon

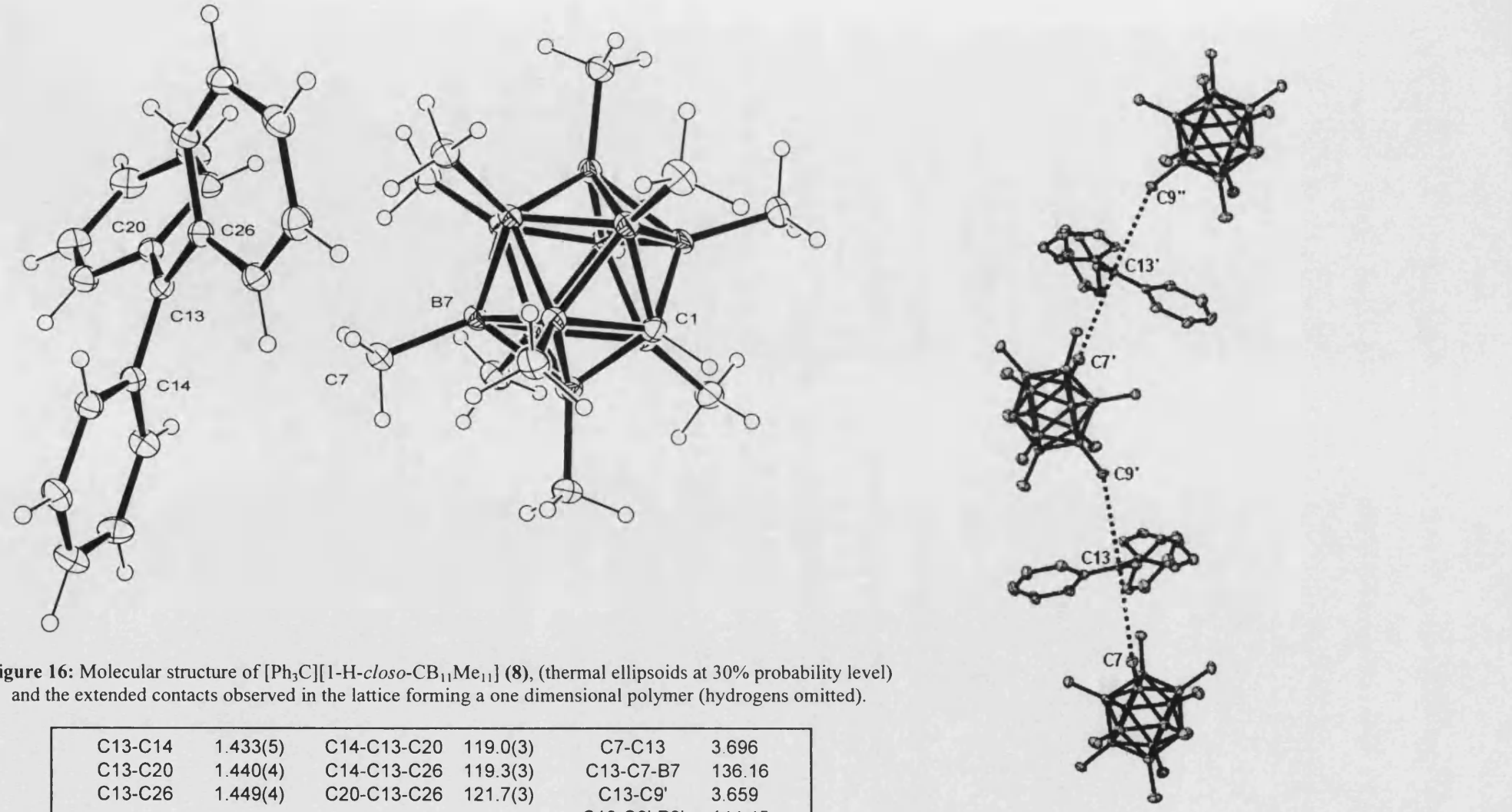

Figure 16: Molecular structure of $[Ph_3C][1\text{-H-}closo\text{-}CB_{11}Me_{11}]$ **(8)**, (thermal ellipsoids at 30% probability level) and the extended contacts observed in the lattice forming a one dimensional polymer (hydrogens omitted).

C13-C14	1.433(5)	C14-C13-C20	119.0(3)	C7-C13	3.696
C13-C20	1.440(4)	C14-C13-C26	119.3(3)	C13-C7-B7	136.16
C13-C26	1.449(4)	C20-C13-C26	121.7(3)	C13-C9'	3.659
				C13-C9'-B9'	144.45

Table 1: Selected bond lengths (Å) and angles (°) for **(8)**.

and CH_3. A further contact in the extended lattice from an adjacent anion (C9'-C13 3.66Å) also falls within this limit, resulting in the extended structure propagating into a one-dimensional polymer (Figure 16). Similar extended structures have been observed for $[Ph_3C]_2[closo\text{-}B_{12}F_{12}]$ and $[Ph_3C][closo\text{-}Me_3NB_{12}F_{11}]$. [60, 61] These complexes also exhibit anion···cation contacts just inside the sum (3.17Å) of van der-Waals radii of carbon and fluorine (Figure 17). Inspection of the geometry around the carbocation core in **(8)**, revealed a trigonal planar arrangement, with angles around the central C approximating to 120° and the sum of the three C-C13-C angles is 360.0(3)°. The lack of any distortion does not rule out any interaction *per se* as the symmetrical arrangement of the two C13···H_3C contacts above and below the plane (C7-C13-C9' 176.76°) produces a trigonal bipyramidal arrangement with the same planar Ph_3C core.

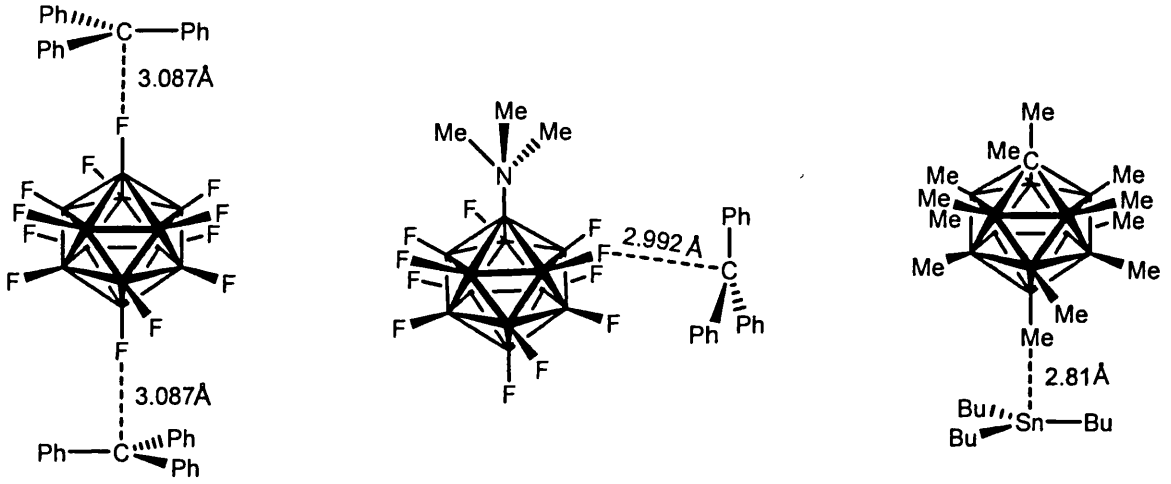

Figure 17: Solid State structures of $[Ph_3C]_2[closo\text{-}B_{12}F_{12}]$, $[Ph_3C][1\text{-}NMe_3\text{-}closo\text{-}B_{12}F_{11}]$ and $Bu_3Sn(closo\text{-}CB_{11}Me_{12})$ with their respective distances to the Group IV cations.

The weak contacts in the perfluorinated borane systems have been ascribed to crystal packing forces due to their longer BF···$^+CPh_3$ (2.992(6) Å, 2.942(6) Å, and 3.087(2) Å) distances when compared to $[Ph_{3-x}C(p\text{-}OMe\text{-}C_6H_4)_x][BF_4]$ (x = 1 and 2, 2.68 Å and 2.58 Å respectively) where the contacts are significant.[62] The isoelectronic

to **(8)** complex, $^{n}Bu_3Sn(closo\text{-}CB_{11}Me_{12})$ displays close cation···anion interactions which are significant, but these by contrast to **(8)** are much shorter (2.81 Å) than the combined (3.87 Å) van der-Waals radii of a carbon (1.7Å) and a Sn atom (2.17 Å).[63] The findings from these related complexes strongly suggests that the long contacts observed in **(8)** can be attributed solely to efficient crystal packing rather than any specific interaction.

Solution NMR spectroscopy on complex **(8)** in CD_2Cl_2 is informative as the resonances attributable to the anion methyl vertices in the $^{1}H\{^{11}B\}$ NMR spectrum (-0.21 ppm, -0.40 ppm and –0.62 ppm) are close to that reported for the non-interacting cation $[^{n}Bu_4N]^{+}$ in the same solvent (0.18 ppm, -0.44 ppm and –0.56 ppm). The carbocation resonance in the $^{13}C\{^{1}H\}$ at 212 ppm is also close to that reported for analogous complexes with the weakly coordinating fluorinated boranes, $[CN\{B(C_6F_5)_3\}_2]^{-}$, and $[B(C_6F_5)_4]^{-}$ anions (211 ppm, 210 ppm and 211 ppm respectively).[45, 60, 61, 64] The similarity of the solution $^{13}C\{^{1}H\}$ NMR resonances combined with the lack of any chemical shift change in the $^{1}H\{^{11}B\}$ NMR spectrum shows that the long contacts observed in the solid state do not persist in solution. Heating a toluene solution of **(8)** overnight resulted in no cage decomposition (*vide infra*). This is a further indication of the absence of intimate anion···cation contacts, as the $[Li]^{+}$ and the $[Ag]^{+}$ (see Chapter one) salts where close cation anion interactions have been characterised undergo cage activation at raised temperatures.[65]

The three complexes, **(8)**, $[1\text{-}H\text{-}closo\text{-}CB_{11}Me_{11}]^{\bullet}$, and $[HNMe_2Ph][1\text{-}H\text{-}closo\text{-}CB_{11}Me_{11}]$ will be used throughout the remainder of this chapter as reagents for introducing the highly alkylated carborane anion to metal centres. The neutral radical

[1-H-*closo*-$CB_{11}Me_{11}$]$^{\bullet}$ has excellent solubility in hydrocarbon solvents, but the $[Ph_3C]^+$ and $[HNMe_2Ph]^+$ cations possess no detectable solubility in hydrocarbon solvents, similar to the Ag(I) salts reported in Chapter 2.

3.2.2: Partnering [1-H-*closo*-$CB_{11}Me_{11}$]$^-$ with Zirconium alkyl complexes.

3.2.2.1: Cp_2ZrMe_2

The reaction of equimolar quantities of **(8)** (or [1-H-*closo*-$CB_{11}Me_{11}$]$^{\bullet}$) with the simple zirconocene Cp_2ZrMe_2 in arene solvents (*e.g.*, benzene, toluene or fluorobenzene, (C_6H_5F)) rapidly produced a bright yellow solution in dilute concentrations. In higher concentrations the formation of higher aggregates and the precipitation of an oil phase occurs, as reported for the activation of zirconocenes by the fluorinated borates, Lewis acidic boranes and MAO.[45, 66] Recrystallisation of a dilute C_6H_5F solution by the slow diffusion of pentanes at -20°C yielded large yellow crystals suitable for X-ray diffraction studies. This revealed that the asymmetric unit consisted of the contact ion pair Cp_2ZrMe(1-H-*closo*-$CB_{11}Me_{11}$), **(9)**, and a molecule of disordered fluorobenzene, readily modelled by equal occupancy of two separate sets of sites (Figures 18 and 19).

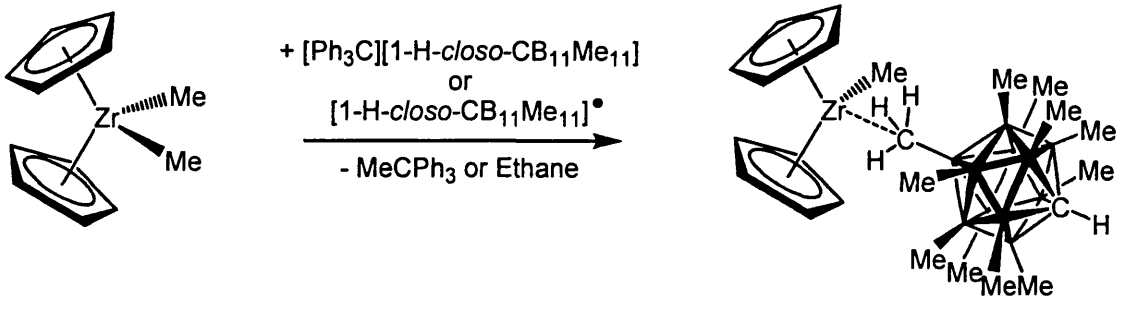

Figure 19: The formation of **(9)**, via the reaction of Cp_2ZrMe_2 with **(8)**, or the neutral radical [1-H-*closo*-$CB_{11}Me_{11}$]$^{\bullet}$.

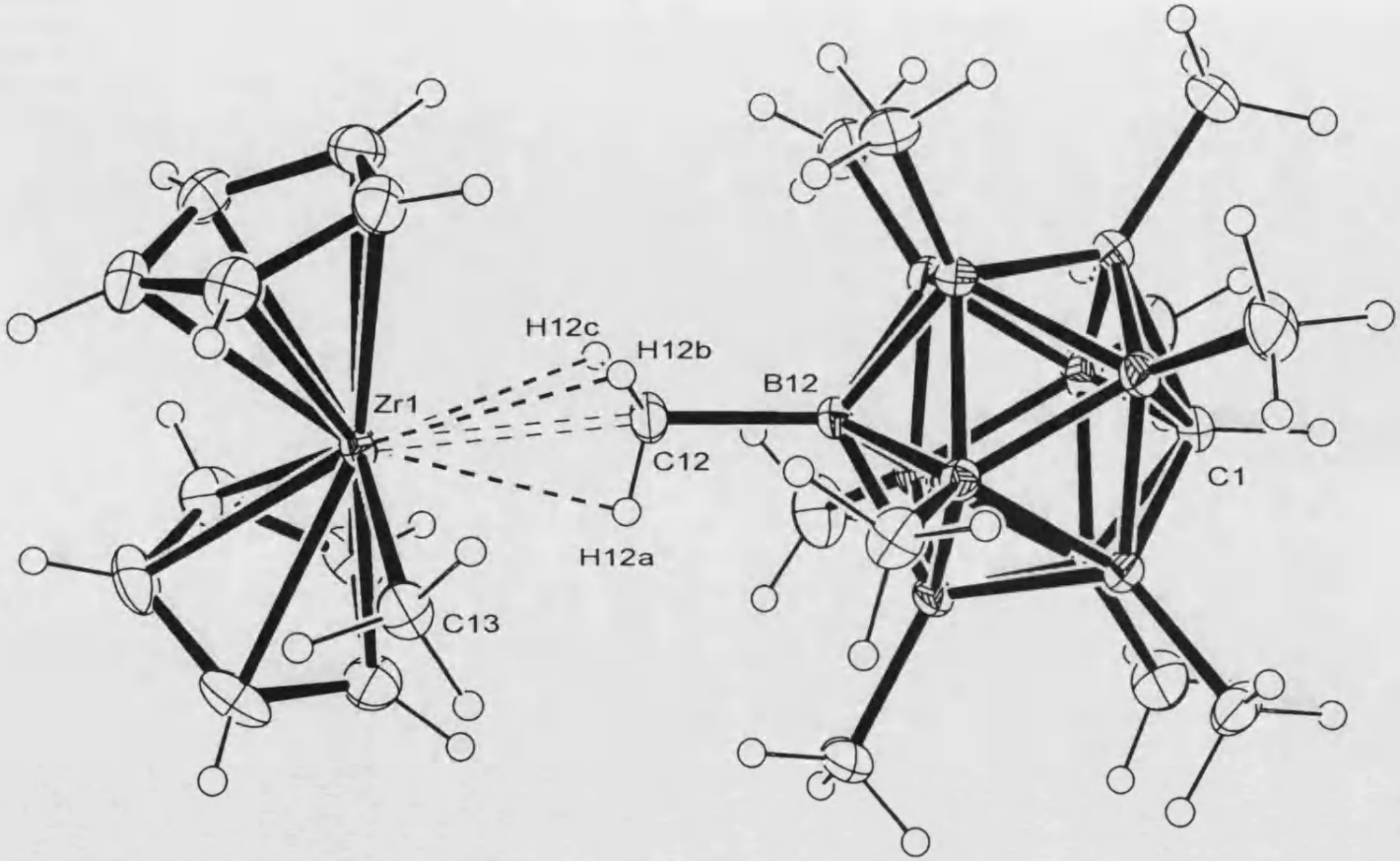

Zr1-C13	2.2612(15)
Zr1-C12	2.516(2)
Zr1-H12a	2.38(2)
Zr1-H12b	2.34(2)
Zr1-H12c	2.45(2)
Zr1-C12-B12	172.2(1)
B12-C12	1.6235(19)
C12-H12a	0.84(2)
C12-H12b	0.97(2)
C12-H12c	0.99(2)
B12-C12-H12a	103(1)
B12-C12-H12b	109(1)
B12-C12-H12c	113(2)
C12-Zr1-C13	89.1(1)

Table 2: Selected bond lengths (Å) and angles (°) for **(9)**.

Figure 18: Molecular structure of $Cp_2ZrMe(1\text{-}H\text{-}closo\text{-}CB_{11}Me_{11})$, **(9)** (thermal ellipsoids shown at the 30% probability level), a disordered molecule of solvent co-crystallite (C_6H_5F) is not shown for clarity.

Complex **(9)** consists of a bent sandwich structure with the Cp rings canted away from the anion, this structural feature is common throughout the zwitterionic metallocene complexes (*e.g.*, $(1,2\text{-}Me_2Cp)_2ZrMe(\mu\text{-}Me)B(C_6F_5)_3$ and $Cp^*_2ZrMe(\mu\text{-}Me)B(C_6F_5)_3$).[25] The anion···cation interaction is through the antipodal $BCH_3(12)$ vertex of the anion and generates a Zr-(μ-Me)-B bridging moiety reminiscent of the $[MeB(C_6F_5)_3]^-$ analogoues.[2, 25] The H_3C···Zr distance is close, with a Zr1-C12 distance of 2.516(2) Å, comparable to that of Zr metallocenes partnered with $[MeB(C_6F_3)_3]^-$ (which range from 2.549(3) Å and 2.640(7) Å) and is significantly longer (by 0.255 Å) than the terminal Zr-Me distance (2.2612(15) Å). A direct comparison with the analogous complex $[Cp_2ZrMe(\mu\text{-}Me)B(C_6F_5)_3]$ is particularly relevant as any differences in the structural metrics will originate solely from the change in the anion. The molecular structure with pertinent bond lengths and angles is shown in Figure 20.[67]

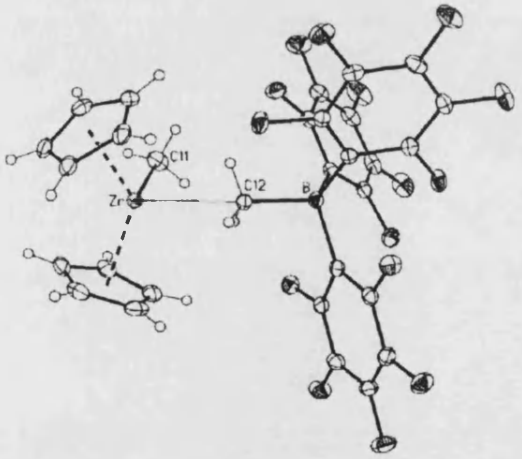

Zr-C11	2.251(3)
Zr-C12	2.556(2)
C11-Zr-C12	87.70(9)
C12-B	1.667(3)
Zr-C12-B	169.10(16)

Figure 20: Molecular Structure of $Cp_2ZrMe(\mu\text{-}Me)B(C_6F_5)_3$ and selected bond lengths (Å) and angles (°).

The Zr-bridging methyl distance in **(9)** is shorter by 0.04 Å, whilst the Zr-terminal Me is longer in **(9)** by 0.01 Å. These differences taken together suggest that the $[1\text{-H-}closo\text{-}CB_{11}Me_{11}]^-$ anion is interacting slightly more strongly with the cationic zirconium than its $[MeB(C_6F_3)]^-$ counterpart. The Zr-C12-B12 linkage in **(9)** is

essentially linear (172.2(1)°) and is close to that reported for $Cp_2ZrMe(\mu\text{-}Me)B(C_6F_5)_3$ (169.10(16)°), suggesting that the intermolecular bonding in **(9)** is unaffected by steric interactions, unlike the bulkier metallocene $(1,2\text{-}Me_2Cp)_2ZrMe(\mu\text{-}Me)B(C_6F_5)_3$, which has a Zr-(μ-Me)-B angle of 161.8(2)°. It also infers that there are no additional intermolecular interactions to anions adjacent in the lattice, as is the case for a number of $\{PR_3Ag\}^+$ complexes. Examination of the extended structure reveals that the closest additional Zr-H_3C contact at 4.546 Å is considerably longer than would be expected for any significant contact. The B12-C12 bond length (1.6235(19) Å) shows no elongation when compared to the same vertex in non-interacting complexes (*e.g.*, Complex **(5)**, $[(Ph_3PAg(OEt_2)_2][1\text{-H-}\textit{closo}\text{-}CB_{11}Me_{11}]$ 1.6233(14) Å).

The data collection for **(9)** was of sufficient quality to allow for the free refinement of the hydrogen positions associated with the interacting vertex. This revealed three equally close (within errors) Zr-H contacts (average 2.39 Å). These are significantly longer than that found in the β-agostic complex $[(MeC_5H_4)_2Zr(CH_2CH_3)PMe_3][BPh_4]$ (2.16 Å, no error reported) suggesting that the anion binding in **(9)** is weaker than this agostic interaction.[68] These Zr-H distances are however comparable to that in $Cp_2ZrMe(\mu\text{-}Me)B(C_6F_5)_3$, though in this case there are only two reported close contacts averaging to 2.38 Å. The tetrahedral geometry around C12 is not perturbed, with the associated bond angles and lengths (Figure 18) close to the ideal sp^3 (within the significant errors). Calculations on the closely related $[MeB(C_6F_5)_3]^-$ bound complexes determined that the interaction between the $\{Cp_2ZrMe\}$ and $\{MeB(C_6F_5)_3\}$ fragments was predominantly electrostatic in origin.[2] In **(9)** due to the lack of any distortion of the binding B-CH_3 vertex the same conclusion can be reached for $[1\text{-H-}\textit{closo}\text{-}CB_{11}Me_{11}]^-$.

It is of interest to investigate the solution behaviour of **(9)**, particular to determine if the close contact ion pair observed in the solid-state structure persists in solutions of weakly coordinating solvents. On dissolution in d_8-toluene, complex **(9)** affords a bright yellow solution that exhibits a single Cp resonance in the $^1H\{^{11}B\}$ NMR spectrum at 5.55 ppm and a terminal Zr-Me signal at 0.29 ppm, similar to that observed for $Cp_2ZrMe(\mu\text{-}Me)B(C_6F_5)_3$.[25] The C_{5V} symmetry of the cage is maintained in solution, indicated by both ^1H and ^{11}B NMR spectroscopy. Moreover, the $Zr\cdots H_3C$ contact persists in solution, with a significant chemical shift change observed for the $B\text{-}CH_3$ resonances in comparison to a non-interacting cation ($[(PPh_3)_2Rh(NBD)]^+$) in an identical solvent (Figure 21).

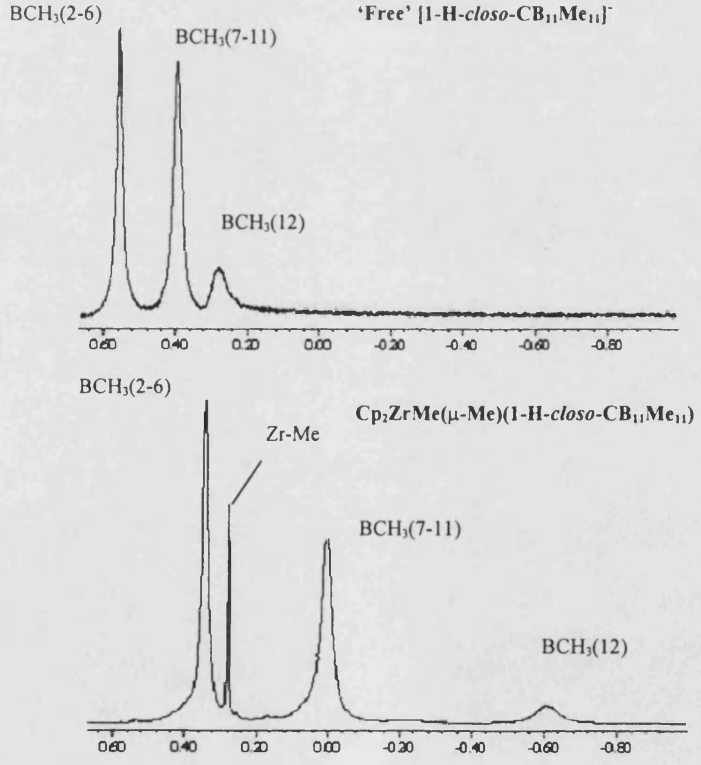

Figure 21: A comparison of the anion CH_3 region in the $^1H\{^{11}B\}$ NMR spectra for free [1-H-*closo*-$CB_{11}Me_{11}]^-$ and **(9)**, both in d_8-toluene.

A comparison of the two spectra shows the methyl resonances for **(9)** to be significantly broadened and the individual chemical shifts moved to higher field. The unambiguous assignment of the individual vertices was achieved by a combination of ^{11}B-^{11}B COSY and ^{1}H-^{11}B HMQC NMR spectroscopy. The change in chemical shift in the $^{1}H\{^{11}B\}$ NMR spectrum of **(9)** in comparison to that of free [1-H-*closo*-$CB_{11}Me_{11}$]$^-$ is significant for all three vertices and consistently upfield. The CH_3(12) vertex experiences the greatest shift (-0.91 ppm), followed by CH_3(7-11) (-0.42 ppm) and CH_3(2-6) the least (-0.24 ppm). A similar pattern is observed for the degree of broadening (pwhm) associated with each resonance; (CH_3(12) 14.2 Hz, CH_3(7-11) 6.7 Hz and CH_3(2-6) 3.4 Hz) compared to ~1 Hz for the free anion overall. This suggests that in solution the interaction between the anion and cationic zirconium fragment is primarily through the 12 and 7-11 BCH_3 vertices. Chemical shift changes of a similar magnitude have been observed for this anion partnered with $\{(PR_3)Ag\}^+$ fragments, though in this case in an opposite direction (Chapter Two). An upfield chemical shift change of equally large magnitude ($\Delta\delta = -1.14$ ppm) has been reported for the analogous $Cp_2ZrMe(\mu\text{-}Me)B(C_6F_5)_3$ (B-Me, 0.10 ppm) when compared to 'free' $[MeB(C_6F_5)_3]^-$ (B-Me, 1.24 ppm).[25, 39] The $^{13}C\{^{1}H\}$ NMR spectrum of **(9)** is uninformative with the anion CH_3 groups appearing as a very broad signal.

Cooling a d_8-toluene solution of **(9)** to progressively lower temperatures results initially in the CH_3(12) resonance broadening (at 273 K), followed by a significant sharpening at 223 K. Concomitantly the chemical shift for this vertex moves further upfield, ultimately to δ -1.00 ppm (223 K) with the signals for CH_3(2-6) and CH_3(7-11) moving in the opposite direction, approaching that observed for the free anion. The Cp resonances also shifts to 5.23 ppm. The upfield chemical shift change to the CH_3(12)

vertex at low temperature implies that there is some freezing out of a fluxional process. This low temperature structure approaches that observed in the solid state, *i.e.* $Cp_2ZrMe(12\text{-}\mu\text{-}Me\text{-}1\text{-}H\text{-}closo\text{-}CB_{11}Me_{10})$ as $CH_3(12)$ is shifted, but $CH_3(2\text{-}11)$ are not. Alongside this major compound are resonances at approximately 10% relative intensity (at 223 K) including a second Cp signal at 5.30 ppm and six observable broad low intensity anion methyl resonances between δ0.65 and –0.90 ppm in the $^1H\{^{11}B\}$ NMR spectrum. This is suggestive of a second compound in which the anion has lost the C_{5V} symmetry seen in the room temperature spectrum and also for the 12-isomer. This compound is assigned as the 7-isomer, $Cp_2ZrMe(7\text{-}\mu\text{-}Me\text{-}1\text{-}H\text{-}closo\text{-}CB_{11}Me_{10})$ (Figure 22), presumably the un-observed BCH_3 signal is coincident with one of more intense 12-isomer resonances.

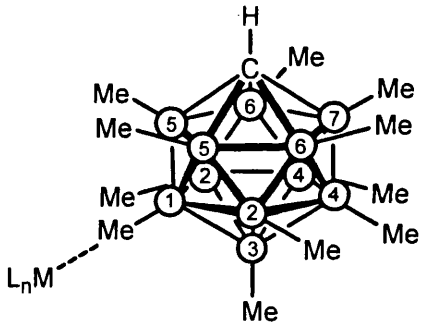

Figure 22: The 7 inequivalent B-CH_3 vertices in $[1\text{-}H\text{-}closo\text{-}CB_{11}Me_{11}]^-$ resulting on metal coordination through the 7 position.

Returning the solution to 298 K resulted in the original spectrum with only one Cp resonance observed. Therefore, a dynamic equilibrium exists between the two isomers (Figure 23) that is frozen out at 223 K.

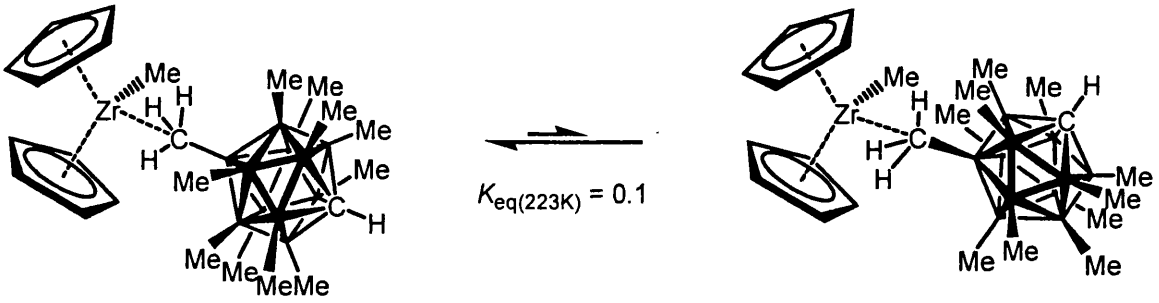

Figure 23: The dynamic equilibrium between two possible isomers of $Cp_2ZrMe(1\text{-}H\text{-}closo\text{-}CB_{11}Me_{11})$.

The presence of two isomeric forms agrees with calculations on the charge distribution across BCH_3 vertices in the $[1\text{-}H\text{-}closo\text{-}CB_{11}Me_{11}]^-$ anion, with the $BCH_3(7\text{-}11)$ and $BCH_3(12)$ vertices being approximately equally negative, whilst the $BCH_3(2\text{-}6)$ positions have an overall positive charge (see Chapter One).[63, 69] The related anion $[closo\text{-}CB_{11}H_{12}]^-$ has also been demonstrated to bind as two isomers in the complexes $CpMo(CO)_3(closo\text{-}CB_{11}H_{12})$ and $CpFe(CO)_2(closo\text{-}CB_{11}H_{12})$.[70, 71]

Compound **(9)** is stable at room temperature for days in arene solvents, similar to that reported for non bulky Cp systems partnered with the $[MeB(C_6F_5)_3]^-$ anion. Prolonged standing in solution results in the gradual decomposition of **(9)** (weeks) which is significantly accelerated on heating. The decomposition of a series of zirconcenes partnered with $[1\text{-}H\text{-}closo\text{-}CB_{11}Me_{11}]^-$ will be discussed in section **3.2.4.**

The reaction of complex **(9)** with hydrogen results in no change in the $^1H\{^{11}B\}$ NMR spectrum, with anion coordination still observed as determined by the distinctive upfield shift of the anion CH_3 resonances. No hydride resonances were detected and the Zr-Me signal at δ 0.29 ppm was still present. This is in contrast to the reaction of H_2 with $Cp_2ZrMe(\mu\text{-}Me)B(C_6F_5)_3$, in which the $[MeB(C_6F_5)_3]^-$ anion is displaced from the Zr coordination sphere by H_2, initiating the stepwise hydrogenolysis to ultimately

produce $Cp_2Zr(H)(\mu\text{-}H)B(C_6F_5)_3$ and two equivalents of methane.[25] The lack of reactivity observed implies, that with respect to the $\{Cp_2ZrMe\}^+$ fragment, the [1-H-*closo*-$CB_{11}Me_{11}$]$^-$ is more coordinating than H_2 and $[MeB(C_6F_5)_3]^-$. In contrast, the reaction of the stronger Lewis base MeCN does cleanly displace the [1-H-*closo*-$CB_{11}Me_{11}$]$^-$ anion and forms $[Cp_2ZrMe(MeCN)]$[1-H-*closo*-$CB_{11}Me_{11}$] as the only product (by $^1H\{^{11}B\}$ NMR spectroscopy and comparison to $[Cp_2Zr(R)MeCN][BPh_4]$).[10]

Attempts to generate **(9)** via the protonation of Cp_2ZrMe_2 with the ammonium salt, $[HNMe_2Ph]$[1-H-*closo*-$CB_{11}Me_{11}$] in an analogous manner to that using $[HNMe_2Ph][B(C_6F_5)_4]$,[21] failed. The resultant complex showed only a single Cp resonance in the $^1H\{^{11}B\}$ NMR spectrum but anion CH_3 resonances indicative of a non-coordinated cage. Hlatky and Turner have previously reported that the reaction of $[HNR_3][BPh_4]$ with less substituted metallocenes (including Cp_2ZrMe_2) underwent secondary reactions after the initial protonation step to give catalytically inactive materials.[15, 20] Furthermore, neutral amine coordination to the cationic metal centre partnered with the weakly coordinating $[B(C_6F_5)_4]^-$ anion has been reported for a mono-Cp titanium catalyst $[\{(C_5Me_4)Si(Me)_2N(^tBu)\}Ti(Me)(NR_3)]^+$ and two non-Cp zirconium complexes (Figure 24).[16, 17, 72]

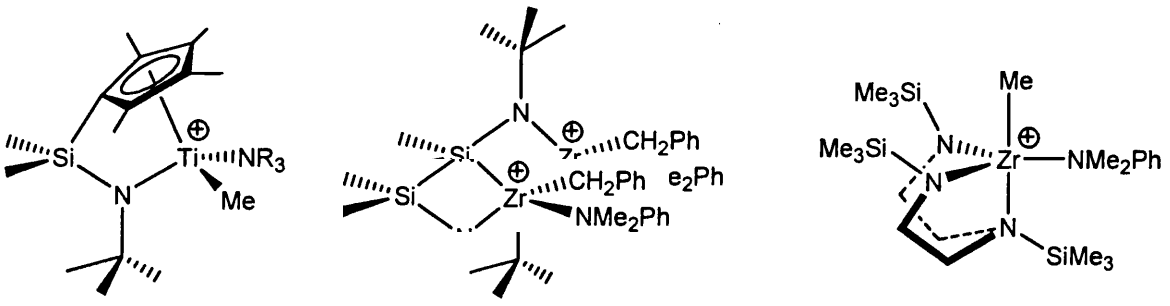

Figure 24: Examples of cationic d^0 metal cations stabilised by coordinated amine.

No attempts were made to isolate the product from the reaction of $[HNMe_2Ph][1\text{-}H\text{-}closo\text{-}CB_{11}Me_{11}]$ and Cp_2ZrMe_2 due to the absence of any cage interactions. It is plausible that amine coordination followed by subsequent secondary reactions occur in a related manner.

The reaction of Cp_2ZrMe_2 with ½ an equivalent of $[Ph_3C][1\text{-}H\text{-}closo\text{-}CB_{11}Me_{11}]$ produces $[\{Cp_2ZrMe\}_2(\mu\text{-}Me)][1\text{-}H\text{-}closo\text{-}CB_{11}Me_{11}]$, **(10)** as the major product (*vide infra*). Compound **(10)** is also synthesised as the major product by the addition of an excess of Cp_2ZrMe_2 to **(9)** (Figure 25).

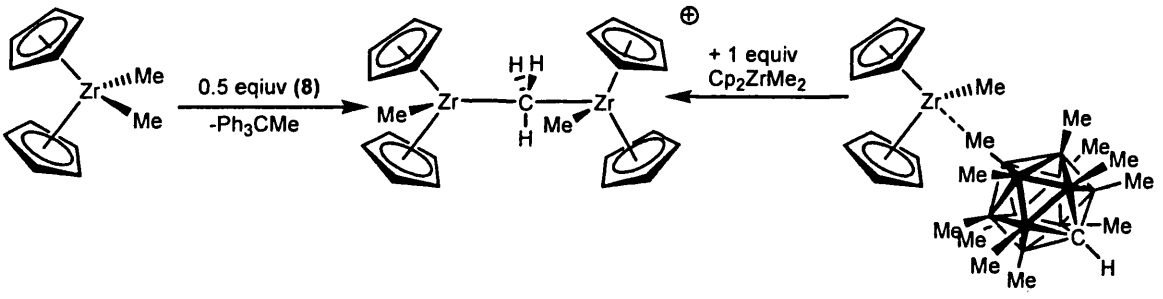

Figure 25: The synthetic routes to $[\{Cp_2ZrMe\}_2(\mu\text{-}Me)][1\text{-}H\text{-}closo\text{-}CB_{11}Me_{11}]$.

The $^1H\{^{11}B\}$ NMR spectrum shows no cage interactions with anion resonances identical to that for the free anion in d_8-toluene (though compound **(10)** is only sparingly soluble in non-polar hydrocarbon solvents – as previously reported for the $[B(C_6F_5)_4]^-$ analogue).[22] The resonances for the cation portion of **(10)** are as reported previously for the $[B(C_6F_5)_4]^-$ and PBB anions.[45, 73] Crystals suitable for an X-ray diffraction study were obtained by the slow diffusion of pentane into a dilute C_6H_5F solution at -20°C. The asymmetric unit of **(10)** consisted of a well-separated discrete anion and two Cp_2ZrMe_2 moieties (Figure 26). The bridging methyls are on special positions, that when the symmetry operations are performed generate two

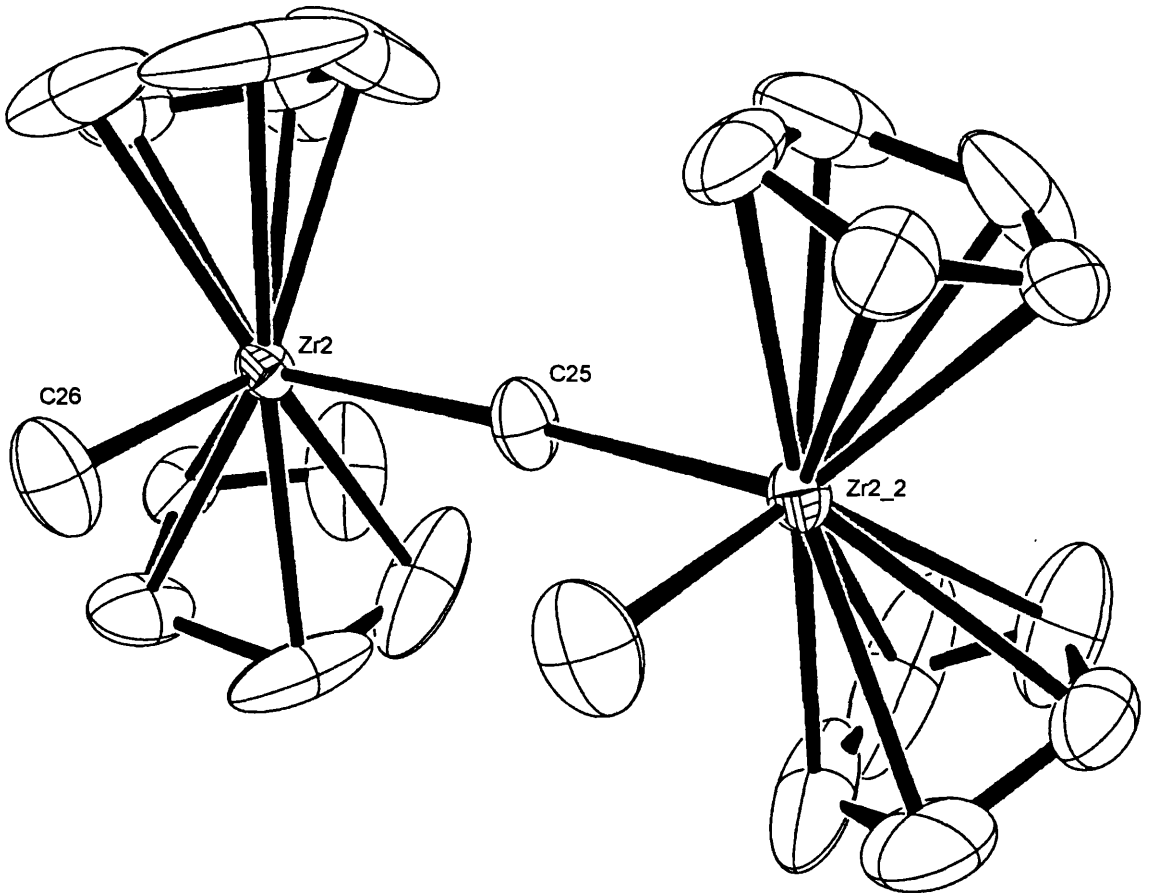

Zr1-C13	2.4182(16)
Zr1-C14	2.259(7)
Zr1a-C13a	2.351(1)
Zr1a-C14	2.748(17)
C14-Zr1-C13	89.6(3)
Zr1-C13-Zr1_2	164.4(5)
Zr1a-C13a-Zr1a_2	152(3)
Zr2-C25	2.4243(15)
Zr2-C26	2.266(7)
Zr2a-C25a	2.265(12)
Zr2a-C26	2.68(2)
C26-Zr2-C25	90.6(6)
Zr2-C25-Zr2_2	175.4(12)
Zr2a-C25a-Zr2a_2	176(6)

Table 3: Selected bond lengths (Å) and angles (°) for **(10)**.

Figure 26: The molecular structure of $[(Cp_2ZrMe)_2(\mu\text{-}Me)][1\text{-}H\text{-}closo\text{-}CB_{11}Me_{11}]$, **(10)** (only one of the two crystallographically independent dimers shown (thermal ellipsoids shown at the 30% probability level, hydrogens are removed for clarity). A disordered molecule of solvent co-crystallite (C_6H_5F), and the disordered cation component are not shown. Symmetry transformations used to generate the equivalent atoms (denoted by _2):(x+1,y,-z+1/2) and (-x,y,-z+1/2).

crystallographically inequivalent $[\{Cp_2ZrMe\}_2(\mu\text{-}Me)]^+$ fragments. Both cation fragments are disordered across the Zr-Me-Zr bridges; this is readily modelled in each case by a 50% occupancy of the two sites. Due to the disorder and the large thermal ellipsoids present in the structure of **(10)** only the gross structural metrics can be discussed with any confidence. The two $\{Cp_2ZrMe\}$ portions of each individual dimer are by definition identical to each other and the two crystallographically independent dimers are grossly similar. One of the dimers approaches linearity (Zr2-C25-Zr2_2 175.4(12)° and Zr2a-C25a-Zr2a_2 176(6)°) comparable to that reported for the only other reported (μ-Me) metallocene dimer $[\{(C_5Me_2H_3)_2ZrMe\}_2(\mu\text{-}Me)][MePBB]$ (170.9(4)°);[73] however, the second is notably more bent (Zr1-C13-Zr1_2 164.4(5)° and Zr1a-C13a-Zr1a_2 152(3)°). This does suggest that the bridging CH_3 moiety is sp^2 hybridised, with a symmetrical interaction. This is supported by the similar chemical shifts observed for **(10)** and $[\{(C_5Me_2H_3)_2ZrMe\}_2(\mu\text{-}Me)][MePBB]$.[22] A valid comparison of the terminal and bridging Zr-Me distances is not warranted due to the difference between the two Zr-terminal Me distances (*e.g.*, Zr1-C14 2.259(7)Å versus Zr1a-C14 2.748(17)Å) generated by the disorder in **(10)**. The only major disparity in the structures of **(10)** and $[\{(C_5Me_2H_3)_2ZrMe\}_2(\mu\text{-}Me)][MePBB]$ worth noting is in the respective orientation of the terminal methyls, eclipsed in **(10)**, compared to staggered in $[\{(C_5Me_2H_3)_2ZrMe\}_2(\mu\text{-}Me)][MePBB]$. The staggered methyl geometry reported may well be necessitated by the bulkier ($C_5Me_2H_3$) groups forcing the geometry to a '*trans*' (staggered) arrangement (with respect to the angling of the Cp_2Zr moieties around the 'linear Zr-Me-Zr core). In the less hindered congener **(10)**, the eclipsed formation is not sterically unfavourable and the unsubstituted Cp rings can be bent into the same plane (Figure 27).

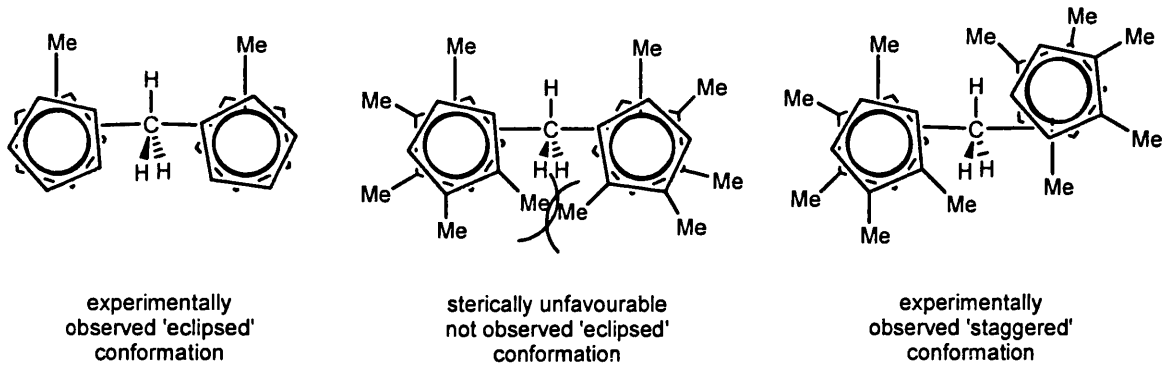

Figure 27: Schematic demonstrating the unfavourable Me···Me interactions in the eclipsed geometry of the $[\{(C_5Me_2H_3)_2ZrMe\}_2(\mu\text{-}Me)]^+$ cation and the two other experimentally observed structures.[10]

Compound **(10)** can be converted to the contact ion pair complex **(9)** by the reaction with a second half an equivalent of $[Ph_3C][1\text{-}H\text{-}\textit{closo}\text{-}CB_{11}Me_{11}]$. Thus, the reaction pathway to form **(9)** can be expected to pass through **(10)** as an intermediate, as previously shown for the $[B(C_6F_5)_4]^-$ systems (Figure 28), and thus places the anionic $[1\text{-}H\text{-}\textit{closo}\text{-}CB_{11}Me_{11}]^-$ as less coordinating than the neutral zirconocene Cp_2ZrMe_2.

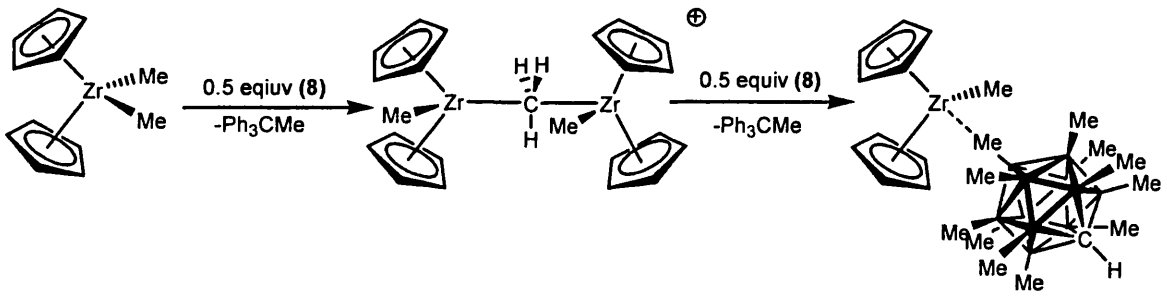

Figure 28: The stepwise reaction mechanism for the formation of **(9)** via the $[\{Cp_2ZrMe\}_2(\mu\text{-}Me)]^+$ cation.

Whilst this stepwise behaviour is similar to that observed for the $[MeB(C_6F_5)_3]^-$ and the $[B(C_6F_5)_4]^-$ anion analogues, moving to the even bulkier $[MePPB]^-$ anion results in the reaction being terminated at the intermediate stage and the $(\mu\text{-}CH_3)$ dimer isolated excusively.[31]

3.2.2.2: $(C_5H_4Me)_2ZrMe_2$

In an attempt to determine the strength of the binding interaction between the [1-H-*closo*-$CB_{11}Me_{11}$]$^-$ anion and the cation in these zirconcene complexes a symmetry probe was introduced into the Cp rings. Replacing the unfunctionalised cyclopentadienyl for the mono methylated C_5H_4Me (Cp'), introduces the possibility of diastereotopic Cp' proton signals in an analogous manner to that utilised by Marks and co-workers in $(C_5H_3Me_2)_2ZrMe(\mu\text{-}Me)B(C_6F_5)_3$.[2, 25, 26] In C_S symmetrical systems *i.e.* the starting dimethyl complex Cp'_2ZrMe_2 there is a mirror plane bisecting the Me-Zr-Me angle resulting in only two proton resonances for the Cp' ring. In an asymmetric system $Cp'_2Zr(X)(Y)$ (*e.g.*, $Cp'_2Zr(Me)$(1-H-*closo*-$CB_{11}Me_{11}$)) there is loss of this mirror plane, consequentially the Cp' protons are now inequivalent and four resonances can be expected in the ^{1}H NMR spectrum (Figure 29).

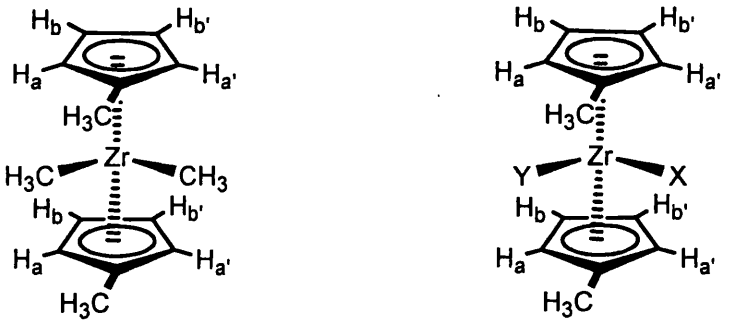

Figure 29: Symmetric and asymmetric substituted zirconocenes, resulting in an increase in the number of aromatic signals in the ^{1}H NMR spectrum.

If the there is tight ion pairing in $Cp'_2Zr(Me)$(1-H-*closo*-$CB_{11}Me_{11}$) then the ^{1}H NMR spectrum will display four aromatic signals. If the anion···cation interaction is weak and the dissociation/rebinding fast on the NMR timescale the X and Y positions

become equivalent through time averaging and a *pseudo* mirror plane is induced in the zirconocene (Figure 30).

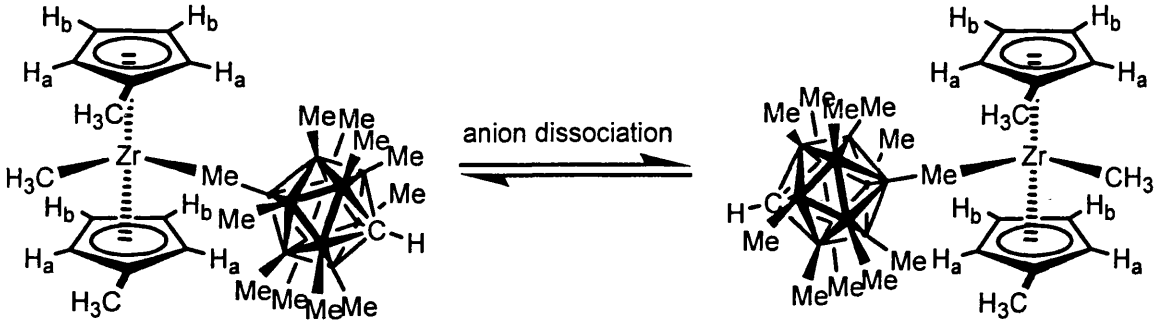

Figure 30: The equilibrium expected on anion dissociation to produce a time averaged mirror plane.

The reaction of Cp'_2ZrMe_2 with one equivalent of **(8)** in d_8-toluene results in a single major product that is assigned as the close contact ion pair $Cp'_2ZrMe(1\text{-}H\text{-}closo\text{-}CB_{11}Me_{11})$, **(11)**. Characterisation is based on an upfield chemical shift (relative to the free anion) and broadening in the $^1H\{^{11}B\}$ NMR spectrum for the anion CH_3 resonances (CH_3(2-6) 0.14 ppm, CH_3(7-11) 0.0 3ppm and CH_3(12) –0.57 ppm) as observed for **(9)**. Further confirmation is provided by the Zr-Me signal in the $^1H\{^{11}B\}$ NMR spectrum that resonates at 0.30 ppm, almost identical to that reported for **(9)** (0.29 ppm). The degree of chemical shift change implies that in compound **(11)**, the anion···cation interaction is similar to that in **(9)**. Importantly the four diasteroetopic Cp' aromatic resonances observed, show that the anion binding is static at room temperature (Figure 31). A ^1H COSY NMR spectrum and the presence of only one Cp' methyl signal in the $^1H\{^{11}B\}$ spectrum confirm that there is only one $\{Cp'_2Zr\}$ complex present in solution.

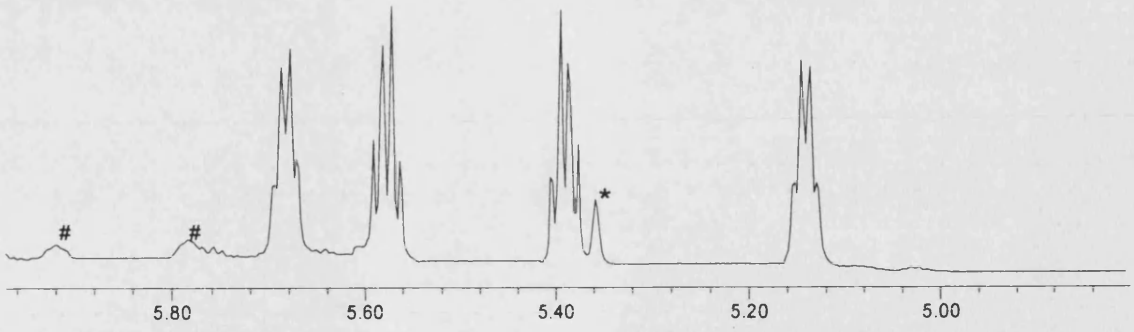

Figure 31: The aromatic Cp region of the $^{1}H\{^{11}B\}$ NMR spectrum of **(11)**, * denotes an unknown impurity, # signifies a decomposition product.

The tight anion binding and lack of fluxionality at room temperature in complex **(11)**, is as observed for the related complex $(C_5H_3Me_2)_2ZrMe(\mu\text{-}Me)B(C_6F_5)_3$ which shows no signal broadening below 40°C.[25] In an attempt to facilitate anion dissociation a d^8-toluene solution of compound **(11)** was gradually heated. At temperatures above 60°C rapid decomposition takes places, whilst below this temperature no discernable signal broadening occurred, frustrating attempts to obtain thermodynamic values for the $\Delta H^{\ddagger}$ and $\Delta S^{\ddagger}$ of anion dissociation. The earlier onset of signal broadening observed in $(C_5H_3Me_2)_2ZrMe(\mu\text{-}Me)B(C_6F_5)_3$ when compared to **(11)**, ranks the $[MeB(C_6F_5)_3]^-$ as more weakly coordinating than the [1-H-*closo*-$CB_{11}Me_{11}]^-$ anion with respect to zirconocene cations. This is in line with the respective solid-state structures, where there is a shorter Zr(μ-Me) bond length in **(9)** than in $Cp_2ZrMe(\mu\text{-}Me)B(C_6F_5)_3$. The decomposition product from heating a solution of **(11)**, showed a severely decomposed anion region in the $^{1}H\{^{11}B\}$ and ^{11}B NMR spectra (see section **3.2.4** for further discussion). A number of constrained geometry complexes of the general formula $(CGC)Zr(Me)(\mu\text{-}Me)B(C_6F_5)_3$ also undergo thermal decomposition at low temperatures.[2] It is interesting to note that for the related compound $Cp'_2ZrMe(\eta^1\text{-}$*closo*-$CB_{11}H_{12})$ a fluxional process is occurring, generating a C_S solution structure and

only two resonances for the Cp' protons.[7] The solid-state structural metrics and the poor polymerisation activity both indicate a strong anion···cation interaction. This implies that an alternative mechanism to anion dissociation is causing the observed C_S symmetry

Repeated attempts to obtain crystalline material of $Cp'_2ZrMe(1\text{-}H\text{-}closo\text{-}CB_{11}Me_{11})$ to allow for a solid-state comparison with **(9)** failed. Similarly, the analogous reaction of **(8)** with the bulkier metallocene, $Cp^*_2ZrMe_2$ repeated yielded a mixture of products (as judged by the number of Cp* CH_3 resonances observed in the $^1H\{^{11}B\}$ NMR spectrum), and a decomposed anion region. Attempts to partner the related anion, $[closo\text{-}CB_{11}H_{12}]^-$ to zirconocenes other than $[Cp_2ZrMe]^+$ and $[(Cp')_2ZrMe]^+$ equally failed due to the instability of the products.[7]

3.2.3: Polymerisation Studies.

Polymerisation studies discussed herein were performed at the University of East Anglia by Professor Manfred Bochmann and co-workers. The pre-catalyst $(SBI)ZrMe_2$ (SBI = *rac*-$Me_2Si(indenyl)_2$, Figure 32) has previously been used to provide highly reactive polymerisation catalysts (over three times the productivity compared to Cp_2ZrMe_2)[74] on the addition of a suitable co-catalyst (*e.g.*, $B(C_6F_5)_3$, $[Ph_3C][B(C_6F_5)_4]$, $[Ph_3C][\{B(C_6F_5)_3\}_2CN]$, Figure 32).[45] The anion partnering the cationic complex has a considerable effect on the activity of the cationic zirconocene, with dissociation of the weakly coordinating anion the entry point into the catalytic cycle.[75-77]

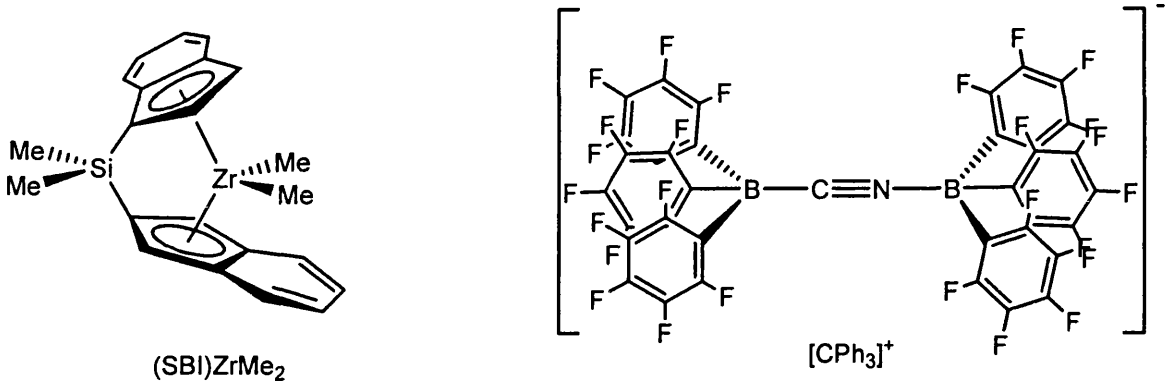

(SBI)$ZrMe_2$

Figure 32: The structure of the pre-catalyst (SBI)$ZrMe_2$ and the co-catalyst $[CPh_3][\{B(C_6F_5)_3\}_2CN]$.

The activity of metal catalysts partnered with a variety of anions is another method for determining their relative co-ordinating ability. (SBI)$ZrMe_2$ on reaction with **8** in toluene gave an overall activity of 45 kg mol^{-1} h^{-1} bar^{-1} for the polymerisation of ethylene (at room temperature). This value shows that the $\{(SBI)ZrMe\}^+$/[1-H-*closo*-$CB_{11}Me_{11}]^-$ combination produces a moderately active catalyst based on the scale of merit proposed by Gibson and co-workers.[1] To put this value in context, however, the highest activity reported for the (SBI)$ZrMe_2$/co-catalyst combination for the production of polyethylene (without AlR_3 scavenger) is 20,400 kg mol^{-1} h^{-1} bar^{-1} using $[CPh_3][\{B(C_6F_5)_3\}_2CN]$ (albeit at the raised temperature of 60°C).[74] This clearly shows that the coordinating nature of the [1-H-*closo*-$CB_{11}Me_{11}]^-$ anion drastically impairs the catalyst active site, whereas the very weakly interacting $[\{B(C_6F_5)_3\}_2CN]^-$ anion has a much higher activity. A more valid comparison is with the $[MeB(C_6F_5)_3]^-$ anion congeners, unfortunately all the reported (SBI)$ZrMe_2$/$B(C_6F_5)_3$ polymerisation studies also involved tri-alkyl aluminium scavengers (to react with trace impurities that can readily deactivate the active catalyst). For example an identical (SBI)$ZrMe_2$/$[Ph_3C][\{B(C_6F_5)_3\}_2CN]$ combination with 1000 equivalents of Al^iBu_3

scavenger gives an increased activity of 760,400 kg mol^{-1} h^{-1} bar^{-1} (again at the raised temperature of 60°C).[45] Marks and co-workers have performed scavenger-free ethylene polymerisation studies using $Cp_2ZrMe(\mu\text{-}Me)B(C_6F_5)_3$ which results in an activity of 4,500 kg mol^{-1} h^{-1} bar^{-1}.[25] This is a hundred-fold higher than that found for the (SBI)$ZrMe_2$/[Ph_3C][1-H-*closo*-$CB_{11}Me_{11}$] combination, demonstrating again the greater nucleophilcity of the [1-H-*closo*-$CB_{11}Me_{11}$]$^-$ anion. However, it should be noted that the rapid anion decomposition observed on the reaction of $Cp^*_2ZrMe_2$ with [CPh_3][1-H-*closo*-$CB_{11}Me_{11}$] may indicate that the lower activity recorded here is due to catalyst decomposition. The possibility of anion decomposition is further supported by the fact that complexes partnered with the more coordinating anion [*nido*-$C_2B_9H_{12}$]$^-$ has a greater activity (*e.g.*, Cp_2ZrMe(*nido*-$C_2B_9H_{12}$) 265 kg^{-1} mol^{-1} h^{-1} bar^{-1}).[13] An alternative possibility for the significantly lower activity in [1-H-*closo*-$CB_{11}Me_{11}$]$^-$ partnered complexes is their reduced solubility in non-polar hydrocarbons (*e.g.*, toluene), which may have resulted in an artificially reduced concentration.

3.2.4: Anion Decomposition.

3.2.4.1: Reaction with Arenes

In all the cationic zirconocene complexes that have been partnered with the [1-H-*closo*-$CB_{11}Me_{11}$]$^-$ anion decomposition occurs, albeit at varying rates (slowly for **(9)**, but rapid with the $\{Cp^*_2ZrMe\}^+$ fragment). Heating these complexes further accelerates the degradation and generates similar NMR spectra to that observed by room temperature decomposition. The Cp and Cp' congeners behave in a closely related manner and they will be discussed together in this section.

The complete loss of all resonances associated with **(9)** occurs within an hour when a toluene solution is heated at 60°C. The ^{1}H NMR spectrum shows numerous Cp resonances (5.86 ppm, 5.67 ppm and 5.50 ppm) and a complex cage region. Figure 33 shows the resultant ^{11}B and ^{1}H NMR spectra (anion and Zr-Me region only) from the heating of a toluene solution of **(9)** at 70°C for 1 hour.

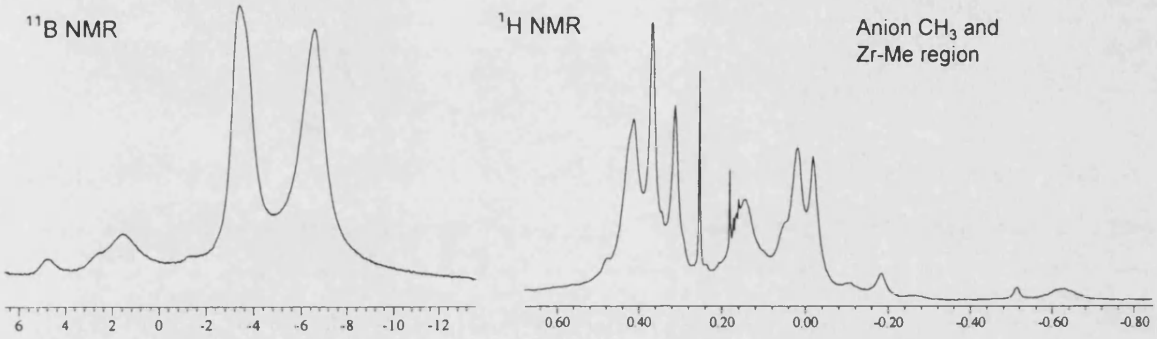

Figure 33: The ^{11}B and ^{1}H NMR spectrum for a d_8-toluene sample of **(9)** heated at 70°C for 1 hour, showing anion B-CH_3 region only – a representative spectrum of the anion decomposition products.

The Cp resonances of the decomposition products are not assignable to **(9)** or Cp_2ZrMe_2. The ^{11}B NMR spectrum gives clues to the products formed, showing that the C_{5V} symmetry is maintained, but with a number of broad antipodal signals between 5 and 0 ppm. Mass spectrometry (FAB-) shows three anionic products: the unfunctionalised cage $[1\text{-H-}closo\text{-}CB_{11}Me_{11}]^-$ (297.5 m/z); a signal at 360.5 m/z attributable to $[1\text{-H-12-Ph-}closo\text{-}CB_{11}Me_{10}]^-$ (to remain C_{5V} symmetric the anion must be substituted in the 12 position as indicated by ^{11}B spectroscopy) and a signal at 375.5 m/z that is assignable to $[1\text{-H-12-}(CH_3C_6H_4)\text{-}closo\text{-}CB_{11}Me_{10}]^-$ (Figure 34). The 12-tolyl substituted cage can exist as a number of isomers (adding to the ^{1}H NMR spectrum complexity), although to keep the local C_{5V} symmetry the cage must again be only 12-substituted. The only identifiable signal in the FAB+ mode on a number of attempts was assigned as $\{Cp_2ZrMe(OH_2)\}^+$ (283.1 m/z,) (Figure 34).

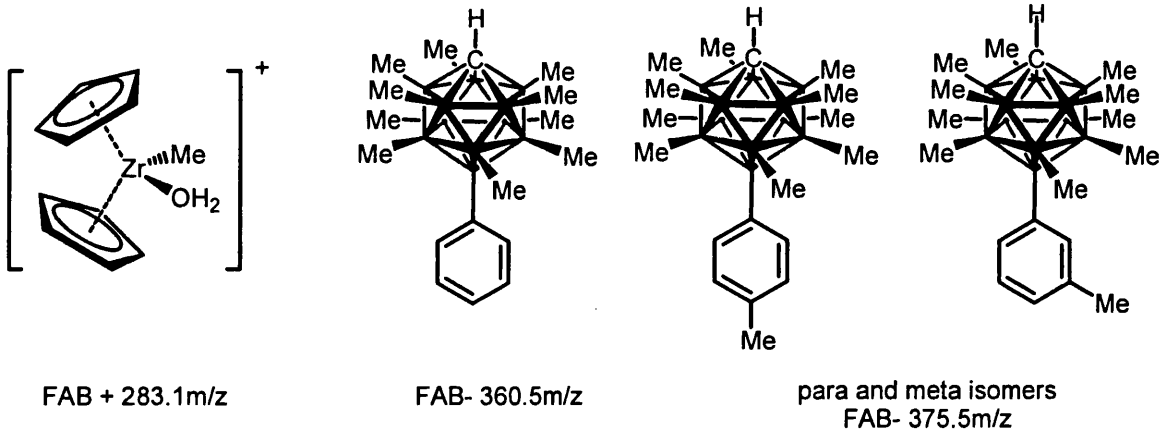

Figure 34: Observed cation and anion complexes from the decomposition of **(9)** in toluene.

Metal···anion coordination must play a central role in the deactivation pathway as the $[MeB(C_6F_5)_3]^-$ analogue is stable at 80°C for hours, ruling out a coordinated solvent decomposition mechanism.[2] Secondly, heating the non-coordinating salt Cs[1-H-*closo*-$CB_{11}Me_{11}$] in C_6H_5F/toluene mix results in no decomposition. The initial step on a proposed decomposition pathway is the anion···Zr complexation via the 12 position as observed in the solid state structure of **(9)**. Two plausible mechanisms are then conceivable. (i) Decomposition could be initiated by the thermal abstraction of a methide to generate Cp_2ZrMe_2 and the reactive borenium ylide {1-H-*closo*-$CB_{11}Me_{11}$}, reported previously.[65, 78] The borenium ylide will then react further with a molecule of solvent (toluene), producing a H^+ (or CH_3^+) via an S_E2 mechanism (Figure 35). This would then go on to react with Cp_2ZrMe_2, generating CH_4 (or C_2H_6). The resultant zirconocene cation would then not undergo any further reaction due to the improved stability provided by coordination to an anion bound arene. Complexes based on $\{Cp_2ZrMe\}^+$ are well documented to bind to anionic arene containing complexes (*e.g.*, $[BPh_4]^-$, $[B(4\text{-R-Ph})_4]^-$).[79-81] (ii) Alternatively, anion coordination to the metal centre could activate the B-C bond to undergo formal σ bond metathesis with the toluene

solvent forming the aryl substituted cage and the cation Cp_2ZrMe^+ which could react further as detailed above.

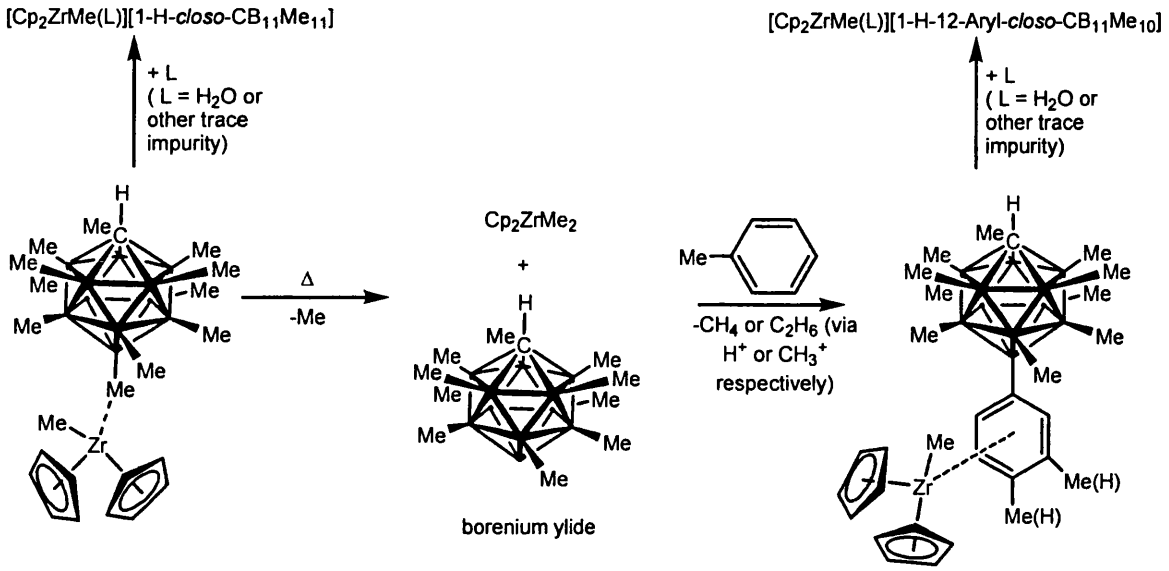

Figure 35: a proposed mechanism for the metal mediated anion activation, accounting for the observed anion and cation fragments observed in the FAB mode Mass spectroscopy

Both of these mechanisms have been proposed previously in the lithium mediated Me/aryl exchange. This involves the exchange of a B – CH_3 moiety for a B-*para*-C_6H_4Br moiety with the concomitant loss of $SiMe_4$ (Figure 36).

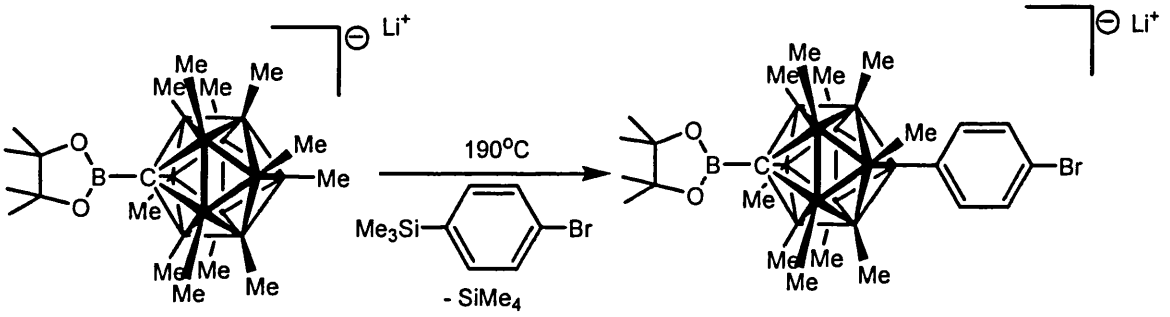

Figure 36: The B-Me/Aryl-Si exchange reaction that takes place on heating the Li salt of [1-$Me_4C_2O_2B$-*closo*-$CB_{11}Me_{11}$]$^-$.

The presence of $[Cp_2ZrMe(OH_2)]^+$ and unfunctionalised [1-H-*closo*-$CB_{11}Me_{11}$]$^-$ is not unexpected as the fiercely electrophilic $\{Cp_2ZrMe\}^+$ will readily scavenge any trace water and on doing will shut down the metal mediated decomposition pathway.

An analogous decomposition is observed when $Cp^*_2ZrMe_2$ is reacted with **(8)** at low temperatures in C_6H_5F, the only anion signal in the FAB- mode mass spectrum being that for the twice-activated cage [1-H-*closo*-$CB_{11}Me_9(C_6H_4F)_2]^-$. The FAB+ mode spectrum exhibits a signal correspond to $Cp^*_2Zr(Me)F$ (Figure 37).

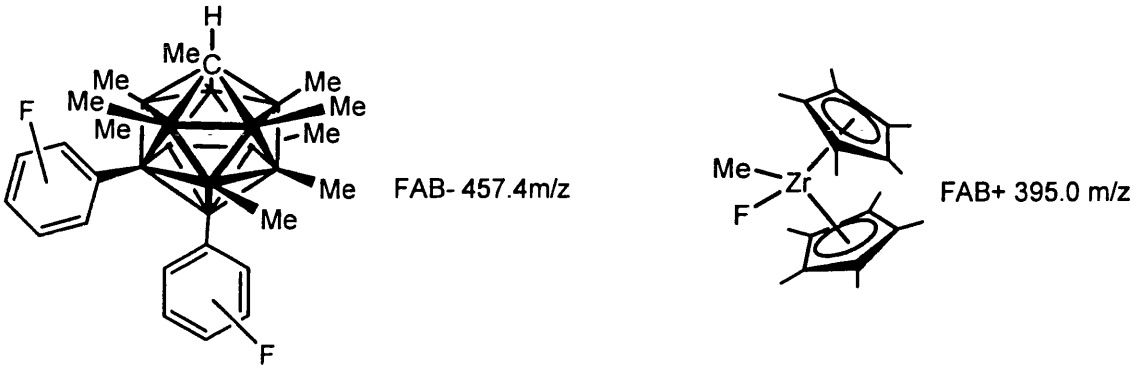

Figure 37: The observed molecular ions from the reaction of $[CPh_3][1\text{-H-}closo\text{-}CB_{11}Me_{11}]$ and $Cp^*_2ZrMe_2$ in C_6H_5F

NMR spectroscopy was not informative in the unambiguous assignment of these compounds and attempts to obtain pure material failed. Nevertheless a similar decomposition mechanism similar to that discussed previously is feasible, the key intermediate again being the neutral borenium ylide [1-H-*closo*-$CB_{11}Me_{10}$], proposed previously by Michl and co workers.[65, 78]

3.2.4.2: Reaction with Dichloromethane.

On dissolution of **(9)** or **(10)**, in CD_2Cl_2 rapid compound decomposition also occurs to give an anion CH_3 region in the $^1H\{^{11}B\}$ NMR spectrum of high complexity. The ^{11}B NMR spectrum is also significantly altered from that of **(9)**, with an increased number of peaks indicating loss of anion C_{5V} symmetry. Mass spectroscopy again was useful in helping to elucidate the structures of both anion and cation products. The FAB+ mode consisted of two major compounds, identified as $\{Cp_2Zr(Me)Cl\}^+$ and

$\{Cp_2ZrCl\}^+$ (Figure 38), chloride inclusion clearly indicating solvent activation is taking place.

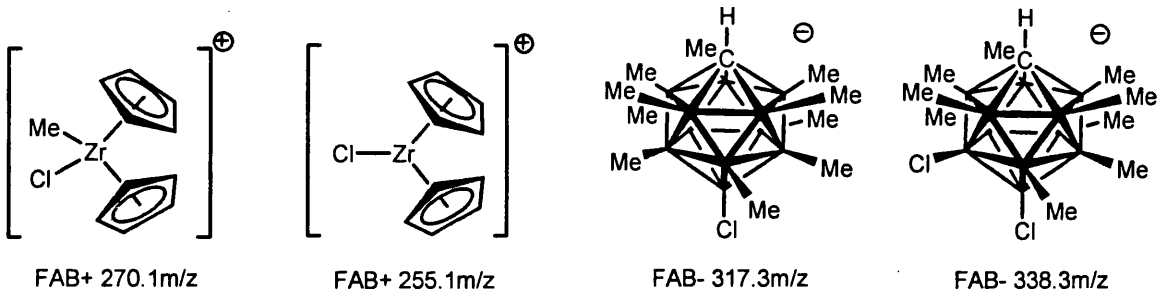

Figure 38: The major identifiable products from the FAB mass spectra of **(9)** decomposed in CD_2Cl_2.

The FAB mass spectrum also clearly showed chloride incorporation on the cage anion, with the major product being [1-H-*closo*-$CB_{11}Me_9Cl_2$]$^-$, which is not C_{5v} symmetric, explaining the greater complexity observed in the ^{11}B spectrum. The second minor product (again by mass spec. only) was the mono chlorinated derivative [1-H-*closo*-$CB_{11}Me_{10}$]$^-$. There are two possible activation steps in dichloromethane, the first is the previously hypothesised methyl abstraction from the anion by the cationic zirconocene. This is unlikely as in hydrocarbon solvents the intimate ion pair **(9)** is stable at room temperature for days. More likely is the displacement of the [1-H-*closo*-$CB_{11}Me_{11}$]$^-$ anion from the zirconium coordination sphere and the formation of a transient dichloromethane adduct that rapidly decomposes via chloride abstraction (Figure 39).

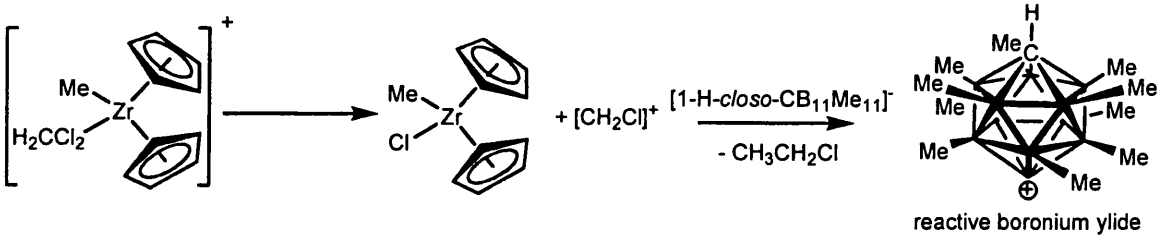

Figure 39: Schematic showing the formation of the boronium ylide by methyl abstraction by a highly reactive $\{CH_2Cl\}^+$ cation.

This would generate a reactive $\{CH_2Cl\}^+$ fragment that could then activate the cage by methyl abstraction to form CH_3CH_2Cl and the borenium ylide. Alternatively, the decomposition of the CH_2Cl_2 complex may be assisted by the attack of a weak base at the carbon of the coordinated CH_2Cl_2, in this case the anion [1-H-*closo*-$CB_{11}Me_{11}$]$^-$. A related mechanism has been proposed for the decomposition of a CH_2Cl_2 coordinated complex in the highly electrophilic compound $[(PR_3)Re(CO)_4(Cl_2CH_2)]^+$.[82] Here nucleophilic attack of Et_2O results in the formation of the chloride analogue $(PR_3)Re(CO)_4Cl$ and the oxonium cation $[ClCH_2OEt_2]^+$ (Figure 40).

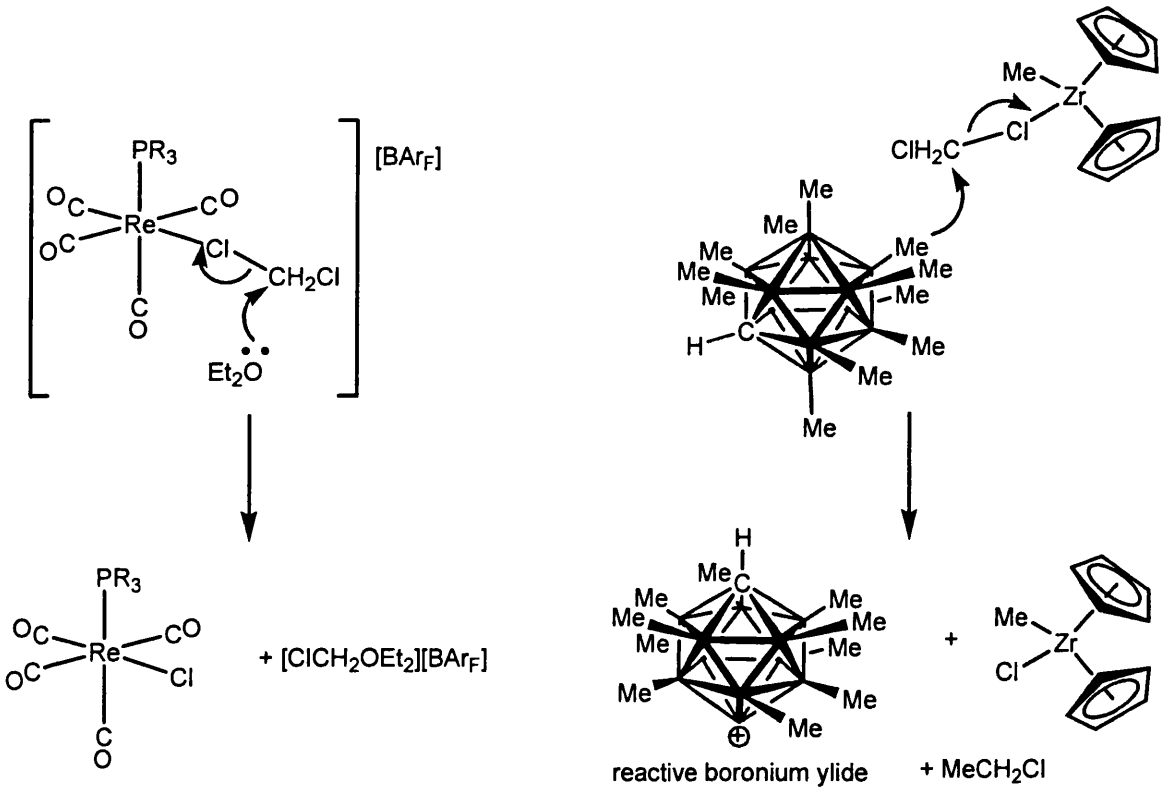

Figure 40: The etherate nucleophilic attack on a Rhenium DCM complex proposed by Kubas and co workers and a related mechanism plausible for the decomposition of the **(9)** in CH_2Cl_2 solution.

The binding of CH_2Cl_2 in favour of [1-H-*closo*-$CB_{11}Me_{11}$]$^-$ has precedent, in the formation of $[(PPh_3)Ag(Et_2O)_2]^+$ (see Chapter One) and a series of dichloromethane adducts with rhodium or rhenium cations (discussed further in Chapter Four). Furthermore cationic zirconium complexes partnered with weakly coordinating anions

are documented to form chloride complexes by solvent activation with no anion decomposition.[83]

Confirmation of the identity of both cation and anion complexes identified by the FAB mode mass spectra was obtained on moving to the $Cp^*_2ZrMe_2$ system. The reaction of equimolar equivalents of $Cp^*_2ZrMe_2$ and **8**, followed by recrystallisation from the slow diffusion of pentane into a CH_2Cl_2 solution yielded pale yellow crystals of suitable quality for X-ray diffraction analysis. This revealed the compound to be $[Cp^*_2Zr(OH_2)Cl][1\text{-}H\text{-}7,12\text{-}Cl_2\text{-}\textit{closo}\text{-}CB_{11}Me_9]$, with no close anion···cation contacts and no anion disorder allowing for the assignment of the cage carbon vertex (Figure 41). The Zr-O distance (2.2210(16) Å) is comparable with other Zr(IV) water complexes *e.g.*, $[Cp_2Zr(C_7H_7SO_3)(H_2O)_2]^+$ (2.276(5) Å and 2.242(5) Å)[84] and $[Cp_2Zr(H_2O)_3]^{2+}$ (2.261(7) Å, 2.195(7) Å and 2.239(7) Å).[85] The anion clearly showed substitution of two B-Me vertices (B7 and B12) for chlorides. The B-Cl distances (B7-Cl1 1.818(2) Å and B12-Cl2 1.843(2) Å) are slightly longer than that reported for identical B-Cl vertices in $[1\text{-}H\text{-}\textit{closo}\text{-}CB_{11}Br_5Cl_6]^-$ (B7-C7 1.790(8) Å and B12-C12 1.782(9) Å) and in $[1\text{-}H\text{-}\textit{closo}\text{-}CB_{11}Cl_{11}]^-$ (B7-Cl7 1.776(3) Å and B12-Cl12 1.775(3) Å).[86] The substitution occurring in the 7 and 12 positions is consistent with the charge density calculations performed on this anion (Chapter two), with the transient $\{CH_2Cl\}^+$ attacking the positions of greatest electron density (BCH_3(7-11) and BCH_3(12)). The formed borenium ylide will then abstract chloride from the solvent.[65] The second $\{CH_2Cl\}^+$ reactive fragment then produced can either abstract a methyl from the functionalised cage (producing the observed di-chlorinated cage anion) or with $Cp_2ZrMe(Cl)$ resulting in the cation $[Cp_2ZrCl]^+$. This ultimately scavenges water to produce the observed $[Cp_2Zr(H_2O)Cl]^+$.

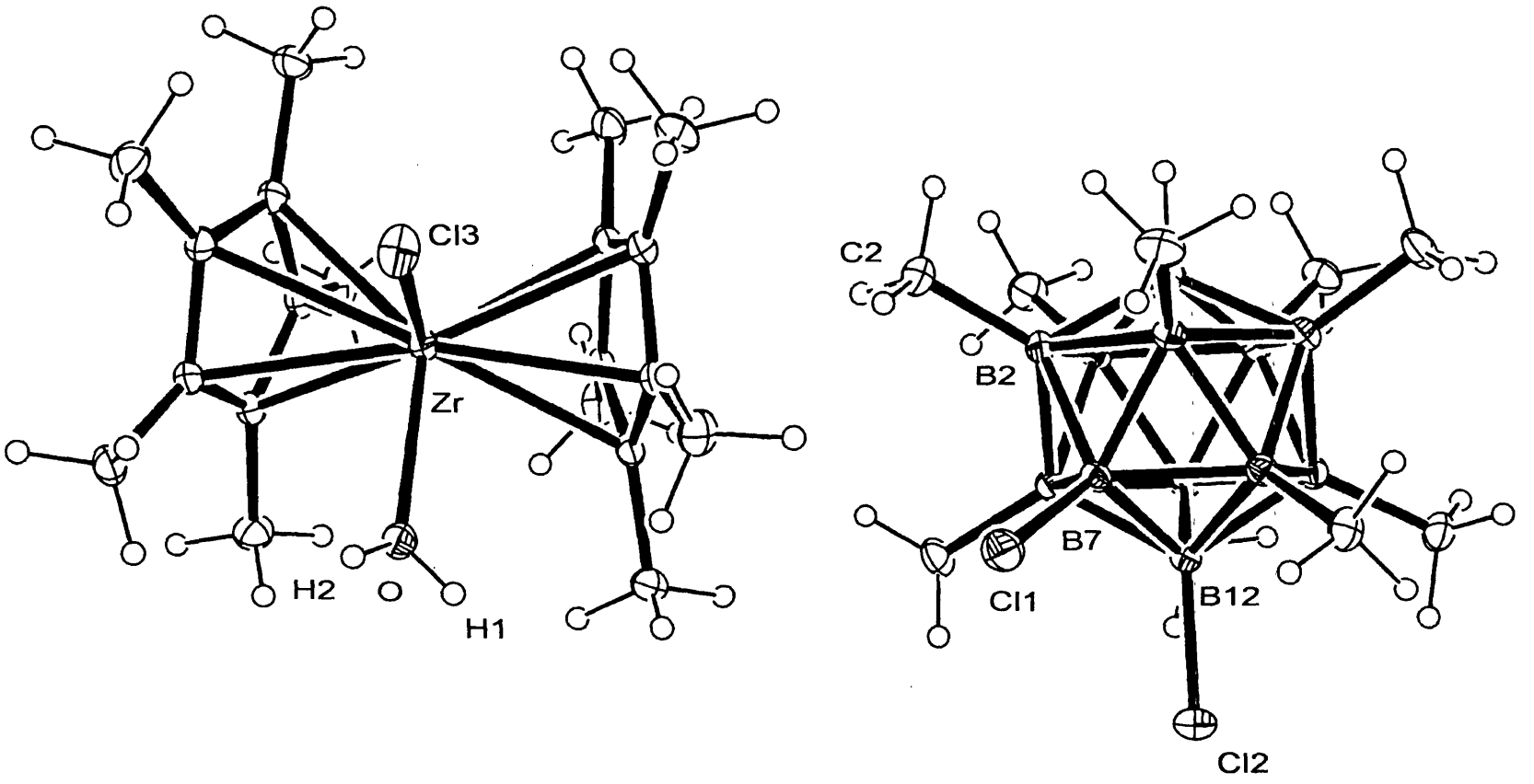

Figure 41: The Molecular structure of $[Cp^*_2Zr(OH_2)Cl][1\text{-H-}7,12\text{-}Cl_2\text{-}closo\text{-}CB_{11}Me_9]$ (thermal ellipsoids are shown at 30% probability level).

Zr-O	2.2210(16)	O-Zr-Cl3	90.6(1)	Cl1-B7	1.818(2)
Zr-Cl3	2.4226(6)	O-H(1)	0.79(4)	Cl2-B12	1.843(2)
		O-H(2)	0.81(4)		

Table 4: Selected bond lengths (Å) and angles (°) for $Cp^*_2Zr(OH_2)Cl[1\text{-H-}7,12\text{-}Cl_2\text{-}closo\text{-}CB_{11}Me_9]$.

In depth mechanistic discussion is not appropriate due the unclean nature of the reaction and the failure to observe any of the intermediates, or the expected by-product, CH_3CH_2Cl by NMR spectroscopy or GC/MS.

The $^1H\{^{11}B\}$ NMR spectrum of $[Cp^*_2Zr(OH_2)Cl][1\text{-}H\text{-}7,12\text{-}Cl_2\text{-}closo\text{-}CB_{11}Me_9]$ exhibits the 5 expected signals in the anion CH_3 region from 0.348 ppm to 0.165 ppm (Figure 42).

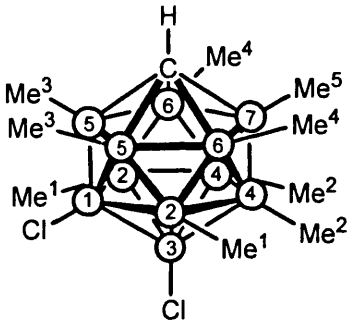

Figure 42: The inequivalent boron and methyl positions in $[1\text{-}H\text{-}7,12\text{-}Cl_2\text{-}closo\text{-}CB_{11}Me_9]^-$.

The coordinated H_2O molecule resonates at 1.821 ppm, shifted downfield from that of free H_2O in CD_2Cl_2 (1.60 ppm) as expected on coordination to an electrophilic metal. The ^{11}B NMR spectrum only shows five broad signals for the anion, with two resonances presumably being coincident.

3.2.5: Partnering [1-H-*closo*-$CB_{11}Me_{11}$]$^-$ with Cobalt Complexes.

In an attempt to partner the cationic 16 electron fragment $\{CpCo(PPh_3)Me\}^+$ with [1-H-*closo*-$CB_{11}Me_{11}$]$^-$, the dialkyl precursor, $CpCo(PPh_3)Me_2$ was reacted with an equimolar quantity of $[Ph_3C][1\text{-H-}closo\text{-}CB_{11}Me_{11}]$ in CD_2Cl_2. Rapid gas evolution was observed and the $^1H\{^{11}B\}$ NMR spectrum of the resultant purple solution showed broad, poorly defined signals in the anion CH_3 and cation PPh_3 aromatic regions, indicative of quadrupolar broadening by a paramagnetic complex. The $^{31}P\{^1H\}$ NMR spectrum displayed no observable signal. Recrystallisation of a CH_2Cl_2 solution of the reaction mixture by the slow diffusion of pentanes produced two major sets of crystals (amber cuboids and purple platelets) in equal quantities. Both sets were of suitable quality for X-ray diffraction studies to be undertaken. On analysis, the amber cuboids were identified as the paramagnetic, 17 electron, Co(II) complex, $[CpCo(PPh_3)_2][1\text{-H-}closo\text{-}CB_{11}Me_{11}]$, **(12)**. The asymmetric unit (Figure 43) consisted of a well separated ion pair (the closest Co···H_3C is 5.068 Å), with no observed disorder. The Co(II) centre is approximately C_s symmetric with the cyclopentadienyl group sitting on top of a $\{CoL_2\}$ fragment. The P1-Co-P2 bond angle (100.64(2)°) is similar to that for the only other characterised $[CpCo(PR_3)_2]^+$ complex, $[CpCo(PEt_3)_2][BF_4]$ (101.21(3)°), that also crystallises with approximate C_s symmetry.[87] The Co-C average distance in **(12)** (2.101 Å) is further comparable to that in $[CpCo(PEt_3)_2][BF_4]$ (2.083 Å), as is the average Co-P distance in **(12)** (2.231 to 2.230 Å in $[CpCo(PEt_3)_2][BF_4]$). No direct solid-state comparison with $[CpCo(PPh_3)_2]$ complexes was possible, due to the lack of any structurally determined examples. Characterisation of paramagnetic **(12)**, explains the poorly resolved $^1H\{^{11}B\}$ NMR spectrum and the absence of any resonance in the $^{31}P\{^1H\}$ NMR spectrum. A disproportionation mechanism must be occurring in solution, with free PPh_3 capturing the unsaturated 15 electron fragment

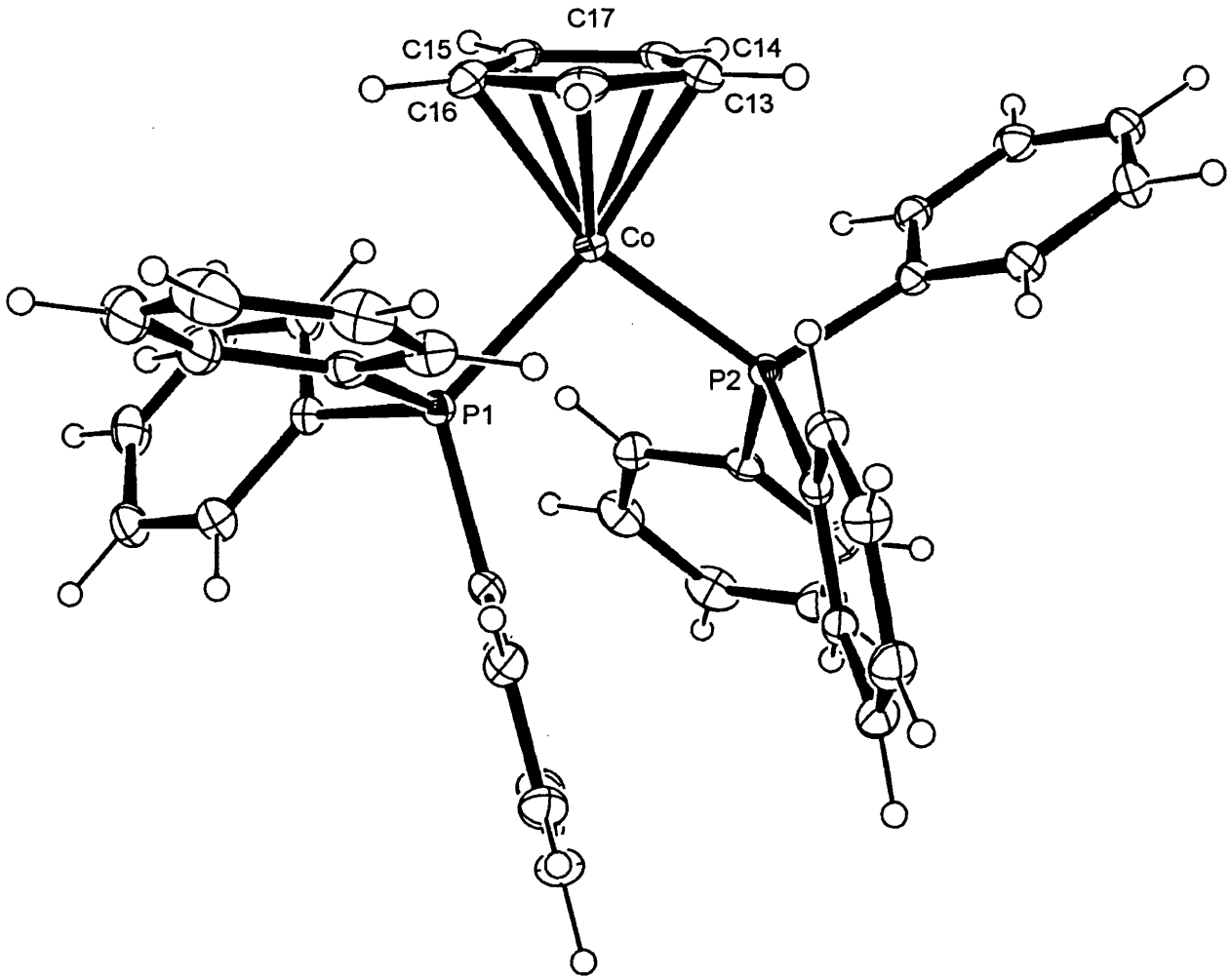

Figure 43: Molecular structure of the cation portion of $[CpCo(PPh_3)_2][1\text{-H-}closo\text{-}CB_{11}Me_{11}]$, **(12)**, thermal ellipsoids shown at the 30% probability level.

Co-P1	2.2108(6)
Co-P2	2.2519(2)
P1-Co-P2	100.64(2)
Co-C13	2.098(2)
Co-C14	2.087(2)
Co-C15	2.118(2)
Co-C16	2.083(2)
Co-C17	2.118(2)

Table 5: Selected Selected bond lengths (Å) and angles (°) for **(12)**.

$\{CpCo^{II}(PPh_3)\}^+$. This suggests that the other crystallised product, present in equal proportion, would involve no phosphine ligation.

An X-ray Diffraction study on the purple platelets revealed the molecular structure to be the discrete ion pair, $[CpCo(\eta^5\text{-}CPh_3)][1\text{-}H\text{-}\textit{closo}\text{-}CB_{11}Me_{11}]$, **(13)**, the $[BF_4]^-$ salt of which has been previously characterised only by NMR spectroscopy.[88] Thus the overall reaction observed is as shown in Figure 44.

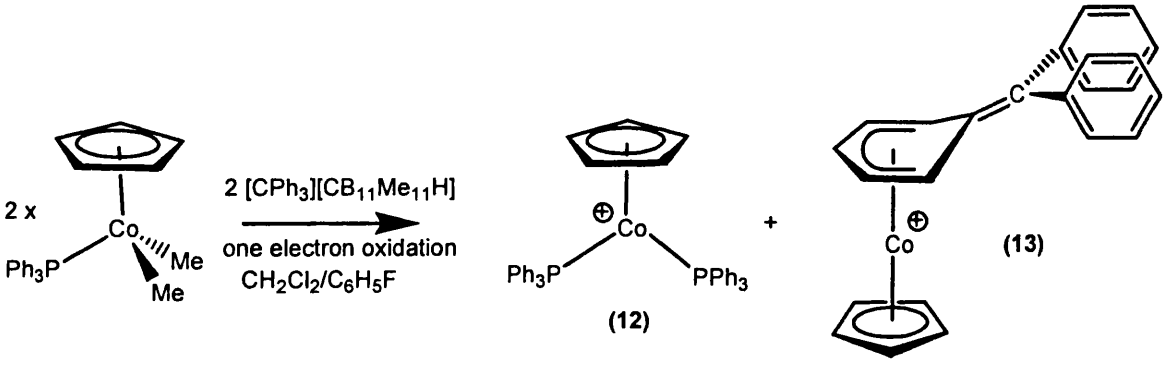

Figure 44: An overall reaction scheme for the addition of **(8)** to $CpCo(PPh_3)Me_2$.

The cation portion of compound **(13)** was heavily disordered, with the Cp and coordinated C_6H_5 phenyl ring occupying two sites in a 3:1 ratio. Figure 45 displays the structure of $[CpCo(\eta^5\text{-}CPh_3)]^+$, with only the positions corresponding to the major occupancy species shown. The structural metrics of both disordered sets are identical (within experimental errors) and only those for the 75% occupancy sites will be discussed here. The anion displays no structural disorder, with the cage carbon unambiguously identified. No anion···cation interactions were observed in the extended lattice (closest Co···H_3C contact at 5.361 Å). The triphenylmethane (trityl) group is coordinated to the Co centre through a single phenyl ring in an η^5 manner, forming a 'half open' cobaltacinium sandwich complex. This binding motif for trityl has been

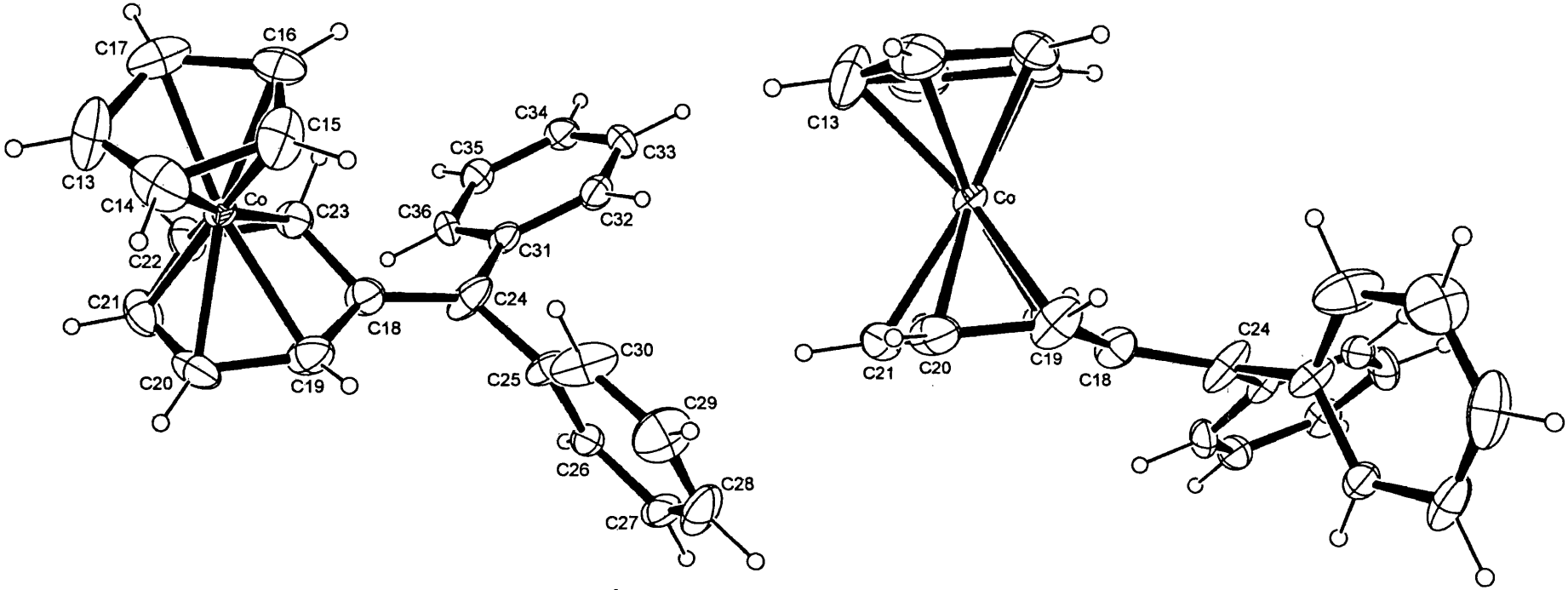

Figure 45: Molecular structure of the cation portion of $[CpCo(\eta^5CPh_3)][1\text{-H-}closo\text{-}CB_{11}Me_{11}]$, **(13)**, (two views) only one of the two disordered sets shown for the Cp and the coordinated phenyl ring (disorder at 75%:25%), the greater probability positions shown. The structural metrics for the 25% occupancy set of disordered positions are identical within errors. Thermal ellipsoids at 30% probability level.

Co-C18	2.522(6)	C18-C19	1.457(5)	C18-C24-C31	122.1(4)	C24-C18	1.369(6)	C32-C33	1.367(5)
Co-C19	2.121(4)	C18-C23	1.454(5)	C18-C24-C25	124.0(4)	C24-C31	1.504(5)	Co-C13	1.987(6)
Co-C20	2.088(5)	C19-C20	1.410(6)	C31-C24-C25	113.5(3)	C24-C25	1.528(6)	Co-C14	2.021(5)
Co-C21	2.101(6)	C20-C21	1.384(10)	C23-C18-C19	107.3(3)	C25-C26	1.366(6)	Co-C15	2.072(4)
Co-C22	2.056(7)	C21-C22	1.402(11)	C19-C18-C23-C24	170.8	C26-C27	1.381(7)	Co-C16	2.014(4)
Co-C23	2.122(4)	C22-C23	1.407(9)	C32-C32-C36	117.8(3)	C31-C32	1.380(4)	Co-C17	1.976(7)

Table 6: Selected bond lengths (Å) and angles (°) for **(13)**.

previously determined in the solid state structures of $[Ti(CO)_4\{\eta^5\text{-}CPh_3\}]^-$, and $Re(CO)_3(\eta^5\text{-}CPh_3)$ (Figure 46).[89, 90]

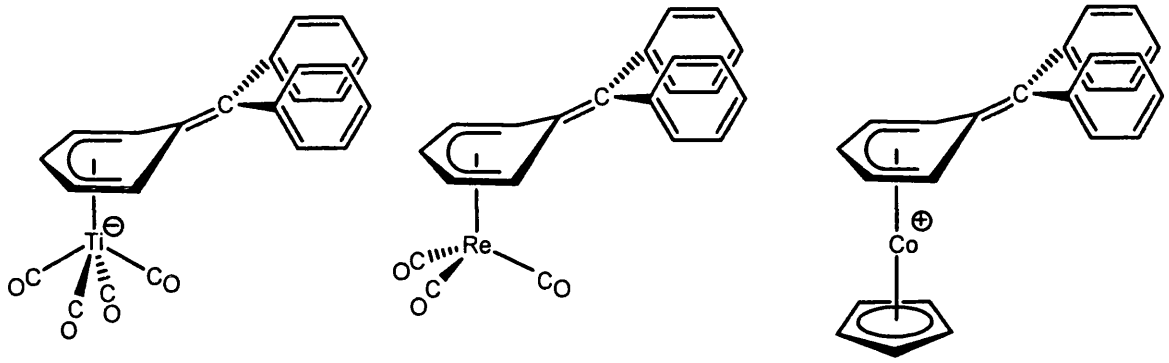

Figure 46: The structurally characterised η^5-trityl coordinated metal complexes, $[Ti(CO)_4\{\eta^5\text{-}CPh_3\}]^-$, $Re(CO)_3(\eta^5\text{-}CPh_3)$ and **(13)**.

The structural metrics of the coordinated trityl clearly indicate that the phenyl ring is bound in a η^5- manner to the Co (Co-C19 to Co-C23 distances ranging from 2.056(7) Å to 2.122(4) Å compared to Co-C18 2.522(6) Å). The coordinated phenyl ring is folded at the C19 and C23 positions (dihedral angle 33.1°), similar foldings are reported for $[Ti(CO)_4\{\eta^5\text{-}CPh_3\}]^-$, $Re(CO)_3(\eta^5\text{-}CPh_3)$ and $CpFe(\eta^5\text{-}C_6Me_5CH_2)$[91] (14.9°, 22° and 33° respectively). Noteworthy is the latter example, the isoelectronic {CpFe} complex, where the coordinated ring experiences an almost identical deformation. The C-C distances around the central trityl carbon indicate the double bond character between C24 and C18, with the two non-bonding phenyl rings having significantly longer C24-C bonds (1.528(6) Å and 1.504(5) Å) than C24-C18 (1.369(6) Å). Analogous distances are found in the two examples of η^5-phenyl rings coordinated to $\{(CO)_4Ti\}$ fragments.[89] The four bonds of the coordinated η^5 phenyl moiety are all equivalent (within experimental errors, C-C average 1.401 Å) and are significantly shorter than the two non-aromatic C-C bonds (C18-C19 1.457(5) Å and 1.454(5) Å). Both of these sets of C-C bond lengths are similar to that reported for $[Ti(CO)_4(\eta^5\text{-}CPh_3)]^-$ (a C-C aromatic average of 1.396 Å and a C-C single bond average of 1.458 Å).

Complex **(13)** is best described as a $\{CpCo^{III}\}$ unit bound to a (η^5-dienyl) group with little indication of any ring slippage to an η^3 allyl complex, as determined by the similar Co-C bond lengths for the five coordinated positions. The structural metrics of the $[CpCo(\eta^5\text{-dienyl})]^+$ in **(13)** (average C-Co distance to the η^5-dienyl ligand, 2.098 Å and average Co-C distance to the Cp ligand, 2.014 Å) bear excellent resemblance to those reported previously for $[CpCo(\eta^5\text{-}C_7H_9)][BPh_4]$ (2.06 Å and 2.05 Å respectively), and $[\{CpCo\}_2\{\eta^5,\eta^5\text{-}3,8\text{-}(CH_3)_2(C_{10}H_{10})\}][PF_6]_2$ (2.074 Å and 2.049 Å).[92, 93] Dissolution of pure crystalline **(13)** in CD_2Cl_2 produced a purple solution with a NMR spectrum that correlates well that reported previously for the $[BF_4]^-$ congener that has not been structurally characterised. $[CpCo(\eta^5\text{-}CPh_3)][BF_4]$ is formed by the displacement of two molecules of ethene (or a diene) from a neutral precursor – with a one electron oxidation of the cobalt centre by $[CPh_3]^+$proposed, facilitating diene dissociation.[88]

It is possible to postulate a mechanism (Figure 47) for the observed formation of **(12)** and **(13)**, with **(8)** acting as a one electron oxidant in the initial step, a role trityl salts are well documented to fulfill.[94] This would produce a transient Co(IV) complex **(A)**, that reductively eliminates ethane to generate a 15 electron Co(II) fragment $\{CpCo(PPh_3)\}^+$, **(B)**. A similar process occurs on the oxidation of $Cp^*Rh(PPh_3)Me_2$, that loses ethane intramolecularly and ultimately yields $[Cp^*Rh(PPh_3)(solv)_2]^{2+}$ (solv = acetone, acetonitrile or THF).[95] This reactive fragment is stabilised in solution by the formation of the an η^3-adduct with the triphenylmethane radical to generate the 18 electron complex $[CpCo(\eta^3\text{-}CPh_3)(PPh_3)][1\text{-H-}closo\text{-}CB_{11}Me_{11}]$, **(C)**. There is good precedence for the η^3 coordination of trityl radicals to metal centres, with a number of

structurally characterised complexes reported (*e.g.*, $(\eta^3\text{-}CPh_3)Re(CO)_4$ and $M(\eta^3\text{-}CPh_3)(acac)$ M = Pt or Pd).[96, 97] Eighteen electron complexes based around $\{CpCo(PPh_3)\}$ are well established to be fluxional in solution, primarily via the ready dissociation of PPh_3.[51, 53, 54, 98, 99]

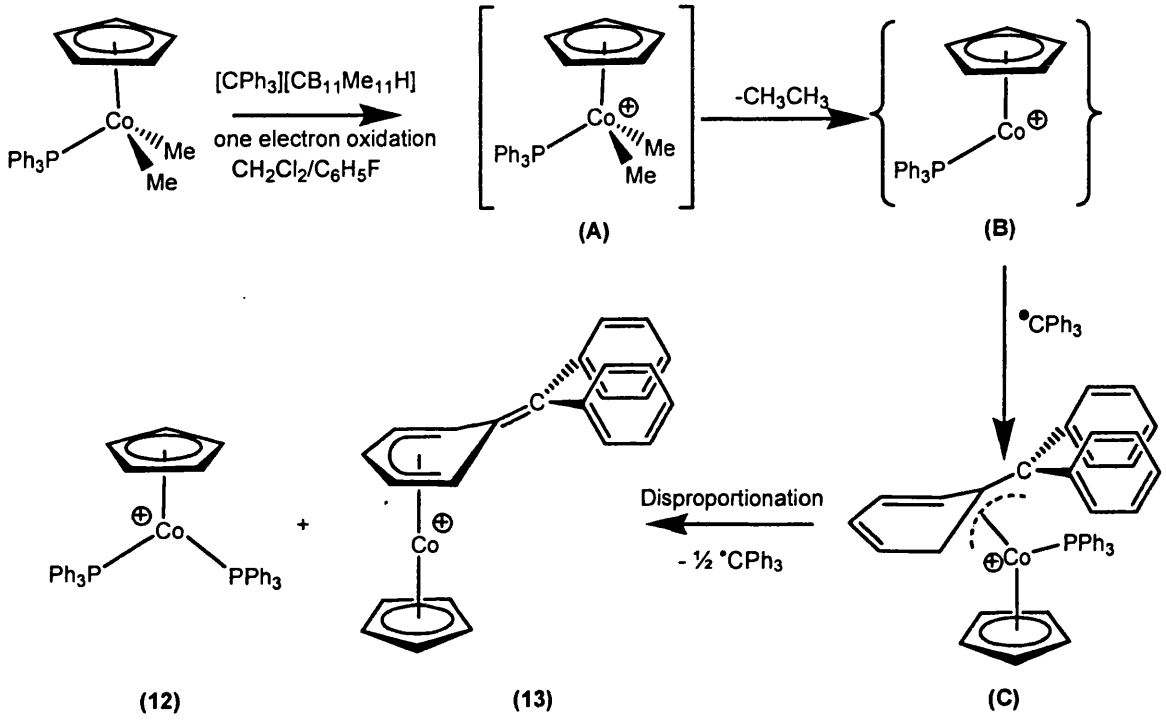

Figure 47: A plausible mechanism explaining the formation of the observed products $[CpCo(PPh_3)_2]^+$ and $[CpCo(\eta^5\text{-}CPh_3)]^+$.

The 'free' PPh_3 present in solution will then displace the coordinated trityl, generating the observed Co(II) complex, $[CpCo(PPh_3)_2][1\text{-}H\text{-}\textit{closo}\text{-}CB_{11}Me_{11}]$. In $(\eta^3\text{-}CPh_3)Re(CO)_4$, the coordinated trityl is facilely displaced by reaction with a number of Lewis bases, *e.g.*, CO, Cl^- and PR_3 (R = low Tolman angle groups).[96] The disproportionation reaction can only produce a maximum of ½ equivalent of the $[CpCo(PPh_3)_2]^+$. The remaining $\{CpCo(\eta^3\text{-}CPh_3)\}^+$ can then undergo a $\{CpCo\}$ to CPh_3 electron transfer, to generate the diamagnetic η^5-adduct $[CpCo(\eta^5\text{-}CPh_3)]^+$. Again literature precedence for an η^3 to η^5 isomerisation of the coordinated trityl ligand is

available with (η^3-CPh_3)$Re(CO)_4$ on heating, losing a molecule of CO to produce (η^5-CPh_3)$Re(CO)_3$ quantitatively.[90]

In rigorously dried solvents a small quantity of air stable yellow crystals are also produced (~5%). Isolation, revealed that these crystals were [Cp_2Co][1-H-*closo*-$CB_{11}Me_{11}$], by comparison of the $^1H\{^{11}B\}$ NMR spectrum to the known complexes [Cp_2Co][BPh_4] and [Cp_2Co][PF_6].[100, 101] The formation of the cobaltacinium cation, indicates that a competing disproportionation reaction is also occurring in solution. It is plausible that the 18-electron cation [$CpCo(\eta^3$-$CPh_3)(PPh_3)]^+$ discussed earlier (or equally some unreacted starting material, $CpCo(PPh_3)Me_2$) can dissociate cyclopentadienyl. This can then go on to displace the η^5-bound $[CPh_3]^-$ ligand, which has previously been demonstrated to substitutionally labile,[89] forming the observed $[Cp_2Co]^+$. Cyclopentadienyl exchange has been unambiguously shown to occur between the compounds $(C_5H_4Me)Co(PPh_3)Me_2$ and $CpCo(PPh_3)_2$,[53] thus a related Cp dissociation process is certainly feasible here.

More interestingly, in CH_2Cl_2 distilled under N_2 instead of argon, the identical reaction between $CpCo(PPh_3)Me_2$ and [CPh_3][1-H-*closo*-$CB_{11}Me_{11}$] yielded a different minor product, blue crystalline material and no [Cp_2Co][1-H-*closo*-$CB_{11}Me_{11}$]. Isolation of this complex, termed here '$CpCo(PPh_3)$' produced a ^1H NMR spectrum in CD_2Cl_2 that strongly suggested a Co···H_3C interaction – judged by the chemical shift change in comparison to [$^nBu_4N$][1-H-*closo*-$CB_{11}Me_{11}$] (Figure 48).

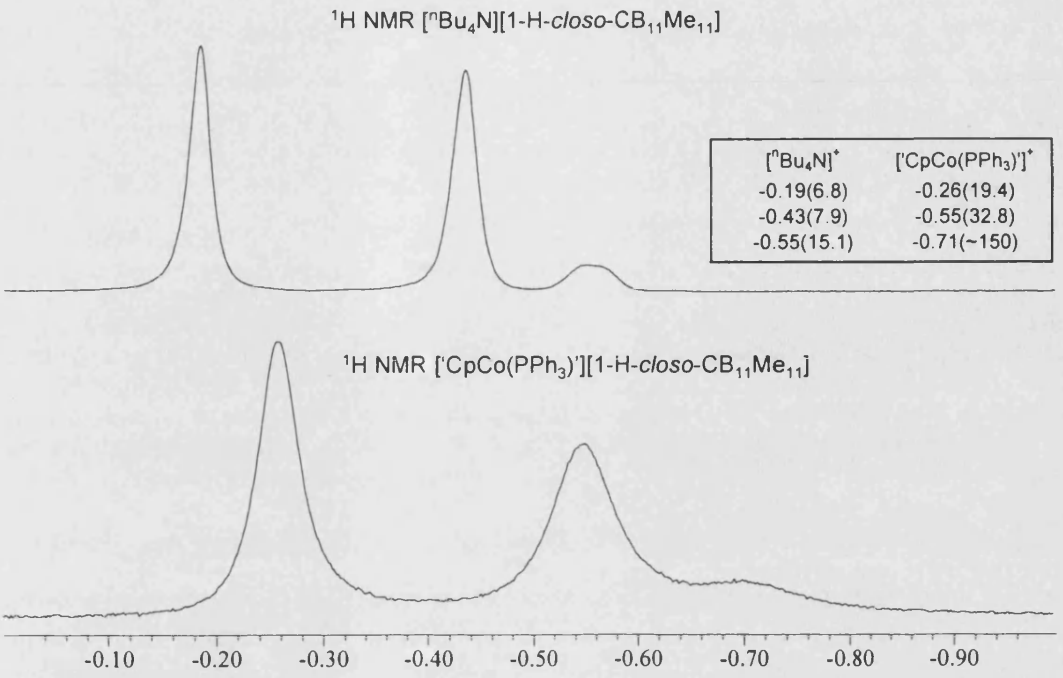

Figure 48: The ^{1}H NMR spectra of [^{n}Bu$_4$N]$^+$ and ['CpCo(PPh$_3$)']$^+$ salts of [1-H-*closo*-CB$_{11}$Me$_{11}$]$^-$ in CD_2Cl_2. Chemical shifts are giving in ppm and the values in parenthesis are the pwhm (Hz) (a satisfactory value for the BCH_3(12) for the cobalt compound was not obtained due to overlapping signals).

The ^{1}H NMR spectra on comparison clearly show an upfield shift and a significant broadening of all the anion CH_3 resonances. Other resonances in the spectrum of ['CpCo(PPh)$_3$']$^+$ (including the triplet due to $CDHCl_2$) are well resolved. Similar chemical shift changes and signal broadening have been reported for complex **(9)**, where close anion···cation pairing has been unambiguously proved. The only other signals in the ^{1}H NMR spectrum are in the aromatic region where three broadened singlets are observed – probably due to PPh_3. No resonance for the Cp protons is visible and in the ^{31}P{^{1}H} NMR spectrum no signal at all is detectable, even after a large number of scans (5000). The ^{11}B NMR spectrum shows the expected three signals, signifying that the compound has C_{5V} symmetry in solution. A plausible structure for this complex is shown in Figure 49.

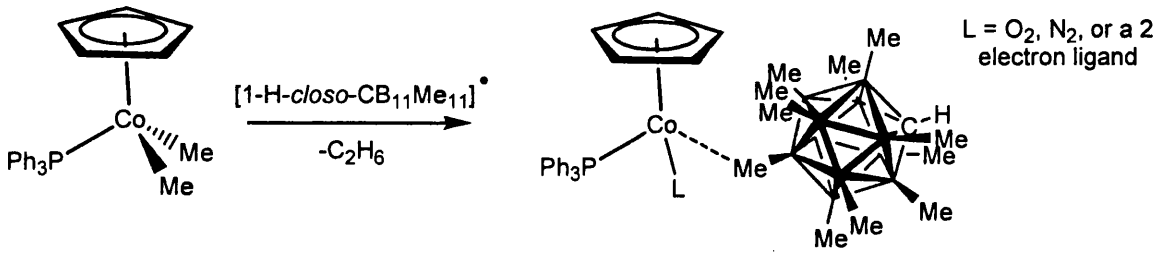

Figure 49: The reaction scheme for the formation of and a possible structure of the blue crystals, 'CpCo(PPh_3)'.

The tentative formulation of the blue crystals as CpCo(PPh_3)L(1-H-*closo*-$CB_{11}Me_{11}$) (L = N_2, O_2, or another 2 electron donor) is based on a number of facts. (i) The anion CH_3 resonances in the $^1H\{^{11}B\}$ NMR spectrum experiencing a significant line broadening and chemical shift change. (ii) The presence of three broad signals in the aromatic region of the $^1H\{^{11}B\}$ NMR spectrum indicative of PPh_3 bound to a Co(II) centre – a similar broadening is observed in the spectrum of **(12)**. (iii) The absence of any Cp signal in the $^1H\{^{11}B\}$ NMR spectrum and the lack of any signals in the $^{31}P\{^1H\}$ NMR spectrum is also seen for **(12)**, a Co(II) compound that has been unambiguously assigned as ligated by Cp and PPh_3. (iv) The requirement of an impurity in the CH_2Cl_2 apparently prevents cyclopentadienyl dissociation and the formation of $[Cp_2Co][1\text{-H-}closo\text{-}CB_{11}Me_{11}]$.

In an attempt to improve the yield of these blue crystals and allow for their further characterisation, the oxidation of the starting compound CpCo(PPh_3)Me_2 was attempted with $[1\text{-H-}closo\text{-}CB_{11}Me_{11}]^•$. This will prevent the formation of the trityl coordinated compound **(12)**, whilst still activating CpCo(PPh_3)Me_2. As expected the reaction of CpCo(PPh_3)Me_2 and $[1\text{-H-}closo\text{-}CB_{11}Me_{11}]^•$ in the same 'impure' CH_2Cl_2 equally evolved gas and on recrystallisation produced the blue crystalline compound ['CpCo(PPh_3)'] in larger quantities. Numerous batches of crystalline material of suitable

quality for X-ray diffraction analysis were synthesised, but due to the highly disordered nature of the structure, diffraction did not extend past a 2θ angle of 20°, insufficient for structure solution. Frustratingly, this still proved to be the case when the higher flux X-rays from synchotron source radiation was used – preventing the identification of this interesting compound. It is possible to postulate a structure of the compound where there is a clear anion···cation interaction, but beyond this the remaining ligand set is unfortunately ambiguous. Though it is clear that the presence of oxygen or an extra ligand present in the poorly purified CH_2Cl_2 is critical in the formation of this complex.

3.4: Summary.

This chapter reports the synthesis of the complexes, $[HNMe_2Ph][1\text{-H-}closo\text{-}CB_{11}Me_{11}]$, $[1\text{-H-}closo\text{-}CB_{11}Me_{11}]^{\bullet}$ and $[Ph_3C][1\text{-H-}closo\text{-}CB_{11}Me_{11}]$. The latter two have been used to introduce the anion to the coordination sphere of zirconium cations. $Cp_2ZrMe(1\text{-H-}closo\text{-}CB_{11}Me_{11})$, **(9)**, has been cleanly synthesised and demonstrated in the solid-state to involve an intimate Zr···H_3C interaction from the antipodal position of the anion. It can be viewed as a $[1\text{-H-}closo\text{-}CB_{11}Me_{11}]^-$ analogue to the active polymerisation catalyst, $Cp_2ZrMe(\mu\text{-Me})B(C_6F_5)_3$.[2] The nature of the metal···anion contact again has been shown to be predominantly ionic in origin, as previously observed for the Group 1 metal cations,[35] the phosphine stabilised silver complexes (see Chapter two) and the related $[MeB(C_6F_5)_3]^-$ coordinated compounds.

The Zr···H_3C interactions have been unambiguously proven to persist in aromatic hydrocarbon solutions, with significant chemical shift changes and broadening of the anion CH_3 vertices observed. The coordinating nature of the [1-H-*closo*-

$CB_{11}Me_{11}]^-$ anion has been investigated, and found to be more nucleophilic than dihydrogen and the $[MeB(C_6F_5)_3]^-$ anion with respect to $\{Cp_2ZrMe\}^+$. It has though been shown to be less coordinating than the neutral alkyl complex Cp_2ZrMe_2, and than stronger Lewis bases (*e.g.*, MeCN).

The decomposition chemistry of the zirconocene/[1-H-*closo*-$CB_{11}Me_{11}]^-$ contact ion pairs have been studied. With the anion being susceptible to methyl abstraction, either initiated by a cationic metal centre, or an electrophilic solvent derived fragment. A number of the anionic decomposition products have been identified and substitution demonstrated to occur in the 12 and 7-11 cage positions, consistent with an electrophilic substitution mechanism – via the postulated borenium ylide reactive intermediate.[78]

Attempts to partner [1-H-*closo*-$CB_{11}Me_{11}]^-$ with a cobalt cation via reaction with the trityl salt was shown to yield predominantly the disproportionation product, **(12)** and the η^5-trityl coordinated compound, **(13)**. A possible mechanism for the formation of these observed species has been discussed. Alongside this, the initial characterisation of a Co···H_3C(anion) complex has been reported that can be synthesised reproducibly in good yield using [1-H-*closo*-$CB_{11}Me_{11}]^\bullet$. Attempts to further characterise this interesting compound have been frustrating by the weakly diffracting nature of its crystalline form.

The investigations into M···H_3C interactions in both the solid-state and solution phase are important due to the role of metal alkane complexes as intermediates in numerous C-H activation reactions. The complexes characterised here can be presented

as a model for these interactions (Figure 50), as Group IV and IX metal compounds have been documented to be intimately involved in C-H activation processes.[102]

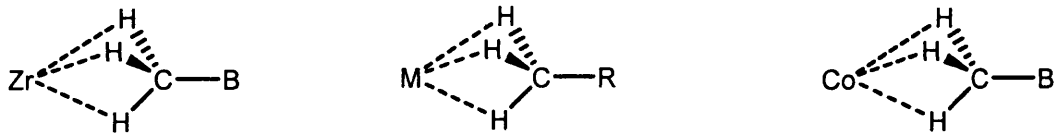

d^0 Model Complex | Alkane σ Complex | d^7 Model Complex (postulated)

Figure 50: A comparison between the model complexes discussed in this chapter and metal alkane complexes

3.5: References.

1 G. J. P. Britovsek, V. C. Gibson, and D. F. Wass, *Angew. Chem., Int. Ed. Engl.*, 1999, **38**, 428.

2 E. Y. X. Chen and T. J. Marks, *Chem. Rev.*, 2000, **100**, 1391

3 S. H. Strauss, *Chem. Rev.*, 1993, **93**, 927.

4 A. Anderson, H. G. Cordes, H. Herwig, W. Kaminsky, A. Merk, R. Mottweiler, J. Pein, H. Sinn, and H. J. Volmer, *Angew. Chem., Int. Ed. Engl.*, 1976, **15**, 630.

5 R. Srinivasa and S. Sivaram, *Prog. Polym. Sci*, 1995, **20**, 309.

6 M. Brookhart, B. Grant, and A. F. Volpe, *Organometallics*, 1992, **11**, 3920.

7 D. J. Crowther, S. L. Borkowsky, D. Swenson, T. Y. Meyer, and R. F. Jordan, *Organometallics*, 1993, **12**, 2897.

8 R. F. Jordan, W. E. Dasher, and S. F. Echols, *J. Am. Chem. Soc.*, 1986, **108**, 1718.

9 R. F. Jordan, C. S. Bajgur, R. Willett, and B. J. Scott, *J. Am. Chem. Soc.*, 1986, **108**, 7410.

10 R. F. Jordan, R. E. Lapointe, C. S. Bajgur, and R. Willett, *J. Am. Chem. Soc.*, 1987, **109**, 4111.

11 M. Bochmann, L. M. Wilson, M. B. Hursthouse, and R. L. Short, *Organometallics*, 1986, **6**, 2556.

12 M. Bochmann and L. M. Wilson, *J. Chem. Soc. Chem. Commun.*. 1986, 1610.

13 G. G. Hlatky and H. W. Turner, *J. Am. Chem. Soc.*, 1989, **111**, 2728.

14 X. Yang, W. A. King, M. Sabat, and T. J. Marks, *Organometallics*, 1993, **12**, 4254.

15 G. G. Hlatky, R. R. Eckman, and H. W. Turner, *Organometallics*, 1992, **11**, 1413.

16 A. D. Horton and J. de-With, *Organometallics*, 1997, **16**, 5424.

[17] A. D. Horton, J. de-With, A. J. v. d. Linden, and H. v. d. Weg, *Organometallics*, 1996, **15**, 2672.
[18] J. C. W. Chien, W.-M. Tsai, and M. D. Rausch, *J. Am. Chem. Soc.*, 1991, **113**, 8570.
[19] J. A. Ewen and M. J. Elder, in 'Eur. Pat. Appl. 0.426.637', 1991.
[20] H. W. Turner, in 'Eur. Pat. Appl. EP 0.277.004 A1', 1988.
[21] X. Yang, C. L. Stern, and T. J. Marks, *Organometallics*, 1991, **10**, 840.
[22] M. Bochmann and S. J. Lancaster, *Angew. Chem., Int. Ed. Engl.*, 1994, **33**, 1634.
[23] M. Ichinohe, H. Fukui, and A. Sekiguchi, *Chem. Lett.*, 2000, 600.
[24] A. Sekiguchi, M. Tsukamoto, and M. Ichinohe, *Science*, 1997, **275**, 60.
[25] X. Yang, C. L. Stern, and T. J. Marks, *J. Am. Chem. Soc.*, 1994, **116**, 10015.
[26] X. Yang, C. L. Stern, and T. J. Marks, *J. Am. Chem. Soc.*, 1991, **13**, 3623.
[27] W. E. Piers and T. Chivers, *Chem. Soc. Rev*, 1997, **26**, 345.
[28] M.-Y. He, G. Xiong, P. J. Toscano, R. L. Burwell, and T. J. Marks, *J. Am. Chem. Soc.*, 1985, **107**, 641.
[29] A. H. Cowley, G. S. Hair, B. G. McBurnett, and R. A. Jones, *Chem. Commun.*. 1999, 437.
[30] Y.-X. Chen, M. V. Metz, J. L. Li, C. L. Stern, and T. J. Marks, *J. Am. Chem. Soc*, 1998, **120**, 6287.
[31] Y.-X. Chen, S. Yang, C. L. Stern, and T. J. Marks, *J. Am. Chem. Soc.*, 1996, **118**, 12451.
[32] M. Bochmann, M. L. H. Green, A. K. Powell, J. Sausmann-Shausen, M. U. Triller, and S. J. Wocadlo, *J. Chem. Soc., Dalton Trans.*, 1999, 43.
[33] L. Li and T. J. Marks, *Organometallics*, 1998, **17**, 3996.
[34] R. Baumann, W. M. Davis, and R. R. Schrock, *J. Am. Chem. Soc.*, 1997, **119**, 3830.
[35] B. T. King, B. C. Noll, and J. Michl, *Collect. Czech. Chem. Commun.*, 1999, **64**, 1001.
[36] A. J. Clarke, M. J. Ingleson, G. Kociok-Kohn, M. F. Mahon, N. J. Patmore, J. P. Rourke, G. D. Ruggiero, and A. S. Weller, *J. Am. Chem. Soc.*, 2004, **126**, 1503.
[37] M. J. Ingleson, M. F. Mahon, N. J. Patmore, G. D. Ruggiero, and A. S. Weller, *Angew. Chem., Int. Ed. Engl.*, 2002, **41**, 3694.
[38] M. Bochmann, S. J. Lancaster, M. B. Hursthouse, and K. M. A. Malik, *Organometallics*, 1994, **13**, 2235.
[39] C. L. Beswick and T. J. Marks, *Organometallics*, 1999, **18**, 2410
[40] X. Yang, C. L. Stern, and T. J. Marks, *Angew. Chem., Int. Ed. Engl.*, 1992, **31**, 1375.
[41] L. Jia, X. Yang, C. L. Stern, and T. J. Marks, *Organometallics*, 1997, **16**, 842.
[42] R. Gomez, M. L. H. Green, and J. L. Haggit, *J. Chem. Soc., Dalton Trans.*, 1996, 939.
[43] D. J. Gillis, M.-J. Tudoret, and M. C. Baird, *J. Am. Chem. Soc.*, 1993, **115**, 2543.
[44] S. J. Lancaster, O. B. Robinson, and M. Bochmann, *Organometallics*, 1995, **14**, 2456.
[45] J. Zhou, S. J. Lancaster, D. A. Walker, S. Beck, M. Thornton-Pett, and M. Bochmann, *J. Am. Chem. Soc.*, 2001, **123**, 223.
[46] V. C. Gibson and S. K. Spitzmesser, *Chem. Rev.*, 2003, **103**, 283.
[47] L. K. Johnson, C. M. Killian, and M. J. Brookhart, *J. Am. Chem. Soc.*, 1995, **117**, 6414.
[48] G. F. Schmidt and M. Brookhart, *J. Am. Chem. Soc.*, 1985, **107**, 1443.
[49] O. Daugulis, M. Brookhart, and P. S. White, *Organometallics*, 2003, **22**, 4699.

[50] E. R. Evitt and R. G. Bergmann, *J. Am. Chem. Soc.*, 1979, **101**, 3973.
[51] A. H. Janowicz and R. G. Bergmann, *J. Am. Chem. Soc.*, 1981, **103**, 2488.
[52] E. R. Evitt and R. G. Bergmann, *J. Am. Chem. Soc*, 1980, **102**, 7003.
[53] H. E. Bryndza and R. G. Bergmann, *Inorg. Chem.*, 1981, **20**, 2988.
[54] H. E. Bryndza, E. R. Evitt, and R. G. Bergmann, *J. Am. Chem. Soc*, 1980, **102**, 4948.
[55] M. Brookhart, A. F. J. Volpe, D. M. Lincoln, I. T. Horvarth, and J. M. Millar, *J. Am. Chem. Soc.*, 1990, **112**, 5634.
[56] V. C. Gibson, M. J. Humphries, K. P. Tellmann, D. F. Wass, A. J. P. White, and D. J. Williams, *Chem. Commun.*. 2001, 2252.
[57] S. Geftakis and G. E. Ball, *J. Am. Chem. Soc.*, 1998, **120**, 9953
[58] X. Z. Sun, D. C. Grills, S. M. Nikiforov, M. Poliakoff, and M. W. George, *J. Am. Chem. Soc.*, 1997, **119**, 7521.
[59] B. T. King, B. C. Noll, A. J. McKinley, and J. Michl, *J. Am. Chem. Soc.*, 1996, **118**, 10902.
[60] S. V. Ivanov, S. M. Miller, O. P. Anderson, K. A. Solntsev, and S. H. Strauss, *J. Am. Chem. Soc.*, 2003, **125**, 4694.
[61] S. V. Ivanov, J. A. Davis, S. M. Miller, O. P. Anderson, and S. H. Strauss, *Inorg. Chem.*, 2003, **42**, 4489.
[62] T. Laube, *Chem. Rev.*, 1998, **98**, 1277.
[63] I. Zharov, B. T. King, Z. Havlas, A. Pardi, and J. Michl, *J. Am. Chem. Soc.*, 2000, **122**, 10253.
[64] Z. W. Xie, T. Jelinek, R. Bau, and C. A. Reed, *J. Am. Chem. Soc.*, 1994, **116**, 1907.
[65] Z. Janousek, U. Lehmann, J. Castulik, I. Cisarova, and J. Michl, *J. Am. Chem. Soc.*, 2004, **126**, 4060.
[66] E. P. Talsi, J. L. Eilertsen, M. Ystenes, and E. Rytter, *J. Organomet. Chem.*, 2003, **677**, 10.
[67] I. A. Guzei, R. A. S. Jr., and R. F. Jordan, *Acta Cryst. Sec. C*, 2000, **56**, 635.
[68] R. F. Jordan, P. K. Bradley, N. C. Baenziger, and R. E. Lapointe, *J. Am. Chem. Soc.*, 1990, **112**, 1289.
[69] M. L. McKee, *J. Am. Chem. Soc.*, 1997, **119**, 4220
[70] N. J. Patmore, M. F. Mahon, J. W. Steed, and A. S. Weller, *J. Chem. Soc., Dalton Trans.*, 2001, 277.
[71] D. J. Liston, Y. J. Lee, W. R. Scheidt, and C. A. Reed, *J. Am. Chem. Soc.*, 1989, **111**, 6643.
[72] R. E. Campbell, USA Pat. 5,066,741, 1991.
[73] Y.-X. Chen, M. V. Metz, L. Li, C. L. Stern, and T. J. Marks, *J. Am. Chem. Soc.*, 1998, **120**, 6287.
[74] S. J. Lancaster, D. A. Walker, M. Thorton-Pett, and M. Bochmann, *Chem. Commun.*. 1999, 1533.
[75] F. Schaper, A. Geyer, and H. H. Brintzinger, *Organometallics*, 2002, **21**, 473.
[76] R. F. Jordan, *Adv. Organomet. Chem*, 1991, **32**, 325.
[77] M. J. Bochmann, *J. Chem. Soc., Dalton Trans.*, 1996, 255.
[78] B. T. King, I. Zharov, and J. Michl, *Chemical Innovation*, 2001, **31**, 23.
[79] A. D. Horton and A. G. Orpen, *Organometallics*, 1991, **10**, 3910.
[80] A. D. Horton and J. H. G. Frijins, *Angew. Chem., Int. Ed. Engl.*, 1991, **30**, 1152.
[81] M. Bochmann, A. J. Jagger, and J. C. Nicholls, *Angew. Chem., Int. Ed. Engl.*, 1990, **29**, 780.
[82] J. Huhmann-Vincent, B. L. Scott, and G. J. Kubas, *Inorg. Chem.*, 1999, **38**, 115.

[83] R. Gomez, M. L. H. Green, and J. L. Haggitt, *J. Chem. Soc., Dalton Trans.*, 1996, 939.
[84] W. Lasser and U. Thewalt, *J. Organomet. Chem.*, 1986, **302**, 201.
[85] U. Thewalt and W. Lasser, *J. Organomet. Chem.*, 1984, **276**, 341.
[86] C. W. Tsang, Q. Yang, E. T. P. Sze, T. C. W. Mak, D. T. W. Chan, and Z. Xie, *Inorg. Chem.*, 2000, **39**, 3582.
[87] R. L. Harlow, R. J. McKinney, and J. F. Whitney, *Organometallics*, 1983, **2**, 1839.
[88] T. D. Newbound and R. D. Ernst, *J. Organomet. Chem.*, 1986, **316**, 213.
[89] P. J. Fischer, K. Ahrendt, V. G. Young, and J. E. Ellis, *Organometallics*, 1998, **17**, 13.
[90] L. S. Crocker and M. D. Heinekey, *J. Am. Chem. Soc.*, 1989, **111**, 405.
[91] J. R. Hamon, D. Astruc, and E. Roman, *J. Am. Chem. Soc.*, 1981, **103**, 2431.
[92] M. A. Bennett, J. C. Nicholls, A. K. F. Rahman, A. D. Redhouse, and J. L. Spencer, *J. Chem. Soc. Chem. Commun.*. 1989, 1328.
[93] W.-Q. Weng, A. M. Arif, and R. D. Ernst, *Organometallics*, 1998, **17**, 4240.
[94] N. G. Connelly and W. E. Geiger, *Chem. Rev.*, 1996, **96**, 877.
[95] A. Pedersen and M. Tilset, *Organometallics*, 1993, **12**, 56.
[96] L. S. Crocker, B. M. Mattson, M. D. Heinekey, and G. K. Schulte, *Inorg. Chem.*, 1988, **27**, 3722.
[97] A. Sonoda, P. M. Bailey, and P. M. Maitlis, *J. Chem. Soc., Dalton Trans.*, 1979, 346.
[98] A. H. Janowicz and R. G. Bergmann, *J. Am. Chem. Soc.*, 1982, **104**, 352.
[99] E. R. Evitt and R. G. Bergmann, *J. Am. Chem. Soc.*, 1980, **102**, 7003.
[100] A. N. Nesmeyanov, N. S. Kochetkova, E. V. Leonova, E. I. Fedin, and P. V. Petrovskii, *J. Organomet. Chem.*, 1972, **39**, 173.
[101] R. B. Materikova, V. N. Babin, I. R. Lyatifov, R. M. Salimov, E. I. Fedin, and P. V. Petrovskii, *J. Organomet. Chem.*, 1981, **219**, 259.
[102] A. E. Shilov and G. B. Shul'pin, 'Activation and Catalytic Reactions of Saturated Hydrocarbons in the Presence of Metal Complexes', Kluwer Academic, 2000.

4 [1-H-*closo*-$CB_{11}Me_{11}$]$^-$ as a weakly coordinating anion susceptible to B-C bond cleavage.

4.1 Background.

Until recent years, synthetic chemists considered dichloromethane (CH_2Cl_2) as a polar, but non-coordinating solvent.[1, 2] The earliest indication that CH_2Cl_2 could act as a ligand towards cationic metal centres came from the pioneering work of Beck and Sünkel.[3, 4] This centred on the investigation into the coordination behaviour of a range of anions with the cationic fragment {$CpMo(CO)_3$}$^+$, showing that a number of 'classically' weakly nucleophilic anions[5] (*e.g.* [OTf]$^-$, [BF_4]$^-$, [AsF_6]$^-$ and [SbF_6]$^-$)[6-8] were interacting with the metal centre. However, with the anion [PF_6]$^-$, an equilibrium between the anion and the CH_2Cl_2 coordinated complexes was established (Figure 1), with the dichloromethane complex favoured at low temperature.[3, 4]

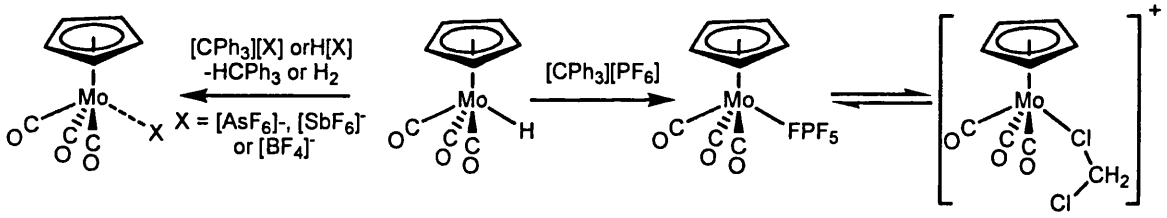

Figure 1: The anion dependence involved in the formation of contact ion pairs or solvent separated ion pairs for the {$CpMo(CO)_3$}$^+$ cationic fragment

Recent work on this system has expanded the number of anions that form contact ion pairs with the {$CpMo(CO)_3$}$^+$ fragment, with [*closo*-$CB_{11}H_{12}$]$^-$ and [12-Br-*closo*-$CB_{11}H_{11}$]$^-$ both being demonstrated to be closely associated with the metal centre.[9, 10] Use of the more weakly coordinating, [*closo*-$CB_{11}H_6Br_6$]$^-$ anion[11] results in a more complicated outcome, producing three complexes, identified as the hydride bridged dimer, [($CpMo(CO)_3$)$_2${μ-H}][*closo*-$CB_{11}H_6Br_6$], the anion coordinated $CpMo(CO)_3$(*closo*-$CB_{11}H_6Br_6$) and the solvent separated ion pair

$[CpMo(CO)_3(ClCH_2Cl)][closo\text{-}CB_{11}H_6Br_6]$ (Figure 2). Unfortunately, no direct evidence for the coordination of dichloromethane was obtainable for this system by standard spectroscopic techniques.

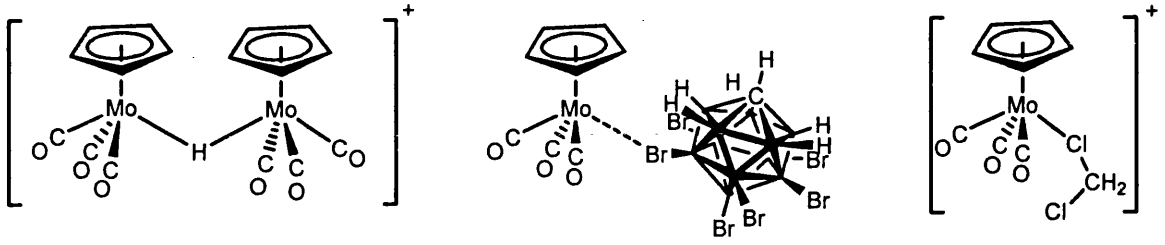

Figure 2: The three molybdenum containing products from the reaction of $CpMo(CO)_3H$ and $[Ph_3C][closo\text{-}CB_{11}H_6Br_6]$ in CD_2Cl_2.

The first, definitive solution characterisation of a metal bound CH_2Cl_2 molecule was obtained by Gladysz *et al.* in 1989. Protonation of the methyl group in $CpRe(NO)(PPh_3)Me$ by the etherate acid of either the $[BF_4]^-$ or $[PF_6]^-$ anions generated the cationic complex $[CpRe(NO)(PPh_3)(ClCH_2Cl)]^+$, **A** (Figure 3).[12] The coordination of CH_2Cl_2 was unequivocally characterised by low temperature ^{13}C NMR spectroscopy, which showed a signal that was shifted downfield with respect to free CH_2Cl_2 ($\Delta\delta$ +24.3 ppm) and coupled to phosphorus.

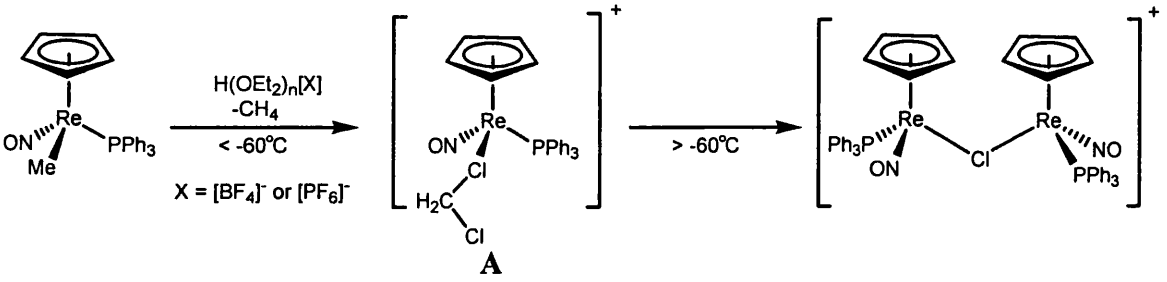

Figure 3: The synthesis and subsequent decomposition of the cation $[CpRe(NO)(PPh_3)(Cl_2CH_2)]^+$.

The coordinated CH_2Cl_2 was readily displaced by stronger Lewis bases, (*e.g.*, CH_3CN, $OPPh_3$, $[CN]^-$, $[Br]^-$, CO or ethene), whilst compound **A** rapidly decomposes at

ambient temperatures to generate the chloride bridged dimer, [{CpRe(NO)(PPh_3)}$_2$(μ-Cl)][X] by chloride abstraction from CH_2Cl_2. The thermal instability of the parent dichloromethane complex precluded attempts to obtain material suitable for X-ray diffraction analysis.

The solid-state determination of a mononuclear $M^+\cdots CH_2Cl_2$ complex was reported soon after for the mixed metal complex, $Ag_2(CH_2Cl_2)_4Pd(OTeF_5)_4$, with each silver centre coordinated by two CH_2Cl_2 molecules in a bidentate manner (Figure 4).[1]

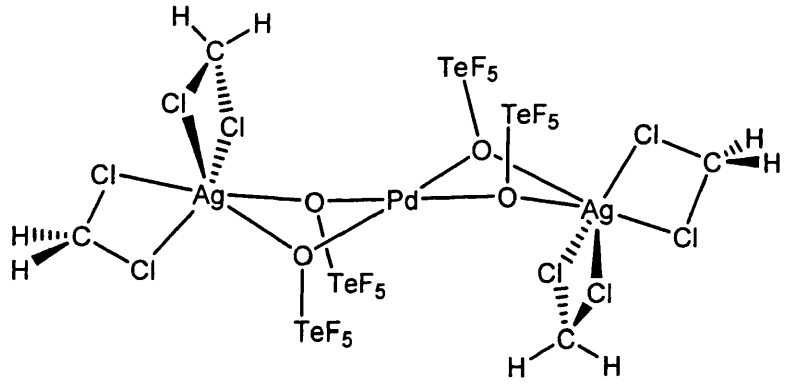

Figure 4: The molecular structure of $Ag_2(CH_2Cl_2)_4Pd(OTeF_5)_4$.

Here the Ag^+ cation is coordinated by both CH_2Cl_2 and the anion ($[OTeF_5]^-$). Since this publication, five further compounds exhibiting $Ag\cdots ClCH_2Cl$ interactions have been structurally determined. They include a mixture of η^1 and η^2 CH_2Cl_2 coordination modes, mixed CH_2Cl_2/anion coordination and purely CH_2Cl_2 Ag^+ coordination, with no anion involvement.[13-17] The presence of intimate $Ag\cdots ClCH_2Cl$ interactions found in these systems is in contrast to the simple silver salt and the phosphine stabilised silver salts of the [1-H-*closo*-$CB_{11}Me_{11}$]$^-$ anion (see Chapter Two).

Aside from these Ag(I) examples, a number of other metal dichloromethane complexes have been structurally characterised, involving a variety of metals from

across the periodic table. There are three related d^6, Group VII, metal cationic complexes, that in each case exhibit a mono dentate M···$ClCH_2Cl$ interaction and require the use of the weakly coordinating anion $[BAr_F]^-$ (Figure 5).[18-21]

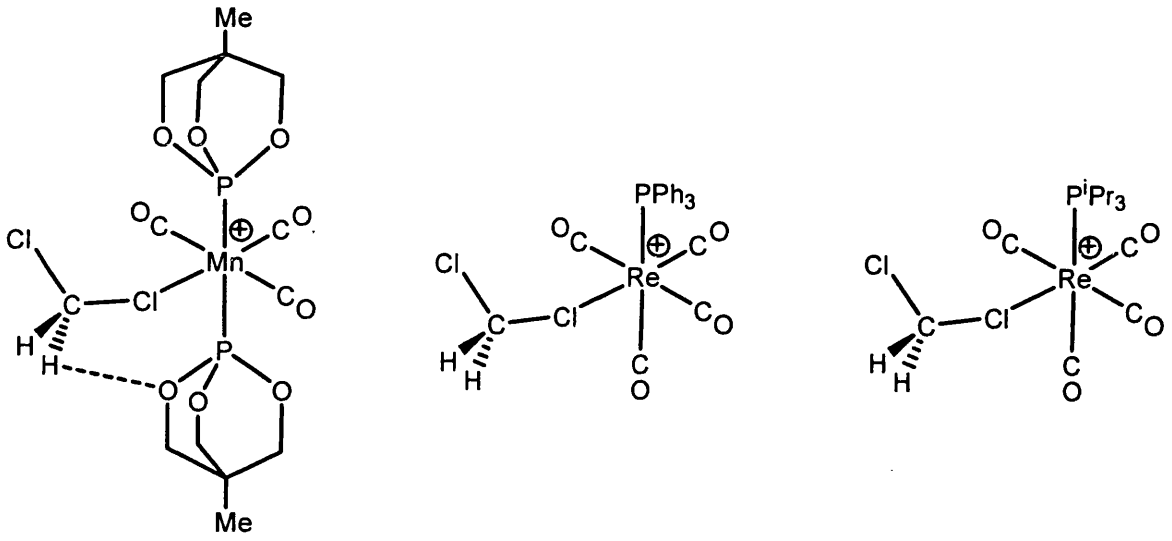

Figure 5: The three group VII CH_2Cl_2 complexes structurally characterised, in each case the $[BAr_F]^-$ anion has been omitted.

In the case of the manganese complex, there is an additional stabilising hydrogen bonding interaction between an acidic proton from the coordinated CH_2Cl_2 and one oxygen from a phosphite ligand. A number of other related complexes have been synthesised and characterised by solution spectroscopic methods only. It is important to note that in these systems the product formed is highly anion dependent. On moving to the analogous complexes partnered with other weakly coordinating anions (*e.g.*, $[BF_4]^-$, $[OTeF_5]^-$ or $[OTf]^-$) intimate ion pairs are formed (*e.g.*, *cis*-$Re(CO)_4(PPh_3)(FBF_3)$, *cis*-$Re(CO)_4(PPh_3)(OTeF_5)$ and *mer*-$Mn(CO)_3(P(OEt)_3)_2(\eta^1$-OTf).[22-24] The CH_2Cl_2 coordinated compounds again all decompose at ambient temperatures to generate chloride bridged dimers analogous to that previously observed by Gladysz, some anion decomposition was also observed.[12] Furthermore, it is

noteworthy that an increase in the steric bulk around the metal centre (albeit with a concomitant reduction in the electrophilicity of these cationic centres) results in these systems relieving their coordinative unsaturation via an agostic interaction rather than CH_2Cl_2 binding (*e.g.*, [*trans*-$(PR_3)_2Re(CO)_3$][BAr_F] R = Ph, Cy or ^iPr, and *trans*-[$(PCy_3)_2Mn(CO)_3$][BAr_F] (Figure 6)).[25-27]

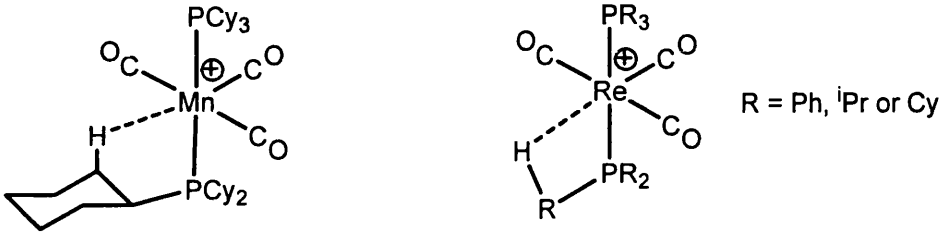

Figure 6: Cation portions of group VII cations stabilised by agostic interactions.

These agostic complexes, like their related CH_2Cl_2 congeners, require the robust, weakly coordinating anion [BAr_F]$^-$, use of [OTf]$^-$ results in anion coordination, whilst the [BF_4]$^-$ analogue suffers from rapid decomposition even at low temperatures.[26]

Four d^6 metal complexes of CH_2Cl_2 have also been structurally characterised, [$RuH(CO)(CH_2Cl_2)(P^tBu_2Me)_2$][$BAr_F$]$^-$, [$Cp^*M(PMe_3)Me(CH_2Cl_2)$][$BAr_F$]$^-$ (M = Rh or Ir) and [$RhCl(CH_2Cl_2)$(dimethyl-benzyl-bis-oxazaline)][BAr_F] (Figure 7).[28-31]

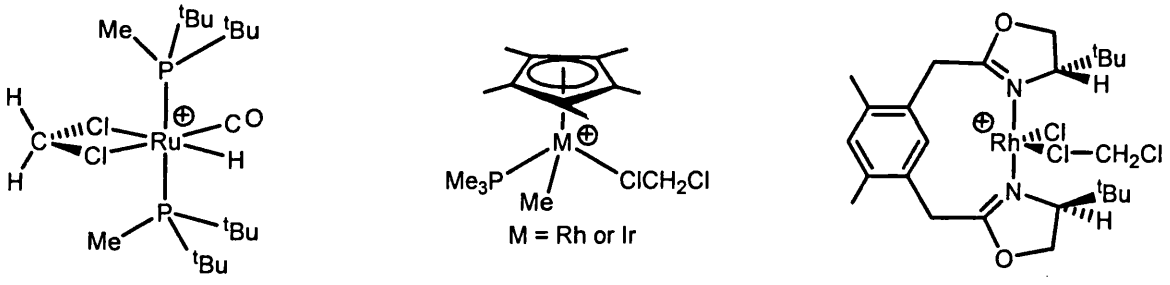

Figure 7: The remaining d^6 metal··· Cl_2CH_2 complexes (cation portions only) structurally characterised.

All of these complexes are readily synthesised by salt metathesis reactions from their analogous triflate coordinated precursors. The complexes shown in Figure 7,

whilst being extremely air and moisture sensitive, are more stable with respect to chloride abstraction when compared to the Groups VII examples, presumably due to the reduced electrophilicity at the metal centre (i.e. no strongly π – acidic groups).

The final structurally characterised $M\cdots Cl_2CH_2$ complex is based on the d^8 square planar cationic fragment, $\{trans\text{-}(^iPr_3P)_2PtH\}^+$,[32] again partnered with the $[BAr_F]^-$ anion. The dichloromethane adduct is readily accessible by two routes (Figure 8).

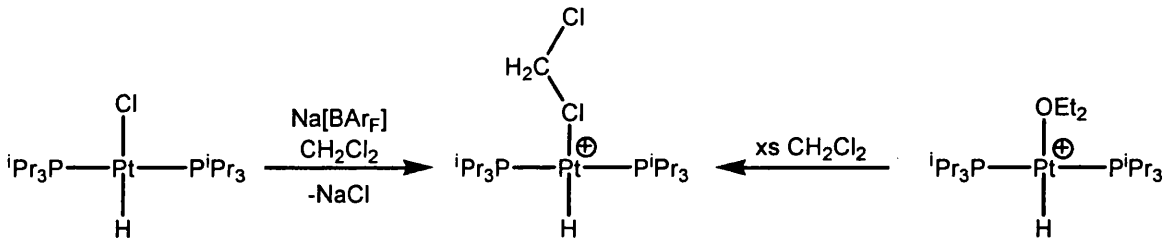

Figure 8: The synthetic routes to the CH_2Cl_2 coordinated complex $[trans\text{-}(^iPr_3P)_2Pt(H)(CH_2Cl_2)][BAr_F]$.

This dichloromethane complex is surprisingly stable persisting even in the presence of O_2 and adventitious H_2O for days, although the addition of a twofold excess of a stronger Lewis base, (L) effects the clean conversion to new products of the general formula $[(^iPr_3P)_2Pt(H)(L)]^+$. Decomposition of the CH_2Cl_2 complex requires forcing conditions and again proceeds via chloride abstraction.

The complexes discussed herein are not meant to be an exhaustive list of all the known dichloromethane complexes, rather it is meant to highlight the important and the structurally characterised examples that will be investigated further in this chapter.

4.1.1 Scope of Chapter:

Chapters Two and Three detailed examples where M···H_3C interactions between a number of metal complexes and the anion [1-H-*closo*-$CB_{11}Me_{11}$]$^-$ have been characterised, and crucially, shown to persist in dichloromethane solutions. These findings demonstrate that, for certain cationic metal-ligand sets, [1-H-*closo*-$CB_{11}Me_{11}$]$^-$ can be more coordinating than CH_2Cl_2. This chapter discusses attempts to synthesise a number of complexes partnered with the [1-H-*closo*-$CB_{11}Me_{11}$]$^-$ anion instead of the [BAr_F]$^-$ anion. These would have the potential of either producing intimate ion pair complexes or, the analogous *solvento* complexes. Further precedence for this methodology is that in a number of these systems CH_2Cl_2 is displaced from a metal's coordination sphere by 'classically' weakly coordinating anions (*e.g.*, [$OTeF_5$]$^-$, [BF_4]$^-$ and [OTf]$^-$). As [1-H-*closo*-$CB_{11}Me_{11}$]$^-$ has been demonstrated previously to be more coordinating than [BAr_F]$^-$ then the displacement of CH_2Cl_2 by this anion is also feasible.

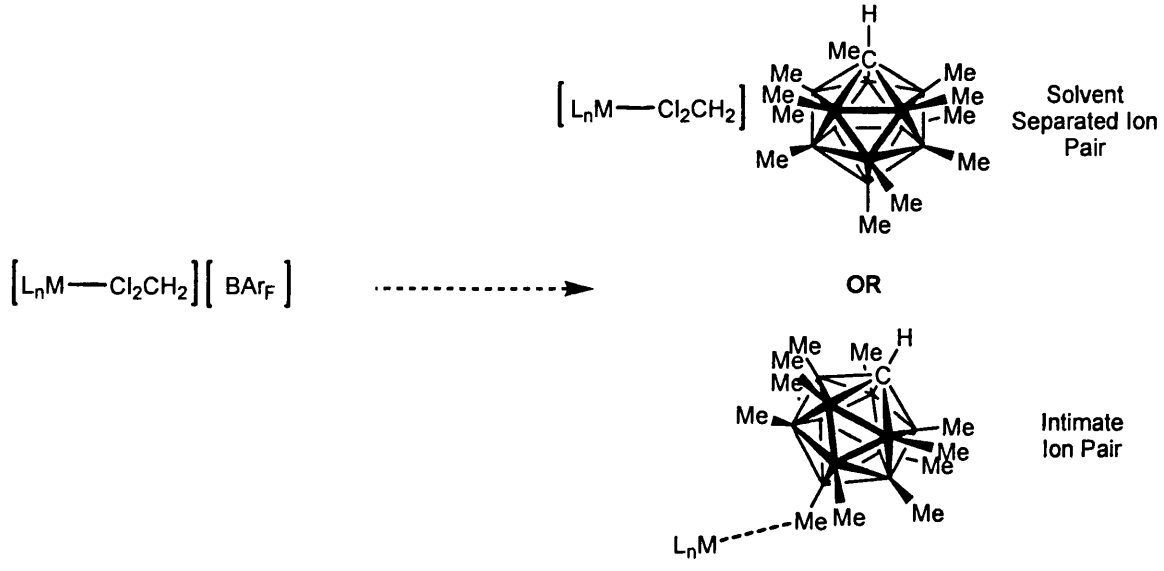

Figure 10: The two possible results expected on synthesising known CH_2Cl_2 complexes partnered with [1-H-*closo*-$CB_{11}Me_{11}$]$^-$.

On the successful synthesis of these analogous complexes partnered with [1-H-*closo*-$CB_{11}Me_{11}$]$^-$ two possible outcomes can be envisaged (Figure 10): (i) Solvent

separated ion pairs that would be analogous to the reported $[BAr_F]^-$ complexes. (ii) Intimate ion pair complexes that by necessity would involve M···H_3C interactions and provide a further model for metal alkane interactions.

4.2: Results and Discussion:

4.2.1: Attempts to partner [1-H-*closo*-$CB_{11}Me_{11}$]$^-$ with {$CpMo(CO)_3$}$^+$.

Following the seminal work by Beck[3, 4, 7, 8] and the success at partnering the 16 electron {$CpMo(CO)_3$}$^+$ fragment with the carborane mono-anions [*closo*-$CB_{11}H_{12}$]$^-$, [12-Br-*closo*-$CB_{11}H_{11}$]$^-$ (and to a limited extent [*closo*-$CB_{11}H_6Br_6$]$^-$),[9, 10, 33, 34] a number of synthetic pathways to introduce the [1-H-*closo*-$CB_{11}Me_{11}$]$^-$ anion were studied (Figure 11).

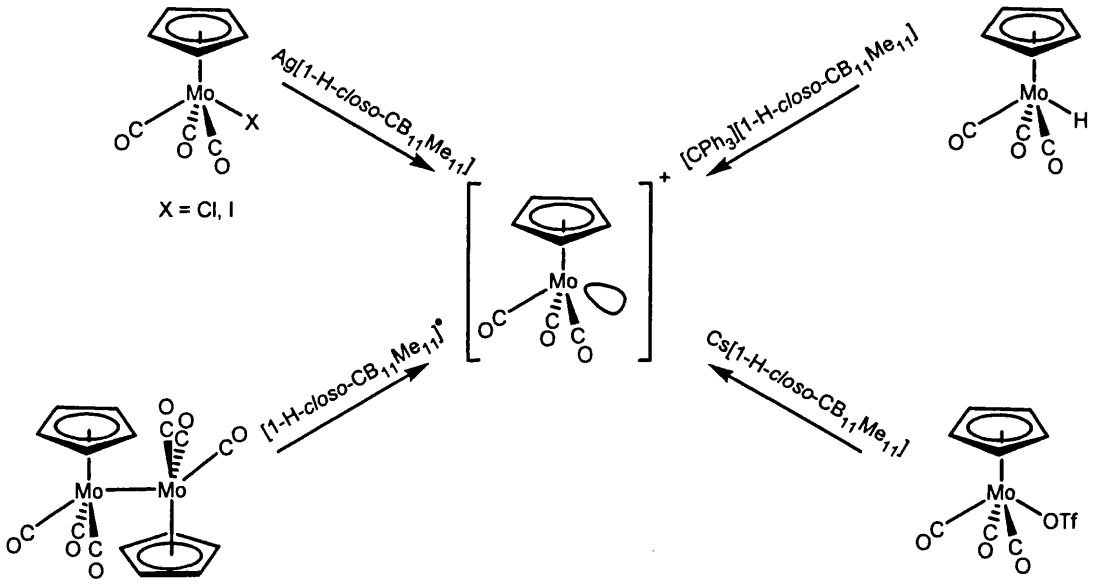

Figure 11: Synthetic routes to generate the cationic fragment {$CpMo(CO)_3$}$^+$, the vacant site depicted in reality would be occupied either, by a solvent molecule or an anion interaction.

4.2.1.1: Silver Salt Metathesis reactions.

Metathetical reactions employing the silver salt of the closely related anion, [*closo*-$CB_{11}H_6Br_6$]$^-$ have been reported to have mixed success in generating metal cations. In the $CpMo(CO)_3X$ system (X = halide) the reaction is arrested, not proceeding past an intermediate stage (Figure 12).[9] In contrast, the reaction of

$CpFe(CO)_2I$ with $Ag[closo\text{-}CB_{11}H_6Br_6]$ was reported to result in the complete metathesis to give $CpFe(CO)_2(closo\text{-}CB_{11}H_6Br_6)$, although this compound was only identified by IR spectroscopy.[35] Thus, the halide abstraction from $CpMo(CO)_3X$ utilising $Ag[1\text{-}H\text{-}closo\text{-}CB_{11}Me_{11}]$ was explored.

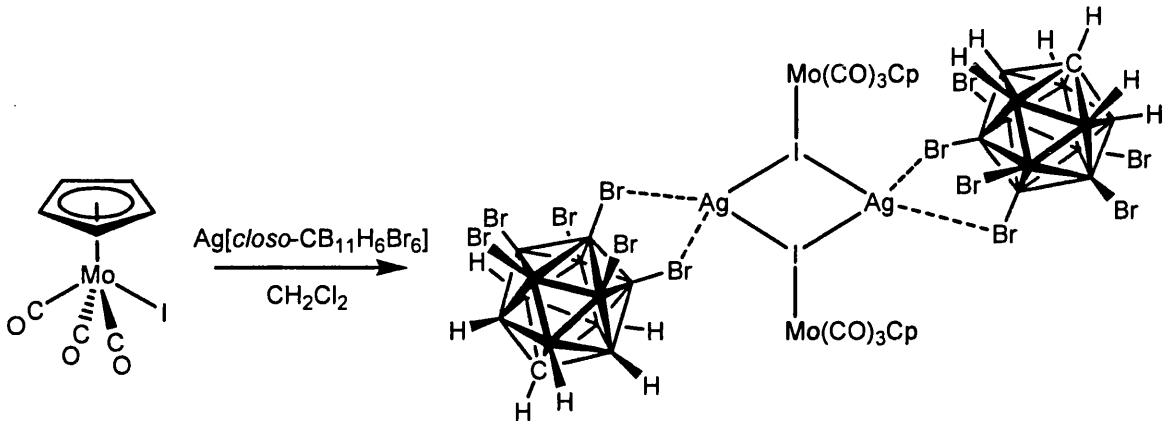

Figure 12: The retarded metathesis reaction of $CpMo(CO)_3I$ with $Ag[closo\text{-}CB_{11}H_6Br_6]$, terminated at the intermediate stage.

The reactivity discussed herein will focus on the salt metathesis reactions when, X = I although similar results were obtained with X = Cl (*vide infra*). Consistently with $CpMo(CO)_3Cl$, however, the reactions showed a number of other unidentified products (totalling to ~15% overall content, based on the combined Cp resonances in the ^1H NMR spectrum) along with some anion decomposition.

The addition of one equivalent of $Ag[1\text{-}H\text{-}closo\text{-}CB_{11}Me_{11}]$ to $CpMo(CO)_3I$ in a CD_2Cl_2 solution resulted in a ^1H NMR spectrum with a single Cp resonance at δ 5.76 ppm, shifted downfield from that of $CpMo(CO)_3I$ in the same solvent (δ 5.67 ppm). The IR spectrum of a CH_2Cl_2 solution of this complex showed a number of CO stretching bands (2055, 2043 and 1966 cm^{-1}). This is a more complex spectrum to those reported for the anion coordinated compounds with $\{Ag_2I_2\}$ cores observed in the analogous

silver salt metathesis reactions with [*closo*-$CB_{11}H_{12}]^-$ (2054 and 1973 cm^{-1}), and [*closo*-$CB_{11}H_6Br_6]^-$ (2055 and 1975 cm^{-1}),[9, 34] suggesting a different structure. Crystals of this complex suitable for an X-ray diffraction analysis were obtained by the slow diffusion of hexanes into a CH_2Cl_2 solution at -20°C (some white powder – later characterised as Ag[1-H-*closo*-$CB_{11}Me_{11}$] was also observed). This revealed the structure (Figure 13) to also have a dicationic $\{Ag_2I_2\}$ core, but in contrast to the three structurally characterised carborane coordinated intermediate complexes (Figure 14), the silver coordination spheres are completed by two further 'terminal' interactions to $CpMo(CO)_3I$ to give $[Ag_2\{CpMo(CO)_3I\}_6][1\text{-H-}closo\text{-}CB_{11}Me_{11}]_2$, **14-I**.

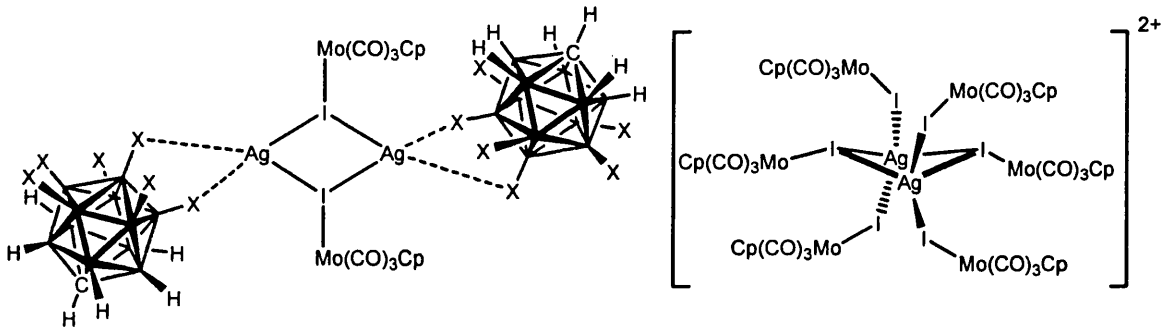

Figure 14: The structural disparity between the carborane bound intermediates (X = Br or H, bound via η^1 or η^2 linkages, dependent on anion) and the $CpMo(CO)_3I$ 'ligated' Ag adduct, **14-I** .

There are two [1-H-*closo*-$CB_{11}Me_{11}]^-$ anions present for charge balance, but no close M···anion contacts are observed. The two symmetry related Ag^+ cations in **14-I** are in an approximate tetrahedral geometry generated by four iodine atoms, two bridging and two terminal (Figure 15).

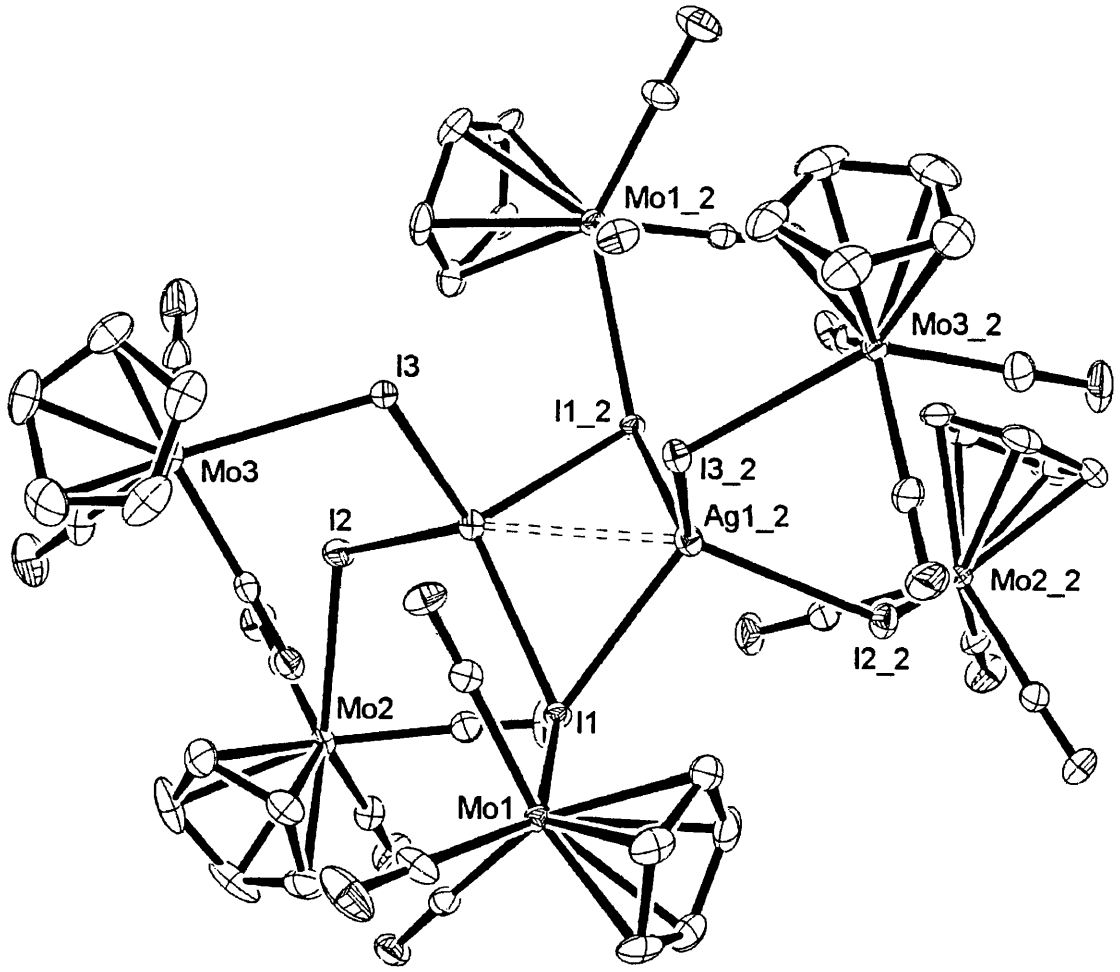

Figure 13: Molecular structure of the di-cationic portion of compound **14-I**, hydrogens omitted for clarity. Symmetry transformations used to generate equivalent atoms: -x+1 y -z+1/2. Thermal ellipsoids shown at the 30% probability level.

Ag1-I1	2.9123(4)
Ag1-I2	2.8171(4)
Ag1-I3	2.7872(4)
Mo1-I1	2.8704(5)
Mo2-I2	2.8578(5)
Mo3-I3	2.8537(5)
Ag1-I1-Mo1	108.507(13)
Ag1_2-I1-Mo1	124.805(14)
Ag1-I2-Mo2	115.451(15)
Ag1-I3-Mo3	105.866(13)
Ag1_2-I1	2.8918(4)
Ag1-Ag1_2	3.0376(6)
I3-Ag1-I1_2	120.361(15)
I3-Ag1-I2	124.805(14)
I3-Ag1-I1	108.417(14)
I2-Ag1-I1_2	109.977(14)
I(1_2)-Ag-I1	104.342(13)
I2-Ag1-I1_2	103.137(14)
I1-Ag1-Ag1_2	58.114(12)
I3-Ag1-Ag1_2	100.863(9)

Table 1: Selected bond lengths (Å) and angles (°) for Compound **14-I**.

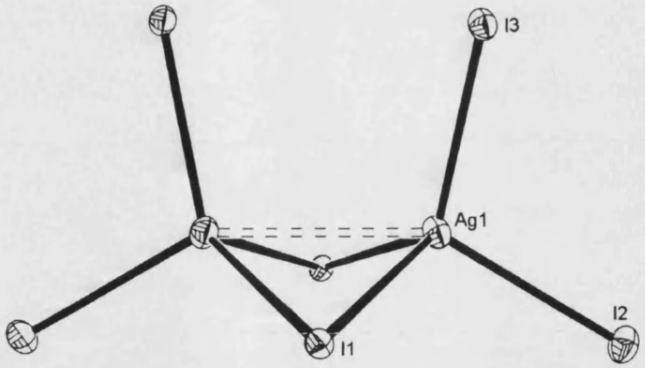

Figure 15: The immediate environment around each silver centre, demonstrating the tetrahedral geometry about Ag^{+}.

A similar tetrahedral arrangement has been observed in $[Ag\{CpW(CO)_3I\}_4][BF_4]$ (Figure 16),[36] which is another example where a neutral organometallic metal halide complex has displaced a counterion from the Ag^{+} coordination sphere. This can be viewed as a monomeric version of compound **14-I** (albeit with an extra molecule of $CpW(CO)_3I$).

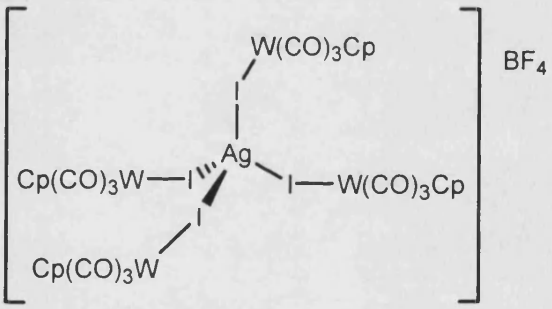

Figure 16: The molecular structure of $[Ag\{CpW(CO)_3I\}_4][BF_4]$.

The $\{Ag_2I_2\}$ core is significantly deviated away from planarity, approaching a butterfly geometry, hinged around the I1 – I1_2 vector by 63.1°, similar to that observed for the structure of $[CpMo(CO)_3I{:}Ag(\eta^1\text{-}closo\text{-}CB_{11}H_{12})]_2$ (hinge angle of 56.8°).[34] In contrast planar cores $\{Ag_2I_2\}$ have been found for $[CpMo(CO)_3I{:}Ag(\eta^2\text{-}12\text{-}Br\text{-}closo\text{-}CB_{11}H_{11})]_2$ and $[CpMo(CO)_3I{:}Ag(\eta^3\text{-}closo\text{-}CB_{11}H_6Br_6)]_2$.[9]

The Ag···Ag separation at 3.0376(6) Å lies within that of the combined van der Waals radii of two silver atoms (3.44Å),[37] indicative of a ligand supported argentophilic interaction.[38] The four Ag-I bond lengths in **14-I** are disparate, with the two terminal interactions being shorter (Ag1-I2 2.8171(4) Å, Ag1-I3 2.7872(4) Å) than the two bridging bonds (Ag1-I1 2.9123(4) Å and 2.8918(4) Å) as would be expected. Though these bond lengths are within in the range (2.8 to 2.9 Å) expected for dative R-I···Ag bonds and are comparable to that in $[Ag\{CpW(CO)_3I\}_4][BF_4]$ (2.832(1) Å).[36, 39] Furthermore, the Mo-I distance of the bridging $CpMo(CO)_3I$ moiety (2.8704(5) Å) is stretched to some extent in comparison to the two terminal fragments (2.8578(5) Å and 2.8537(5) Å), possibly indicating a slight activation of this Mo-I bond to halide abstraction.

The solid state structure of **14-I** possesses two inequivalent $CpMo(CO)_3I$ environments (terminal and bridging) in a 2:1 ratio. This inequivalence is not observed in the solution phase NMR spectra. On the dissolution of a crystalline sample of **14-I** into CD_2Cl_2 the resultant ^1H NMR spectrum shows only one Cp signal at δ 5.76 ppm and a Cp : anion ratio of 3:1. The anion resonances in both the ^1H and ^{11}B NMR spectra exhibit the expected 3 signals (signifying C_{5V} symmetry is maintained in solution), with the chemical shifts and line widths effectively identical to that observed for $[^nBu_4N][1\text{-}H\text{-}closo\text{-}CB_{11}Me_{11}]$, indicating no M···anion interactions. Cooling the sample to -60°C resulted in no significant changes in the ^1H NMR spectrum, indicating a fast fluxional process is making all the $CpMo(CO)_3I$ molecules equivalent. It is unlikely that this process occurs through the cleavage of a Mo-I bond – rather a more probable mechanism would involve the scission of the $\{Ag_2I_2\}$ core into 'monomeric' fragments (Figure 17).

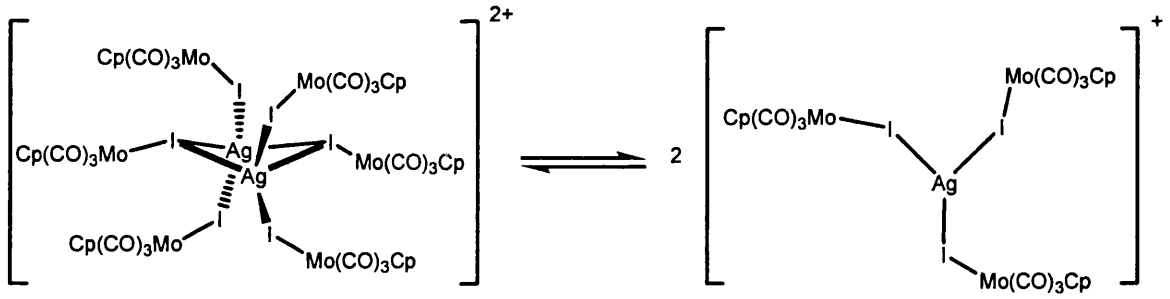

Figure 17: A possible fluxional process that would result in the single Cp resonance observed in the ^{1}H NMR spectrum

Precedence for this proposed equilibrium and the existence of a monomeric $[Ag\{CpMo(CO)_3I\}_3]^+$ cation comes from the characterisation of the closely related $[Ag\{CpW(CO)_3I\}_4]^+$ cation that has a central Ag^+ surrounded by four $CpW(CO)_3I$ ligands.

Continuation of the reaction over the course of a further 14 days results in a gradual disappearance of the CO stretching bands in the IR spectrum corresponding to complex **14-I**, with them ultimately being completely displaced by a more complex set of new stretching bands between 2066 and 1963 cm^{-1}. A white precipitate is also observed, which we assign to AgI. The ^{1}H NMR spectrum showed the presence of a single Cp signal at δ 5.77 and, in combination with the IR spectrum, allowed for the formulation of this new compound as $[\{CpMo(CO)_3\}_2(\mu\text{-I})][1\text{-H-}closo\text{-}CB_{11}Me_{11}]$, **15-I** by comparison to previously reported $[\{CpMo(CO)_3\}_2(\mu\text{-I})][BPh_4]$ complex.[40] Definitive identification of the final metathesis product as $[\{CpMo(CO)_3\}_2(\mu\text{-X})][1\text{-H-}closo\text{-}CB_{11}Me_{11}]$, **15**, was obtained by an X-ray diffraction analysis for the chloride congener, **15-Cl** (prepared in an identical manner to the iodide – albeit with a significant proportion of cage decomposition present, ~20%), Figure 18. The structure is unremarkable with the Cl^- symmetrically bridging two $\{CpMo(CO)_3\}^+$ fragments (Mo1-

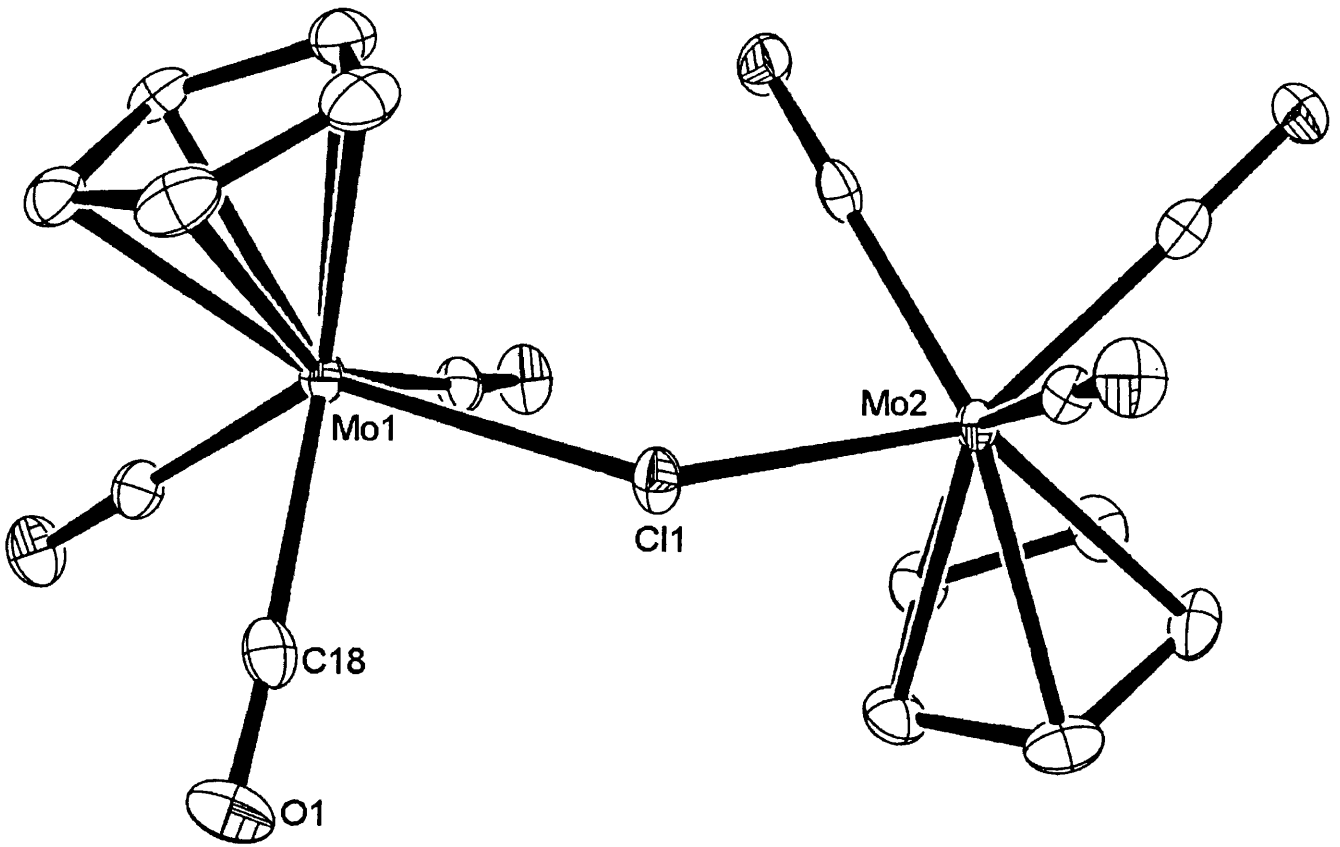

Figure 18: Molecular structure of cationic portion of Compound **15-Cl**, hydrogens omitted for clarity. Thermal ellipsoids shown at the 30% probability level.

Mo1-Cl1	2.5390(11)
Mo2-Cl1	2.5393(10)
Mo1-Cl1-Mo2	128.61(4)
Mo1-C18	2.049(5)
C18-O1	1.127(5)

Table 2: Selected bond lengths (Å)and angles (°) for Compound **15-Cl**.

Cl1 2.5390(11) Å and Mo2-Cl1 2.5393(10) Å), that are arranged in a *trans* orientation to each other. The Mo-Cl-Mo angle is large (128.61(4)°) eliminating, as expected, the possibility of any Mo···Mo bonding, a similar M-X-M angle has been reported for $[\{CpFe(CO)_2\}_2(\mu\text{-}I)][BF_4]$ (110.8(1)°),[41,42] Complexes **15**, are presumably formed by the halide abstraction from $CpMo(CO)_3X$ to generate the 16 electron fragment $\{CpMo(CO)_3\}^+$ which is then trapped by the remaining $CpMo(CO)_3X$. Intermediate **14** and the final metathesis product **15** are the only Cp containing species formed, even when a large excess of Ag[1-H-*closo*-$CB_{11}Me_{11}$] is used. The intermediacy of **14** on the pathway to **15** is demonstrated in the 1:1 reaction of Ag[1-H-*closo*-$CB_{11}Me_{11}$]:$CpMo(CO)_3I$ by two findings, the first being examination of the relative mole fractions of **14** and **15** (calculated by ^1H NMR spectroscopy, integrating the respective Cp resonances to an internal standard). Figure 19 demonstrates the immediate formation of the intermediate species, **14-I**, followed by its slow conversion to produce the halide bridged dimer; importantly the mass balance is constant throughout the transformation indicating that **14** is converted cleanly to **15**.

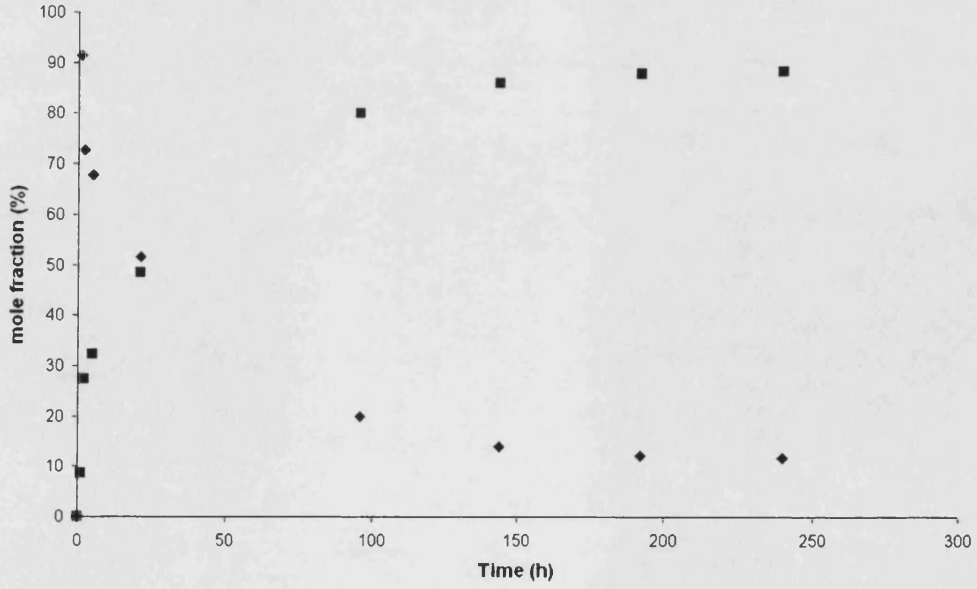

Figure 19: Plot of mole fraction versus time for compounds **14-I** (◆) and **15-I** (■).

Secondly dissolution of crystalline **14-I** in CD_2Cl_2 resulted, after a period of days in two Cp containing products, the final metathesis product **15-I**, and $CpMo(CO)_3I$ (by comparison to an independently synthesised sample), along with the precipitation of a white solid –AgI (Figure 20).

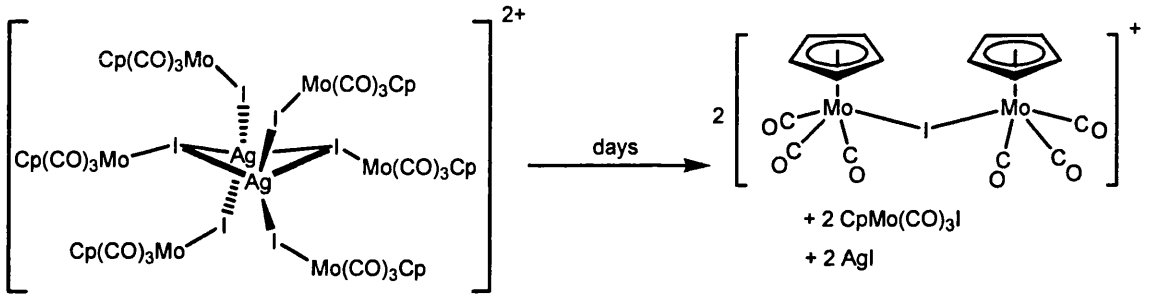

Figure 20: The overall reaction stoichiometry for the reaction of **14-I** to generate the final metathesis product.

$CpMo(CO)_3I$ is formed as a by-product in this reaction due to insufficient Ag[1-H-*closo*-$CB_{11}Me_{11}$]. In a 1:1 reaction of $CpMo(CO)_3I$ and Ag[1-H-*closo*-$CB_{11}Me_{11}$], **15** is the only CpMo containing product ultimately formed. Addition of an excess (10 fold) of Ag[1-H-*closo*-$CB_{11}Me_{11}$] does not result in complete metathesis to $CpMo(CO)_3$(1-H-*closo*-$CB_{11}Me_{11}$), the reaction being arrested at the halide bridged dimer. This is in contrast to [{$CpFe(CO)_2$}$_2$(μ-I)][BF_4], that on the addition of one equivalent of Ag[BF_4] does progress to give the complete metathesis product, $CpFe(CO)_2(BF_4)$.[42] This strongly implies that anion nucleophilicity is an important factor in driving halide metathesis through to completion – with weakly coordinating anions only proceeding slowly, if at all. [43]

A related investigation into the chloride abstraction from a bulky platinum diimine system [(N-N-chelate)Pt(Me)Cl] with Ag[BF_4] revealed a similar phenomenon

(Figure 21), with the initial formation of a dimeric Ag bridged dimer, that in non-coordinating solvents proceeds to give the chloride bridged dimer.[44] The formation of only two Cl···Ag contacts, in contrast to **14**, presumably arises due to the greater steric bulk around the metal centre, thus preventing any higher aggregation.

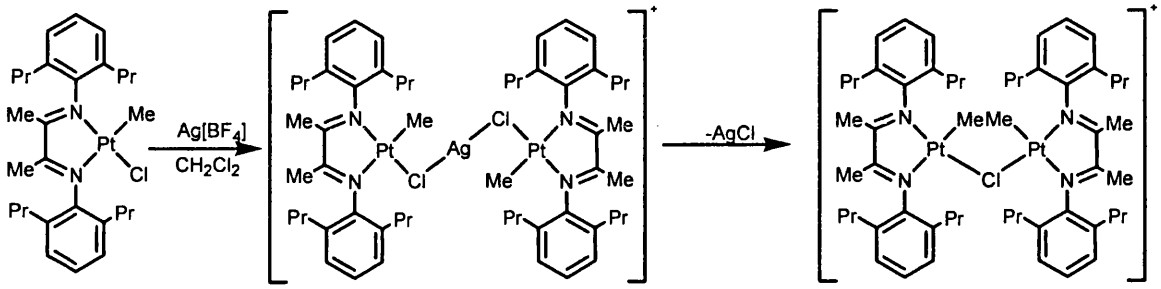

Figure 21: Reaction scheme leading to the chloride bridged platinum dimer.

Following the absence of a metathesis product in the analogous [*closo*-$CB_{11}H_6Br_6]^-$ system, it was somewhat surprising to observe any further reaction with the less coordinating [1-H-*closo*-$CB_{11}Me_{11}]^-$ anion to afford the halide bridged dimer **15**. The lack of any further reaction beyond the intermediate $\{Ag_2I_2\}$ complex in the [*closo*-$CB_{11}H_6Br_6]^-$ congener has been previously ascribed to the significant steric bulk associated with [*closo*-$CB_{11}H_6Br_6]^-$. This prevents any anion attack on the molybdenum centre and consequently metathesis consummation. Metathesis reactions occurring via the intermediate complexes **14** do by contrast, proceed, presumably due to the significantly decreased steric congestion associated with the iodide from $CpMo(CO)_3I$, allowing it to attack the Mo centre.

4.2.1.2: Hydride Abstraction Reactions:

Following the failure of the silver salt metathesis pathway to generate $\{CpMo(CO)_3\}^+$ an alternative route, the hydride abstraction from $CpMo(CO)_3H$ by the

trityl salt, $[Ph_3C][1\text{-H-}closo\text{-}CB_{11}Me_{11}]$ (reported in Chapter Three) was investigated. This methodology has had previous success in introducing the anions $[12\text{-Br-}closo\text{-}CB_{11}H_{11}]^-$, $[closo\text{-}CB_{11}H_6Br_6]^-$ $[PF_6]^-$, $[SbF_6]^-$ and $[BF_4]^-$ to the metal coordination sphere (Figure 22).[4, 9, 45]

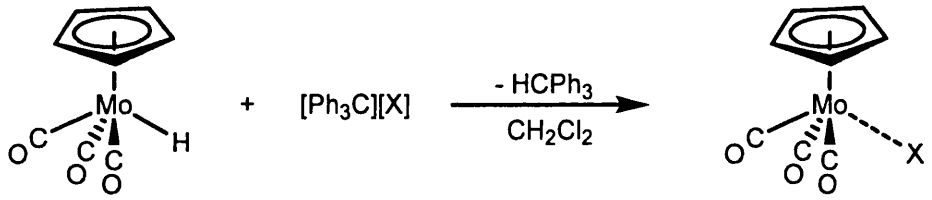

X = $[12\text{-Br-}closo\text{-}CB_{11}H_{11}]^-$, $[closo\text{-}CB_{11}H_6Br_6]^-$, $[PF_6]^-$, $[SbF_6]^-$ or $[BF_4]^-$

Figure 22: A general schematic for the formation of the anion bound complexes $CpMo(CO)_3\cdots X$.

The reaction of $[Ph_3C][1\text{-H-}closo\text{-}CB_{11}Me_{11}]$ with one equivalent of $CpMo(CO)_3H$ in CD_2Cl_2 resulted in $[\{CpMo(CO)_3\}_2(\mu\text{-H})][1\text{-H-}closo\text{-}CB_{11}Me_{11}]$ as the major product. In addition to this product unreacted $[Ph_3C][1\text{-H-}closo\text{-}CB_{11}Me_{11}]$ and some cage methyl decomposition products (~10% based on the ^1H and ^{11}B NMR spectra) were also observed. The hydride-bridged dimer was consistently the major product, despite attempts with different concentrations, slow addition of a $CpMo(CO)_3H$ solution and using a large excess of $[Ph_3C][1\text{-H-}closo\text{-}CB_{11}Me_{11}]$. In an analogous manner (albeit much faster) to the formation of compound **15**, hydride abstraction results in the formation of the unsaturated 16 electron fragment $\{CpMo(CO)_3\}^+$ which rapidly reacts with the strongest nucleophile present in solution, $CpMo(CO)_3H$, generating the observed product. The small percentage of cage decomposition product may arise from a $\{CpMo(CO)_3\}^+$ fragment that coordinates and subsequently activates CD_2Cl_2 (or alternatively the anion). FAB mass spectroscopy identified the anion $[HCB_{11}Me_{10}Cl]^-$ in the reaction mixture, seen previously (Chapter Three) and a similar mechanism of formation is feasible here. The rapid formation of

the stable hydride bridged dimer and the absence of any observed anion coordinated compound places the [1-H-*closo*-$CB_{11}Me_{11}$]$^-$ anion as less nucleophilic than [*closo*-$CB_{11}H_6Br_6$]$^-$ with respect to the {$CpMo(CO)_3$}$^+$ fragment. Hydride abstraction in the presence of a good Lewis base (L = acetone, H_2O or 3-pentanone) cleanly results in the formation of [$CpMo(CO)_3L$][1-H-*closo*-$CB_{11}Me_{11}$] as the only Cp containing product (by ^1H NMR spectroscopy).[6]

The clean formation of [$CpMo(CO)_3(O{=}CEt_2)$][1-H-*closo*-$CB_{11}Me_{11}$] and (see Experimental) its mono-phosphine congener, [$CpMo(CO)_2(PPh_3)(O{=}CEt_2)$][1-H-*closo*-$CB_{11}Me_{11}$] allows for the investigation of their potential in the transfer hydrogenation catalytic cycle developed by Bullock (Figure 23).[46, 47]

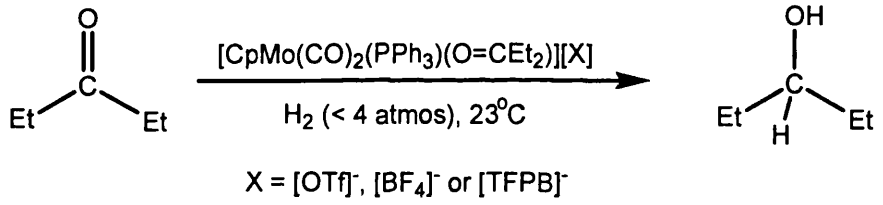

Figure 23: The transfer hydrogenation of 3-pentanone catalysed by [$CpMo(CO)_2(PPh_3)(O{=}CEt_2)$][X].

Importantly, in this system a direct relationship between catalyst activity and the coordinating ability of the anion has been demonstrated. The very weakly coordinating anion, [BAr_F]$^-$ generated a more active catalyst than congeners with the 'classically' weakly coordinating anions [PF_6]$^-$ and [BF_4]$^-$.[46] The published protocol for the hydrogenation of 3-pentanone outlined by Bullock was closely followed and allows for the comparison of the relative nucleophilicity of the anions [BAr_F]$^-$, [*closo*-$CB_{11}H_6Br_6$]$^-$ and [1-H-*closo*-$CB_{11}Me_{11}$] in a catalytic process.[47] Figure 24 shows the number of catalyst turnovers with respect to time for the hydrogenation of 3-pentanone to 3-

pentanol, under 4 atmospheres of H_2 and catalysed by $[CpMo(CO)_3(O{=}CEt_2)][1\text{-H-}closo\text{-}CB_{11}Me_{11}]$ (generated *in situ* from the reaction of $CpMo(PPh_3)(CO)_2H$ and $[Ph_3C][1\text{-H-}closo\text{-}CB_{11}Me_{11}]$, in the presence of 10 equivalents of 3-pentanone). In addition the catalytic efficiency for the analogous compounds partnered with $[BAr_F]^-$ and $[closo\text{-}CB_{11}H_6Br_6]^-$ are also shown.

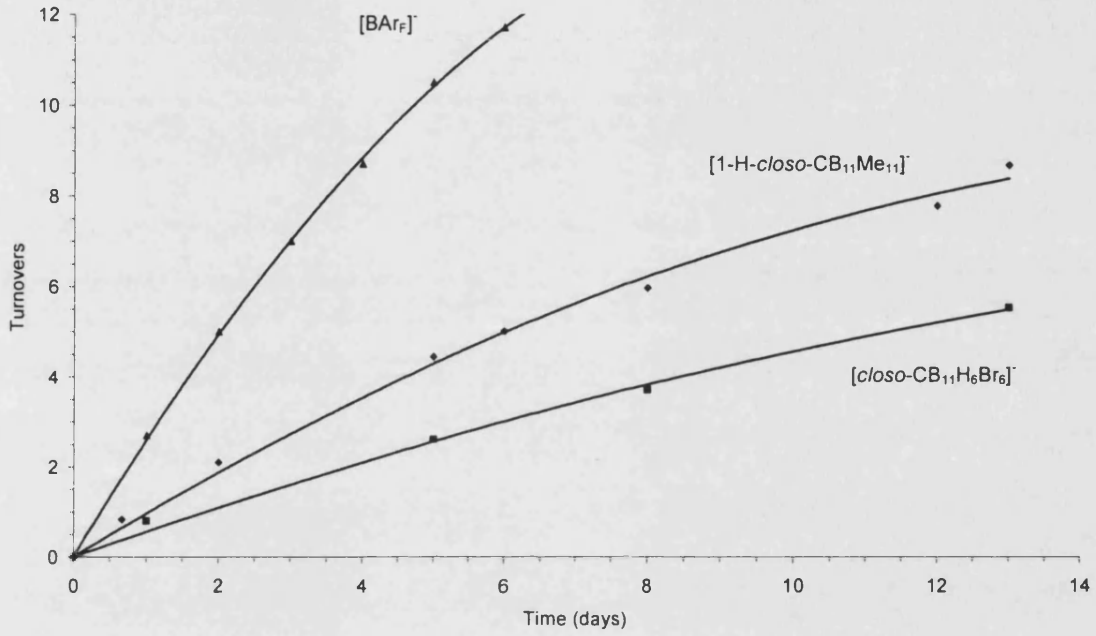

Figure 24: The respective number of turnovers for the hydrogenation of $O{=}CEt_2$ by H_2 catalysed by $[CpMo(PPh_3)(CO)_2(O{=}CEt_2)][X]$, X = $[BAr_F]^-$ (▲), $[1\text{-H-}closo\text{-}CB_{11}Me_{11}]^-$ (◆) and $[closo\text{-}CB_{11}H_6Br_6]^-$ (■).

With the $[1\text{-H-}closo\text{-}CB_{11}Me_{11}]^-$ anion (8 turnovers after 12 days) the catalyst outperforms the $[closo\text{-}CB_{11}H_6Br_6]^-$ analogue (5 turnovers after 12 days), but is significantly slower than the $[BAr_F]^-$ system (12 turnovers after 6 days). This allows for the anions to be ranked in a decreasing order of nucleophilicity, $[closo\text{-}CB_{11}H_6Br_6]^-$ > $[1\text{-H-}closo\text{-}CB_{11}Me_{11}]^-$ > $[BAr_F]^-$ with respect to the $\{CpMo(CO)_2(PPh_3)\}^+$ fragment. An identical ordering was found for the coordinating ability of these three anions with respect to the $\{(PR_3)Ag\}^+$ cationic fragment (Chapter Two). Direct comparison against the $[BF_4]^-$ and $[PF_6]^-$ anions was not possible, as qualitative measurements only, were

reported for these two systems. They were though, determined to be considerably less active than their $[BAr_F]^-$ counterpart on the basis of the final yield of product.[46] Use of other anions including, [*closo*-$CB_{11}H_{12}]^-$, [12-Br-*closo*-$CB_{11}H_{11}]^-$ and $[OTf]^-$ generated catalytically inactive compounds, confirming that they are significantly more co-ordinating.[33]

4.2.1.3: Alternative methods to introduce [1-H-*closo*-$CB_{11}Me_{11}]^-$ to $\{CpMo(CO)_3\}^+$.

With the formation of the dimeric complexes **15** and [$\{CpMo(CO)_3\}_2(\mu$-H)][1-H-*closo*-$CB_{11}Me_{11}$] preventing the isolation and subsequent investigation into the coordination behaviour of [$CpMo(CO)_3$][1-H-*closo*-$CB_{11}Me_{11}$] a further two alternative routes were looked at that cannot form analogous bridged complexes: (i) the oxidative cleavage of the dimer $\{CpMo(CO)_3\}_2$ by the neutral radical [1-H-*closo*-$CB_{11}Me_{11}]^\bullet$, and (ii) the salt metathesis of $CpMo(CO)_3(OTf)$ with Cs[1-H-*closo*-$CB_{11}Me_{11}$] (Figure 25).

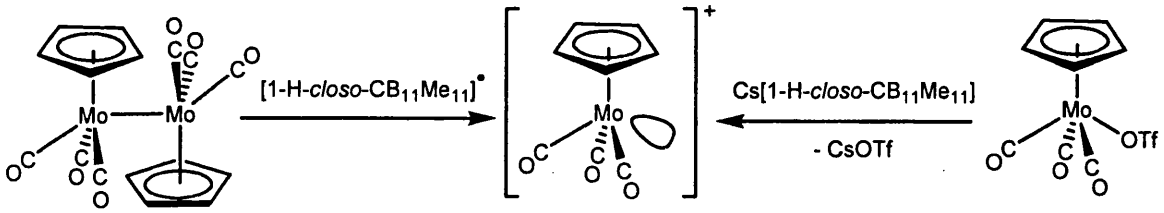

Figure 25: Further attempts to form the 16 electron fragment, $\{CpMo(CO)_3\}^+$.

Due to the similar reactivity patterns observed for these two systems they shall be discussed together. In CD_2Cl_2, both the ^1H and ^{11}B NMR spectra showed that the attempted formation of the monomeric cationic compound resulted in a highly complex anion region. This was even the case with samples synthesised at low temperatures (-78°C), implying that the compound formed is highly reactive, undergoing rapid anion decomposition. A plausible mechanism involves the formation of a $[Mo\cdots Cl_2CH_2]^+$

complex, that initiates the anion decomposition, either by direct chloride abstraction, or via a nucleophilic attack on the coordinated CH_2Cl_2 by [1-H-*closo*-$CB_{11}Me_{11}$]$^-$ (see Chapter Three). Complexes of the general formula $[CpMo(CO)_3(ClCH_2Cl)]^+$ are well documented, having been reported previously partnered with $[PF_6]^-$ and [*closo*-$CB_{11}H_6Br_6]^-$[3, 4, 9].

In order to gain further insight into a possible mechanism for the electrophilic metal induced decomposition of [1-H-*closo*-$CB_{11}Me_{11}$]$^-$ in CH_2Cl_2, a similar system, $[(PCy_3)Re(CO)_4(CH_2Cl_2)][BAr_F]$, was investigated that has been previously demonstrated to undergo anion decomposition via a CH_2Cl_2 coordinated complex.[21]

4.2.2: Reactions of [1-H-*closo*-$CB_{11}Me_{11}$]$^-$ with $[(PR_3)_xRe(CO)_{5-x}(CH_2Cl_2)]^+$ (x = 1, R = Ph or Cy, x = 2, R = $P(OCH_2)_3CCH_3$).

The reaction of $[Ph_3C][1\text{-H-}closo\text{-}CB_{11}Me_{11}]$ with three different rhenium complexes, $(PCy_3)Re(CO)_4Me$, $(PPh_3)Re(CO)_4Me$ and $(P(OCH_2)_3CCH_3)_2Re(CO)_3Me$ in CH_2Cl_2 generated, in each case, a dichloromethane coordinated complex analogous to the previously reported $[BAr_F]^-$ congeners (Figure 26).[19, 20, 48]

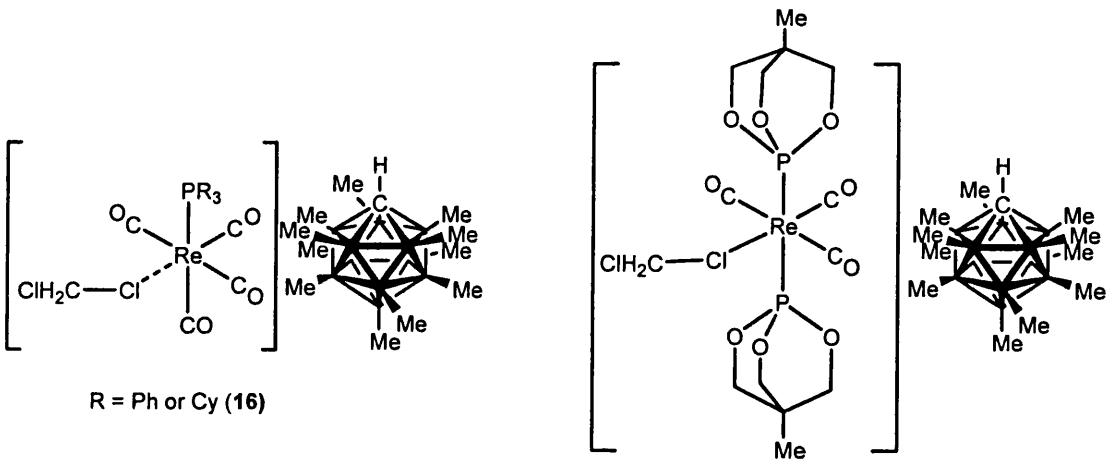

Figure 26: The three synthesised Re-dichloromethane adducts.

The characterisation of these compounds was based on ^{1}H and $^{31}P\{^{1}H\}$ NMR spectroscopy which were identical to the $[BAr_F]^-$ analogues (apart from the differences associated with the change of counterion).[19-21] The further reactivity of these three complexes is similar and therefore, the following discussion will focus solely on the decomposition of $[(PCy_3)Re(CO)_4(\eta^1\text{-}ClCH_2Cl)][1\text{-}H\text{-}\textit{closo}\text{-}CB_{11}Me_{11}]$, **16**, the findings though are equally applicable.

Complex **16** is formed, as the major product following the methide abstraction from $(PCy_3)Re(CO)_4Me$ at low temperature (-78°C) in CD_2Cl_2 (~ 90% by ^{1}H NMR spectroscopy). On standing at room temperature in CD_2Cl_2 solution, the $^{31}P\{^{1}H\}$ NMR resonance associated with **16** decreases, until after **8** hours no signal attributable to **16** is observed. Concomitant to the disappearance of **16**, is the formation of one new major signal (~ 70%) in the $^{31}P\{^{1}H\}$ NMR spectra that by comparison to the $[BAr_F]^-$ analogue,[21] is readily identified as the chloro-bridged dimer $[\{(PCy_3)Re(CO)_4\}_2(\mu\text{-}Cl)]^+$. A number of other unidentified minor signals were also observed in the $^{31}P\{^{1}H\}$ NMR spectrum. Alongside this change in the $^{31}P\{^{1}H\}$ spectrum, there is activation of the anion, with the ^{1}H and ^{11}B NMR spectra exhibiting an increased complexity in the anion B-CH_3 regions (Figure 26).

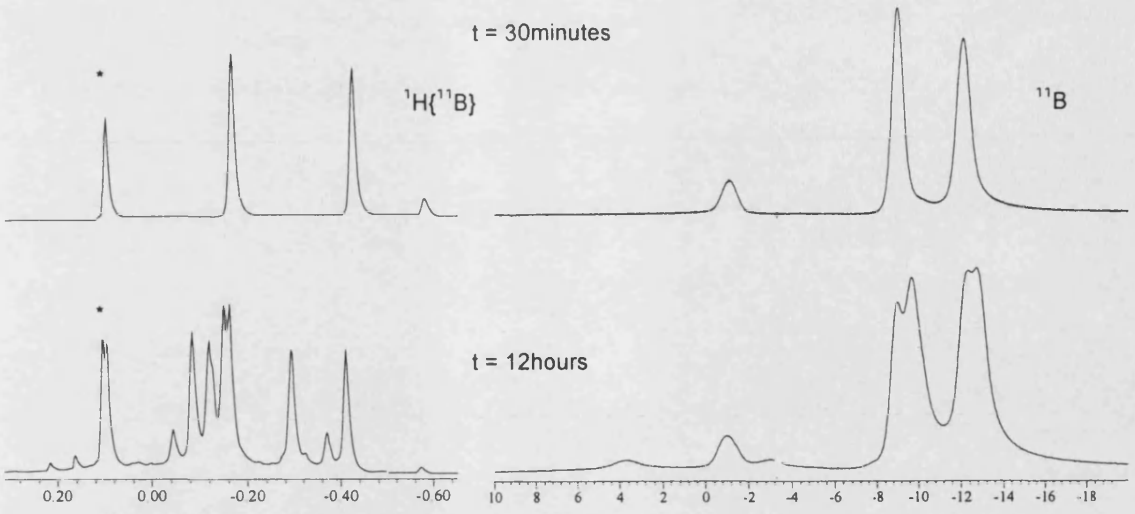

Figure 26: The cage region of the $^{1}H\{^{11}B\}$ and ^{11}B NMR spectra for the reaction of $[(PCy_3)Re(CO)_4Me]$ with $[Ph_3C][1\text{-H-}closo\text{-}CB_{11}Me_{11}]$ in CD_2Cl_2, after 30 minutes and 12 hours respectively, * = vacuum grease.

FAB- mass spectroscopy confirmed the presence of three anionic cage species: the unfunctionalised cage $[1\text{-H-}closo\text{-}CB_{11}Me_{11}]^-$, a monochlorinated cage $[H\text{-}CB_{11}Me_{10}Cl]^-$ and a bischloriniated cage $[H\text{-}CB_{11}Me_9Cl_2]^-$. A plausible mechanism to explain the observed products is outlined in Figure 27.

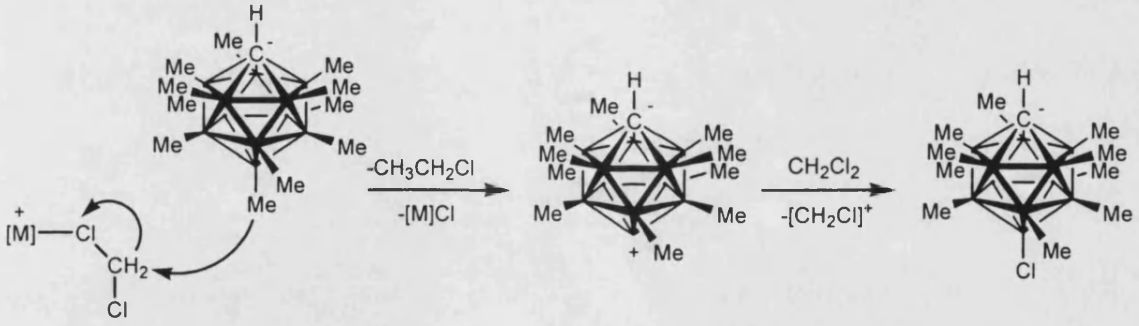

Figure 27: Possible decomposition mechanism for $[(PCy_3)Re(CO)_4(Cl_2CH_2)][1\text{-H-}closo\text{-}CB_{11}Me_{11}]$.

The first step in this proposed pathway, the attack on the coordinated dichloromethane by a weak nucleophile (in this case the anion, $[1\text{-H-}closo\text{-}CB_{11}Me_{11}]^-$), has precedence. Gladysz has previously observed the nucleophilic attack of X^- (X = Cl, Br) on $[CpRe(NO)(PPh_3)(Cl_2CH_2)]^+$ to produce $CpRe(NO)(PPh_3)Cl$ and $ClCH_2X$.[49]

Furthermore, it has been previously shown that in the analogous $[BAr_F]^-$ complex to **16**, Et_2O readily attacks the coordinated dichloromethane, producing the neutral chloride compound and the ethyloxonium ion $[ClCH_2OEt_2]^+$ (Figure 28).[21] In general the coordination of a halocarbon to a metal centre, even though it is a weak interaction, greatly increases its susceptibility to attack by nucleophiles.[2]

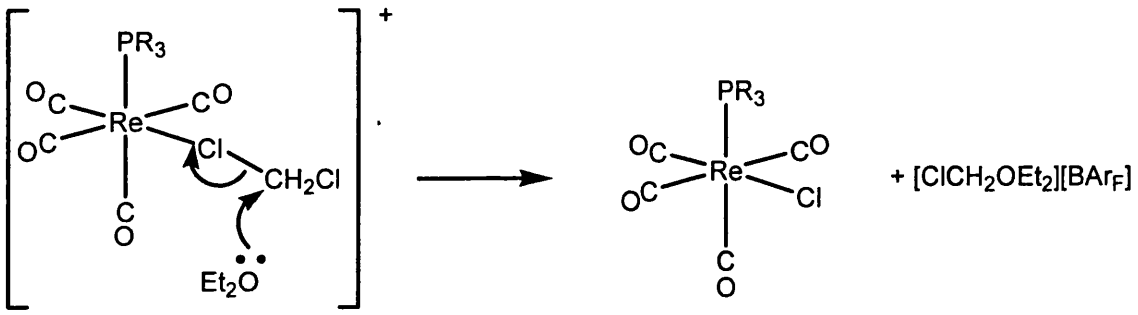

Figure 28: Ether attack on a cationic dichloromethane complex.

In the decomposition of **16** the anion would have to be the nucleophile, with [1-H-*closo*-$CB_{11}Me_{11}]^-$ attacking in a manner analogous to Et_2O in Figure 28. The 12 vertex of [*closo*-$CB_{11}Me_{12}]^-$ is nucleophilic enough to coordinate to $[Sn(^nBu)_3]^+$, forming a Sn···H_3C interaction with some covalent character,[50] demonstrating that [1-H-*closo*-$CB_{11}Me_{11}]^-$ can have appreciable nucleophilic behaviour. An S_N2 type attack would generate the neutral chloride complex and the neutral borenium ylide (Figure 27), via the elimination of chloroethane from the transient complex, [12-$ClCH_2CH_3$-1-H-*closo*-$CB_{11}Me_{10}$]. The borenium ylide would then readily abstract chloride from CH_2Cl_2 to generate the observed anion. Repeated attempts to detect the presence of chloroethane by GC/MS and NMR techniques unfortunately failed.

The presence of the two other anions, [1-H-*closo*-$CB_{11}Me_{11}]^-$ and [1-H-*closo*-$CB_{11}Me_9Cl_2]^-$ observed by NMR and MS techniques can be readily rationalised. The initially formed [1-H-12-Cl-*closo*-$CB_{11}Me_{10}]^-$ would compete with [1-H-*closo*-

$CB_{11}Me_{11}]^-$ with respect to the nucleophilic attack on a second molecule of $[(PCy_3)Re(CO)_4(Cl_2CH_2)]^+$. This would then yield the bis functionalised product and, prevent all of the [1-H-*closo*-$CB_{11}Me_{11}]^-$ from undergoing mono-chlorination.

The methide abstraction from the Heinekey bis-phosphine analogue,[26] $[(PCy_3)_2Re(CO)_3Me]$ by $[Ph_3C][1\text{-H-}closo\text{-}CB_{11}Me_{11}]$ in CD_2Cl_2 led to the agostic compound [*trans-mer*-$(PCy_3)_2Re(CO)_3$][1-H-*closo*-$CB_{11}Me_{11}$] (*vide infra*), as previously determined for the $[BAr_F]^-$ analogue (Figure 29).[27] This agostic complex undergoes no anion decomposition, further implicating a coordinated CH_2Cl_2 complex as initiating anion decomposition.

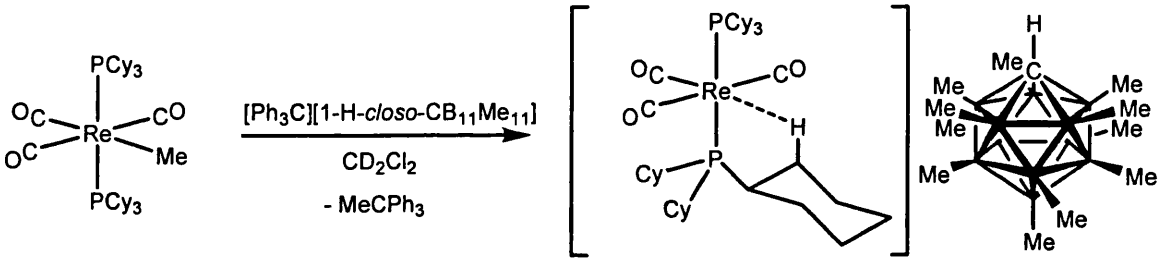

Figure 29: The formation of the γ -agostic compound, [*trans-mer*-$(PCy_3)_2Re(CO)_3$][1-H-*closo*-$CB_{11}Me_{11}$].

Following the findings that the highly electrophilic metal CH_2Cl_2 complexes result in the rapid anion B-C bond cleavage, it becomes necessary to utilise complexes that are less fiercely electrophilic (*i.e.*, no π acidic ligands) whilst still being electronically unsaturated. Examples of them are the two fragments $\{Cp^*Rh(PMe_3)Me\}^+$ and $\{Pt(^iPr_3P\}_2H\}^+$, [30, 32] that have been demonstrated to bind weak donor molecules readily when the counterion is $[BAr_F]^-$ and they do not undergo facile decomposition of the coordinated CH_2Cl_2. The formation of analogous compounds partnered with the [1-H-*closo*-$CB_{11}Me_{11}]^-$ anion will be discussed next.

4.2.3: Attempts to partner [1-H-*closo*-$CB_{11}Me_{11}$]$^-$ with [Cp*Rh(PMe_3)Me]$^+$.

The reaction of Cp*Rh(PMe_3)Me(OTf)[30] with one equivalent of Cs[1-H-*closo*-$CB_{11}Me_{11}$]$^-$ in CH_2Cl_2 led to the formation of the previously characterised dichloromethane coordinated complex [Cp*Rh(PMe_3)Me($ClCH_2Cl$)][1-H-*closo*-$CB_{11}Me_{11}$], **17** (Figure 30).[30] No decomposition of compound **17** was observed over a period of days in solution. The increased stability of **17** in contrast to **16** and can be attributed to the reduced electrophilicity at the metal centre resulting in a coordinated CH_2Cl_2 molecule that is less activated towards nucleophilic attack.

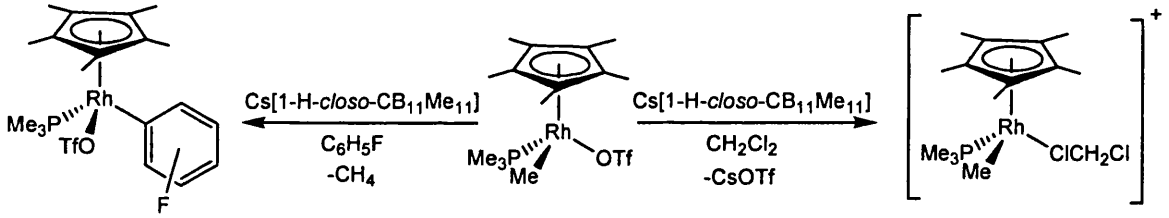

17

Figure 30: The observed products from the salt metathesis reactions between Cs[1-H-*closo*-$CB_{11}Me_{11}$] and Cp*Rh(PMe_3)Me(OTf) in CH_2Cl_2 and C_6H_5F respectively.

When performed in fluorobenzene (C_6H_5F), the rapid C-H activation of the solvent results followed by the loss of methane (observed at δ 0.20 ppm) and the formation of an isomeric mixture of the triflate coordinated complexes (Figure 30). Similar arene, and halo arene activation has been reported for the analogous iridium complex, Cp*Ir(PMe_3)Me(OTf), including the C-H activation of 1,2-difluorobenzene.[51] Interestingly, the use of 1,2-di-substituted arenes prevented the formation of isomeric products with only the meta positions activated.[51] It was anticipated that use of a polar, 1,3,5 substituted arene would prevent any C-H activation by sterically blocking the arene C-H bonds. In this manner, the analogous reaction was attempted with 5-fluoro-

meta-xylene as the solvent. No gas evolution was observed and a white precipitate rapidly formed. On removal of the solvent *in vacuo* and dissolution in CD_2Cl_2 a compound with chemical shifts identical to that of **17** was produced, the further precipitation of a small quantity of white solid was also noted. This result was initially interpreted as the formation of a cationic rhodium complex containing an interaction weaker that of the Rh···$ClCH_2Cl$ contact (Figure 31).

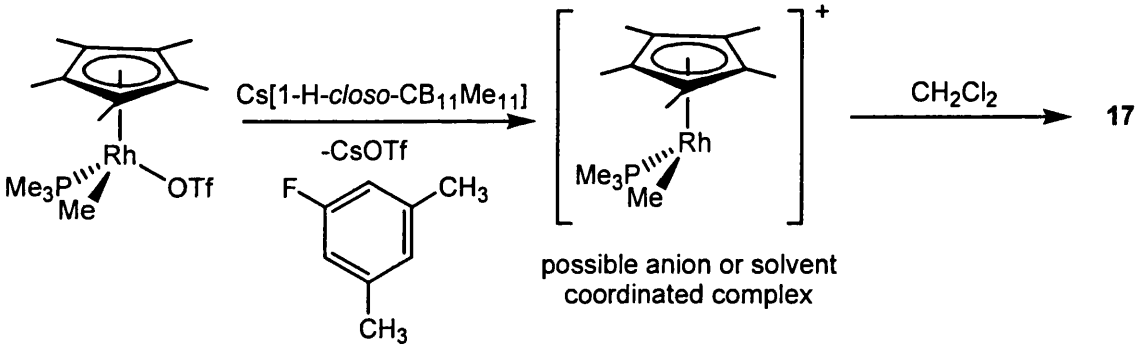

Figure 31: The proposed reactivity for the salt metathesis reaction carried out in 5-fluro-*meta*-xylene.

Crystalline material was obtainable from a 5-fluoro-*m*-xylene solution by the slow diffusion of pentanes at -20°C, though of insufficient quality for an X-ray diffraction study. Dissolution of these into CD_2Cl_2 gave an unexpected ratio of Cp* : [1-H-*closo*-$CB_{11}Me_{11}$]$^-$ of 2:1 (by ^1H NMR spectroscopy). The $^{31}P\{^1H\}$ NMR spectrum showed a single resonance at δ4.8ppm with a ^1J Rh-P coupling constant of 165.7 Hz, different from that of complex **17**, (δ3.2 ppm (163.2 Hz)). The ^{19}F NMR spectrum displayed one singlet at δ –78.69 ppm, shifted downfield from that of the monomeric starting material Cp*Rh(PMe_3)Me(OTf) in CD_2Cl_2 (δ-79.1 ppm),[30] significantly it also does not correspond to that of 'free' triflate (-79.0 ppm for [(^{n}Hex)$_4$N][OTf] in CD_2Cl_2).[51] Addition of an excess of Cs[1-H-*closo*-$CB_{11}Me_{11}$] to this sample resulted in the clean formation of **17** and the precipitation of a white solid, classified as CsOTf.

These combined findings led to the characterisation of the isolated crystals as the retarded metathesis complex [{Cp*Rh(PMe_3)Me}$_2$(μ-OTf)][1-H-*closo*-$CB_{11}Me_{11}$] (Figure 32). The initial misleading observation of the clean formation of **17** from this reaction, presumably arose from the presence of unreacted Cs[1-H-*closo*-$CB_{11}Me_{11}$] that on dissolution in a more coordinating solvent, CD_2Cl_2, completed the metathesis, explaining the further precipitation also observed. For the complete metathesis to occur there again appears to be a minimum nucleophilicity required for the attacking molecule without which only a retarded salt exchange or no reaction at all takes place (*i.e.* CH_2Cl_2 Vs 5-fluoro-m-xylene/[1-H-*closo*-$CB_{11}Me_{11}$]$^-$). This is analogous to the behaviour observed in the silver salt metathesis reactions between $CpMo(CO)_3X$ and Ag[1-H-*closo*-$CB_{11}Me_{11}$]$^-$ described earlier in this chapter.

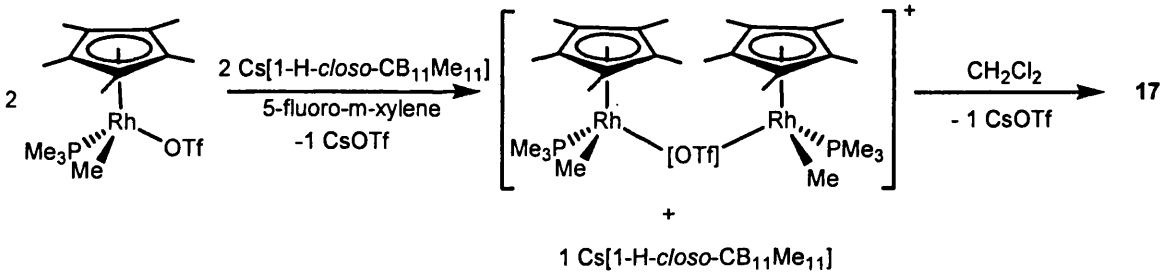

Figure 32: The role of solvent in the metathesis reaction between Cs[1-H-*closo*-$CB_{11}Me_{11}$] and Cp*Rh(PMe_3)Me(OTf).

The ability of [OTf]$^-$ to act as a bridging anion is well documented, with a large number of ligand supported and unsupported bridging triflate complexes structurally characterised with a range of metals, including cationic d^6 complexes.[52-57] Furthermore, the bidentate binding mode of [OTf]$^-$ has been characterised recently in a unsaturated rhodium fragment ($^iPr_3P)_2Rh(\eta^2$-OTf).[58]

Compound **17** is also accessible from $Cp^*Rh(PMe_3)Me_2$ by reaction with either the trityl salt, $[Ph_3C][1\text{-H-}closo\text{-}CB_{11}Me_{11}]$ or the neutral radical $[1\text{-H-}closo\text{-}CB_{11}Me_{11}]^\bullet$ (albeit in each case the reaction is not as clean as via the $Cp^*Rh(PMe_3)Me(OTf)$ route). The radical mechanism for the formation of the related anion coordinated complex, $Cp^*Rh(PPh_3)Me(PF_6)$ (from $Cp^*Rh(PPh_3)Me_2$ and $[Cp_2Fe][PF_6]$) has previously been determined by Tilset to occur via a two electron oxidation of $Cp^*Rh(PPh_3)Me_2$, with the concomitant intramolecular loss of ethane to generate $[Cp^*Rh(PPh_3)(solv)_2]^{2+}$ followed by a rapid intermolecular methyl transfer from $Cp^*Rh(PPh_3)Me_2$.[59] It is reasonable to assume that the generation of **17** via the radical $[1\text{-H-}closo\text{-}CB_{11}Me_{11}]^\bullet$ proceeds by a closely related mechanism (Figure 33), as the formation of ethane (singlet δ 0.86 ppm) is confirmed by the ^1H NMR spectrum.

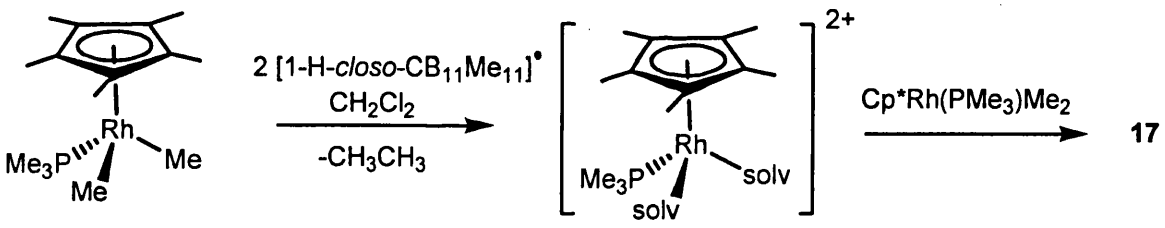

Figure 33: Proposed radical mechanism for the formation of **17**.

With the formation of **17** possible from two neutral compounds, $Cp^*Rh(PMe_3)Me_2$ and $[1\text{-H-}closo\text{-}CB_{11}Me_{11}]^\bullet$, the reaction was attempted in cyclohexane. Immediate gas evolution was observed followed by the precipitation of a tan solid; there were no detectable Rh containing products in the cyclohexane solution. Dissoluionof the tan solid in CD_2Cl_2 resulted in a rapid colour change to vermillion and NMR spectra consistent with the formation of **17** as the predominant product (~ 70% based on the Cp* resonance). The minor products presumably arise from C-H activation

of the alkane solvent, as reported for $Cp^*Ir(PMe_3)Me(OTf)$. There was no cage decomposition observed.[51, 60] A number of 'layer' reactions were attempted to isolate crystalline material of the tan solid. This consisted of one reactant in cyclohexane layered with the other compound dissolved in pentane. On diffusion this yielded only a fine precipitate, therefore a buffer solution of hexane was introduced between the two reactant carrying layers to prevent a rapid reaction, but no crystalline material was formed despite repeated attempts under a range of conditions. The lack of a suitable solvent has frustrated further attempts to identify this compound, with CH_2Cl_2, THF and other weakly basic solvents coordinating to the metal, facile C-H activation preventing the use of arenes and haloarenes and C-H activation occurring with saturated alkanes. It is tempting to suggest that this 'tan solid' is attributable to a anion coordinated complex (Figure 34), however an agostic complex is also feasible.

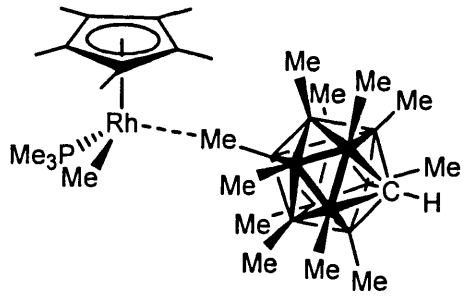

Figure 34: A suggested structure for the 'tan solid' complex isolated.

4.2.4: Attempts to Partner [1-H-*closo*-$CB_{11}Me_{11}$]$^-$ with [*trans*-(^{i}Pr$_3$P)$_2$PtMe]$^+$.

The final CH_2Cl_2 system investigated is based on that reported by Kubas *et al.*, [*trans*-Pt(Me)($ClCH_2Cl$)(^{i}Pr$_3$P)$_2$][BAr_F], which is an extremely stable, well characterised dichloromethane complex.[32] A major drawback for the formation of the analogous compound partnered with [1-H-*closo*-$CB_{11}Me_{11}$]$^-$ stems from the synthesis requiring the etherate acid [$H(OEt_2)_2$][BAr_F]. This is not feasible for the [1-H-*closo*-

$CB_{11}Me_{11}]^-$ anion due to the instability of the anion to strong acid environments, frustrating attempts to synthesise $[H(OEt_2)_2][1\text{-H-}closo\text{-}CB_{11}Me_{11}]$.[61] An alternative synthesis published involved the salt metathesis of *trans*-$Pt(H)Cl(^iPr_3P)_2$ with $Na[BAr_F]$, this is also not viable due to the formation of retarded metathesis products previously observed when utilising $Ag[1\text{-H-}closo\text{-}CB_{11}Me_{11}]$ and $Cs[1\text{-H-}closo\text{-}CB_{11}Me_{11}]$ (see earlier this Chapter). Instead the readily synthesised *cis*-$(^iPr_3P)_2PtMe_2$ was used as a starting point to investigate the coordination chemistry of $[1\text{-H-}closo\text{-}CB_{11}Me_{11}]^-$ with respect to unsaturated 14-electron $\{(^iPr_3P)_2PtL\}^+$ fragments.

The reaction of equimolar quantities of *cis*-$(^iPr_3P)_2PtMe_2$ with $[Ph_3C][1\text{-H-}closo\text{-}CB_{11}Me_{11}]$ in either CH_2Cl_2 or fluorobenzene (C_6H_5F) resulted in the formation of *trans*-$[PtMe(^iPr_3P)_2][1\text{-H-}closo\text{-}CB_{11}Me_{11}]$, **18** and $MeCPh_3$ (Figure 35). Complex **18** is also produced on reaction with the one electron oxidant $[1\text{-H-}closo\text{-}CB_{11}Me_{11}]^\bullet$, producing, one equivalent of methane (δ 0.20 ppm) consistent with a one electron homolysis reaction.[62]

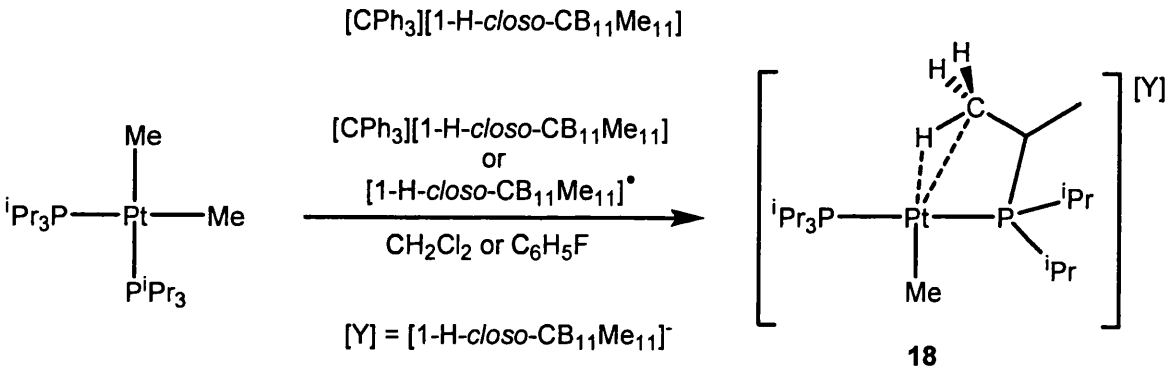

Figure 35: The various routes to access the agostic complex, **18**.

The $[MeB(C_6F_5)_3]^-$ analogue of **18** is also accessible by the reaction of *cis*-$(^iPr_3P)_2PtMe_2$ with $B(C_6F_5)_3$. Crystals suitable for an X-ray diffraction study, obtained via the $[1\text{-H-}closo\text{-}CB_{11}Me_{11}]^\bullet$ route were grown by the slow diffusion of pentanes into a C_6H_5F solution. This revealed the structure to be a T–shaped planar platinum (II)

cation, stabilised by one γ agostic interaction, with the anion, [1-H-*closo*-$CB_{11}Me_{11}$]$^-$ not proximate in the lattice (Figure 36). Similar d^8 T-shaped metal complexes have been previously structurally characterised for Rh,[63] Pd[64] and Pt.[65]

The geometry around the Pt(II) centre is *pseudo* square planar (the sum of angles about the Pt centre is equal to 360.0°) generated by two *trans* phosphine, the methyl and one close agostic approach of a CH_3 group from one phosphine (Pt1-C31 2.858(6)Å). There is no close approach of the anion in the extended lattice, and no solvent co-crystallite. The hydrogen atoms attached to C31 were located in the final difference map and refined subject to being restrained at a distance of 0.89 Å from C31. This resulted in a bonding motif where one hydrogen is directed towards (Pt1-H31a 2.24(4) Å) and two hydrogens directed away from the Pt(II) centre, with the latter showing significantly longer non-bonding distances (Pt1-H31b 3.67(5) Å and Pt1-H31c 2.94(4) Å). The closest Pt-C distance is a long agostic interaction, significantly greater than that observed for the related complexes, [Pt{PCy_2(2,6-$Me_2C_6H_3$)}{PCy_2(2-Me-6-CH_2-C_6H_3)}]$^+$, **B** (Figure 37),[65] that has a Pt-C distance of 2.432(6) Å and the β-agostic Pt complexes (Pt-C distances of 2.28(2) Å and 2.309(5) Å).[66-68] There is no observed lengthening of the agostic C-H bond, which within errors is identical to the non agostic C-H bonds, consistent with the limited C-H elongation (5-10%) observed for agostic interactions.[69]

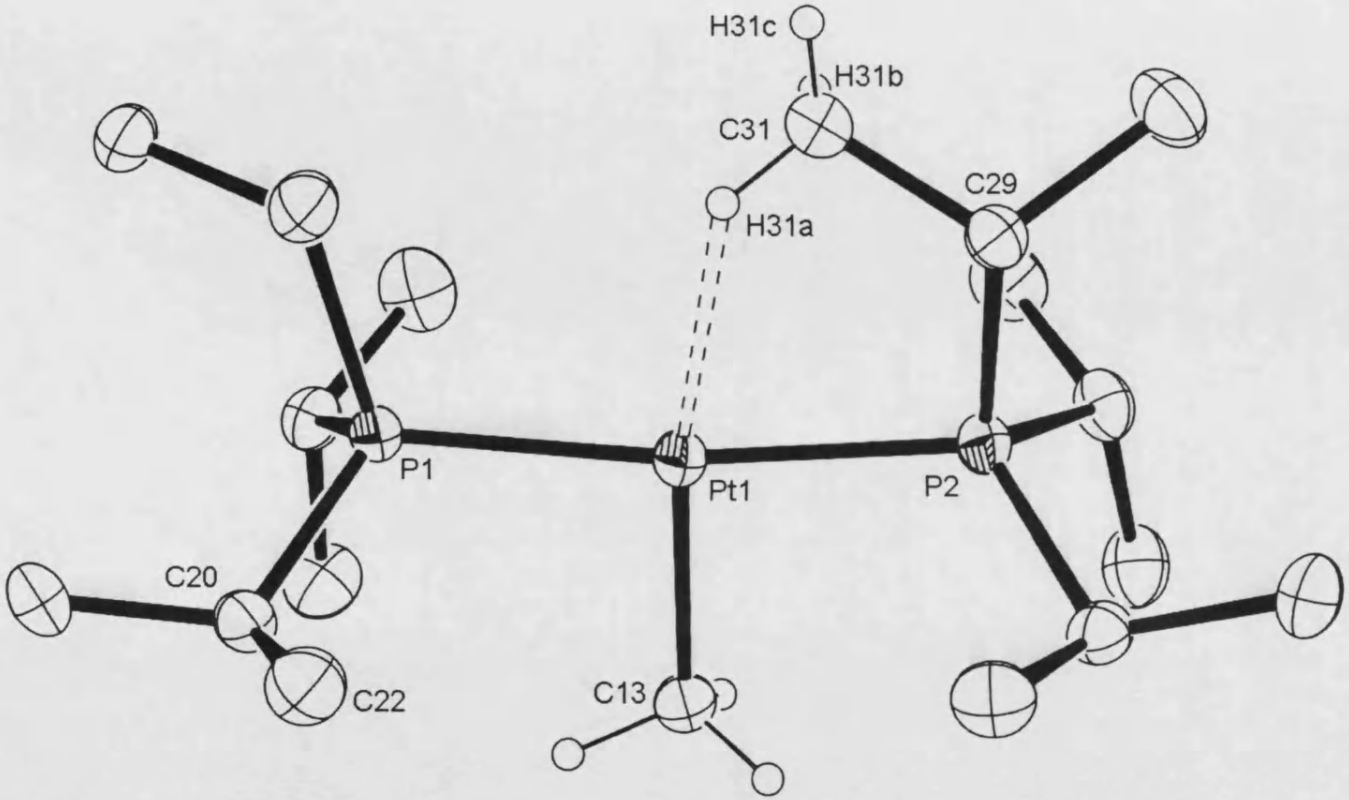

Pt1-P1	2.3161(12)
Pt-P2	2.3024(12)
Pt1-C13	2.026(5)
Pt1-H31a	2.24(4)
Pt-C31	2.858(6)
C13-Pt1-H31a	164.0(11)
P1-Pt1-P2	171.08(4)
C13-Pt1-P1	93.36(15)
C13-Pt1-P2	94.81(15)
C31-C29-P2	108.2(4)
C29-P2-Pt1	97.99(16)
C20-P1-Pt1	106.67(15)
C22-C20-P1	111.9(3)

Table 3: Selected Bond Lengths (Å) and Angles (°) for **18**.

Figure 36: Cationic portion of complex **18**. Hydrogen atoms apart from those associated with C13 and C31 are omitted. Thermal ellipsoids are shown at the 30% probability level.

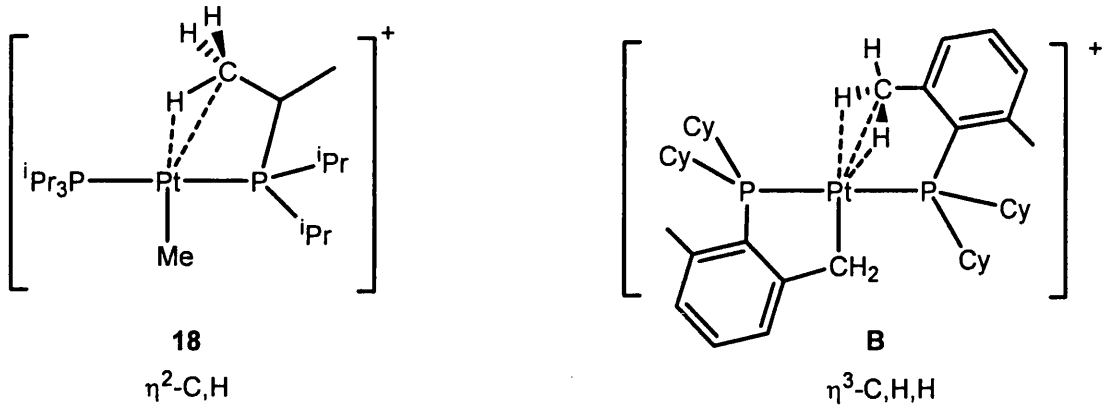

Figure 37: The differing Pt-H_3C agostic interactions characterised in **18** and [Pt{PCy_2(2,6-$Me_2C_6H_3$)}{PCy_2(2-Me-6-CH_2-C_6H_3)}][BAr_F], **B** (anions not shown).[65]

Comparison of the CH_3 binding modes involved in the agostic interactions for complexes **18** and **B** is noteworthy and valid (given the usual caveats) as both data sets allowed for the free refinement of the associated hydrogen positions. Complex **18**, involving a γ agostic interaction, shows a η^2-C,H binding motif (see Chapter One) whilst the δ agostic interaction in **B**, presents two hydrogens equally towards the metal (Pt-H distances of 2.085 Å and 2.057 Å respectively) resulting in a symmetrical η^3-C,H,H mode. This, as recently outlined by Barratta *et al.* [70] is as expected, as complex **18** has to undergo significant ligand distortion to achieve the favoured geometry for agostic bonding, thus allowing for the close approach of only a single C-H bond. This ligand deformation is clearly visible on inspection of the relative phosphine geometries (Figure 36). The agostically bound phosphine is bent towards the Pt centre (Pt1-P2-C29, 97.99(16)°), being significantly distorted compared to that of the non agostically bound phosphine ligand (*e.g.*, Pt1-P1-C20, 106.67(15)°) and the average Pt-P-C_α angle in [(^{i}Pr_3P)$_2$Pt(Me)N_3] (112.7°).[71] The long agostic interaction in compound **18** relative to **B**, implies that it is inherently weaker. This is consistent with the short *trans* Pt-σ bonded methyl distance of 2.026(5) Å, that lies at the short end of Pt(II)-Me bonds.[72]

Complex **18** in a CD_2Cl_2 solution possesses C_s symmetry at room temperature (by ^1H and $^{31}P\{^1H\}$ NMR spectroscopy), presumably due to the rapid intramolecular exchange of the agostic C-H bond, thereby making equivalent the CH_3 groups on both phosphines. Cooling to 190 K does not result in any significant change in the NMR spectra, indicating a facile exchange process and a weaker interaction to that found in **B**, in which the fluxionality is frozen out at 178 K.[65] The value of the $^2J(PtCH_3)$ coupling constant (106 Hz) is large in comparison to complexes with more strongly bound *trans* ligands, *e.g.*, *trans*-$PtMeCl(^iPr_3P)_2$ (83 Hz) and *trans*-$PtMe(OTf)(^iPr_3P)_2$ (96 Hz).[73] Furthermore the Pt-CH_3 resonance in **18** is shifted notably downfield (δ1.69 ppm) when compared to both the $[Cl]^-$ and $[OTf]^-$ congeners in the same solvent (δ0.47 ppm and 0.81 ppm respectively).[73]

The closely related cation $[PtH(^iPr_3P)_2]^+$,[32] binds a range of solvent molecules (PhBr, PhI, CH_2Cl_2, Et_2O and THF) in preference to the formation of an agostic interaction. Definitive proof that the agostic contact, which is structurally characterised in complex **18**, persists in CD_2Cl_2 is provided by the addition of 5 equivalents of CH_2Cl_2 to a C_6H_5F solution of **18**. This resulted in no change in the chemical shifts or in the coupling constants (a more sensitive indicator to the identity of the *trans*-to methyl ligand), with both $^1J(PtP)$ and the $^2J(Pt\text{-}CH_3)$ remaining unaltered. Addition of a stronger Lewis base *e.g.*, THF to a C_6H_5F solution of complex **18** contrastingly provided a significant shift in the NMR resonances and coupling constants (discussed later). The disparity in the coordination behaviour of these two closely related 14 electron cationic fragments, $\{PtMe(^iPr_3P)_2\}^+$ and $\{PtH(^iPr_3P)_2\}^+$ is suggested to be essentially steric in origin. Close examination of the orientation of the *trans* phosphine

ligands reveal that in $\{PtH(^{i}Pr_3P)_2\}^+$ they are bent towards the hydride ligand reducing the steric crowding and allowing the approach of an extra ligand (Figure 38).

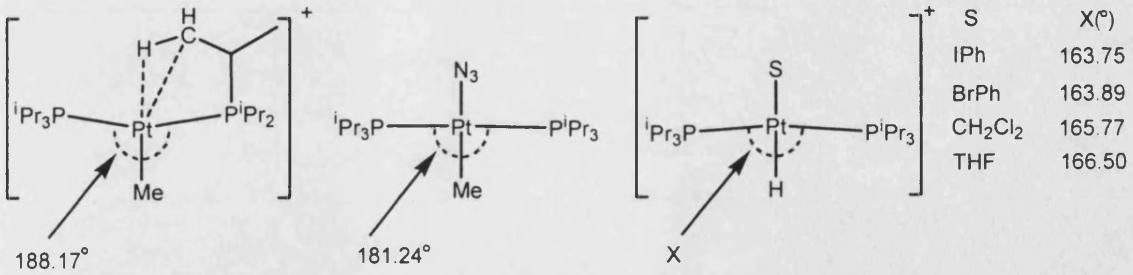

Figure 38: The effect of the cis ligands on the P-Pt-P bond angle.

By contrast, in compound **18** the phosphines are angled away from the methyl ligand, shielding the Pt more effectively. This change in angle is not completely an artefact of the agostic interaction deforming the phosphine ligand geometry, as it is present (albeit to a lesser extent) in the azide bound complex $(^{i}Pr_3P)_2Pt(Me)N_3$,[71] thus is a real factor. This effect is further demonstrated by examination of the space-filling diagram for the related compounds (Figure 39).

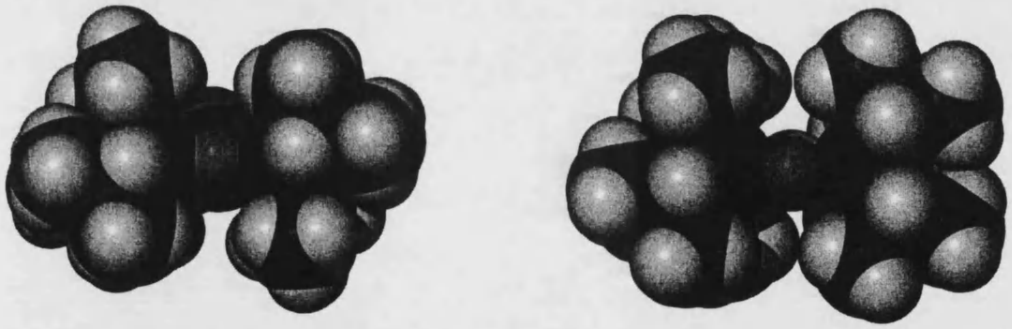

Figure 39: Space filling diagrams for the $\{PtMe(^{i}Pr_3P)_2\}^+$ cation (looking down the Pt-C axis) and the $\{PtH(^{i}Pr_3P)_2\}^+$ cation (looking down the Pt-H axis). Both generated from their respective 4 coordinate compounds with the fourth ligand removed.

As is clearly visible in the structure of the $\{PtH\{^{i}Pr_3P\}_2\}^+$ cation there is a more open environment *trans* to the hydride, allowing for the ready access of a small, fourth ligand to the platinum centre. In contrast, the structure of $\{PtMe(^{i}Pr_3P)_2\}^+$ is much more

sterically congested, explaining the observed preference of the agostic bond spectroscopically characterised over the binding of weak ligands (*e.g.* CH_2Cl_2). This is further supported by the related congener, $[PtH(^tBu_3P)_2][BAr_F]$ (where $^iPr_3P$ has been replaced by the electronically similar but sterically bulkier phosphine, $^tBu_3P$),[74] spectroscopically characterised as a three coordinate compound, presumably stabilised by an agostic interaction analogous to complex **18**.[32] A similar steric controlled bonding regime has been observed in the complexes $[(PCy_3)_xRe(CO_3)_{5-x}]^+$, when x = 1, CH_2Cl_2 binding is favoured, whilst on increasing the steric crowding about the metal (*i.e.* x = 2), an agostic interaction is preferred.[21, 26]

The structure of complex **18** was also investigated by gas phase DFT calculations at the B3LYP//LANL2DZ level using the Gaussian 03 package of programs (calculations performed by Dr Gus Ruggerio).[75] The resulting calculated structure shows good correlation to the solid-state structure, including only one close Pt-H contact (Figure 40).

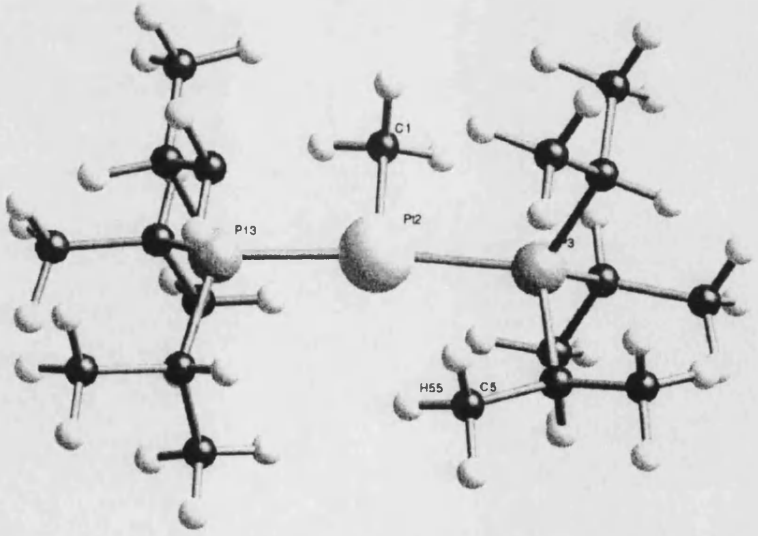

Figure 40. DFT calculated structure for 1. Selected bond lengths and angles: Pt2-C1 2.053 Å, Pt2-P3 2.430 Å, Pt2-P13 2.436 Å, Pt2-C5 3.245 Å, Pt2-H55 2.610 Å. P-Pt-P 171.55°

Compound **18** in a CD_2Cl_2 solution is not significantly changed after 10 days heating at 40°C, whilst heating at 70°C overnight in C_6H_5F led to a mixture of intractable products and some cage decomposition (by ^1H and ^{11}B NMR spectroscopy). Addition of two equivalents of $[^nBu_4N][closo\text{-}CB_{11}H_6Br_6]$ resulted in no change in the $^{31}P\{^1H\}$ NMR spectrum indicating the persistence of the agostic interaction. This is not surprising when you consider the weakly coordinating nature and large size of the anion $[1\text{-}H\text{-}closo\text{-}CB_{11}H_6Br_6]^-$, [11] in conjunction with the sterically crowded environment around the Pt(II) centre. The agostic interaction in complex **18** is displaced by smaller Lewis bases, stronger than CD_2Cl_2. Addition of 1 atmosphere of H_2 to a CD_2Cl_2 solution of **18** yielded an equilibrium between the two previously characterised complexes, *trans*-$[PtH(^iPr_3P)_2(\eta^2\text{-}H_2)]^+$ and *trans*-$[PtH(^iPr_3P)_2(ClCH_2Cl)]^+$ as well as methane (Figure 41).[32] This presumably occurs via the activation of a dihydrogen adduct, and this mechanism is supported by the formation of CH_3D (a 1:1:1 triplet at δ 0.19 ppm) when the hydrogenolysis is carried out with D_2 (no CH_4 is observed). A similar reactivity has been observed for the Pt-agostic complex **B**, that undergoes hydrogenolysis and Pt-C bond cleavage, generating a platinum hydride complex.[65]

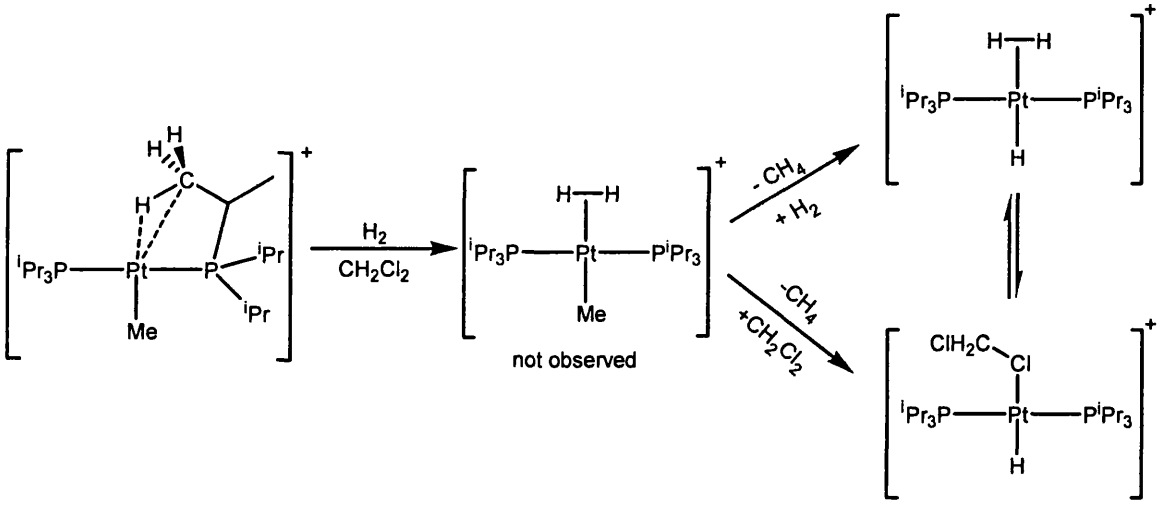

Figure 41: The displacement of the agostic interaction in **18** and the subsequent hydrogenolysis.

Addition of 5 equivalents of THF to a CD_2Cl_2 solution of **18** resulted in a significant chemical shift alteration and signal broadening in the ^1H and $^{31}P\{^1H\}$ NMR spectra, indicative of fluxionality. Cooling the solution to 230 K resulted in a freezing out of the exchange process and two sets of signals in the ^1H and $^{31}P\{^1H\}$ NMR spectra. The minor set corresponded to the agostic complex **18** at this temperature, the major compound we assign as the THF adduct $[PtMe(THF)\{^iPr_3P\}_2]^+$, **19**. Two THF environments were observed, free THF and one set of resonances for the coordinated THF molecule that were shifted downfield (δ 3.90 and 1.90 ppm in the ^1H NMR spectrum) compared to that of free THF (δ 3.60 and 1.82 ppm). The displacement of agostic interactions by THF is well documented (*e.g.*, the reaction of $[Cp^*_2Ti][BPh_4]$ with THF),[76] including examples where the THF molecule is only weakly bound and highly labile, as found in complex **19**.[77] The equilibrium distribution at this temperature is one that favours the THF adduct over the agostic compound in a 4:1 ratio.

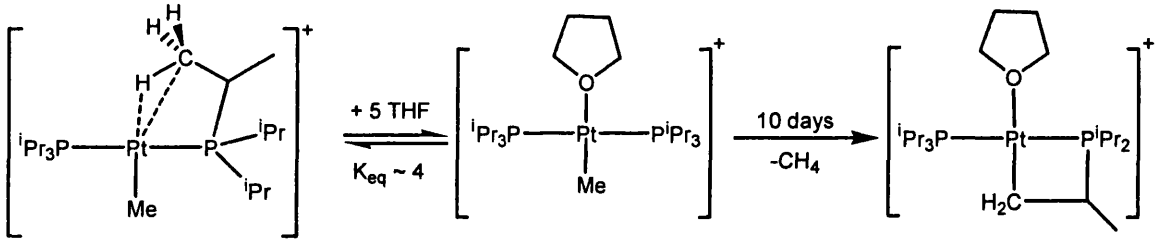

18 **19** **20**

Figure 42: The formation of the cyclometallated product **20**, from the formal C-H activation of **19**.

On standing (10 days) this solution slowly undergoes cyclometallation of one of the CH_3 groups of one phosphine, with the reaction cleanly generating $[Pt(^iPr_3P)(^iPr_2PC(H)MeCH_2)(THF)]^+$, **20** (characterised by comparison to the complex $Pt(^iPr_3P)(^iPr_2PC(H)MeCH_2)(OTf))$[73], along with methane (Figure 42). Complex **20** represents the formal C-H activation of a pendant CH_3 group, followed by the rapid loss

of methane (observed at δ 0.20 ppm). THF is essential to the reaction, as complex **18** is stable in CH_2Cl_2 solution for weeks at room temperature, with no detectable cyclometallation even on heating at 40°C for 7 days. Previous work on the closely related compound $PtMe(^iPr_3P)_2(OTf)$, which is equally stable to cyclometallation, showed that catalytic quantities of acid was required to form the cyclometallated product, $Pt(^iPr_3P)(^iPr_2PC(H)MeCH_2)(OTf)$.[73] A combination of results led us to conclude that the presence of a catalytic quantity of an unknown and adventitious acid similarly is initiating cyclometallation. (i) Addition of 10mol % of HCl to the **18/19** equilibrium mixture led to the accelerated formation of **20** as the major product, with a minor compound detected that was characterised as $PtCl_2(^iPr_3P)_2$.[73] (ii) Compound **18**, in the presence of 5 equivalents of THF and the hindered base 2,6-di-tert-butyl pyridine does not cyclometallate. The source of the acid is uncertain, though the most likely possibility is from the presence of adventitious water, the acidity of which would be drastically increased on coordination to a cationic $\{Pt(II)\}^+$ centre, and such aqua complexes are well known.[78] A full mechanism supported by these findings and consistent with previous studies on C-H activation in mono and dicationic Pt(II) systems is outlined in Figure 43.[73, 79-81]

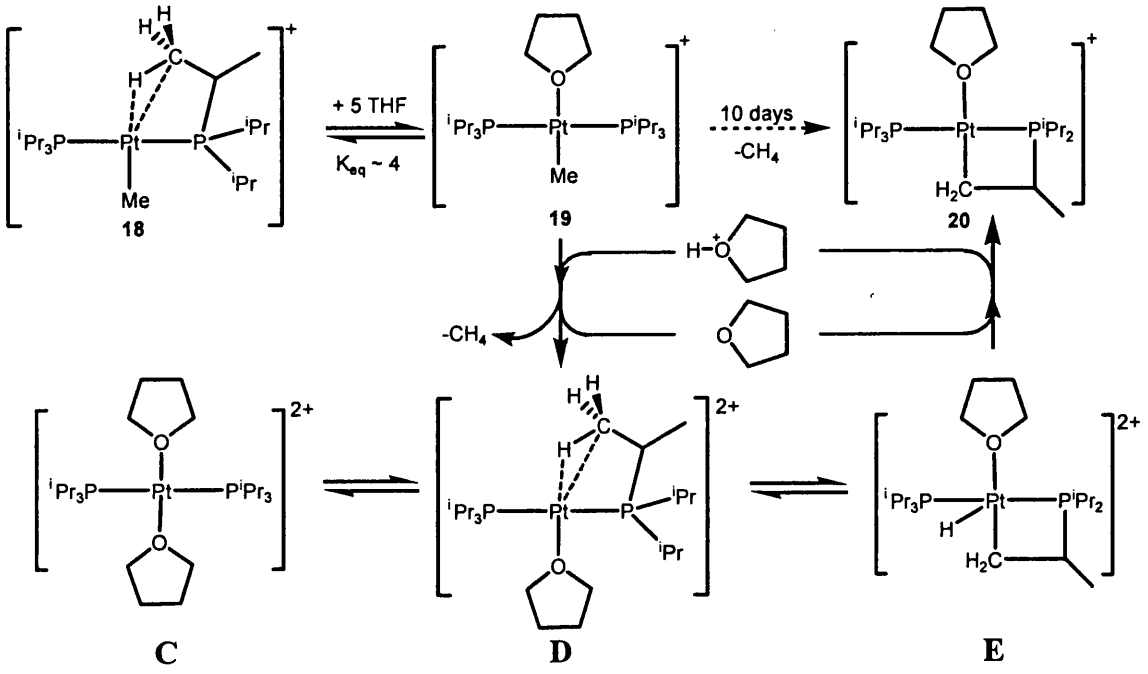

Figure 43: A plausible mechanism for the acid catalysed formation of the metallocycle **20**.

THF plays a critical role in this reaction, acting as both a Brønsted base and a Lewis base. Furthermore, THF free samples of complex **18** show no susceptibility to protonation. This can be attributed to the THF adduct, **19** being more electron rich than the agostic compound **18**, and is supported by their respective $^2J(Pt\text{-}CH_3)$ coupling constants, 86 Hz for **19** and 106 Hz for **18**. Similar findings have been reported previously, with the complex $[PtMe(Cl)(^iPr_3P)_2]$ readily undergoing protonation, but $[PtMe(OTf)(^iPr_3P)_2]$ proving stable in this respect in acidic media.[73] Complexes related to intermediates **C – E** have been previously proposed by Labinger and Bercaw in the mechanism of intramolecular C-H activation in the presence of base by Pt(II) dications bearing α-diimine ligands.[80] The slow nature of the reaction (10 days) could be attributable to two different factors: (i) the formation of the cationic complex Pt(II)-OH_2 complex, which is postulated as the acid source. It has been previously reported that H_2O has to be added in 2 equivalents to achieve complete displacement of coordinated

CH_2Cl_2 in $[Pt(H)(ClCH_2Cl)(^iPr_3P)_2]^+$, thus as water in these reactions is present in low concentrations (rigorously dried solvents) it would compete unfavourably against complexes **18** and **19**, resulting in an extremely low concentration of the aqua complex. (ii) A slow protonation step. The protonation of compound **19** by trace acid would be expected to be slow as it is documented that cationic Pt(II) alkyls are relatively stable to protonlysis.[79, 80, 82]

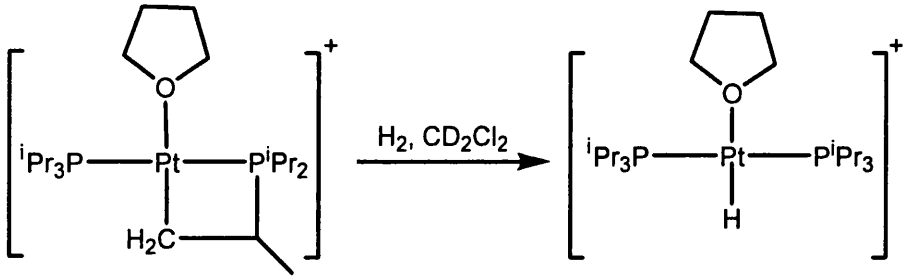

Figure 43: The hydrogenolysis of the cyclometallated complex **20**.

Complex **20** readily reacts with H_2, resulting in the opening of the metallacycle to generate $[PtH(THF)(^iPr_3P)_2]^+$, previously characterised by Kubas *et al.* (Figure 44).[32] Analogous reactivity of other cationic Pt(II) cyclometallated complexes with H_2 has been reported, including with the related compound **B**, that also undergoes Pt-C bond cleavage in the presence of H_2.[65, 83]

4.2.5: Attempts to generate $[Pt(^iPr_3P)_2][1\text{-H-}closo\text{-}CB_{11}Me_{11}]_2$

Following the formation of the agostic complex **18**, attempts where made to remove the second methide group from $[PtMe(^iPr_3P)_2]^+$ thereby generating a formally 12 electron Pt(II) di-cation that may exhibit cation···anion contacts. The reaction of **18** with one equivalent of $[Ph_3C][1\text{-H-}closo\text{-}CB_{11}Me_{11}]$ in CD_2Cl_2 resulted in no change in the ^1H and $^{31}P\{^1H\}$ NMR spectra after 7 days. However, addition to this reaction

mixture of 5 equivalents of THF resulted in the immediate formation (< 5 minutes) of the cyclometallated complex **20** (Figure 45).

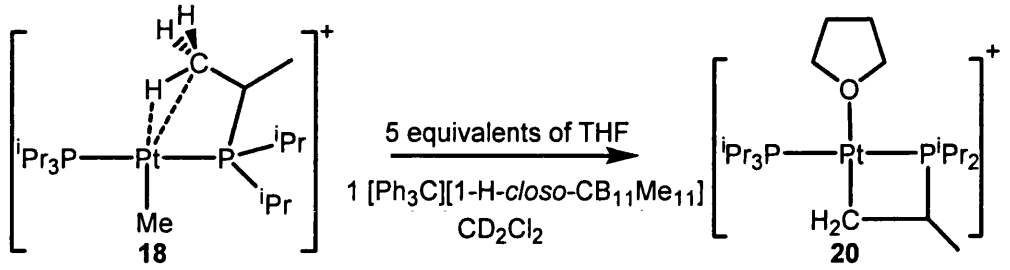

Figure 45: The rapid cyclometallation of compound **18** on the addition of one equivalent of $[CPh_3][1\text{-}H\text{-}closo\text{-}CB_{11}Me_{11}]$ in the presence of THF.

The dramatic rate acceleration in the formation of **20** is presumably due to an increased acid concentration. This can be generated by adventitious H_2O reacting with the free trityl salt generating Ph_3COH and H^+. $[Ph_3C]^+$ salts are well documented to react with moisture, even in the solid state.[84] However, there is no direct evidence for the formation of the resultant carbinol, Ph_3COH by NMR spectroscopy. With H_2O present in low concentrations this would consequently result in low, perhaps undetectable levels of Ph_3COH. Along with the formation of complex **20** via this route there remains the presence of nearly one equivalent of unreacted $[Ph_3C][1\text{-}H\text{-}closo\text{-}CB_{11}Me_{11}]$ (by ^1H NMR spectroscopy) discounting an alternative mechanism via direct methide abstraction from the THF adduct **19**. An analogous rate acceleration is observed when $[Ph_3C][1\text{-}H\text{-}closo\text{-}CB_{11}Me_{11}]$ is replaced with $B(C_6F_5)_3$. This presumably is also by the reaction of the Lewis acid with trace H_2O, forming the strong acid $H[HOB(C_6F_5)_3]$, that has been previously reported to readily protonate Pt-Me bonds.[85] No $[MeB(C_6F_5)_3]^-$ was observed, consistent with this.

Complex **20** is not stable in CH_2Cl_2, frustrating efforts to obtain crystalline material (attempts in other solvent mixtures *e.g.*, C_6H_5F led only to oils). Complex **20**, on standing in CH_2Cl_2 solutions, undergoes a gradual decomposition predominantly generating (~80% by $^{31}P\{^1H\}$ NMR spectroscopy) one phosphorus containing product. This has been identified as the chloride bridged dimer, $[\{Pt(^iPr_3P)_2(\mu\text{-}Cl)\}_2][1\text{-H-}closo\text{-}CB_{11}Me_{11}]_2$, due in part to chloride abstraction from the solvent (Figure 46).

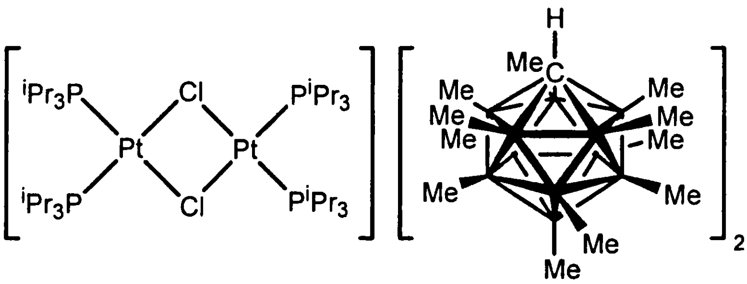

Figure 46: The chloride bridged dimer formed on complex **20** standing in CH_2Cl_2 solutions.

Confirmation that the decomposition product was indeed $[\{Pt(^iPr_3P)_2(\mu\text{-}Cl)\}_2][1\text{-H-}closo\text{-}CB_{11}Me_{11}]_2$ was attained by an X-ray diffraction study on suitable crystals grown by the slow diffusion of hexanes into a CH_2Cl_2 solution (Figure 47). The asymmetric unit consisted of one cationic $\{PtCl(^iPr_3P)_2\}^+$ fragment, one $[1\text{-H-}closo\text{-}CB_{11}Me_{11}]^-$ (that was not proximate), and a molecule of CH_2Cl_2 of solvation. The anion shows no positional disorder, with the cage carbon freely refined, the CH_3 isopropyl groups are equally disordered over two sites that is readily modelled by 50% occupancies. On performance of the associated symmetry operations the dimeric dicationic $[\{Pt(^iPr_3P)_2\}_2(\mu\text{-}Cl)_2]^{2+}$ is formed, with the vacant site observed in the asymmetric unit occupied by an additional bridging chloride. The geometry at the Pt(II)

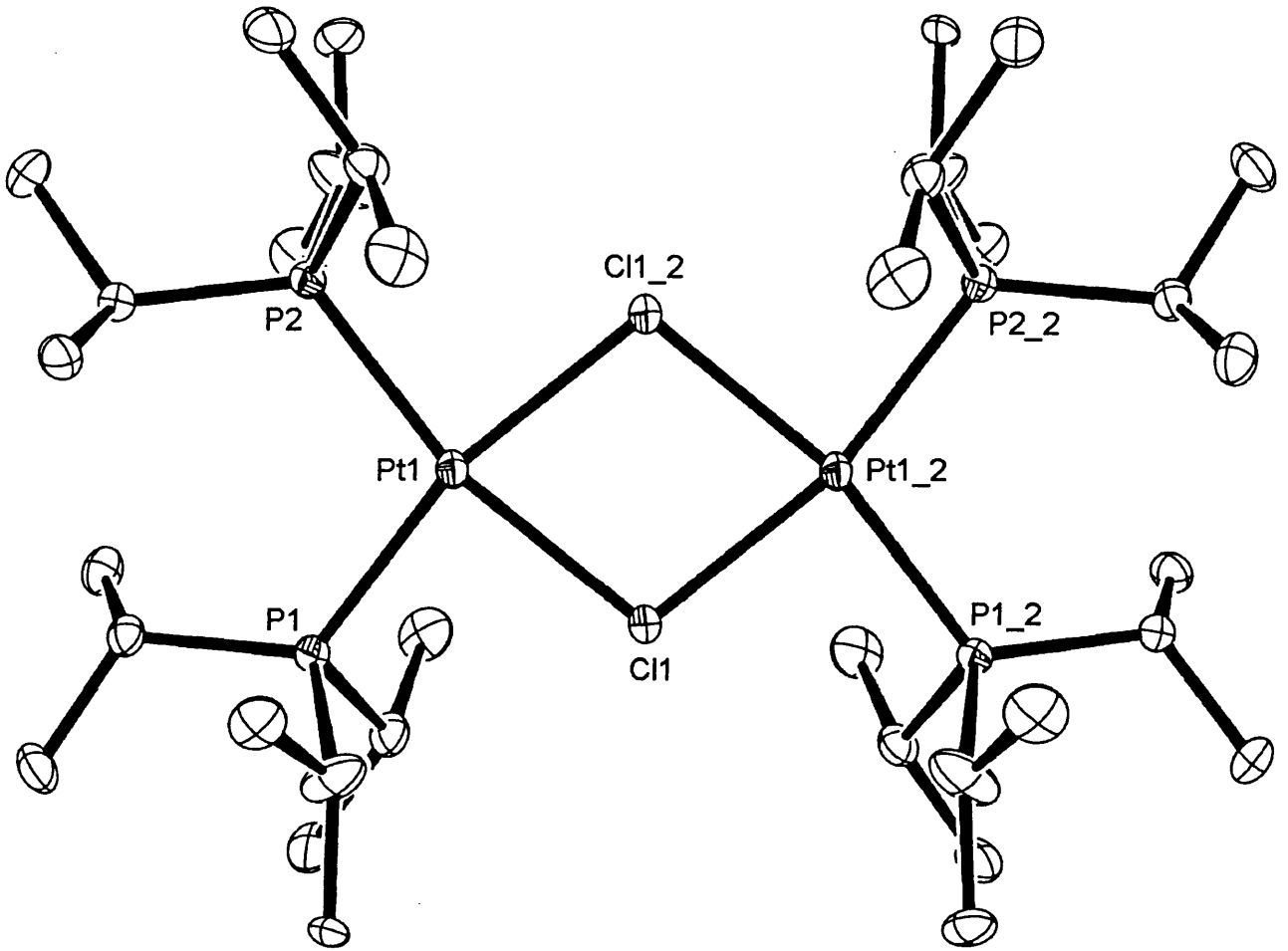

Figure 47: The molecular structure of the dication $[\{Pt(^{i}Pr_3P)_2\}_2(\mu\text{-}Cl)_2]^{2+}$, only one component of the disordered isopropyl methyls are shown. Hydrogen atoms omitted for clarity. Symmetry transformations used to generate equivalent atoms, x+1,-y,-z+1 and -x,-y,-z. Thermal ellipsoids shown at the 30% probability level.

Pt1-P1	2.2915(8)
Pt1-P2	2.3007(8)
Pt1-Cl1	2.4032(8)
Pt1-Cl1_2	2.4147(8)
P1-Pt1-P2	106.52(3)
P1-Pt1-Cl1	87.55(3)
P2-Pt1-Cl1_2	87.19(3)
Cl1-Pt1-Cl1_2	78.74(3)

Table 4: Selected bond lengths (Å) and angles (°) for $[\{Pt(^{i}Pr_3P)_2\}_2(\mu\text{-}Cl)_2]^{2+}$.

centre is distorted square planar (sum of angles = 360°), with the Cl1-Pt1-Cl1_2 angle compressed (78.74(3)°) by the greater steric demand of the terminal $^{i}Pr_3P$ groups. The geometric parameters related to the $\{P_2PtCl\}_2$ core are unremarkable and bare excellent agreement with the closely related complex $[\{Pt(dbpp)\}_2(\mu\text{-}Cl)_2][BF_4]_2$ (dbpp = di-tert-butylphosphinopropane).[86] A related decomposition has been reported for the similar *solvento* Pt(II) species, $[PtMe(solv)(tmeda)]^+$ (solv = Et_2O or THF) that on standing at room temperature in CH_2Cl_2 solutions formed the analogous chloride bridged dimer $[\{Pt(tmeda)\}_2(\mu\text{-}Cl)_2][BAr_F]_2$ and methane.[87, 88] Bercaw *et al.* suggests the possible intermediacy of the isolated hydrido-carbene complexes $[(tmeda)PtH\{(=C(Me)(OEt)\}]^+$ and $[(tmeda)PtH(=CCH_2CH_2CH_2O)]^+$ (Figure 48) formed via the double α-H abstraction of the coordinated solvent molecule. A related mechanism is possible here, though due to the unclean nature of the decomposition and failure to identify any intermediates further in-depth discussion is not appropriate.

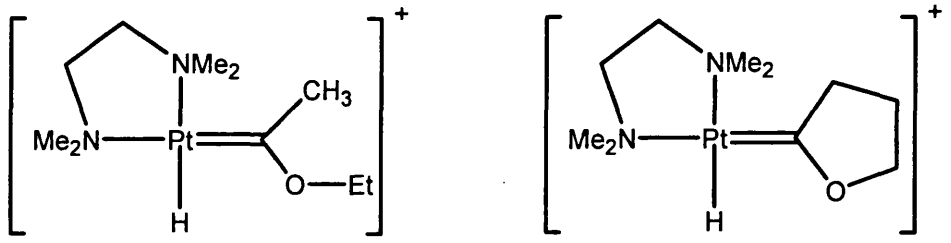

Figure 48: The hydrido carbene complexes formed from the decomposition of $[(tmeda)Pt(Me)(solv)]^+$ (solv = Et_2O or THF), that ultimately in CH_2Cl_2 gives the chloride bridged dimer.

Complex **18** was likewise treated with one equivalent of the neutral radical [1-H-*closo*-$CB_{11}Me_{11}]^{\bullet}$ in an another attempt to generate the $\{Pt(^{i}Pr_3P)_2\}^+$fragment. In CH_2Cl_2 solutions the reaction proceeded immediately, generating one phosphorus containing compound by $^{31}P\{^{1}H\}$ NMR, that was identified as the dication

$[\{Pt(^{i}Pr_3P)_2\}_2(\mu\text{-}Cl)_2]^{2+}$ by comparison to the earlier characterised sample. However, this time anion functionalisation had also occurred (as determined by ^{1}H and ^{11}B NMR spectroscopy) to give predominantly one product in which the 12-vertex of the anion had undergone methyl substitution.

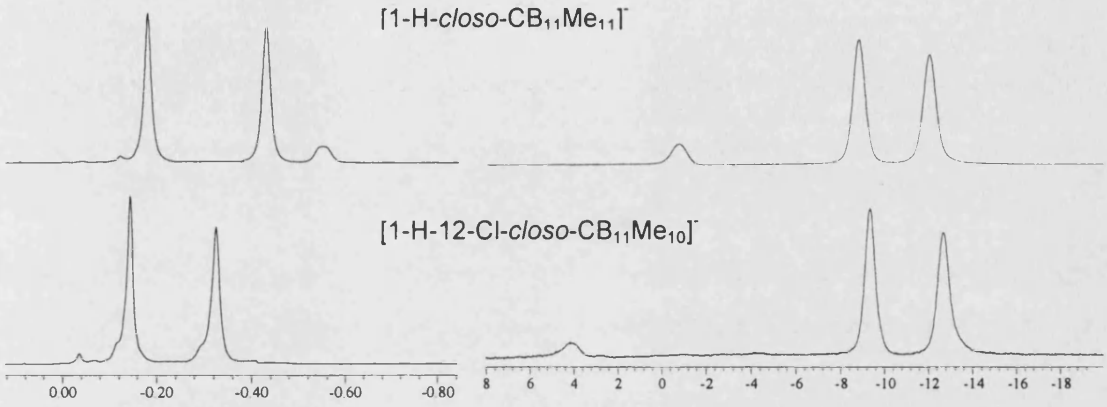

Figure 49: A comparison of the ^{1}H (left) and ^{11}B (right) NMR spectra in CD_2Cl_2 of [1-H-*closo*-$CB_{11}Me_{11}]^-$ and [1-H-12-Cl-*closo*-$CB_{11}Me_{10}]^-$ generated from the reaction of **18** with one equivalent of [1-H-*closo*-$CB_{11}Me_{11}]^{\bullet}$.

There is no observable signal in the ^{1}H NMR spectrum for the antipodal methyl, concomitantly the antipodal signal in the ^{11}B spectrum had shifted downfield significantly (Figure 49). Mass spectroscopy (FAB- mode) allowed for the characterisation of the functionalised anion as the mono chlorinated derivative, $[HCB_{11}Me_{10}Cl]^-$ (317.2m/z) and in conjunction with the C_{5V} symmetry observed by NMR techniques, functionalisation solely takes place in the 12 position generating [1-H-12-Cl-*closo*-$CB_{11}Me_{10}]^-$. Corroboration of this assignment was forthcoming from an X-ray diffraction study on yellow crystals grown by the slow diffusion of pentane into a DCM solution at room temperature. The dicationic core is identical (within errors) to that reported for $[\{Pt(^{i}Pr_3P)_2\}_2(\mu\text{-}Cl)_2][1\text{-}H\text{-}closo\text{-}CB_{11}Me_{11}]_2$, whilst the anion shows chloride functionalisation in the twelve position (Figure 50). The B-Cl distance in [1-H-12-Cl-*closo*-$CB_{11}Me_{10}]^-$ at 1.823(7) Å is slightly longer than that reported for the

identical B-Cl vertices in [1-H-*closo*-$CB_{11}Br_5Cl_6$]$^-$ (B12-Cl12 1.782(9) Å) and in [1-H-*closo*-$CB_{11}Cl_{11}$]$^-$ (B12-Cl12 1.775(3) Å).[89] Whilst the B-CH_3 distances in [1-H-12-Cl-*closo*-$CB_{11}Me_{10}$]$^-$ are each effectively identical to that observed for the unfunctionalised cage [1-H-*closo*-$CB_{11}Me_{11}$]$^-$.

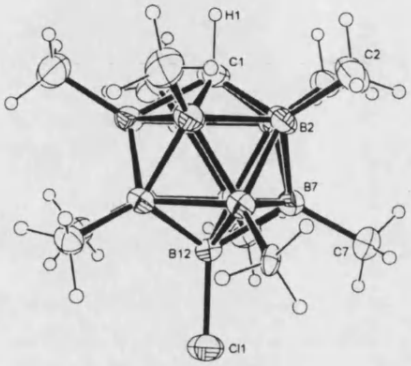

B2-C2	1.600(10)
B7-C7	1.771(9)
B12-Cl1	1.823(7)

Figure 50: The molecular structure of [1-H-12-Cl-$CB_{11}Me_{10}$]$^-$, with selected bond lengths (Å). Thermal ellipsoids are shown at the 30% probability level.

As to the mechanism of formation, the neutral radical [1-H-*closo*-$CB_{11}Me_{11}$]$^\bullet$ is stable in CH_2Cl_2 for days, with no diminishing of its intense colour. Furthermore, on addition of one equivalent of ferrocene to a CH_2Cl_2 solution of [1-H-*closo*-$CB_{11}Me_{11}$]$^\bullet$ the compound [Cp_2Fe][1-H-*closo*-$CB_{11}Me_{11}$] was immediately formed as the only product, indicating that anion decomposition requires a suitable metal fragment. The mechanism of anion functionalisation is believed to occur via the formation of the solvent stabilised dicationic complex, [$Pt(Cl_2CH_2)(^iPr_3P)_2$]$^{2+}$ (Figure 51). The formation of dicationic Pt(II) *solvento* complexes are well documented.[80]

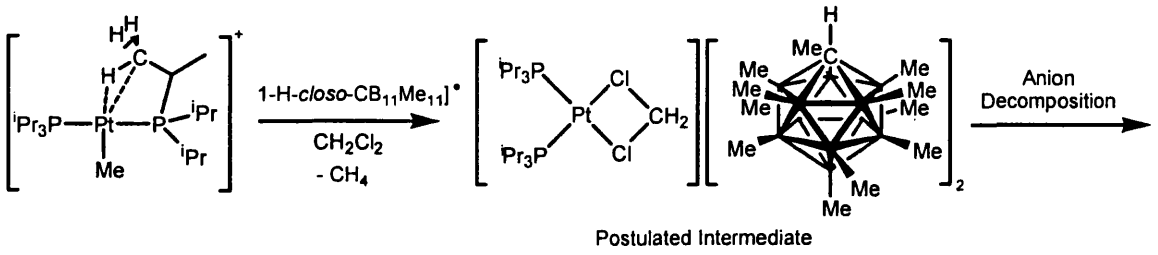

Figure 51: The formation of the dicationic CH_2Cl_2 complex, a possible intermediate in the radical initiated anion decomposition reaction.

Highly electrophilic cationic metals like the proposed $[Pt(ClCH_2Cl)(^iPr_3P)_2]^{2+}$ have also previously been shown to decompose in CH_2Cl_2 solution to generate chloride bridged dimers and neutral metal chlorides.[90] A similar process is feasible here. Chloride abstraction in $[Pt(Cl_2CH_2)(^iPr_3P)_2]^{2+}$ would generate $\{PtCl(^iPr_3P)_2\}^+$, that then dimerises to give the observed cationic product. Concurrently, the by-product, the fragment $\{CH_2Cl\}^+$ could then activate the cage as described previously via a borenium ylide mechanism.[91, 92] A direct activation of the [1-H-*closo*-$CB_{11}Me_{11}$]$^-$ anion by the electrophilic Pt(II) centre is equally feasible, as is a radical process. The reaction is not catalytic, as addition of only 10 mol % of [1-H-*closo*-$CB_{11}Me_{11}$]$^\bullet$ to complex **18** led to functionalisation of only a small percentage of the anion and the major phosphine containing product remained the agostic complex **18**. The cage substitution occurring at the 12 position is consistent with the charge density calculations performed on this anion (Chapter Two).

The analogous reaction was carried out in the non-chlorinated solvent, C_6H_5F, to avoid formation of the stable chloride bridged dimer. This was transferred to CD_2Cl_2 for NMR analysis. This showed two phosphine containing products (by $^{31}P\{^1H\}$ NMR spectroscopy), and a complex anion region (in both the ^1H and ^{11}B NMR spectra). The observed $^{31}P\{^1H\}$ NMR spectrum resonances **did not** correspond to $[\{Pt(^iPr_3P)_2\}_2(\mu$-

$Cl)_2]^{2+}$, $PtMe(Cl)(^iPr_3P)_2$ or $PtCl_2(^iPr_3P)_2$ (*vide infra*), and attempts to isolate pure material from this reaction failed. However, mass spectroscopy was useful in allowing for the characterisation of a number of products.

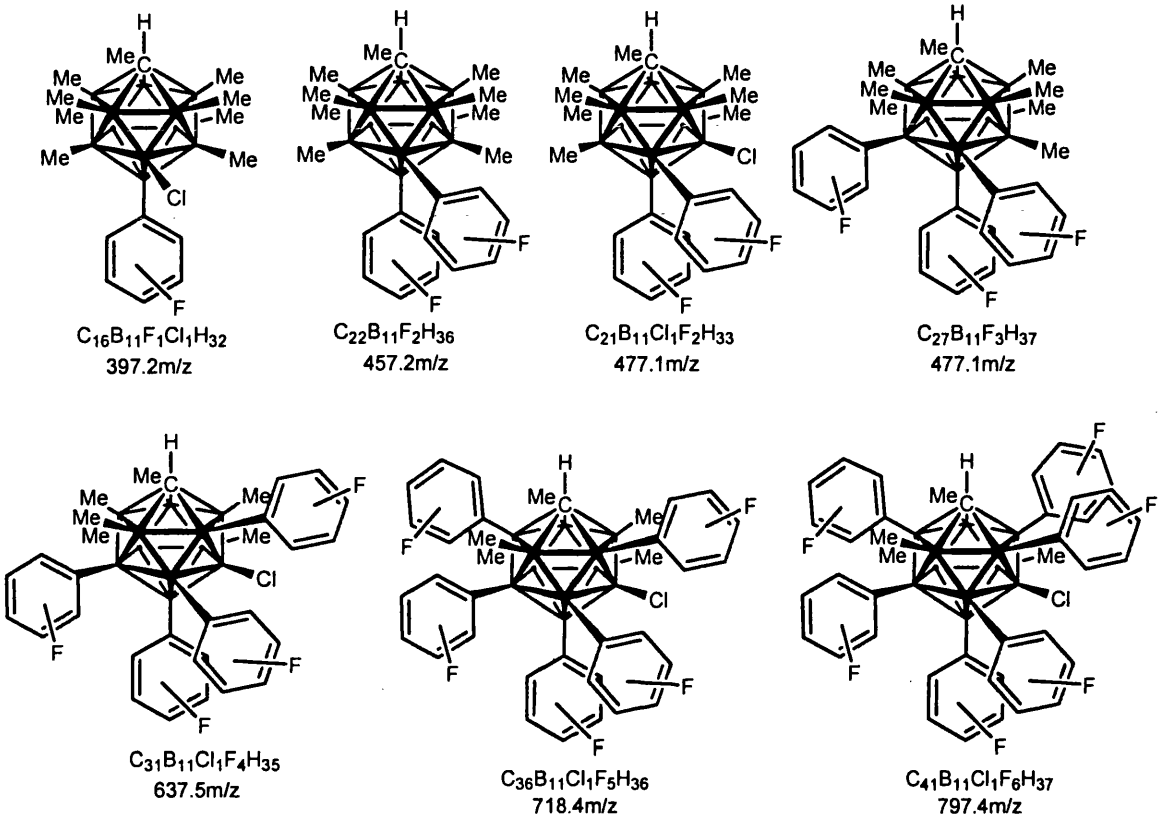

Figure 52: The range of anions observed from the reaction of $[1\text{-H-}closo\text{-}CB_{11}Me_{11}]^{\bullet}$ with complex **18**, in C_6H_5F, followed by dissolution in CD_2Cl_2- substitution positions are arbitrary.

The FAB- mode showed the formation of seven different functionalised anions, including anions that had undergone up to seven substitutions. The identified anions are shown in Figure 52, with substitutions shown in arbitrary positions

As for the previous cage functionalisation, the involvement of the Pt(II) complex is crucial as the radical $[1\text{-H-}closo\text{-}CB_{11}Me_{11}]^{\bullet}$ is stable in C_6H_5F solution for days. The reaction is clearly catalytic with up to seven functionalisations occurring. A possible mechanism for this would be again to invoke the formation of the borenium ylide, this

time possibly formed on methide abstraction by the electrophilic $\{Pt(^{i}Pr_3P)_2\}^+$ complex. The reactive borenium ylide can then undergo reaction with the solvent, C_6H_5F analogous to the Li^+ mediated B-CH_3 activation.[91] Importantly, this generates one equivalent of H^+ for each functionalisation – thus providing the catalytic turnover of H^+ required in this reaction. The anion, [1-H-*closo*-$CB_{11}Me_{11}$]$^-$ is known to be sensitive to strong acid environment, undergoing B-C bond protonlysis.[61] The incorporation of Cl into the cage periphery must occur on dissolution of the reaction mixture into CD_2Cl_2.

4.3: Summary

This Chapter reports efforts to form intimate contact ion pairs between [1-H-*closo*-$CB_{11}Me_{11}$]$^-$ and a range of cationic metal centres. This was frustrated by: (i) retarded metathesis reactions due to the low nucleophilicity of the anion, resulting in the failure to generate the desired unsaturated cationic metal centre; (ii) the preferential binding of CH_2Cl_2 to the metal centre over [1-H-*closo*-$CB_{11}Me_{11}$]$^-$; (iii) the formation of cationic agostic complexes; and finally (iv) the susceptibility of [1-H-*closo*-$CB_{11}Me_{11}$]$^-$ to decomposition, preventing the isolation of reactive metal cations that may have contained M···H_3C interactions.

The mechanism of cage activation is still unclear, but probably occurs via the borenium ylide reactive intermediate. The large range of cationic metal complexes that have been demonstrated to initiate anion decomposition has implications with respect to the use of [1-H-*closo*-$CB_{11}Me_{11}$]$^-$ as a weakly coordinating anion. The lack of robustness of this anion towards electrophilic B-C cleavage will therefore be an

important consideration in any future attempts to partner [1-H-*closo*-$CB_{11}Me_{11}$]$^-$ with metal cations.

4.4: References.

1 T. D. Newbound, M. R. Colsman, M. M. Miller, G. P. Wulfsberg, O. P. Anderson, and S. H. Strauss, *J. Am. Chem. Soc.*, 1989, **111**, 3762

2 R. H. Crabtree, 'The Organometallic Chemistry of the Transition Metals', Wiley Inter-Science, 2001.

3 K. Sunkel, W. Beck, and G. Urban, *J. Organomet. Chem.*, 1983, **252**, 187.

4 K. Sunkel, U. Nagel, and W. Beck, *J. Organomet. Chem.*, 1983, **251**, 227.

5 S. H. Strauss, *Chem. Rev.*, 1993, **93**, 927.

6 W. Beck, K. Schloter, K. Sunkel, and G. Urban, *Inorg Synth*, 1989, **26**, 96.

7 M. Appel, K. Schloter, J. Heidrich, and W. Beck, *J. Organomet. Chem.*, 1987, **322**, 77.

8 W. Beck and K. Sunkel, *Chem. Rev.*, 1988, **88**, 1405

9 N. J. Patmore, M. J. Ingleson, M. F. Mahon, and A. S. Weller, *J. Chem. Soc., Dalton Trans.*, 2003, 2894.

10 N. J. Patmore, M. F. Mahon, J. W. Steed, and A. S. Weller, *J. Chem. Soc., Dalton Trans.*, 2001, 277.

11 C. A. Reed, *Acc. Chem. Res.*, 1998, **31**, 133.

12 J. M. Fernandez and J. A. Gladysz, *Organometallics*, 1989, **8**, 207.

13 D. M. Van-Seggen, P. K. Hurlburt, O. P. Anderson, and S. H. Strauss, *Inorg. Chem.*, 1995, **34**, 3453

14 I. Krossing, *Chem. Eur. J.*, 2001, **7**, 490

15 J. Fornies, F. Martinez, R. Navarro, and E. P. Urriolabeitia, *Organometallics*, 1996, **15**.

16 M. R. Colsman, T. D. Newbound, L. J. Marshall, M. D. Noirot, M. M. Miller, G. P. Wulfsberg, J. S. Frye, O. P. Anderson, and S. H. Strauss, *J. Am. Chem. Soc.*, 1990, **112**.

17 D. M. v. Seggen, P. K. Hurlburt, O. P. Anderson, and S. H. Strauss, *J. Am. Chem. Soc.*, 1992, **114**, 10995.

18 X. G. Fang, J. Huhmann-Vincent, B. L. Scott, and G. J. Kubas, *J. Organomet. Chem.*, 2000, **609**, 95.

19 X. G. Fang, B. L. Scott, K. D. John, and G. J. Kubas, *Organometallics*, 2000, **19**, 4141.

20 J. Huhmann-Vincent, B. L. Scott, and G. J. Kubas, *J. Am. Chem. Soc.*, 1998, **120**, 6808.

21 J. Huhmann-Vincent, B. L. Scott, and G. J. Kubas, *Inorg. Chem.*, 1999, **38**, 115.

22 S. T. Brewer, L. A. Buggey, J. H. Holloway, and E. G. Hope, *J. Chem. Soc., Dalton Trans.*, 1995, 2941.

[23] T. Y. Cheng and R. M. Bullock, *Organometallics*, 1995, **14**, 4031.
[24] G. Albertin, S. Antoniutti, M. Bettiol, E. Bordignon, and F. Busatto, *Organometallics*, 1997, **16**, 4959.
[25] A. Toupadakis, G. J. Kubas, W. A. King, B. L. Scott, and J. Huhmann-Vincent, *Organometallics*, 1998, **17**, 5315.
[26] M. D. Heinekey, C. E. Radzewich, M. H. Voges, and B. M. Schomber, *J. Am. Chem. Soc.*, 1997, **119**, 4172.
[27] M. D. Heinekey, B. M. Schomber, and C. E. Radzewich, *J. Am. Chem. Soc.*, 1994, **116**, 4515.
[28] H. Dejian, J. C. Huffman, J. C. Bollinger, O. Eisenstein, and K. G. Caulton, *J. Am. Chem. Soc.*, 1997, **119**, 7398.
[29] B. A. Arndtsen and R. G. Bergmann, *Science*, 1995, **270**, 1970.
[30] F. L. Taw, H. Mellows, P. S. White, F. J. Hollander, R. G. Bergmann, M. Brookhart, and M. D. Heinekey, *J. Am. Chem. Soc.*, 2002, **124**, 5100.
[31] J. R. Krumper, M. Gerisch, J. M. Suh, R. G. Bergman, and T. D. Tilley, *J. Org. Chem*, 2003, **68**, 9705.
[32] M. D. Butts, B. L. Scott, and G. J. Kubas, *J. Am. Chem. Soc.*, 1996, **118**, 11831.
[33] N. J. Patmore, 'Transition Metal Complexes of Icosahedral MonoCarborane Anions: Synthesis to Catalysis', Thesis, University of Bath, Bath, 2002.
[34] N. J. Patmore, J. W. Steed, and A. S. Weller, *Chem. Commun.*. 2000, 2173.
[35] Z. W. Xie, T. Jelinek, R. Bau, and C. A. Reed, *J. Am. Chem. Soc.*, 1994, **116**, 1907.
[36] T. N. Sal'nikova, V. G. Andrianov, and Y. T. Struchkov, *Koord. Khim.*, 1976, **2**, 537.
[37] A. Bondi, *J. Phys. Chem*, 1964, **68**, 441.
[38] C.-M. Che, M.-C. Tse, M. C. W. Chan, K.-K. Cheung, D. L. Phillips, and K.-H. Leung, *J. Am. Chem. Soc.*, 2000, **122**, 2464.
[39] J. Powell, M. J. Horvath, and A. Lough, *J. Chem. Soc., Dalton Trans.*, 1996, 1669.
[40] J. C. T. R. Burckett-St.Laurent, J. S. Field, R. J. Haines, and M. McMahon, *J. Organomet. Chem.*, 1979, **181**, 3186.
[41] F. A. Cotton, B. A. Frenz, and A. J. White, *J. Organomet. Chem.*, 1973, **60**, 147.
[42] B. M. Mattson and W. A. G. Graham, *Inorg. Chem.*, 1981, **20**, 3186.
[43] D. J. Liston, Y. J. Lee, W. R. Scheidt, and C. A. Reed, *J. Am. Chem. Soc.*, 1989, **111**, 6643.
[44] V. G. Albano, M. Di-Serio, M. Monari, I. Orabona, A. Panunzi, and F. Ruffo, *Inorg. Chem.*, 2002, **41**, 2672.
[45] W. Beck and K. Schloter, *Z. Naturforsch*, 1978, **33**, 1214.
[46] M. H. Voges and R. M. Bullock, *Dalton Trans.*, 2002, 759.
[47] R. M. Bullock and M. H. Voges, *J. Am. Chem. Soc.*, 2000, **122**, 12594.
[48] J. Huhmann-Vincent, B. L. Scott, and G. J. Kubas, *Inorg. Chim. Acta*, 1999, **294**, 240.
[49] C. H. Winter and J. A. Gladysz, *J. Organomet. Chem.*, 1988, C33.
[50] I. Zharov, B. T. King, Z. Havlas, A. Pardi, and J. Michl, *J. Am. Chem. Soc.*, 2000, **122**, 10253.
[51] D. M. Tellers, C. M. Yung, B. A. Arndtsen, D. R. Adamson, and R. G. Bergman, *J. Am. Chem. Soc.*, 2002, **124**, 1400.
[52] F. A. Cotton, J. Lu, and A. Yokochi, *Inorg. Chim. Acta*, 1998, **275-276**, 447.
[53] R. C. Schnabel and D. M. Roddick, *Organometallics*, 1993, **12**, 704.

[54] C. R. Baar, L. P. Carbray, M. C. Jennings, and R. J. Puddephatt, *Organometallics*, 2000, **19**, 2482.
[55] S. Schlecht, J. Magull, D. Fenske, and K. Dehnicke, *Angew. Chem., Int. Ed. Engl.*, 1997, **36**, 1994.
[56] P. Leoni, A. Albinati, F. Lianza, H. Ruegger, and P. S. Pregosin, *Organometallics*, 1993, **12**, 4503.
[57] G. A. Lawrence, *Chem. Rev.*, 1986, **86**, 17.
[58] R. Goikhman and D. Milstein, *Angew. Chem., Int. Ed. Engl.*, 2001, **40**, 1119.
[59] A. Pedersen and M. Tilset, *Organometallics*, 1993, **12**, 56.
[60] P. Burger and R. G. Bergman, *J. Am. Chem. Soc.*, 1993, **115**, 10462.
[61] B. T. King, Z. Janousek, B. Gruner, M. Trammell, B. C. Noll, and J. Michl, *J. Am. Chem. Soc.*, 1996, **118**, 3313.
[62] L. Johansson, O. B. Ryan, C. R. Romming, and M. Tilset, *Organometallics*, 1998, **17**, 3957.
[63] H. Urtel, C. Meier, F. Eisentrager, F. Rominger, J. P. Joschek, and P. Hofmann, *Angew. Chem., Int. Ed. Engl.*, 2001, **40**, 781.
[64] J. P. Stambuli, M. Buhl, and J. F. Hartwig, *J. Am. Chem. Soc.*, 2002, **124**, 9346.
[65] W. Baratta, S. Stoccoro, A. Doppiu, E. Herdtweck, A. Zucca, and P. Rigo, *Angew. Chem., Int. Ed. Engl.*, 2003, **42**, 105.
[66] L. Mole, J. L. Spencer, N. Carr, and A. G. Orpen, *Organometallics*, 1991, **10**, 49.
[67] N. Carr, L. Mole, A. G. Orpen, and J. L. Spencer, *J. Chem. Soc., Dalton Trans.*, 1992, 2653.
[68] N. Carr, B. J. Dunne, A. G. Orpen, and J. L. Spencer, *J. Chem. Soc. Chem. Commun.*. 1988, 926.
[69] D. Braga, F. Grepioni, K. Biradha, and G. Desiraju, *J. Chem. Soc., Dalton Trans.*, 1996, 3925.
[70] W. Baratta, C. Mealli, E. Herdtweck, A. Ienco, S. A. Mason, and P. Rigo, *J. Am. Chem. Soc.*, 2004, **126**, 5549
[71] S. Schlecht, N. Faza, W. Massa, S. Dapprich, G. Frenking, and K. Dehnicke, *Z. Anorg. Allg. Chem*, 1998, **624**, 1011.
[72] C. M. Haar, S. P. Nolan, W. J. Marshall, K. G. Moloy, A. Prock, and W. P. Gierang, *Organometallics*, 1999, **18**, 474.
[73] D. L. Thorn, *Organometallics*, 1998, **17**, 348.
[74] C. A. Tolman, *Chem. Rev.*, 1977, **77**, 313.
[75] M. J. Frisch, G. W. Trucks, H. B. Schlegel, G. E. Scuseria, M. A. Robb, J. R. Cheeseman, V. G. Zakrzewski, J. A. Montgomery, R. E. Stratmann, J. C. Burant, S. Dapprich, J. M. Milliam, A. D. Daniels, K. N. Kudin, M. C. Strain, O. Farkas, J. Tomasi, V. Barone, M. Cossi, R. Cammi, B. Mennucci, C. Pomelli, C. Adamo, S. Clifford, J. Ochterski, G. A. Petersson, P. Y. ayala, Q. Cui, K. Morokuma, D. K. Malick, A. D. Rabuck, K. Raghavachari, J. B. Foreman, J. Cioslowski, J. V. Ortiz, A. G. Baboul, B. B. Stefanov, G. Liu, A. Liashenko, P. Piskorz, I. Komaromi, R. Gomperts, R. L. Martin, D. L. Fox, T. Keith, M. A. Al-Laham, C. Y. Peng, A. Nanayakkara, M. Challacombe, P. M. W. Gill, B. Johnson, W. Chen, M. W. Wong, J. L. Anders, C. Gonsalez, M. Head-Gordon, E. S. Replogle, and J. A. Pople, *Gaussian 98, revision A.9; Gaussian, Inc. Pittsburgh*, 1998.
[76] M. W. Bouwkamp, J. d. Wolf, I. d. H. Morales, J. Gercama, A. Meetsma, S. I. Troyanov, B. Hessen, and J. H. Teuben, *J. Am. Chem. Soc.*, 2002, **124**, 12956.

[77] H. J. Wasserman, G. J. Kubas, and R. R. Ryan, *J. Am. Chem. Soc.*, 1986, **108**, 2294.
[78] M. A. Bennett and A. Rokick, *Inorg Synth*, 1989, **25**, 100.
[79] H. A. Zhong, J. A. Labinger, and J. E. Bercaw, *J. Am. Chem. Soc.*, 2002, **124**, 1378.
[80] A. G. Wong-Foy, L. M. Henling, M. Day, J. A. Labinger, and J. E. Bercaw, *J. Mol. Catal. A.*, 2002, **189**, 3.
[81] U. Fekl and K. I. Goldberg, *Adv. Inorg. Chem.*. 2003, **54**, 259.
[82] L. Johansson, O. B. Ryan, and M. Tilset, *J. Am. Chem. Soc.*, 1999, **121**, 1974.
[83] M. E. v. d. Boom, J. Ott, and D. Milstein, *Organometallics*, 1998, **17**, 4263.
[84] N. G. Connelly and W. E. Geiger, *Chem. Rev.*, 1996, **96**, 877.
[85] G. S. Hill, L. Manojlovic-Muir, K. W. Muir, and R. J. Puddephatt, *Organometallics*, 1997, **16**, 525.
[86] S. A. Litster, L. Mole, A. D. Redhouse, and J. L. Spencer, *Acta Cryst. Sec. C*, 1992, **48**, 913.
[87] M. W. Holtcamp, L. M. Henling, M. W. Day, J. A. Labinger, and J. E. Bercaw, *Inorg. Chim. Acta*, 1998, **270**, 467.
[88] M. W. Holtcamp, J. A. Labinger, and J. E. Bercaw, *J. Am. Chem. Soc.*, 1997, **119**, 848.
[89] C.-W. Tsang, Q. Yang, E. T.-P. Sze, T. C. W. Mak, D. T. W. Chan, and Z. Xie, *Inorg. Chem.*, 2000, **39**, 5851
[90] R. Gomez, M. L. H. Green, and J. L. Haggit, *J. Chem. Soc., Dalton Trans.*, 1996, 939.
[91] Z. Janousek, U. Lehmann, J. Castulik, I. Cisarova, and J. Michl, *J. Am. Chem. Soc.*, 2004, **126**, 4060.
[92] B. T. King, I. Zharov, and J. Michl, *Chemical Innovation*, 2001, **31**, 23.

5: The hydrogenation of group 9 metal di-olefin complexes partnered with [1-H-*closo*-$CB_{11}Me_{11}$]$^-$ and [BAr_F]$^-$.

5.1: Background.

The complexes [L_2M(diene)][anion] (L = phosphine or nitrogen donor, M = Rh or Ir, diene = COD (cyclooctadiene) or NBD (norbornadiene), Figure 1) have attracted considerable attention as they are pre-catalysts for the transition metal catalysed hydrogenation of alkenes.[1-6] One of the most important of these is the Crabtree catalyst, [(pyridine)(PCy_3)Ir(COD)][PF_6], that is highly effective for the hydrogenation of sterically hindered internal alkenes at room temperature and low H_2 pressures (Figure 1).[7, 8]

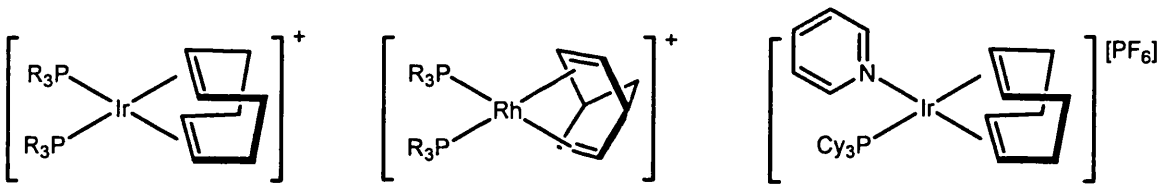

[$(PR_3)_2$Ir(COD)]$^+$ [$(PR_3)_2$Rh(NBD)]$^+$ Crabtree's Catalyst

Figure 1: Some generic cationic hydrogenation catalyst precursors, including the Crabtree catalyst.

The chemistry of the Crabtree catalyst (and its monodentate bisphosphine analogues) has been studied in depth and the 'resting' state of these catalysts in coordinating media has been shown to be [LL'Ir$(H)_2(solv)_2$]$^+$ (solv = acetone, THF or ethanol), which are accessed simply by hydrogenation of the COD precursor. [1, 7]

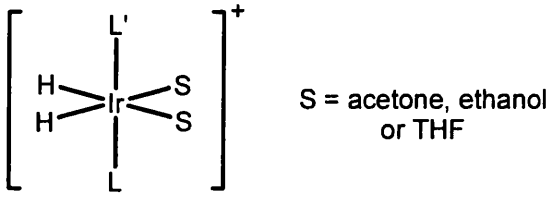

Figure 2: The resting state for the active hydrogenation catalyst formed on the hydrogenation of [LL'Ir(COD)]$^+$ precursors in coordinating solvents.

These active catalysts have proved to be highly electrophilic yet remarkably stable to $CHCl_3$ and CH_2Cl_2, solvents that normally react with late transition metal hydrides rendering them inactive to hydrogenation.[9] In non-coordinating solvents (*e.g.*, CH_2Cl_2) the active catalyst is not stabilised by a strongly binding solvent, allowing for more facile alkene coordination and concomitantly, a drastic acceleration in the rate of hydrogenation. The increase in activity, however, comes at the expense of catalyst longevity: and on complete hydrogenation of the olefin the inactive dimer, $[\{IrH(PR_3)_2\}_2(\mu\text{-}H)_3]^+$, is formed along with one equivalent of HX (X = $[PF_6]^-$, Figure 3).

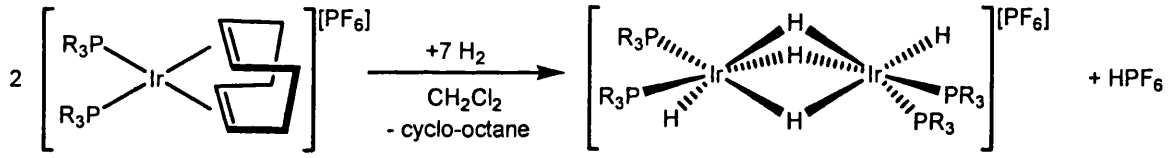

Figure 3: The deactivation products on the hydrogenation of $[(PR_3)_2Ir(COD)][PF_6]$

Mixed ligand systems such as Crabtree's catalyst decompose in a similar manner to yield a trinuclear analogue (Figure 4).[10] Crabtree proposed that the precursors to these deactivation complexes were mono-cationic complexes $[LL'IrH_6]^+$ (the identification of the hydride ligands as the classically or non-classically bonded congeners was not reported), and it was shown that these complexes, on deprotonation by NEt_3, lead to $[\{IrH(PR_3)_2\}_2(\mu\text{-}H)_3][PF_6]$.[1] $[L_2IrH_6]^+$ complexes can be accessed by the protonation of the polyhydride complex, $[(PCy_3)_2IrH_5]$ which yielded $[(PCy_3)_2Ir(H_2)_2(H)_2]^+$, as characterised by T_1 NMR measurements (Figure 4).[11]

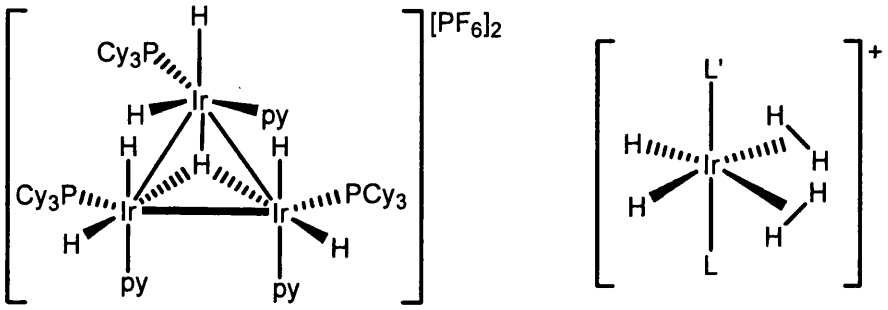

Figure 4: The decomposition product (left) isolated from Crabtree's catalyst (py = pyridine) and the proposed intermediate (right), L and L' = phosphine or nitrogen 2 electron donor.

Cationic dihydrogen complexes, $[LL'M(H_2)]^+$, are well documented to be highly acidic, with some complexes even having an acidity higher than triflic acid.[12] Furthermore, cationic iridium dihydrogen complexes have been demonstrated to readily lose a proton to the anion (*e.g.*, in $[(triphos)Ir(H_2)(H)_2][BPh_4]$ where protonation of the anion generates the trihydride, $(triphos)Ir(H_3)$, BPh_3 and benzene).[13] The dihydrogen ligands in $[(PCy_3)_2Ir(H_2)_2(H)_2]^+$ have also been shown to be labile, easily displaced by coordinating solvents generating $[Ir(H)_2(PCy_3)_2(solv)_2]^+$ (solv = MeCN or acetone). A closely related complex stabilised by two agostic interactions has also been reported.[14, 15] This complex has been shown to add dihydrogen stepwise via a coordinatively unsaturated dihydrogen-dihydride complex ultimately to give the $[(P^tBu_2Ph)_2Ir(H_2)_2H_2]^+$ complex (Figure 5).[16]

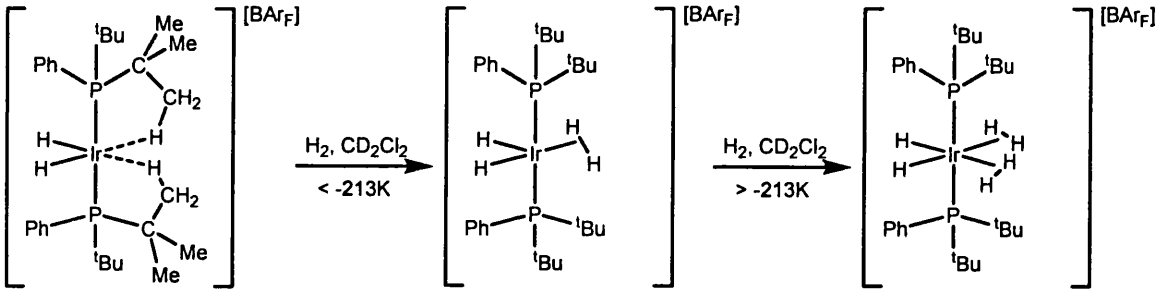

Figure 5: The bis-agostic complex, $[Ir(H)_2(P^tBu_2Ph)_2][BAr_F]$ which undergoes stepwise addition of two molecules of dihydrogen.

Similar investigations have also been carried out on analogous rhodium systems, especially the Schrock-Osborn hydrogenation catalyst precursors, $[L_2Rh(NBD)][anion]$ (Figure 1).[5] The catalytic cycle for these complexes has been previously elucidated, with hydrogenation in coordinating solvents resulting in complexes of the general formula, $[(PR_3)_2Rh(H)_2(solv)_2]^+$ (solv = MeCN, 2-butanone, dimethylacetamide and EtOH).[17] No rhodium complexes analogous to the polyhydride iridium complexes, $[(PR_3)_2Ir(H_2)_2(H)_2]^+$ have been reported. Studies on the $[(PR_3)_2RhH_2(solv)_2]^+$ complexes have shown that in addition to being highly active hydrogenation catalysts for simple olefins they are also effective as olefin isomerisation catalysts. The activity of these complexes in isomerisation has been previously ascribed to their acidic nature, which generates the catalytically active mono-hydride species by loss of a proton (Figure 6).[18]

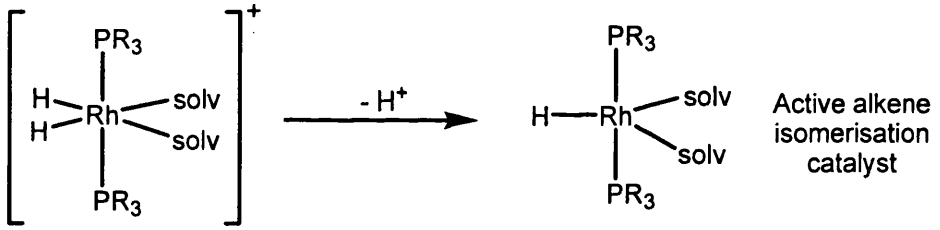

Figure 6: The acidic nature of complexes of the general formula $[(PR_3)_2RhH_2(solv)_2]^+$.

Since these precursors are cationic in nature it is necessary to partner them with a suitable anion. The counterion in the catalytically active specie is 'non-innocent', with significant activity increases in the hydrogenation of olefins and improved enantioselectivities achieved simply by alteration of the anion.[19-22] Anion effects have been reported in a number of systems based on the Schrock-Osborn catalyst precursors.[23-25] An example that exemplifies the importance of the counterion in the activity of these systems utilises the pre-catalyst $[(dppb)Rh(COD)]^+$ (dppb = diphenylphosphinobutane) developed by van Koten (Figure 7).[25]

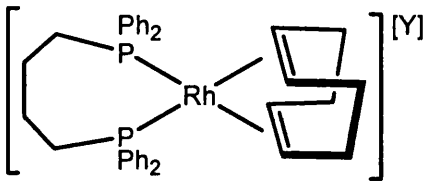

Catalyst activity in the hydrogenation of 1-Octene

Y	TOF (hr^{-1})
$[BPh_4]$	12
$[BF_4]$	67
$[BAr_F]$	80

Figure 7: Anion effects on the hydrogenation of 1-Octene.

An inverse correlation was observed between the coordinating power of the anion and the turnover frequency (TOF), with the weakest coordinating anion, $[BAr_F]^-$, generating a catalyst with the highest activity. This is a strong indicator that the catalytic cycle at some stage involves a cation···anion interaction, which with more coordinating anions (*e.g.*, $[BPh_4]^-$) lowers the catalysts' activity by binding to the metal centre in competition to the substrate. Support for this comes from the isolation of the intimate ion pair, (dppb)Rh(η^6-$PhBPh_3$) formed from hydrogenation of the COD precursor, with the anion binding in favour to H_2 and CH_2Cl_2.[26] Other contact ion pairs have also been formed from analogous reactions with precursors partnered with the perchlorate anion ($[ClO_4]^-$), and a range of sulfonates.[21, 27]

A number of derivatives of [*closo*-$CB_{11}H_{12}]^-$ have been paired with the Schrock-Osborn and iridium pre-catalysts and their reactivity towards hydrogen investigated.[22, 28] Differing reactivity pathways have been found depending on the anion's coordinating ability. For the precursors $[(PPh_3)_2Rh(NBD)][Y]$ (Y = [*closo*-$CB_{11}H_{12}]^-$, [12-Br-*closo*-$CB_{11}H_{11}]^-$, [*closo*-$CB_{11}H_6Br_6]^-$ and [1-H-*closo*-$CB_{11}Me_{11}]^-$) two distinct sets of compounds were synthesised, contact ion pairs and arene bridged dimers (Figure 8).[22, 29]

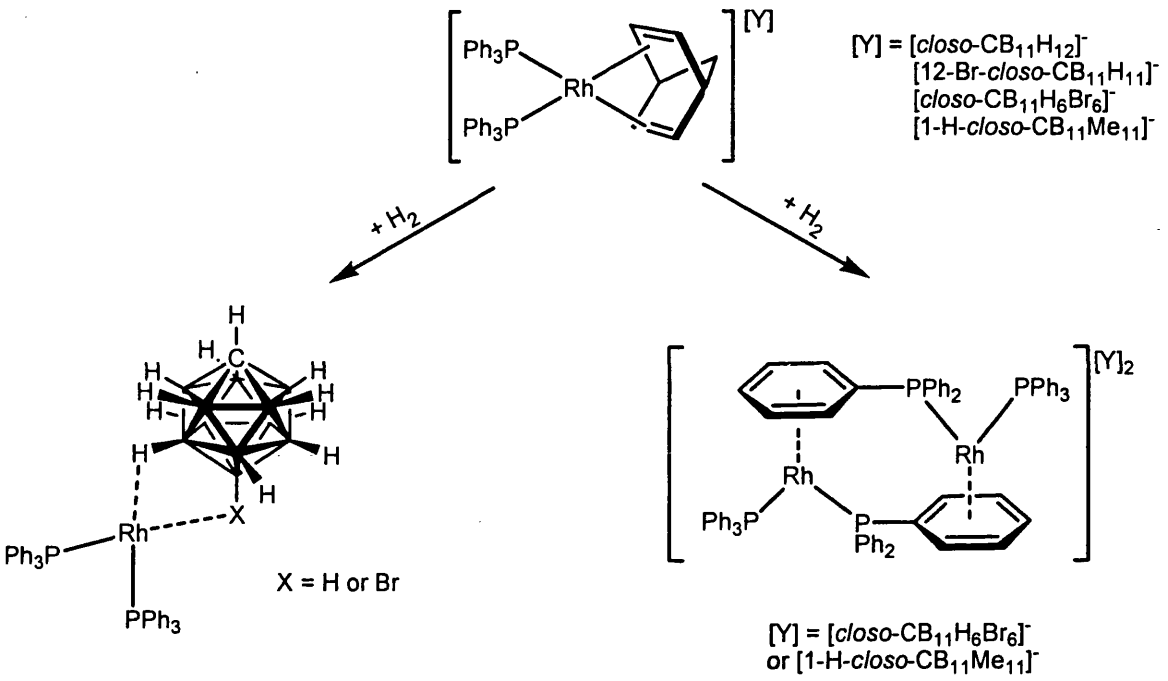

Figure 8: The two sets of compounds formed on the hydrogenation of $[(PPh_3)_2Rh(NBD)]^+$ partnered with $[closo\text{-}CB_{11}H_{12}]^-$ and its derivatives.

Contact ion pairs are formed with the relatively coordinating $[closo\text{-}CB_{11}H_{12}]^-$ and $[12\text{-}Br\text{-}closo\text{-}CB_{11}H_{11}]^-$ anions,[30] whilst with the more weakly coordinating $[closo\text{-}CB_{11}H_6Br_6]^-$ and $[1\text{-}H\text{-}closo\text{-}CB_{11}Me_{11}]^-$ anions the $\{(PPh_3)_2Rh\}^+$ fragment dimerises through a phosphine based arene ring in preference to forming Rh···anion interactions. Related monomeric arene coordinated complexes have also been reported, $[(PPh_3)_2Rh(\eta^6\text{-}C_6H_5Me)][closo\text{-}CB_{11}H_6Br_6]$ and $[(dppe)Rh(\eta^6\text{-}C_6H_6)][BF_4]$.[22, 31]

The use of the arene bridged dimer, $[(PPh_3)(PPh_2\text{-}\eta^6\text{-}C_6H_5)Rh]_2[closo\text{-}CB_{11}H_6Br_6]_2$ in hydrogenation reactions led to the isolation and characterisation of a deactivation product, $[\{Rh(H)(PPh_3)_2\}_2(\mu\text{-}Cl)_2(\mu\text{-}H)][closo\text{-}CB_{11}H_6Br_6]$ (Figure 9),[22] similar to that observed in the iridium congener.[1]

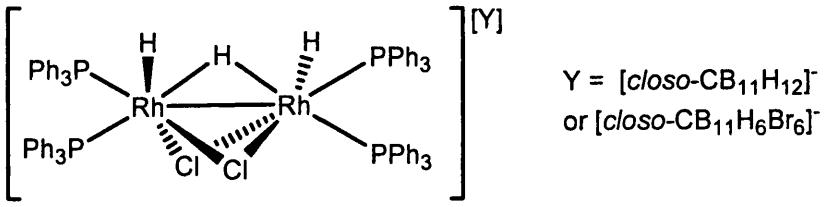

Figure 9: The cation portion of the deactivation product, $[\{Rh(H)(PPh_3)_2\}_2(\mu\text{-}Cl)_2(\mu\text{-}H)]^+$.

The chlorides incorporated into this deactivation product must originate from activation of the solvent, CH_2Cl_2. An analogous iridium product, $[\{IrH(PPh_3)_2\}_2(\mu\text{-}Cl)_2(\mu\text{-}H)]^+$, has been previously synthesised by the addition of HCl to the dimer $[\{IrH(PPh_3)_2\}_2(\mu\text{-}H)_3]^+$ (Figure 10).[32] This implies that the formation of the rhodium deactivation product may well be a consequence of a decomposition pathway that produces H^+.

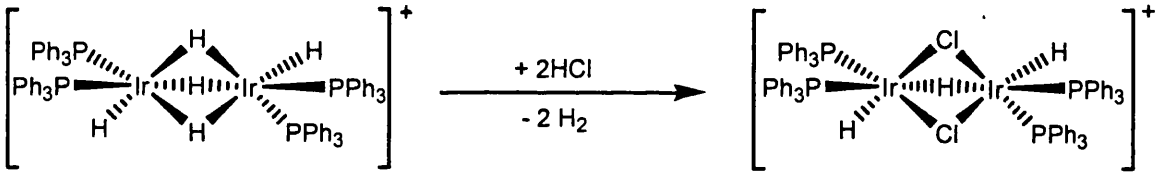

Figure 10: The formation of the iridium dimer, $[\{IrH(PPh_3)_2\}_2(\mu\text{-}Cl)_2(\mu\text{-}H)]^+$ by the action of HCl on the hydrogenation deactivation product $[\{IrH(PPh_3)_2\}_2(\mu\text{-}H)_3]^+$.

The importance of the anion in these systems is further exemplified by the recent isolation and characterisation of the contact ion pair complex $(PPh_3)_2Ir(H)_2$(*closo*-$CB_{11}H_6Br_6$) (Figure 11).[33]

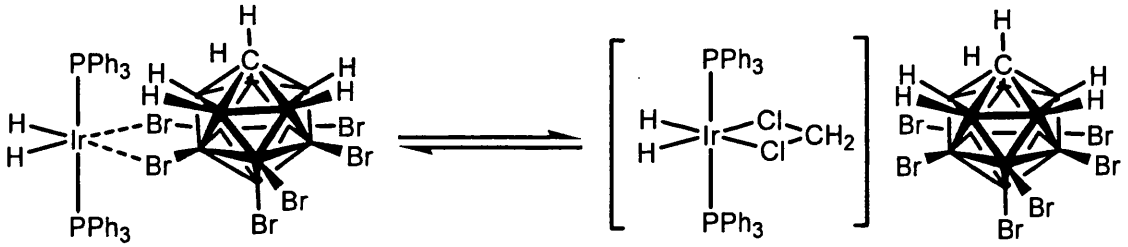

Figure 11: The low temperature equilibrium between the contact ion pair ($(PPh_3)_2Ir(H)_2$(*closo*-$CB_{11}H_6Br_6$) and the solvent separated ion pair.

The [*closo*-$CB_{11}H_6Br_6$]$^-$ anion plays a crucial role in stabilising this system, with the anion coordinating in favour of dihydrogen, this intimate ion pair then prevents the decomposition observed with the more weakly coordinating anions (*e.g.*, $[BAr_F]^-$, $[BF_4]^-$ and $[PF_6]^-$). In the absence of H_2 ($(PPh_3)_2IrH_2$(*closo*-$CB_{11}H_6Br_6$) has been demonstrated to be in equilibrium at low temperatures with the DCM coordinated compound (Figure 11). This is contrast to the agostic complex, $[(P^tBu_2Ph)_2Ir(H)_2][BAr_F]$, formed in CH_2Cl_2 when the phosphine contains the superior agostic bond donor group, ^{t}Bu. [14]

To circumvent the formation of arene-bridged dimers and thereby allow for further studies into the coordination behaviour of $\{(PR_3)_2Rh\}^+$ fragments it is necessary to move away from PPh_3 to saturated phosphine analogues. A number of *exo-closo* rhodacarboranes complexes, $(PR_3)_2Rh$(*closo*-$CB_{11}H_{12}$) (R = OMe and Cy) have been synthesised with saturated phosphines (Figure 12, left), again via the hydrogenation of the NBD precursor.[28] Unfortunately, the analogous complexes with anions more weakly coordinating than [*closo*-$CB_{11}H_{12}$]$^-$, (*e.g.*, [*closo*-$CB_{11}H_6Br_6$]$^-$ or $[BAr_F]^-$) have not yet been reported.

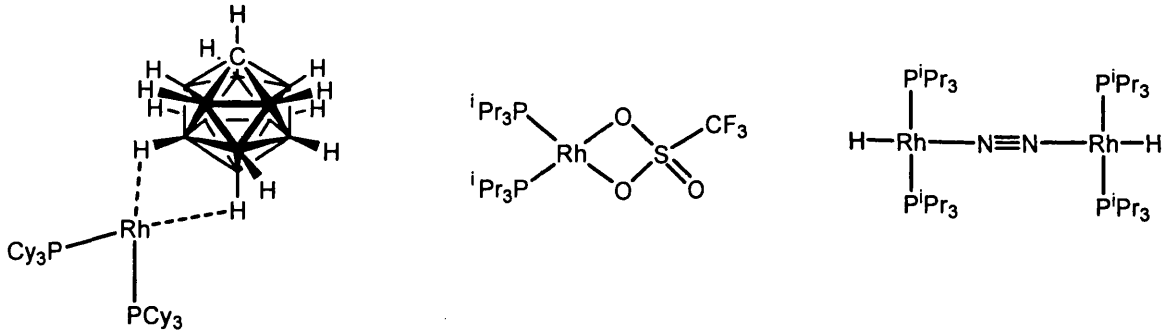

Figure 12: Anion and small molecule coordination to rhodium bis-(saturated)-phosphine complexes.

A triflate coordinated analogue and a N_2 bridging adduct have also been isolated using the $\{(PR_3)_2Rh\}^+$ scaffold (R = $^iPr_3P$, Figure 12).[34-36]

5.1.1 Scope of Chapter

The following chapter discusses the hydrogenation of two sets of compounds, $[(PPh_3)_2Ir(COD)][1\text{-H-}closo\text{-}CB_{11}Me_{11}]$ and $[(PR_3)_2Rh(NBD)][Y]$ (R = Cy or ^iPr, Y = $[1\text{-H-}closo\text{-}CB_{11}Me_{11}]^-$ or $[BAr_F]^-$). On hydrogenation of the diene, reactive 14 electron fragments ($\{(PR_3)_2MH_2\}^+$ or $\{(PR_3)_2M\}^+$) can be expected to be generated. Similar unsaturated fragments have been previously shown to alleviate their coordinative unsaturation in a number of ways: (i) anion coordination, generating contact ion pairs; (ii) *solvento* complexes (in coordinating media); (iii) intramolecular interactions, either by an agostic bond or via dimerisation through a pendant arene ring; and (iv) dihydrogen binding.

For the iridium system the reactivity of $[(PPh_3)_2Ir(COD)][1\text{-H-}closo\text{-}CB_{11}Me_{11}]$ will be determined by the coordinating ability of the $[1\text{-H-}closo\text{-}CB_{11}Me_{11}]^-$ anion, which if nucleophilic enough will form a contact ion pair analogous to

$(PPh_3)_2IrH_2(closo\text{-}CB_{11}H_6Br_6)$.[33] Alternatively if dihydrogen binds in favour, then a reactivity similar to that previously elucidated for the $[BF_4]^-$ and $[BAr_F]^-$ anions can be expected (Figure 13).

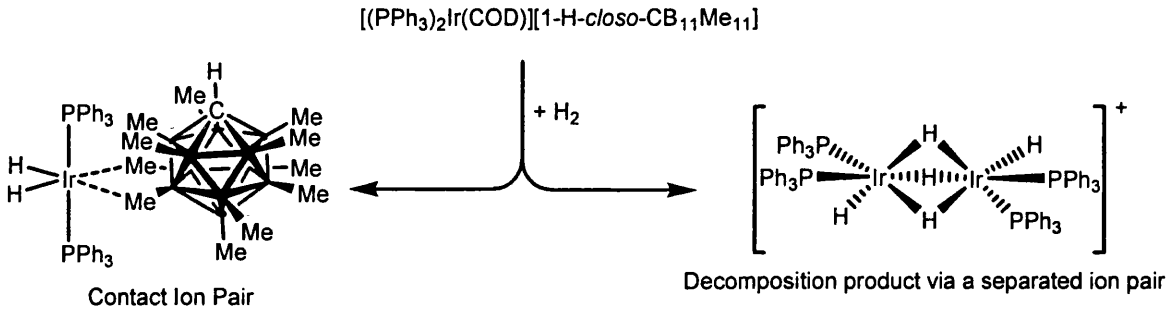

Figure 13: The two expected possible outcomes from the hydrogenation of $[(PPh_3)_2Ir(COD)][1\text{-}H\text{-}closo\text{-}CB_{11}Me_{11}]$.

The four possibilities mentioned earlier are all equally feasible as methods for the $\{(PR_3)_2RhH_2\}^+$ or $\{(PR_3)_2Rh\}^+$ fragments to alleviate their coordinative unsaturation (Figure 14), and the results from these Rh systems will be discussed in the second half of this chapter.

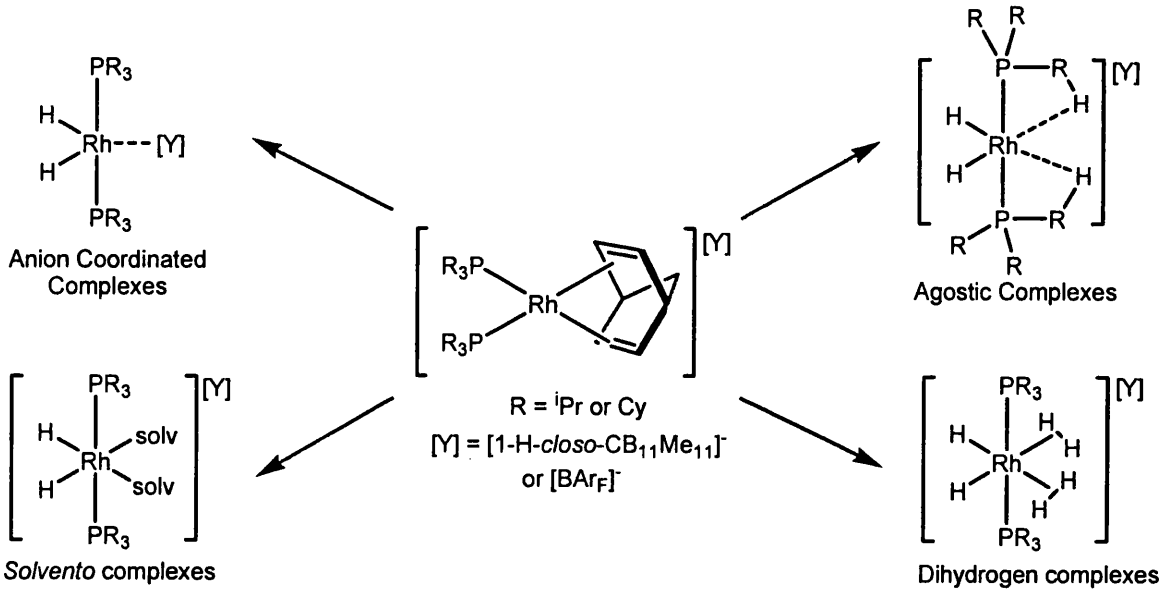

Figure 14: The possible outcomes from the hydrogenation reactions of $[(PR_3)_2Rh(NBD)][Y]$.

5.2: Results and Discussions:

5.2.1: Hydrogenation Reactions of $[(PPh_3)_2Ir(COD)][1\text{-}H\text{-}closo\text{-}CB_{11}Me_{11}]$.

The precursor complex $[(PPh_3)_2Ir(COD)][1\text{-}H\text{-}closo\text{-}CB_{11}Me_{11}]$ is readily prepared in a two step synthesis from $[Ir(COD)Cl]_2$ in an analogous manner to the $[closo\text{-}CB_{11}H_6Br_6]$ congener.[33] Deep red crystalline material is readily obtainable from the diffusion of hexanes into a saturated CH_2Cl_2 solution. Treatment of a stirred solution of $[(PPh_3)_2Ir(COD)][1\text{-}H\text{-}closo\text{-}CB_{11}Me_{11}]$ in CD_2Cl_2 with H_2 resulted in the reduction of the diene and formation of a yellow solution. The ^1H NMR spectrum of this solution showed a hydride region corresponding to the clean formation of the cation, $[\{IrH(PPh_3)_2\}_2(\mu\text{-}H)_3]^+$.[3] In an attempt to observe any intermediate compounds the hydrogenation was carried out at -80°C in CD_2Cl_2. At this temperature the only hydrogenation product in the ^1H NMR spectrum was attributable to $[(PPh_3)_2Ir(H)_2(COD)][1\text{-}H\text{-}closo\text{-}CB_{11}Me_{11}]$, by comparison to the known $[PF_6]^-$ salt (Figure 15).[37, 38]

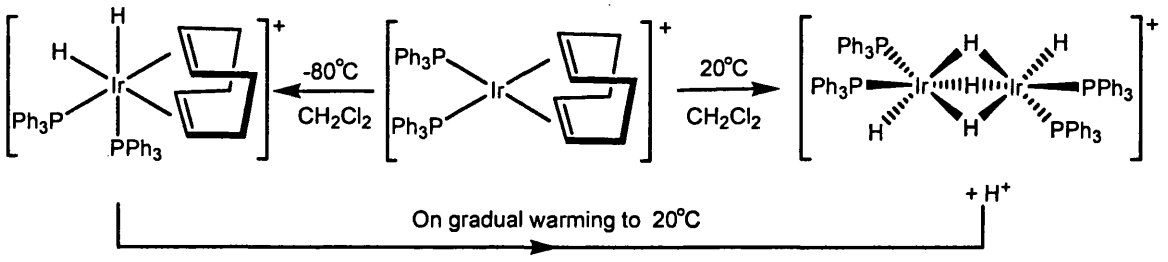

Figure 15: The reactivity of $[(PPh_3)_2IrCOD][1\text{-}H\text{-}closo\text{-}CB_{11}Me_{11}]$ on hydrogenation in CH_2Cl_2.

On warming to ambient temperature the COD is hydrogenated followed by the immediate formation of $[\{IrH(PPh_3)_2\}_2(\mu\text{-}H)_3]^+$, with no detectable intermediates, again as seen for the $[PF_6]^-$ analogue.[3] On standing, CH_2Cl_2 solutions of $[\{IrH(PPh_3)_2\}_2(\mu\text{-}H)_3][1\text{-}H\text{-}closo\text{-}CB_{11}Me_{11}]$ and the acid by-product, "$H[1\text{-}H\text{-}closo\text{-}CB_{11}Me_{11}]$", undergo

a further reaction, with cage decomposition observed (with complex anion resonances in both the ^{1}H and ^{11}B NMR spectra). After 24 hours the reaction is complete with no [1-H-*closo*-$CB_{11}Me_{11}$]$^-$ remaining. Mass spectroscopy (FAB- mode) showed the presence of [$HCB_{11}Me_{10}Cl$]$^-$ and [$HCB_{11}Me_9Cl_2$]$^-$ that presumably form via the borenium ylide mechanism discussed previously (Chapter Four).[39] Along with this anion functionalisation, [{$IrH(PPh_3)_2$}$_2$(μ-H)$_3$]$^+$ is cleanly converted to [{$IrH(PPh_3)_2$}$_2$(μ-H)(μ-Cl)$_2$]$^+$ (by NMR and mass spectroscopy), a reaction that also occurs on the addition of HCl to [{$IrH(PPh_3)_2$}$_2$(μ-H)$_3$][PF_6] (Figure 16).[38]

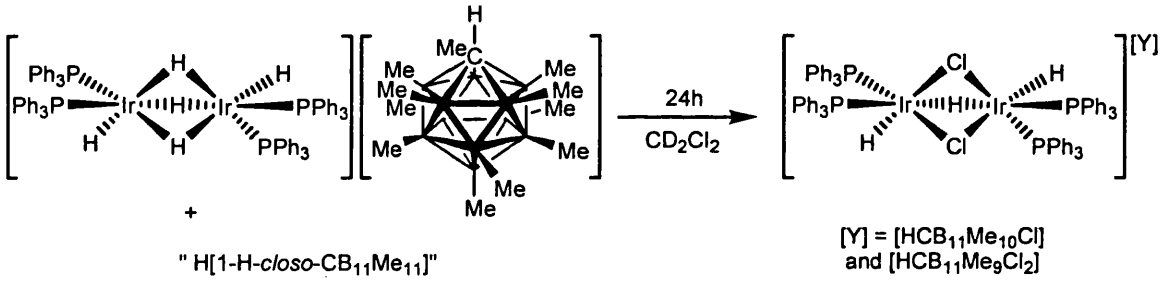

Figure 16: The acid initiated decomposition of [{$IrH(PPh_3)_2$}$_2$(μ-H)$_3$][1-H-*closo*-$CB_{11}Me_{11}$].

With the failure to observe any anion coordinated compound and the activation of CH_2Cl_2, hydrogenation of [$(PPh_3)_2Ir(COD)$][1-H-*closo*-$CB_{11}Me_{11}$] using C_6H_5F as the solvent was next investigated. The initial hydrogenation predominantly (~90% by ^{1}H NMR spectroscopy in CD_2Cl_2 after removal of the C_6H_5F) generated [{$IrH(PPh_3)_2$}$_2$(μ-H)$_3$][1-H-*closo*-$CB_{11}Me_{11}$] presumably along with "H[1-H-*closo*-$CB_{11}Me_{11}$]". A number of other products, present in low yield, were also detected. Numerous resonances were observed in the $^{31}P\{^{1}H\}$ NMR spectrum and in the hydride region of the ^{1}H NMR spectrum. Recrystallisation of this crude mixture allowed for the isolation of a small number of yellow crystals suitable for an X-ray diffraction study.

This showed them to be $[(PPh_3)_2Ir(H)\{1\text{-}H\text{-}12\text{-}(\eta^6\text{-}C_6H_4F)\text{-}closo\text{-}CB_{11}Me_{10}\}][1\text{-}H\text{-}closo\text{-}CB_{11}Me_{11}]$, **21** (Figure 17).

The solid-state structure shows that the $[1\text{-}H\text{-}closo\text{-}CB_{11}Me_{11}]^-$ anion has undergone a B-CH_3 bond cleavage reaction with C_6H_5F, the solvent, to afford the arene-substituted anion. There is no disorder in the anion methyl positions, with the cage carbon unambiguously identified, revealing that the anion functionalisation has occurred at the 12 position affording $[1\text{-}H\text{-}12\text{-}(C_6H_4F)\text{-}closo\text{-}CB_{11}Me_{10}]^-$ (Figure 18). Related 12-aryl substituted derivatives of $[1\text{-}R\text{-}closo\text{-}CB_{11}Me_{11}]^-$ have been synthesised by a $[Li]^+$ Lewis-acid catalysed reaction, generating the anion $[1\text{-}(C_6H_{12}O_2)B\text{-}12\text{-}(4'\text{-}Br\text{-}C_6H_4)\text{-}closo\text{-}CB_{11}Me_{10}]^-$ that has also been structurally characterised (Figure 18 and Chapter One for synthetic details).[40] DFT calculations show that the lower hemisphere of the cage bares the most negative charge, and this is consistent with the B-CH_3 activation at this position by a Lewis-acid (see Chapter Two).[41]

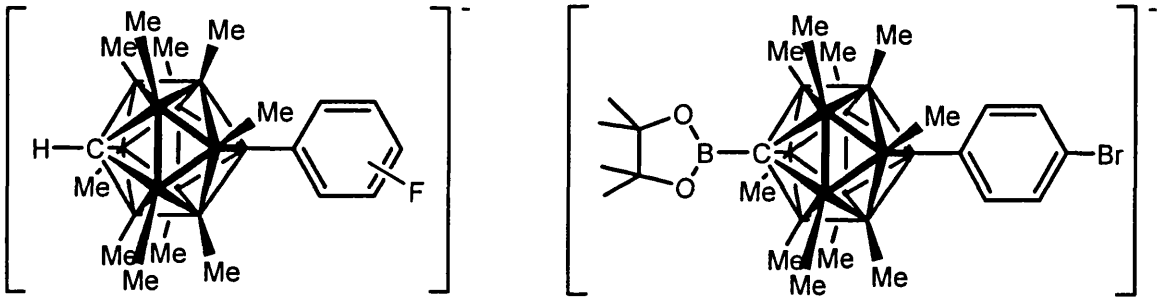

85%:15% ratio *meta:para* (by X-ray) 100% *para*-isomer

Figure 18: The two related crystallographically characterised $[1\text{-}R\text{-}12\text{-}aryl\text{-}closo\text{-}CB_{11}Me_{10}]^-$ anions.

In compound **21** the fluorine occupies three sites (two *meta* and one *para*), resulting in an overall occupancy ratio determined by X-ray crystallography

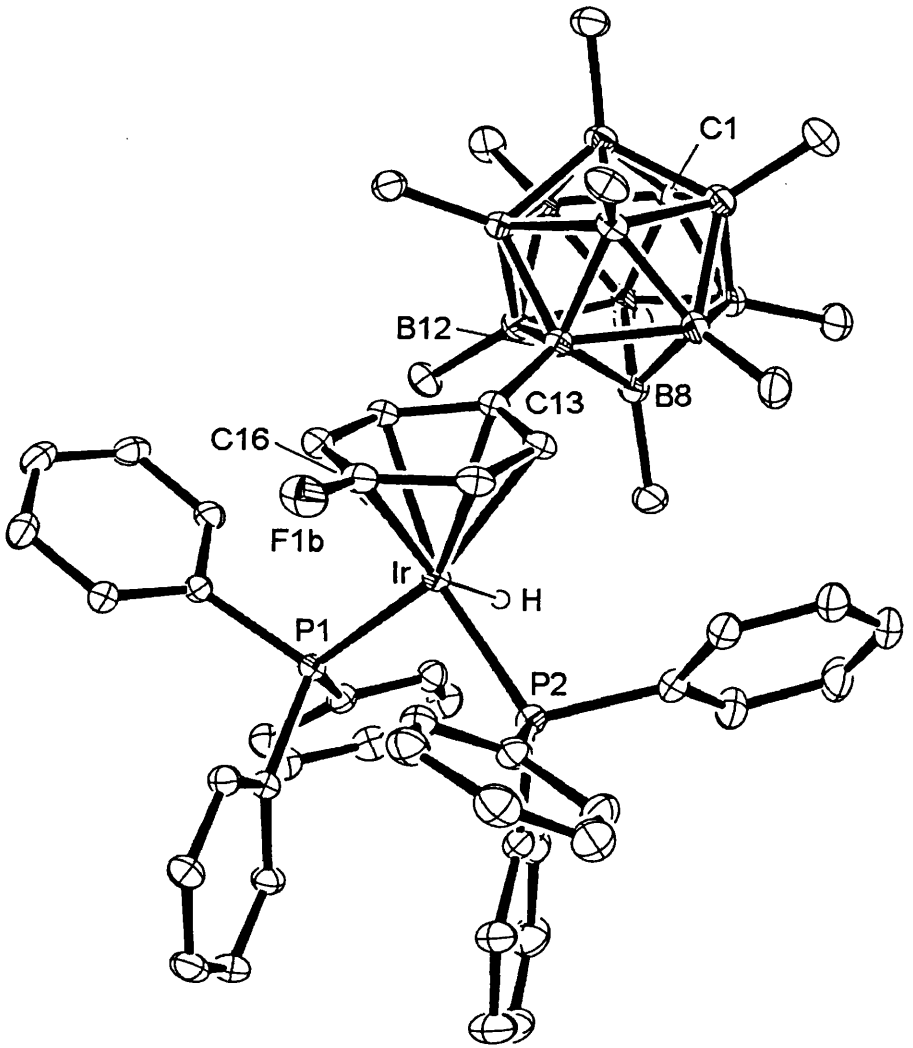

Figure 17: Molecular structure of the cationic portion of complex **(21)**, the fluorine is disordered over *meta* and *para* sites, with only the *para* position shown. Hydrogen atoms apart from the Ir-H are not shown for clarity. Thermal ellipsoids are shown at the 30% probability level.

Ir-P1	2.3138(6)
Ir-P2	2.3159(6)
Ir-H	1.41(3)
P1-Ir-P2	97.83(2)
P1-Ir-H	84.3(14)
P2-Ir-H	80.5(14)
B12-C13	1.591(3)
Ir-C13	2.438(2)
Ir-C14	2.332(2)
Ir-C15	2.373(2)
Ir-C16	2.384(2)
Ir-C17	2.285(2)
Ir-C18	2.309(2)
C13-C14	1.421(3)
C13-C18	1.427(3)
C14-C15	1.407(3)
C15-C16	1.393(4)
C16-C17	1.411(4)
C17-C18	1.408(3)

Table 1: Selected bond Lengths (Å) and Angles (°) for complex **(21)**.

of 85%:15% (*meta*:*para*). This is in contrast to [1-($C_6H_{12}O_2$)B-12-(4'-Br-C_6H_4)-*closo*-$CB_{11}Me_{10}$]$^-$, which is formed cleanly as the *para* isomer. The B-C_{aryl} bond length in **21** (1.591(3) Å) is similar to that in [1-($C_6H_{12}O_2$)B-12-(4'-Br-C_6H_4)-*closo*-$CB_{11}Me_{10}$]$^-$ (1.597(3) Å). The bound arene in **21** is asymmetrically η^6 coordinated to the $\{(PPh_3)_2IrH\}^{2+}$ fragment (all C-C distances are the same within errors), with Ir-C_{aryl} distances ranging from 2.285(2) Å to 2.438(2) Å. The asymmetric nature of this coordination presumably helps minimise the steric repulsion between the two PPh_3 groups and the bulky anion. The cage bound aryl carbon (C12, Figure 17) has the longest Ir-C length (2.438(2) Å), consistent with this the carborane also moves away from the PPh_3 ligands, tilted by 7.3° above the arene plane. The hydride ligand was located and freely refined in the final electron difference map. The Ir-H distance is 1.41(3) Å comparable, within errors, to that of the related complex, [(N-C^5-N-Tp-H)Ir(PPh_3)$_2$H][BF_4] (1.52(7) Å, Figure 19 - **A**), where the hydride was also located.[42] Both phosphines in **21** are bent back from lying orthogonal to the arene ring, consistent with the presence of a hydride and generating a *pseudo* octahedral environment around the iridium, with the carborane functionalised arene capping one face. This produces a compound geometrically analogous to [(N-C^5-N-Tp-H)Ir(PPh_3)$_2$H][BF_4] (Figure 19).[42]

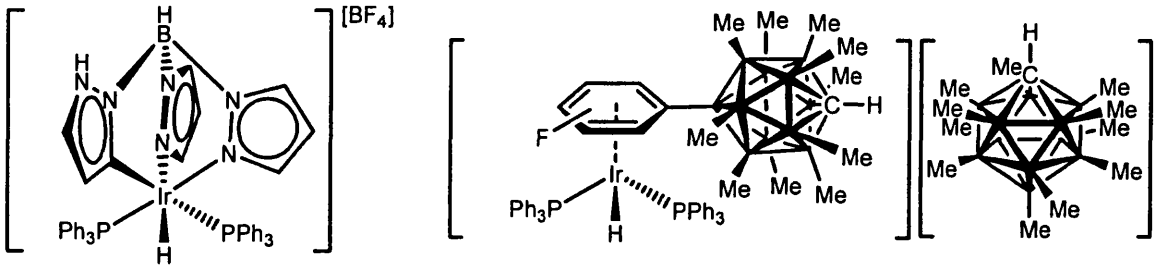

Figure 19: The geometrically and chemically related complexes, [(N-C^5-N-Tp-H)Ir(PPh_3)$_2$H][BF_4] and **21**.

The overall formulation as an Ir(III) centre comes from the presence of two anions in the asymmetric unit, a coordinated arene functionalised anion and a non-proximate, unfunctionalised anion. Compound **21**, as far as we are aware, is the first characterised Ir-fluorobenzene complex (or a derivative thereof); Ru(II), Cr(0), and Rh(I) fluorobenzene complexes are known.[43-45] Cationic iridium phosphino-hydride complexes have been reported to coordinate with other more electron rich arenes (*e.g.*, $[Ir(\eta^6\text{-}1,3,5\text{-}Me_3\text{-}C_6H_3)(^iPr_3P)(H)_2][BF_4]$).[46] Mass spectroscopy on the crystalline material revealed the presence of the parent cation $[(PPh_3)_2Ir(H)\{1\text{-}H\text{-}12\text{-}(\eta^6\text{-}C_6H_4F)\text{-}closo\text{-}CB_{11}Me_{10}\}]^+$ (FAB+ mode, m/z 1095.5 with the correct isotopic distribution pattern) and the free functionalised anion $[1\text{-}H\text{-}12\text{-}(\eta^6\text{-}C_6H_4F)\text{-}closo\text{-}CB_{11}Me_{10}]^-$ (FAB- mode, m/z 377.3) in addition to the unsubstituted anion $[HCB_{11}Me_{11}]^-$ (m/z 297.3). Due to the small number of crystals of complex **21** isolated it was not possible to obtain any further clean spectroscopic data, thus definitive characterisation resides only on the solid-state structure and mass spectroscopy.

Repeated attempts to obtain a larger quantity of crystalline material of complex **21** for complete spectroscopic analysis failed. NMR spectra run on crude samples showed a mixture of compounds, the predominant component always being $[\{IrH(PPh_3)_2\}_2(\mu\text{-}H)_3]^+$. However, by comparison with the closely related complex **A**, (Figure 19), it was possible to identify a hydride signal in the ^1H NMR spectrum potentially ascribable to complex **21**. The major isomer, as based on the crystallographically determined *meta:para* ratio, present in solution will be the *meta* fluorinated arene anion. This isomer of **21** possesses inequivalent phosphine environments, making the expected hydride signal a doublet of doublets. In a C_6D_6 solution of the crude reaction mixture the only hydride signal in the ^1H NMR that is not

assigned to the dimer $[\{IrH(PPh_3)_2\}_2(\mu\text{-}H)_3]^+$ is a doublet of doublets at δ -23.90 ppm, shifted upfield from that in **A**, (δ −18.91 ppm). The coupling constants of this signal ($^2J(PH)$ 13 and 23 Hz) are comparable to that reported for **A** ($^2J(PH)$ 12 and 20 Hz), suggesting that this is the hydride signal associated to **21**. A hydride signal with identical $^2J(PH)$ coupling constants is also observed in CD_2Cl_2 solution at δ -24.36 ppm. Unfortunately, no information could be obtained from the $^{31}P\{^1H\}$ spectrum, due to complex overlapping signals in the region **21** would expect to resonate (δ +15 to δ 0 ppm).

The mechanism for the formation of complex **21** is probably acid based, with one equivalent of H^+ generated for each $[\{IrH(PPh_3)_2\}_2(\mu\text{-}H)_3]^+$ formed (present as the major product). This unsupported proton would then effect B-C bond cleavage by protonlysis, generating the borenium ylide (as discussed in Chapters Three and Four) that could then react with the solvent, C_6H_5F, in an electrophilic substitution reaction producing the observed anion, [1-H-12-(C_6H_4F)-*closo*-$CB_{11}Me_{10}$]$^-$. The trapping of a $\{(PPh_3)_2IrH\}^{2+}$ fragment would then form **21**. The related anion, [*closo*-$CB_{11}Me_{12}$]$^-$ has been previously reported to undergo acid mediated cage decomposition.[39, 47] $[\{IrH(PPh_3)_2\}_2(\mu\text{-}H)_3]$[1-H-*closo*-$CB_{11}Me_{11}$] does not react on standing in C_6H_5F to generate **21**, ruling out this as an intermediate on the pathway to **21**. This means the hydride bridged dimer and **21** must form by parallel routes.

With a reactivity pattern for the hydrogenation of $[(PPh_3)_2Ir(COD)]$[1-H-*closo*-$CB_{11}Me_{11}$] similar to that reported for the $[PF_6]^-$ and $[BAr_F]^-$ analogues (albeit with cage decomposition also observed) [1-H-*closo*-$CB_{11}Me_{11}$]$^-$ can be classed as less coordinating than [*closo*-$CB_{11}H_6Br_6$]$^-$ with respect to the $\{(PPh_3)_2IrH_2\}^+$ fragment. In an

attempt to produce more stable complexes that may exhibit M···anion interactions the related rhodium precursors were synthesised and their reactivity with H_2 investigated.

5.2.2: Hydrogenation Reactions of $[(PR_3)_2Rh(NBD)][Y]$ (R = ^{i}Pr or Cy, Y = [1-H-*closo*-$CB_{11}Me_{11}]^-$ or $[BAr_F]^-$).

The precursor complexes $[(PR_3)_2Rh(NBD)][Y]$ (R = ^{i}Pr or Cy, Y = [1-H-*closo*-$CB_{11}Me_{11}]^-$ or $[BAr_F]^-$) are readily prepared in a two step synthesis from $[(NBD)RhCl]_2$ in an analogous manner to the [*closo*-$CB_{11}H_{12}$] congener.[28] Orange crystalline material is obtainable in reasonable yield (~ 50%) for each compound from the diffusion of hexanes into a saturated CH_2Cl_2 solution.

5.2.2.1:$[(^iPr_3P)_2Rh(H_2)_x(H)_2][Y]$ (x = 1 or 2).

Treatment of a stirred solution of $[(^iPr_3P)_2Rh(NBD)][1\text{-H-}closo\text{-}CB_{11}Me_{11}]$ in CD_2Cl_2 with ~ 4 atmospheres of H_2 (generated by backfilling a degassed sample with H_2 at 77 K, the pressure on warming to room temperature should be *ca.* 4 atmospheres, 298/77 = 3.9) resulted in the reduction of the diene and the rapid formation of a pale yellow solution. The ^{1}H NMR spectrum at 298 K showed one set of signals for the ^{i}Pr groups, and one broad hydride signal centred at δ –8.62 ppm of integral 3.6 H (compared to the ^{i}Pr signals), no resonance for free dihydrogen (δ 4.60 ppm) was observed, suggesting a fluxional process involving free and coordinated H_2. Similar room temperature ^{1}H NMR spectra are reported for the complexes $(^iPr_3P)_2Ru(H_2)_2(H)_2$ (δ ^{1}H hydride, -8.31 ppm) and $[(PCy_3)_2Ir(H_2)_2(H)_2]^+$ (δ ^{1}H hydride, broad singlet –8.3

ppm).[11, 48] The $^{31}P\{^{1}H\}$ NMR spectrum showed the formation of a single phosphine containing product, a broadened doublet centred at δ60.4ppm (^{1}J(RhP) 107 Hz). Cooling this sample below 220 K resulted in the freezing out of some of the exchange processes and the $^{31}P\{^{1}H\}$ NMR spectrum at 200 K showed two phosphine containing products, both doublets (δ 68.4 ppm ^{1}J(RhP) 92 Hz and δ62.1 ppm ^{1}J(RhP) 100 Hz), with the ratio of the resonances approximately 2:1. The ^{1}H NMR spectrum at this temperature showed five new resonances in the hydride region (Figure 20).

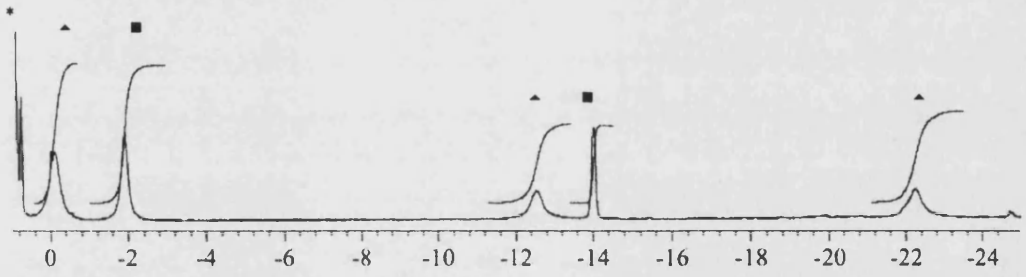

Figure 20: The hydride region of the ^{1}H NMR spectrum at 200K of the products from the hydrogenation of $[(^{i}Pr_3P)_2RhNBD][Y]$. * = ^{i}Pr CH_3 groups. ▲ = $[(^{i}Pr_3P)_2Rh(H_2)(H)_2(CH_2Cl_2)]^+$ and ■ = $[(^{i}Pr_3P)_2Rh(H_2)_2(H)_2]^+$.

By comparison to the related compounds, $[(PR_3)_2Ir(H_2)_xH_2][Y]$ (where Y is a weakly coordinating anion and x = 1 or 2),[11, 15, 16, 48] these two complexes are formulated as the mono cations, $[(^{i}Pr_3P)_2Rh(H_2)_2(H)_2]^+$, **22-($H_2$)$_2$** (■) and $[(^{i}Pr_3P)_2Rh(H_2)(H)_2(CH_2Cl_2)]^+$, **22-($H_2$)** (▲) in a 1:2 ratio (Figure 21). The assignment of the sixth ligand in the mono-dihydrogen adduct, **22-(H_2)** as a molecule of dichloromethane is tentative as there is no direct spectroscopic evidence for coordinated CH_2Cl_2, though it should be noted that this is often the case.[49-51] However, an agostic interaction can be ruled out, as for octahedral complexes analogous to **22**, hydrides *trans* to an agostic interaction or a 'vacant' site resonate significantly further upfield in the ^{1}H NMR spectrum (*e.g.*, $[(P^{t}Bu_2Ph)_2Ir(H_2)(H)_2][BAr_F]$ (-41.2 ppm)[16] and $[(P^{t}Bu_2Ph)_2Ir(H)_2I]$ (-44.4 ppm)[52]) to that observed in **22-(H_2)** (-22.42 ppm). In contrast,

hydride ligands *trans* to coordinated CH_2Cl_2 molecules (*e.g.*, $[(PPh_3)_2Ir(H)_2(CH_2Cl_2)][closo\text{-}CB_{11}H_6Br_6]$, {-23.2 ppm} and $[(^iPr_3P)_2Pt(H)(Cl_2CH_2)][BAr_F]$, {-22.8 ppm}) do resonate in this region.[33, 49]

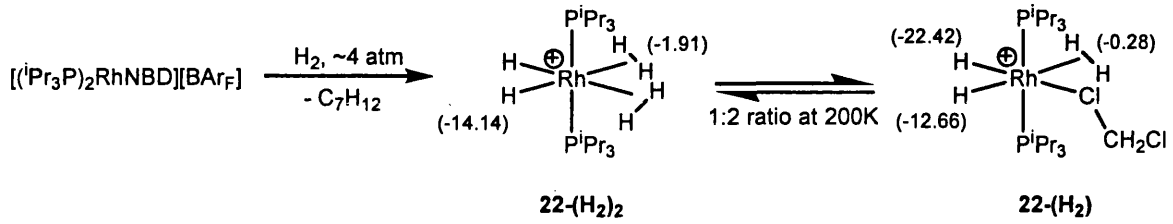

Figure 21: The products from hydrogenation of $[(^iPr_3P)_2Rh(NBD)]^+$ under 4 atmospheres of H_2 (NMR chemical shifts of the hydride resonances at 200K are shown in parentheses).

These assignments were confirmed both by T_1 measurements at 200 K (400 MHz) and the observation of a HD coupling constant in partially deuterated samples. The T_1 values (Figure 22) are consistent with the three hydride resonances between –12.66 ppm and –22.42 ppm being classical hydrides (> 80 ms) and the resonance at –1.91 ppm corresponding to a coordinated dihydrogen ligand (<50 ms).[53] Unfortunately, the T_1 measurement for the resonance at –0.28 ppm (94 ms) is outside the range normally seen for η^2-H_2 ligands, although this may though be due to the presence of vacuum grease that is coincident with this signal, formulation as a Rh(V) complex is unreasonable though.

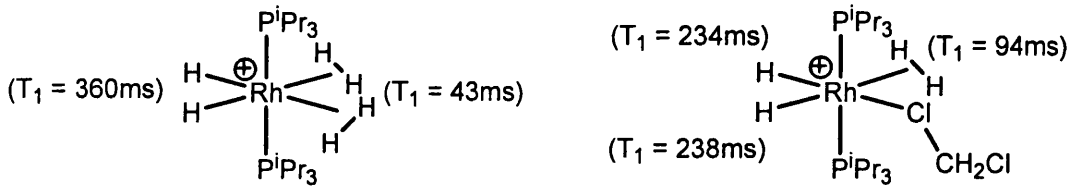

Figure 22: The T_1 measurements for **22-(H$_2$)$_2$** and **22-(H$_2$)** at 200 K and 400 MHz.

All the hydride/dihydrogen rhodium complexes previously reported exhibit only a single hydride resonance at all accessible temperatures,[51, 54-56] preventing any direct comparison of their respective T_1 values. The values for **22-(H_2)** and **22-(H_2)$_2$** are in contrast to that reported for $[(PCy_3)_2Ir(H_2)_2(H)_2]^+$ (48 ms IrH_2 and 73 ms IrH), [11] where the T_1 values are believed to be significantly time averaged and not therefore 'true' values for the individual sites.

Degassing a CD_2Cl_2 sample of **22** by three freeze/pump/thaw cycles and subsequently backfilling with D_2 (~ 4 atm.) resulted in a decrease in intensity for all the hydride resonances. The η^2-H_2 resonance corresponding to **22-(H_2)$_2$** in the ^1H NMR spectrum below 220 K was now observed as a broad triplet due to HD coupling, (Figure 23). The asymmetric nature of the triplet is the result of residual dihydrogen, the spectrium of **22-(H_2)$_2$** is super-imposed.

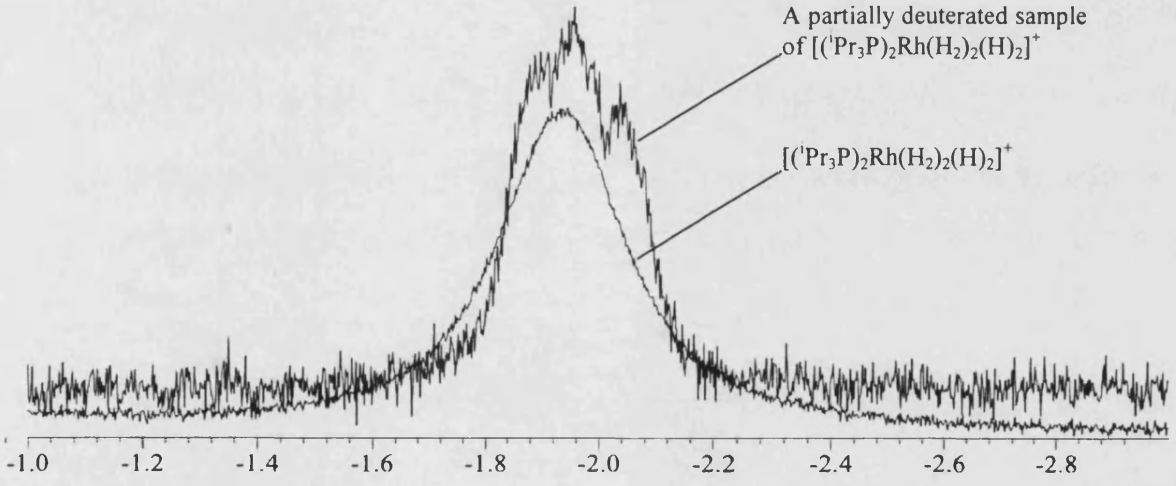

Figure 23: The dihydrogen region of the ^1H NMR spectra at 190 K of the partially deuterated and non-deuterated sample of **22-(H_2)$_2$**.

The formation of HD must occur via a fluxional process affecting the exchange of a coordinated D_2 molecule with a *cis* hydride. An extensive experimental and theoretical treatment of this process has been performed on the related system

$[(P^tBu_2Ph)_2Ir(H_2)_2(H)_2]^+$, where the formation of HD is also observed on the addition of D_2 to $[(P^tBu_2Ph)_2Ir(H)_2]^+$.[16] The fluxional process for site exchange between a cis hydride and H_2 ligands has been proposed to occur via a 'M-H_3' transition state and energy barriers as low as 1.5 kcal/mol have been reported (Figure 24).[12, 57]

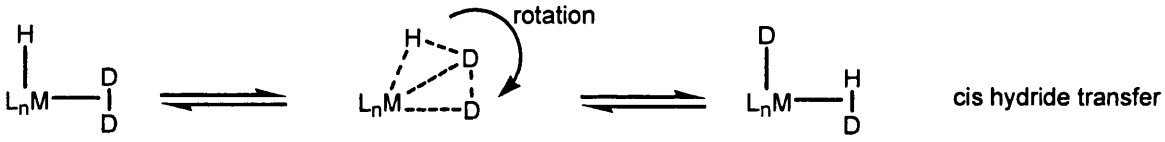

Figure 24: A possible fluxional process explaining the formation of HD via a cis-hydride transfer.

The broad nature of the triplet in Figure 23 is due to the overlapping unresolved resonances for the large number of possible isotopomers that result on the partial deuteration of **22** ($[(^iPr_3P)_2RhH_{6-x}D_x]^+$). Complex, yet well resolved, overlapping isotopomer patterns have previously been observed and accurately simulated in a number of systems, allowing for $^1J(HD)$ coupling constants to be extracted.[48, 51] The inherently broad nature of the dihydrogen resonance associated with the *protio* **22-(H_2)$_2$** and the large number of possible isotopomers prevents a similar well-resolved system being observed here. An accurate value for the ^1J HD coupling constant in **22** therefore was not obtainable, although an approximate value of 29 Hz is obtainable from the broad triplet – but in-depth interpretation of this value (i.e. calculation of the H-H distance) is not valid. Nevertheless, the observation of a HD coupling constant in **22-(H_2)$_2$** is further proof of the existence of an intact H_2 ligand, as classical hydrides would exhibit very small (<2 Hz) (HD) coupling. No triplet was observable for the (H_2) signal in the mono dihydrogen complex, **22-(H_2)**, over the temperature range 180 K-210 K, with deuteration only resulting in a general broadening of this resonance.

An Isotopic Perturbation of Resonance (IPR) is observed for the partially deuterated sample of **22-$(H_2)_2$**, with the broadened triplet (centred at approximately –1.95 ppm), shifted upfield by 44 ppb compared to that of the *perprotio* isotopomer. Similar upfield IPRs have been observed in the cationic rhodium system $[Cp^*Rh(PMe_3)H(H_2)]^+$, showing upfield shifts of 31 ppb (d_1 isotopomer) and 121 ppb (d_2 isotopomer), and in the partially deuterated isotopomers of the isoelectronic $(^iPr_3P)_2Ru(H_2)_2(H)_2$ (40 ppb upfield).[48] A smaller IPR of 20 ppb was also observed for **22-(H_2)** (though there are significant errors inherent in this values due to the extremely broad nature of this resonance), confirming that this signal is indeed due to a dihydrogen ligand.

No deuterium was incorporated into the phosphine iso-propyl groups in **22** in contrast to $(^iPr_3P)_2Ru(H_2)(H)_2$, where H/D exchange occurs and is postulated to proceed via the C-H activation of an agostic complex (Figure 25).[48] Similarly no deuterium was incorporated into the phosphine groups on addition of D_2 to $[(P^tBu_2Ph)_2Ir(H_2)][BAr_F]$ even after prolonged heating.[15]

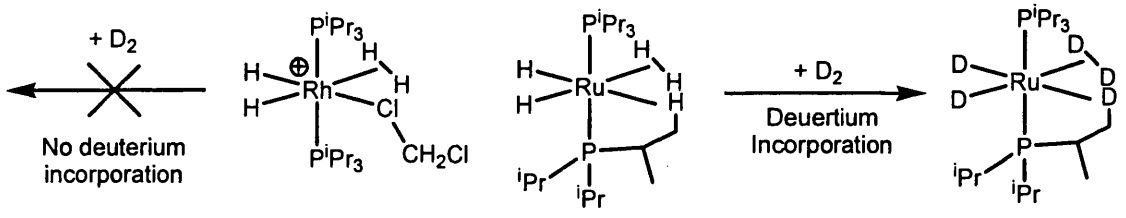

Figure 25: Reactions of the isoelectronic complexes, $[(^iPr_3P)_2Rh(H_2)(H)_2(CH_2Cl_2)]^+$ and $(^iPr_3P)_2Ru(H_2)(H)_2$ with deuterium.

Close examination of the hydride region of **22** over the range 180 K – 200 K revealed a product distribution that was highly temperature dependent (Figure 26).

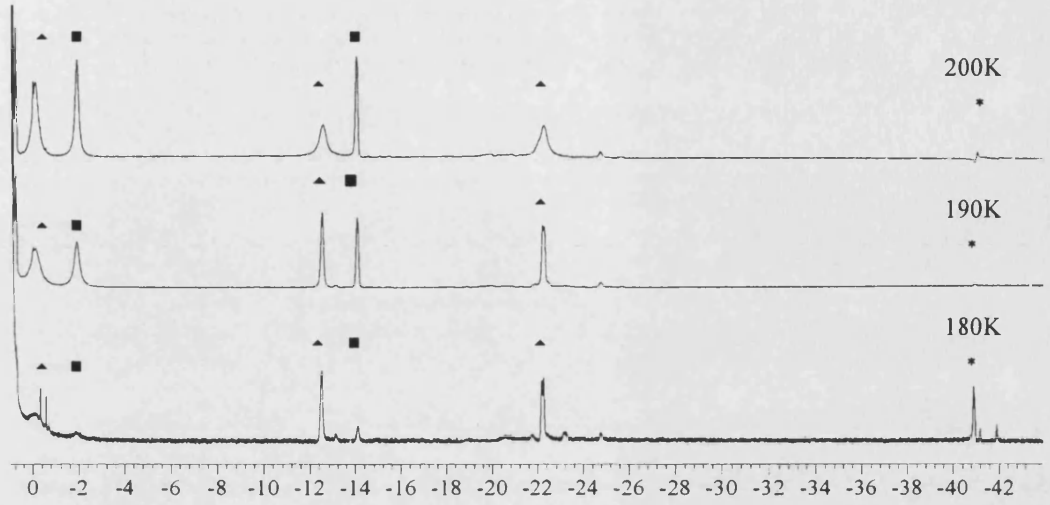

Figure 26: The product distribution of the $\{(^{i}Pr_3P)_2Rh(H)_2\}^+$ fragment under 4 atmospheres of H_2 over the temperature range 180 K to 200 K. ■ = **22-(H_2)$_2$**. ▲ = **22-(H_2)**. * = hydride *trans* to a vacant/agostic site in **22-(H_2)**.

The ^1H NMR spectra at 200 K and 190 K consist of predominantly two complexes, **22-(H_2)$_2$** and **22-(H_2)** as discussed. Interestingly, in each of these spectra there is also a small hydride resonance at –40.9 ppm. On cooling further to 180 K this resonance increases in intensity, concomitant with a significant decrease in **22-(H_2)$_2$**. The reduction in the concentration of **22-(H_2)$_2$** is attributable to a decrease in the solubility of H_2 in CD_2Cl_2 at very low temperatures.[58] The hydride resonance at –40.9 ppm is assigned to a hydride ligand *trans* to a vacant/agostic site in the mono-dihydrogen complex $[(^{i}Pr_3P)_2Rh(H_2)(H)_2]^+$, (Figure 27).

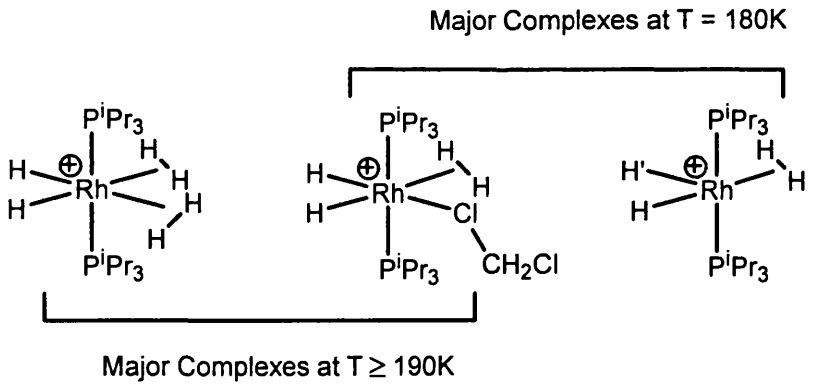

Figure 27: The various complexes observed in the variable temperature ^1H NMR spectra for $\{(^iPr_3P)_2Rh(H)_2\}^+$ under 4 atmospheres of H_2 pressure.

The assignment of this third complex at low temperature is based on the comparison of the chemical shift with other well-characterised Group IX cationic octahedral complexes where a hydride is *trans* to a vacant/agostic site, (*e.g.*, $[(P^tBu_2Ph)_2Ir(H_2)(H)_2][BAr_F]$ {-41.2 ppm},[16] $[(P^tBu_2Ph)_2Ir(H)_2(CO)][BAr_F]$ {-36.5 ppm},[59] $[(P^tBu_2Ph)_2Ir(H)_2][BAr_F]$ {-37.1 ppm}[15] and $(P^tBu_2Ph)_2Ir(H)_2I$ {-44.4 ppm}[52]).

On warming the sample above 220 K, the two hydride resonances assigned to **22-(H_2)** coalesce without any broadening of the dihydrogen resonance. This is consistent with a two-site hydride exchange process through a five coordinate transition state with C_{2v} symmetry (Figure 28), this is an exchange mechanism that for $[(P^tBu_2Ph)_2Ir(H_2)H_2]^+$ has been calculated to have low energetic barriers.[59]

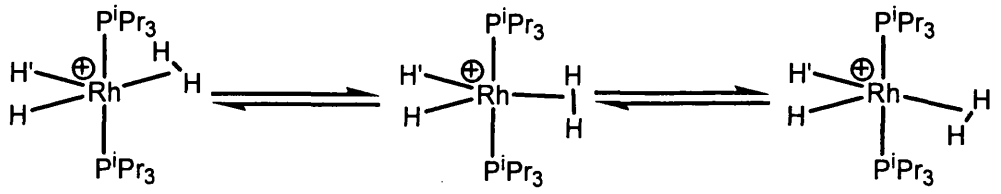

Figure 28: A schematic of the fluxional process that makes the two hydride resonances equivalent in **22-(H_2)**.

Complex **22** is extremely sensitive, decomposing rapidly in the presence of traces of H_2O or O_2 to generate a mixture of unidentified products. It is, however, stable in dichloromethane solutions under a H_2 atmosphere for days at low temperature. This is in contrast to the ruthenium analogues that abstract chloride from CH_2Cl_2 to form $(PR_3)_2Ru(H_2)(H)Cl$.[48, 60] Attempts to isolate solid material of these dihydrogen adducts repeatedly failed, whilst solution IR spectroscopy was not useful in the characterisation of these compounds, with no M-H stretching bands observed. At room temperature under 4 atmospheres of H_2 a gradual decomposition of **22** occurs, that is accelerated on heating, the resultant products of which will be discussed in Chapter 6. Addition of 5 equivalents of MeCN to a freshly prepared sample of **22** resulted in the clean displacement of the dihydrogen ligands and the formation of one new compound, $[(^iPr_3P)_2Rh(H)_2(MeCN)_2]^+$, with the hydride region changing to a well resolved doublet of triplets (centred at δ -19.1 ppm) and a $^{31}P\{^1H\}$ NMR spectrum with a doublet now centred at 59.7 ppm (108 Hz). Analogous dihydrogen displacement by MeCN has been reported for $[(PCy_3)_2Ir(H_2)_2(H)_2]^+$.[11]

In the 180 K ^1H NMR spectrum of **22** under 4 atmospheres of H_2, a further hydride signal of low intensity at 23.11 ppm (Figure 26) is also visible, while the $^{31}P\{^1H\}$ NMR spectrum at this temperature also shows a doublet at 54.5 ppm (^1J (RhP) 111 Hz). This is the only product after the removal of H_2 *in-vacuo*. The ^1H NMR spectrum shows a single integral two hydride resonance at a similar position (δ -23.18 ppm) that is now fully resolved into a doublet of triplets. This new complex is assigned as a dichloromethane adduct, **22-DCM** (Figure 29).

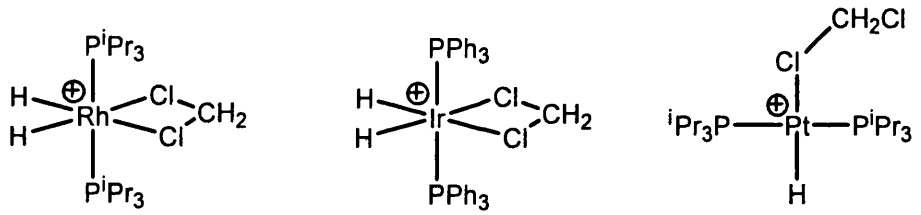

Hydride Chemical Shift (298K)	-24.36ppm (22-DCM)	-23.2ppm	-22.8ppm

Figure 29: Cationic metal-dichloromethane complexes with a *trans*-hydride geometry, along with their respective chemical shifts.

At room temperature the doublet of triplets remains, though shifted upfield to –24.36ppm. This resonance is in a similar region to that reported for known cationic complexes where a hydride is *trans* to a coordinated dichloromethane molecule (*e.g.*, $[(PPh_3)_2Ir(H)_2(CH_2Cl_2)][closo\text{-}CB_{11}H_6Br_6]$, {-23.2 ppm} and $[(^iPr_3P)_2Pt(H)(CH_2Cl_2)][BAr_F]$, {-22.8 ppm}, Figure 29).[33, 49] An anion coordinated complex can be discounted due to the identical spectra observed (apart from the anion resonances) on moving from $[1\text{-}H\text{-}closo\text{-}CB_{11}Me_{11}]^-$ to $[BAr_F]^-$. A formulation as a bis-agostic complex is also unfavoured due to the absence of any extremely high field resonance such as are observed for the hydrides in the cation $[(P^tBu_2Ph)_2Ir(H)_2]^+$ {-36.5 ppm}.[15] However, no resonances attributable to coordinated dichloromethane were observable by NMR spectroscopy at 180 K. The formation of a dichloromethane adduct, **22-DCM** when **22** is not stored under H_2 is in contrast to the behaviour of $(^iPr_3P)_2Ru(H_2)_2(H)_2$, which under vacuum forms the hydride bridged dimer, $(^iPr_3P)_2(H)Ru(\mu\text{-}H)_3Ru(H)_2(^iPr_3P)_2$, (Figure 30).[48]

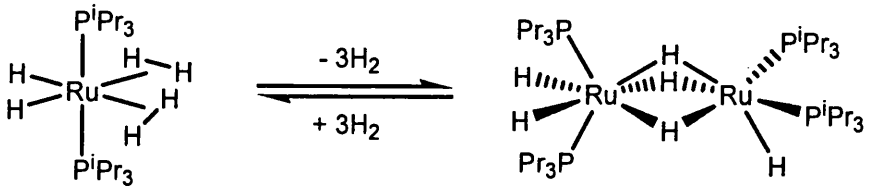

Figure 30: The reversible formation of the hydride bridged dimer resulting when $(^iPr_3P)_2Ru(H_2)_2(H)_2$ is not kept under a H_2 atmosphere.

The facile loss of H_2 from **22-(H_2)$_2$** is also different to the iridium complex $[(PCy_3)_2Ir(H_2)_2(H)_2]^+$ which exists only as the bis-dihydrogen adduct at -80°C under no H_2 pressure. This is probably due to the stronger bonds that 5d metals form when compared to their respective 4d metal complex.[51] Addition of 4 atmospheres of H_2 to **22-DCM** results in room temperature NMR spectra consistent with the reformation of the mono and bis dihydrogen adducts, the displacement of coordinated CH_2Cl_2 by H_2 in Group IX cationic metals has been previously documented[15, 51] and in fact is an established route to dihydrogen complexes of the transition metals.[12, 50]

Attempts to isolate the postulated dichloromethane complex, **22-DCM** repeatedly failed with both the $[BAr_F]^-$ and [1-H-*closo*-$CB_{11}Me_{11}]^-$ anions. This is possibly due to its inherent instability, with decomposition of **22-DCM** fully occurring in solution within 24 hours to give a complex mixture (*vide infra*). Some yellow crystals of sufficient quality for an X-ray diffraction study were obtained from the $[BAr_F]^-$ analogue in small quantity on recrystallisation of the decomposition products. This allowed for the identification of one of the decomposition products as $[\{(^iPr_3P)_2Rh(H)\}_2(\mu\text{-}Cl)_2][BAr_F]_2$, **23** (Figure 31). The asymmetric unit consists of a folded $(^iPr_3P)_2Rh(\mu\text{-}Cl)_2Rh(^iPr_3P)_2$ dimer, with two non-proximate $[BAr_F]^-$ anions, making the dimer dicationic overall. The Rh-Rh distance (3.5892(3) Å) and the large hinge angle (153.8° at the Cl···Cl vector) precludes any metal-metal interaction. Two possible explanations can equally account for the dicationic nature of the dimer. (i) A mixed Rh(I)/Rh(III) dimer, and such dimers structurally similar to **23** are documented (Figure 32).[61, 62] (ii) A Rh(III)/Rh(III) dimer with two hydrides, similar to the iridium and rhodium dimers, $[\{M(H)(PPh_3)_2\}_2(\mu\text{-}Cl)_2(\mu\text{-}H)]^+$ (M = Rh or Ir). NMR

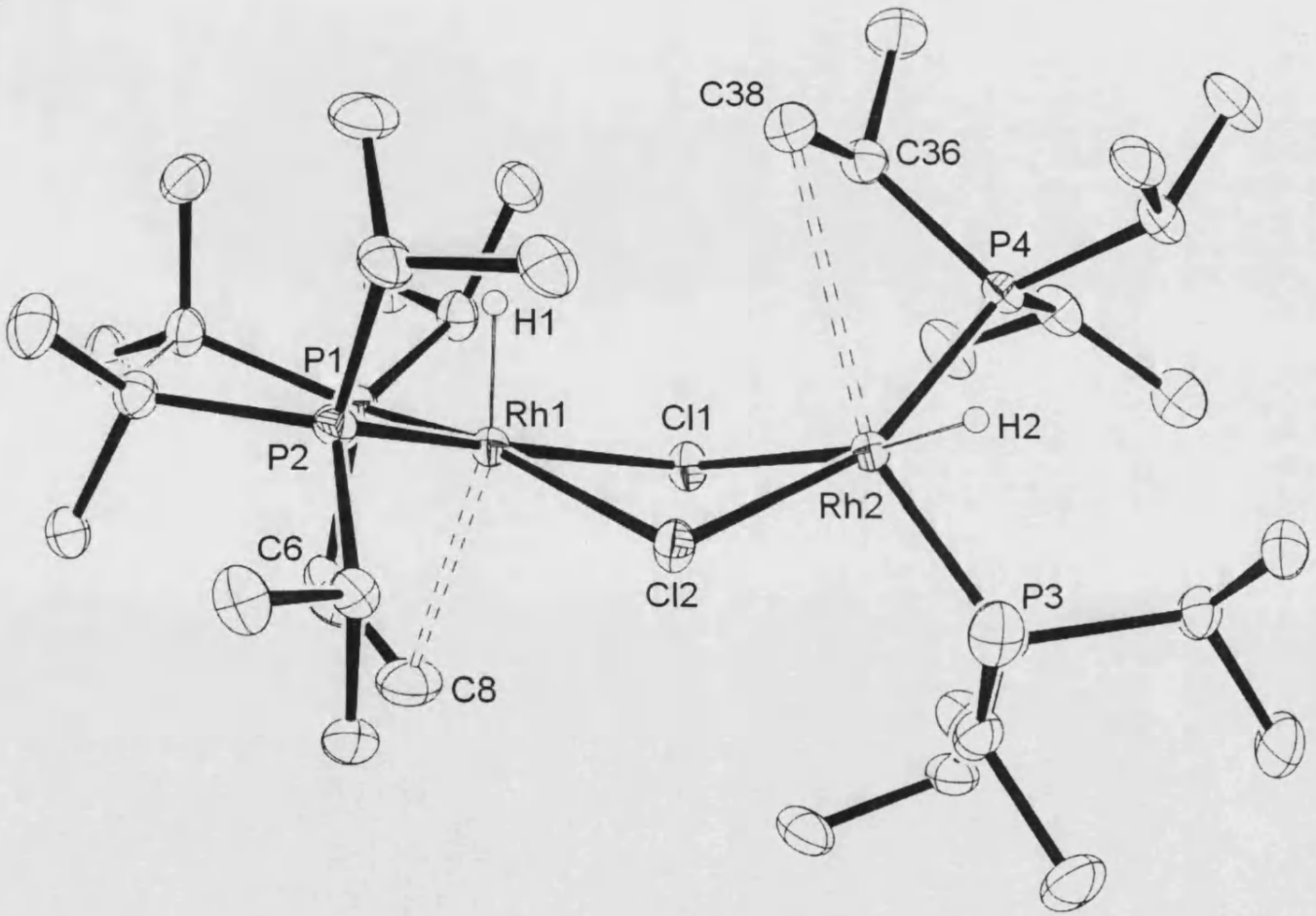

Figure 31: The molecular structure of the dicationic portion of complex **(23)**. Hydrogens atoms, apart from the two rhodium hydrides are not shown for clarity. Thermal ellipsoids are shown at the 30% probability level.

Rh1-Cl1	2.4069(8)
Rh1-Cl2	2.4342(8)
Rh1-P1	2.3194(9)
Rh1-P2	2.3216(9)
Rh1-H1	1.40(5)
Rh1-C8	2.980(4)
Rh1-Rh2	3.5892(3)
Rh1-P1-C6	100.19(12)
P1-C6-C8	111.9(3)
P1-Rh1-P2	106.82(3)
C8-Rh1-H1	152(2)
Rh2-Cl1	2.4737(8)
Rh2-Cl2	2.4066(8)
Rh2-P3	2.2227(9)
Rh2-P4	2.2918(8)
Rh2-H2	1.52(4)
Rh2-C38	3.154(4)
Rh2-P4-C36	94.55(12)
P4-C36-C38	112.6(3)
P3-Rh2-P4	104.48(3)
C38-Rh2-P3	155.66(8)
H2-Rh2-Cl1	170.1(15)

Table 2: Selected bond Lengths (Å) and Angles (°) for complex **(23)**.

spectroscopy could easily distinguish between these two sets of complexes, but unfortunately the few remaining crystals of **23** rapidly melted at room temperature resulting in their recombination with the crude oil that had also formed. A ^{1}H NMR spectrum of this mixture did show two hydride resonances, but due to the unclean nature of the system it is impossible to assign either to **23** with any confidence, therefore the characterisation of **23** is based solely on the X-ray crystallography study as repeated attempts to grow and isolate crystalline material of **23** were unsuccessful. Two hydrides could be located and freely refined in the final electron difference map (given the usual caveats about the observation and location inherent from the low scattering factor of hydrides) and one found to be terminally bound to each rhodium

Formulation as a Rh(I)/Rh(III) dimer is further discounted after close examination of the geometry around each rhodium centre. The environment around Rh2 is clearly not square planar with P3 appearing to occupy an axial position of a distorted octahedron. The situation involving Rh1 is less straightforward with a square planar geometry observed (sum of angles about Rh1 of 360.8°), consistent with that expected for a mixed Rh(I)/Rh(III) dimer. However, the P_2RhCl_2 core is not planar as expected for a Rh(I) centre, (*e.g.*, in the solid state structure of $\{(^{i}Pr_3P)_2Rh(\mu\text{-}Cl)\}_2$ and $RhCl(PCP)(\mu\text{-}Cl)_2Rh(COD)$ Figure 32))[61, 63] with a P1-Rh1-Cl2 angle bent out of the plane (163.04(3)°).

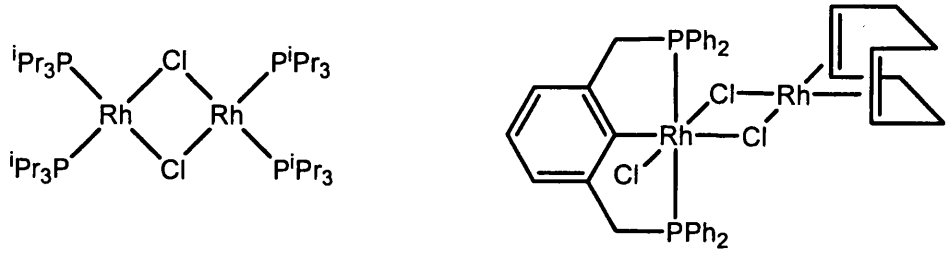

Figure 32: Examples of planar Rh_2Cl_2 cores in a Rh(I)/Rh(I) and a Rh(I)/Rh(III) dimer.

In addition the Rh-P bond lengths are significantly greater in **23** (Rh1-P1 2.3194(9) Å and Rh1-P2 2.3216(9) Å) than that for $\{(^{i}Pr_3P)_2Rh(\mu\text{-}Cl)\}_2$, (2.262(2) Å and 2.246(2) Å).[63] Finally, one of the pendant CH_3 groups of a phosphine has a close approach to the rhodium centre (Rh1-C8 2.980(4) Å), which whilst greater than the sum (2.81 Å) of the ionic radius for Rh(III) (0.81 Å) and the van der Waals radius of CH_3 (2.00 Å) is significant due to the considerable deformation of the involved ^{i}Pr group (Rh1-P1-C6 100.19(12)°), in comparison to those non bonded (average Rh1-P-C angle of 114.6°). These findings combined with the predominance of M(III)/M(III) dimers as the decomposition products resulting from the hydrogenation of diene precursors strongly suggest that Rh1 is equally in the +3 oxidation state. To achieve charge balance two hydrides therefore must also be associated with the dimer. Examination of the penultimate electron difference map indeed revealed the presence of two hydrides (given the usual caveats for the detection of hydrides using X-ray data), one terminally bound to each rhodium. This is in contrast to the related mono-cationic decomposition product, $[\{Rh(H)(PPh_3)_2\}_2(\mu\text{-}Cl)_2(\mu\text{-}H)]^+$ (Figure 33), where the two rhodium centres are bridged in addition to two chlorides by a hydride and a metal-metal bond. The formation of which also involves activation of CH_2Cl_2, the solvent.[22] Importantly, $[\{Rh(H)(PPh_3)_2\}_2(\mu\text{-}Cl)_2(\mu\text{-}H)]^+$ and a related iridium decomposition product, $[\{IrH(PR_3)_2\}_2(\mu\text{-}H)_3][PF_6]$.[1] were formed under H_2 pressure – possibly accounting for the additional bridging hydride present in each.[22]

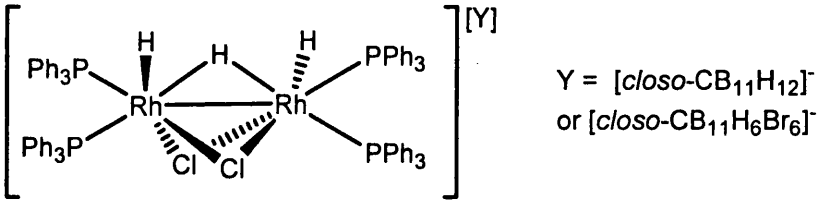

Figure 33: The cation portion of the deactivation product, $[(PPh_3)_2HRh(\mu\text{-}Cl)_2(\mu\text{-}H))RhH(PPh_3)_2]^+$

In **23** the hydride associated with Rh2 is located *trans* to a bridging chloride (Cl1-Rh2-H2 170.1(15)°), and the large *trans* effect of the hydride ligand is clearly visible in the lengthening of the *trans* Rh-Cl bond (Rh2-Cl1 2.4737(8) Å, in comparison to Rh2-Cl2 2.4066(8) Å), confirming its correct location. A similar effect is observed in $RhCl(PCP)(\mu\text{-}Cl)_2Rh(COD)$, where the bridging chloride *trans* to the larger *trans* effect ligand (phenyl) has a considerably longer bond length (2.555(3) Å) than that *trans* to a terminal chloride (2.377(2) Å).[61] The second hydride, H1 is located *trans* to the β agostic interaction and completes the distorted octahedral environment around Rh1. The octahedral geometry around Rh2 is equally completed by one very long β agostic bond, (Rh2-C38 3.154(4) Å). The two agostic interactions in **23** are long in comparison to the only other six coordinate Rh(III) agostic compound, $Rh(2,4,6\text{-}Me_3\text{-}C_6H_2)_3$ (Figure 34),[64] where there are three agostic interactions with Rh(III)···H_3C distances of 2.78, 2.78 and 2.79 Å (no errors reported), implying that those in **23** are at best only weak contacts.

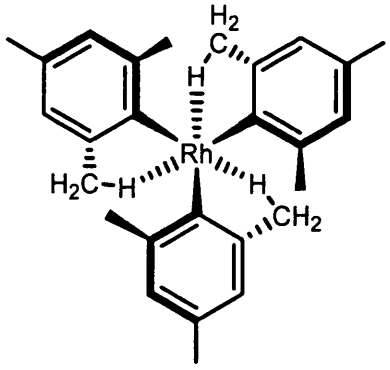

Figure 34: The only other structurally characterised Rh(III) six coordinate agostic complex, $Rh(2,4,6\text{-}Me_3\text{-}C_6H_2)_3$.

The arrangement of the two sets of phosphine groups in **23** respectively 'perpendicular' to each other minimises the unfavourable steric congestion and this is the most likely cause of the deviation away from a pure octahedral geometry observed

at both rhodium centres. The numerous other products formed alongside **23** precludes any in-depth discussion into a mechanism, but the substitution of a hydride for a chloride on a metal centre utilising chlorinated solvents is well documented and is likely to be taking place here (Figure 35).[65]

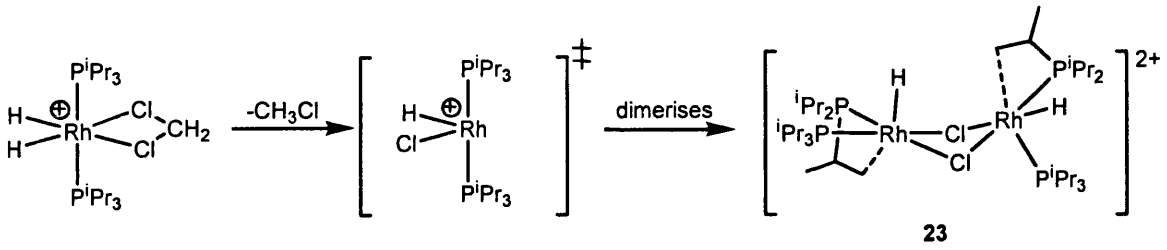

Figure 35: A possible mechanism accounting for the formation of the observed dimer, **23**.

A further attempt to obtain crystalline material of a *solvento* complex of the fragment $\{(^{i}Pr_3P)_2Rh(H)_2\}^+$ from C_6H_5F and pentane led to the formation of yellow needles suitable for an X-ray diffraction study. The asymmetric unit (Figure 36) contains two crystallographically inequivalent molecules of the compound $[(\eta^6\text{-}C_6H_5F)Rh(^{i}Pr_3P)_2][BAr_F]$, **24**, the structural metrics of which are identical within errors, therefore only one will be discussed here. The C_6H_5F molecule in **24** is η^6 coordinated to the $\{(^{i}Pr_3P)_2Rh\}^+$ fragment (with all C-C distances effectively identical) and the arrangement of the phosphines is planar with respect to the Rh-arene vector. The combination of the η^6 bonded arene and the planar P-Rh-P arrangement further precludes the presence of any hydride ligands in **24**. Similar capping of $\{(PR_3)_2Rh\}^+$ fragments by arenes has been previously reported, though with the more electron rich arenes, $C_6H_5CH_3$ and $C_6H_2(CH_3)_4$. [31, 66] As discussed earlier for complex **21**, C_6H_5F complexes has been documented to bind to cationic metal centres.[43, 44] The only other structurally characterised Rh(I)-C_6H_5F adduct shows significantly different coordination behaviour, with either a monomeric η^4 or a bridging *anti*-μ-η^4-η^4 fluorobenzene

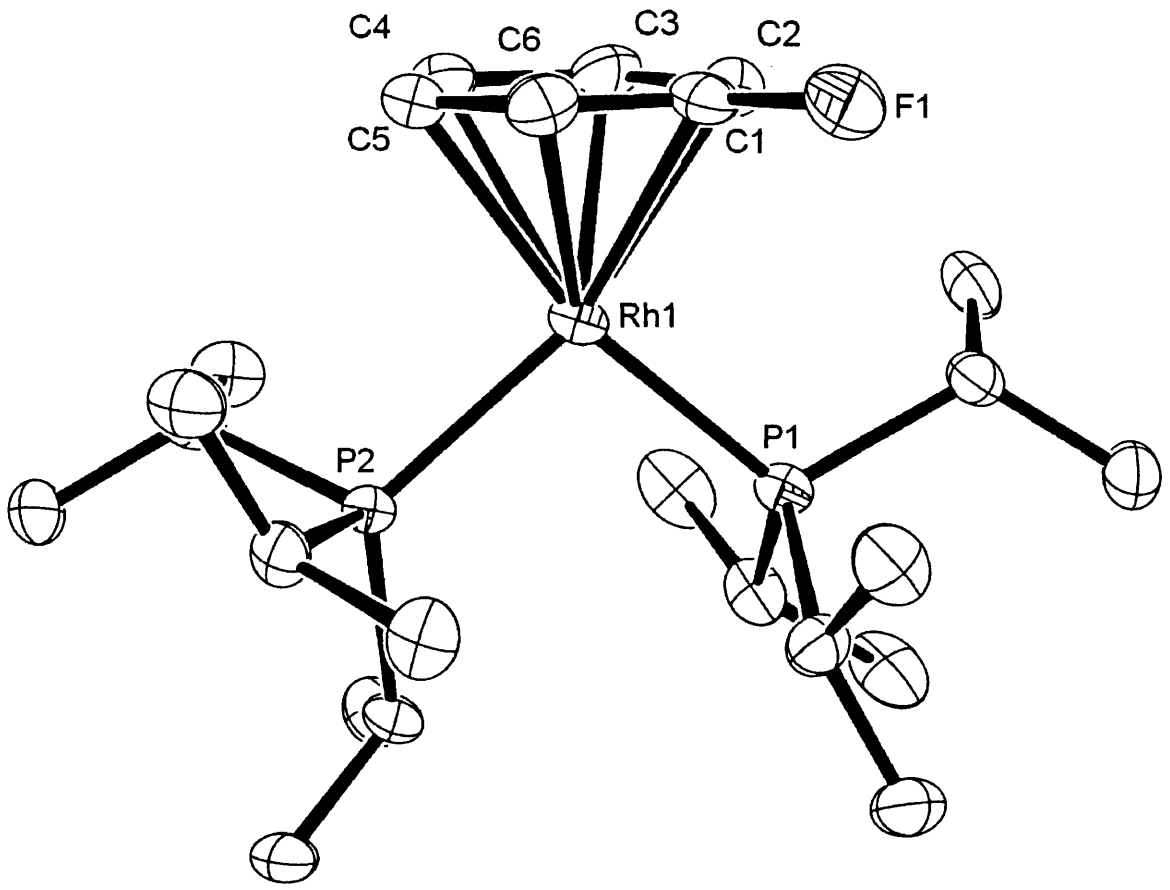

Figure 36: Molecular structure of one of the crystallographically inequivalent cationic portions from the ASU of complex **(24)**. Hydrogens atoms are not shown for clarity. Thermal ellipsoids are shown at the 30% probability level.

Rh1-P1	2.304(2)
Rh1-P2	2.326(2)
Rh1-C1	2.362(9)
Rh1-C2	2.313(9)
Rh1-C3	2.338(9)
Rh1-C4	2.311(9)
Rh1-C5	2.302(9)
Rh1-C6	2.361(8)
C1-F1	1.342(12)
P1-Rh-P2	98.19(7)

Table 3: Selected bond Lengths (Å) and angles (°) for complex **(24)**.

complex formed, (Figure 37), the considerable steric demand of the β-diiminate ligand is responsible for these unusual bonding motifs.[67]

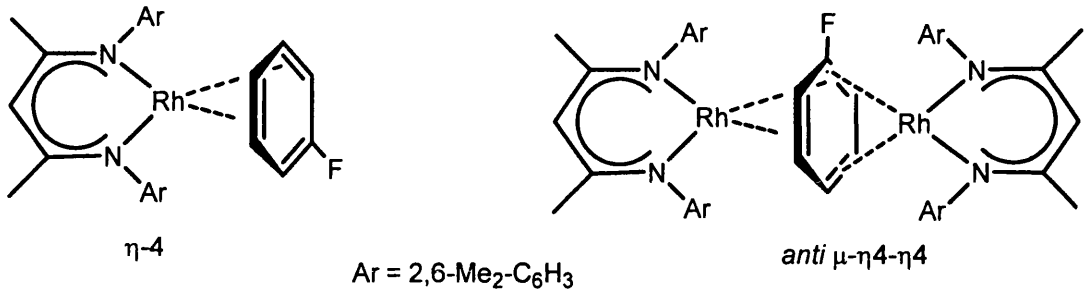

Figure 37: The coordination modes of C_6H_5F to the bulky {(β-diiminate)Rh} fragment.

The formation of both **23** and **24** lends further credence to the fact that the cationic fragment $\{(^{i}Pr_3P)_2Rh(H)_2\}^+$ forms *solvento* complexes in preference to anion bound complexes, thereby frustrating attempts to explore the properties of Rh···H_3C anion interactions.

The analogous hydrogenation was also attempted with the $[(PMe_3)_2Rh(NBD)][1\text{-H-}closo\text{-}CB_{11}Me_{11}]$ precursor, however this led to intractable mixtures of unidentified products. In an attempt to obtain solid material of the dihydrogen adducts to allow for complete characterisation (i.e. solid state and IR spectroscopy) and for direct comparison to Crabtree's $[(PCy_3)_2Ir(H_2)_2(H)_2]^+$, the hydrogenation of the analogous PCy_3 precursor was investigated, the results of which are discussed next.

5.2.2.2:[$(PCy_3)_2Rh(H_2)_2(H)_2$][Y] (Y = [1-H-*closo*-$CB_{11}Me_{11}$]$^-$ or [BAr_F]$^-$).

In an analogous manner to the $^iPr_3P$ congener, [$(PCy_3)_2$Rh(NBD)][1-H-*closo*-$CB_{11}Me_{11}$] was treated with 4 atmospheres of H_2, resulting in a gradual colour change (~5 minutes) from orange to yellow. The resultant ^1H and $^1H\{^{31}P\}$ NMR spectra at 298 K displayed no hydride signals. The $^{31}P\{^1H\}$ NMR spectrum showed the clean formation of one compound, a significantly broadened doublet centred at 54.3 ppm. An identical spectrum (apart from the differences in those associated with the anion) is obtained on the hydrogenation of [$(PCy_3)_2$Rh(NBD)][BAr_F] under the same conditions. In both cases, no resonance was observed for free dihydrogen (δ 4.60 ppm), indicating that a fluxional process is taking place involving free and coordinated H_2.[49] On cooling to 200 K the $^{31}P\{^1H\}$ NMR spectrum displays a sharp, well-resolved doublet at δ 60.1 ppm (^1J(RhP) 92.4 Hz). The hydride region of the ^1H NMR spectrum (Figure 38) now consisted of a singlet at –14.14 ppm (integral 2.2 H) and a broader resonance at –1.81 ppm (integral 4 H, relative to the anion resonances), in addition a broad singlet corresponding to free dihydrogen was also visible downfield at 4.50 ppm.

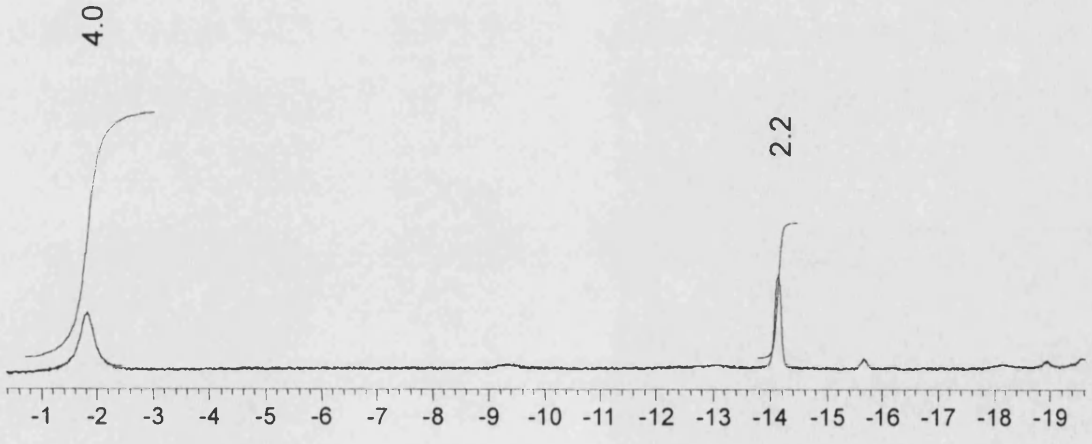

Figure 38: The hydride region of the ^1H NMR spectrum resulting from the hydrogenation of [$(PCy_3)_2$Rh(NBD)][Y], in CD_2Cl_2 at 200 K (integrated against the anion and $^iPr_3$ resonances).

By comparison of the chemical shifts and relative integrals of the two observed hydride resonances to the isoelectronic complex, $[(PCy_3)_2Ir(H_2)_2H_2]^+$ (Figure 39)[11] and the $^iPr_3$ congener, **22**, this new complex is formulated as $[(PCy_3)_2Rh(H_2)_2(H)_2]^+$, **25-$(H_2)_2$**. The highfield signals are assigned as a hydride ligand (-14.14 ppm) and a dihydrogen ligand (-1.81 ppm) respectively. This compound is an important addition to a series of analogous iso-electronic di-hydrogen complexes previously reported (Figure 39).[11, 60]

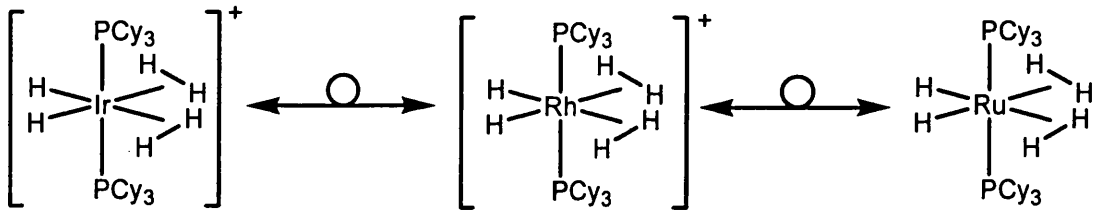

25-$(H_2)_2$

Figure 39: The three iso-electronic compounds, $[(PCy_3)_2M(H_2)_2(H)_2]^{n+}$ (M = Ir, Rh, n = 1, M = Ru, n =0).

In the $^1H\{^{31}P\}$ NMR spectrum the signal at –14.14 ppm splits into a doublet (^1J(RhH), 21.6 Hz) at this temperature, although the dihydrogen ligand is still a broad singlet. As for the $^iPr_3$ analogue an unresolved fluxional process presumably accounts for the broadness of the hydride resonances in **25-$(H_2)_2$**.

Measurement of the T_1 values for **25-$(H_2)_2$** at 190 K (at 400 MHz) allows for the unambiguous assignment of the highfield signals as a dihydrogen and a hydride ligand (20.8 ms, Rh-(H_2) –1.81 ppm and 259.7 ms, Rh-(H) –14.14 ppm) respectively. These relaxation times are comparable to other Group IX, d^6 non-time averaged hydride/dihydrogen complexes (*e.g.*, $[IrH(H_2)(bq)(PPh_3)_2]^+$ (bq = benzoquinone) T_1 (500 MHz, 188 K) (H_2) = 30ms, (H) = 390 ms).[11] We were not successful in observing

any HD coupling constant for complex **25-(H_2)$_2$** on addition of D_2. Infrared spectroscopy (in both H_2 saturated CH_2Cl_2 and C_6H_5F solutions) was not useful in the characterisation of **25-(H_2)$_2$**, with no signals in the terminal Rh-H region (1500 – 2300 cm^{-1}) of the spectra. This is possibly due to a very weak Rh-H stretching band, as documented for the iridium congener.[68] The lack of any M-H stretching bands in both **25-(H_2)$_2$** and its iridium analogue is in contrast to the neutral ruthenium analogue, for which two strong bands (1927 and 1890 cm^{-1}) are observed. Complex **25-(H_2)$_2$** is extremely sensitive to dihydrogen pressure, with the clean formation only occurring under 4 atmospheres of pressure. Under lower pressures (1 and ~2 atmospheres of H_2) different, more complex ^1H and $^{31}P\{^1H\}$ NMR spectra were recorded at low temperatures (Figures 40 and 41).

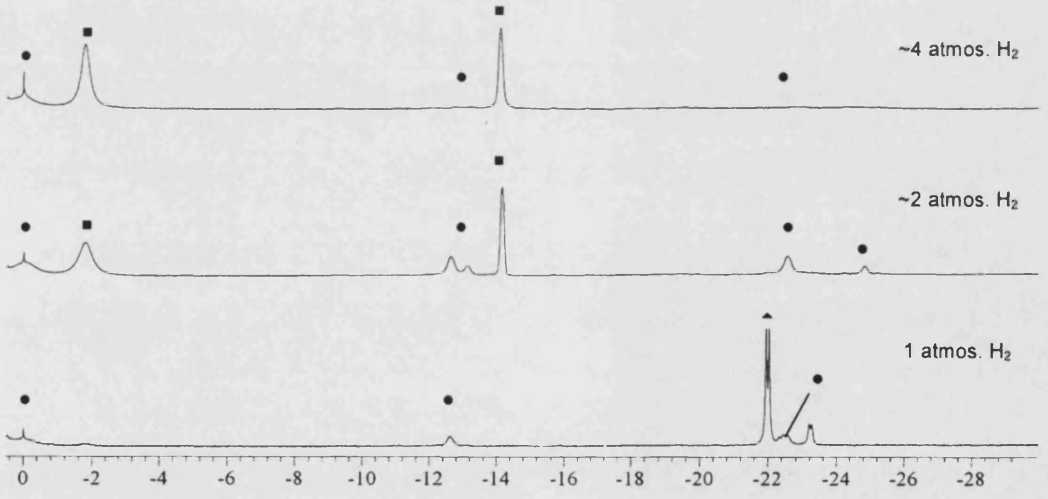

Figure 40: The ^1H NMR spectra in CD_2Cl_2 at 190 K of $\{(PCy_3)_2RhH_2\}^+$ at varying H_2 pressures, the sharp singlet at ~ 0ppm = vacuum grease. ■ = **25-(H_2)$_2$**, ● = $[(PCy_3)_2Rh(H_2)(H)_2L]^+$, **(25)-($H_2$)** and ▲ = the peak attributable to $[(PCy_3)_2Rh(H)_2(CH_2Cl_2)]^+$, **25-DCM**.

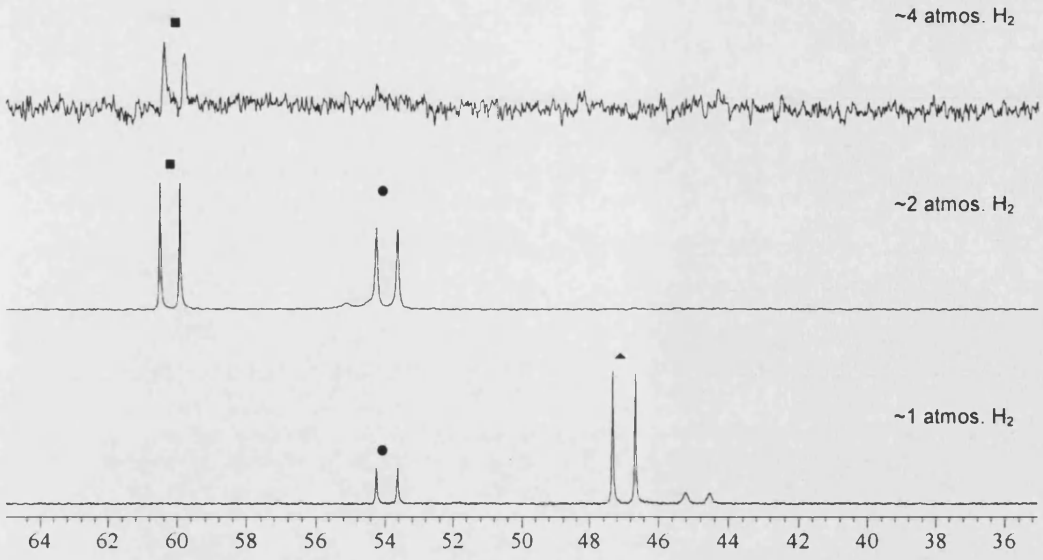

Figure 41: $^{31}P\{^1H\}$ NMR spectra in CD_2Cl_2 at 180K of $\{(PCy_3)_2RhH_2\}^+$ at varying H_2 pressures. ■ = **25-(H_2)$_2$**, ● = $[(PCy_3)_2Rh(H_2)(H)_2L]^+$, **25-($H_2$)** and ▲ = $[(PCy_3)_2Rh(H)_2(CH_2Cl_2)]^+$, **25-DCM**.

These sets of spectra, along with their the relative integrals, T_1 measurements and comparison with $[(PR_3)_2Ir(H_2)_x(H)_2][BAr_F]$ (x = 1, 2)[11, 16, 59] and **22** allow for the identification of a number of these products. Under 4 atmospheres of H_2, the predominant complex observed is **25-(H_2)$_2$**. On lowering the H_2 pressure to ~2 atmospheres, two major compounds are visible by $^{31}P\{^1H\}$ NMR spectroscopy, one being **25-(H_2)$_2$**. The ^1H NMR spectrum at this pressure exhibits a broad resonance with a chemical shift of δ –0.11 ppm, which, again by comparison, can be assigned to the (H_2) ligand in a mono-dihydrogen complex, $[(PCy_3)_2Rh(H_2)(H)_2]^+$, which is the second doublet in the $^{31}P\{^1H\}$ NMR spectrum. The sixth coordination site on the rhodium centre appears to be occupied by two different ligands in a ratio 2:1 (determined by integration of the separate sets of hydride resonances). An agostic interaction can again be ruled out due to the significant downfield chemical shift characteristic of hydrides that are *trans* to agostic interactions The major sets of hydride signals (at –0.11, -12.63 and –22.58 ppm) we tentatively assign as the dichloromethane adduct (Figure 42),

however, no direct evidence for a coordinated dichloromethane molecule was observed by low temperature NMR spectroscopy. The minor set of signals possibly arises from an impurity present in low concentration (*e.g.*, N_2 or H_2O).

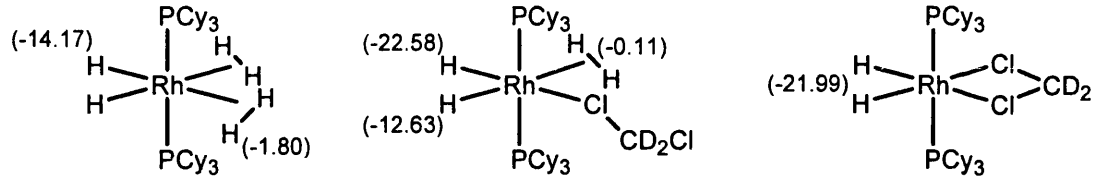

$\delta^{31}P\{^1H\}$ (190K) 60.2ppm 53.9ppm 47.0ppm

Figure 42: The assignment and chemical shifts of the major complexes formed with $\{(PCy_3)_2RhH_2\}^+$ in CD_2Cl_2 solutions at various H_2 pressures (cationic portions only shown).

At one atmosphere of dihydrogen there is no **25-$(H_2)_2$** remaining and the mono-dihydrogen adduct is drastically reduced in intensity (by ^1H NMR spectroscopy). In their place a doublet at δ -22.99 ppm is now the major product (along with a smaller doublet further upfield). Two new resonances are also seen in the $^{31}P\{^1H\}$ NMR spectrum. The major hydride signal (δ -21.99 ppm) is tentatively assigned as the dichloromethane adduct, $[(^iPr_3P)_2Rh(H)_2(CD_2Cl_2)]^+$ (Figure 42), with a chemical shift comparable to that reported for known cationic complexes where a hydride is *trans* to a coordinated dichloromethane molecule (*e.g.*, $[(PPh_3)_2Ir(H)_2(CH_2Cl_2)][closo\text{-}CB_{11}H_6Br_6]$, {-23.2 ppm} and $[(^iPr_3P)_2Pt(H)(Cl_2CH_2)][BAr_F]$, {-22.8 ppm}).[33, 49] Anion coordinated complexes can be ruled out due to the similar spectra observed on moving between the $[BAr_F]^-$ and $[1\text{-H-}closo\text{-}CB_{11}Me_{11}]^-$ anions. Increasing the hydrogen pressure in this sample to 2 atmospheres or above returns the spectra to those of a mixture of mono and bis-dihydrogen adducts (Figure 43).

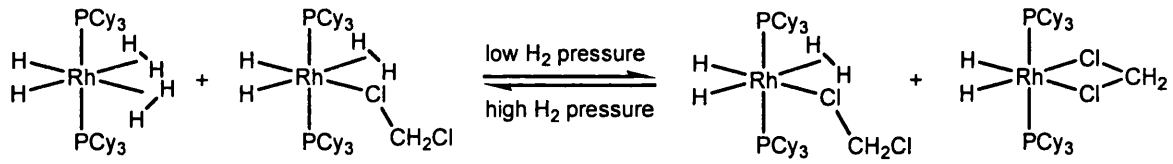

Figure 43: The hydrogen pressure dependency of the products observed from the hydrogenation of $[(PCy_3)_2Rh(NBD)][Y]$ ([Y] = $[BAr_F]$ or [1-H-*closo*-$CB_{11}Me_{11}]^-$.

Under 4 atmospheres of dihydrogen pressure complex **25-$(H_2)_2$** is stable at low temperature for days. At room temperature **25-$(H_2)_2$** is stable for hours and heating to 50°C further accelerates this decomposition. The products resulting from this decomposition will be discussed in Chapter 6. Complex **25**, under dihydrogen does not react with chlorinated solvents, in contrast to the ruthenium analogue that rapidly produces $(PCy_3)_2RuHCl(H_2)_x$ (x = 1 or 2) on standing in CD_2Cl_2, even at low temperatures.[69] Attempts to isolate bulk solid material of **25** invariable failed, due to the requirement of high H_2 pressures, the mixture of products and its inherent instability. However, crystalline material of only adequate quality was obtained of the [1-H-*closo*-$CB_{11}Me_{11}]^-$ salt and an X-ray diffraction study carried out. Whilst the nature of the crystal and the significant disorder in the final refinement prevented a fully satisfactory result, the gross structural parameters of **25** were determinable (Figure 44). Analogous to $(PR_3)_2Ru(H_2)_2(H)_2$ (R = Cy[48] or ^{i}Pr[70]) the phosphines are located *trans* to each other (P-Rh-P 179.65(15)°) with a 'normal' P-Rh distance, 2.352(3)Å (*e.g.*, compared to 2.336(3)Å and 2.357(3)Å in $[(PCy_3)_2Rh(\{E\}\text{-}CH{=}CHCy)(acac)][BF_4]$).[71] No further information is obtainable, though importantly no significant residual electron density is located near the rhodium centre, strongly suggesting that this is a di-hydrogen adduct, $(PCy_3)_2RhH_x$.

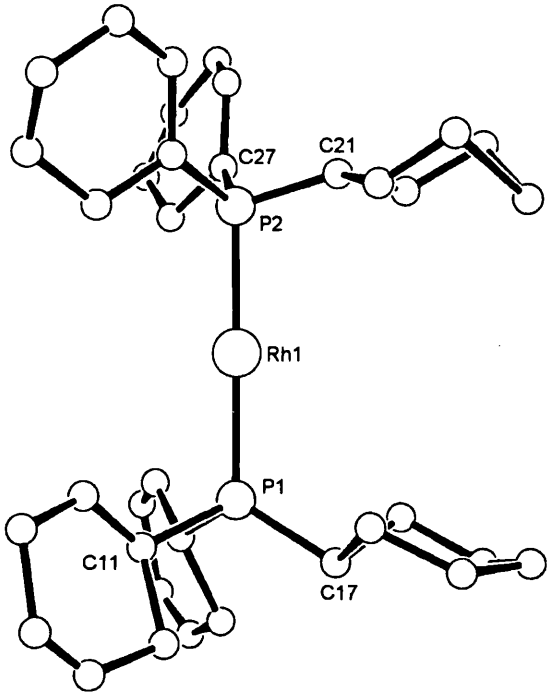

Figure 44: The molecular structure of the cationic portion of **25-$(H_2)_X$**, the poor data set prevented the location of the hydrides (see text). Only one set of two equally occupied cyclohexyl phosphine positions are shown for clarity.

The reactivity of complex **25** is similar to that of **22**, being highly sensitive to H_2O and O_2. The dihydrogen ligands are labile, rapidly displaced on the addition of MeCN to form $[(PCy_3)_2Rh(H)_2(MeCN)_2]^+$, with the hydride region changing to a well-resolved doublet of triplets (centred at δ -18.9 ppm). Attempts to form the dihydrogen free fragment $\{(PCy_3)_2Rh(H)_2\}^+$, by pumping *in vacuo*, appeared to give similar results to **22**, with hydride resonances in similar region of the spectra to **22-DCM** and equally no indication of any anion interaction as expected.

5.3: Summary.

This chapter reports the hydrogenation of Group IX bisphosphine precursors partnered initially with the [1-H-*closo*-$CB_{11}Me_{11}$]$^-$ anion, in an attempt to engender

contact ion pair formation and allow for the further investigate of the M···H_3C interaction. In the iridium precursors the reactivity of the [1-H-*closo*-$CB_{11}Me_{11}$]$^-$ congener closely follows that previously reported for the [BAr_F]$^-$ and [PF_6]$^-$ anions, with no metal anion interactions formed. This is in contrast to the [*closo*-$CB_{11}H_6Br_6$]$^-$ anion that forms an intimate ion pair complex, allowing for the rating of these weakly nucleophilic anions with respect to the $\{(PPh_3)_2Ir(H)_2\}^+$ fragment as follows; [*closo*-$CB_{11}H_6Br_6$]$^-$ > [1-H-*closo*-$CB_{11}Me_{11}$]$^-$ ≈ [PF_6]$^-$ ≈ [BAr_F]$^-$. An anion decomposition product involving anion B-C and solvent C-H activation was also isolated, presumably forming via an acid catalysed mechanism.

The analogous rhodium systems partnered with [1-H-*closo*-$CB_{11}Me_{11}$]$^-$ afforded dihydrogen complexes of the general formula $[(PR_3)_2Rh(H_2)_x(H)_2]^+$ (x = 1 or 2 R = ^{i}Pr or Cy). These dihydrogen adducts were demonstrated to be extremely sensitive to temperature, dihydrogen pressure and to the presence of Lewis bases. The [BAr_F]$^-$ congener was found to equally produce a mixture of dihydrogen complexes. Characterisation by T_1 measurements, HD coupling constant and solid state studies show these complexes to be closely related to the known iridium analogues and structurally similar to $(PCy_3)_2Ru(H_2)_2(H)_2$. On the removal of dihydrogen from these complexes, solvent coordinated species are suggested to form, in preference to intimate ion pairs. An interesting DCM activated dimeric decomposition product, $[\{(^iPr_3P)_2(H)Rh\}_2(\mu\text{-}Cl)_2]^{2+}$ that has two agostic interactions was also isolated. A decomposition product, the octahedral rhodium clusters, $[(PR_3)_6Rh_6H_X]^{2+}$, that gradually forms when the mixture of dihydrogen adducts are left standing under a H_2 atmosphere will be discussed next, along with some initial reactivity studies.

5.4 References.

1 R. H. Crabtree, *Acc. Chem. Res.*, 1979, **12**, 331.

2 A. Lightfoot, P. Schnider, and A. Pflatz, *Angew. Chem., Int. Ed. Engl.*, 1998, **37**, 2897.

3 R. H. Crabtree, A. Gautier, G. Giordano, and T. Khan, *J. Organomet. Chem.*, 1977, **141**, 113.

4 H. Brunner, 'Hydrogenation in Applied Homogeneous Catalysis with Organometallic Compounds', ed. B. Cornils and W. A. Hermann, Wiley-VCH, 2000.

5 R. R. Schrock and J. A. Osborn, *J. Am. Chem. Soc.*, 1976, **98**, 2134.

6 R. Noyori, 'Asymmetric Catalysis in Organic Synthesis', Wiley, 1994.

7 R. Crabtree, P. C. Demou, D. Eden, J. M. Milhelcic, C. A. Quirk, and G. E. Morries, *J. Am. Chem. Soc.*, 1982, **104**, 6994.

8 H. M. Lee, T. Jiang, E. D. Stevens, and S. P. Nolan, *Organometallics*, 2001, **20**, 1255.

9 J. A. Osborn, F. H. Jardine, J. F. Young, and G. Wilkinson, *J. Chem. Soc. A*, 1966, 1711.

10 D. F. Chodsch, R. H. Crabtree, H. Felkin, and G. E. Morris, *J. Organomet. Chem.*, 1978, **161**, C67.

11 R. H. Crabtree and M. Lavin, *Chem. Commun.*. 1985, 1661.

12 G. J. Kubas, 'Metal Dihydrogen and Sigma Bond Complexes. Structure, Theory and Reactivity.' Kluwer, 2001.

13 C. Bianchini, S. Moneti, M. Peruzzini, and F. Vizza, *Inorg. Chem.*, 1997, **36**, 5818.

14 A. C. Cooper, E. Clot, J. C. Huffman, W. E. Streib, F. Maseras, O. Eisenstein, and K. G. Caulton, *J. Am. Chem. Soc.*, 1999, **121**, 97.

15 A. C. Cooper, W. E. Streib, O. Eisenstein, and K. G. Caulton, *J. Am. Chem. Soc.*, 1997, **119**, 9069.

16 A. C. Cooper, O. Eisenstein, and K. G. Caulton, *New. J. Chem*, 1998, 307.

17 J. R. Shapley, R. R. Schrock, and J. A. Osborn, *J. Am. Chem. Soc.*, 1969, **91**, 2816.

18 T. C. Morrill and C. A. D'Souza, *Organometallics*, 2003, **22**, 1626.

19 T. Ohta, H. Ikegami, T. Miyake, and H. Takaya, *J. Organomet. Chem.*, 1995, **502**, 169.

20 E. Y. X. Chen and T. J. Marks, *Chem. Rev.*, 2000, **100**, 1391

21 J. M. Buriak and J. A. Osborn, *Organometallics*, 1996, **15**, 3161.

22 A. Rifat, N. J. Patmore, M. F. Mahon, and A. S. Weller, *Organometallics*, 2002, **21**, 2856.

23 J. M. Buriak, J. C. Klein, D. G. Herrington, and J. A. Osborn, *Chem. Eur. J.*, 2000, **6**, 139.

24 J. M. Leitner, H. Brown, and S. J. Brunner, *J. Am. Chem. Soc.*, 1993, **115**, 152.

25 J. v. d. Broeke, E. d. Wolf, B. J. Deelman, and G. v. Koten, *Adv. Synth. Catal.*, 2003, **345**, 625.

26 Z. Zhou, G. Facey, B. R. James, and H. Alper, *Organometallics*, 1996, **15**, 2496.

27 D. P. Fairlie and B. Bosnich, *Organometallics*, 1988, **7**, 936.

28 A. Rifat, V. E. Laing, G. Kociok-Kohn, M. F. Mahon, G. D. Ruggiero, and A. S. Weller, *J. Organomet. Chem.*. 2003, **680**, 127.

[29] A. Rifat, 'Exo-Closo Carborane Complexes of rhodium and iridium. Synthesis and Evaluation as Hydrogenation Catalysts.' University of Bath, 2003.
[30] C. A. Reed, *Acc. Chem. Res.*, 1998, **31**, 133.
[31] E. T. Singewald, C. S. Slone, C. L. Stern, C. A. Mirkin, C. G. P. A. Yap, L. M. Liable-Sands, and A. L. Rheingold, *J. Am. Chem. Soc.*, 1997, **119**, 3048.
[32] R. H. Crabtree, C. A. Parnell, and R. J. Uriate, *Organometallics*, 1987, **6**, 696.
[33] A. Rifat, G. Kociok-Kohn, J. W. Steed, and A. S. Weller, *Organometallics*, 2004, **23**, 428.
[34] R. Goikhman and D. Milstein, *Angew. Chem., Int. Ed. Engl.*, 2001, **40**, 1119.
[35] T. Yoshida, T. Okano, D. L. Thorn, T. H. Tulip, S. Otsuka, and J. A. Ibers, *J. Organomet. Chem.*, 1979, **181**, 183.
[36] H. Werner, M. Bosch, M. E. Schneider, C. Hahn, F. Kukla, M. Manger, B. Windmuller, B. Weberndorfer, and M. Laubender, *J. Chem. Soc., Dalton Trans.*, 1998, 3549.
[37] R. H. Crabtree, H. Felkin, T. Fillebeen-Khan, and G. E. Morris, *J. Organomet. Chem.*, 1979, **168**, 183.
[38] R. H. Crabtree, H. Felkin, and G. E. Morris, *J. Organomet. Chem.*, 1977, **141**, 205.
[39] B. T. King, Z. Janousek, B. Gruner, M. Trammell, B. C. Noll, and J. Michl, *J. Am. Chem. Soc.*, 1996, **118**, 3313.
[40] Z. Janousek, U. Lehmann, J. Castulik, I. Cisarova, and J. Michl, *J. Am. Chem. Soc.*, 2004, **126**, 4060.
[41] M. L. McKee, *J. Am. Chem. Soc.*, 1997, **119**, 4220
[42] J. S. Wiley, W. J. Oldham, and D. M. Heinekey, *Organometallics*, 2000, **19**, 1670.
[43] H. Arieetha, M. Jimenez-Tenorio, M. C. Puerta, P. Valerga, V. N. Sapunov, R. Schmid, K. Kirchner, and K. Mereiter, *Organometallics*, 2002, **21**, 5334.
[44] S. T. H. Willems, P. H. M. Budzelaar, N. N. P. Moonen, R. de-Gelder, L. M. M. Smits, and A. W. Gal, *Chem. Eur. J.*, 2002, **8**, 1310.
[45] A. Khaleel and K. J. Klabunde, *Inorg. Chem.*, 1996, **35**, 3223.
[46] F. Torres, E. Sola, M. Martin, J. A. Lopez, F. J. Lahoz, and L. A. Oro, *J. Am. Chem. Soc.*, 1999, **121**, 10632.
[47] B. T. King, I. Zharov, and J. Michl, *Chemical Innovation*, 2001, **31**, 23.
[48] K. Abdur-Rashid, D. G. Gusev, A. J. Lough, and R. H. Morris, *Organometallics*, 2000, **19**, 1652.
[49] M. D. Butts, B. L. Scott, and G. J. Kubas, *J. Am. Chem. Soc.*, 1996, **118**, 11831.
[50] X. G. Fang, J. Huhmann-Vincent, B. L. Scott, and G. J. Kubas, *J. Organomet. Chem.*, 2000, **609**, 95.
[51] F. L. Taw, H. Mellows, P. S. White, F. J. Hollander, R. G. Bergmann, M. Brookhart, and M. D. Heinekey, *J. Am. Chem. Soc.*, 2002, **124**, 5100.
[52] B. E. Hauger, D. Gusev, and K. G. Caulton, *J. Am. Chem. Soc.*, 1994, **116**, 208.
[53] R. H. Crabtree, *Acc. Chem. Res.*, 1990, **23**, 95.
[54] U. E. Bucher, T. Lengweiler, D. Nanz, W. v. Philipsborn, and L. M. Venanzi, *Angew. Chem., Int. Ed. Engl.*, 1990, **29**, 548.
[55] W. J. O. Jr., A. S. Hinkle, and D. M. Heinekey, *J. Am. Chem. Soc.*, 1997, **119**, 11028.
[56] V. I. Bakhmutov, C. Bianchini, M. Peruzzini, F. Vizza, and E. V. Vorontsov, *Inorg. Chem.*, 2000, **39**, 1655.
[57] P. G. Jessop and R. H. Morris, *Coord. Chem. Rev*, 1992, **121**, 155.
[58] D. W. Lee and C. M. Jensen, *J. Am. Chem. Soc.*, 1996, **118**, 8749.

[59] A. C. Cooper and K. G. Caulton, *Inorg. Chem.*, 1998, **37**, 5938.
[60] S. Sabo-Etienne and B. Chaudret, *Coord. Chem. Rev*, 1998, **178-180**, 381.
[61] J. Yao, W. T. Wong, and G. Jia, *J. Organomet. Chem.*, 2000, **598**, 228.
[62] A. A. H. v. d. Zeijden, G. v. Koten, R. Luijk, K. Vrieze, C. Slob, H. Krabbendam, and A. L. Spek, *Inorg. Chem.*, 1988, **27**, 1014.
[63] P. Binger, J. Haas, G. Glaser, R. Goddard, and C. Kruger, *Chem. Ber.*, 1994, **127**, 1927.
[64] R. S. Hay-Motherwell, B. Hussain-Bates, M. B. Hursthouse, and G. Wilkinson, *J. Chem. Soc. Chem. Commun.*. 1990, 1242.
[65] R. H. Crabtree, 'The Organometallic Chemistry of the Transition Metals', Wiley Inter-Science, 2001.
[66] J. R. Bleeke and A. J. Donaldson, *Organometallics*, 1988, **7**, 1588.
[67] P. H. M. Budzelaar, N. N. P. Moonen, R. de-Gelder, J. M. M. .Smits, and A. W. Gal, *Chem. Eur. J.*, 2000, **6**, 2740.
[68] R. H. Crabtree, M. Lavin, and L. Bonneviot, *J. Am. Chem. Soc.*, 1986, **108**, 4032.
[69] M. L. Christ, S. Sabo-Ettienne, and B. Chaudret, *Organometallics*, 1994, **13**, 3800.
[70] A. F. Borowski, B. Donnadieu, J.-C. Daran, S. Sabo-Etienne, and B. Chaudret, *Chem. Commun.*. 2000, **2000**, 543.
[71] M. A. Esteruelas, F. J. Lahoz, E. Onate, L. A. Oro, L. Rodruguez, P. Steinert, and H. Werner, *Organometallics*, 1996, **15**, 3436.

6: High hydride content octahedral clusters from the decomposition of rhodium dihydrogen complexes.

6.1 Background:

The previous chapter described the characterisation of a number of new cationic rhodium dihydrogen adducts. The general reactivity of the coordinated H_2 in such complexes can be split into three distinct processes: oxidative addition, heterolytic cleavage and elimination of H_2. Of importance towards the decomposition of the $[(PR_3)_2Rh(H_2)_x(H)_2]^+$ cations is the second process: heterolytic cleavage of coordinated H_2. A full and comprehensive review of the other two processes has also been published,[1] and an excellent recent in-depth review of the heterolytic splitting of H_2 has just been published.[2] This introduction shall therefore only cover the salient points involved in the decomposition of **22-$(H_2)_x$** and **25-$(H_2)_x$**.

Heterolytic cleavage of H_2, otherwise termed 'deprotonation of coordinated H_2', has been demonstrated to be favoured in the presence of 'super' electrophilic metal centres that are invariably cationic.[3] In these complexes the coordinated dihydrogen becomes extremely polarised, $H^{\delta+}$-$H^{\delta-}$, and is often highly acidic.[4, 5] A number of general properties are required for dihydrogen complexes to exhibit strong acidity: short H-H bonds (*i.e.*, no M to H_2 σ^* back bonding); a cationic metal centre; and a labile H_2 molecule. Molecules which meet these requirements are $[Cp^*Re(H_2)(CO)(NO)]^+$ and $[Re(H_2)(CO)_4(PR_3)]^+$.[6, 7] Following the breaking of the H-H bond into H^+ and H^- fragments the hydride binds to the metal centres whilst the proton is transferred to a Lewis base, which can be the anion, ancillary ligand or solvent (Figure 1).

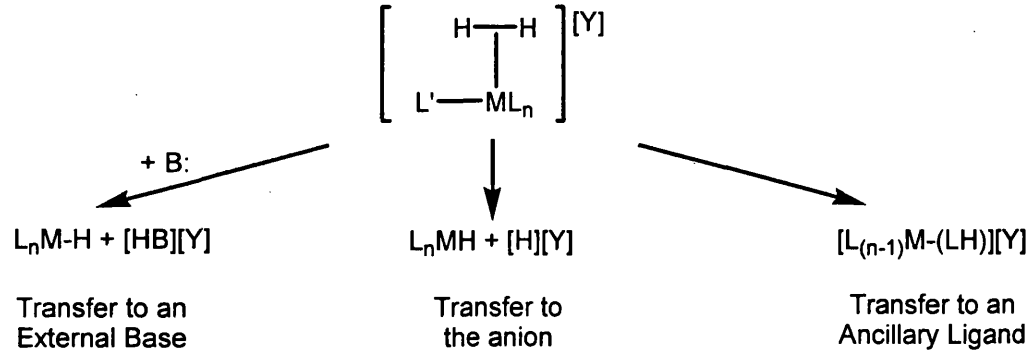

Figure 1: The possible protonation routes following the heterolytic cleavage of H_2 coordinated to an electrophilic metal.

The transfer of a proton from coordinated dihydrogen to an ancillary ligand (L) followed by the dissociation of HL^+, results in a coordinatively unsaturated metal centre, with the two electrons originally present in the H-H bond transferred to the M-H bond. This process is comparable to the role that hydrogenases play in nature, catalysing the reversible transformation of H_2 into H^+ (Figure 2), via the splitting of a coordinated dihydrogen molecule.

$$H_2 \rightleftharpoons 2H^+ + 2e^-$$

Figure 2: The equilibrium process catalysed by hydrogenases.

The heterolytic cleavage of coordinated H_2 should be important in complexes **22-$(H_2)_X$** and **25-$(H_2)_X$** that clearly possess the necessary criteria discussed above for the coordinated H_2 to be significantly acidic. As we will show the decomposition products formed from these adducts result from the heterolytic cleavage of H_2 which forms unsaturated fragments that self-assemble to generate higher nuclearity rhodium clusters.

A number of mid and late transition metal mononuclear complexes have been reacted directly with dihydrogen (presumably via a transient coordinated H_2 species) generating metal clusters. The octahedral cluster $W_6(H)_5(C\text{-}^iPr)(O\text{-}^iPr)_{12}$ is formed from

the reaction of H_2 with $W_2(^iBu)_2(O\text{-}^iPr)_4$, and is believed to form via the heterolytic cleavage of H_2 (Figure 3).[8, 9]

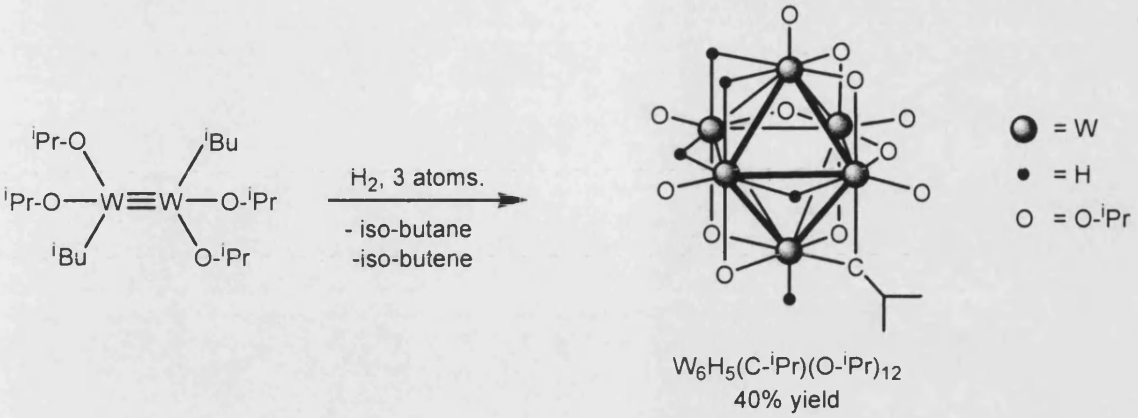

Figure 3: Formation of the octahedral cluster, $W_6(H)_5(C\text{-}^iPr)(O\text{-}^iPr)_{12}$.

Reactivity studies on $W_6(H)_5(C\text{-}^iPr)(O\text{-}^iPr)_{12}$ have demonstrated that it catalyses H/D exchange in ethene, undergoes site-selective alcoholysis, hydrogenolysis and reversible hydrogenation (Figure 4).[10, 11] With chelating phosphines a dimer, $W_2(H)_2(O\text{-}^iPr)_4(dmpe)_2$ and a tetramer, $W_4(H)_4(O\text{-}^iPr)_8(dmpm)_3$have been isolated.[11]

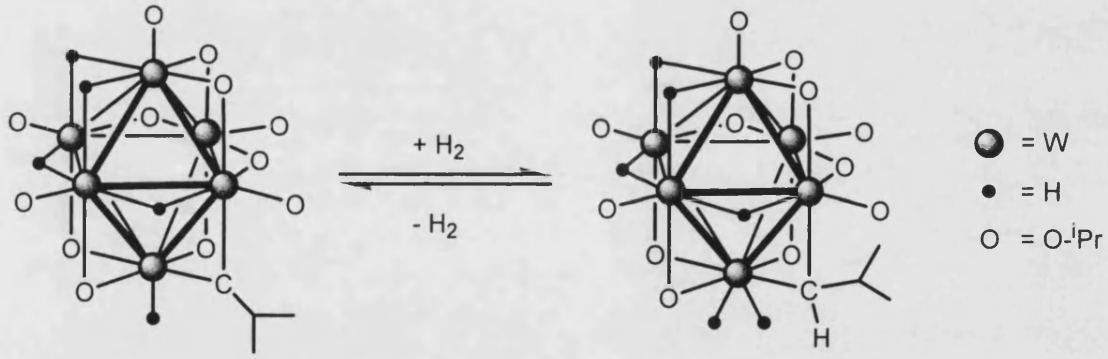

Figure 4: The reversible hydrogenation of the $W_6(H)_5(C\text{-}^iPr)(O\text{-}^iPr)_{12}$ cluster.

The platinum precursors $(PR_3)Pt(C_2H_4)_2$ also react with H_2 (albeit under high pressure ~ 300 atmospheres) giving a number of Pt-hydride clusters, the nuclearity of which is highly dependent on the phosphine steric bulk (Figure 5).[12-14]

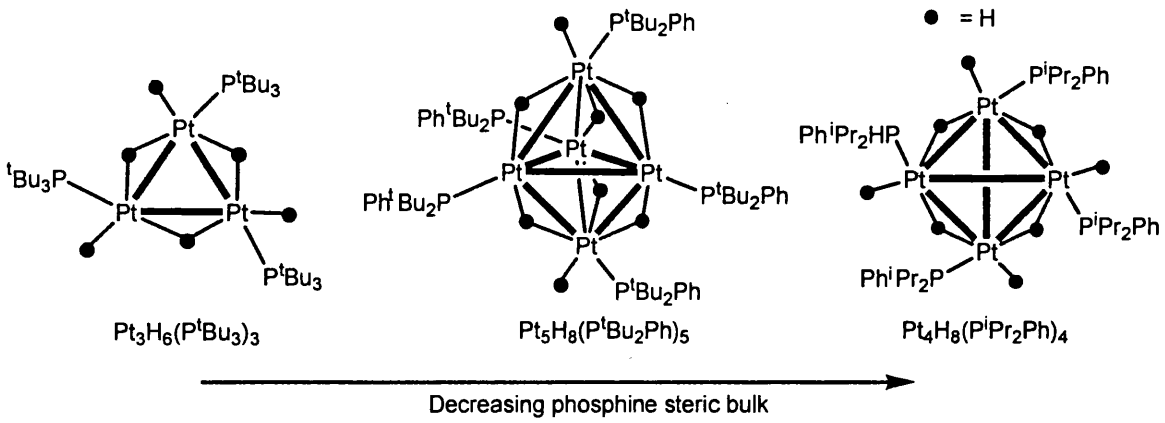

Figure 5: The clusters resulting from the hydrogenation of a number of $(PR_3)Pt(C_2H_4)_2$ precursors.

These were the first, well characterised, clusters reported where the H : M ratio exceeds unity, i.e., there are more hydrides than metal centres in the cluster. Previous work on the copper polyhydrides, $(PR_3)_6Cu_6H_6$, had set the benchmark for this ratio.[15, 16] On the loss of a number of the hydrides (by the use of ethene as a hydrogen acceptor) $Pt_3H_6(P^tBu_3)_3$ condenses further to form the higher nuclearity cluster $Pt_4H_2(P^tBu_3)_4$.[13]

Of particular relevance to the work described in this chapter are clusters resulting from the hydrogenation of the Rh(I) allyl precursors, $(\eta^3\text{-}C_3H_5)Rh(PR_3)_2$,[17-19] that can be viewed as neutral analogues of the Schrock-Osborn pre-catalysts studied in Chapter 5. On exposure to hydrogen these neutral precursors rapidly evolved propane and form highly fluxional dimeric or trimeric complexes, again depending on the bulk of the R substituent. These complexes react further with dihydrogen, with each oligomer reversibly binding one molecule of H_2 to form higher hydride content species (Figure 6). Reaction stoichiometries were determined by hydrogen titrations, although definitive identification of each complex was not reported. NMR spectroscopic and reactivity studies strongly suggests that the structure of the dimer product to be $(PR_3)_2(H)Rh(\mu\text{-}H)_3Rh(PR_3)_2$.[18]

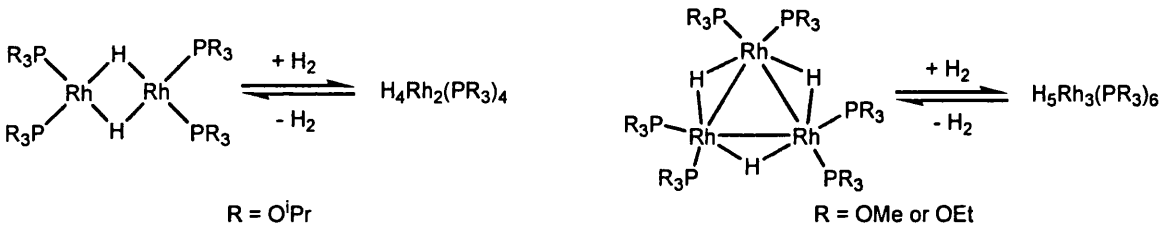

Figure 6: The rhodium phosphine oligomers formed on the hydrogenation of $(\eta^3\text{-}C_3H_5)Rh(PR_3)_2$.

A Group IX complex with a hydride : metal ratio of 2 : 1 has also been recently reported, though this was not formed via the hydrogenolyisis of a monomeric precursor.[20] Treatment of $Ir_4(CO)_{12}$ with PPh_3 under a H_2 atmosphere produced in quantitative yield two isomers of the cluster compound, $Ir_4H_8(CO)_4(PPh_3)_4$ (Figure 7), that is an unusually stable high hydride cluster, showing no reactivity to base or CO.

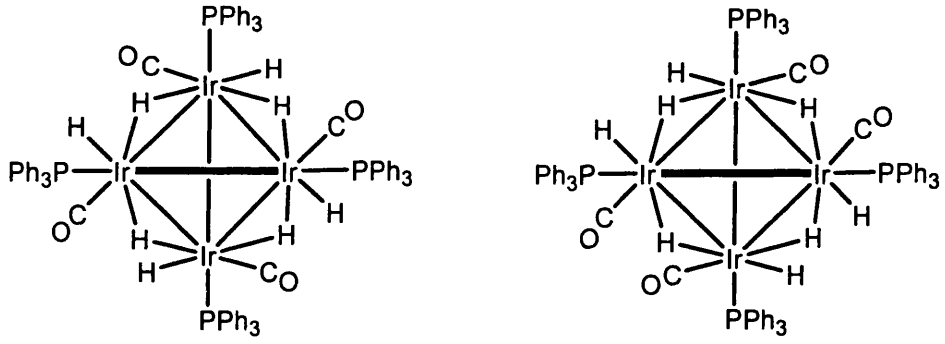

Figure 7: The two isomers of $Ir_4H_8(CO)_4(PPh_3)_4$.

A decomposition product from the hydrogenation of the widely used Crabtree catalyst, $[(PCy_3)(py)Ir(COD)][PF_6]$, has also been structurally characterised and shown to be a hydride capped tri-iridium cluster (Figure 8).[21]

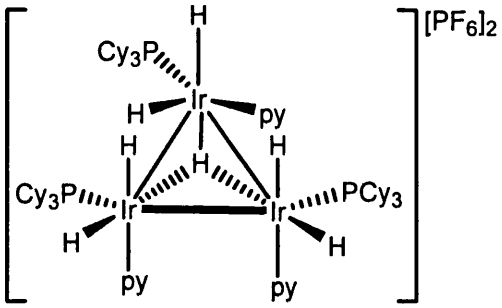

Figure 8: The tri nuclear iridium cluster formed from the hydrogenation of the Crabtree catalyst in CH_2Cl_2.

Finally, a tetrahedral cluster, $[Ru_4H_6(C_6H_6)_4]^{2+}$, has also been reported that is ligated by both classical and non-classical hydrides (based on T_1 measurements), and is synthesised by the reaction of molecular hydrogen with $[(C_6H_6)RuCl_2]_2$.[22] This reaction has been shown to be pressure sensitive with low (1.5 atmospheres) H_2 pressures resulting in the tetra hydride analogue that is also dicationic, $[Ru_4H_4(C_6H_6)_4]^{2+}$. In both cases heterolytic cleavage of dihydrogen is intimately involved in the cluster formation, with six equivalents of acid (HCl) formed for each tetramer. Interestingly, the hexa hydride, $[Ru_4H_6(C_6H_6)_4]^{2+}$, does not lose dihydrogen even under high vacuum; instead, dioxygen is required to effect formal reductive elimination, with the concomitant formation of H_2O. (Figure 9).[23]

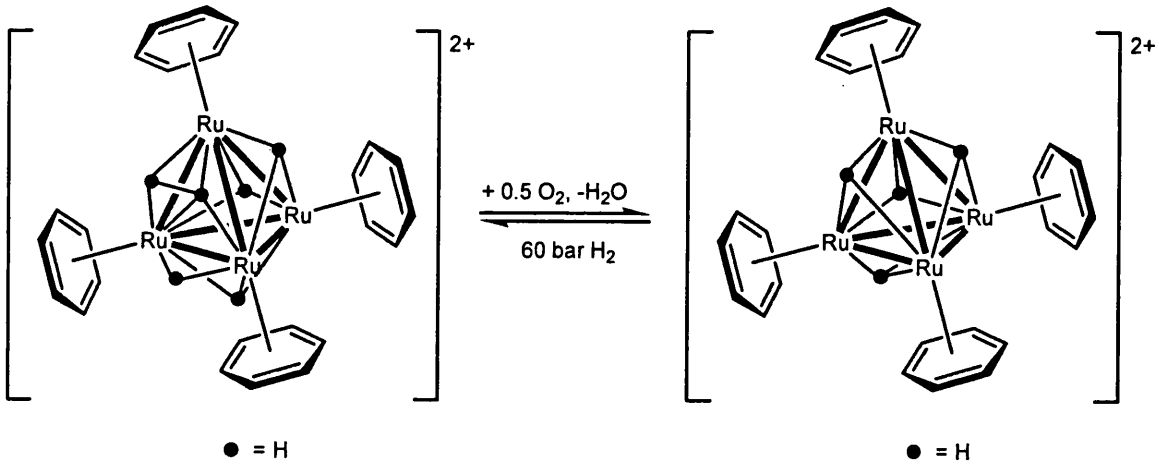

Figure 9: The reversible dehydrogenation of $[Ru_4H_6(\eta^6\text{-}C_6H_6)_4]^{2+}$.

More sterically bulky arenes shield the cluster core and significantly slow this reversible process. This complex is an active catalyst for the biphasic hydrogenation of benzene to cyclohexane.[24] The reversible addition of H_2 to a cluster to form dihydrides has been reported in a number of other systems and can occur with or without significant alteration to the cluster framework.[25-28]

6.1.1: Scope of Chapter

This chapter will discuss the decomposition products formed when $[(PR_3)_2Rh(H_2)_x(H)_2]^+$ (x = 1 or 2, R = ^{i}Pr or Cy) is kept under an atmosphere of dihydrogen. Characterisation of high hydride content $\{Rh_6\}$ clusters will be presented, along with some theoretical comparison to more 'classical' cluster complexes. Initial insights into the mechanism of formation and some early reactivity studies will also be discussed.

6.2: Results and Discussion.

6.2.1: $[(^iPr_3P)_6Rh_6H_{12}][Y]_2$ (Y = [1-H-*closo*-$CB_{11}Me_{11}$]$^-$ or $[BAr_F]^-$).

6.2.1.1:Characterisation and Discussion.

Complex **22** (either as the [1-H-*closo*-$CB_{11}Me_{11}$]$^-$ or $[BAr_F]^-$ salt) on standing in a C_6H_5F solution at room temperature under a dihydrogen atmosphere undergoes a gradual darkening in colour, from pale yellow through to brown. The NMR spectra after the colour change displayed resonances in the ^1H and $^{31}P\{^1H\}$ NMR spectra that

corresponded to the cation, $[HP(^{i}Pr)_3]^+$, **26Pr** ($\delta^{31}P\{^1H\}$ 46.6 ppm singlet, δ^1 H 5.31 ppm d of q $^1J(PH)$ 336 Hz, $^3J(HH)$ 4.4 Hz).[29] Concomitant with this, two doublets, one being at very low field (110.5 ppm and 59.8 ppm respectively in CD_2Cl_2) were also observed in the $^{31}P\{^1H\}$ NMR spectrum. The ^1H NMR spectrum of this sample showed only two phosphine environments, with one set of $^{i}Pr_3P$ signals ascribable to **26Pr**, and the two remaining phosphine containing products presumably resonating coincidentally. The hydride region showed two resonances, a doublet of triplets centred at –24.9 ppm and a broad singlet at –21.40 ppm. Recrystallisation of the $[BAr_F]^-$ counterion reaction mixture, under an atmospheric pressure of dihydrogen, yielded dark red crystals suitable for X-ray diffraction (in 45% yield based on rhodium content *vide infra*). The asymmetric unit consisted of a Rh_3 triangular unit and one anion that was not proximate. The performance of the associated symmetry operations generated a $[Rh_6]$ core and a second anion, making the cluster dicationic. The molecular structure is a regular octahedron formed from six {PRh} fragments (Figure 10), the Rh-Rh bond lengths are identical within errors, with the triangular faces approximating to equilateral triangles and three equivalent square planes completing the geometrical facets of this cluster. The Rh-Rh distances (average 2.719 Å) are similar to those found in the 'classical' Rh_6 octahedral cluster, $Rh_6(CO)_{16}$ (2.794 Å).[30] Examination of the penultimate electron difference map revealed six edge-bridging hydrogens in the asymmetric unit (given the usual caveats about the location and positioning of hydrogens using X-ray crystallography), with each refining satisfactorily as having a full occupancy. The molecular structure of the $\{(^{i}Pr_3P)Rh\}_6$ cluster is therefore completed by twelve edge bridging hydrides, resulting in an overall formulation as $[(^{i}Pr_3P)_6Rh_6(H)_{12}]^{2+}$, **27-$H_{12}$**. The closest H-H distance (2.042 Å) precludes the possibility of coordinated dihydrogen, and identifies all twelve as "classical" hydrides.

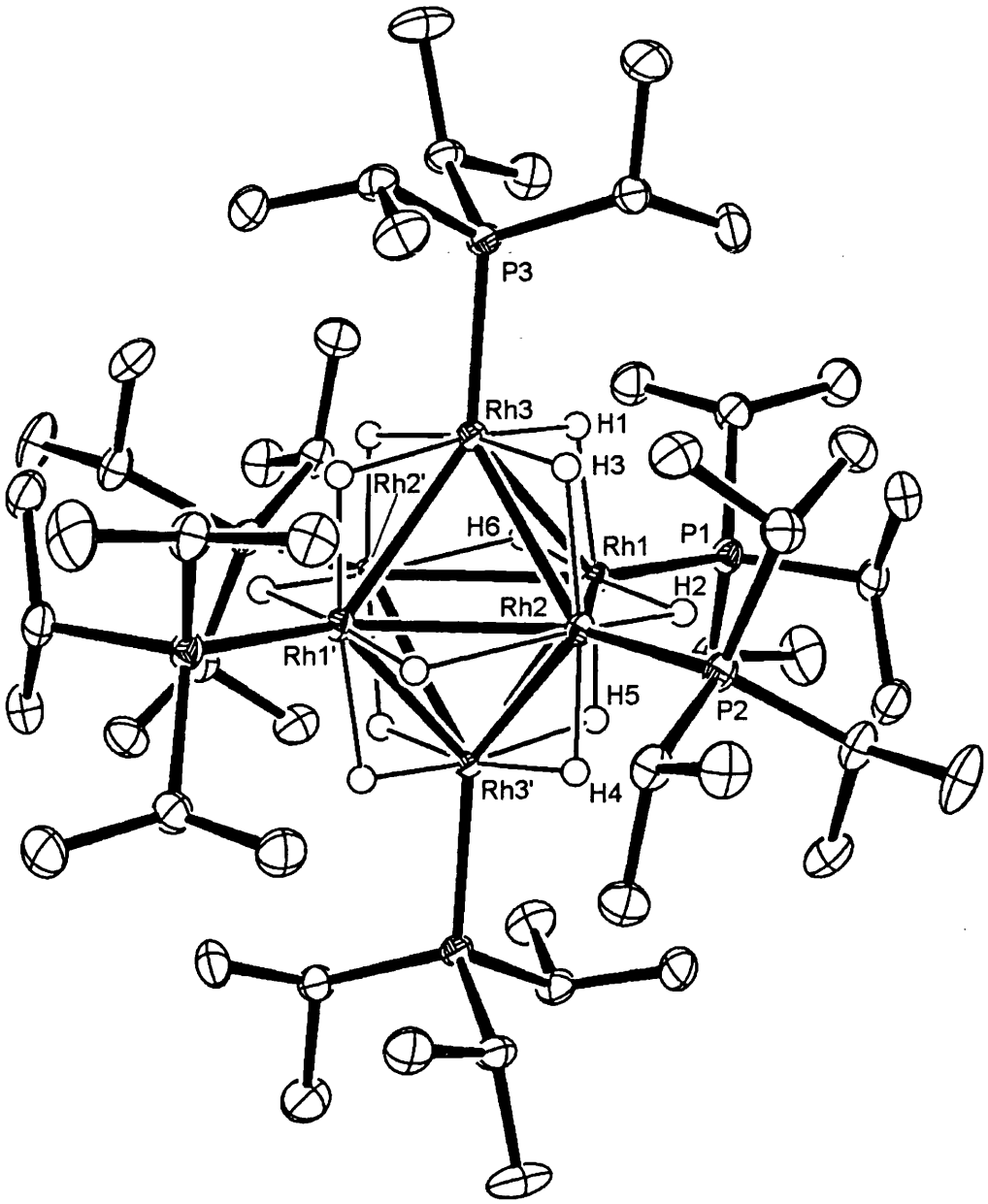

Figure 10: The molecular structure of the dicationic portion of $[(^{i}Pr_3P)_6Rh_6H_{12}][BAr_F]_2$, **27-$H_{12}$**, symmetry related positions generated by the following transformations, -x,-y,-z+2 and -x+1,-y+1,-z+1. Hydrogen atoms except the bridging hydrides removed for clarity. Thermal ellipsoids shown at the 30% probability level.

Rh1-Rh2	2.7142(2)	Rh1-Rh2-Rh3	59.967(6)	Rh1-H6	1.59(4)	Rh3-H3	1.96(3)
Rh1-Rh3	2.7209(2)	Rh1-Rh3-Rh2	60.206(6)	Rh2-H2	1.38(3)	Rh3'-H4	1.64(4)
Rh2-Rh3	2.7303(2)	Rh2-Rh1-Rh3	60.309(6)	Rh2-H3	1.70(3)	Rh3'-H5	1.86(3)
Rh1-P1	2.2461(6)	Rh1-H1	1.82(3)	Rh2-H4	1.85(4)	Rh1-Rh2-Rh1'	89.601(7)
Rh2-P2	2.2450(6)	Rh1-H2	2.04(3)	Rh2'-H6	1.93(4)	Rh1'-Rh1-Rh2	90.399(7)
Rh3-P3	2.2444(6)	Rh1-H5	1.66(3)	Rh3-H1	1.66(3)	Rh3-Rh2-Rh3'	89.433(7)

Table 1: Selected bond lengths (Å) and angles (°) for compound **27-H_{12}**.

The [1-H-*closo*-$CB_{11}Me_{11}$]$^-$ analogue may be prepared in the same way, and on recrystallisation yielded dark red crystals and a set of colourless crystals, both of which were suitable for X-ray diffraction studies. A crude data collection (resulting in a wR_1 = 10.6%) on the colourless crystals confirmed the formation of [$HP(^iPr)_3$][1-H-*closo*-$CB_{11}Me_{11}$] as a by-product (Figure 11).

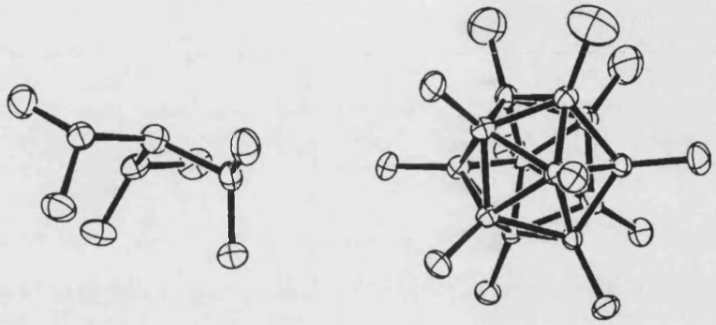

Figure 11: The molecular structure of [$HP(^iPr_3)$][1-H-*closo*-$CB_{11}Me_{11}$], hydrogen atoms are not shown and thermal ellipsoids are at the 30% probability level. The anion is disordered and the cage carbon atom was not located.

The identification of **27-H_{12}** was supported by an X-ray diffraction study performed on the dark red crystals, again revealing a dicationic Rh_6 octahedron which possessed similar gross structural parameters to the [BAr_F]$^-$ analogue, equally supported by six phosphines and twelve hydrides. A simplified schematic of this cluster is shown in Figure 12, with only the $P_6Rh_6H_{12}$ core structure shown.

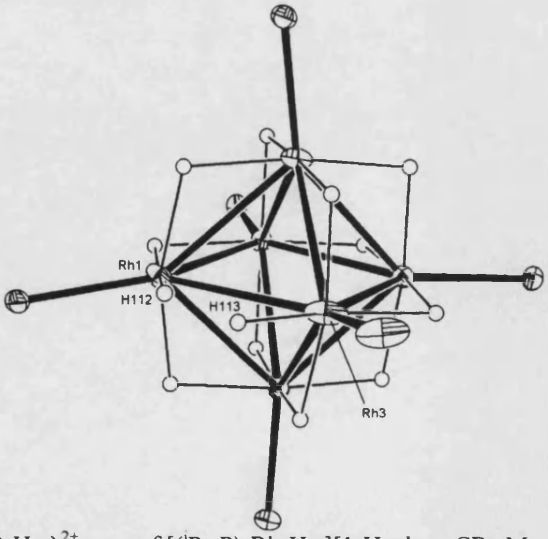

Figure 12: The $\{Rh_6P_6H_{12}\}^{2+}$ core of [$(^iPr_3P)_6Rh_6H_{12}$][1-H-*closo*-$CB_{11}Me_{11}$]$_2$, with the disordered hydride environment labelled.

However, there are some minor, structural differences in the two dicationic clusters structurally characterised. $[(^{i}Pr_3P)_6Rh_6H_{12}][1\text{-H-}closo\text{-}CB_{11}Me_{11}]_2$ does not reside on a centre of inversion, making all Rh-P and Rh-Rh vertices inequivalent and the range of Rh-Rh distances in this octahedron is noticeably greater (2.7181(3) – 3.0597(5) Å). The twelve bridging hydrides were still located in this structure, eleven readily refined with full occupancy as edge bridging hydrides, the final bridging position, involving the Rh1 and Rh3 edge is not spanned by a hydride. Instead the refinement revealed a positional disorder, with the expected bridging hydride apparently disordered over two terminal sites. It is interesting to note that this unique hydride arrangement is also the location of the longest Rh-Rh distance (Rh1-Rh3 3.0597(5) Å compared to an average = 2.794 Å). The phosphine associated with Rh1 is also disordered over two sites of equal occupancy. These slight differences are not believed to infer a different complex, though the two terminal hydride positions could be treated as fully occupied, generating a cluster with 13 hydrides, without any detrimental effect on the refinement. However, based on the solution chemistry of this cluster (discussed next), particularly the observed diamagnetism of these crystals, formulation as a 12 hydride-containing cluster is still favoured (both a H_{13} and a $H_{11}(\mu\text{-}H_2)$ cluster would have 77 cluster valence electrons and therefore be paramagnetic). The relatively small distortions compared to the $[BAr_F]^-$ congener are ascribed to crystal packing effects resulting from the change in the anion, and the large degree of positional disorder in the immediate environment around Rh1.

Due to the limitations inherent in the location of hydrides using X-ray diffraction data it was important to unambiguously confirm the number of hydrides

associated with these clusters, this was achieved by three complimentary techniques. Firstly, HYDEX[31] analysis (performed by Professor Paul Raithby, Department of Chemistry, University of Bath) confirmed that the lowest energy positioning of 12 hydrides around a $\{Rh_6P_6\}^{2+}$ core is as all edge bridging, with no hydrides in terminal positions, further suggesting that the two terminal sites observed in the [1-H-*closo*-$CB_{11}Me_{11}]^-$ solid-state structure are an artefact of disorder. Attempts to fit 8 face capping hydrides with four other terminal hydrides, or placing all twelve hydrides as terminal resulted in the experimentally observed structure with twelve bridging hydrides (Figure 13).

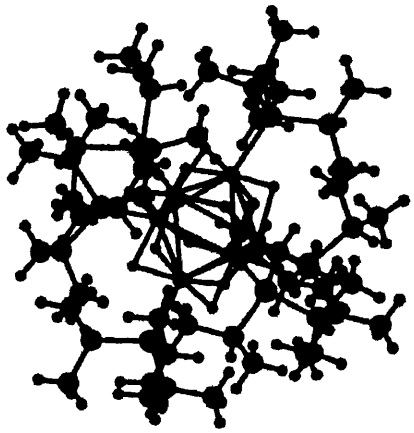

Figure 13: The calculated hydride positions in **27-H_{12}** from HYDEX analysis.

This analysis, however, only gives limited support to the experimental location of the 12 hydrides as edge bridging and it does not prove that the twelve hydrides observed are actually real and not, for example, ten fluxional edge bridging hydrides disordered over twelve positions.

In solution, both salts (bar the signals associated with the anion) display identical spectra, with the $^{31}P\{^1H\}$ NMR spectrum showing only one phosphorus environment (δ 110.5 ppm ^1J(RhP) 140 Hz) and a single broad hydride resonance at –

21.44 ppm in the ^{1}H NMR spectrum. The integral of this hydride resonance was 12H (repeatedly found for both salts, on independently synthesised samples and with a 5 s relaxation time to prevent saturation). The identical spectra for both salts and most importantly a matching 12 H integral hydride signal, confirm that both solid-state structures correspond to **27-H_{12}**. Definitive confirmation of the presence of 12 hydrides was forthcoming from mass spectrometry (FAB+ mode), with the radical cation, $[(^iPr_3P)_6Rh_6H_{12}]^{\bullet+}$, observed at 1590.3 m/z with the expected isotope pattern for $Rh_6C_{54}H_{138}P_6$ (Figure 14).

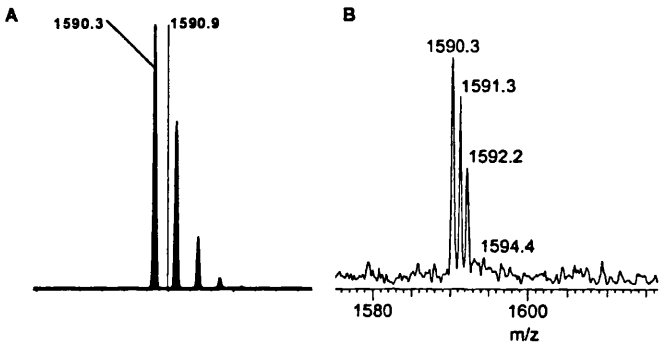

Figure 14: Calculated (A) and observed (B) mass spectrum for the radical cation $[(^iPr_3P)_6Rh_6H_{12}]^{\bullet+}$.

Progressively cooling a sample of **27-H_{12}** to 200 K in CD_2Cl_2 resulted in a gradual broadening of the hydride resonance, until at 210 K it broadens into the base line. The slow exchange regime was not obtained, indicating a rapid fluxionality of the hydrides over the surface of the cluster. The hydride resonance remained a broad singlet in the $^1H\{^{31}P\}$ NMR spectrum at 200 K, with no Rh-H or P-H coupling observed. With the unequivocal formulation of **27-H_{12}** now in hand, a full discussion of this cluster is possible. The structure of **27-H_{12}** bares striking resemblance to that for the early transition metal halides with edge bridging π donor ligands, exemplified by $[Nb_6(\mu\text{-}Cl)_{12}Cl_6]^{4-}$ (Figure 15)[32] as opposed to the late transition metal clusters (*e.g.*, $Rh_6(CO)_{16}$, Figure 15). A further link between **27-H_{12}** and the early transition metal halide clusters

is found on performing a cluster valence electron count (c.v.e) on **27-H_{12}**. This revealed an identical number of c.v.e (76) when compared to $[Nb_6(\mu\text{-}Cl)_6Cl_2]^{4-}$, again in contrast to that expected for late transition metal octahedrons (*e.g.*, $Rh_6(CO)_{16}$ has 86 c.v.e).

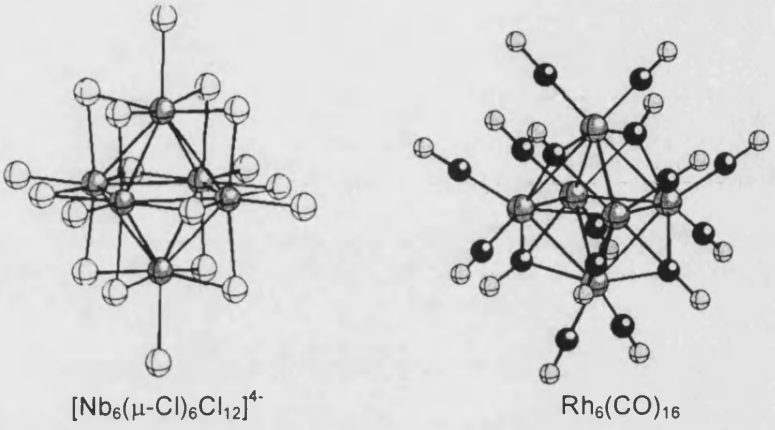

Figure 15: The solid-state structures of $[Nb_6(\mu\text{-}Cl)_6Cl_{12}]^{4-}$ and $Rh_6(CO)_{16}$.

That complex **27-H_{12}** has 76 c.v.e rather than 86 and shows a structural resemblance to $[Nb_6(\mu\text{-}Cl)_{12}Cl_6]^{4-}$ can be rationalised readily. Shifting from chlorides in the Nb cluster to hydrides and phosphines in **27-H_{12}** generates a deficiency of 24 electrons for cluster bonding. This shortfall is exactly offset by the move from Nb to Rh, which produces a net increase in metal electrons of 24 electrons, resulting in the observed identical c.v.e counts and therefore the close structural connection. This is an example of the electron count driving structure.

An even closer structural relationship is observed on comparison of **27-H_{12}** to a neutral $Zr_6Cl_{12}P_6H_2$ cluster (Figure 16),[33, 34] although in this case the cluster is supported by the considerably less bulky phosphine PMe_2Ph (respective cone angles PMe_2Ph = 121°, $^iPr_3P$ = 160°).[35] The c.v.e count for this closely related cluster is 74 electrons, two lower than that for **27-H_{12}**.

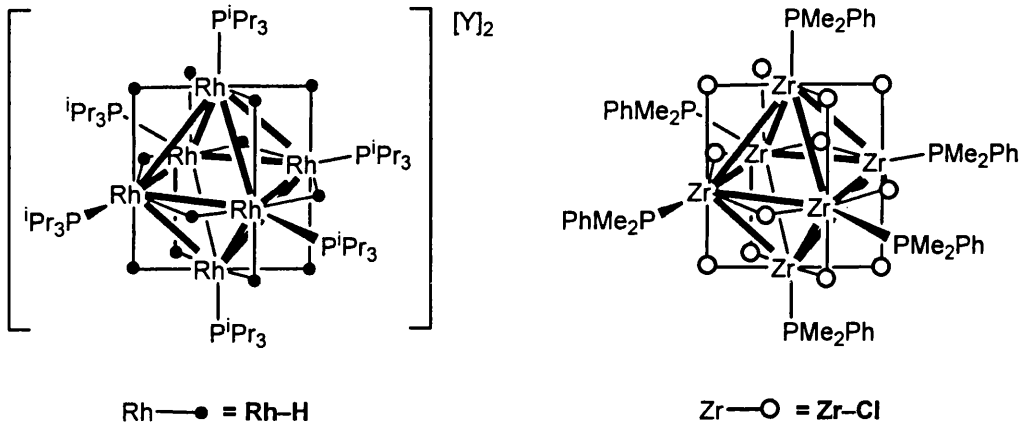

Figure 16: The close structural similarity between **27-H_{12}** and $Zr_6(\mu\text{-}Cl)_{12}H_2(PMe_2Ph)_6$ (hydride positions not known).

Along with the isolation of $Zr_6(\mu\text{-}Cl)_{12}H_2(PMe_2Ph)_6$ a cationic analogue was also synthesised, $[Zr_6(\mu\text{-}Cl)_{12}H_3(PEt_3)_6]^+$. The hydrides were not located in either of these 74 c.v.e count cluster solid state structures, though by comparison to closely related analogues, $[Zr_6Cl_{18}H_4]^{4-}$ and $[Zr_6Cl_{18}H_5]^{3-}$ (equally 74 c.v.e clusters) it is probable that they are face bridging in a (μ-3) mode.[36] Hexa-nuclear clusters with the $[Nb_6(\mu\text{-}Cl)_{12}Cl_6]^{4-}$ type atomic arrangement can exist equally with c.v.e. counts of 74 and 76, dependent on the metal-ligand set involved. The cluster $[Ta_6Cl_{12}(OTf)_6]^{n-}$ (n = 2, 3 or 4) can exist as both of these c.v.e counts, being reversibly reduced electrochemically in two one-step processes to the 76 c.v.e cluster (Figure 17),[37] although only the 74 and the paramagnetic 75 c.v.e count clusters have been isolated.[38]

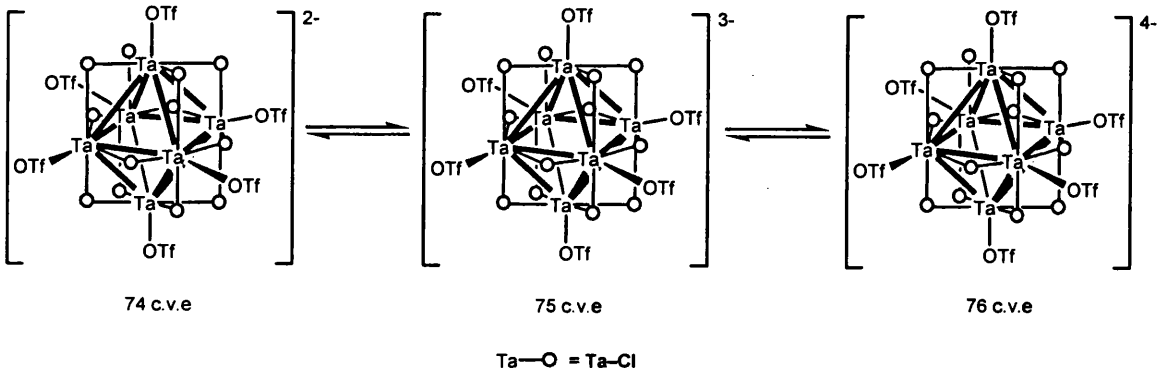

Figure 17: The reversible reduction of the $[Ta_6Cl_{12}(OTf)_6]^{2-}$ cluster.

6.2.1.2: Preliminary Mechanistic Studies

Deuteration studies on the decomposition of **22-$(H_2)_X$** have unambiguously demonstrated that the proton source in the formation of **26Pr** is external dihydrogen, with the replacement of H_2 for D_2 in the synthesis of **22** affording $[DP^iPr_3][Y]$, as shown by a 1:1:1 triplet (δ46.1 ppm, $^1J(DP)$ 68 Hz) in the $^{31}P\{^1H\}$ NMR spectrum. The formation of **27-H_{12}** therefore clearly involves the heterolytic activation of coordinated dihydrogen, as seen previously in the synthesis of $[Ru_4H_6(\eta^6\text{-}C_6H_6)]^{2+}$,[22] with the transfer of a proton to the phosphine generating **26Pr**. Intramolecular transfer of a proton from coordinated H_2 to an ancillary ligand is well known (*e.g.*, $[Os(\eta^2\text{-}H_2)(CO)(\text{pyridine-2-thiolate})(PPh_3)_2][BF_4]$, Figure 18),[2, 39] although to the best of our knowledge there are no examples of this process involving a phosphine.

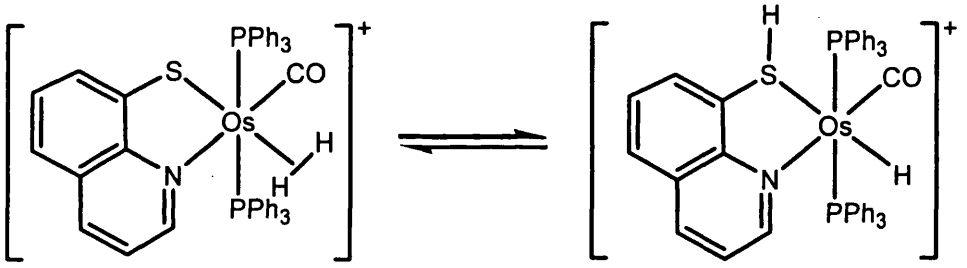

Figure 18: The reversible proton transfer from coordinated dihydrogen.

For proton transfer to occur in **22** a dihydrogen adduct (either the mono or the bis complex) has to be more acidic than $[HP^iPr_3]^+$, which has a pK_a of 9.0. Extensive work has been performed on the estimation of the pK_a's of dihydrogen complexes,[40] and complexes that are cationic are significantly more acidic than their neutral counterparts. **22-$(H_2)_2$** also must have a considerably lower pK_a than the neutral $[(^iPr_3P)_2Ru(H_2)_2(H)_2]$ (pK_a = 39), in which protonated phosphine does not form.[41]

Following the characterisation of **26Pr** there are still a number of possible mechanisms that could account for the formation of **27-H_{12}**. Hexa-nuclear clusters are well documented to self-assemble spontaneously from unsaturated mono nuclear precursors,[37] such as the fragment $\{(^{i}Pr_3P)Rh(H)_x\}$ that may well be formed after the loss of **26Pr** (Figure 19).

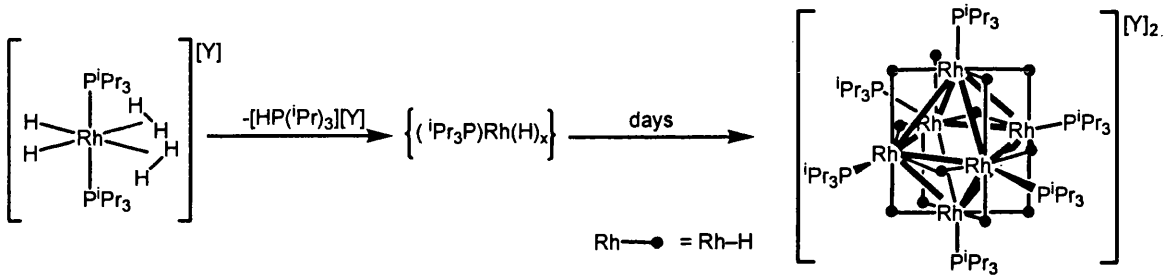

Figure 19: Cluster formation possibly via a $\{(^{i}Pr_3P)Rh(H)_X\}$ fragment.

This aggregation may occur directly from a mono-nuclear compound or via an intermediate cluster that would then undergo an equally well known fragment condensation reaction.[40] To elucidate this process the decomposition of **22** in C_6H_5F under 4 atmospheres of H_2 was monitored periodically by $^{31}P\{^{1}H\}$ NMR spectroscopy. Unfortunately the lack of suitable deuterated solvent (C_6D_5F) prevented the acquisition of suitable ^{1}H NMR spectra, whilst CD_2Cl_2 was not used due to side reactions that occur in competition to cluster formation, resulting in a more complex spectrum. The array of $^{31}P\{^{1}H\}$ NMR spectra are shown in Figure 20 for the duration of the cluster synthesis (monitoring for longer times resulted in no further change in the spectra).

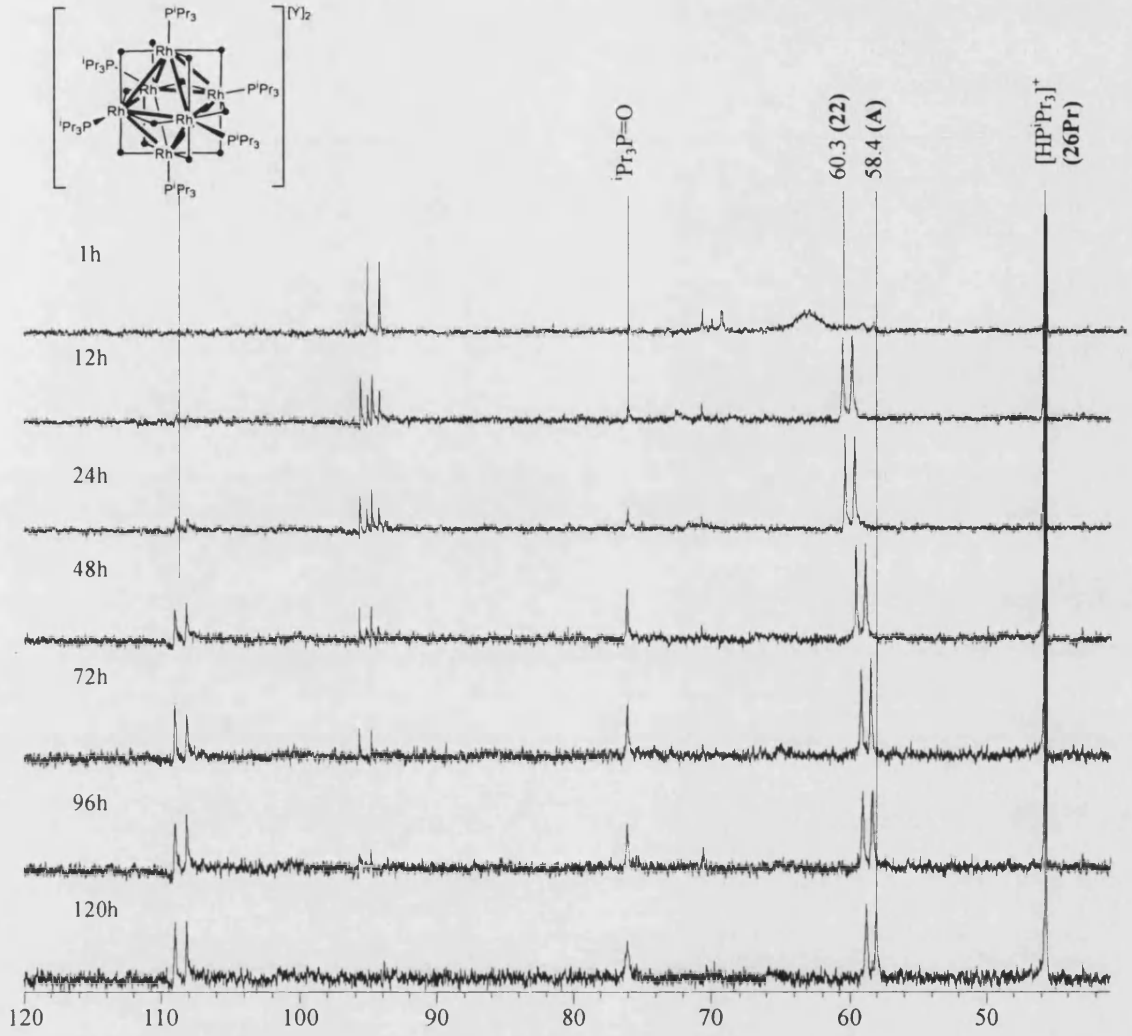

Figure 20: The $^{31}P\{^1H\}$ NMR spectra for the decomposition at 40°C of **22** in C_6H_5F under 4 atmospheres of H_2.

A number of important points can be taken from the analysis of these spectra: (i) after five days (120 h) the reaction is complete, with three major phosphine containing products, **26Pr**, **27-H$_{12}$**, and a doublet at 58.4 ppm (^{1}J(RhP) 115 Hz, Complex **A**) being observed; (ii) after 12 hours, the reaction shows the presence of significant quantities of **26Pr**, along with two intermediates at ~95 ppm; (iii) the intermediates are gradually converted into **27-H$_{12}$** over the course of the next 96 hours (confirmed by an examination of the mass balance of the system – Figure 21); (iv) the higher field doublet (initially at 60.3 ppm **(22)**, ^{1}J(RhP) 112 Hz) gradually shifts upfield over the course of

the reaction, until it is centred at 58.4 ppm (^{1}J(RhP) 115 Hz), with a concomitant growth of the resonance attributable to **26Pr**.

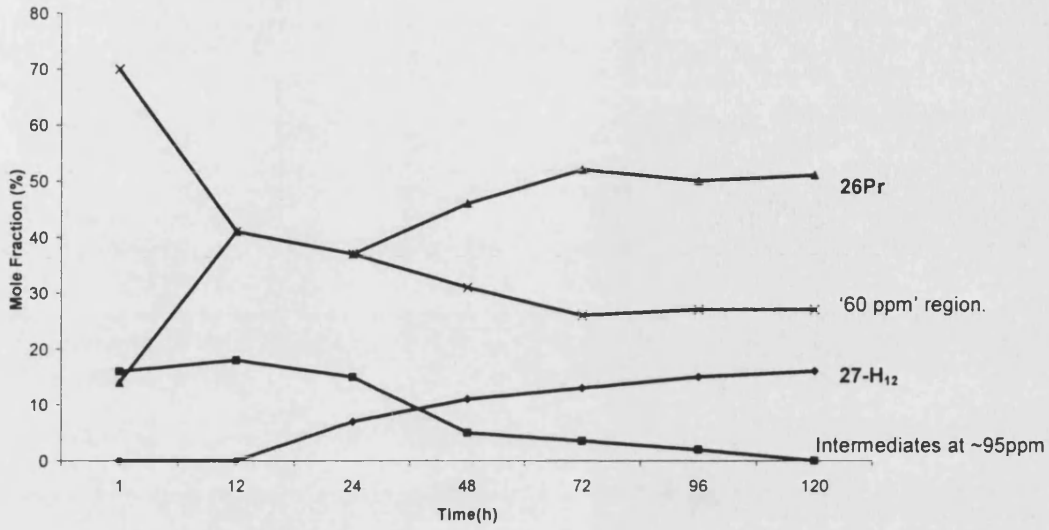

Figure 21: Mass balance for the various phosphine containing products in the decomposition at 40°C of **22** in C_6H_5F under 4 atmospheres of H_2 (values for ^{i}Pr$_3$P=O omitted for clarity). ■ = the intermediates at ~95ppm, ◆ = **27-H$_{12}$**, X = doublet in the range 58.4 to 60.0, ▲ = **26Pr**.

Inspection of the mass balance of this system (Figure 21) suggests that the intermediate complexes forms via the heterolytic cleavage of coordinated dihydrogen, with both the intermediate and **26Pr** present in equal concentration after 1 hour. The formula of the neutral rhodium fragment formed after loss of **26Pr** would be {(^{i}Pr$_3$P)RhH$_3$}, this could exist as a mono nuclear species further ligated by dihydrogen, generating a mixed hydride/dihydrogen complex (perhaps the 18 electron complex (^{i}Pr$_3$P)Rh(H)$_3$(η^2-H$_2$)$_2$). A more plausible formulation for this complex is as a tri-nuclear cluster formed from the unsaturated {(^{i}Pr$_3$P)RhH$_3$} fragment. The chemical shift (~95 ppm) for this complex is shifted downfield significantly away from the region expected for mono-nuclear complexes. Late-transition metal tri-nuclear clusters formed from the hydrogenation of mono-nuclear precursors are well-documented (see section **6.1**) and generally have a low c.v.e count of 42 electrons (*e.g.*, Pt$_3$H$_6$(P^{t}Bu$_3$)$_3$ and Rh$_3$H$_3$(POMe$_3$)$_6$ – unfortunately no ^{31}P{^{1}H} NMR spectra were reported for this

rhodium trimer)[13, 19] or 44 electrons (*e.g.*, $[Ir_3H_7(PCy_3)_2(py)_3]^{2+}$)[21]. This is compared to more classical electron precise trimers that have 48 c.v.e. An analogous structure with 42 c.v.e can be drawn for the intermediate in this system (Figure 22), which could then react further, possibly via an electronically unsaturated cationic species (generated by reaction with the acid by-product or the acidic **22-$(H_2)_x$** adducts) ultimately giving **27-H_{12}**.

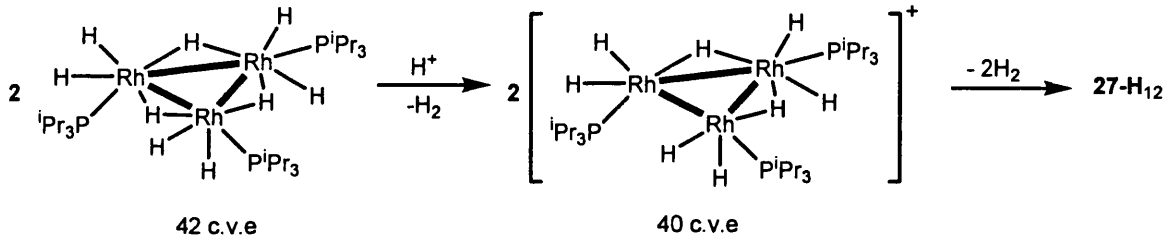

Figure 22: A postulated mechanism for the formation of **27-H_{12}** via the two observed intermediate complexes.

The 42 c.v.e count trimer shown in Figure 22 is also analogous to the early transition metal clusters, *e.g.*, $[Nb_3Cl_{10}(PR_3)_3]^-$,[34, 42] that have the same number of cluster electrons. Trimeric clusters with this c.v.e count generally are stable with respect to further agglomeration; therefore, for further fragment condensation to occur, an unsaturated intermediate compound is probably required. Examination of the intermediate region of the $^{31}P\{^1H\}$ NMR spectra (Figure 20) shows two products, one that initially predominates, but gradually reduces in intensity, with a concomitant growth in the other intermediate. This could be due to a process like that shown in Figure 22. The coalescence of two trimeric clusters yielding a hexa-nuclear cluster is documented[37] and often occurs with ligand expulsion, (*e.g.*, in the synthesis of $[Mo_6S_8(PEt_3)_6]$ by the reductive dimerization of two trinuclear molybdenum chloro-sulfido clusters).[43] The conversion of an intermediate oligomeric complex into a hexameric cluster has also been postulated to account for the formation of

$W_6(H)_5(C^iPr)(O^iPr)_{12}$, with the fusion of a number of reactive dimers yielding the octahedral cluster.[11] Specific precedence for a lower nuclearity cluster forming a higher one by the loss of hydrides is found when the tri-nuclear Pt cluster, $Pt_3H_6(P^tBu_3)_3$, self assembles on dehydrogenation to form the cluster $Pt_4H_2(P^tBu_3)_4$.[12-14] However, without further physical data on the structure of the intermediates involved in the formation of **27-H_{12}** this remains conjecture.

Equally importantly in this system is the elucidation of the by-product (termed complex **A** from here on), that accounts for approximately 50% of the rhodium content in this system. The ^1H NMR spectrum of **A** on removal of all free hydrogen has a hydride resonance at –24.90 ppm that on phosphorus decoupling collapses from a doublet of triplets to a doublet ($^1J(RhH)$ = 37 Hz). Therefore, the single hydride environment in this complex is coupling to two equivalent phosphines ($^2J(PH)$ 14 Hz) and one rhodium. Complex **A** is not the *solvento* complex **22-DCM**, due to different chemical shifts and coupling constants in both the ^1H and $^{31}P\{^1H\}$ NMR spectra. An accurate determination of the number of hydrides in **A** is frustrated by the constant presence of residual cluster, **27-H_{12}**, preventing a precise integration against the anion or $^iPr_3P$ resonances. An integral value corrected for the concentration of **27-H_{12}** gives a value of ~1.5 hydrides per $\{(^iPr_3P)_2Rh\}$ fragment. This could be interpreted in a number of ways, as either a $\{(^iPr_3P)_2RhH\}$ fragment, a $\{(^iPr_3P)_2RhH_2\}^+$ fragment or a cluster compound averaging to this ratio. The $\{(^iPr_3P)_2RhH\}$ fragment has been previously reported to form from the decomposition of $\{(^iPr_3P)_2(H)Rh\}_2(\mu\text{-}N_2)$, and is only transient, eventually resulting in the formation of unidentified complexes that are postulated to be oligomeric clusters in nature.[44] Complex **A** is not the mono-nuclear compound $(^iPr_3P)_2RhH$,[45] or in fact any monomeric Rh(I) complex due to the small

^{1}J(RhP) coupling constant (112 Hz) observed in the ^{31}P{^{1}H} NMR spectra ($Rh(I)(P^iPr_3)_2$ complexes generally have coupling constants in the region of ~150 Hz).[44] The dimeric compound $\{(^iPr_3P)_2RhH\}_2$ can also be ruled out, as this compound has a hydride resonance centred at –14.5 ppm, significantly downfield from that in **A**.[45] Furthermore, complex **A** is not the Rh(III) compound $(^iPr_3P)_2RhH_3$, (where the hydrides resonate as a broad singlet at –12.5 ppm).[44] It is also not assignable as **22-$(H_2)_x$** (x =1 or 2). We thus tentatively assign **A** as a trimeric, 42 c.v.e count cluster, either $Rh_3H_3(^iPr_3P)_6$ or $[Rh_3H_6(^iPr_3P)_6]^{3+}$ (Figure 23), similar to the known compounds $Rh_3H_3(POMe_3)_6$ and $Pt_3H_6(PBu_3)_3$ respectively.[13, 18] However, in **A** the hydrides have to be in terminal positions as a bridging mode would lead to a multiplicity drastically higher than that observed.[18] A cationic μ-3 hydride capped trimer analogous to the decomposition product from Crabtree's catalyst can also be discounted due to the observation of only one, non-fluxional, hydride environment in **A**. Mass spectrometry was not useful in characterising these complexes, as only a signal due to the fragment $\{(^iPr_3P)_2Rh\}^+\}$ was observed.

Figure 23: Postulated structures of complex **A**, both are terminal hydride Rh trimers with cluster valence electron count of 42.

An unsaturated cluster with a valence electron count of 42 is favoured as the chemical shifts corresponding to **A** change under a dihydrogen atmospheres, with a

downfield shift of the doublet observed in the $^{31}P\{^{1}H\}$ NMR spectrum (to 61.80 ppm, $^{1}J(RhP)$ 112 Hz). The hydride resonance previously observed as a doublet of triplets is now not detectable at room temperature, the resonance for free dihydrogen is also not observed, again indicating that a fluxional exchange process is occurring. This exchange is extremely facile, not being frozen out at 195 K. The observed reaction with dihydrogen may well be producing a $Rh_3H_5(P^iPr_3)_6$ or $[Rh_3H_8(P^iPr_3)_6]^{3+}$, this reactivity is consistent with 42 c.v.e count trimers, that can readily accept two electron donors to reach the equally stable count of 44 c.v.e.[46] An analogous addition of dihydrogen is also observed for $Rh_3H_3(POMe_3)_6$, which is also a 42 c.v.e rhodium trimer.[18] Due to the repeated failure to isolate crystalline material of **A** there is considerable uncertainty in its identity, precluding any further discussion.

A number of attempts were made to improve on the synthesis of the cluster compound **27-H_{12}** by varying H_2 pressure, temperature, and the solvent used. On moving to higher H_2 pressures (10 atmos.) there was a decrease in the amount of **27-H_{12}** formed (yield only 20%, the by-product was still complex **A** formed in 80% yield). This is in contrast to the copper polyhydrides and the $(R_3P)_xPt_xH_y$ clusters that need high H_2 pressures (up to 300 atm.) to form in good yield.[12-15] The reaction at a lower H_2 pressure (~1 atmosphere) did not greatly affect the outcome, with the synthesis leading to a 40% : 60% ratio of **27-H_{12}** : **A**. The presence of excess dihydrogen is vital, as an attempt to form **27-H_{12}** under an argon atmosphere led to no observable cluster products. All further reactions were performed under the apparent optimum of 4 atmospheres of H_2 pressure. At low temperatures (268 K) no detectable decomposition to **27-H_{12}** had occurred after 5 days, with the predominate rhodium containing product remaining **22-$(H_2)_X$**, although small quantities of the intermediate complexes (~5%, by $^{31}P\{^{1}H\}$ NMR

spectrum) were observed. At higher temperatures, (refluxing C_6H_5F, 368 K) a much quicker colour change was observed, with all the starting **22-$(H_2)_X$** consumed within 15 minutes, a new complex at 60.4 ppm in the $^{31}P(^1H\}$ NMR spectrum (doublet ^1J(RhP) 118 Hz) was the only rhodium containing product observed, along with 2 equivalents of **26Pr**. Attempts to recrystallise this product failed. Longer refluxing times led to only the resonance associated with **26Pr** being present in the $^{31}P\{^1H\}$ NMR spectrum, with metallic rhodium also deposited. At 323 K, reduced yields of **27-H_{12}** were observed *(vide infra)*, thus it was concluded that 313 K was the optimum temperature for this reaction. An attempt was also made in replacing fluorobenzene for dichloromethane. This led to the formation of **27-H_{12}**, but only in a low yield; a number of other products were also observed in the $^{31}P\{^1H\}$ and ^1H NMR spectra. These presumably arise from chloride abstraction (as found for **22-DCM**) by the unsaturated reactive intermediates. Once formed, however, cluster **27-H_{12}** and complex **A** are stable for weeks in CH_2Cl_2 solutions. Other anions (*e.g.*, $[PF_6]^-$ and $[BF_4]^-$) are not suitable for this system, with anion decomposition preventing cluster formation. On extended heating (14 days) of a solution of complex **A** under H_2, no **27-H_{12}** is formed; therefore, **A** is not an intermediate on the pathway to **27-H_{12}**. The optimum conditions were found to be ~4 atmospheres of H_2, C_6H_5F as the solvent, 5 days duration, 40°C heating and with a robust, weakly coordinating anion also essential.

6.2.1.3:Reactivity of $[(^iPr_3P)_6Rh_6H_{12}][Y]_2$.

In solution **27-H_{12}** is stable for days, but on evacuation for several hours, both the ^1H and $^{31}P\{^1H\}$ NMR spectrum show a significant change. The hydride resonance in the ^1H NMR spectrum shifts from -21.40 to –25.50 ppm, concomitantly the associated

integral decreases from 12 H to 10 H (again relative to the anion and ^{i}Pr resonances, determined on a number of different samples, with a 5 s delay to prevent pre-saturation). The $^{31}P\{^{1}H\}$ NMR spectrum had also changed, now showing a doublet centred at 107.5 ppm with a much reduced coupling constant (^{1}J(RhP) 110 Hz). This process is reversible, as on addition of dihydrogen **27-H$_{12}$** is cleanly reformed (Figure 24). The observation of a single hydride resonance suggests a fluxional system where the hydrides are in rapid exchange as it is impossible to arrange 10 bridging ligands around a L_6M_6 core and maintain O_h symmetry. Attempts to confirm the number of hydrides by mass spectrometry failed, with no cluster compound seen at all, and attempts to obtain crystalline material were not successful. Despite this, the complex can be assigned as the ten-hydride species, $[(^{i}Pr_3P)_6Rh_6H_{10}]^{2+}$, **27-H$_{10}$** with reasonable confidence solely from NMR spectroscopy.

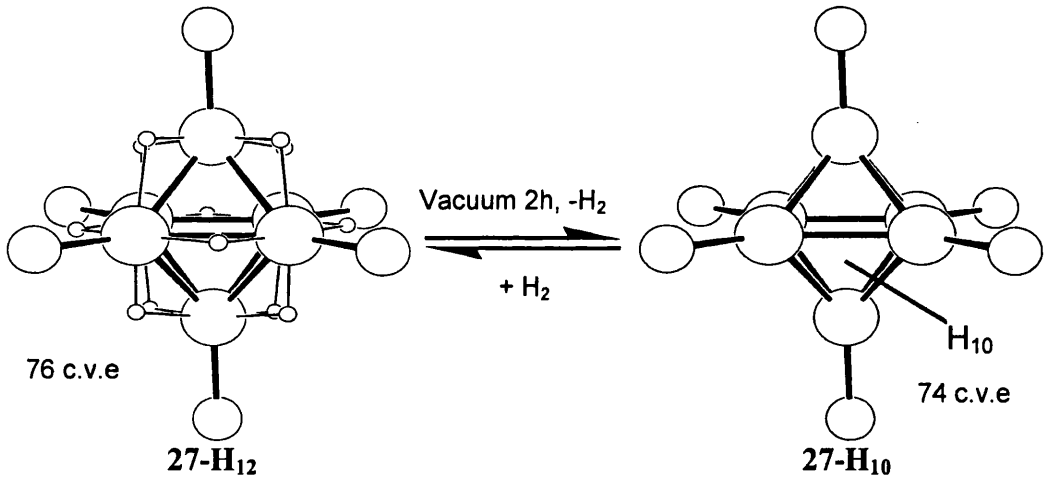

Figure 24: The reversible loss of H_2 from **27-H$_{12}$**, generating **27-H$_{10}$** (hydride locations not known).

The isolation of these two closely related stable clusters, differing by only two hydrides is achievable due to the two possible stable cluster valence electrons counts (74 and 76 respectively) for the octahedrons with this geometric arrangement. Clusters that are able to co-exist as each of these two c.v.e counts have been previously reported (*e.g.*, the $[Ta_6Cl_{12}(OTf)_6]$ cluster that can exist as the 2- or the 4- complex).[38, 47] The

reversible loss/addition of H_2 to a cluster framework has also been reported.[11, 22] The loss of a number of the inner hydride ligands (here the bridging ligands are termed inner and the terminal ligands axial) in **27-H_{12}** is unusual for $[M_6(\mu^2\text{-}X)_{12}Y_6]^n$ systems, as in the plethora of early transition metal clusters with comparable geometries the inner ligands are substitutionally inert, whilst the axial ligands are labile.[38] This disparity may well be due to the differing electron donor properties, with bridging halides acting as a three electron donor in comparison to H^-, a one electron donor.

Extended evacuation of **27-H_{12}** (5 days) resulted in the complete loss of the resonances associated with the cluster in both the ^1H and the $^{31}P\{^1H\}$ NMR spectra. In fact, no hydride resonances in the ^1H NMR spectrum and no rhodium containing products in the $^{31}P\{^1H\}$ NMR spectrum were observed. This reaction is irreversible as recharging the solution with H_2 did not result in the regeneration of either **27-H_{10}** or **27-H_{12}**. This decomposition must be initiated by further vacuum induced loss of dihydrogen.

Deuteration studies on **27-H_{12}** showed that placing a solution of **27-H_{12}** under a D_2 atmosphere resulted in no reduction in the intensity of the associated hydride signal. This clearly shows that there is no exchange between the hydrides on **27-H_{12}** and D_2, a finding that is supported by the observation of individual signals for both **27-H_{12}** and free H_2 (4.60 ppm) in the ^1H NMR spectrum when placed under a H_2 atmosphere. However, placing a sample of **27-H_{10}** under a D_2 atmosphere resulted in a hydride resonance (-21.38 ppm) very similar to that observed for the *perprotio* isotopomer, **27-H_{12}** (-21.44 ppm) and a $^{31}P\{^1H\}$ NMR spectrum corresponding to the high hydride cluster, while the hydride resonance still integrated to 10 H. This is consistent with the

formation of the isotopomer, $[(^{i}Pr_3P)_6Rh_6(H)_{10}(D)_2]^{2+}$ (Figure 25). In each of the deuterium reactions no free H_2 or HD was observed.

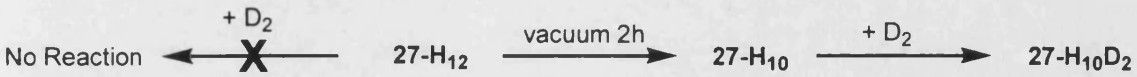

Figure 25: The respective reactivities of **27-H_{12}** and **27-H_{10}** towards D_2.

Complexes **27-H_{12}** and **27-H_{10}** are stable to significant concentrations of weak acid (in the form of the protonated phosphine **26PR**, pKa of 9.0),[40] with no protonation occurring. The reactivity of the related zirconium clusters, $[Zr_6X_{18}H_5]^{3-}$ (X = Cl or Br) was found to be dependent on the steric shielding supplied by the bridging halides, with $[Zr_6Br_{18}H_5]^{3-}$ considerable more stable than its chloride congener.[36] A similar steric protection could well be the source of the stability of **27-H_{12}**, as the space filling diagram reveals an almost complete encapsulation of the Rh_6H_{12} core by the alkyl periphery (Figure 26).

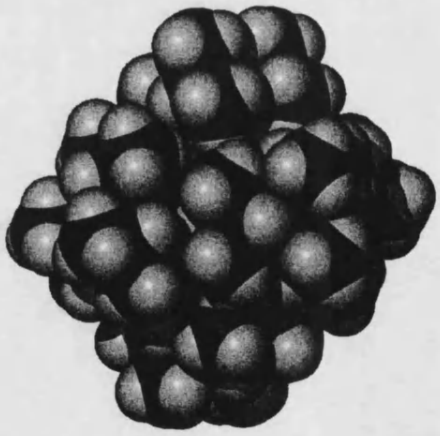

Figure 26: The space filling diagram of the dicationic portion of **27-H_{12}**.

The cluster, **27-H_{12}**, however does react with acetonitrile to generate a mixture of unidentified products as determined by $^{31}P\{^{1}H\}$ and ^{1}H NMR spectroscopy. Addition

of an excess (100 fold) of 1-hexene to a dihydrogen saturated solution of **27-H_{12}** resulted in the complete hydrogenation to hexane (by G.C. analysis); however, the system is not recyclable with no activity to a second batch of 1-hexene. NMR spectroscopy on the post-hydrogenation solution showed that no **27-H_{12}** remained, furthermore no signals were detected in the hydride region of the ^{1}H NMR spectrum or in the $^{31}P\{^{1}H\}$ NMR spectrum.

In an attempt to isolate crystalline material of the postulated Rh_3 cluster (complex **A**) the decomposition of the dihydrogen adduct with a bulkier phosphine, PCy_3 was investigated. The significant steric crowding around the periphery of **27-H_{12}** suggests that an increase in the Tolman cone angle of 10° may also be sufficient to prevent the condensation of the intermediate complexes, allowing for their isolation and full characterisation. Importantly, by analogy to the early transition metal clusters the use of the more electron donating phosphine, PCy_3, may also stabilise clusters with a lower valence electron count (i.e., a 8 hydride analogue of **27** with a c.v.e of 72). In the early transition metal cluster analogues the electron donor strength of the axial ligand is the primary factor in influencing the relative stabilies of the possible formal oxidation states of the M_6X_{12} core.[38] This is exemplified by the niobium series (Figure 27), that with π acceptor ligands (phosphines, $[CN]^-$) favour the 76 c.v.e count, with π donor ligands (*e.g.*, halide) the 74 c.v.e count and very basic ligands (*e.g.*, primary amines) resulting in a significant alteration in the octahedral structure, changing from twelve edge bridging halides to eight face capping halides.[48-50]

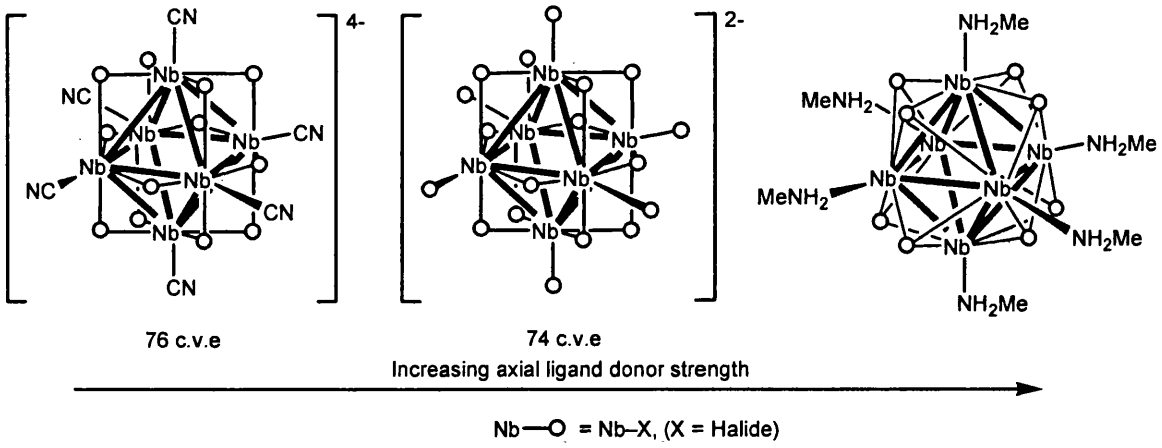

Figure 27: The effect of axial ligand π donor ability on the geometry of stable octahedral Niobium halide clusters.

6.2.2:[$(PCy_3)_6Rh_6H_X$][Y]$_2$ (Y = [1-H-*closo*-$CB_{11}Me_{11}$]$^-$ or [BAr_F]$^-$).

The ^{1}H and ^{31}P{^{1}H} NMR spectra of **23-$(H_2)_x$** on standing in CD_2Cl_2 solutions at ambient conditions under 4 atmospheres of H_2 showed the slow formation of [$HPCy_3$][Y] (**26Cy**) in an analogous manner to **22-$(H_2)_x$**. A heterolytic cleavage of coordinated dihydrogen is therefore again occurring, which is accelerated on heating fluorobenzene solutions of **23-$(H_2)_x$** to 50°C. After 5 days the ^{31}P{^{1}H} NMR spectrum of the brown solution (in H_2 saturated CD_2Cl_2) appeared to show four products, (**26Cy**), a broad doublet centred at 52.73 ppm (^{1}JRhP 101 Hz, the major rhodium containing product ~ 85%), a broad singlet at 88.5 ppm and finally another broad singlet at 109.6 ppm. The hydride region of the ^{1}H NMR spectrum however consisted of only two resonances, a major and a minor, both broad singlets at –24.50 and –21.63 ppm respectively. In addition to the resonances associated with **26Cy** and that attributable to cyclohexyl phosphine (1.01 to 2.19 ppm), at approximately 0.50 ppm a very broad singlet was also observed. The spectra were identical for both the [1-H-*closo*-$CB_{11}Me_{11}$]$^-$ and the [BAr_F]$^-$ anions. Recrystallising a concentrated C_6H_5F sample of the

[1-H-*closo*-$CB_{11}Me_{11}$]$^-$ reaction mixture by the slow diffusion of pentanes at room temperature under a dihydrogen atmosphere yielded a set of brown crystals and a set of colourless crystals. ^1H and $^{31}P\{^1H\}$ NMR spectroscopy on the colourless crystals allowed them to be characterised as **26Cy**. An X-ray diffraction study on the brown crystals (isolated in only 10% yield) revealed that the asymmetric unit consisted of a $\{(PCy_3)Rh\}_6$ cluster core, analogous to that observed in **27-H_{12}**, two anions (that showed no positional disorder) and one molecule of CH_2Cl_2. Figure 28 shows the molecular structure of the dicationic cluster core with pertinent bond distances and angles.

Despite a decent data set (wR_1 = 5.7%) the hydrides could not be refined reliably and thus were not considered in the final stages of refinement. Examination of the structural metrics revealed an essentially symmetrical dicationic $\{PRh\}_6$ octahedral core, however the Rh3 apex does appear to be slightly elongated. The Rh-Rh bond lengths range from 2.7201(8) to 3.1315(9) Å, possibly suggesting an inequivalent hydride substitution pattern on the cluster core. However, considering that the solid state structure of the [1-H-*closo*-$CB_{11}Me_{11}$]$^-$ salt of **27-H_{12}** had an equally wide range of Rh-Rh distances (2.7181(3) – 3.0597(5) Å) this is probably a packing artefact.

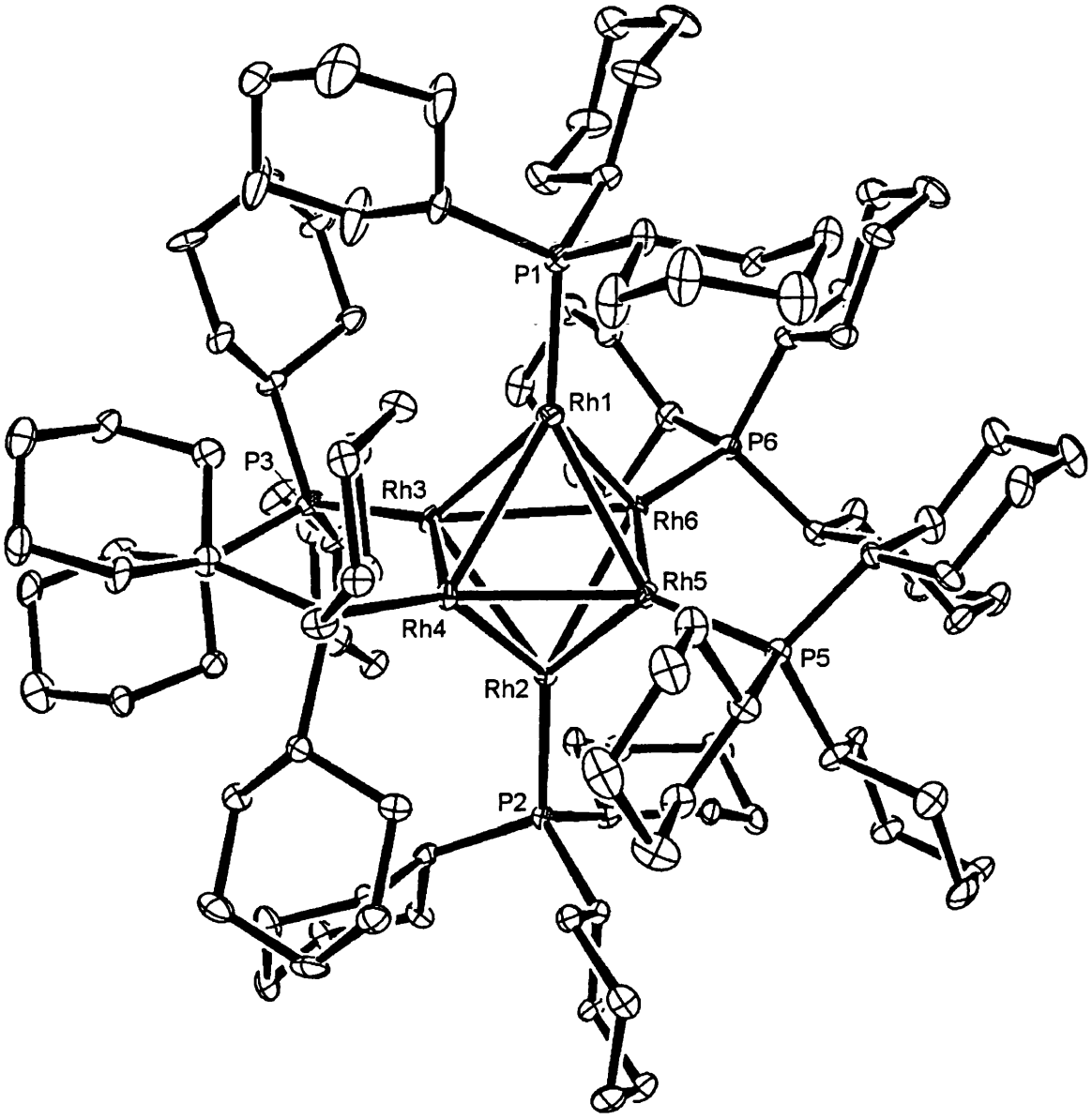

Figure 28: The molecular structure of the dicationic portion of $[(PCy_3)_6Rh_6H_X][1\text{-H-}closo\text{-}CB_{11}Me_{11}]_2$, **28-H$_X$**, hydrogen atoms associated with the cluster were not located, and all hydrogens are omitted for clarity. Thermal ellipsoids shown at the 30% probability level.

Rh1-Rh3	3.1315(9)	Rh2-Rh5	2.7201(8)	Rh1-P1	2.2347(19)	Rh4-Rh1-Rh5	58.326(18)
Rh1-Rh4	2.777(1)	Rh2-Rh6	2.7585(7)	Rh2-P2	2.2482(17)	Rh4-Rh1-Rh6	85.77(2)
Rh1-Rh5	2.8116(7)	Rh3-Rh4	2.9244(7)	Rh3-P3	2.2478(19)	Rh5-Rh2-Rh4	59.961(18)
Rh1-Rh6	2.8648(7)	Rh3-Rh6	2.7984(7)	Rh4-P4	2.2710(19)	Rh5-Rh1-Rh3	86.07(2)
Rh2-Rh3	2.7922(7)	Rh4-Rh5	2.7235(7)	Rh5-P5	2.2466(19)	Rh5-Rh2-Rh3	94.95(2)
Rh2-Rh4	2.7301(7)	Rh5-Rh6	2.7436(7)	Rh6-P6	2.2628(18)	Rh4-Rh2-Rh6	88.80(2)

Table 2: Selected bond lengths (Å) and angles (°) for compound **28-H$_X$**.

The $[BAr_F]^-$ congener, $[(PCy_3)_6Rh_6H_x][BAr_F]_2$ (Figure 29) was also recrystallised in an analogous manner (again requiring a dihydrogen atmosphere and again in poor yield). As for complex **27-H_{12}** this anion produces a more symmetrical octahedral core. The asymmetric unit consists of a Rh_3 triangular face, and one heavily disordered anion that is remote.

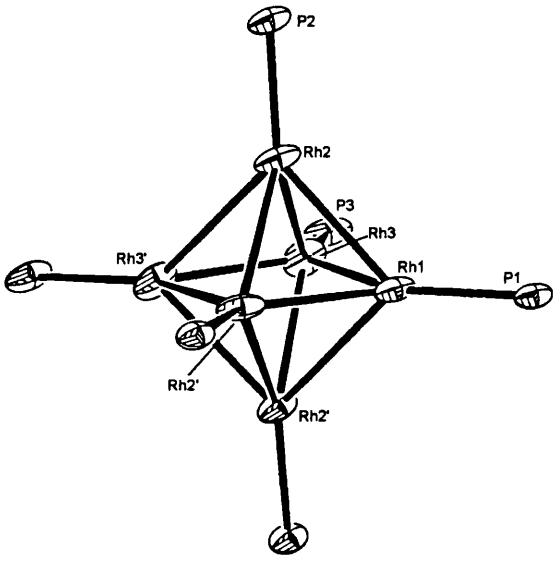

Rh1-Rh2	2.8034(9)
Rh1-Rh3	2.8493(9)
Rh2-Rh3	2.8841(10)
Rh1-Rh2-Rh3	60.11(2)
Rh1-Rh3-Rh2	58.54(2)
Rh2-Rh1-Rh3	61.35(2)
Rh1-P1	2.248(2)
Rh2-P2	2.236(2)
Rh3-P3	2.246(3)
Rh1-Rh3-Rh3'	89.96(3)
Rh1'-Rh1-Rh3	89.99(3)
Rh1'-Rh2-Rh3	89.66(3)

Table 3: Selected bond lengths (Å) and angles (°) for $[(PCy_3)_6Rh_6H_X][BAr_F]_2$.

Figure 29: The $\{PRh\}_6$ core of $[(PCy_3)_6Rh_6H_X][BAr_F]_2$, thermal ellipsoids at the 30% probability level.

Definitive characterisation of the number of hydrides present in these clusters is based on a combination of NMR and mass spectroscopy. The ^1H NMR spectrum of crystals of the $\{PRh\}_6^{2+}$ cluster under a dihydrogen atmosphere displayed a broad hydride resonance at –21.53 ppm, that is not in exchange with free dihydrogen (observed at 4.60 ppm). In addition to the signals corresponding to the anion and PCy_3 there is an additional broad resonance at 0.50 ppm. The integration of these signals (repeated on numerous independently synthesised samples, with a 5 second delay) gave a relative integral (in comparison to the anion resonances) of approximately 2 : 12 (0.50

ppm and –21.53 ppm resonances respectively Figure 30). The spectra are independent of the anion utilised.

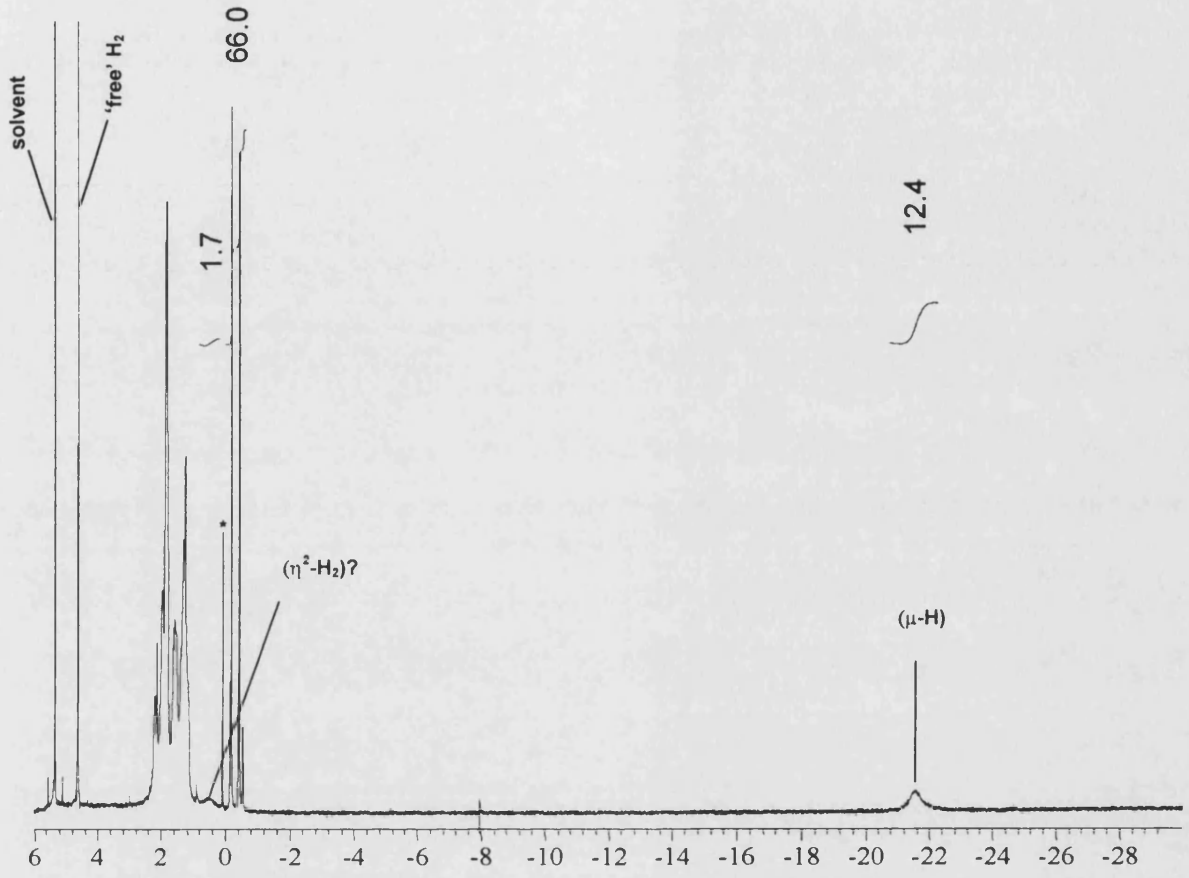

Figure 30: The ^{1}H NMR spectrum (in CD_2Cl_2) of the $[(PCy_3)_6Rh_6H_X][1\text{-H-}closo\text{-}CB_{11}Me_{11}]_2$ cluster under a dihydrogen atmosphere, (* = resonance attributable to vacuum grease).

The observed ^{1}H NMR spectrum suggests the presence of twelve hydrides (possibly edge bridging) as previously seen for **27-H_{12}** that are also not in exchange with free H_2 (δ 4.60 ppm). However, there is also an integral two, broad resonance at 0.5 ppm, which is in the range expected for coordinated dihydrogen.[1] This allows for a tentative formulation as $[(PCy_3)_6Rh_6H_{12}(H_2)][Y]_2$, **28-$H_{14}$**, with 12 edge bridging hydrides and two hydrides (possibly of the non-classical variety) in a different chemical environment. The calculation of T_1 values on these two hydrides confirmed that the

resonance at –21.53 ppm is a hydride (with a relaxation time of 157 ms), however the T_1 value for the 0.50ppm resonance was unobtainable, possibly due to its broadness and proximity to the PCy_3 resonances. A $^1H\{^{31}P\}$ NMR spectrum was effectively identical to the non decoupled spectrum. Dihydrogen can coordinate to clusters, as shown in the compound $[Ru_4H_6(C_6H_6)_4]^{2+}$ where one hydride resonance is characterised as an intact η^2-H_2 ligand by the short T_1 value of 34 ms.[22] The $^{31}P\{^1H\}$ NMR of **28-H_{14}** showed two broad resonances at 88.5 ppm and at 109.6 ppm, in a relative ratio of 2:1, demonstrating two inequivalent phosphine environments in this cluster. Support for the number of hydrides around the $\{PRh\}_6^{2+}$ core was forthcoming from mass spectroscopy, which identified the molecular di-cation $[(PCy_3)_6RhH_{14}]^{2+}$ at 1158.3 m/z (Figure 31).

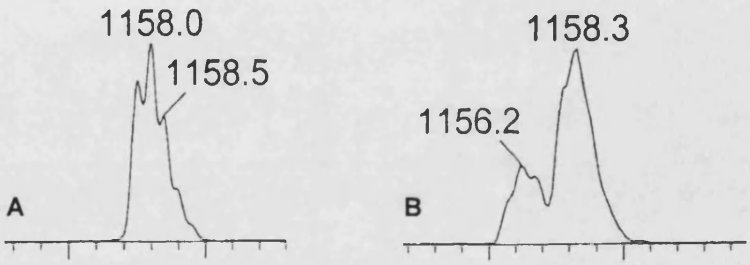

Figure 31: **A** theoretical, **B** observed isotope pattern for $[(PCy_3)_6Rh_6H_{14}]^{2+}$, **28-$H_{14}$**, (1158.3m/z), the observed 'shoulder' at 1156.2 is assignable to $[(PCy_3)_6Rh_6H_{10}]^{2+}$ (1156.2m/z)

As well as providing confirmation of the hydride count in **28-H_{14}** the mass spectrum also suggests that **28-H_{14}** can lose a number of hydrides to form a ten hydride complex (*e.g.*, as observed for **27-H_{10}**). Cluster **28-H_{14}** does lose a number of hydrides under vacuum, though this takes considerably longer than for **27-H_{12}**. After 2 days evacuating there is still a significant amount of **28-H_{14}** as well as two new equally broad hydride resonances at –26.51 ppm and -28.45 ppm, interestingly these two signals are in a respective ratio of 8 : 2. Further evacuation (> 3 days) results in the complete loss of resonances attributable to **28-H_{14}**, cleanly forming one product as determined by the

$^{31}P\{^{1}H\}$ NMR spectrum this time a single sharp doublet at 92.1 ppm (^{1}J(RhP) 97.8 Hz). The two hydride resonances observed in the ^{1}H NMR spectrum were repeatably integrated to 8 H and 2 H respectively (again on a number of samples each with a 5 second delay). This allows for the formulation of the low hydride cluster as $[(PCy_3)_6Rh_6H_{10}][Y]_2$, **28-$H_{10}$**, again with two inequivalent hydride positions. The integral eight hydride signal may well be attributable to eight face bridging hydrides, in an analogous manner to that observed for the halides in $Nb_6I_8(NH_2Me)_6$ and for the seven hydrides in $Th_6Br_{15}H_7$ (here the seven hydrides are disorder over the eight faces).[50, 51] This reaction is reversible (Figure 32), with **28-H_{14}** quantitatively reformed on exposure of a solution of **28-H_{10}** to a dihydrogen atmosphere. No intermediate cluster complex with 12 hydrides, analogous to **27-H_{12}** is observed in either the ^{1}H or the $^{31}P\{^{1}H\}$ NMR spectra.

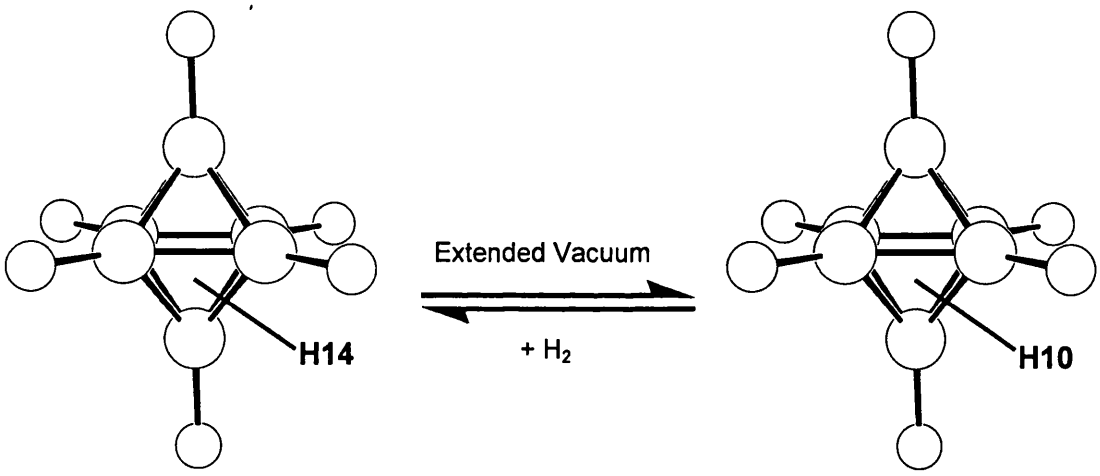

28-H_{14} **28-H_{10}**

Figure 32: The reversible addition/loss of dihydrogen to the $\{(PCy_3)_6Rh_6\}$ cluster core.

The observation of both sets of hydride signals after 2 days vacuum rules out a rapid room temperature equilibrium between the two clusters, **28-H_{14}** and **28-H_{10}**. The formation of a ten hydride cluster octahedral was expected as this would result in a 74

c.v.e count, a known stable electronic configuration for these systems and is analogous to **27-H_{10}**. However, the formation of a 14 hydride cluster certainly was not, as this formally counts to 78 c.v.e an unprecedented value (a paramagnetic $[Nb_6Cl_{18}]^{5-}$ cluster has been previously reported with a c.v.e. count of 77).[37] A possible explanation that may account for this unusually high cluster count comes from some preliminary EHMO calculations (performed by Dr A. S. Weller) which reveals a small HOMO LUMO gap for a model complex. Therefore, it is feasible that a small 2 electron donor (like H_2) that can penetrate the cyclohexyl periphery could bond with the cluster. An early transition metal cluster with 20 ligands around the M_6 core, $[Zr_6Cl_{12}(PR_3)_6H_2]$ has been reported and suggested to have 2 face bridging hydrides as well as the unambiguously characterised twelve edge bridging chlorides.[36] An analogous structure could be suggested in **28-H_{14}**, with twelve edge bridging hydrides and either two hydrides or one dihydrogen molecule face bridging. However, the positioning and the nature (classical or non-classical) of these hydrides will not be unambiguously resolved until a full neutron diffraction analysis has been performed.

The disparity in the behaviour of the respective (^{i}Pr_3P and PCy_3) high hydride content $\{PRh\}_6^{2+}$ clusters is further highlighted by the reaction of **28-H_{14}** with D_2. The ^{1}H NMR spectrum of a degassed sample of **28-H_{14}** when placed under an atmosphere of D_2 shows a hydride signal in the expected region (-21.58 ppm), however the associated integral has been reduced to 9.8 H. Furthermore, both free H_2 (4.60 ppm) and HD (triplet ^{1}J(DH) 42 Hz at 4.57 ppm) are observed (Figure 33).

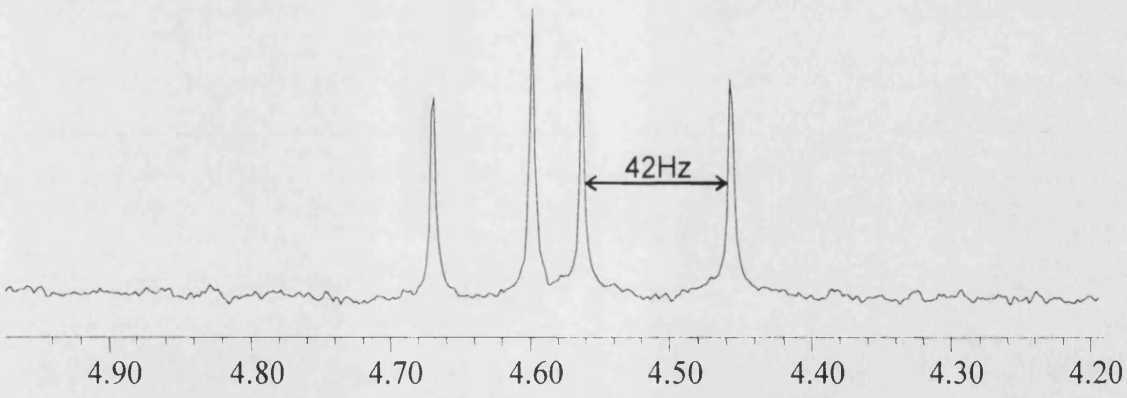

Figure 33: The uncoordinated dihydrogen region of the ^{1}H NMR spectrum of a degassed solution of **28-H_{14}** under D_2.

Unsurprisingly no resonance is now observed at 0.50ppm (the position of the proposed dihydrogen ligand), this would be expected to be the weakest bound, and thus most readily displaced by D_2 (or lost under vacuum). The formation of D_2 must involve the cleavage of a molecule of coordinated D_2, this probably occurs on the unsaturated cluster, **28-H_{10}**, as **28-H_{14}** does not undergo an exchange process with free H_2.

In contrast to the ^{i}Pr$_3$P analogue the loss of hydrides resulting in the conversion of **28-H_{14}** to **28-H_{10}** is not facile, requiring a number of days under high vacuum to complete the transformation. Therefore, dissolution of the bulk crystalline sample previously used in the X-ray diffraction analysis can be relied upon to give a representative spectrum, importantly with a reliable hydride environment. Crystals of both the [1-H-*closo*-$CB_{11}Me_{11}$]$^-$ and [BAr_F]$^-$ congeners on dissolution in CD_2Cl_2 unambiguously show a signal at 0.50 ppm and –21.53 ppm, identifying them both as the high hydride cluster, **28-H_{14}**.

The fluxionality of **28-H_{14}** was also examined, with a CD_2Cl_2 sample under 4 atmospheres of H_2 progressively cooled down to 195 K. At 250 K in the ^{1}H NMR

spectrum the tentatively assigned coordinated dihydrogen resonance has shifted downfield to approximately 0.75 ppm, an accurate integration at this temperature is not possible due to it partially overlapping with the broad PCy_3 resonances. The hydride resonance has become more complex, splitting into five broad singlets between –16.5 and –27.6 ppm and one very broad signal approximately centred at –21.3 ppm. This indicates that one of the fluxional processes has been frozen out, though the extremely broad hydride resonance indicates that the slow exchange regime has not been reached. The $^{31}P\{^1H\}$ NMR spectrum still consists of two broad singlets, again in a 1:2 ratio. The inequivalent hydride environments could well be associated with the additional H_2 ligand, as this is not seen for **27-H_{12}** at this temperature. Further cooling to 195 K resulted in no significant change in the $^{31}P\{^1H\}$ NMR spectrum, but there is another increase in the complexity of the hydride region (Figure 34).

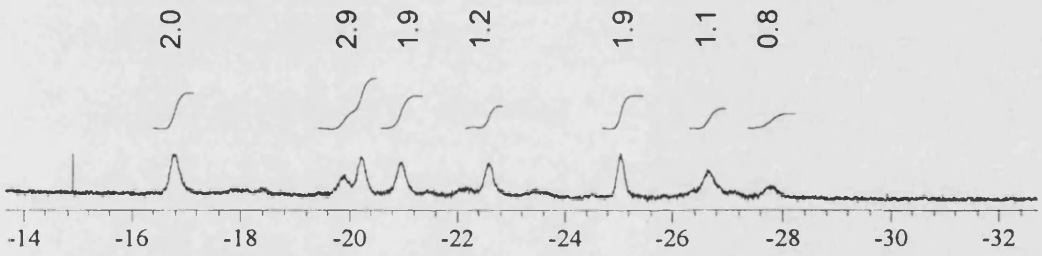

Figure 34: The hydride region of the ^1H NMR spectrum of **28-H_{14}** at 195K (integrated against anion resonances).

Eight signals now are observed between –16.78 ppm and –27.89 ppm, integrating each results in a 2:1:2:2:1:2:1:1 ratio, totalling 12 protons as expected from the room temperature spectra. The 'dihydrogen' resonance is not observed, possibly due to it now being coincident with the broadened, complex, PCy_3 signal. The $^1H\{^{31}P\}$ spectra shows no significant change in the hydride region, with eight major resonances still observed. Therefore, the binding of the additional hydrides in **28-H_{14}** in comparison

to **27-H_{12}** has resulted in two different phosphine environments (ratio 2:1), and eight (possibly edge bridging) different hydride environments (2:1:2:2:1:2:1:1 ratio). Due to the complexity of the system and the uncertainty in whether the addition ligand(s) is two hydrides or a dihydrogen molecule means that any discussion about the location of individual hydrides at low temperature is not possible. The important point is that coordination of an extra ligand has occurred on alteration of the phosphine to PCy_3, resulting in a cluster that is chemically very different to the $^iPr_3P$ congener. This is shown by addition of an excess of acetonitrile to **28-H_{14}**, on which the ^1H NMR spectrum still shows one broad hydride signal, that is slightly shifted to –21.56 ppm, (in comparison to **28-H_{14}** –21.53 ppm), however a broad resonance is still observed at 0.5ppm indicating that the cluster, **28-H_{14}**, has persisted. This is further supported by the lack of free dihydrogen in the ^1H NMR spectrum, which would be expected if a H_2 molecule has been displaced by MeCN. Furthermore, **28-H_{10}** is stable under vacuum for 14 days in contrast to **27-H_{10}**. The disparity in the behaviour of **28-H_{14}** when compared to **27-H_{12}** may have two origins, steric or electronic: (i) the additional two electron donor ligand(s) (η^2-H_2 or $(H)_2$) stabilises the cluster core and prevents attack of an external Lewis base by donation into a low lying LUMO, or (ii) an increased steric protection due to the bulkier phosphine. A comparison of the space filling diagrams of **27** and **28** show an extremely congested periphery in **28** with the cyclohexyl rings interlocked, which must provide a better steric shield than the $^iPr_3P$ 'shroud' where there appears to be less steric crowding (Figure 35). This is analogous to the increase in cluster stability found on moving to a bulkier halide in $[Zr_6X_{18}H_5]^{3-}$ (X = Cl or Br).[36]

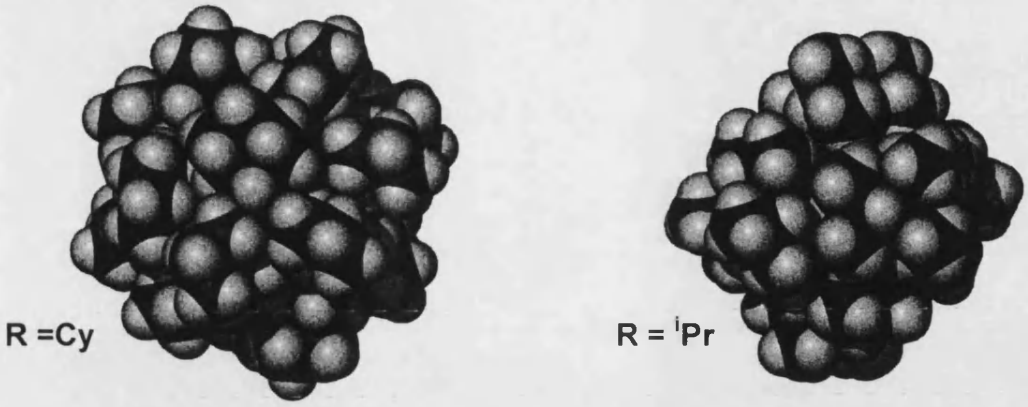

Figure 35: A comparison of the respective space filling diagrams for the $\{(PR_3)Rh\}_6$ clusters (R = Cy and ^{i}Pr).

The severe steric crowding in **28** may also be the source of the significantly poorer yield consistently observed (maximum isolated yields **28-H_{14}** ~10%, **27-H_{12}** repeatably above 40%), with the other complex (possibly a trimer) that presumably is less sterically crowded, forming as the major product for **28**.

Unfortunately, as found for the ^{i}Pr$_3$P system, attempts to isolate crystalline material associated with the other doublet observed in the $^{31}P\{^1H\}$ NMR spectrum from the crude reaction mixture repeatably failed. Due to the similarity of the two phosphine systems (both resulting in $\{PRh\}_6$ clusters) these by-products are probably closely related, thus the discussion in the earlier section about possible structures is equally valid here. Attempts to synthesise these clusters from the analogous PMe_3 precursors failed, forming an intractable mixture of unidentified products.

6.3. Summary

This chapter has elucidated a number of the decomposition products from the dihydrogen adducts **22-$(H_2)_x$** and **23-$(H_2)_X$**, one of which has been shown

unambiguously by a mixture of X-ray diffraction, NMR and mass spectroscopy to be the high hydride containing rhodium octahedron $[(PR_3)_6Rh_6H_{12}][Y]_2$ (R = ^{i}Pr). A by-product in the formation of these clusters has been isolated and characterised as the protonated phosphine $[HPR_3]^+$, **26**. This allowed for the mode of decomposition of the dihydrogen adducts to be clearly identified as a heterolytic cleavage process with proton transfer to an ancillary ligand. Thus, the cationic dihydrogen adducts have a pK_a lower than that of **26** (9.0). The clusters have been demonstrated to reversibly lose a number of their hydrides, with **27** existing as either 12 (76 c.v.e) or 10 hydrides (74 c.v.e). An analogy between the structure and reactivity of **27** and the early transition metal clusters that can equally reversibly shuttle between 76 and 74 c.v.e counts has been highlighted. The compound **27-H_{12}** has been demonstrated to be an active hydrogenation catalyst for simple linear alkenes and as such can be viewed as a molecular model for the colloidal group 9 hydrogenation catalysts.[52, 53] The synthesis of **27-H_{12}** has been currently optimised to yield between 40 and 50% crystalline product (based on rhodium content).

The cyclohexyl phosphine cluster **28** has shown significantly different behaviour to its ^{i}Pr$_3$P analogue, existing as a dicationic $\{PRh\}_6$ cluster ligated by either 10 or 14 hydrides. The 14 hydride cluster formally counts to 78 c.v.e, an unprecedented value for octahedral clusters of this geometric arrangement. Furthermore, this cluster is considerably more resistant to hydride loss and exhibits no cluster break down in the presence of an excess of MeCN. The hydride environment has also been shown to be significantly different to **27**, with inequivalent hydride environments in both **28-H_{14}** and **28-H_{10}**. The presence of an intact dihydrogen bonded to the cluster has also been suggested. The synthesis of this cluster is currently not optimised with yields of only *circa* 10%.

Both these sets of clusters by reversibly uptaking and releasing dihydrogen can be viewed as models for hydrogen storage devices.[54] Significant further works needs to be performed on these clusters to elucidate further the mechanism of formation and to investigate what should be a wide and interesting reactivity. Definitive confirmation of the hydride bonding mode and identification of their location in these clusters still needs to be obtained.

6.4: References

1 G. J. Kubas, 'Metal Dihydrogen and Sigma Bond Complexes. Structure, Theory and Reactivity.' Kluwer, 2001.

2 G. Kubas, in 'Advances In Inorganic Chemistry 56: Heterolytic Splitting of H-H, Si-H and Other Sigma Bonds on Electrophilic Metal Centres', ed. R. van-Eldik, 2004.

3 P. J. Brothers, *Prog. Inorg. Chem.*, 1981, **28**, 1.

4 L. S. van-der-Sluys, M. M. Miller, G. J. Kubas, and K. G. Caulton, *J. Am. Chem. Soc.*, 1991, **113**, 2513.

5 P. G. Jessop and R. H. Morris, *Coord. Chem. Rev*, 1992, **121**, 155.

6 X. G. Fang, B. L. Scott, K. D. John, and G. J. Kubas, *Organometallics*, 2000, **19**, 4141.

7 X. G. Fang, J. Huhmann-Vincent, B. L. Scott, and G. J. Kubas, *J. Organomet. Chem.*, 2000, **609**, 95.

8 M. H. Chisholm, K. S. Kramer, and W. E. Streib, *J. Am. Chem. Soc.*, 1992, **114**, 3571.

9 M. H. Chisholm, K. S. Kramer, and W. E. Streib, *J. Am. Chem. Soc.*, 1995, **117**, 6152.

10 M. H. Chisholm and K. S. Kramer, *Chem. Commun.*. 1996, 1331.

11 M. H. Chisholm, K. Folting, K. S. Kramer, and W. E. Streib, *J. Am. Chem. Soc.*, 1997, **119**, 5528.

12 R. J. Goodfellow, E. M. Hamon, J. A. K. Howard, J. L. Spencer, and D. G. Turner, *J. Chem. Soc. Chem. Commun.*. 1984, 1604.

13 P. W. Frost, J. A. K. Howard, J. L. Spencer, D. G. Turner, and D. Gregson, *J. Chem. Soc. Chem. Commun.*. 1981, 1104.

14 D. Gregson, J. A. K. Howard, M. Murray, and J. L. Spencer, *J. Chem. Soc. Chem. Commun.*. 1981, 716.

[15] G. V. Goeden and K. G. Caulton, *J. Am. Chem. Soc.*, 1981, **103**, 7354.
[16] T. h. Lenmen, K. Folting, J. C. Huffman, and K. G. Caulton, *J. Am. Chem. Soc.*, 1985, **107**, 7774.
[17] V. W. Day, M. F. Fredrich, G. S. Reddy, A. J. Sivak, W. R. Pretzer, and E. L. Muetterties, *J. Am. Chem. Soc.*, 1977, **99**, 8091.
[18] A. J. Sivak and E. L. Muetterties, *J. Am. Chem. Soc.*, 1979, **101**, 4878.
[19] R. K. Brown, J. M. Williams, A. J. Sivak, and E. L. Muetterties, *Inorg. Chem.*, 1980, **19**, 370.
[20] L. Garlaschelli, F. Greco, G. Peli, M. Manassero, M. Sansoni, R. Gobetto, L. Salassa, and R. D. Pergola, *Eur. J. Inorg. Chem.*. 2003, 2108.
[21] D. F. Chodsch, R. H. Crabtree, H. Felkin, and G. E. Morris, *J. Organomet. Chem.*, 1978, **161**, C67.
[22] G. Suss-Fink, L. Plasseraud, A. Maisse-Francois, H. Stoeckli-Evans, H. Berke, T. Fox, R. Gautier, and J.-Y. Saillard, *J. Organomet. Chem.*, 2000, **609**, 196.
[23] G. Meister, G. Rheinwald, H. Stoeckli-Evans, and G. Suss-Fink, *J. Chem. Soc., Dalton Trans.*, 1994, 3215.
[24] L. Plasseraud and G. Suss-Fink, *J. Organomet. Chem.*, 1997, **539**, 163.
[25] A. M. Arif, T. A. Bright, R. A. Jones, and C. M. Nunn, *J. Am. Chem. Soc.*, 1988, **110**, 6894.
[26] N. Lugan, G. Lavigne, J.-J. Bonnet, R. Reau, D. Neibecker, and I. Tkatchenko, *J. Am. Chem. Soc.*, 1988, **110**, 5369.
[27] M. J. Breen, M. R. Duttera, G. L. Geoffroy, G. C. Novotnak, D. A. Roberts, P. M. Shulman, and G. R. Steinmetz, *Organometallics*, 1982, **1**, 1008.
[28] L. J. Farrugia, M. Green, D. R. Hankey, A. G. Orpen, and G. A. Stone, *J. Chem. Soc. Chem. Commun.*. 1983, 310.
[29] F. Torres, E. Sola, M. Martin, J. A. Lopez, F. J. Lahoz, and L. A. Oro, *J. Am. Chem. Soc.*, 1999, **121**, 10632.
[30] D. H. Farrar, E. V. Grachova, A. Lough, C. Patirana, A. J. Poe, and S. P. Tunik, *Dalton Trans.*, 2001, 2015.
[31] A. G. Orpen, *Dalton Trans.*, 1980, 2509.
[32] D. M. P. Mingos and D. J. Wales, 'Introduction to Cluster Chemistry', Prentice Hall, 1990.
[33] L. Chen and F. A. Cotton, *Inorg. Chim. Acta*, 1997, **257**, 105.
[34] F. A. Cotton, P. A. Kibala, and W. J. Roth, *J. Am. Chem. Soc.*, 1988, **110**, 298.
[35] C. A. Tolman, *Chem. Rev.*, 1977, **77**, 313.
[36] L. Chen, F. A. Cotton, W. T. Klooster, and T. F. Koetzle, *J. Am. Chem. Soc.*, 1997, **119**, 12175.
[37] T. G. Gray, *Coord. Chem. Rev*, 2003, **243**, 213.
[38] N. Prokopuk, V. O. Kennedy, C. L. Stern, and D. F. Shriver, *Inorg. Chem.*, 1998, **37**, 5001.
[39] M. Schlaf, A. J. Lough, and R. H. Morris, *Organometallics*, 1996, **15**, 4423.
[40] K. Abdur-Rashid, T. P. Fong, B. Greaves, D. G. Gusev, J. G. Hinman, S. E. Landau, A. J. Lough, and R. H. Morris, *J. Am. Chem. Soc.*, 2000, **122**, 9155.
[41] K. Abdur-Rashid, D. G. Gusev, A. J. Lough, and R. H. Morris, *Organometallics*, 2000, **19**, 1652.
[42] F. A. Cotton, M. P. Diebold, and W. J. Roth, *J. Am. Chem. Soc.*, 1987, **109**, 2833.
[43] T. Saito, N. Yamamoto, T. Yamagata, and H. Imoto, *J. Am. Chem. Soc.*, 1988, **110**, 1646.

[44] T. Yoshida, D. L. Thorn, T. Okano, S. Otsuka, and J. A. Ibers, *J. Am. Chem. Soc.*, 1980, **102**, 6451.
[45] T. Yoshida, T. Okano, D. L. Thorn, T. H. Tulip, S. Otsuka, and J. A. Ibers, *J. Organomet. Chem.*, 1979, **181**, 183.
[46] F. A. Cotton, *Inorg. Chem.*, 1964, **3**, 1217.
[47] V. O. Kennedy, C. L. Stern, and D. F. Shriver, *Inorg. Chem.*, 1994, **33**, 5967.
[48] B. Yan, H. Zhou, and A. Lachgar, *Inorg. Chem.*, 2003, **42**, 8818.
[49] N. Prokopuk, C. S. Weinert, V. O. Kennedy, D. P. Siska, H.-J. Jeon, C. L. Stern, and D. F. Shriver, *Inorg. Chim. Acta.*, 2000, **300**, 951.
[50] F. Stollmaier and A. Simon, *Inorg. Chem.*, 1985, **24**, 168.
[51] A. Simon, F. Bottcher, and J. K. Cockcroft, *Angew. Chem., Int. Ed. Engl.*, 1990, **30**, 101.
[52] P. J. Dyson, *Dalton Trans.*, 2003, 2964.
[53] J. A. Windegren and R. G. Finke, *Inorg. Chem.*, 2002, **41**, 1558.
[54] P. Braunstein, L. A. Oro, and P. R. Raithby, 'Metal Clusters in Chemistry', Wiley-VCH, 1999.

7 EXPERIMENTAL

7.1 Experimental techniques

7.1.1 General

All manipulations were performed under an inert atmosphere of argon, using standard Schlenk-line and glove box techniques. Glassware was dried in an oven at 130°C overnight and flamed with a blowtorch, under vacuum, three times before use. CH_2Cl_2, $C_4H_8SO_2$,, CH_3CN and pentane were distilled from CaH_2. C_6H_5F was distilled from P_2O_5, toluene and hexane from sodium, THF and diethyl ether from sodium wire /benzophenone ketal indicator. C_6D_6 and d_8-toluene were dried over a potassium mirror; CD_2Cl_2 was distilled under vacuum from CaH_2. Microanalyses were performed by Mr. Alan Carver (University of Bath Microanalytical Service). Gas Chromotography was performed on a Perkin-Elmer Autosystem XL. Mass spectrometry were performed by Mr Chris Cryer (University of Bath Mass Spectrometry Service) and the EPSRC National Mass Spectrometry Service Centre, University of Wales, Swansea

7.1.2 NMR spectroscopy

^{1}H, ^{11}B, ^{13}C and ^{31}P NMR spectra were recorded on Varian 400 MHz, Bruker Avance 400 MHz or Bruker Avance 300 MHz FT-NMR spectrometers. Residual protio solvent was used as reference for ^{1}H NMR spectra (CD_2Cl_2: $\delta = 5.32$, C_7D_8: $\delta = 2.10$, C_3D_6O: $\delta = 2.09$)

and ^{13}C NMR spectra (CD_2Cl_2: $\delta = 53.8$). ^{11}B and ^{31}P NMR spectra were referenced against $BF_3.OEt_2$ (external) and 85% H_3PO_4 (external) respectively. Chemical shifts are quoted in ppm. Coupling constants are given in Hz.

7.1.3 Infrared spectroscopy

Infrared spectra were recorded on a Nicolet NEXUS FT-IR spectrometer. Solid-state samples were prepared using oven-dried potassium bromide. Solution spectra were recorded using a 0.1mm solution cell.

7.1.4 Crystallographic studies

Crystallographic measurements for all structures were recorded on a Nonius Kappa CCD diffractometer with Mo κ_α radiation (0.71073 Å). Structure solution followed by full-matrix least-squares refinement was performed by using the SHELX suite of programs throughout. Hydrogens were included in calculated positions unless otherwise stated.

7.2 Syntheses and characterisation

7.2.1 Starting materials

The starting materials Cs[*closo*-$CB_{11}H_{12}$],[1] [1-H-*closo*-$CB_{11}Me_{11}$]$^{\bullet}$,[2] $HN(Me)_2Ph$[1-H-*closo*-$CB_{11}Me_{11}$],[3] Cs[*closo*-$CB_{11}Me_{12}$],[3] Cs[*closo*-$CB_{11}H_6Br_6$],[4] CPh_3[*closo*-$CB_{11}H_6Br_6$],[5] $^{n}Bu_4N$[*closo*-$CB_{11}H_6Br_6$],[5] $MoCp(CO)_3Cl$,[6] $MoCp(CO)_3I$,[6] $MoCp(CO)_3Me$,[7]

$CpMo(CO)_3H$,[8] $CpMo(CO)_2(PPh_3)H$,[9, 10] $(CpMo(CO)_3)_2$,[11] $(CpW(CO)_3)_2$,[11] $CpMo(CO)_3(OTf)$,[12] $\{(NBD)RhCl\}_2$,[13] $\{(COD)IrCl\}_2$,[14] $Cp^*Rh(PMe_3)(Me)Cl$,[15] $Cp^*Rh(PMe_3)Me_2$,[16] $Cp^*Rh(PMe_3)Me(OTf)$,[16] Cp'_2ZrMe_2 (Cp = C_5H_5, C_5H_4Me or C_5Me_5),[17] $K[BAr_F]$,[18] $^nBu_4N[BAr_F]$,[18] $(PCy_3)Re(CO)_4Me$,[19] $(PPh_3)Re(CO)_4Me$,[19] $(PPh_3)_2Re(CO)_3Me$,[20] $(PCy_3)_2Re(CO)_3Me$,[20] $(CH_3C(CH_2O)_3P)_2Re(CO)_3Me$,[21] $CpCo(PPh_3)Me_2$[22] and $(^iPr_3P)_2PtMe_2$[23] were all prepared by previously published methods or a variation thereof. All other chemicals were used as received from Aldrich, Acros, Alfa Aesar, Fisher, Fluka, or Strem Chemicals.

7.2.2 Synthesis

Satisfactory microanalyses on a majority of the compounds containing the highly alkylated carborane anion were unobtainable, consistently being low in carbon content despite repeated attempts with pure crystalline samples.

$Cs[1\text{-}H\text{-}closo\text{-}CB_{11}Me_{11}]$: A modified preparation based on that reported[24] previously by Michl *et al.* was used. $Cs[closo\text{-}CB_{11}H_{12}]$ (1.5 g, 5.4 mmol) and CaH_2 (8.66 g, 216 mmol) are loaded into a 250 ml three necked round bottom flask and sulfalone, ~25ml was added via syringe. This reaction mixture was then heated in an oil bath to ~35°C, (NOTE it is important not to go higher than this as MeOTf is volatile and boils at 41°C) and ~12 ml MeOTf was extracted into a 20 ml syringe and added at a rate of addition of 0.707 ml/h via a syringe pump. After three days of stirring a second portion of MeOTf (~6 ml) and $C_4H_8SO_2$ (~10 ml) was added to ensure full conversion. The reaction mixture was sealed and stirred for a further two days whilst monitoring the reaction daily by ^{11}B NMR. If after

2 further days the reaction has not reached clean methylation then a further 6 mls of MeOTf was added via syringe in one portion and the stirring continued for a further day. When complete cage functionalisation had occurred the reaction mixture was opened to the atmosphere, **CARE must be taken as both MeOTf and a large amount of CaH_2 will still be present**. The product is extracted from the reaction mixture by the addition of 2 x 200 ml portions of CH_2Cl_2, filtering each through a sintered glass frit into a round bottom flask (500 ml) to leave a colourless solution and a white solid. To the combined (~400 ml) DCM solution was added 100 ml of NH_4OH and the heterogeneous solution stirred for 5 mins. The CH_2Cl_2 was then removed *in vacuo*. The remaining NH_4OH solution was extracted with 3 x 50 ml Et_2O, the ether portions are then combined. The white solid isolated earlier was transferred to a 250 ml flask and cooled in an ice bath, then a 10% HCl solution was slowly added until the mixture is ~pH 7. Once neutralised, the aqueous solution is extracted with 3 x 50 ml portions of ether. The ether portions are combined with those from earlier. The combined etherate extractions are converted to the Cs salt by washing with 3 x 50 ml portions of CsCl 10% w/v aqueous solution. The H_2O washings are combined and in turn extracted with 3 x 50 ml portions of Et_2O. All Et_2O solutions are combined and the solvent removed *in vacuo* to leave an off-white solid. Residual sulfolane is removed by vacuum distillation at 180°C. The remaining solid is dissolved in boiling water and filtered hot and on cooling yields crystalline white solid that is washed x 2 with cold aliquots of H_2O and dried *in vacuo* to yield 1.67 g of pure Cs[1-H-*closo*-$CB_{11}Me_{11}$].

Yield: 72%

δ $^1H\{^{11}B\}$ (298 K, d_6 -acetone): δ 1.27 (1H, s, C_{cage} – H), -0.02 (15H, s, B(2)CH_3-B(6)CH_3), -0.25 (15H, s, B(7)CH_3 – B(11)CH_3) and –0.34 (3H, s, B(12)CH_3).

δ ^{11}B (298 K, d_6 - acetone): -0.73 (1B, s B(12)), -8.86 (5B, s B(7)-B(11)), -12.22 (5B, s, B(2)-B(6)).

[Ag(1-H-*closo*-$CB_{11}Me_{11}$)], (1): Cs[1-H-*closo*-$CB_{11}Me_{11}$] (407 mg, 0.95 mmol) was dissolved in Et_2O (30ml) treated with three 30 ml portions of 10% w/v $AgNO_3$ aqueous solution. The combined aqueous layers were extracted with 3 aliquots of Et_2O (25 ml). The combined Et_2O portions were evaporated to dryness *in vacuo*. The resultant off-white solid was redissolved in CH_2Cl_2 (20ml) filtered and the solvent removed *in vacuo* to leave a white solid that was dissolved in minimum CH_2Cl_2, layered with hexanes at –30°C in the dark. Colourless crystals of [Ag(1-H-*closo*-$CB_{11}Me_{11}$)] (303 mg, 0.75 mmol) were isolated.

Yield: 79%

δ ^{1}H{^{11}B} (298 K,d_6-acetone): δ 1.09 (1H, s, C_{cage}-H), -0.16 (15H, s, B(2)CH_3-B(6)CH_3), -0.39 (15H, s, B(7)CH_3-B(11)CH_3), -0.51 (3H, s, B(12)CH_3).

δ ^{11}B (298 K, d_6-acetone): -0.66 (1B, s, B(12)), -8.84 (5B, s, B(7)-B(11)), -12.22 (5B, s, B(2)-B(6)).

δ ^{1}H{^{11}B} (298 K, CD_2Cl_2): δ 1.27 (1H, s, C_{cage}-H), -0.15 (15H, s, B(2)CH_3-B(6)CH_3), -0.33 (15H, s, B(7)CH_3-B(11)CH_3), -0.54 (3H, s, B(12)CH_3).

δ ^{11}B (298 K, CD_2Cl_2): 1.5 (1B, s, B(12)), -5.9 (5B, s, B(7)-B(11)), -8.5 (5B, s, B(2)-B(6)).

Elemental Analysis: Calcd. for $C_{12}H_{34}B_{11}Ag_1$: %C 35.6; %H 8.40. Found: %C 33.1; %H 8.31.

Ag(PPh_3)(1-H-*closo*-$CB_{11}Me_{11}$), (2): PPh_3 (60mg, 0.23mmol) was dissolved in CH_2Cl_2 (5ml) and added dropwise to a foil covered Schlenk flask charged with Ag[1-H-*closo*-

$CB_{11}Me_{11}$] (92mg, 0.23mmol). The resulting solution was stirred for 16 h, cannula filtered and the solvent removed *in vacuo*. The white solid formed was redissolved in the minimum volume of CH_2Cl_2, layered with hexanes, then placed in a freezer overnight at –30°C to afford 122 mg (0.183 mmol) of $Ag(PPh_3)$(1-H-*closo*-$CB_{11}Me_{11}$) as colourless crystals.

Yield: 81%

δ $^1H\{^{11}B\}$ (298 K, CD_2Cl_2): 7.66 – 7.36 (15H, m, C_6H_5), 1.26 (1H s, CH_{cage}), -0.14 (15H, br. s, BCH_3), -0.22 (3H, br. s, BCH_3), -0.28 (15H, br. s, BCH_3).

δ ^{11}B (298 K, CD_2Cl_2 assignments from ^{11}B-^{11}B COSY): -1.31 (1B, s), -9.03 (5B, s), -12.05 (5B, s).

δ $^{13}C\{^1H\}$ (298 K, CD_2Cl_2): 133.93 (s, C_{phenyl}), 132.33 (s, C_{phenyl}), 130.00 (s, C_{phenyl}), 128.23 [d, C_{phenyl}, J(CP) 37], 61.33 (s, C_{cage}), -0.74 - -6.00 (br. m, CH_3).

δ $^{31}P\{^1H\}$ (298 K, CD_2Cl_2): 18.21 [dd, $J(^{109}AgP)$ 853, $J(^{107}AgP)$ 794].

IR (KBr): ν = 2921, 2895, 2829, 2736cm^{-1}.

Elemental Analysis: Calc. for $C_{30}H_{49}Ag_1B_{11}P_1$: %C, 54.0; %H, 7.35. Found: %C, 53.4; %H, 7.30.

$Ag(PCy_3)$(1-H-*closo*-$CB_{11}Me_{11}$), (3): The procedure for $Ag(PPh_3)$(1-H-*closo*-$CB_{11}Me_{11}$) was followed except that 60 mg, (0.11 mmol) of PCy_3 and 43mg (0.11 mmol) of Ag[1-H-*closo*-$CB_{11}Me_{11}$] were used. This afforded 34 mg (0.05 mmol) of colourless crystals.

Yield: 46%

δ $^{1}H\{^{11}B\}$ (298 K, CD_2Cl_2): δ 2.01 – 1.75 (18H, m, Cy), 1.37 - 1.21 (16H, m, Cy and C_{cage}-H), -0.13 (15H, br s, B(7)CH_3-B(11)CH_3), -0.23 (18H, v.br s B(12)CH_3 and B(2)CH_3-B(6)CH_3).

δ ^{11}B (298 K, CD_2Cl_2,): -1.81 (1B, s B(12)), -9.16 (5B, s, B(7)-B(11)), -11.77 (5B, s, B(2)-B(6)).

δ $^{31}P\{^{1}H\}$ (298 K, CD_2Cl_2): 49.88 [dd, $J(Ag^{109}P)$ 821, $J(Ag^{107}P)$ 711].

IR (KBr): ν = 2932, 2893, 2856, 2827 cm^{-1}.

Elemental Analysis: Calcd. for $C_{30}H_{67}Ag_1B_{11}P_1$: %C, 52.6; %H, 9.8. Found: %C, 52.0, %H, 9.8.

Ag(P({3,5-$(CH_3)_2C_6H_3$}$_3$)(1-H-closo-$CB_{11}Me_{11}$), (4): The procedure for Ag(PPh_3)(1-H-*closo*-$CB_{11}Me_{11}$) was followed except that 39 mg, (0.11 mmol) of P({3,5 - $(CH_3)_2C_6H_3$}$_3$ and 50 mg (0.12 mmol) of Ag[1-H-*closo*-$CB_{11}Me_{11}$] were used. This afforded 53 mg (0.07 mmol) of **(4)** as colourless crystals.

Yield: 63%

δ $^{1}H\{^{11}B\}$ (298 K, CD_2Cl_2,): δ 7.28 – 7.02 (9H, m, Ph), 2.39 (18H, s, Ph-CH_3), 1.30 (1H, s, C_{cage}-H), -0.08 (15H, br s, B(7)CH_3-B(11)CH_3), -0.21 (3H, br s, B(12)CH_3), and –0.23 (15H, br s, B(2)CH_3 – B(6)CH_3).

δ ^{11}B (298 K, CD_2Cl_2): -1.73 (1B, s B(12)), -9.12 (5B, s B(7)-B(11)), -11.79 (5B, s, B(2)-B(6)).

δ $^{31}P\{^{1}H\}$ (298 K, CD_2Cl_2): 19.14 [br d, Av. J(AgP) 731,].

Elemental Analysis: Calcd. for $C_{36}H_{61}Ag_1B_{11}P_1$: %C 57.6; %H 8.13. Found: %C 58.1; %H 8.42.

$[(OEt_2)_2Ag(PPh_3)(1\text{-H-closo-}CB_{11}Me_{11})]$, (5): Crystalline $PPh_3Ag(1\text{-H-}closo\text{-}CB_{11}Me_{11})$ (30 mg,) was dissolved in Et_2O (5 ml) in a Young's tube and layered with pentane. Recrystallisation in the dark at -30°C resulted in colourless crystals suitable for X-ray diffraction. The crystalline material immediately starts to lose diethyl ether on removal from the mother liquor and thus, satisfactory microanalysis and yield were not obtainable.

δ ^{1}H (298 K, CD_2Cl_2): 7.65 – 7.37 (15H, m, Ph), 3.55 (8H, q, O-CH_2), 1.26 (12H, t, CH_3) 1.17 (1H, s, C_{cage}-H), -0.16 (15H, s, B(2)CH_3-B(6)CH_3), -0.38 (15H, s, B(7)CH_3-B(11)CH_3), -0.45 (3H, s, B(12)CH_3).

δ ^{11}B (298 K, CD_2Cl_2): 1.98 (3H, s, 12B), -5.72 (15H, s, B7-11), -8.63 (15H, s, B2-6)

δ ^{31}P{^{1}H} (298 K, CD_2Cl_2): 18.95 (dd, $^1J(Ag^{109}P)$ 858, $^1J(Ag^{107}P)$ 774).

$(PPh_3)_2Ag[1\text{-H-}closo\text{-}CB_{11}Me_{11}]$, (6): PPh_3 (144 mg, 0.28 mmol) was dissolved in CH_2Cl_2 (5 ml) and added drop wise to a foil covered Schlenk flask charged with $Ag[1\text{-H-}closo\text{-}CB_{11}Me_{11}]$ (56 mg, 0.14 mmol). The resulting solution was stirred for 16 hours, cannula filtered and solvent removed *in vacuo*. The white solid formed was redissolved in minimum CH_2Cl_2, layered with hexanes, then placed in a freezer overnight at –30°C to afford 68 mg (0.07 mmol) of $Ag(PPh_3)_2(1\text{-H-}closo\text{-}CB_{11}Me_{11})$ as colourless crystals.

Yield: 53%

δ ^{1}H{^{11}B} (298 K, CD_2Cl_2): 7.70 – 7.40 (30H, m, C_6H_5), 1.16 (1H s, CH_{cage}), -0.16 (15H, s, BCH_3), -0.44 (15H, s, BCH_3), -0.51 (3H, s, BCH_3).

δ ^{11}B (298 K, CD_2Cl_2): -0.9 (1B, s), -8.9 (5B, s), -12.2 (5B, s).

δ ^{31}P {^{1}H } (298 K, CD_2Cl_2): 17.421 [dd, $J(^{109}AgP)$ 580, $J(^{107}AgP)$ 502].

Elemental Analysis: Calcd. for $C_{48}H_{64}Ag_1B_{11}P_2$: %C, 62.0; %H, 6.94. Found: %C, 60.1; %H, 6.91.

[Ag(P({3,5-$(CH_3)_2C_6H_3$}$_3$)$_2$(1-H-*closo*-$CB_{11}Me_{11}$)]: Synthesis as for $(PPh_3)_2Ag$[1-H-*closo*-$CB_{11}Me_{11}$].

δ $^1H\{^{11}B\}$ (298 K, CD_2Cl_2): 7.27 – 7.03 (18H, m, Ph), 2.34 (36H, s, Ph-Me), 1.15 (1H, s, C_{cage}-H), -0.17 (15H, s, B(2)CH_3-B(6)CH_3), -0.39 (15H, s, B(7)CH_3-B(11)CH_3), -0.51 (3H, s, B(12)CH_3)

δ ^{11}B (298 K, CD_2Cl_2): -0.99 (1B, s, B(12)), -8.95 (5B, s, B(7)-B(11)), -12.14 (5B, s, B(2)-B(6)).

δ $^{31}P\{^1H\}$ (298 K, CD_2Cl_2): 18.66 (dd, $^1J(Ag^{109}P)$ 577, $^1J(Ag^{107}P)$ 500).

$(Ag(PPh_3)_4)[(Ag\{1\text{-H-}closo\text{-}CB_{11}Me_{11}\}_2)]$, (7): $Ag(PPh_3)$(1-H-*closo*-$CB_{11}Me_{11}$) (30 mg, 0.05 mmol) was dissolved in 5 ml CH_2Cl_2 and to it was added a CH_2Cl_2 solution of PPh_3 (13 mg, 0.05 mmol). The resulting solution was stirred for 16 hours in the dark, cannula filtered and the solvent removed *in vacuo* yielding of 31 mgs of white powder. Redissolving in minimum CH_2Cl_2 and layering with hexanes at –30°C resulted in colourless crystals of both polymorphs.

Yield: 74%

NMR and IR data identical to that reported for $[Ag(PPh_3)_2$(1-H-*closo*-$CB_{11}Me_{11}$)].

[^{n}Bu$_4$N][1-H-*closo*-$CB_{11}Me_{11}$]: Cs[1-H-*closo*-$CB_{11}Me_{11}$] (150 mg, 0.35 mmol) was dissolved in 30 ml of Et_2O and washed three times with ^{n}Bu$_4$NBr (560 mgs, 1.75 mmol)

dissolved in 100 ml of H_2O. The aqueous portion was extracted three times with 20 ml portions of Et_2O. The ether washing were combined and evaporated to dryness to yield 105 mg of white solid.

Yield: 57%

δ $^1H\{^{11}B\}$ (298 K, d_6 -acetone): δ 3.65 – 3.51 (8H, m, N-CH_2), 2.08 – 1.93 (8H, m, CH_2), 1.67 – 1.48 (8H, m, CH_2), 1.27 (1H, s, C_{cage} – H) 1.19 – 1.11 (12H, t, CH_3) -0.02 (15H, s, B(2)CH_3-B(6)CH_3), -0.25 (15H, s, B(7)CH_3 – B(11)CH_3) and –0.34 (3H, s, B(12)CH_3).

δ ^{11}B (298 K, d_6 - acetone): -0.73 (1B, s B(12)), -8.86 (5B, s B(7)-B(11)), -12.22 (5B, s, B(2)-B(6)).

δ $^1H\{^{11}B\}$ (298 K,CD_2Cl_2, selected): 1.22 (1H, s, C_{cage} – H) -0.184 (15H, s, B(2)CH_3-B(6)CH_3), -0.435 (15H, s, B(7)CH_3 – B(11)CH_3) and –0.555 (3H, s, B(12)CH_3).

[Me_4N][1-H-*closo*-$CB_{11}Me_{11}$]: This was synthesised as for the [$^nBu_4N$]$^+$ salt. Chemical shifts for (1-H-*closo*-$CB_{11}Me_{11}$) were identical to those for [$^nBu_4N$][1-H-*closo*-$CB_{11}Me_{11}$].

δ $^1H\{^{11}B\}$ (selected, 298 K, d_6 -acetone): 3.25 (12H, s, NMe_4).

Calculation Details (performed by Dr G. Ruggerio). Gas-phase geometry optimisation for all multi-nuclear solutes were performed using the Gaussian 98 program[25] using DFT at the B3LYP hybrid method[26] with the DZVP basis sets.[27] Geometry optimisation for minimas used the Berny routine. No symmetry constraints were imposed. The charge distributions were obtained from the DFT wavefunction employing a natural population analysis. The silver complex study used the double-zeta-valence-polarisation (DZVP) basis set developed for DFT. Previous work on metals using this basis set has shown that DZVP

produces structures and energies comparable to those obtained using the better tested basis set, 6-31+G(d).[28] In the original communication,[29] we reported that the 7 isomer was slightly favoured energetically over the 12-isomer by *ca* 1.4 kcal mol^{-1} – the opposite of that reported here. Subsequent refinements of the model since have revealed new local minima, and the 12-isomer is in fact 1.9 kcal mol^{-1} *more* stable than the 7-isomer. This is now consistent with calculations previously reported for $[Me_3Sn][closo\text{-}CB_{11}Me_{12}]$.[30] Since the potential energy surface for the isomers of **2** is quite flat, great care must be taken with geometry optimisation to ensure convergence towards stationary points with zero gradients. Even though the RMS residual force in our original calculations was well below the usual standard exit threshold for convergence they may not be the lowest energies possible when investigating large flexible systems, such as those discussed here. By tightening the cut-offs on forces (opt=tight keyword) and the step size that are used to determine convergence it was possible to lower the gradient and energy of the system so that modest (ca. 3 $kcalmol^{-1}$) improvements where made over our original calculations. Nevertheless, the conclusion is still exactly the same: interaction of the metal fragment with those $\{BCH_3\}$ vertices on the lower hemisphere of the cage is energetically favored over those on the upper part, fully consistent with the observed chemical shift changes of the methyl groups in the ^1H NMR spectra.

$[Ph_3C][1\text{-}H\text{-}closo\text{-}CB_{11}Me_{11}]$, (8): $Cs[1\text{-}H\text{-}closo\text{-}CB_{11}Me_{11}]$ (0.351 g, 0.82 mmol) was dissolved in 15 ml toluene/MeCN (1:2 mix) and added in one portion to a solution of Ph_3CBr (0.265 g, 0.82 mmol) in toluene. Immediately, a yellow solution formed and stirred for two hours. Solvents removed *in vacuo* to leave a brown oil and some white precipitate.

15 ml of dry DCM added and the solution was cannula filtered. The CH_2Cl_2 layer was concentrated to 2ml and layered with hexanes at –30°C to afford 0.296 g (0.55 mmol) of $[Ph_3C][1\text{-H-}closo\text{-}CB_{11}Me_{11}]$ as brown block crystals.

Yield: 67%

δ $^1H\{^{11}B\}$ (298 K CD_2Cl_2): 7.6-8.25 (15H, 3 multiplets trityl arene H's), 1.00 (1H s cage CH), -0.21 (15H s B2-6 CH_3), -0.40 (15H s B7-11 CH_3), -0.62 (3H s B12 CH_3).

δ ^{11}B (298 K CD_2Cl_2): -0.87 (1B s), -8.90 (5B s), -12.19 (5B s).

δ $^{13}C\{^1H\}$ (298 K CD_2Cl_2): 211.55 (s, C^+), 144.41 (s, C_{phenyl}), 143.53 (s, C_{phenyl}), 140.69 (s, C_{phenyl}), 131.49 (s, C_{phenyl}).

Elemental Analysis: Calcd. for $C_{31}H_{49}B_{11}$: %C: 68.9, %H: 9.1 %N: 0. Found %C: 66.7, %H: 8.92, %N: 0.

Despite numerous attempts with crystalline samples that were pure by NMR spectroscopy, satisfactory microanalysis could not be obtained.

Accurate Mass Spec: (FAB+) calcd for $C_{19}H_{15}$: 243.1174; Found: 243.1174m/z

$Cp_2ZrMe(1\text{-H-}closo\text{-}CB_{11}Me_{11})$, (9): A Young's tube was charged with $[Ph_3C][1\text{-H-}closo\text{-}CB_{11}Me_{11}]$ (0.041 g, 0.076 mmol) and Cp_2ZrMe_2 (0.019 g, 0.076 mmol). Fluorobenzene was cooled to 243 K and 5 ml added by cannula to give a yellow solution. The sample was then layered with n-pentane at 243 K to yield 0.020 g of yellow crystalline solid of $Cp_2ZrMe(1\text{-H-}closo\text{-}CB_{11}Me_{11})$.

Yield: 48%.

δ $^1H\{^{11}B\}$ (298 K, d_8-tol): 5.55 (10H, s, Cp), 1.48 (1H, s, cage C-H), 0.36 (15H, s, B-CH_3 (2-6)), 0.29 (3H, s, Zr-Me), 0.02 (15H, s, B-CH_3(7-11)) and –0.59 (3H, s, B-CH_3(12).

δ ^{11}B (298 K, d_8-tol): 3.6 (1H, s, B12), -3.6 (5H, s, B7-11), -5.9 (5H, s, B2-6),

δ ^{13}C{^{1}H} (298 K, d_8-tol): 119.9 (Cp), 68.0 (v. br CH_{cage}), 44.4 (Zr-Me, s), 3.9 (v. br B-CH_3)

IR (fluorobenzene ν(CH_3), cm^{-1}): 2962 vs, 2929 s, 2873 s.

[($Cp_2ZrMe)_2$(μ-Me)][1-H-*closo*-$CB_{11}Me_{11}$], (10): A Young's NMR tube was loaded with [Ph_3C][1-H-*closo*-$CB_{11}Me_{11}$] (0.020 g) and two equivalents of Cp_2ZrMe_2 (0.019 g) followed by 0.35 ml of C_6D_6. The resultant NMR spectra showed [($Cp_2ZrMe)_2$(μ-Me)]$^+$ as the sole cationic product by comparison to the previously reported [BAr_F]$^-$ analogue.[31]

δ ^{1}H{^{11}B} (298 K, d_8-tol): 5.59 (s, 20H, Cp,), 1.44 (1H, s, cage C-H), 0.57 (15H, s, B-CH_3 (2-6)), 0.39 (15H, s, B-CH_3(7-11)),0.32 (3H, s,B-CH_3(12)), -0.19 (6H, s, Zr-CH_3), -1.22 (s, 3H Zr-(μ-Me)).

δ ^{11}B (298 K, d_8-tol): 3.3 (1H, s, B12), -3.5 (5H, s, B7-11), -6.1 (5H, s, B2-6).

($C_5H_4Me)_2$Zr(Me)(1-H-*closo*-$CB_{11}Me_{11}$), (11): This compound was synthesised in an analogous manner to the Cp derivative; repeated attempts to obtain solid material all failed. Characterisation was performed on the isolated oil.

δ ^{1}H{^{11}B} (298 K, d_8-tol): 5.69 (2H, Cp, dd, ^{3}J(HH) 4.5, ^{4}J(HH) 2.3), 5.59 (2H, Cp, dd, ^{3}J(HH) 5.6 ^{4}J(HH) 2.9), 5.40 (2H Cp, dd, ^{3}J(HH) 5.6, ^{4}J(HH) 2.6), 5.15 (2H, Cp, dd, ^{3}J(HH) 4.6, ^{4}J(HH) 2.3), 1.69 (s, 6H, CpMe), 1.48 (1H, s, cage C-H), 0.35 (15H, s, B-CH_3 (2-6)), 0.30 (3H, s, Zr-Me), 0.03 (15H, s, B-CH_3(7-11)) and –0.57 (3H, s, B-CH_3(12).

δ ^{11}B (298 K, d_8-tol): 3.7 (1H, s, B12), -3.6 (5H, s, B7-11), -5.9 (5H, s, B2-6).

[Cp*$_2$Zr(OH$_2$)Cl][1-H-7,12-Cl$_2$-*closo*-CB$_{11}$Me$_9$]: A Young's tube was charged with Cp*$_2$ZrMe$_2$ (0.020 g, 0.05 mmol) and 27 mgs of [Ph$_3$C][1-H-*closo*-CB$_{11}$Me$_{11}$] and dissolved in 3 ml of C_6H_5F. The resultant yellow solution was reduced to dryness *in vacuo* and redissolved in CH_2Cl_2 and layered with hexanes at -20°C. A small number of pale yellow crystals formed alongside a dark yellow oil.

δ ^{1}H{^{11}B} (298 K,CD_2Cl_2): 1.82 (s, 2H, OH_2), 1.63 (s, 30H, Cp*,), 1.29 (1H, s, cage C-H), 0.35 (6H, s, B-CH_3), 0.26 (6H, s, B-CH_3),0.25 (6H, s, B-CH_3), 0.24 (6H, s, B-CH_3), 0.165 (s, 3H B-CH_3).

δ ^{11}B (298 K,CD_2Cl_2): 2.82 (s), -4.47 (s), -8.99 (s), -9.79 (s) and –12.58 (s).

Polymerisation Studies (performed at the University of East Anglia): A 250ml all glass reactor vessel was flame-dried *in vacuo* and then charged with toluene (50ml). This was placed under an atmosphere of ethylene and allowed to saturate. A solution of [Ph$_3$C][1-H-*closo*-CB$_{11}$Me$_{11}$] (0.011g) in toluene (4ml) was added. Finally a solution of (SBI)ZrMe$_2$ (SBI = *rac*-Me$_2$Si(Indenyl)$_2$, 0.08g) was added. The colour became yellow (from orange) and some precipitated polymer was observed. After 5 minutes the reaction was terminated by the injection of methanol (5ml). The polymer was precipitated into methanol (300ml) and HCl, collected *via* filtration and dried at 50°C for 16h. The final yield of polyethylene was 76mg.

Activity: 45kg mol^{-1} h^{-1} bar^{-1} (a moderate value from comparison to literature data).[32]

[CpCo(PPh$_3$)$_2$][1-H-*closo*-CB$_{11}$Me$_{11}$], (12) and [CpCo(η^5-Ph-CPh$_2$)][1-H-*closo*-CB$_{11}$Me$_{11}$], (13):

A Young's tube was loaded with $CpCo(PPh_3)Me_2$ (0.030 g, 0.08 mmol) and $[Ph_3C][1\text{-H-}closo\text{-}CB_{11}Me_{11}]$ (0.045 g, 0.08 mmol) and dissolved in 5 ml of CH_2Cl_2. Immediate gas evolution occurs and the solution changes from an orangey/brown to a purple colour. Recrystallisation by the slow diffusion of pentanes at room temperature yielded crystalline material of $[CpCo(\eta^5\text{-}PhCPh_2)][1\text{-H-}closo\text{-}CB_{11}Me_{11}]$ and $[CpCo(PPh_3)_2][1\text{-H-}closo\text{-}CB_{11}Me_{11}]$. No NMR data for $[CpCo(PPh_3)_2]^+$ can be reported due to the rapid relaxation times inherent in paramagnetic complexes.

$[CpCo(\eta^5\text{-}PhCPh_2)][1\text{-H-}closo\text{-}CB_{11}Me_{11}]$:

δ $^1H\{^{11}B\}$ (298 K, CD_2Cl_2): 7.80 (t of t, *para*-coordinated-phenyl, J(HH) 5, J(HH) 1), 7.74 – 7.38 (6H, m, Ph), 7.14 – 7.11 (4H, m, Ph), 5.79 (2H, d of d, J(HH) 5.6 and 7.6), 5.68 (2H, d of d, J(HH) 7.6 and 1), 5.50 (5H, s Cp), 1.15 (1H, s cage C-H), -0.18 (15H, s, $B_{2\text{-}6}CH_3$), -0.43 (15H, s, $B_{7\text{-}11}CH_3$) and -0.55 (3H, s, $B_{12}CH_3$).

δ ^{11}B (298 K, CD_2Cl_2): -0.90 (1B, s, B_{12}), -8.94 (5B, s, $B_{7\text{-}11}$) and -12.13 (5B, s, $B_{2\text{-}6}$).

$[\{CpMo(CO)_3I\}_3{\cdot}Ag(1\text{-H-}closo\text{-}CB_{11}Me_{11})]_2$, (14-I): The compounds $[CpMo(CO)_3I]$ (0.027 g, 0.07 mmol) and $Ag[1\text{-H-}closo\text{-}CB_{11}Me_{11}]$ (0.029 g, 0.07 mmol) were stirred in CH_2Cl_2 in the dark for one hour. The dark red solution was filtered and the solvent removed *in vacuo* to leave a dark red light sensitive oil. Crystals suitable for X-ray diffraction were grown by dissolving the solid in minimum CH_2Cl_2, layering with hexanes and placing in a –30°C freezer overnight. This yielded dark red crystals and some dark red powder – this intermediate compound could not be isolated cleanly due to the presence of some metathesis product after recrystallisation. The NMR data is from an *in situ* preparation monitored after 1 h and showed only one product (judged by the number of Cp rings).

δ $^{1}H\{^{11}B\}$(298 K, CD_2Cl_2): 5.76 (15H, s, Cp), 1.15 (1H, s cage C-H), -0.18 (15H, s, $B_{2\text{-}6}CH_3$), -0.43 (15H, s, $B_{7\text{-}11}CH_3$) and -0.55 (3H, s, $B_{12}CH_3$).

δ ^{11}B (298 K, CD_2Cl_2): -0.88 (1B, s, B_{12}), -8.92 (5B, s, $B_{7\text{-}11}$) and -12.18 (5B, s, $B_{2\text{-}6}$).

IR (CH_2Cl_2 ν(CO) (cm^{-1})): 2055sh, 2043s and 1966s.

[{$CpMo(CO)_3$}$_2$(μ-Cl)][1-H-*closo*-$CB_{11}Me_{11}$], (14-Cl): A Young's NMR tube was charged with Ag[1-H-*closo*-$CB_{11}Me_{11}$] (0.020g) and $CpMo(CO)_3Cl$ (0.014g) to which 0.3ml of CD_2Cl_2 was added to give a deep red solution. The reaction was kept in the dark and was periodically monitored by $^{1}H\{^{11}B\}$ NMR spectroscopy until after 7 d there was primarily only one Cp resonance. The solution was transferred to a Young's tube and layered with n-hexanes to give 0.010g of dark red powder.

Yield: 25%

δ $^{1}H\{^{11}B\}$ (298 K, CD_2Cl_2): 5.81 (5H, s, Cp), 1.15 (1H, s, cage C-H), -0.18 (15H, s, $B_{2\text{-}6}CH_3$), -0.43 (15H, s, $B_{7\text{-}11}CH_3$) and -0.55 (3H, s, $B_{12}CH_3$).

δ ^{11}B (298 K, CD_2Cl_2): -0.96 (1B, s, B_{12}), -8.94 (5B, s, $B_{7\text{-}11}$) and -12.19 (5B, s, $B_{2\text{-}6}$).

IR (CH_2Cl_2,ν(CO) (cm^{-1}): 2073s, 2065sh, 1999br.

[{$CpMo(CO)_3$}$_2$(μ-I)][1-H-*closo*-$CB_{11}Me_{11}$], (15-I): A Young's NMR tube was charged with Ag[1-H-*closo*-$CB_{11}Me_{11}$] (0.024 g, 0.06 mmol) and $CpMo(CO)_3I$ (0.022 g, 0.06 mmol) and dissolved in 0.3 ml of CD_2Cl_2 to give a deep red solution. The reaction was kept in the dark and was periodically monitored by $^{1}H\{^{11}B\}$ NMR spectroscopy until after 12 days there was primarily only one Cp resonance. The solution was transferred to a Young's tube and layered with n-hexanes to give 0.014 g of dark red crystals.

Yield: 53%

δ $^{1}H\{^{11}B\}$ (298 K, CD_2Cl_2): 5.82 (5H, s, Cp), 1.15 (1H, s, cage C-H), -0.18 (15H, s, $B_{2\text{-}6}CH_3$), -0.43 (15H, s, $B_{7\text{-}11}CH_3$) and -0.55 (3H, s, $B_{12}CH_3$).

δ ^{11}B (298 K, CD_2Cl_2): -0.91 (1B, s, B_{12}), -8.93 (5B, s, $B_{7\text{-}11}$) and -12.17 (5B, s, $B_{2\text{-}6}$).

IR (KBr,ν(CO) (cm^{-1}): 2066s, 2054s, 1992br, 1981br and 1963sh.

Accurate Mass Spec: Calcd: 617.004m/z, Found: 617.00m/z

$[(CpMo(CO)_3)_2(\mu\text{-}H)][1\text{-}H\text{-}closo\text{-}CB_{11}Me_{11}]$, (15-Cl): *In a typical reaction*: A Young's NMR tube was charged with $CpMo(CO)_3H$ (0.014 g), $[Ph_3C][1\text{-}H\text{-}closo\text{-}CB_{11}Me_{11}]$ (0.030 g) and CD_2Cl_2 (0.3 cm^3) to produce primarily $[(CpMo(CO)_3)_2(\mu\text{-}H)][1\text{-}H\text{-}closo\text{-}CB_{11}Me_{11}]$ and one half an equivalent of unreacted $[Ph_3C][1\text{-}H\text{-}closo\text{-}CB_{11}Me_{11}]$. An alternative synthesis using a 2:1 ratio of $CpMo(CO)_3H$: $[Ph_3C][1\text{-}H\text{-}closo\text{-}CB_{11}Me_{11}]$ produced $[(CpMo(CO)_3)_2(\mu\text{-}H)][1\text{-}H\text{-}closo\text{-}CB_{11}Me_{11}]$ with no remaining $[Ph_3C][1\text{-}H\text{-}closo\text{-}CB_{11}Me_{11}]$. Attempts to isolate solid analytically pure material repeatedly failed. By NMR spectroscopy, the hydride-bridged dimer was always the predominant product. Addition over a range of temperatures (-78°C to 25°C) gave the same ratio of products.

δ ^{1}H (298 K, CD_2Cl_2): 5.55 (10H, s, Cp), -0.12 (15H, s, $B_{2\text{-}6}CH_3$), -0.40 (15H, s, $B_{7\text{-}11}CH_3$) and -0.52 (3H, s, $B_{12}CH_3$), -21.26 (1H, s, Mo-H-Mo).

δ ^{11}B (298 K, CD_2Cl_2): -0.97 (1B, s), -8.93 (5B, s), -12.10 (5B, s).

$[(CpMo(PPh_3)(CO)_2(CH_3CH_2C(O)CH_2CH_3)][1\text{-}H\text{-}closo\text{-}CB_{11}Me_{11}]$, and ^{1}H NMR reaction monitoring of the hydrogenation of 3-Pentanone to 3 Pentanol:

$CpMo(CO)_2(PPh_3)H$ (0.050 g, 0.11 mmol) and $[Ph_3C][1\text{-H-}closo\text{-}CB_{11}Me_{11}]$ (0.059 g, 0.11 mmol) and $O{=}CEt_2$ (0.11 ml, 1.1 mmol) were added to a Young's NMR tube and dissolved in 0.3 ml CD_2Cl_2. This gave a clean mixture of the *cis* and *trans* isomers of $[(CpMo(PPh_3)(CO)_2(CH_3CH_2C(O)CH_2CH_3)][1\text{-H-}closo\text{-}CB_{11}Me_{11}]$ (55%:45% by ^1H NMR spectroscopy) the NMR data for the cation corresponds to that previously reported by Bullock *et al.*[33] The solution was then degassed by three freeze/pump/thaw cycles and backfilled at 77 K with H_2. The pressure of H_2 in the tube on warming to room temperature should be *ca.* 4 atmospheres (298/77 = 3.9). The pressure was maintained periodically by recharging with H_2 at 77 K. To ensure thorough diffusion of gas into the solvent the tube was slowly spun using a mechanical stirring motor. ^1H NMR measurements were periodically taken over the course of 14 days and the number of catalyst turnovers was monitored by measuring the disappearance of the $O{=}CEt_2$ peak at $\delta = 2.47$ (q, CH_2) versus the appearance of Et_2CHOH peaks at $\delta = 5.54$ (m, CH) and $\delta = 0.97$ (t, CH_3).

$[(PCy_3)Re(CO)_4(CH_2Cl_2)][1\text{-H-}closo\text{-}CB_{11}Me_{11}]$, (16): A Young's NMR tube was charged with $(PCy_3)Re(CO)_4Me$ (0.028 g) and $[Ph_3C][1\text{-H-}closo\text{-}CB_{11}Me_{11}]$ (0.025 g). 0.3 ml of CD_2Cl_2 was vacuum transferred in and the solution was warmed to -78°C to generate a pale yellow solution. Characterisation was carried out by NMR studies run immediately at 25°C and the cation signals are identical to that reported for the $[BAr_F]^-$ analogue.[19]

$[((PCy_3)Re(CO)_4)_2(\mu\text{-Cl})][Y]$ (Y = a number of functionalised cages): A CD_2Cl_2 solution of $[(PCy_3)Re(CO)_4(CH_2Cl_2)][1\text{-H-}closo\text{-}CB_{11}Me_{11}]$ decomposes at 25°C to give predominantly one phosphine containing product identified by comparison to the $[BAr_F]^-$

analogue and accurate mass spec to be $[((PCy_3)Re(CO)_4)_2(\mu\text{-}Cl)]^+$.[19] Along with the formation of this chloride bridged dimer there is decomposition of the anion to give [1-H-12-Cl-*closo*-$CB_{11}Me_{10}$] and other unidentified products.

[1-H-12-Cl-*closo*-$CB_{11}Me_{10}$]:

δ ^{11}B (298 K, CD_2Cl_2): 3.82 (s, 1B), -8.84 (s, 5B), -12.33 (s, 5B).

Mass Spec: Calcd: 317.7 m/z. Found: 317.3 m/z

[$(P(OCH_2)_3CMe)_2Re(CO)_3(CH_2Cl_2)$][1-H-*closo*-$CB_{11}Me_{11}$]: A Young's NMR tube was charged with $(P(OCH_2)_3CMe)_2Re(CO)_3Me$ (0.015 g) and $[Ph_3C]$[1-H-*closo*-$CB_{11}Me_{11}$] (0.014 g). 0.3 ml of CD_2Cl_2 was vacuum transferred in and the solution was warmed to -78°C to generate a yellow solution. Characterisation was carried out by NMR studies run immediately at 25°C and the cation signals are identical to those reported for the $[BAr_F]^-$ analogue.[21]

[$(PCy_3)_2Re(CO)_3$][1-H-*closo*-$CB_{11}Me_{11}$]: A Young's NMR tube was charged with 0.025 g of $(PCy_3)_2Re(CO)_3Me$ and 0.016 g of $[Ph_3C]$[1-H-*closo*-$CB_{11}Me_{11}$] and 0.3 ml of CD_2Cl_2 was vacuum distilled in. On warming to room temperature an orange solution rapidly formed whose formulation as the agostic complex $[(PCy_3)_2Re(CO)_3]$[1-H-*closo*-$CB_{11}Me_{11}$] is consistent with that reported previously by Heinekey.[34]

[Cp*Rh(PMe_3)(Me)(CH_2Cl_2)][1-H-*closo*-$CB_{11}Me_{11}$], (17): Cs[1-H-*closo*-$CB_{11}Me_{11}$] (0.020 g) and Cp*Rh(PMe_3)(Me)(OTf) (0.022 g) were dissolved in CH_2Cl_2 in a Young's ampoule. The resultant red solution was stirred for 15 mins, filtered to remove CsOTf and

the solvent removed *in vacuo*. Redissolving in CD_2Cl_2 allowed characterisation *vide infra* by comparison to the previously reported $[BAr_F]^-$ analogue.[16] The yield was quantitative by NMR spectroscopy.

[(Cp*Rh(PMe$_3$)Me)$_2$(μ-OTf)][1-H-*closo*-CB$_{11}$Me$_{11}$]: Cs[1-H-*closo*-$CB_{11}Me_{11}$] (0.018 g) and Cp*Rh(PMe_3)(Me)(OTf) (0.020 g) were dissolved in 5-fluoro–m-xylene in a Young's ampoule and the resultant red orange solution was stirred for 15 minutes and filtered into a Young's recrystallisation tube. Red/orange crystals were grown by the slow diffusion of pentane into a saturated 5-fluoro-m-xylene solution at -20°C.

Yield: 44%

δ ^{1}H (298 K, CD_2Cl_2): 1.66 (d, 30H, ^{3}J(RhH) 2.4), 1.51 (d, 18H, ^{2}J(PH) 10), 1.14 (s, 1H, CH_{cage}), 0.83 (dd, 6H, ^{2}J(RhH) 6.0, ^{3}J(PH) 1.2), -0.19 (s, 15H, B-CH_3(2-6)), -0.44 (s, 15H, B-CH_3(7-11)), -0.56 (s, 3H, B-CH_3(12)).

δ ^{31}P{^{1}H} (298 K, CD_2Cl_2): 3.8 (d, ^{1}J(RhP) 165.7)

δ ^{19}F (298 K, CD_2Cl_2): -78.69 (s)

[(^{i}Pr$_3$P)$_2$Pt(Me)][1-H-*closo*-CB$_{11}$Me$_{11}$], (18): A Young's ampoule was charged with equimolar quantities of [(^{i}Pr$_3$P)$_2$PtMe$_2$] (0.020 g) and [1-H-*closo*-$CB_{11}Me_{11}$]$^\bullet$ (0.011 g) (or alternatively 0.020 g of [Ph_3C][1-H-*closo*-$CB_{11}Me_{11}$] and 5 ml of C_6H_5F was added, resulting in the formation of a yellow solution. Yellow crystals were obtained by the slow diffusion of pentane at -20°C.

δ ^{1}H (298 K, CD_2Cl_2): 2.56 (m, 6H, ^{i}Pr CH), 1.69 (t, 3H, Pt-Me, ^{2}J(PtH) 106, ^{3}J(PH) 5.6), 1.34 (dd, 36H, ^{i}Pr CH_3, ^{3}J(PH) 14.8 ^{3}J(HH) 7.6), 1.15 (s, 1H CH_{cage}), -0.18 (s, 15H, B-

CH_3(2-6)), -0.43 (s, 15H, B-CH_3(7-11)), -0.55 (s, 3H, B-CH_3(12)).

δ $^{31}P\{^1H\}$ (298 K, CD_2Cl_2): 47.1 (^{1}J(PtP) 2757)

δ ^{11}B (298 K, CD_2Cl_2): -0.51 (s, 1B), -8.60 (s, 5B), -11.90 (s, 5B).

δ $^{13}C\{^1H\}$ (298 K, CD_2Cl_2): 60.19 (s, Cage C), 23.24 (t, ^{1}J(PC) 14, ^{i}Pr_3P C-H), 18.82 (s, ^{i}Pr_3P CH_3), -3.82 (br s, B-CH_3), -14.11 (s, ^{1}J(PtC) 755, Pt-CH_3).

Accurate Mass Spec (ES+): Theoretical for $C_{19}H_{45}P_2Pt_1$ = 530.2639 m/z. Experimentally Observed = 530.2637 m/z

[*trans*-(^{i}Pr_3P)$_2$Pt(Me)(THF)][1-H-*closo*-$CB_{11}Me_{11}$], (19): To a solution of [(^{i}Pr_3P)$_2$Pt(Me)][1-H-*closo*-$CB_{11}Me_{11}$] (prepared *in situ*) in CD_2Cl_2 was added via syringe 5 equivalents of THF (20 μl). The room temperature NMR spectra are fluxional, with only one sets of broadened signals visible in the $^{31}P\{^1H\}$ NMR, the Me *trans* to the fluxional site is also significantly broadened. At 230 K, the fluxionaility is frozen out and two sets of signals are visible – one is the agostic complex, [(^{i}Pr_3P)$_2$Pt(Me)][1-H-*closo*-$CB_{11}Me_{11}$]. The other is assigned as [*trans*-(^{i}Pr_3P)$_2$Pt(Me)(THF)][1-H-*closo*-$CB_{11}Me_{11}$], also present in the ^{1}H NMR spectra are the signals for free THF.

δ ^{1}H (298 K, CD_2Cl_2): 2.56 (m, 6H, ^{i}Pr CH), 1.58 (br s, 3H, Pt-Me, ^{2}J(PtH) 98), 1.33 (dd, 42H, ^{i}Pr CH_3, ^{3}J(PH) 14.8 ^{3}J(HH) 7.2), 1.14 (s, 1H CH_{cage}), -0.18 (s, 15H, B-CH_3(2-6)), -0.43 (s, 15H, B-CH_3(7-11)), -0.55 (s, 3H, B-CH_3(12)).

δ $^{31}P\{^1H\}$ (298 K, CD_2Cl_2): 46.1 (br s^{1}J(PtP) 2771)

Low Temperature Data:

δ ^{1}H (230 K, CD_2Cl_2): 3.90 (m, 4H, THF), 2.33 (m, 6H, ^{i}Pr CH), 1.90 (m, 4H THF), 1.28

(vt, 42H, ^{i}Pr CH_3, ^{3}J(PH) 13.4 ^{3}J(HH) 6.7), 1.11 (s, 1H CH_{cage}), 0.76 (t, 3H, Pt-Me ^{2}J(PtH) 86Hz, ^{3}J (PtP) 5.2)-0.25 (s, 15H, B-CH_3(2-6)), -0.54 (s, 15H, B-CH_3(7-11)), -0.67 (s, 3H, B-CH_3(12)).

δ ^{31}P{^{1}H} (230 K, CD_2Cl_2): 40.3 (^{1}J(PtP) 2820)

[(^{i}Pr$_3$P)(THF)Pt{κ^2-P(^{i}Pr$_2$)(CH(CH$_3$)CH$_2$)}][1-H-*closo*-CB$_{11}$Me$_{11}$], (20): 5 equivalent of THF is added via a syringe to 20 mgs of [*trans*-(^{i}Pr$_3$P)$_2$Pt(Me)][1-H-*closo*-$CB_{11}Me_{11}$] dissolved in CD_2Cl_2. On standing the solution gradually lightened in colour from yellow to colourless over the course of 10 days (periodically monitoring of the reaction by ^{31}P{^{1}H} NMR spectroscopy until only one complex is present) to produce quantitatively (by ^{1}H{^{31}P}, ^{31}P{^{1}H} and ^{13}C{^{1}H} NMR spectroscopy) [(^{i}Pr$_3$P)(THF)Pt{κ^2-P(^{i}Pr$_2$)(CH(CH$_3$)CH$_2$)}][1-H-*closo*-$CB_{11}Me_{11}$]. Solid material was unobtainable despite repeated attempts. Facile loss of the coordinated THF molecule prevented satisfactory microanalysis.

δ ^{1}H{^{31}P} (220 K, CD_2Cl_2): 3.92 (m. 4H, THF O(**C**H$_2$CH$_2$)$_2$), 2.97 (1H, m, PtCH$_2$**C**HMeP) 2.58 (2H, m, PtCH$_2$CHMeP(**C**HMe$_2$)$_2$), 2.21 (3H, m , Pt-P(**C**HMe$_2$)$_3$, 1.92 (6H, m, O(CH$_2$C**H**$_2$) THF and PtC**H**$_2$CHMeP), 1.41 – 1.05 (34H, 7 sets of d, PtCH$_2$CH**Me**P, Pt-P(CH**Me**$_2$)$_3$ and PtCH$_2$CHMeP(CH**Me**$_2$)$_2$ and an obscured cage C-H) [1,41 (d, ^{3}J(HH) 7), 1.38 (d, ^{3}J(HH) 7), 1.29, (d, ^{3}J(HH) 7), 1.24 (d, ^{3}J(HH) 7), 1.15 (d, ^{3}J(HH) 7), 1.12 (d, ^{3}J(HH) 7) and 1.05 (d, ^{3}J(HH), 7)], -0.21 (s, 15H, B-CH_3(2-6)), -0.46 (s, 15H, B-CH_3(7-11)), -0.59 (s, 3H, B-CH_3(12)).

δ ^{31}P{^{1}H} (220 K, CD_2Cl_2): 41.8 (d, ^{2}J (PtP) 358 ^{1}J(PtP) 3010), -15.8 (d, ^{2}J(PtP) 358, ^{1}J(PtP) 2124)

δ ^{11}B (298 K, CD_2Cl_2): -0.60 (s, 1B), -8.75 (s, 5B), -12.08 (s, 5B).

δ ^{13}C{^{1}H} (220 K, CD_2Cl_2): 75.25 (s, THF), 59.79 (s, Cage C), 34.19 (d, 31 J(PC)), 29.99 to 17.46 (complex overlapping isopropyl signals and remaining THF signal), -3.20 (br s, B-CH_3), -17.40 (d, ^{2}J(PC) 22, ^{1}J(PtC) not observed, Pt-CH_2).

Accurate Mass Spec (ES+): Theoretical for $C_{18}H_{41}P_2Pt_1$ (M^+ -THF) = 514.2331 m/z. Experimentally Observed = 514.23312 m/z.

[(^{i}Pr$_3$P)$_2$Pt(μ-Cl)]$_2$[1-H-12-Cl-*closo*-$CB_{11}Me_{10}$]$_2$: A Young's ampoule was charged with [(^{i}Pr$_3$P)$_2$PtMe$_2$] (0.020 g, 0.037 mmol) and two equivalents of [1-H-*closo*-$CB_{11}Me_{11}$]$^•$ (0.022 g, 0.074 mmol) and 5ml of CH_2Cl_2 was added, resulting in the formation of a yellow solution (the reaction can alternatively be carried out by the sequential addition of [1-H-*closo*-$CB_{11}Me_{11}$]$^•$ - which proceeds via the agostic complex [(^{i}Pr$_3$P)$_2$PtMe][1-H-*closo*-$CB_{11}Me_{11}$]). Yield is quantitative by ^{31}P{^{1}H} NMR spectroscopy. Yellow crystals (0.028 g) were obtained by the slow diffusion of pentane at -20°C.

Yield: 70%

δ ^{1}H (298 K, CD_2Cl_2): 2.48 (m, 12H, ^{i}Pr CH), 1.50 (dd, 72H, ^{i}Pr CH_3, ^{3}J(PH) 15.6 ^{3}J(HH) 7.2), 1.17 (s, 2H CH_{cage}), -0.14 (s, 30H, B-CH_3(2-6)), -0.32 (s, 30H, B-CH_3(7-11)),

δ ^{31}P{^{1}H} (298 K, CD_2Cl_2): 38.5 (^{1}J(PtP) 3706)

δ ^{11}B (298 K, CD_2Cl_2): 3.97 (s, 1B), -9.35 (s, 5B), -12.67 (s, 5B).

Mass Spec: FAB- Calcd: 317.7 m/z. Found: 317.3 m/z

[(PPh_3)$_2$Ir(C_8H_{12})][1-H-*closo*-$CB_{11}Me_{11}$]: [(COD)IrCl]$_2$ (0.083 g) was loaded into a beaker with PPh_3 (0.129 g) and 15 ml of ethanol. The suspension was stirred for 15 mins

during which time a homogeneous red solution is formed. Upon addition of Ag[*closo*-1-H-$CB_{11}Me_{11}$] (0.100 g) dissolved in 5 ml of ethanol an immediate precipitate was observed. The ethanol was removed *in vacuo* and the residue redissolved in 5 ml of CH_2Cl_2. AgCl is removed by filtration and the product recrystallised by the slow diffusion of hexanes into the CH_2Cl_2 solution at 25°C to afford 0.145 g of red crystalline solid.

Yield: 52%

δ ^{1}H ($CDCl_3$, 298 K): 7.30 (m, 30H, C_6H_5), 4.16 (s, 4H, C_8H_{12}), 2.20 (m, 4H, C_8H_{12}), 1.95 (m, 4H, C_8H_{12}), 1.28 (s, 1H, CH_{cage}), -0.04 (s, 15H, B-CH_3(2-6)), -0.27 (s, 15H, B-CH_3(7-11)), -0.45 (s, 3H, B-CH_3(12)).

δ ^{11}B (298 K, $CDCl_3$): -0.61 (s, 1B), -8.75 (s, 5B), -12.08 (s, 5B).

δ ^{31}P{^{1}H} (298 K, $CDCl_3$): 18.9 (s)

Elemental Analysis: Calcd: %C 55.7; %H 6.77; Found: %C 54.1, %H 6.62

[(^{i}Pr$_3$P)$_2$Rh(NBD)][BAr$_F$]: A Schlenk flask was charged with {(NBD)RhCl}$_2$ (0.100 g, 0.22 mmol) and 15 ml of CH_2Cl_2 was added. A hexane solution of ^{i}Pr$_3$P (0.86 mmol) was added in one portion and the resultant solution stirred for 15 minutes. K[BAr$_F$] (0.392 g, 0.44 mmol) in CH_2Cl_2 was added in one portion followed by a 15 ml portion of degassed H_2O. The biphasic mixture was vigorously mixed for 15 minutes and the H_2O layer extracted. Hexane was added to the point of cloudiness and cooled to -20°C resulting in the formation of 0.320 g of vermilion crystalline material.

Yield: 54%

δ ^{1}H (298 K, CD_2Cl_2): 7.74 (8H, s, o-Ar BAr_F), 7.57 (4H, s, m-Ar BAr_F), 4.82 (4H, s alkene NBD), 3.91 (2H, s, NBD), 2.19 (6H, septet, ^{i}Pr), 1.55 (2H, s, NBD), 1.38 (36H d of d, ^{i}Pr).

δ ^{11}B (298 K, CD_2Cl_2): -5.88.

δ ^{31}P {^{1}H} (298 K, CD_2Cl_2): 33.82 (d, ^{1}J-RhP 146)

Elemental Analysis: Calculated: C 49.7%; H: 4.5%; Found: C 49.4%; H: 4.5%.

[(^{i}Pr$_3$P)$_2$Rh(NBD)][1-H-*closo*-$CB_{11}Me_{11}$]: An identical method to the $[BAr_F]^-$ salt was followed starting with 0.057 g of {(NBD)RhCl}$_2$ and 0.100 g of Ag[1-H-*closo*-$CB_{11}Me_{11}$], on recrystallisation resulted in 0.136 g.

Yield: 64%

NMR Data for the cationic portion identical to that for [(^{i}Pr$_3$P)$_2$Rh(NBD)][BAr_f].

δ ^{1}H{^{11}B} (298 K, CD_2Cl_2): 1.13 (1H, br. s C-H_{cage}), -0.15 (15H, s, BCH_3), -0.38 (15H, s, BCH_3), -0.55 (3H, s, BCH_3).

δ ^{11}B (298 K, CD_2Cl_2): 0.12 (1B, s), -7.92 (5B, s), -11.19 (5B, s).

[(PCy_3)$_2$Rh(NBD)][1-H-*closo*-$CB_{11}Me_{11}$]: {(NBD)RhCl}$_2$ (0.050 g, 11 mmol), Ag[1-H-*closo*-$CB_{11}Me_{11}$] (0.088 g, 11 mmol) and 2,5-norbornadiene (15 μl, 15 mmol) were stirred in CH_2Cl_2 for 2 h. The resultant vermilion solution was filtered and the solvent removed *in vacuo* to leave a red/orange solid, which was redissolved in CH_2Cl_2 and a CH_2Cl_2 solution of PCy_3 (0.122g .43mmol) was added drop wise and the mixture wasstirred for 30 minutes. The compound was crystallized by the addition of hexanes.

Yield: 0.096 g (41%)

δ $^{1}H\{^{11}B\}$ (298 K, CD_2Cl_2): 4.75 (s, 4H, C_7H_8), 3.9 (s, 2H, C_7H_8), 2.2 – 1.3 (m 66H PCy_3, 2H C_7H_8 and 1H cage C-H). -0.05 (15H, s, BCH_3), -0.38 (15H, s, BCH_3), -0.55 (3H, s, BCH_3).

δ ^{11}B (298 K, CD_2Cl_2): -0.8 (1B, s), -8.9 (5B, s), -12.2 (5B, s).

δ $^{31}P\{^{1}H\}$ (298 K, CD_2Cl_2): 23.340 J(RhP) 145

Elemental Analysis: Calcd: %C; 62.7, %H 10.3. Found: %C 62.1, %H 10.1.

IR (CH_2Cl_2, ν(1-H-*closo*-$CB_{11}Me_{11}$) cm^{-1}): 2928, 2892, 2853.

[$(PCy_3)_2Rh(NBD)$][BAr_F]: A Schlenk flask was charged with $\{(NBD)RhCl\}_2$ (0.080 g, 0.17 mmol) and dissolved in 15 ml of CH_2Cl_2. A CH_2Cl_2 solution of PCy_3 (0.194 g, 34 mmol) was added in one portion and the resultant solution stirred for 15 minutes. K[BAr_F] (0.313 g, 0.35 mmol) in CH_2Cl_2 was added in one portion followed by a 15 ml portion of degassed H_2O. The biphasic mixture was vigorously mixed for 15 minutes and the H_2O layer extracted. Hexane was added to the point of cloudiness and the sample was cooled to -20°C resulting in the precipitation of 346 mgs of an orange crystalline solid.

Yield: 62%

NMR data for the cationic portion is identical to that found for [$(PCy_3)_2Rh(NBD)$][1-H-*closo*-$CB_{11}Me_{11}$]

δ ^{1}H (selected 298 K, CD_2Cl_2): 7.72 (8H, ortho aromatic BAr_F), 7.57 (4H, para aromatic BAr_F).

δ ^{11}B (298K, CD_2Cl_2): -5.90 (s,)

Elemental Analysis: Calculated: C 55.6%; H 5.4%. Found: C 55.8%; H 5.4%.

$[(^{i}Pr_3P)_2Rh(H_2)_xH_2][Y]$: (x = 1 (22-$(H_2)$) or 2 (22-$(H_2)_2$) and Y = [1-H-*closo*-$CB_{11}Me_{11}]^-$ or $[BAr_F]^-$)

A typical experiment consisted of charging a Young's NMR tube with 0.015g of $[(^{i}Pr_3P)_2Rh(NBD)][Y]$. Addition of 0.3 ml of CD_2Cl_2 generated an orange solution. The sample was freeze/pumped/thawed three times before being backfilled with H_2 at 77 K (~ 4 atmospheres of H_2). On thawing the solution rapid changes colour from orange to pale yellow. Attempts to isolate solid material repeatedly failed.

Yield: Quantitatively by NMR spectroscopy

δ ^{1}H (CD_2Cl_2, 298 K for Y = BAr_F): 7.73 (s, 8H, ortho arene), 7.57 (s, 4H, para arene), 2.31 (m, 6H, ^{i}Pr bridgehead ^{3}J (HH) 7.14), 1.25 (vq, 36H, CH_3 ^{3}J(HH) 7.14, ^{3}J(PH) 14.83), -8.62 (v. br 3.6H, (H_2)/H).

δ ^{31}P{^{1}H} (CD_2Cl_2, 298 K): 60.4 (d, ^{1}J(RhP) 107).

δ ^{11}B NMR (CD_2Cl_2, 298 K): –5.9 (s).

Mass Spec: (FAB+ NOBA Matrix) Calcd for $[(^{i}Pr_3P)_2Rh(H)_2(H_2)]^+$: 427.4145 m/z Found: 427.3.

Ratio of x = 1:x = 2 at **190K** ~4:1

$[(^{i}Pr_3P)_2Rh(H_2)H_2][BAr_F]$ (22-(H_2)):

δ ^{1}H NMR (CD_2Cl_2, 190 K): δ 7.61 (s, 8H, ortho arene), 7.46 (s, 4H, para arene), 2.08, (m, 6H, ^{i}Pr bridgehead), 1.02 (m, 36H, CH_3), -0.28 (br 2H (η^2-H_2), T_1 94ms), -12.66 (s br, 1H, T_1 238ms), -22.42 (s br, 1H T_1 234ms).

δ ^{31}P{^{1}H} (CD_2Cl_2, 190 K): 62.1 (d, ^{1}J (RhP) 100)

$[(^{i}Pr_3P)_2Rh(H_2)_2H_2][BAr_F]$ (22-$(H_2)_2$):

δ ^{1}H NMR (CD_2Cl_2, 190 K): δ 7.61 (s, 8H, ortho arene), 7.46 (s, 4H, para arene), 2.08, (m, 6H, ^{i}Pr bridgehead), 1.02 (m, 36H, CH_3), -2.06 (v. br 4H (η^2-H_2), T_1 43 ms), -14.23 (s br, 1H, T_1 360 ms),

δ $^{31}P\{^1H\}$ (CD_2Cl_2, 190 K): δ 68.4 (d, ^{1}J(RhP) 92)

Assignment of the hydrides in each complex comes from T_1 measurements at 190 K using the software provided with a Bruker Advance 400MHz spectrometer using the best fit curves and comparison of observed chemical shifts with the previously reported complexes $[(R_3P)_2Ir(H_2)_xH_2][BAr_F]$ (x = 1, 2).[35, 36]

$[(^{i}Pr_3P)_2Rh(HD)_xH_2][BAr_F]$: A solution of $[(^{i}Pr_3P)_2Rh(H_2)_xH_2][Y]$ in CD_2Cl_2 in a Young's NMR tube was frozen in liquid nitrogen, evacuated and then sealed and warmed to room temperature, the solution was then refrozen and D_2 added at low temperature. All other NMR signals in the ^{1}H and $^{31}P\{^1H\}$ spectra were identical to $[(^{i}Pr_3P)_2Rh(H_2)_xH_2][Y]$.

δ ^{1}H (190 K, CD_2Cl_2) (for x =2): 1.95 (t, ^{1}J(DH) 29).

The HD coupling for the (x=1) dihydrogen adduct could not be resolved at any temperature, due to overlap of signals from the broad ^{i}Pr CH_3 resonances.

$[(^{i}Pr_3P)_2RhH_2][Y]$, (22-DCM) Y = [1-H-*closo*-$CB_{11}Me_{11}$] or $[BAr_F]$:

A sample of $[(^{i}Pr_3P)_2Rh(H_2)_xH_2][Y]$ was formed *in situ* by the hydrogenation of $[(^{i}Pr_3P)_2Rh(NBD)][Y]$ in C_6H_5F. The solvent was evaporated to dryness and pumped on for 5 hours to leave a dark yellow oil. Attempts to obtain solid material repeatedly failed due to the ready decomposition of this compound. NMR data shown for Y = $[BAr_f]^-$

δ ^{1}H (CD_2Cl_2, 298 K): 7.72 (s, 8H, ortho arene), 7.56 (s, 4H, para arene), 2.33 (m, 6H, ^{i}Pr bridgehead), 1.25 (vq, 36H, CH_3 ^{3}J(HH) 7.6, ^{3}J(PH) 14.4), -24.36 (d of t 2H, ^{1}J(RhH) 40.4, ^{2}J(PH) 14.4).

δ ^{31}P{^{1}H} (CD_2Cl_2, 298 K): 57.6 (d, ^{1}J(RhP) 104).

δ ^{11}B NMR (CD_2Cl_2, 298 K): –5.9 (s).

Mass Spec: (FAB+ NOBA Matrix) Calcd for $[(^{i}Pr_3P)_2Rh(H)_2]^{+}$: 423.4 m/z Found: 423.3.

$[(^{i}Pr_3P)_2Rh(\eta^{6}\text{-}C_6H_5F)][BAr_F]$ (24): 0.030 g of $[(^{i}Pr_3P)_2Rh(NBD)][BAr_F]$ was loaded into a Young's ampoule and dissolved in 5 ml of C_6H_5F. The orange solution was thoroughly degassed by three freeze/pump/thaw cycles and backfilled with H_2 at 77 K. On liquefying the solution rapidly turned yellow and was stirred for 15 minutes. The solvent was then removed *in vacuo* and the resulted brown oil pumped to dryness. Redissolving in 3 ml of C_6H_5F produced a dark yellow solution that was layered with pentane at -20°C. Slow diffusion of pentane resulted in a mixture of yellow crystals and brown oil. Extraction of the yellow crystals that melted at room temperature, cleanly gave $[(^{i}Pr_3P)_2Rh(\eta^{6}\text{-}C_6H_5F)][BAr_F]$.

δ ^{1}H (298 K, CD_2Cl_2): 7.72 (s, 8H, ortho arene BAr_F), 7.56 (s, 4H, para arene BAr_F), 7.36 (m, 2H, C_6H_5F), 7.15 (m, 1H, C_6H_5F) 7.06 (m, 2H, C_6H_5F), 2.32 (m, 6H, ^{i}Pr CH), 1.27 (m, 42H, ^{i}Pr CH_3).

δ ^{31}P{^{1}H} (298 K, CD_2Cl_2): 57.6 (d, ^{1}J(RhP) 109)

δ ^{11}B (298 K, CD_2Cl_2): -6.6

δ ^{19}F (298 K, CD_2Cl_2): -62.91 (CF_3 BAr_F), -113.95 (C_6H_5F)

$[(PCy_3)_2Rh(H_2)_2(H)_2][Y]$ (25-$(H_2)_2$): (Y = 1-H-*closo*-$CB_{11}Me_{11}$ or BAr_F)

A typical experiment consisted of charging a Young's NMR tube with 0.020 g of $[(PCy_3)_2Rh(NBD)][Y]$, addition of 0.3 ml of CD_2Cl_2 generated an orange solution. The sample was freeze/pumped/thawed three times before being backfilled with H_2 at 77 K (~ 4 atmospheres of H_2). On thawing the solution rapid changes colour from orange to pale yellow. Attempts to isolate solid material repeatedly failed.

Yield: Quantitatively by NMR spectroscopy

δ ^{1}H (CD_2Cl_2, 298 K for Y = BAr_F): 7.73 (s, 8H, ortho arene), 7.57 (s, 4H, para arene), 2.24 – 1.05 (m, 66H, PCy_3), no hydride signal visible

δ $^{31}P\{^1H\}$ (CD_2Cl_2, 298 K): 54.3 (br d, ^1J(RhP) 109.6).

δ ^{11}B (CD_2Cl_2, 298 K): –5.9 (s).

Selected δ ^{1}H NMR (CD_2Cl_2, 180 K): –1.80 (br 4H (η^2-H_2), T_1 21 ms (400MHz)), -14.17 (s br, 2H, T_1 260 ms (400 MHz)).

Selected δ ^{1}H NMR (CD_2Cl_2, 200 K): –1.81 (br 4H (η^2-H_2), T_1 58 ms), -14.14 (s br, 2H, T_1 147 ms).

δ $^{31}P\{^1H\}$ (CD_2Cl_2, 200 K): 60.1 (d, ^1J(RhP) 92.4)

$[(Cy_3P)_2RhH_2][Y]$, (25-DCM) Y = [1-H-*closo*-$CB_{11}Me_{11}$] or [BAr_F]:

A sample of $[(Cy_3P)_2Rh(H_2)_2H_2][Y]$ was formed *in situ* by the hydrogenation of $[(Cy_3P)_2Rh(NBD)][Y]$ in C_6H_5F. The solvent was evaporated to dryness and pumped on for 5 hours to leave a dark yellow oil. Attempts to obtain solid material repeatedly failed due to the ready decomposition of this compound. NMR data shown for Y = $[BAr_f]^-$

δ ^{1}H (CD_2Cl_2, 298 K): 7.74 (s, 8H, ortho arene), 7.54 (s, 4H, para arene), 2.46 – 1.27 (m, 66H, PCy_3) -24.03 (br d. 2H, ^{1}J(RhH) 41.5).

δ ^{31}P{^{1}H} (CD_2Cl_2, 298 K): 53.9 (d, ^{1}J(RhP) 111.3).

δ ^{11}B NMR (CD_2Cl_2, 298 K): –5.9 (s).

[($^{i}Pr_3P)_6Rh_6H_{12}$][1-H-*closo*-$CB_{11}Me_{11}$]$_2$ + 4 [HP(^{i}Pr)$_3$][1-H-*closo*-$CB_{11}Me_{11}$]:

A Young's tube was charged with (0.030 g, $3.7x10^{-5}$ mol) [($^{i}Pr_3P)_2$Rh(NBD)][1-H-*closo*-$CB_{11}Me_{11}$] and C_6H_5F (5 ml) was added. This was fully degassed by three freeze-pump-thaw cycles then immediately backfilled with H_2 at 4 atmospheres pressure (77 K) resulting in a colour change from orange to yellow. Stirring for 4 days yielded a further gradual darkening of the solution to brown. The solvent was layered with pentane under 1 atmosphere of H_2 at room temperature and yielded black and colourless crystals (co-product [HP(^{i}Pr)$_3$][1-H-*closo*-$CB_{11}Me_{11}$] that were separated manually. A second crop of crystalline [($^{i}Pr_3P)_6Rh_6H_{12}$][1-H-*closo*-$CB_{11}Me_{11}$]$_2$ was isolated by redissolving the non-crystalline product in C_6H_5F and combining with the supernatant and layering with pentane at room temperature under 1 atmosphere of H_2.

[($^{i}Pr_3P)_6Rh_6H_{12}$][1-H-*closo*-$CB_{11}Me_{11}$]$_2$ (27-H_{12}):

δ ^{1}H (298 K, CD_2Cl_2): 2.31 (br, m 18H, C-H ^{i}Pr), 1.28 (m, 108H, CH_3 ^{i}Pr), 1.16 (s, 2H $cage_{C\text{-}H}$), -0.17 (s, 30H), -0.43 (s, 30H), -0.54 (s, 6H), -21.44 (br s, 12 H relative to ^{i}Pr signals, 5 s delay to avoid saturation, integration consistent over 4 independently synthesized samples).

δ ^{11}B (298 K, CD_2Cl_2): 0.17 (s, 1B), -7.89 (s, 5B), -11.14 (s, 5B),

δ $^{31}P\{^1H\}$ (298 K, CD_2Cl_2): 110.5 (d, 140)

Accurate Mass Spec: (FAB+ CH_2Cl_2 Matrix): Calcd. $[Rh_6(^iPr_3P)_6H_{12}]^{\bullet+}$: 1590.96 m/z, Found: m/z 1590.3.

$[HP(^iPr)_3][1\text{-H-}closo\text{-}CB_{11}Me_{11}]$ (26Pr): (Anion signals coincident to that in $[(^iPr_3P)_6Rh_6H_{12}][1\text{-H-}closo\text{-}CB_{11}Me_{11}]_2$.

δ ^1H (298 K, CD_2Cl_2): 5.31 (1H, d of q ^1J(PH) 336, ^3J(HH) 4.4), 2.68 (3H, m ^{i}Pr C-H) and 1.56 (18H, dd, ^3J(PH) 17.4, ^3J(HH) 7.8).

δ $^{31}P\{^1H\}$ (298 K, CD_2Cl_2): 46.6 (s)

$[(^iPr_3P)_6Rh_6H_{12}][BAr_F]_2$ (27-H_{12})

Synthesis as for $[(^iPr_3P)_6Rh_6H_{12}][1\text{-H-}closo\text{-}CB_{11}Me_{11}]_2$, starting with 0.100 g of $[(^iPr_3P)_2Rh(NBD)][BAr_F]$, yielded 0.014 g of dark red crystals from the initial recrystallisation and a further 0.003 g from a repeated recrystallisation of the supernatant.

δ ^1H (298 K, CD_2Cl_2): 7.63 (s, 16H, ortho arene) 7.47 (s, 8H, para arene), 2.35 (m, 18H, ^{i}Pr bridgehead) 1.26 (m, 108H, CH_3), -21.40 (br, s, 12H).

δ ^{11}B(298 K, CD_2Cl_2): –5.9 (s)

δ $^{31}P\{^1H\}$ (298 K, CD_2Cl_2): 110.5 (d, J(RhP) 140)

Elemental Analysis:

Yield: 37% (first crop),

8% (second crop)

$[(^{i}Pr_3P)_6Rh_6H_{10}][Y]_2$ (Y = [1-H-*closo*-$CB_{11}Me_{11}$] or [BAr_F]) (27-H_{10}): A Young's NMR tube was charged with crystalline $[(^{i}Pr_3P)_6Rh_6H_{10}][Y]_2$ and dissolved in 0.5 ml of CH_2Cl_2, removal of the solvent *in vacuo* and evacuating for 2 hours cleanly gave $[(^{i}Pr_3P)_6Rh_6H_{10}][Y]_2$. Attempts to obtain solid material with either anion repeatably failed. The yield was quantitative by ^{1}H and $^{31}P\{^{1}H\}$ NMR spectroscopy (NMR data for the cation portion only listed, the anion NMR data is identical to that reported for the $[(^{i}Pr_3P)_6Rh_6H_{12}][BAr_F]_2$ and $[(^{i}Pr_3P)_6Rh_6H_{12}][1\text{-H-}closo\text{-}CB_{11}Me_{11}]_2$ complexes respectively). The hydride content has been determined only by numerous integrations on different samples of $[(^{i}Pr_3P)_6Rh_6H_{10}][Y]_2$ and consistently integrates to 10H relative to the ^{i}Pr signals (128 scans, 3seconds delay to avoid saturation). No accurate Mass Spec data was obtainable.

δ ^{1}H (298 K, CD_2Cl_2): 2.23 (m, 18H, ^{i}Pr bridgehead) 1.22 (m, 108H, CH_3), -25.50 (br, s, 10H).

δ $^{31}P\{^{1}H\}$ (298 K, CD_2Cl_2): 107.5 (d, J(RhP) 110)

$[(PCy_3)_6Rh_6H_{14}][Y]_2$ (28-H_{14}): The synthesis is identical to that for $[(^{i}Pr_3P)_6Rh_6H_{12}][Y]_2$, except the precursor compound $[(PCy_3)_2Rh(H_2)_2(H)_2][Y]$ is heated at 50°C.

$[(PCy_3)_6Rh_6H_{14}][Y]_2$: (Anion shifts identical to that reported earlier)

δ ^{1}H (selected, 298 K, CD_2Cl_2): 2.19 – 1.01 (m 198H, PCy_3) 0.51 (v. br, s 2H) -21.53 (br s, 12H).

δ $^{31}P\{^{1}H\}$ (298 K, CD_2Cl_2): 109.6 (br s), 88.5 (br, s)

Mass Spec: (FAB+ NOBA Matrix): Calcd $[(PCy_3)_6Rh_6H_{14}]^{2+}$: 1158.0 m/z, Found: 1158.3 m/z.

$[(PCy_3)_6Rh_6H_{10}][Y]_2$ (28-H_{14}): This was prepared by a related synthesis as for the $^iPr_3$ derivative, though evacuation for 3 days was required to reduce the hydride content fully. Solid material is unobtainable for this H_{10} cluster. Yield is also quantitative by ^1H NMR and $^{31}P\{^1H\}$ spectroscopy. The hydride content has been determined by numerous integrations on different samples of $[(PCy_3)_6Rh_6H_{10}][Y]_2$ and consistently integrates to 8 H: 2 H relative to the PCy_3 and anion signals (128 scans, 5 s delay to avoid saturation) Cation NMR shifts only listed.

δ ^1H (selected, 298 K, CD_2Cl_2): 2.28 – 1.14 (m 198H, PCy_3), –26.51 (br s, 8H), -28.45 (br s, 2H)

δ $^{31}P\{^1H\}$ (298 K, CD_2Cl_2): 92.1 (d, ^1J(RhP) 97.8)

Mass Spec: (FAB+ NOBA Matrix): Calcd. $[Rh_6(PCy_3)_6H_{10}]^{2+}$: 1156.0 m/z, Found: 1156.2 m/z.

7.3: References

1 K. Shelly, D. C. Finster, Y. L. Lee, W. R. Scheidt, and C. A. Reed, *J. Am. Chem. Soc*, 1985, **107**, 5955.

2 B. T. King, B. C. Noll, A. J. McKinley, and J. Michl, *Journal of the American Chemical Society*, 1996, **118**, 10902.

3 B. T. King, Z. Janousek, B. Gruner, M. Trammell, B. C. Noll, and J. Michl, *Journal of the American Chemical Society*, 1996, **118**, 3313.

4 T. Jelinek, J. Plesek, S. Hermanek, and B. Stibr, *Collect. Czech. Chem. Commun.*, 1985, **51**, 819.

5 Z. W. Xie, T. Jelinek, R. Bau, and C. A. Reed, *Journal of the American Chemical Society*, 1994, **116**, 1907.

6 T. S. Piper and G. Wilkinson, *J. Inorg. Nucl. Chem.*, 1957, **3**, 104.

7 R. B. King and M. B. Bisnette, *J. Organomet. Chem.*. 1976, **8**, 287.

8 R. B. King and F. G. A. Stone, *Inorg. Synth*, 1963, **7**, 99.

9 A. Bainbridge, P. J. Craig, and M. Green, *J. Chem. Soc. A*, 1968, 2715.

[10] W. Beck, K. Schloter, K. Sunkel, and G. Urban, *Inorg Synth*, 1989, **26**, 96.
[11] K. M. Kadish, D. A. Lacombe, and J. E. Anderson, *Inorg. Chem.*, 1986, **25**, 2246.
[12] M. Appel, K. Schloter, J. Heidrich, and W. Beck, *J. Organomet. Chem.*, 1987, **322**, 77.
[13] R. Schrock and J. A. Osborn, *J. Am. Chem. Soc.*, 1971, **93**, 2397.
[14] G. Winkhaus, *Inorg. Synth*, 1974, **15**, 18.
[15] W. D. Jones and F. J. Feher, *Organometallics*, 1983, **2**, 562.
[16] F. L. Taw, H. Mellows, P. S. White, F. J. Hollander, R. G. Bergmann, M. Brookhart, and M. D. Heinekey, *J. Am. Chem. Soc.*, 2002, **124**, 5100.
[17] J. Manriques, D. R. McAlister, R. D. Sanner, and J. E. Bercaw, *J. Am. Chem. Soc.*, 1978, **100**, 2716.
[18] W. E. Buschmann and J. S. Miller, *Inorg Synth*, 2002, **33**, 85.
[19] J. Huhmann-Vincent, B. L. Scott, and G. J. Kubas, *Inorg. Chem.*, 1999, **38**, 115.
[20] M. D. Heinekey, C. E. Radzewich, M. H. Voges, and B. M. Schomber, *J. Am. Chem. Soc.*, 1997, **119**, 4172.
[21] X. G. Fang, B. L. Scott, K. D. John, and G. J. Kubas, *Organometallics*, 2000, **19**, 4141.
[22] E. R. Evitt and R. G. Bergmann, *J. Am. Chem. Soc.*, 1980, **102**, 7003.
[23] G. M. Whitesides, T. J. McCarthy, and R. G. Nuzzo, *J. Am. Chem. Soc.*, 1981, **103**, 3396.
[24] J. Michl, in 'The Synthesis of Highly Alkylated Carborane Anions', ed. A. S. Weller, 2002.
[25] M. J. Frisch, G. W. Trucks, H. B. Schlegel, G. E. Scuseria, M. A. Robb, J. R. Cheeseman, V. G. Zakrzewski, J. A. Montgomery, R. E. Stratmann, J. C. Burant, S. Dapprich, J. M. Milliam, A. D. Daniels, K. N. Kudin, M. C. Strain, O. Farkas, J. Tomasi, V. Barone, M. Cossi, R. Cammi, B. Mennucci, C. Pomelli, C. Adamo, S. Clifford, J. Ochterski, G. A. Petersson, P. Y. ayala, Q. Cui, K. Morokuma, D. K. Malick, A. D. Rabuck, K. Raghavachari, J. B. Foreman, J. Cioslowski, J. V. Ortiz, A. G. Baboul, B. B. Stefanov, G. Liu, A. Liashenko, P. Piskorz, I. Komaromi, R. Gomperts, R. L. Martin, D. L. Fox, T. Keith, M. A. Al-Laham, C. Y. Peng, A. Nanayakkara, M. Challacombe, P. M. W. Gill, B. Johnson, W. Chen, M. W. Wong, J. L. Anders, C. Gonsalez, M. Head-Gordon, E. S. Replogle, and J. A. Pople, *Gaussian 98, revision A.9; Gaussian, Inc. Pittsburgh*, 1998.
[26] A. D. Becke, *Phys. Rev. A*, 1988, **38**, 3089.
[27] N. Godbout, D. R. Salahub, J. Andzelm, and E. Wimmer, *Can. J. Chem.*, 1992, **70**, 560.
[28] T. Shoeib, R. K. Milburn, G. K. Koyanagi, V. V. Lavrov, D. K. Bohme, K. W. M. Siu, and A. C. Hopkins, *Int. J. Mass Spectrom.*, 2000, **201**, 87.
[29] M. J. Ingleson, M. F. Mahon, N. J. Patmore, G. D. Ruggiero, and A. S. Weller, *Angew. Chem., Int. Ed. Engl.*, 2002, **41**, 3694.
[30] I. Zharov, B. T. King, Z. Havlas, A. Pardi, and J. Michl, *J. Am. Chem. Soc.*, 2000, **122**, 10253.
[31] J. Zhou, S. J. Lancaster, D. A. Walker, S. Beck, M. Thornton-Pett, and M. Bochmann, *J. Am. Chem. Soc.*, 2001, **123**, 223.
[32] G. J. P. Britovsek, V. C. Gibson, and D. F. Wass, *Angew. Chem., Int. Ed. Engl.*, 1999, **38**, 428.

[33] R. M. Bullock and M. H. Voges, *J. Am. Chem. Soc.*, 2000, **122**, 12594.
[34] M. D. Heinekey, B. M. Schomber, and C. E. Radzewich, *J. Am. Chem. Soc.*, 1994, **116**, 4515.
[35] A. C. Cooper, O. Eisenstein, and K. G. Caulton, *New. J. Chem*, 1998, 307.
[36] R. H. Crabtree and M. Lavin, *Chem. Commun.*. 1985, 1661.